Contrôle de l'interaction entre des espèces siliceuses et des espèces aluminosilicatées en présence d'une solution alcaline

Laeticia Vidal

Thèse de doctorat

Université de Limoges

École Doctorale Sciences et Ingénierie en Matériaux, Mécanique, Énergétique et Aéronautique (ED 522)

Laboratoire de Science des Procédés Céramiques et de Traitements de Surface (SPCTS)

Thèse pour obtenir le grade de

Docteur de l'Université de Limoges

Discipline : Matériaux Céramiques et Traitements de Surface

Présentée et soutenue par

Laëticia Vidal

Le 15 septembre 2016

CONTRÔLE DE L'INTERACTION ENTRE DES ESPÈCES SILICEUSES ET DES ESPÈCES ALUMINOSILICATÉES EN PRÉSENCE D'UNE SOLUTION ALCALINE

Thèse dirigée par Sylvie Rossignol

Co-encadrée par Joseph Absi et Emmanuel Joussein

JURY :

Président du jury

M. Patrick Simon, Directeur de recherche, CEMHTI Fédération MATV2L FR3469, CNRS

Rapporteurs

M. Jean Marc Chaix, Directeur de Recherche, SIMAP, Grenoble INP - Phelma

M. Fabien Frizon, Ingénieur de Recherche (HDR), Laboratoire de Physico-Chimie des Matériaux Cimentaires, CEA Marcoule

Examinateurs

M. François Cansell, Professeur des Universités, Bordeaux INP

M. Jean-Louis Gelet, Ingénieur, MERSEN

M. Joseph Absi, Professeur des Universités, SPCTS, Université de Limoges

M. Emmanuel Joussein, Maître de Conférences, GRESE, Université de Limoges

Mme. Sylvie Rossignol, Professeur des Universités, SPCTS, ENSCI

REMERCIEMENTS

Ce travail a été effectué au sein du laboratoire de Science des Procédés Céramiques et de Traitements de Surface (SPCTS) à Limoges en collaboration avec la société MERSEN. Je tiens donc à remercier Monsieur Thierry Chartier, directeur du SPCTS, de m'avoir accueillie au sein de ce laboratoire lors de mes travaux de thèse.

Je tiens à exprimer toute ma gratitude à Monsieur Jean-Marc Chaix, directeur de recherche au SIMAP de Grenoble, et Monsieur Fabien Frizon, Ingénieur de recherche au CEA de Marcoule, d'avoir accepté d'être rapporteurs de mes travaux de thèse, à Monsieur Patrick Simon, directeur de recherche au CEMHTI d'Orléans, d'avoir présidé mon jury de thèse ainsi que Monsieur François Cansell, professeur des Universités à Bordeaux INP, et Monsieur Jean-Louis Gelet, ingénieur chez MERSEN, pour leur participation à mon jury de thèse.

Je souhaite également remercier sincèrement ma directrice de thèse, Madame Sylvie Rossignol, et mes encadrants de thèse, Messieurs Emmanuel Joussein et Joseph Absi pour leur disponibilité, leur confiance, leur aide et leur soutien au cours de ces trois années et de m'avoir confié ce sujet qui m'a permis de découvrir la recherche scientifique ainsi que le côté industriel.

Je tiens également à remercier Messieurs Franck Sarrus et Jean-Louis Gelet de m'avoir accueillie au sein de la société MERSEN à Saint-Bonnet-de-Mure et pour le temps qu'ils m'ont consacré lors de mes déplacements à Saint-Bonnet-de-Mure ainsi que toutes les personnes avec qui j'ai collaboré au sein de l'entreprise.

Un très grand merci à Maggy Colas et Julie Cornette, du SPCTS, pour les manipulations de spectroscopie Raman, pour le temps qu'elles m'ont accordé, pour leur aide et leur gentillesse. Ce fut un plaisir de travailler avec vous.

Je remercie aussi Monsieur Jesus Sanz et Madame Isabel Sobrados pour leur accueil chaleureux à l'ICMM à Madrid mais également pour leur aide, leur gentillesse et leur bienveillance. J'ai beaucoup apprécié de travailler avec vous.

Je souhaite remercier tout le personnel du SPCTS et du CEC d'avoir toujours su se rendre disponible ainsi que pour leur gentillesse et notamment Yann et Patrice pour leur aide lors de mes nombreuses séances de MEB, Mickaël pour sa disponibilité pour les manips de dilatométrie, Sandra, Sylvestre, Stéphane, Jean-Michel, Paméla…

Merci à mes collègues et amis du labo pour tous les bons moments passés ensemble. Julie la basketteuse et Najet moudira, les deux gourmandes avec qui j'ai partagé mon bureau, pour leur bonne humeur (la plupart du temps), pour les soirées entre filles et pour m'avoir supportée pendant ma rédaction. William, fournisseur de caramel, avec qui j'ai partagé de nombreux repas, discussions et de bons moments au labo, je n'oublierai pas les soirées jeux (avec Antoine et Sylvain) et tes pièges informatiques ! Sylvain pour sa bonne humeur, son aide et son humour et Antoine pour sa gentillesse et nos discussions. Un très grand merci à Alessandra pour sa gentillesse, sa bonne humeur et pour m'avoir fait découvrir des spécialités italiennes ! Marie pour les bons moments lors de nos soirées, Ameni notamment pour les visites à Florence, à Madrid et à Vancouver, Ahmed pour sa bonne humeur ainsi que Fabrice, Sophie, Nadine, Aurélie, Perrine, Jérémie, Elmas, Etienne, Jéremy, Rémi, Joseph, Fanny…

Enfin, je remercie sincèrement mes parents, mon frère, mes grands-parents, mes amis et Rémy d'avoir cru en moi ainsi que de leur soutien, leurs encouragements, leur présence à tout moment au cours de ces trois années et sans qui tout cela n'aurait pas été possible.

INTRODUCTION GENERALE

De nos jours, l'un des principaux enjeux des entreprises concerne la production de matériaux plus économiques, plus écologiques et présentant une consommation énergétique moindre. Dans ce contexte, l'entreprise MERSEN, l'un des leaders mondiaux dans la production de fusibles, a initié en 2013 un projet FUI nommé FE^2E (Fusible Ecologiquement et Economiquement Efficace). Le développement industriel de ces nouveaux composants dépendra donc de la connaissance et de la maîtrise des interactions entre les différentes matières premières.

Les fusibles sont des composants électriques utilisés pour la protection contre les surintensités de courant ou les courts-circuits au sein d'une installation électrique. Ils sont constitués d'un corps en céramique et d'un remplissage à base de sable de silice et d'une solution de silicate de sodium, contenant un élément fusible en cuivre ou en argent. Le sable aggloméré et la céramique ont un rôle d'isolation vis-à-vis de l'arc électrique créé lors de la coupure du fusible. Ces matériaux doivent donc présenter des propriétés thermomécaniques suffisantes pour résister en condition normale de fonctionnement du fusible et à la pression induite lors de l'apparition de l'arc électrique. La méthode d'agglomération du sable actuellement utilisée entraîne des problèmes d'hétérogénéité au sein des matériaux induisant de nombreuses pertes lors de la production. De même, les corps en céramiques actuels nécessitent un traitement thermique à haute température coûteux en énergie.

Les solutions de silicate sont des liants minéraux présentant de nombreuses applications industrielles en tant que colles minérales, défloculants, liants, enduits, etc. Différents domaines, tels que les industries électrique et métallurgique, utilisent les solutions de silicate pour l'agglomération du sable. Les caractéristiques des blocs de sable aggloméré à l'aide de silicate dépendent des interactions entre la solution et le sable ainsi que du type de séchage. Le séchage par convection représentant un coût énergétique important, l'industrie métallurgique a récemment opté pour l'utilisation d'un séchage par micro-ondes plus rapide et moins coûteux. Ce type de traitement thermique pourrait également être transposé à la fabrication des composants électriques.

Dans le cadre du projet FE^2E, l'utilisation de géopolymères a été proposée pour remplacer les corps de fusibles actuels. Les géopolymères sont des matériaux qui s'inscrivent dans le développement durable de par leur faible consommation énergétique et leurs faibles émissions de CO_2 du fait de leur consolidation à température ambiante. De nombreuses études

à travers le monde s'intéressent à ces matériaux. Les caractéristiques des matières premières, à savoir la solution de silicate alcalin et la source aluminosilicate, influencent les interactions entre ces matériaux et donc les réactions de polycondensation. Les matériaux géopolymères étant fabriqués à partir d'une solution de silicate, la formation d'une couche de transition pourrait être envisagée entre le bloc de sable aggloméré et le liant géopolymère.

Par conséquent, ce manuscrit s'articule autour de quatre chapitres. Dans un premier temps, une étude bibliographique sur les différents composants électriques, les solutions de silicate et leur interaction avec différents types de matériaux, ainsi que sur les paramètres influençant les propriétés des matériaux consolidés est développée. Le deuxième chapitre concerne les caractéristiques des différentes matières premières, les protocoles expérimentaux et les différentes techniques de caractérisation déployés. Le troisième chapitre correspond à une synthèse des différents résultats concernant la réalisation d'un fusible et d'un busbar plus écologiques et plus économiques. Ensuite, les différents travaux publiés (7 articles, 3 actes, 1 chapitre) seront regroupés dans le quatrième chapitre. Finalement, une conclusion fera la synthèse des différents résultats obtenus au cours de ces travaux de thèse.

ACL 1. Effect of the addition of ammonium molybdate on metakaolin-based geopolymer formation: Shrinkage and crystallization, L. Vidal, E. Joussein, M. Colas, J. Absi, S. Rossignol, Powder Technology, 275, 211-219, 2015.

ACL 2. Recycling of aluminosilicate waste: Impact onto geopolymer formation, N. Essaidi, A. Gharzouni, L. Vidal, F. Gouny, E. Joussein, S. Rossignol, European Physical Journal: Special Topics, 224 (9), 1707-1713, 2015.

ACL 3. Recycling of geopolymer waste: Influence on geopolymer formation and mechanical properties, A. Gharzouni, L. Vidal, N. Essaidi, E. Joussein, S. Rossignol, Materials and Design, 94, 221-229, 2016.

ACL 4. Controlling the reactivity of silicate solution: A FTIR, Raman and NMR study, L. Vidal, E. Joussein, M. Colas, J. Cornette, J. Sanz, I. Sobrados, J.-L. Gelet, J. Absi, S. Rossignol, Colloids and Surfaces A: Physicochemical and Engineering Aspects, 503, 101-109, 2016.

ACL 5. Identification of chains and rings in alkaline silicate solutions by Raman spectroscopy: Effect of alkali cation, L. Vidal, E. Joussein, M. Colas, J. Cornette, J. Absi, S. Rossignol, Spectrochimica Acta Part A: Molecular and Biomolecular Spectroscopy, submitted.

ACL 6. How to counteract the low reactivity of an alkaline solution, L. Vidal, E. Joussein, I. Sobrados, J. Absi, S. Rossignol, Journal of Non-Crystalline Solids, 452, 220-230, 2016.

ACL 7. Coating of unreactive and reactive surface by aluminosilicate binder, L. Vidal, E. Joussein, J. Absi, S. Rossignol, Ceramics International, submitted.

ACLN 1. Role of siliceous species in geopolymer reactant mixture: Interaction with $(NH_4)_2Mo_2O_7$, L. Vidal, A. Autef, S. Selmani, E. Joussein, S. Rossignol, Key Engineering Materials, 617, 46-49, 2014 (2nd International Symposium on Inorganic Environmental Materials, ISIEM 2013, Rennes, France).

ACLN 2. Addition of ammonium molybdate in geopolymer formulation, L. Vidal, E. Joussein, J. Absi, S. Rossignol, Advances in Science and Technology, 92, 8-13, 2014 (CIMTEC 2014, Montecatini Terme, Italie).

ACLN 3. Recycled geopolymer on new formulations, N. Essaidi, L. Vidal, F. Gouny, E. Joussein, S. Rossignol, Ceramic Engineering and Science Proceedings, 36 (8), 49-60, 2016 (39th International Conference on Advanced Ceramics and Composites, ICACC 2015, Daytona Beach, Etats-Unis).

Chapitre. Alkaline silicate solutions: An overview of their structure, reactivity, and applications, L. Vidal, A. Gharzouni, S. Rossignol, dans : L. Klein, M. Aparicio, A. Jitianu, Handbook of Sol-Gel Science and Technology, in press.

CHAPITRE I

Synthèse bibliographique

I. INTRODUCTION

Les propriétés des blocs de sable aggloméré et des liants géopolymères pour l'industrie électrique dépendent des interactions entre les différents matériaux. Cette partie a donc pour but de présenter, dans un premier temps, les composants électriques visés. Les caractéristiques des solutions et leurs interactions avec les différents matériaux seront ensuite analysées. Finalement, les différents paramètres qui influencent les propriétés des matériaux finaux seront développés.

II. DESCRIPTION DES COMPOSANTS ÉLECTRIQUES

Au sein des composants électriques, le fusible et le busbar seront présentés avec notamment les matériaux isolants les constituant.

1. Le fusible

a. Description et rôle du fusible

Un fusible est un composant électrique qui a un rôle de protection vis-à-vis d'une installation électrique et des personnes [1]. En effet, le fusible est placé au sein d'un circuit électrique afin de protéger les différents composants d'une surcharge de courant (court-circuit ou surintensité) qui risquerait de les endommager. Le fusible présente deux fonctions principales : une fonction de conduction et une fonction de coupure [1, 2]. En fonctionnement normal, le fusible laisse passer le courant dans un élément conducteur et, lors d'une surcharge de courant, l'élément conducteur pourra fondre entraînant une coupure du circuit.

Un fusible est composé d'un corps isolant, d'éléments conducteurs, et d'un matériau aggloméré (**Figure 1**) [3]. Le corps isolant est généralement en céramique ou en plastique contenant les éléments fusibles. Ces derniers sont de très bons conducteurs comme le cuivre ou l'argent. Le sable, pouvant être aggloméré par une solution de silicate, entoure les lames métalliques et joue un rôle d'isolant lors de la fusion de l'élément fusible. Finalement, des pièces de raccordement sont placées aux extrémités des fusibles et permettent de les connecter au circuit électrique.

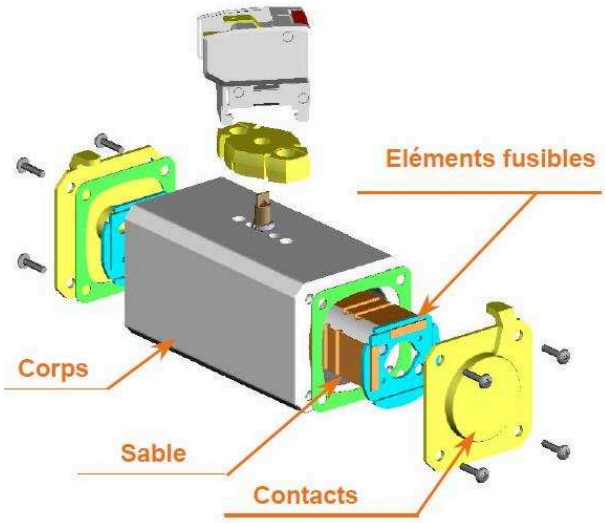

Figure 1 : *schéma de constitution d'un fusible [***3**].

b. Matériaux isolants

Les matériaux isolants constituant un fusible, à savoir le corps en céramique et le bloc de sable aggloméré, vont être détaillés.

L'enveloppe isolante des fusibles participe à différentes fonctions [2] à savoir la conduction et la coupure. Dans le cas de la fonction de conduction, le corps intervient sur la résistance thermique (évacuation de la chaleur générée dans l'élément fusible lors du passage du courant), la tenue en température (résistance à des températures supérieures à 150 °C) et la résistance aux chocs thermiques. Pour la fonction de coupure, l'enveloppe isolante doit absorber l'énergie libérée lors de l'apparition de l'arc électrique. De plus, le corps de fusible doit protéger des manifestations extérieures du fonctionnement et de la coupure.
Les matériaux céramiques généralement utilisés pour la fabrication des corps de fusible sont des silicates de magnésium (stéatites, cordiérites…), des aluminosilicates et également des céramiques à haute teneur en alumine (> 80 %).

L'agglomération du sable doit être préservée durant toute la vie du fusible aussi bien en fonctionnement normal que lors d'une surcharge de courant. Il doit donc répondre aux critères suivants [1, 2] :

(i) Etre capable d'absorber l'énergie calorique de l'arc pour permettre son extinction. Pour les coupures aux courants critiques, il s'agit de pouvoir absorber environ 105 J.

(ii) Conserver son pouvoir isolant lors de la formation du canal d'arc.

(iii) Posséder une porosité optimale. En effet, si l'empilement granulaire n'est pas homogène, les particules ionisées peuvent s'accumuler et entraîner des contraintes locales très fortes capables de détruire le fusible. En cas de compacité faible, la quantité de matière solide (les grains de sable) en contact avec la lame d'argent est plus faible conduisant à une absorption moindre de l'énergie de l'arc. Finalement, le sable doit maintenir une surpression de gaz dans le canal facilitant l'extinction de l'arc. Néanmoins, l'empilement doit être suffisamment modifiable pour permettre la condensation des vapeurs métalliques ionisées au plus loin de la zone d'arc.

(iv) Absorber partiellement les chocs mécaniques subis durant la coupure.

La fabrication des fusibles est réalisée à partir de différents liants de type organique ou minéral permettant l'agglomération du sable en passant par les étapes de séchage à température ambiante [1]. Cependant, la solution minérale à base de silicate de sodium a été privilégiée [4, 5]. De plus, l'agglomération du sable a été optimisée par la technique de la pluviation permettant d'obtenir des échantillons de compacité maximale de façon reproductible [6]. Parallèlement, il a été mis en évidence la possibilité de tasser le sable par vibration pour la fabrication de fusibles [7, 8]. Par conséquent, lors de la fabrication des fusibles, le sable est soit tassé par pluviation, soit par vibration et le liant utilisé est du silicate de sodium.

2. Le busbar

La mise en œuvre de composants électroniques pour l'électrotechnique impose des conditions d'emploi de plus en plus sévères du fait des puissances importantes à contrôler. La condition la plus importante est désignée par l'expression « fonctionnement en commutation » (**Figure 2**). En effet, les dispositifs à semi-conducteur jouent leur rôle d'interrupteur et il est impératif de les faire fonctionner en commutation. Le busbar est donc un composant conducteur, généralement en cuivre ou en aluminium, auquel plusieurs circuits peuvent être reliés séparément, incorporés dans un boîtier en plastique [9]. Il permet de réduire les inductances de câblage des installations assumant un rôle de commutation dans leur fonctionnement permanent [2].

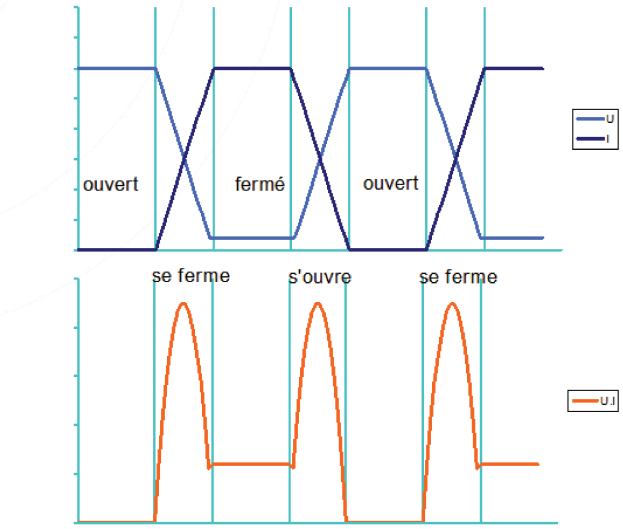

Figure 2 : courbes du courant et de la tension, ainsi que de la puissance lors de la *commutation d'un interrupteur semi*-conducteur.

Même s'*il est facile d'imprégner* du sable par du silicate, il sera nécessaire de trouver *une solution à plus basse température, mais aussi de suppléer l'enveloppe céramique par des matériaux basse température en terme d'innovation.*

III. LES SOLUTIONS DE SILICATE

Au sein de la grande famille des silicates, il existe entre autres les solutions de silicate alcalin (également appelées water glass) [10] ainsi que les verres silicatés [11]. Ces différents composés sont basés sur l'empilement de tétraèdres de silicium issus de la structure cristalline de la silice [12] et présentent de nombreuses applications industrielles en tant que liants, formateurs de gels, enduits, défloculants ou inhibiteurs de corrosion [13, 14]. Les différentes applications utilisant plus particulièrement les solutions silicatées vont dépendre de leur réactivité et donc des espèces siliceuses qu'elles contiennent.

1. Préparation des solutions

Les solutions de silicate peuvent être obtenues selon différents procédés présentant une influence sur les espèces silicatées. Les solutions commerciales sont généralement préparées par dissolution d'un verre silicaté. Le verre peut être obtenu par une réaction entre de la silice et des carbonates alcalins ou des sulfates alcalins réalisée à 1300 °C [15] (**Eq. 1** et **Eq. 2**).

$3\ SiO_2 + M_2SO_4 + ½\ C = ½\ CO_2 + SO_2 + 3\ SiO_2 \cdot M_2O$ **Eq. 1**

$3\ SiO_2 + M_2CO_3 = CO_2 + 3\ SiO_2 \cdot M_2O$ **Eq. 2**

Une autre méthode de préparation consiste à dissoudre des hydroxydes alcalins et de la silice amorphe dans de l'eau [16] (**Eq. 3**). Cette méthode est utilisée pour la fabrication de solutions de silicates alcalins dans les laboratoires.

$2\ MOH + 3\ SiO_2 \rightarrow 3\ SiO_2 \cdot M_2O + H_2O$ **Eq. 3**

La dissolution de ces espèces siliceuses dépend de la valeur de pH, et lorsque celle-ci augmente (i.e. la concentration en cations alcalins augmente), la solubilité de la silice devient plus élevée [17] (**Figure 3**). L'influence de la nature de la silice utilisée (quartz, opale, gel de silice) a été étudiée en fonction de l'équilibre de dissolution de la silice dans l'eau. Iler [15] montre que, pour la silice amorphe, la vitesse de dissolution augmente avec la valeur de pH. Deux processus contrôleraient ce phénomène de dissolution. Pour une valeur de pH inférieure à 11, la silice amorphe est dissoute selon l'**Eq. 4**.

$SiO_2 + 2\ H_2O = H_4SiO_4$ **Eq. 4**

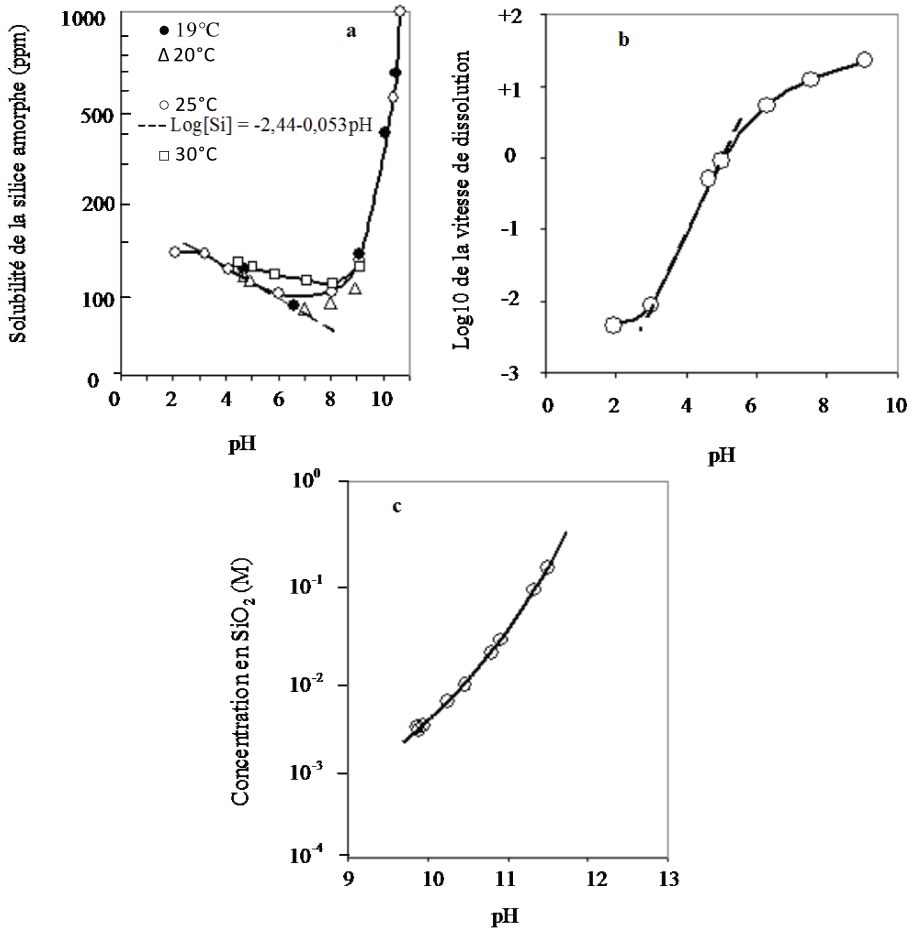

Figure 3 : (a) solubilité de la silice amorphe et **(b)** vitesse de dissolution de la silice pour 2 < pH < 10 [15] et **(c)** concentration en silice pour 9 < pH < 12 [17].

Pour une valeur de pH supérieure à 11, l'attaque de la silice est initiée de la même façon par l'anion OH^-. L'acide silicique (H_4SiO_4) va ensuite se dissocier selon les **Eq. 5** et **Eq. 6**. Plus la valeur de pH augmente, plus le phénomène de dissociation est important engendrant ainsi une augmentation de la dissolution de la silice.

$$H_4SiO_4 + OH^- = H_3SiO_4^- + H_2O \qquad \textbf{Eq. 5}$$

$$H_3SiO_4^- + OH^- = H_2SiO_4^{2-} + H_2O \qquad \textbf{Eq. 6}$$

Par ailleurs, Dietzel [18] a montré que, pour de faibles valeurs de pH, les espèces prédominantes sont monomériques (**Figure 4**). Lorsque la valeur de pH augmente, des acides polysiliciques apparaissent et deviennent stables pour des valeurs de pH supérieures à 10. La formation des acides polysiliciques peut être décrite selon l'**Eq. 7**.

$$\equiv Si\text{-}OH + HO\text{-}Si\equiv = \equiv Si\text{-}O\text{-}Si\equiv + H_2O \qquad \textbf{Eq. 7}$$

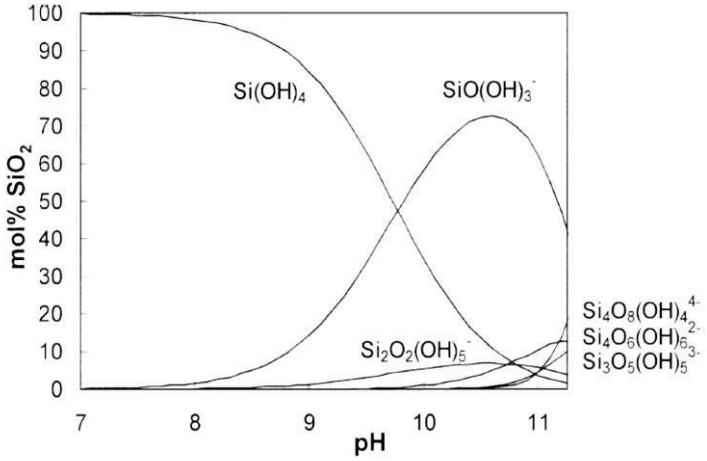

Figure 4 : *variation des espèces d'acide silicique en fonction de la valeur de pH à* température ambiante [18].

2. Structure des solutions

Les solutions de silicates alcalins sont composées de différentes espèces monomériques (SiO_4^{4-}) et polymériques ($Si_2O_7^{6-}$, $Si_3O_9^{6-}$, $(SiO_3^{2-})_n$) et caractérisées par une structure complexe. Ces dernières ont fait l'objet de nombreux travaux structuraux par les techniques spectroscopiques.

La résonnance magnétique nucléaire (RMN) ^{29}Si a largement été utilisée pour la caractérisation des solutions de silicate alcalin. Cette technique permet de distinguer et de quantifier les différentes espèces Q^n. La notation Q^n, utilisée pour décrire les espèces silicatées, a été introduite par Engelhardt et al. [19] (**Figure 5A**). Dans cette notation, Q représente l'atome de silicium connecté à n atomes d'oxygène pontant et (4-n) atomes

d'oxygène non pontant dans un environnement tétraédrique. La variation des différentes espèces Q^n a été déterminée en fonction du rapport Si/M et de la valeur de pH [20, 21] (**Figure 5B**). La présence d'espèces Q^4 est notée pour les solutions de rapport Si/M > 1,6. De plus, la présence des espèces Q^2 et Q^3 en grande quantité semble indiquer l'existence de chaînes simples et ramifiées pour des rapports molaires Si/M élevés. Pour des rapports élevés (Si/M >1), les espèces majoritaires sont les espèces Q^2 et Q^3. En revanche, pour des rapports Si/M <1, les espèces prédominantes sont les entités Q^0 et Q^1. Il est à noter qu'au cours de la dépolymérisation des solutions [22], il y a la formation d'espèces cycliques Q^{2c} et Q^{3c} révélant ainsi la formation d'anneaux au sein de ces solutions (**Figure 6a, b**).

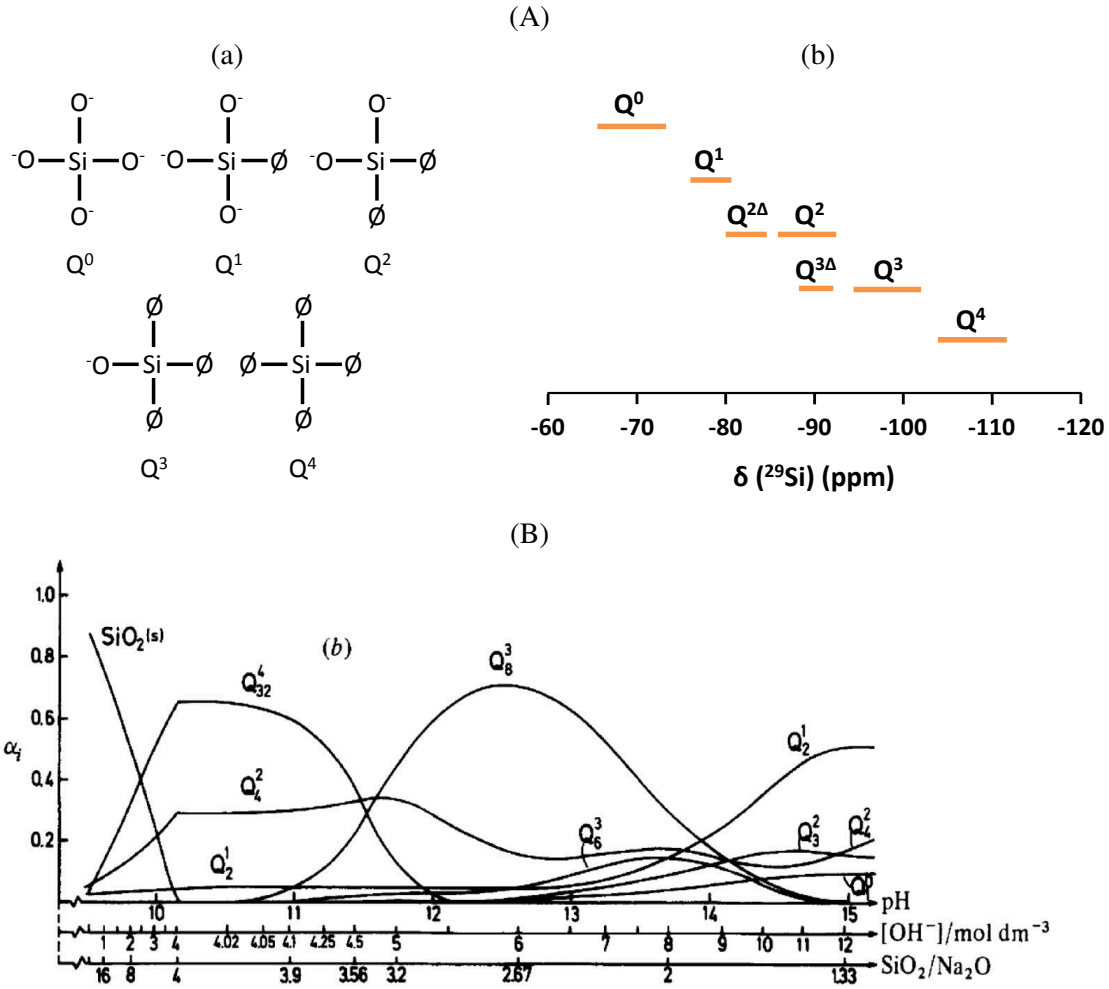

Figure 5 : (A) (a) représentation des différentes espèces Q^n et **(b)** valeur du déplacement chimique relatif aux différentes entités structurales [19] et **(B)** répartition des espèces silicatées Q^n en fonction du rapport molaire SiO_2/Na_2O ([Si]=8 M) [22].

Les pourcentages des différentes espèces déterminés par RMN peuvent ensuite être utilisés pour le calcul du nombre d'atomes d'oxygène non-pontant par tétraèdre [SiO_4] (NBO) selon l'**Eq. 8** [23, 24].

$$NBO/T = (3*Q^1 + 2*Q^2 + Q^3)/100 \qquad \textbf{Eq. 8}$$

L'utilisation de la RMN 2D permet de déterminer l'environnement des différentes entités Q^n. Tognonvi et al. [14] ont ainsi démontré que, pour une solution de silicate de sodium (Si/Na = 1,7), les espèces Q^n sont préférentiellement reliées à des entités Q^n ou Q^{n+1}, i.e. (Q^3-Q^3), (Q^3-Q^4) ou (Q^2-Q^3). Cho et al. [25] ont également pu identifier de nouvelles structures d'oligomères de petites tailles au sein d'une solution de silicate de sodium dépolymérisée (Si/Na = 0,6).

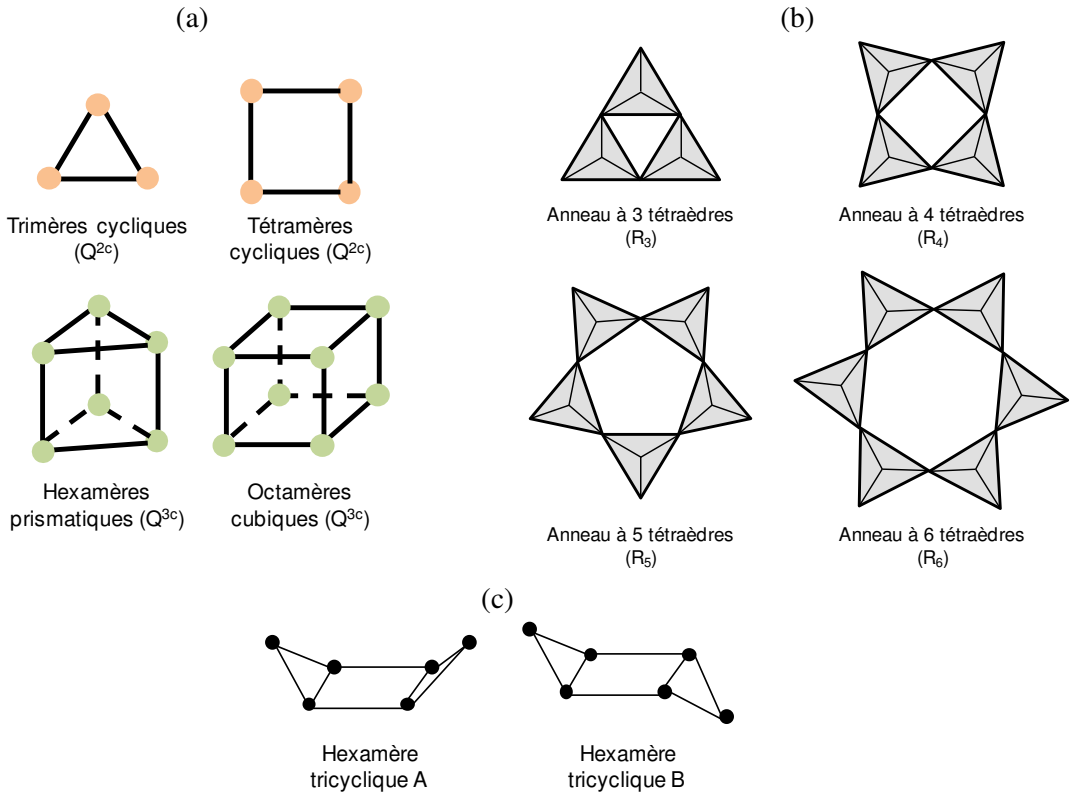

Figure 6 : représentation schématique **(a)** de quelques espèces cycliques contenant les espèces (●) Q^{2c} et (●) Q^{3c}, **(b)** des anneaux de différentes tailles et **(c)** des espèces de *différentes configurations dans l'espace [*25].

Toutes ces études par RMN (1D et 2D) ont permis d'identifier une cinquantaine d'espèces silicatées de diverses formes (linéaires, cycliques, prismatiques, etc.) dans des solutions faiblement concentrées [26] (**Figure 6c**). Il est à noter que, pour compléter ces études, la RMN ^1H pourrait être appliquée, puisque ce noyau est utilisé pour caractériser des gels de silice ainsi que des verres silicatés [27]. L'absence de caractérisation des solutions de silicate

par RMN du proton pourrait être due à la quantité d'eau majoritaire au sein des solutions contrairement aux verres ou aux gels.

La spectroscopie infrarouge à transformée de Fourier (IRTF) a été utilisée afin de déterminer les espèces silicatées présentes au sein des solutions à partir de la large bande attribuée à l'élongation (stretching) antisymétrique des liaisons Si-O-Si. La notation Q^n utilisée pour décrire les espèces silicatées en RMN ^{29}Si ne peut pas être utilisée directement en spectroscopie IRTF mais conventionnellement elle est admise [28] pour différencier les différentes espèces Q^n au sein de la large bande du pic Si-O-Si. Différents auteurs ont ainsi montré que les contributions des espèces Q^4, Q^3 et Q^2 sont respectivement notées à des nombres d'onde de l'ordre de 1150-1200, 1100 et 1000-1030 cm^{-1} [28, 29]. Les bandes attribuées aux espèces Q^1 et Q^0 ont également été respectivement positionnées vers 900-920 et 820-876 cm^{-1} [23].

Afin de compléter les données obtenues par la spectroscopie IRTF, **la spectroscopie Raman** a été développée essentiellement pour les verres sachant que peu d'études relatent des solutions de silicate [30]. Les analyses réalisées sur les verres ont révélé, en plus des différentes contributions précédentes, l'existence de contributions attribuées au mode de respiration des anneaux à 3, 4, 5 tétraèdres ou plus ($R_{3,4,5 \text{ et plus}}$) [31] (**Figure 7a**). La contribution de ces anneaux dépend de la quantité de cations alcalins pouvant entraîner un déplacement de la bande associée aux anneaux à 5 tétraèdres (**Figure 7b**) [32]. Ces phénomènes ont été reliés à une diminution de l'angle Si-O-Si et donc à une diminution de la taille des anneaux [33]. La dépolymérisation des différentes espèces a été démontrée par la teneur en ions alcalins [34]. En effet, l'augmentation de la quantité de cation alcalin entraîne la formation d'espèces Q^3 au détriment des espèces Q^4 et pour des teneurs plus élevées, la formation d'entités Q^2 au détriment des entités Q^3.

Par ailleurs, la complémentarité de la spectroscopie Raman est donc de pouvoir obtenir des informations sur la taille des cycles (à basse fréquence) ainsi que sur les espèces Q^n (à haute fréquence) présentes au sein des verres.

(a)

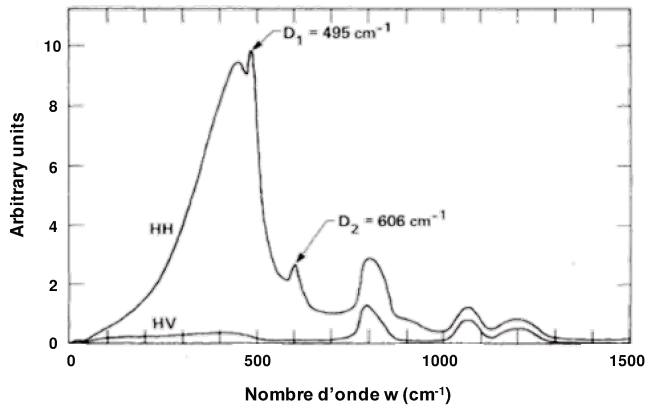

(b)

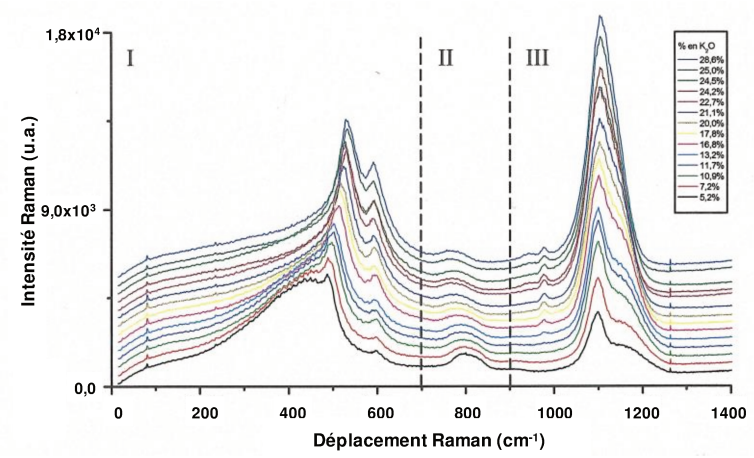

Figure 7 : (a) *spectre Raman d'un verre de silice* [33] et **(b)** évolution des spectres Raman en fonction de la quantité de K_2O (la quantité augmente de bas en haut de 5,2 à 28,6 % de K_2O) [31].

Peu de travaux comparent les données issues des études par spectroscopie IRTF, Raman et RMN 2D. Néanmoins, il peut être cité les travaux de Le Losq [35] qui ont révélé des différences de proportions de liaisons Si-O-Si entre un verre à base de potassium et de sodium confirmés par RMN 2D. Concernant les solutions de silicate alcalin, il semblerait opportun d'étudier leur structure par spectroscopie Raman afin de déterminer l'existence et la taille des chaînes et des anneaux lors de la dépolymérisation.

3. Paramètres régissant les entités structurales

Les différentes études structurales (IRTF, Raman et RMN) ont montré que les espèces Q^n, les anneaux et les chaînes gouvernaient le degré de polymérisation des solutions en relation avec la nature du cation alcalin. Il est également important de connaître l'impact du mode de préparation, du rapport molaire Si/M et du taux d'eau.

Il a été vu précédemment que les solutions de silicate alcalin peuvent être commerciales ou préparées au laboratoire. Les solutions sont donc issues de la dissolution d'un verre silico-alcalin ou d'une silice amorphe. Pour un même rapport Si/M, Prud'homme et al. [36] ont démontré que la solution préparée au laboratoire contient nettement plus d'espèces dépolymérisées Q^0 tandis que le rapport des entités Q^1/Q^2 est similaire pour les deux solutions. Ainsi, la solution provenant d'une solution commerciale est plus polymérisée qu'une solution préparée au laboratoire pour un même rapport Si/M. De même, Gharzouni et al. [23] ont montré que des solutions commerciales, de rapports Si/M compris entre 1,7 et 0,4, contenaient des espèces similaires, mais de contributions différentes en fonction de la quantité d'eau due au cation alcalin. Les solutions présentant des rapports Si/M initiaux plus faibles contiennent plus d'espèces Q^0 que les solutions de rapports Si/M initiaux élevés. Pour des solutions issues de la dissolution d'un verre ou d'une silice colloïdale, Brykov et al. [21] ont démontré que la méthode de préparation de la solution avait peu d'influence sur la connectivité des atomes de silicium. Il semble donc que la méthode de préparation est un paramètre influant sur la quantité des différentes espèces Q^n contenues au sein des solutions.

Quelques études ont mis en évidence l'influence du rapport molaire Si/M sachant que c'est à partir d'une valeur de Si/M = 1 que les phénomènes de dépolymérisation interviennent. Bourlon [20] a démontré par diffusion dynamique de la lumière (DLS) qu'une augmentation de ce rapport entraîne une baisse importante du volume hydrodynamique des espèces. L'auteur a également analysé ces solutions par une étude structurale par rayons X (diffusion et diffraction) et a mis en évidence que l'augmentation du rapport Si/M entraîne une diminution des interactions répulsives entre particules ainsi qu'une augmentation de la taille des particules. Steins [37] a aussi observé ce phénomène par des analyses structurales par rayons X. Par analogie, l'impact du rapport molaire M/Si au sein des verres a été mis en évidence par la valeur du NBO qui augmente quand ce rapport diminue (**Figure 8**) [38]. Le rapport molaire Si/M semble donc influencer l'état de polymérisation des solutions.

De plus, des études ont ainsi mis en évidence que la dilution d'une solution entraîne une polymérisation des anions silicatés. En effet, Lucas et al. [5] ont démontré que la dilution d'une solution entraîne des réactions de polycondensation des espèces silicatées par spectroscopie IRTF. Böschel et al. [39] ont également observé une variation de la taille des particules silicatées lors de la dilution. Tognonvi et al. [14] ont noté que la dilution de la solution entraîne une augmentation de la taille des plus petits colloïdes mais également une diminution de la taille des particules les plus importantes. Ces variations de taille de colloïdes

suggèrent la présence de réactions de polycondensation lors de la dilution. Le taux d'eau contrôle donc le degré de polymérisation et donc la réactivité des solutions de silicate.

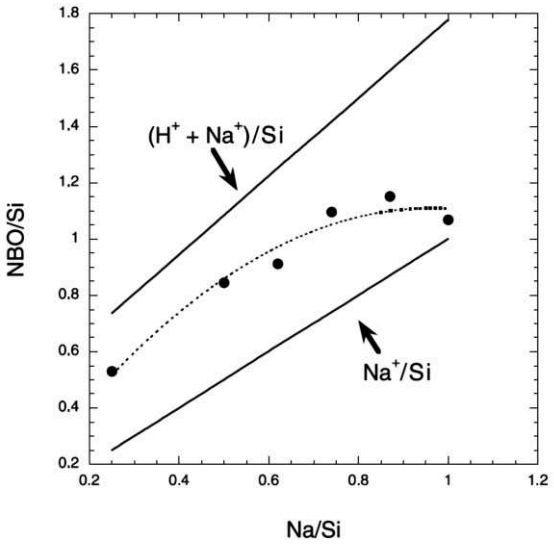

Figure 8 : *variation du nombre d'atomes d'oxygène non*-pontant (NBO) en fonction du rapport molaire Na/Si pour des verres sodo-silicatés [38].

La nature du cation alcalin présente également une faible influence sur les espèces silicatées. En effet, l'augmentation de la taille du cation entraîne la formation d'espèces silicatées légèrement plus protonées ainsi qu'une légère augmentation de la quantité d'espèces Q^{2c} et Q^{3c} [37]. De plus, pour des rapports Si/M variant de 0,6 à 1,5, la polymérisation des solutions de silicate est favorisée par une augmentation de la taille des cations selon l'ordre suivant $Na^+ < K^+ < Rb^+ < Cs^+$ [37]. Ce phénomène est dû à l'augmentation de la sphère d'hydratation lorsque la taille du cation diminue. D'autre part, des travaux sur les solutions ont permis de déterminer le rayon ionique des cations hydratés ainsi que l'effet de ces cations sur les phénomènes de diffusion. Mähler et Persson [40] ont déterminé le rayon ionique des cations Na^+ et K^+ et ils ont montré que la distance Na-O était légèrement plus faible que la distance K-O. Les études de diffusion menées par Melkior et al. [41] ont démontré que le potassium présentait une vitesse de diffusion plus élevée que le cation sodium. Cette différence de vitesse de diffusion a été corrélée au rayon de Stokes (**Figure 9**) lié à la sphère d'hydratation [42]. Plus la sphère d'hydratation est importante, plus la diffusion de ce cation sera ralentie (**Figure 9**). La taille du cation alcalin semble donc avoir une influence sur les espèces silicatées au sein de la solution.

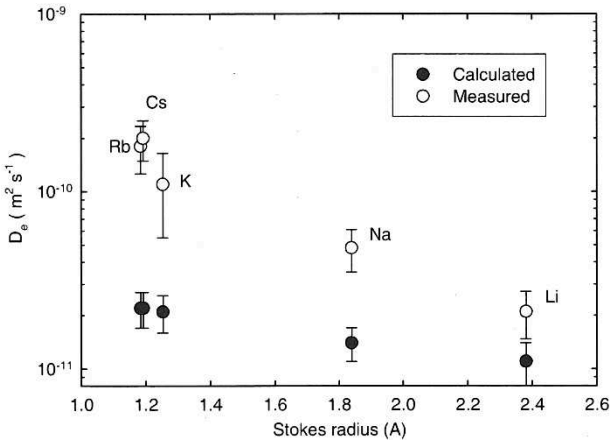

Figure 9 : valeur des coefficients de diffusions expérimentaux et calculés en fonction des rayons de Stokes des différents cations alcalins [41].

Les paramètres contrôlant le taux de polymérisation de la solution sont la méthode de *préparation, le taux d'eau, le rapport Si/M* ainsi que le cation alcalin. Une étude plus *approfondie des solutions par spectroscopie Raman pourrait permettre l'obtention d'informations* pertinentes concernant la présence et la taille des chaînes et des anneaux au sein des solutions.

IV. INTERACTIONS AVEC DIFFÉRENTS COMPOSANTS

L'utilisation des solutions de silicate, pour la fabrication de fusibles ou de liants géopolymères, nécessite la compréhension des interactions en présence de sable, de métakaolins ou de métaux. Ces interactions sont aussi gouvernées par les énergies de surface qui seront déterminées au travers des angles de mouillage.

1. Interactions avec du sable

Les interactions entre une solution alcaline et du sable vont dépendre des paramètres intrinsèques de chaque constituant et de leur interaction.

La dissolution de quartz menée par Schwartzentruber et al. [43] au sein des solutions alcalines à 80 et 90 °C révèle que plus la valeur de pH basique est élevée, plus le taux de dissolution est favorisé. Le modèle cinétique associé, comportant une étape intermédiaire de chimisorption d'ions silicates à la surface du quartz, démontre l'affinité des espèces dissoutes avec la surface. Cette couche adsorbée, pour de faibles concentrations, peut recouvrir une grande partie de la surface, ayant pour effet de retarder le phénomène de dissolution. Lorsque la concentration augmente, il y a également le phénomène de polymérisation des espèces

silicatées [43] dû à la saturation de la solution. L'effet de la valeur de pH et de la force ionique sur la dissolution du quartz a également été étudié par Brady et al. [44]. Les résultats obtenus ont confirmé les tendances observées par Knauss et al. [45] (**Figure 10**). Le taux de dissolution est quasiment inexistant pour des valeurs de pH inférieures à 6 alors qu'au-delà il augmente de façon exponentielle. Ce phénomène de dissolution est lié à la diffusion des différentes espèces favorisée par la température et les forces ioniques de la solution d'attaque. De plus, Nangia et al. [46] expliquent que la dépendance du taux de dissolution en fonction de la valeur de pH est due à l'existence de différents sites à la surface des grains : un site protoné ($\equiv SiOH_2^+$), un site neutre ($\equiv SiOH$) et un site déprotoné ($\equiv SiO^-$). Lors des simulations numériques, les réactions protonées, neutres et déprotonées ont été modélisées respectivement par l'**Eq. 9**, l'**Eq. 10** et l'**Eq. 11**.

$(OH)_3Si\text{-}O\text{-}Si(OH)_3H^+ + H_2O \rightarrow (OH)_3Si\text{-}OH + Si(OH)_3\text{-}OH_2^+$ **Eq. 9**

$(OH)_3Si\text{-}O\text{-}Si(OH)_3 + H_2O \rightarrow (OH)_3Si\text{-}OH + Si(OH)_3\text{-}OH$ **Eq. 10**

$(OH)_3Si\text{-}O\text{-}Si(OH)_2O^- + H_2O \rightarrow (OH)_3Si\text{-}OH + Si(OH)_3\text{-}O^-$ **Eq. 11**

Pour des valeurs de pH proches de 2, le mécanisme prédominant est le neutre. Pour des valeurs de pH en milieu basique, les sites déprotonés contribuent majoritairement au mécanisme de dissolution. Un autre point concerne la relation entre le taux de dissolution et la charge de surface évoluant de façon linéaire selon les travaux de Gratz et al. [47].

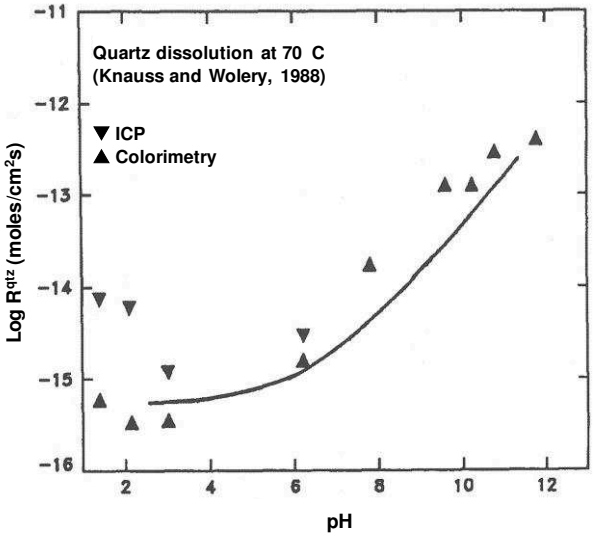

Figure 10 : comparaison des taux de dissolution du quartz (▲, ▼) de Knauss et al. [45] avec la modélisation de Brady et al. [44] (ligne).

Deleuze et al. [48] ont étudié l'influence du cation alcalin sur les mécanismes de dissolution du quartz en milieu basique pour différentes températures selon cet ordre : $Li^+ > Na^+ > K^+$. Ces variations peuvent être expliquées par le pouvoir polarisant et l'effet

d'encombrement stérique dû à la taille du cation. De même, l'augmentation de la valeur de l'angle Si-O-M avec la taille du cation en relation avec la sphère d'hydratation (M = Li, Na ou K) favorise les réactions de dissolution. Comme précédemment énoncé, en présence de solutions proches d'une valeur de pH neutre [49, 50], la taille du cation a un très faible impact sur le taux de dissolution du quartz.

L'influence de la température sur les mécanismes de dissolution du quartz est liée à la solubilité de la silice et aux interactions entre les différentes espèces siliceuses [15, 51]. En effet, à partir d'une valeur de pH supérieure à 9 (**Figure 11**), le nombre des espèces siliceuses croît de façon considérable engendrant la formation de précipités ou de gels. Ces derniers vont être favorisés en fonction de la température par les phénomènes de coalescence. Ceci entraîne des évolutions microstructurales des gels, induisant une augmentation de la taille des pores et de la perméabilité des gels ainsi qu'une réduction de leur surface spécifique [52, 53, 54].

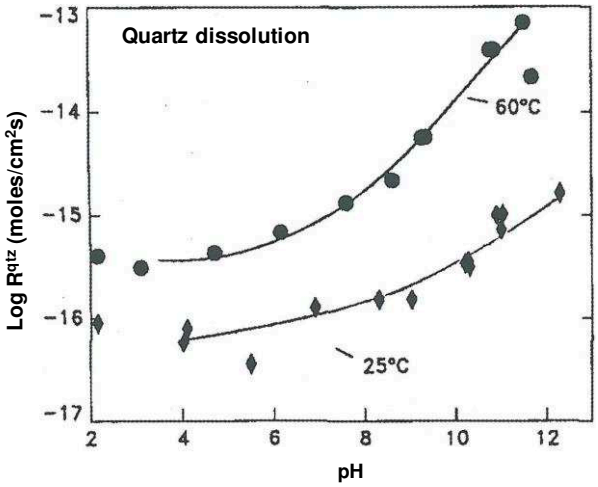

Figure 11 : évolution du taux de dissolution du quartz à (♦) 25 et (●) 60 °C en fonction de la valeur de pH obtenue par Brady et al. [44].

Il a été montré que l'effet de la surface du sable sur les interactions entre une solution et un grain de sable dépendait essentiellement des énergies de surface du sable qui peuvent être activées avec la température [55, 56]. L'érosion des grains de silice est possible par l'existence de cristallites pouvant être extraites en préservant l'énergie de surface. Néanmoins, à terme, ce phénomène pourra induire des modifications de rugosité.

A titre d'exemple, le cristal de Kossel, contenant des faces F (5 liaisons avec d'autres cristaux), S (4 liaisons) et K (3 liaisons), permet de modéliser la réactivité des cristaux (**Figure 12**) [55]. Lors de la dissolution, les premiers cristaux séparés sont ceux de faible énergie, à savoir ceux possédant le moins de liaisons. Le taux de dissolution des faces évolue donc selon l'ordre K > S >> F. La prédominance des faces K et S au détriment des faces F favorise une rugosité plus importante. Ainsi, les grains rugueux énergétiquement plus faibles, vont présenter des taux de dissolution plus élevés impactant la granulométrie finale.

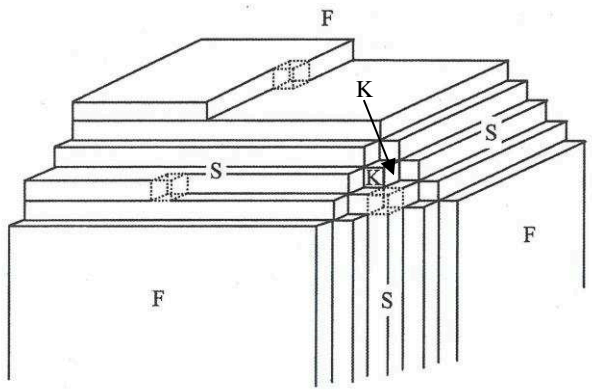

Figure 12 : représentation des trois types de faces F, S et K du cristal de Kossel [55].

Lors de l'interaction entre une solution et des grains de sable, il faudra donc se focaliser essentiellement sur les paramètres de la solution, de la température et la rugosité.

2. Interactions avec des métakaolins

La compréhension des phénomènes qui se produisent au cours de la formation d'un géopolymère impose la connaissance des interactions entre une solution alcaline et un métakaolin.

Différents travaux ont étudié l'influence des différentes caractéristiques des métakaolins (pureté, composition chimique, pourcentage de phase amorphe, structure, granulométrie et mouillabilité) sur leur réactivité. La pureté et la composition chimique du métakaolin présentent une influence sur la granulométrie et le rapport molaire Si/Al. En effet, Autef et al. [57, 58] ont démontré qu'une augmentation de la quantité d'impuretés (i.e. minéraux accessoires) contenues au sein du métakaolin entraîne une diminution de la valeur du d_{50} ainsi que du rapport Si/Al. Les travaux de Gharzouni et al. [59] ont prouvé que la présence d'impuretés induisait une diminution de la réactivité du métakaolin en présence d'une solution alcaline.

La structure du métakaolin présente également une influence sur les interactions entre une solution et un métakaolin. En effet, les travaux de Brykov et al. [60] ont mis en évidence des différences de réactivité en fonction des taux de coordinence des atomes d'aluminium (Al [4], et [6]). Plus la quantité d'Al [5] est élevée, plus les réactivités sont exacerbées.

Cependant, les travaux de Gharzouni et al. [59] ont également démontré que la réactivité de la solution alcaline était capable de contrebalancer l'effet de la réactivité du métakaolin. En effet, il a été démontré qu'en présence d'une solution peu réactive, la réactivité du métakaolin contrôle les réactions. En revanche, une solution alcaline très réactive va contrôler les réactions et inhiber la réactivité du métakaolin.

La réactivité du métakaolin doit être parfaitement contrôlée pour maîtriser la formation d'un géopolymère.

3. Interactions avec les métaux

Lors de la fabrication des busbars [2], les métaux seront mis en contact avec le milieu basique. Il est donc important de regarder l'interaction métal-solution basique.

a. Diagramme de Pourbaix

Afin de comprendre le comportement des différents métaux utilisés (cuivre, cuivre étamé et cuivre nickelé qui sont les métaux classiquement utilisés dans la fabrication de busbars) en fonction de la valeur de pH, les diagrammes de Pourbaix [61, 62] sont reportés à la **Figure 13**. Dans cette partie, il ne sera abordé que le domaine de valeur de pH compris entre 10 et 14. Quel que soit le métal considéré, il faudra prendre en compte la zone de passivation avec la formation d'hydroxyde, la zone d'innocuité et la zone de réactivité avec la présence d'espèces chargées.

En effet, le cuivre est présent sous une forme oxydée (CuO) pour des valeurs de pH inférieures à 10,5 – 11 alors qu'au-delà de cette valeur, il y a l'apparition d'espèces $Cu(OH)_2$. Dans le cas des métaux Sn et Ni, les zones de passivation $Sn(OH)_4$ et $Ni(OH)_2$ sont formées pour des valeurs de pH respectivement comprises entre 9 et 12 et inférieures à 12. Pour des valeurs de pH supérieures, la formation d'espèces ioniques SnO_3^{2-} et $HNiO_2^-$ est observée.

Par conséquent, lors de la fabrication des busbars, il faudra donc utiliser des mélanges de valeur de pH à la limite entre les deux zones, c'est-à-dire proche de 11 et 12 respectivement pour le cuivre et l'étain ou le nickel.

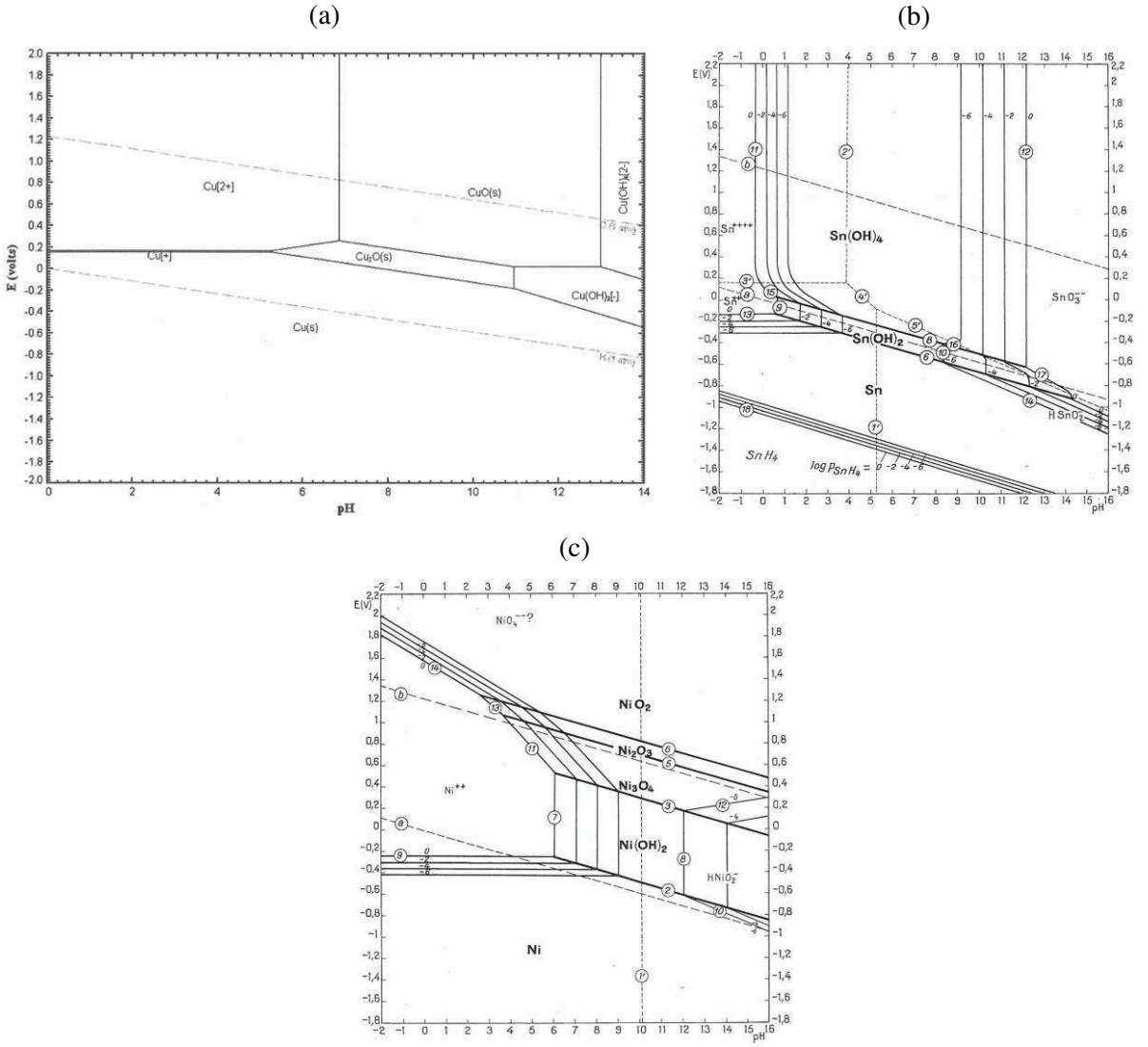

Figure 13 : diagrammes de Pourbaix des systèmes **(a)** cuivre-eau à 25 °C [61], **(b)** étain-eau à 25 °C [62] et **(c)** nickel-eau à 25 °C [62].

b. Métal/liant basique

Quelques travaux ont été menés sur les interactions entre un métal et un liant géopolymère. Parmi ceux-ci, Ranjbar et al. [63] ont analysé l'effet de l'ajout de micro fibres rugueuses en acier enrobées de cuivre au sein d'une matrice basique à base de cendres volantes. Les résultats ont démontré que l'adhésion entre les deux matériaux était due à la formation d'un complexe entre le cuivre et la matrice. Néanmoins, la quantité de fibres entraîne l'apparition de défauts et des problèmes d'adhésion [64].

De même, des dépôts de liants (mélanges de solution d'hydroxyde de sodium et de cendres volantes) sur des plaques en acier ont été menés par Irfan Khan et al. [65]. Il a été mis en évidence que la valeur du rapport Na/Al et la quantité d'eau influençaient l'adhérence du

dépôt sur le substrat métallique. Les compositions ou formulations (rapport eau / solide = 0,33 et 0,8 < Na/Al < 1,2) présentent une stabilité en température et une durabilité satisfaisante.

Une autre étude par Allison et al. [66], relative à l'interface entre un liant géopolymère à base de cendres volantes et un acier, a mis en évidence par nano-indentation l'absence d'interface. Un prétraitement de l'acier par émaillage permet de favoriser l'ancrage du liant au travers d'une couche poreuse.

Ainsi, l'adhésion d'un liant géopolymère sur un métal dépend de l'état de surface du support ainsi que de la nature du métal et de la composition du liant.

4. Les angles de mouillage

La mesure de l'angle de mouillage permet de déterminer la capacité d'un liquide à mouiller une surface idéalement lisse et homogène [67]. Cet angle est formé à l'intersection triple, i.e. à l'endroit où les trois états de la matière (solide S, liquide L et vapeur V) sont en équilibre. Sa valeur peut varier entre 0 et 180°, 0° correspondant à un mouillage parfait et 180° à un liquide non-mouillant. Lorsque l'angle est inférieur à 90°, le liquide est dit mouillant (**Figure 14a**), dans le cas contraire, il est dit non-mouillant (**Figure 14b**). A l'équilibre thermodynamique, l'angle de mouillage θ dépend des énergies superficielles solide-liquide γ_{SL}, solide-vapeur γ_{SV} et liquide-vapeur γ_{LV} selon la relation de Young (**Eq. 12**) [68].

$$\gamma_{SV} = \gamma_{SL} + \gamma_{LV} \cos \theta \qquad \textbf{Eq. 12}$$

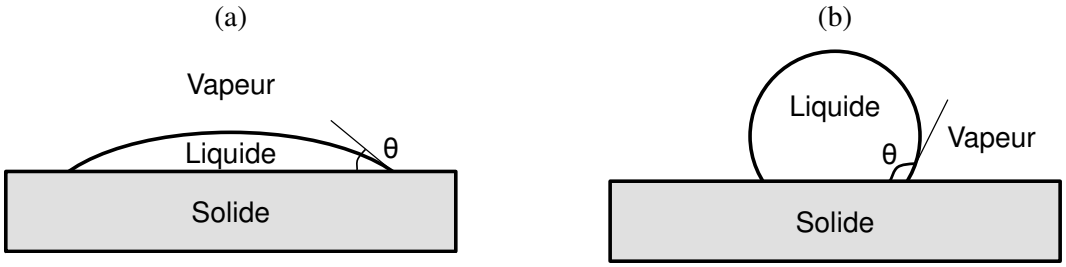

Figure 14 : *schéma de l'angle de mouillage obtenu dans le cas d'un liquide* **(a)** mouillant et **(b)** non-mouillant.

La valeur de l'angle de contact dépend de la présence de défauts à la surface du solide tels que la rugosité du solide (topologie de la surface modifiée) et les hétérogénéités chimiques (variation de la composition de la surface ou présence de contamination [67]). En présence d'une surface de densification partielle (poudre compactée ou dépôt d'une couche de poudre sur un substrat avec ou sans ajout d'adhésif), la technique de la goutte pendante peut être

utilisée mais les valeurs sont seulement qualitatives [69, 70]. Le liquide peut pénétrer au sein de la poudre par les pores causant une incertitude de la mesure de l'angle de mouillage. En effet, dans ce cas, l'énergie interfaciale est différente entraînant des écarts de valeurs. De même, la pression utilisée pour compacter les poudres modifie les caractéristiques de la poudre et présente une influence importante sur les valeurs des angles de mouillage. Les valeurs des angles de mouillage vont donc dépendre d'une part de la composition chimique du liquide et d'autre part de l'état de surface de l'échantillon. Dans le cas de poudres, des analyses comparatives entre différents liquides peuvent être effectuées.

Compte tenu des interactions citées, il était nécessaire d'avoir des données sur les différents matériaux envisagés.

La détermination des angles de contact de différentes solutions salines sur du sable (sec ou mouillé) en tenant compte de la loi de Darcy a été faite par des essais statiques et dynamiques conduisant à des variations [71]. Les valeurs d'angle obtenues par la méthode dynamique pour deux liquides (2° et 21° pour l'eau et la solution de $NaNO_3$) se rapprochent des valeurs acquises en utilisant la loi de Young (0° et 25° pour l'eau et la solution de $NaNO_3$) et sont donc plus représentatives. Leelamanie et al. [72] ont étudié l'influence de l'humidité relative sur la valeur de l'angle de mouillage sur des sables partiellement ou totalement hydrophobes (dû à l'ajout d'acide stéarique). Il a été démontré que l'angle de contact augmente avec la quantité d'acide stéarique ajoutée ainsi qu'avec l'humidité relative. Cependant, l'humidité relative n'a pas d'influence sur la relation entre l'angle de contact et le temps de pénétration du liquide. De plus, une relation entre les angles de contact et la viscosité du liquide, pour la fabrication de blocs de sable aggloméré pour l'industrie métallurgique, a révélé que les liants de faibles viscosités, i.e. des liquides présentant des vitesses de mouillage élevées, favorisent la formation de ponts entre les grains [73].

Concernant les matériaux aluminosilicates, peu ou pas de travaux sur les métakaolins sont mentionnés dans la littérature, seules des études relatives à des céramiques réfractaires et des liquides en fusion ont été réalisées. Ortiz-Covarrubias et al. [74] ont comparé les valeurs des angles de mouillage d'alliages d'aluminium sur des céramiques réfractaires et ont démontré que l'ajout d'un composé contenant du barium entraînait une diminution de la mouillabilité (i.e. une valeur d'angle de mouillage plus élevée). Ibarra Castro et al. [75] avaient précédemment obtenu des résultats similaires en ajoutant du $SrSO_4$ ou du $BaSO_4$ à la mullite.

Récemment, Duan et al [76] ont tenté de modifier la surface de géopolymères afin de les rendre hydrophobes. Des mesures d'angles de mouillage ont été réalisées sur des échantillons

avant et après traitement. La modification de la surface a entraîné une augmentation de la valeur de l'angle de 36° à 132° confirmant l'état hydrophobe de la surface. Les essais ont également mis en évidence que la modification de la surface améliore la tenue à l'eau des échantillons et réduit l'absorption d'eau.

Les interactions entre une solution alcaline et un sable, un métakaolin ou un métal vont *être contrôlées d'une part par la réactivité de la solution*, mais également par la chimie de l'*état solide et les énergies interfaci*ales du sable, du métakaolin et des alliages.

V. APPLICATIONS DES MATÉRIAUX À BASE DE SILICATE.

1. Blocs de sable aggloméré

a. Procédés

L'agglomération du sable est utilisée pour différentes applications telles que la fabrication de moules pour l'industrie métallurgique [77] ou la fabrication de fusibles pour l'industrie électrique [1].

Différents procédés peuvent être utilisés pour la consolidation des mélanges de sable et de solutions de silicate. Les techniques de séchage adoptées pour l'obtention de blocs de sable aggloméré sont des procédés chimiques (consolidation à l'aide de CO_2) ou thermiques (séchage convectif ou par micro-ondes) reportés à la **Figure 15** [78].

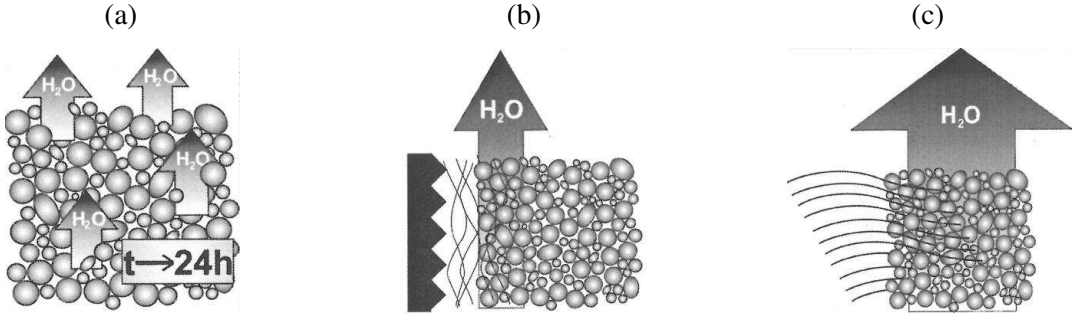

Figure 15 : représentation des procédés de séchage **(a)** chimique *à l'aide de CO_2*, et **(b, c)** thermiques par convection et par micro-ondes selon Stachowicz et al. [78].

La consolidation à l'aide de CO_2 résulte d'un déplacement du domaine de réactivité par la valeur de pH. En effet, la réaction entre la solution de silicate et le gaz carbonique CO_2 entraîne une diminution de la valeur de pH qui conduit à la formation d'un gel de silice et de carbonate de sodium selon l'**Eq. 13** [79]. Cependant, cette technique requiert environ 24 heures afin que l'échantillon soit consolidé.

$$Na_2O{\cdot}2SiO_2{\cdot}xH_2O + CO_2 \rightarrow Na_2CO_3 + 2SiO_2{\cdot}xH_2O \qquad \textbf{Eq. 13}$$

Les procédés thermiques sont reliés à la conductivité thermique du mélange. Le séchage par convection consiste à évaporer progressivement l'eau couche par couche. Cependant, cette technique de séchage consomme du temps et de l'énergie dus aux pertes de chaleur observées au cours du procédé. Dans le cas du séchage par micro-ondes, le liant, qui contient des molécules d'eau polarisées, va s'échauffer en premier permettant par la suite un traitement en volume. L'énergie des ondes électromagnétiques est transformée en énergie thermique favorisant ainsi la formation d'une couche de silicate de sodium amorphe [78]. Cette méthode permet ainsi de diminuer fortement la durée du séchage. La réaction qui se produit lors des procédés thermiques est représentée par l'**Eq. 14** [80].

$$Na_2O, SiO_2, xH_2O \xrightarrow{\text{chaleur}} Na_2SiO_3 + xH_2O_g \qquad \textbf{Eq. 14}$$

La comparaison pour une même solution montre que les résistances mécaniques des blocs de sable aggloméré varient selon le procédé de séchage (**Figure 16**). En effet, la consolidation à l'aide de CO_2 permet l'obtention de faibles résistances mécaniques [81], alors qu'en utilisant les procédés thermiques par convection et par micro-ondes, les valeurs sont similaires et plus élevées.

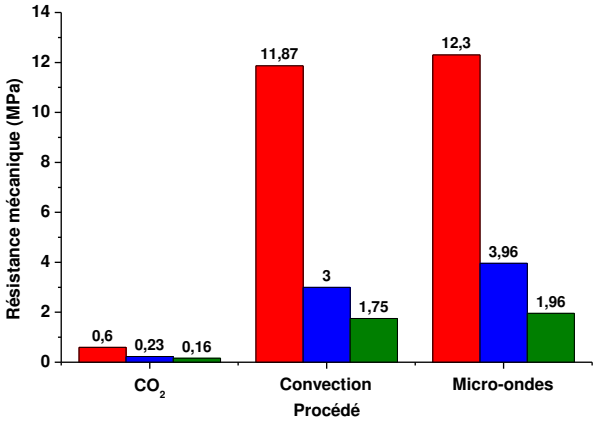

Figure 16 : résistance (▰) en compression, (▰) en flexion et (▰) en traction des blocs de sable aggloméré obtenus avec les différents procédés de consolidation *d'après* les données de Stachowicz et al. [81].

b. Paramètres influents

Toutes les propriétés citées sont néanmoins dépendantes des paramètres de séchage (température et puissance des micro-ondes) mais aussi des paramètres du mélange (rapport Si/M et quantité de solution).

Lucas et al. [5] ont montré que l'élévation de la température de séchage de 70 à 150 °C entraîne une augmentation de la contrainte à la rupture des échantillons séchés par convection.

Deux phénomènes de consolidation ont été proposés pour expliquer ces variations : la formation d'un silicate de sodium amorphe à basse température (70 °C) et la formation d'une phase obtenue par un mécanisme de dissolution-reprécipitation à 150 °C.
Dans le cas du séchage par micro-ondes, l'augmentation de la puissance des micro-ondes de 240 à 400 W améliore les propriétés mécaniques des blocs de sable de façon notable, avec au-delà de 400 W un régime permanent [82].

Quel que soit le procédé de séchage, Granat et al. [83] ont également démontré qu'une diminution du rapport molaire Si/Na de 1,7 à 1,0 conduisait à une augmentation des propriétés mécaniques. Celles-ci peuvent être améliorées lorsque la quantité de silicate au sein de l'échantillon augmente de 0,5 à 5,0 % [84, 85] (**Figure 17**). Néanmoins, dans une gamme de puissance de 300 à 900 W, la quantité de silicate induit une augmentation de la valeur de la résistance. Pour des valeurs inférieures, il existe une teneur maximale en silicate à ne pas dépasser de l'ordre de 3,0 – 3,5 %.

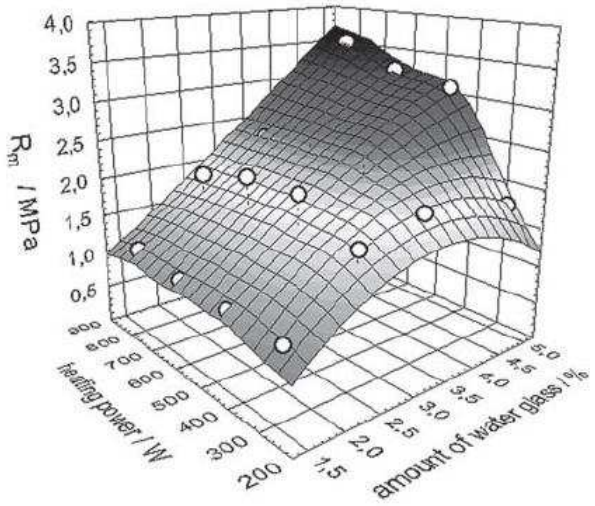

Figure 17 : influence de la quantité de solution de silicate (Si/M = 1,5) et de la puissance des micro-ondes sur la résistance en traction des blocs de sable [85].

Il est à noter que d'autres colles, comme du chlorure de sodium en solution (de 3 à 7 %), ont été utilisées pour obtenir la cohésion d'un matériau granulaire [86]. Un exemple de valeur de compression d'un mélange avec 5 % de solution, avec différents temps de séchage, est présenté sur la **Figure 18**. Deux régimes de cohésion en fonction de la cristallisation dans le matériau ont été mis en exergue : un régime capillaire pour un temps de séchage court (comportement de type plastique ductile) et un régime cimentaire pour un temps de séchage long (comportement fragile). Il a donc pu être démontré la relation entre la résistance mécanique et l'état de cristallisation pour des mélanges de sable et d'une solution saline.

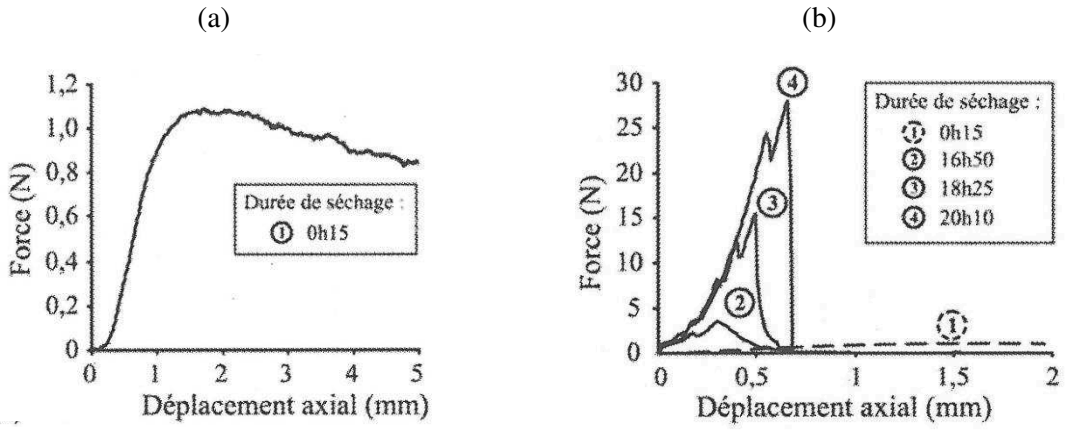

Figure 18 : exemple de courbes force-déplacement pour une teneur en solution de 5 % à un temps de séchage de **(a)** 15 min et **(b)** variant de 15 min à 20 h 10 [86].

***L'agglomération du sable siliceu*x est possible par du séchage par convection et micro-ondes en présence de solutions ioniques. Les paramètres discriminants seront la température et le taux de cristallinité du matériau obtenu.**

2. Géopolymères

Afin de fabriquer des fusibles et des busbars, la mise en forme des liants géopolymères devra être abordée ainsi que leur tenue en température [1].

a. Mise en forme

Les géopolymères ont pour formule $M^{+}_{n}\{(SiO_2)_z,AlO_2\}_n$, w H_2O avec z le rapport molaire Si/Al, M^+ le cation monovalent et n le degré de polymérisation. Ces matériaux sont obtenus en voie liquide par dissolution de sources aluminosilicatées en présence d'une solution basique [87, 88]. Leur formation est régie par des réactions de polycondensation et de géopolymérisation. Leur prise est très rapide et varie de 1 à 48 heures. Récemment, Habert et al. [89] ont étudié l'impact environnemental des liants géopolymères et ont montré que leur production permettrait de réduire d'un facteur 4 les émissions de CO_2.

Les liants géopolymères à l'état frais étant sous forme liquide et présentant différentes valeurs de viscosité, il est donc nécessaire d'utiliser des méthodes de mise en forme proches des solutions et/ou suspensions céramiques [90]. Dans le cas des matériaux céramiques, les principales méthodes utilisant des pâtes liquides ou plastiques sont le dépôt par pulvérisation, l'extrusion et le coulage. Ces différentes techniques diffèrent par la viscosité de la pâte nécessaire pour la mise en forme.

Dans le cas du dépôt par pulvérisation, la viscosité de la pâte doit être très faible afin de pouvoir être transformée en fines gouttelettes et projetée à l'aide d'un pistolet [91]. L'extrusion permet de mettre en forme un mélange en le faisant traverser une filière à l'aide d'une vis sans fin [91] et nécessite une pâte plastique devant garder la forme après extrusion. Ces deux modes requièrent des valeurs de viscosité très différentes difficilement adaptables pour des compositions proches en liant géopolymère [20, 91].

A l'inverse, le mode par coulage peut être utilisé pour différentes viscosités. Cependant, la viscosité doit être suffisamment faible afin que le liquide épouse parfaitement toutes les cavités des moules complexes [91]. Les géopolymères présentent des variations de viscosité en fonction des cinétiques de prise. La mise en forme par coulage semble donc être la méthode la plus appropriée pour la mise en forme de ces liants.

b. Tenue en température

Influence de la composition (cation et Si/Al)

Différents travaux ont étudié les propriétés des géopolymères lors de traitement en température. Les facteurs influençant le comportement en température des géopolymères à base de métakaolin, déterminés par des mesures dilatométriques, sont le cation alcalin et le rapport molaire Si/Al [92].

Duxson et al. [92] ont analysé différentes compositions de géopolymères avec des cations alcalins et des rapports molaires Si/Al différents par dilatométrie (**Figure 19**). Quels que soient les échantillons considérés, quatre phénomènes différents ont été identifiés : (i) l'eau contenue dans les macropores est évacuée sans causer de retrait jusqu'à 100 °C environ, (ii) l'eau libre est évacuée au-delà de 200 °C, (iii) des réarrangements structuraux apparaissent entre 300 et 600 °C et (iv) un retrait important dû au flux visqueux au-delà de 600 °C.

La nature du cation permet de contrôler la température d'apparition du flux visqueux ainsi que le retrait total. En effet, le cation potassium provoque le retard d'apparition du flux visqueux par comparaison avec le cation sodium (**Figure 19 a, b**).

Le rapport molaire Si/Al est également un paramètre à prendre en compte du fait de la compétition entre les atomes de silicium et d'aluminium au sein du réseau. Plus la valeur du rapport Si/Al augmente, plus la quantité de flux visqueux augmente (**Figure 19c**).

Ces phénomènes ont également été observés par He et al. [93] pour des géopolymères à base de potassium et de métakaolin et par des analyses thermiques sur des géopolymères à base de sodium [92, 94**,** 95]. Ces mécanismes ont également été notés par Provis et al. [96] sur des liants à base de cendres volantes.

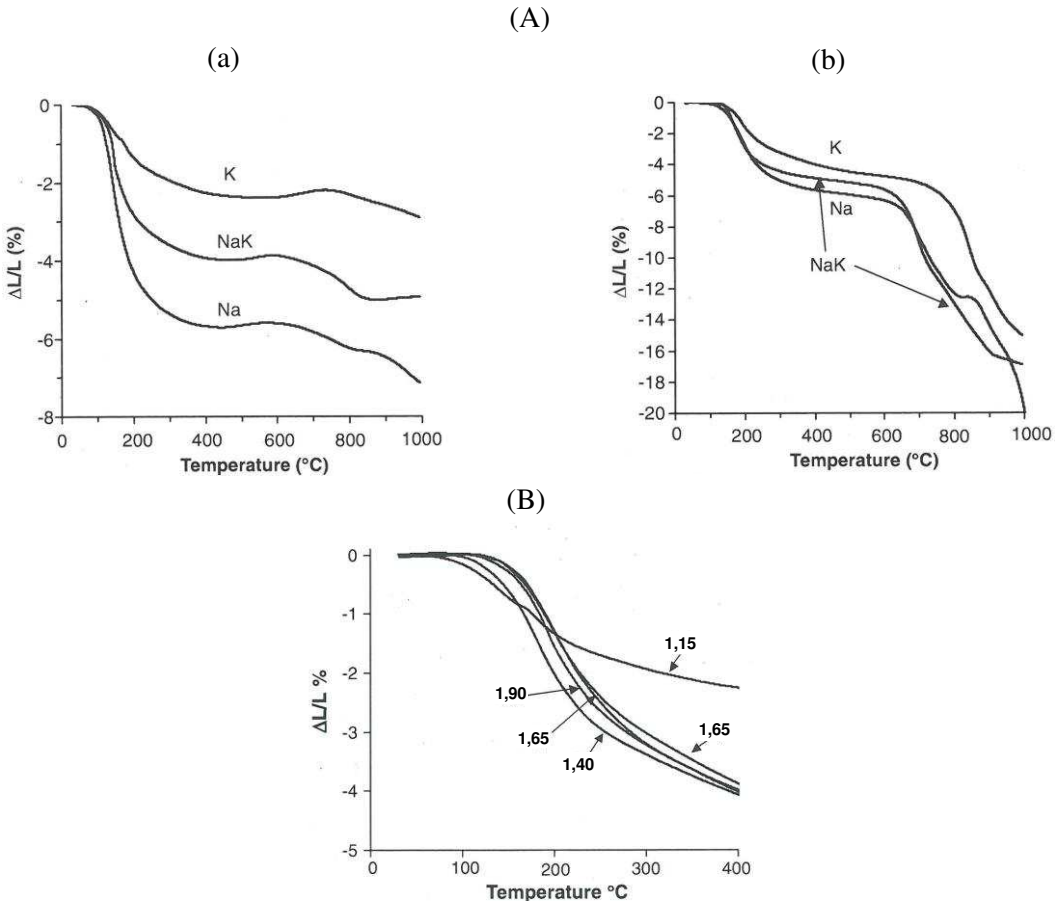

Figure 19 : *courbes dilatométriques présentant (A) l'influence du cation alcalin pour les* géopolymères avec Si/Al = **(a)** 1,15 et **(b)** 2,15 et **(B)** *l'influence du rapport Si/Al pour des* géopolymères à base de potassium [92].

Des analyses par diffraction des rayons X ont également été réalisées sur des géopolymères à base de sodium, de cations mixtes Na-K et de potassium traités à 1000 °C ou plus. Les échantillons à base de sodium conduisent simplement à la cristallisation de néphéline de formule $NaAlSiO_4$ [97, 98] alors que les échantillons à base de potassium et de solution mixte présentent des cristallisations complexes. En effet, pour les échantillons à base de potassium, l'apparition de kalsilite (ou kaliophilite) de formule $KAlSiO_4$ et de leucite de formule $KAlSi_2O_6$ est notée dans la littérature [93, 98, 99]. Dans le cas des échantillons à base de solution mixte (K-Na), les phases observées sont la leucite et la néphéline potassique de formule $K(Na,K)_3Al_4Si_4O_{16}$ [98]. Ces phénomènes de cristallisation dépendent du cation alcalin mais aussi du rapport Si/Al. En effet, dans le cas du sodium, une augmentation du rapport molaire Si/Al entraîne un retard de cristallisation [97] dû à l'apparition du flux visqueux à plus basse température entraînant une densification. En revanche, dans le cas du potassium, des cristallisations de leucite et kalsilite sont notées, dues aux énergies de cristallisation plus stables [92, 98]. Leur existence dépend du rapport Si/Al. Les phases

kalsilite et leucite prédominent respectivement pour une valeur du rapport de Si/Al inférieure à 1,15 et supérieure à 2,15. Pour des valeurs comprises entre 1,40 et 1,90, il y a coexistence des deux phases.

Ainsi, le rapport molaire Si/Al et le cation alcalin présentent une influence importante sur le comportement en température des géopolymères.

Influence de la teneur en eau

Des études ont également déterminé l'influence de la teneur en eau sur le comportement thermique des géopolymères. Des travaux menés par Temuujin et al. [100] ont révélé que la teneur en eau impactait la faisabilité des matériaux, un taux d'eau supérieur à 8,47 était proscrit. Le taux d'eau induit de forts retraits jusqu'à 200 °C au-delà l'effet est moins marqué. De même, Kuenzel et al. [101] ont déterminé par analyse thermique (ATD-ATG) que la perte d'eau jusqu'à 600 °C augmentait avec la teneur en eau initiale. Les mesures dilatométriques à 1000 °C mettent en exergue une valeur de retrait plus élevée pour des teneurs en eau plus importantes. Les auteurs ont relié ce phénomène à l'augmentation de la porosité initiale due à une quantité d'eau plus élevée [101, 102]. Par ailleurs, il a été également montré que les échantillons ne présentent pas de retrait à température ambiante tant que la quantité d'eau au sein du géopolymère est supérieure à 3 % [101].

Ainsi, la teneur en eau initiale conditionne la perte de masse et le comportement en température des géopolymères.

Ajout de renforts

Des renforts peuvent être ajoutés afin d'améliorer les propriétés mécaniques ainsi que la tenue en température des échantillons.

Prud'homme et al. [103] ont montré que l'ajout de renforts tels que du sable, des fibres de lin ou de la sciure de bois favorise la stabilisation des propriétés mécaniques des géopolymères à température ambiante. Une autre étude a également démontré une nette amélioration des propriétés mécaniques par l'ajout de sable enrobé par le géopolymère [104]. Alzeer et al. [105] ont aussi souligné que l'ajout de 10 % de fibres de lin permettait d'augmenter la valeur de contrainte en flexion de 6 à 70 MPa. Concernant le renfort par des fibres de verre, le point délicat est leur dégradation au sein du milieu basique [106].

Pour des applications de résistance au feu, l'ajout de fibres de carbone, de basalte ou de verre a été envisagé par Tran et al. [106]. Les différents échantillons conservaient environ 50 % de la valeur de contrainte en flexion après un traitement thermique d'une heure à 600 et 1000 °C, respectivement pour les fibres à base de basalte et verre et de carbone. Samal et al. [107] ont également observé une diminution des propriétés mécaniques des différents échantillons à base de métakaolin après traitement thermique au-delà de 200 °C, et ce quelles que soient les fibres utilisées (carbone, verre, basalte). Une adhésion correcte a été notée entre la matrice géopolymérique et les fibres avant traitement thermique et après traitement thermique à 600 °C. A la température de 1000 °C, l'apparition du flux visqueux modifie le comportement et l'adhérence matrice – fibre est dépendant des différences de coefficient de dilatation.

Ainsi, les propriétés mécaniques et la tenue en température des géopolymères peuvent être améliorées par l'ajout de renforts au sein de la matrice. Les matériaux présentant les meilleurs résultats sont les fibres de carbone et de basalte.

Du fait de leur viscosité variable, les géopolymères peuvent être mis en forme par coulage. Le cation alcalin et le rapport Si/Al contrôlant la tenue en température, celle-ci peut être améliorée par *l'*ajout de renforts.

VI. OBJECTIFS

L'objectif du projet FE²E est de réaliser un fusible à terme plus écologique et plus économique. Pour répondre à cette problématique, la maîtrise de chaque constituant du fusible ainsi que les interactions entre eux doivent être particulièrement éprouvées. Par conséquent, l'objectif de cette étude est de contrôler les différentes interactions entre les entités silicatées et les espèces siliceuses, aluminosilicates ou métalliques.

Afin de répondre au mieux au critère de diminution de l'énergie pour la fabrication de fusible, les axes d'études ont été de :

(i) Valider la compréhension lors de la prise du sable en présence de différentes solutions alcalines, pour diverses conditions de séchage, afin de valider la condition d'usage.

(ii) Réaliser une pièce en céramique basse température à partir d'une couche intermédiaire contenant une source aluminosilicate, voire de réaliser une pièce par coulage.

(iii) Envisager une rupture technologique, c'est-à-dire de valider la tenue en température de nouvelles pièces et d'appréhender les interactions avec des éléments métalliques.

VII. BIBLIOGRAPHIE

[1] G. Vivier. Relations entre la microstructure des blocs agglomérés et les propriétés électriques des fusibles. Thèse de doctorat, Institut National des Sciences Appliquées de Lyon, 2000.

[2] J.-L. Gelet. Informations pour présenter le fusible et le busbar. Document interne MERSEN, 2016.

[3] Mersen. Introduction à la protection par fusible. Consulté à l'adresse : http://ep-ca.mersen.com/fileadmin/user_upload/_common_/Training_Modules/TM_001_Introduction_To_The_Protection_By_Fuses_FR.pdf le 06.05.2016.

[4] J.-L. Gelet, J.-M. Missiaen. Action of the sand in ultra-fast fuses. Problematic. Consulté à l'adresse http://www.profuseinternational.com/wp-content/uploads/2012/12/28-action-of-the-sand-in-Ultra-fast-fuses.pdf le 07.05.2016.

[5] S. Lucas, M.T. Tognonvi, J.-L. Gelet, J. Soro, S. Rossignol. Interactions between silica sand and sodium silicate solution during consolidation process. Journal of Non-Crystalline Solids, 2011, vol. 357, p. 1310-1318.

[6] E. Roueche. Influence des paramètres de vibrations sur la rhéologie d'un milieu granulaire : application au remplissage des fusibles. Ecole Nationale Supérieure des Mines de Saint-Etienne, Saint-Etienne, 2005.

[7] A. Raihane. Etude du comportement des milieux granulaires vibrés horizontalement. Application au remplissage des fusibles. Ecole Nationale Supérieure des Mines de Saint-Etienne, Saint-Etienne, 2009.

[8] S. Nadler. Comportement d'un milieu granulaire soumis à des vibrations horizontales. Etudes numériques et expérimentales. Ecole Nationale Supérieure des Mines de Saint-Etienne, Saint-Etienne, 2012.

[9] L.G. Hewitson, M. Brown, R. Balakrishnan. Practical power system protection. Elsevier Science, 2004.

[10] R. Calas, P. Pascal, J. Wyart. Nouveau traité de chimie minérale. Tome VIII. Silicium. Masson et C^{ie}, Paris, 1965.

[11] Z.H. Jiang, Q.Y. Zhang. The structure of glass: A phase equilibrium diagram approach. Progress in Materials Science, 2014, vol. 61, p. 144-215.

[12] F. Liebau. Structural chemistry of silicates. Springer-Verlag, Berlin, 1985.

[13] A.C.J.H. Johnson, P. Greenwood, M. Hagström, Z. Abbas, S. Wall. Aggregation of nanosized colloidal silica in the presence of various alkali cations investigated by the electrospray technique. Langmuir, 2008, vol. 24, p. 12798-12806.

[14] M.T. Tognonvi, D. Massiot, A. Lecomte, S. Rossignol, J.-P. Bonnet. Identification of solvated species present in concentrated and dilute sodium silicate solutions by combined ^{29}Si NMR and SAXS studies. Journal of Colloid and Interface Science, 2010, vol. 352, p. 309-315.

[15] R.K. Iler. The chemistry of silica. John Wiley and Sons, New York, 1979.
[16] A. Autef. Formulation géopolymère : influence des rapports molaires Si/K et Si/Al sur les réactions de polycondensation de gels aluminosilicatés. Thèse de doctorat, Université de Limoges, 2013.
[17] L.S. Dent Glasser, N. Kataoka, The Chemistry of A.A.R. Conference On A.A.R. in Concrete, Cape Town, South-Africa, S252/23, 1981.
[18] M. Dietzel. Dissolution of silicates and the stability of polysilicic acid. Geochimica et Cosmochica Acta, 2000, vol. 64 (19), p. 3275-3281.
[19] G. Engelhardt, D. Zeigan, H. Jancke, D. Hoebbel, Z. Weiker. High resolution 29Si NMR of silicates and zeolites. Zeitschrift für Anorganische und Allgemeine Chemie, 1975, vol. 418, p. 17-28.
[20] A. Bourlon. Physico-chimie et rhéologie des géopolymères frais pour la cimentation des puits pétroliers. Thèse de doctorat, Université Pierre et Marie Curie, 2011.
[21] A.S. Brykov, V.V. Danilov, E.Y. Aleshunina. State of silicon in silicate and silica-containing solutions and their binding properties. Russian Journal of Applied Chemistry, 2008, vol. 81, p. 1717-1721.
[22] I.L. Svensson, S. Sjöberg, L.-O. Öhman. Polysilicate equilibria in concentrated sodium silicate solutions. Journal of the Chemical Society, Faraday Transactions 1. 1986, vol. 82, p. 3635-3646.
[23] A. Gharzouni, E. Joussein, B. Samet, S. Baklouti, S. Pronier, I. Sobrados, J. Sanz, S. Rossignol. The effect of an activation solution with siliceous species on the chemical reactivity and mechanical properties of geopolymers. Journal of Sol-Gel Science and Technology, 2014, vol. 73, p. 250-259.
[24] W.J. Malfait, W.E. Halter, Y. Morizet, B.H. Meier, R. Verel. Structural control on bulk melt properties: single and double quantum ^{29}Si NMR spectroscopy on alkali silicate glasses. Geochimica et Cosmochimica Acta, 2007, vol. 71, p. 6002-6018.
[25] H. Cho, A.R. Felmy, R. Craciun, J.P. Keenum, N. Shah, D.A. Dixon. Solution state structure determination of silicate oligomers by ^{29}Si NMR spectroscopy and molecular modeling. Journal of American Chemical Society, 2006, vol. 128, p. 2324-2335.
[26] C.T.G. Knight, R.J. Balec, S.D. Kinrade. The structure of silicate anions in aqueous alkaline solutions. Angewandte Chemie International Edition, 2007, vol. 46, p. 8148-8152.
[27] J. Li, S. Hayakawa, Y. Shirosaki, A. Osaka. Revisiting structure of silica gels from water glass: an ^{1}H and ^{29}Si MAR and CP-MAS NMR study.
[28] S.A. MacDonald, C.R. Schardt, D.J. Masiello, J.H. Simmons. Dispersion analysis of FTIR reflection measurements in silicate glasses. Journal of Non-Crystalline Solids, 2000, vol. 275, p. 72-82.
[29] M.T. Tognonvi, J. Soro, S. Rossignol. Physical-chemistry of silica/alkaline silicate interactions during consolidation. Part 1: Effect of cation size. Journal of Non-Crystalline Solids, 2012, vol. 358, p. 81-87.
[30] J.D. Hunt, A. Kavner, E.A. Schauble, D. Snyder, C.E. Manning. Polymerization of aqueous silica in H_2O-K_2O solutions at 25-200 °C and 1 bar to 20 kbar. Chemical Geology 2011, vol. 283, p. 161-170.

[31] F. Chaimbault. Mise en évidence de transitions de rigidité dans les silicates d'alcalins. Thèse de doctorat, Université d'Orléans, 2004.
[32] N. Trcera. Etude de la structure des verres magnésio-silicatés : approche expérimentale et modélisation. Thèse de doctorat, Université de Paris-Est, 2010.
[33] F.L. Galeener. Planar rings in vitreous silica. Journal of Non-Crystalline Solids, 1982, vol. 49, p. 53-62.
[34] B.O. Mysen, G.D. Cody. Solution mechanisms of H_2O in depolymerized peralkaline melts. Geochimica et Cosmochimica Acta, 2005, vol. 69, p. 5557-5566.
[35] C. Le Losq. Rôle des éléments alcalins et de l'eau sur les propriétés et la structure des aluminosilicates fondus et vitreux : implications volcanologiques. Thèse de doctorat, Université Paris-Diderot, 2012.
[36] E. Prud'homme, A. Autef, N. Essaidi, P. Michaud, B. Samet, E. Joussein, S. Rossignol. Defining existence domains in geopolymers through their physicochemical properties. Applied Clay Science, 2013, vol. 73, p. 26-34.
[37] P. Steins. Influence des paramètres de formulation sur la texturation et la structuration des géopolymères. Thèse de doctorat, Université de Limoges, 2014.
[38] G.D. Cody, B.O. Mysen, S.K. Lee. Structure vs. composition: a solid-state ^{1}H and ^{29}Si NMR study of quenched glasses along the Na_2O-SiO_2-H_2O join. Geochimica et Cosmochimica Acta, 2005, vol. 69, p. 2373-2384.
[39] D. Böschel, M. Janich, H. Roggendorf. Size distribution of colloidal silica in sodium silicate solutions investigated by dynamic light scattering and viscosity measurements. Journal of Colloid and Interface Science, 2003, vol. 267, p. 360-368.
[40] J. Mähler, I. Persson. A study of the hydration of the alkali metal ions in aqueous solutions. Inorganic Chemistry, 2012, vol. 51, p. 425-438.
[41] T. Melkior, S. Yahiaoui, D. Thoby, S. Motellier, V. Barthès. Diffusion coefficients of alkaline cations in Bure mudrock. Physics and Chemistry of the Earth, 2007, vol. 32, p. 453-462.
[42] E. Darmois. Qu'est-ce qu'un ion électrolytique ? Journal de Physique et le Radium, 1941, vol. 2 (1), p. 2-11.
[43] J. Schwartzentruber, W. Fürst, H. Renon. Dissolution of quartz into dilute alkaline solutions at 90 °C: a kinetic study. Geochimica et Cosmochimica Acta, 1987, vol. 51, p. 1867-1874.
[44] P.V. Brady, J.V. Walther. Kinetics of quartz dissolution at low temperatures. Chemical Geology, 1990, vol. 82, p. 253-264.
[45] K.G. Knauss, T.J. Wollery. The dissolution kinetics of quartz as a function of pH and time at 70 °C. Geochimica et Cosmochimica Acta, 1988, vol. 52, p. 43-53.
[46] S. Nangia, B.J. Garrison. Reaction rates and dissolution mechanisms of quartz as a function of pH. Journal of Physical Chemistry A, 2008, vol. 112, p. 2027-2033.
[47] A.J. Gratz, P. Bird. Quartz dissolution: negative crystal experiments and a rate law. Geochimica et Cosmochimica Acta, 1993, vol. 57, p. 965-976.
[48] M. Deleuze, A. Goiffon, A. Ibanez, E. Philippot. Solvent influence on kinetics and dissolution mechanism of quartz in concentrated basic media (NaOH, KOH, LiOH). Journal of Solid-State Chemistry, 1995, vol. 118, p. 254-260.

[49] P.M. Dove, C.J. Nix. The influence of the alkaline earth cations, magnesium, calcium, and barium on the dissolution kinetics of quartz. Geochimica et Cosmochimica Acta, 1997, vol. 61 (16), p. 3329-3340.
[50] A.J. Gratz, P. Bird, G.B. Quiro. Dissolution of quartz in aqueous basic solution, 106-236 °C: surface kinetics of "perfect" crystallographic faces. Geochimica et Cosmochimica Acta, 1990, vol. 54, p. 2911-2922.
[51] J.W. Tester, W.G. Worley, B.A. Robinson, C.O. Grigsby, J.L. Feerer. Correlating quartz dissolution kinetics in pure water from 25 to 625 °C. Geochimica et Cosmochimica Acta, 1994, vol. 58 (11), p. 2407-2420.
[52] M. Yamane, S. Aso, S. Okano, T. Sakaino. Low temperature synthesis of a monolithic silica glass by the pyrolysis of a silica gel. Journal of Marerials Science, 1979, vol. 14, p. 607-611.
[53] G. Reichenauer. Thermal aging of silica gels in water. Journal of Non-Crystalline Solids, 2004, vol. 350, p. 189-195.
[54] S. Hæreid, J.M. Anderson, M.-A. Einarsrud, D.W. Hua, D.M. Smith. Thermal and temporal aging of TMOS-based aerogel precursors in water. Journal of Non-Crystalline Solids, 1995, vol. 185, p. 221-226.
[55] J.-M. Gautier, E.H. Oelkers, J. Schott. Are quartz dissolution rates proportional to B.E.T. surface areas? Geochimica et Cosmochimica Acta, 2001, vol. 65 (7), p. 1059-1070.
[56] A.J. Gratz, P. Bird. Quartz dissolution: theory of rough and smooth surfaces. Geochimica et Cosmochimica Acta, 1992, vol. 57, p. 977-989.
[57] A. Autef, E. Joussein, A. Poulesquen, G. Gasgnier, S. Pronier, I. Sobrados, J. Sanz, S. Rossignol. Influence of metakaolin purities on potassium geopolymer formulation: the existence of several networks. Journal of Colloid and Interface Science, 2013, vol. 408, p. 43-53.
[58] A. Autef, E. Joussein, G. Gasgnier, S. Pronier, I. Sobrados, J. Sanz, S. Rossignol. Role of metakaolin dehydroxylation in geopolymer synthesis. Powder Technology, 2013, vol. 250, p. 33-39.
[59] A. Gharzouni, E. Joussein, B. Samet, S. Baklouti, S. Rossignol. Effect of the reactivity of alkaline solution and metakaolin on geopolymer formation. Journal of Non-Crystalline Solids, 2015, vol. 410, p. 127-134.
[60] A.S. Brykov, A.S. Panfilov, M.V. Mokeev. Effect of metakaolin structure on its binding properties in alkaline hydration. Russian Journal of Applied, 2012, vol. 85 (5), p. 722-725.
[61] Y. Zeng, K. Bai, H. Jin. Thermodynamic study on the corrosion mechanism of copper wire bonding. Microelectronics Reliability, 2013, vol. 53, p. 985-1001.
[62] M. Pourbaix. Atlas d'équilibres électrochimiques à 25 °C. Gauthier-Villars, Paris, 1963.
[63] N. Ranjbar, S. Talebian, M. Mehrali, C. Kuenzel, H.S. Cornelis Metselaar, M.Z. Jumaat. Mechanisms of interfacial bond in steel and polypropylene fiber reinforced geopolymer composites. Composites Science and Technology, 2016, vol. 122, p. 73-81.
[64] N. Ranjbar, M. Mehrali, M. Mehrali, U.J. Alengaram, M.Z. Jumaat. High tensile strength fly ash based geopolymer composite using copper coated micro steel fiber. Construction and Building Materials, 2016, vol. 112, p. 629-638.

[65] M. Irfan Khan, K. Azizli, S. Sufian, Z. Man. Sodium silicate-free geopolymers as coating materials: effects of Na/Al and water/solid ratios on adhesion strength. Ceramics International, 2015, vol. 41, p. 2794-2805.
[66] P.G. Allison, C.A. Weiss jr., R.D. Moser, A.J. Diaz, O.G. Rivera, S.S. Holton. Nanoindentation and SEM/EDX characterization of the geopolymer-to-steel interfacial transition zone for a reactive porcelain enamel coating. Composites Part B, 2015, vol. 78, p. 131-137.
[67] O. Dezellus. Contribution à l'étude des mécanismes de mouillage réactif. Institut National Polytechnique de Grenoble, Grenoble, 2005.
[68] A.W. Adamson. Physical chemistry of surfaces, 5e édition. Wiley, New York, 1990.
[69] K. Saleh, P. Guigon. Caractérisation et analyse des poudres. Propriétés comportementales des solides divisés. *Techniques de l'Ingénieur*, 2009.
[70] A. Alghunaim, S. Kirdponpattara, B.Z. Newby. Techniques for determining contact angle and wettability of powders. Powder Technology, 2016, vol. 287, p. 201-215.
[71] N. Weisbrod, T. McGinnis, M.L. Rockhold, M.R. Niemet. Effective Darcy-scale contact angles in porous media imbibing solutions of various surface tensions. Water Resources Research, 2009, vol. 45, W00D39 p. 1-10.
[72] D.A.L. Leelamanie, J. Karube, A. Yoshida. Relative humidity effects on contact angle and water drop penetration time of hydrophobized fine sand. Soil Science and Plant Nutrition, 2008, vol. 54, p. 695-700.
[73] B. Hutera, D. Drożyński. The effect of chemical structure of foundry binder diluent on surface processes and sand strength. Archives of Metallurgy and Materials, 2011, vol. 56 (1), p. 31- 36.
[74] K.E. Ortiz-Covarrubias, J.M. Almanza-Robles, D.A. Cortés-Hernández, J.C. Escobedo-Bocardo, A. Flores-Valdés. Synthesis of $Al_6Si_2O_{13}$-$BaAl_2Si_2O_8$-ZrO_2-based composites and their wettability by molten Al and an Al-Si alloy. Ceramics International, 2015, vol. 41, p. 4360-4373.
[75] M.N. Ibarra Castro, J.M. Almanza Robles, D.A. Cortés Hernandez, J.C. Escobedo Bocardo, J. Torres Torres. The effect of $SrSO_4$ and $BaSO_4$ on the corrosion and wetting by molten aluminum alloys of mullite ceramics. Ceramics International, 2010, vol. 36, p. 1205-1210.
[76] P. Duan, C. Yan, W. Luo, W. Zhou. A novel surface waterproof geopolymer derived from métakaolin by hydrophobic modification. Materials Letters, 2016, vol. 164, p. 172-175.
[77] R. Matalon. Novel method of making foundry molds and adhesively bonded composites. US 4 226 277. 1980.
[78] M. Stachowicz, K. Granat, D. Nowak. Application of microwaves for innovative hardening of environment-friendly water-glass moulding sands used in manufacture of cast-steel castings. Archives of Civil and Mechanical Engineering, 2011, vol. 11 (1), p. 209-219
[79] A. Rabbii. Sodium silicate glass as an inorganic binder in foundry industry. Iranian Polymer Journal, 2001, vol. 10 (4), p. 229-235.
[80] Y.A. Owusu. Physical-chemical study of sodium silicate as a foundry sand binder. Advances in Colloid and Interface Science, 1982, vol. 18, p. 57-91.

[81] M. Stachowicz, K. Granat, D. Nowak. Effect of hardening method and structure of linking bridges on strength of water glass moulding sands. Archives of Foundry Engineering, 2010, vol. 10 (2), p. 141-146.
[82] K. Granat, D. Nowak, M. Pigiel, M. Stachowicz, R. Wikiera. The influence of microwave heating and water glass king on the properties of molding sands. Archives of Foundry Engineering, 2008, vol. 8 (1), p. 119-122.
[83] K. Granat, D. Nowak, M. Pigiel, M. Stachowicz, R. Wikiera. Microwaves energy in curing process of water glass molding sands. Archives of Foundry Engineering, 2007, vol. 7 (1), p. 183-188.
[84] K. Granat, D. Nowak, M. Pigiel, M. Stachowicz, R. Wikiera. The influence of water glass on the properties of microwave cured molding sands. Archives of Foundry Engineering, 2008, vol. 8 (1), p. 123-126.
[85] M. Stachowicz, K. Granat, D. Nowak. Dielectric hardening method of sandmixes containing hydrated sodium silicate. Metalurgija, 2013, vol. 52 (2), p. 169-172.
[86] J.-Y. Delenne, F. Soulié, M.S. El Youssoufi, C. Saix. Evolution de la cohésion dans un matériau granulaire : de la capillarité à la cimentation. C. R. Mecanique, 2007, vol. 335, p.119-124.
[87] V.D. Glukhovsky. Soil silicates. Gosstroyizdat, Kiev, 1959.
[88] E. Prud'homme. Rôles du cation alcalin et des renforts minéraux et végétaux sur les mécanismes de formation de géopolymères poreux ou denses. Thèse de doctorat, Université de Limoges, 2011.
[89] G. Habert, C. Ouellet-Plamondon. Recent uptade on the environmental impact of geopolymers. RILEM Technical Letters, 2016, vol. 1, p. 17-23.
[90] J.M. Hausonne, J.L. Barton, P. Bowen, C.P. Carry. Traité des matériaux. 16. Céramiques et Verres. Presses polytechniques et universitaires romandes, Lausanne, 2005.
[91] Institut de Céramique Française. Technologie Céramique. I.C.F., Limoges, 2015.
[92] P. Duxson, G.C. Lukey, J.S.J. van Deventer. Thermal evolution of metakaolin geopolymers: Part 1 – Physical evolution. Journal of Non-Crystalline solids, 2006, vol. 352, p. 5541-5555.
[93] P. He, D. Jia, M. Wang, Y. Zhou. Thermal evolution and crystallization kinetics of potassium-based geopolymer. Ceramics International, 2011, vol. 37, p. 59-63.
[94] P. Duxson, G.C. Lukey, J.S.J. van Deventer. Physical evolution of Na-geopolymer derived from metakaolin up to 1000 °C. Journal of Materials Science, 2007, vol. 42 (9), p. 3044-3054.
[95] V.F.F. Barbosa, K.J.D. MacKenzie. Thermal behaviour of inorganic geopolymers and composites derived from sodium polysialate. Materials research Bulletin, 2003, vol. 38, p. 319-331.
[96] J.L. Provis, R.M. Harrex, S.A. Bernal, P. Duxson, J.S.J. van Deventer. Dilatometry of geopolymers as a means of selecting desirable fly ash sources. Journal of Non-Crystalline Solids, 2012, vol. 358, p. 1930-1937.
[97] P. Duxson, G.C. Lukey, J.S.J. van Deventer. Evolution of gel structure during thermal processing of Na-geopolymer gels. Langmuir, 2006, vol. 22, p. 8750-8757.

[98] P. Duxson, G.C. Lukey, J.S.J. van Deventer. The thermal evolution of metakaolin geopolymers: Part 2 – Phase stability and structural development. Journal of Non-Crystalline Solids, 2007, vol. 353, p. 2186-2200.
[99] A. Autef, E. Joussein, A. Poulesquen, G. Gasgnier, S. Pronier, I. Sobrados, J. Sanz, S. Rossignol. Influence of metakaolin purities on potassium geopolymer formulation: the existence of several networks. Journal of Colloid and Interface Science, 2013, vol. 408, p. 43-53.
[100] J. Temuujin, W. Rickard, M. Lee, A. van Riessen. Preparation and thermal properties of fire resistant metakaolin-based geopolymer-type coatings. Journal of Non-Crystalline Solids, 2011, vol. 357, p. 1399-1404.
[101] C. Kuenzel, L. Vandeperre, S. Donatello, A.R. Boccaccini, C.R. Cheeseman. Ambient temperature drying shrinkage and cracking in metakaolin-based geopolymers. Journal of the American Ceramic Society, 2012, vol. 95 (10), p. 3270-3277.
[102] M. Lizcano, A. Gonzalez, S. Basu, K. Lozano, M. Radovic. Effects of water content and chemical composition on structural properties of alkaline activated metakaolin-based geopolymers. Journal of the American Ceramic Society, 2012, vol. 95 (7), p. 2169-2177.
[103] E. Prud'homme, P. Michaud, S. Rossignol. Géomatéeiaux composites synthétisés à partir de produits naturels ou de coproduits industriels. Revue des Composites et des Matériaux Avancés, 2010, vol. 20 (3), p. 335-352.
[104] E. Prud'homme, P. Michaud, E. Joussein, C. Peyratout, A. Smith, S. Rossignol. Consolidated geo-materials from sand or industrial waste. Ceramic Engineering and Science Proceedings, 2010, vol. 30 (2), p. 313-324.
[105] M. Alzeer, K.J.D. MacKenzie. Synthesis and mechanical properties of novel composites of inorganic polymers (geopolymers) with unidirectional natural flax fibres (phormium tenax). Applied Clay Science, 2013, vol. 75-76, p. 148-152.
[106] D.H. Tran, P. Louda, D. Kroisová, O. Bortnovsky, N.T. Xiem. Advances in Composite Materials - Analysis of Natural and Man-Made Materials, Chap. 4. New generation of geopolymer composite for fire-resistance. InTech, 2011.
[107] S. Samal, N.P. Thanh, I. Petríková, B. Marvalová. Improved mechanical properties of various fabric-reinforced geocomposites at elevated temperature. Journal of Metals, 2015, vol. 67 (7), p. 1478-1485.

CHAPITRE II

Matières premières, protocoles expérimentaux et techniques de caractérisation

I. INTRODUCTION

Ce chapitre présente les différentes matières premières utilisées lors de ces travaux. Les protocoles expérimentaux pour la préparation des solutions de silicate, pour la synthèse de blocs de sable aggloméré et de liants géopolymères ainsi que pour les dépôts de liants sur des métaux ou des blocs de sable sont décrits. Ce chapitre présente également les différentes techniques de caractérisations structurales, microstructurales, physico-chimiques et mécaniques mises en œuvre au cours de cette étude.

II. LES DIFFERENTES MATIERES PREMIERES UTILISEES

1. Les précurseurs liquides

De nombreuses solutions de silicate de sodium, de potassium et mixtes (sodium et potassium), soit un total de 61 solutions, ont été étudiées. Pour cela, différents modes de préparation ont été considérés, à savoir des solutions commerciales et des solutions préparées au laboratoire. Seulement les données concernant les solutions commerciales (nomenclature utilisée dans le manuscrit, fournisseurs et données physico-chimiques) sont répertoriées dans le **Tableau 1**, les caractéristiques des autres solutions étant présentées en **Annexe II-1-A**.

2. Les précurseurs solides

Différents types de précurseurs solides ont été utilisés au cours de ces travaux. La synthèse des solutions de silicate laboratoire a été réalisée à l'aide d'hydroxyde de sodium ou de potassium ainsi que de silice amorphe.

Quatre types de sable, de granulométrie différente, ont été utilisés pour la préparation des blocs de sable aggloméré.

La synthèse des différents mélanges réactifs a été effectuée à l'aide de trois métakaolins de pureté et de réactivité différentes et les données sont répertoriées dans le **Tableau 2**.

D'autre part, différents supports métalliques ont été enrobés de liants géopolymères. Il s'agit de plaques de cuivre, de cuivre étamé et de cuivre nickelé. Les données relatives à ces plaques métalliques sont reportées en **Annexe II-1-B**.

Tableau 1 : données relatives aux différentes solutions de silicate commerciales.

	Nom	Fournisseur	Si/M (M = Na et/ou K)	H_2O (% massique)	ρ (g/cm^3)
Silicate de potassium	$_{C2}K^{1,7}$	Chemical labs[1]	1,69	76,0	1,19
	$_{C1}K^{1,7}$	Woellner[2]	1,69	76,0	1,18
	$_{C}K^{1,5}$		1,52	68,7	1,32
	$_{C}K^{0,7}$		0,67	59,4	1,51
	$_{C}K^{0,5}$		0,51	48,0	1,65
Silicate de sodium	$_{C1}Na^{1,7}$	Mersen[3]	1,71	62,7	1,37
	$_{C2}Na^{1,7}$	Woellner	1,71	64,2	1,36
	$_{C}Na^{1,3}$		1,29	55,5	1,53
Silicate mixte	$_{C}KNa^{1,6}$	Woellner	1,58	62,0	1,38

Tableau 2 : caractéristiques des différents précurseurs solides.

	Nom	Fournisseur	Composition / pureté (%)	D_{50} (µm)	Si/Al
Hydroxyde de sodium	NaOH	Sigma-Aldrich	97,0		
Hydroxyde de potassium	KOH		85,2		
Hydroxyde de lithium	LiOH	Alfa Aesar	98,0		
Silice amorphe	Cabosil M5	Sigma-Aldrich	99,9	0,2	
Sable	S_2	SIBELCO	98,4	560,0	
	S_4		98,4	340,0	
	S_8		99,8	250,0	
	S_9		98,6	90,0	
	$ZrSiO_4$ (Zr)	CMMP	> 96,0	131,0	
Métakaolin	M-1000 (M1)	Imerys	SiO_2 : 55,0 Al_2O_3 : 40,0	5,3	1,17
	M-1200S (M2)		SiO_2 : 55,0 Al_2O_3 : 39,0	1,3	1,19
	Metastar 501 (MT)		SiO_2 : 52,4 Al_2O_3 : 45,3	1,2	0,98
	Argeco rose (M5)	Argeco	SiO_2 : 59,9 Al_2O_3 : 35,3	21,0	1,44

[1] Chemical Labs, 605 Springs Road, Bedford, MA 01730 (USA).
[2] Woellner GmbH, Wöllnerstraße 26, D-67065 Ludwigshafen, Germany.
[3] MERSEN, 15 Rue Jacques Vaucanson, 69720 St Bonnet de Mure Cedex, France.

III. PROTOCOLES EXPERIMENTAUX

1. Préparation des solutions de silicate

Le protocole de préparation des différentes solutions de silicate laboratoire ou commerciales est présenté sur la **Figure 1**. Les critères tels que le cation alcalin, le mode de préparation, le rapport molaire Si/M (M = Na et/ou K), le taux d'eau et l'ajout de molybdate d'ammonium ont été analysés.

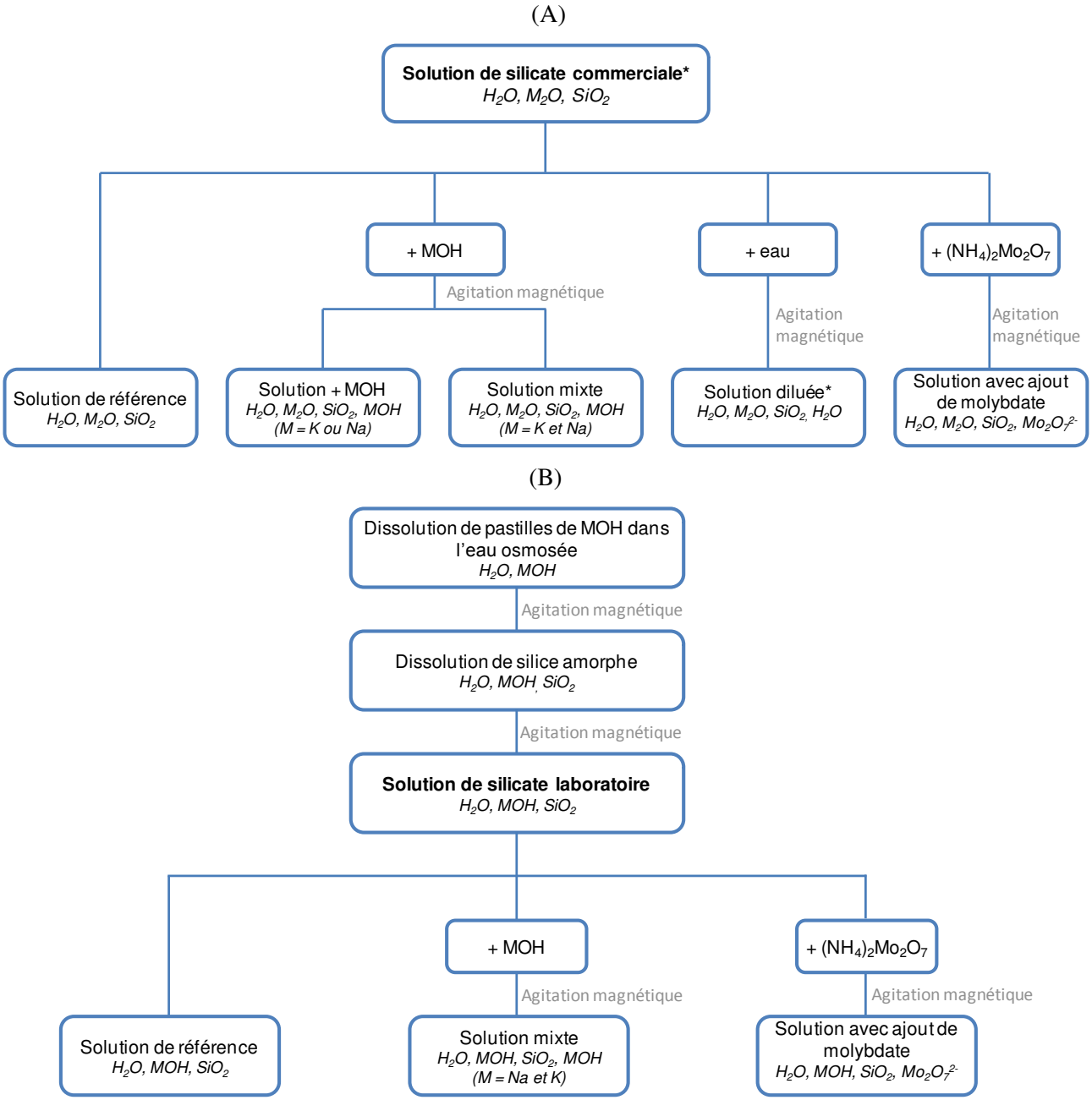

Figure 1 : protocole de préparation des différentes solutions de silicate **(A)** commerciales et **(B)** laboratoires (* : solutions traitées en température).

L'influence **du rapport Si/M** a été étudiée par l'ajout de pastilles d'hydroxyde alcalin au sein des solutions commerciales et par la masse d'hydroxyde alcalin introduite pour des masses de silice et d'eau constantes au sein des solutions laboratoire.

L'influence de la **nature du cation alcalin** a été évaluée par la préparation de solutions mixtes. Pour cela, des pastilles d'hydroxyde alcalin (M différent du cation de la solution initiale) ont été dissoutes au sein des solutions commerciales et fabriquées au laboratoire.

Les solutions commerciales ont également été diluées par ajout de 30 à 70 % d'eau afin **d'évaluer l'influence du taux d'eau**.

Différents ajouts de molybdate d'ammonium ont également été effectués sur des solutions préparées au laboratoire ou commerciales **en tant qu'agent complexant.**

2. Synthèse des blocs de sable aggloméré

Différentes méthodes d'imprégnation ont été utilisées pour la synthèse des blocs de sable aggloméré. La **Figure 2** présente les différents essais d'imprégnation réalisés au cours de l'étude. La **première méthode** correspond au remplissage du moule, sur une table vibrante, avec un mélange de sable S_4 et une solution $^{50}{}_{C}Na^{1,7}$ (**Figure 2a**). Pour **les deux autres méthodes,** le sable a été tassé par pluviation [1]. Le sable a ensuite été imprégné par capillarité (**Figure 2b**) ou par goutte à goutte (**Figure 2c**).

Des essais ont également été réalisés en ajoutant un filtre de nylon ou des fibres de verres avant le remplissage du tube par pluviation afin de favoriser l'imprégnation du bloc de sable.

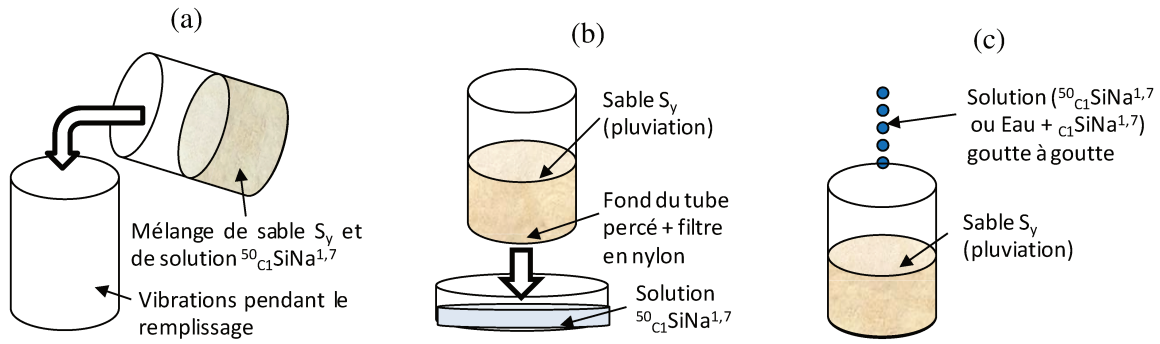

Figure 2 : *protocoles d'imprégnation pour la synthèse des blocs de sable aggloméré.*

Les échantillons imprégnés ont ensuite été séchés selon un **séchage conventionnel ou un séchage micro-ondes**. Les températures de séchage étudiées sont 70, 110 et 150 °C. Pour le séchage conventionnel à 70 °C, les échantillons ont été placés dans une étuve pendant 24 heures alors que, pour les séchages à 110 et 150 °C, les échantillons ont été placés dans une

étuve à la température souhaitée pendant 45 minutes. Finalement, des essais de séchage par micro-ondes et conventionnel à 110 et 150 °C ont également été réalisés chez Mersen.

3. Synthèse des liants géopolymères pour coulage et dépôts

Différents mélanges réactifs ont été réalisés selon le protocole présenté sur la **Figure 3**. Afin d'étudier les interactions entre les solutions et les métakaolins, **des mélanges à base de différentes solutions de silicate et de différents métakaolins (M1, M2 et MT)** ont été effectués. Des solutions de silicate de sodium et de potassium, commerciales ou préparées au laboratoire et de rapports Si/M différents, ont été utilisées. La quantité de métakaolin ajoutée varie de 0,5 à 18 g.

Des liants géopolymères ont également été préparés par dissolution de métakaolin dans une solution de silicate alcalin commerciale.

Des ajouts ont été réalisés sur ces échantillons tels que l'ajout de fibres de verre, de sable ou de tissu de verre. Les fibres de verre ainsi que le sable ont été mélangés au métakaolin avant l'ajout à la solution tandis que le tissu de verre a été placé dans le moule avant d'y ajouter le mélange réactif.

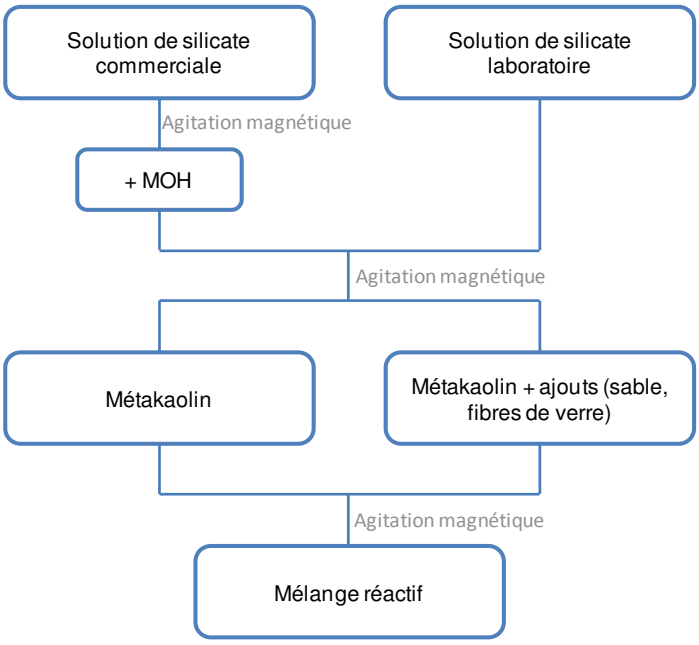

Figure 3 : protocole de synthèse des différents mélanges réactifs réalisés.

Deux méthodes de mise en forme des liants ont été testées. **La première méthode** correspond **à la réalisation de dépôts** sur différents supports tels que des blocs de sable aggloméré ou des métaux. L'enrobage des blocs de sable a été réalisé au pinceau (**Figure 4 Aa**). Une ou deux couches de liant ont été déposées et différents temps de séchage avant le

dépôt de la deuxième couche ont été testés (1 ou 24 heures). Les échantillons enrobés ont ensuite été conservés 7 jours dans une enceinte climatique à 20 °C et 70 % d'humidité, puis ils ont été placés à l'air libre pendant 11 mois.

Dans le cas des métaux, les dépôts ont été effectués au pistolet (**Figure 4Ab**) ou par trempage dans le liant (**Figure 4Ac**). Différentes épaisseurs de liant ont été déposées (une ou deux couches). Dans le cas des échantillons réalisés avec deux couches de liant, le temps de séchage avant le dépôt de la deuxième couche est de 24 heures.

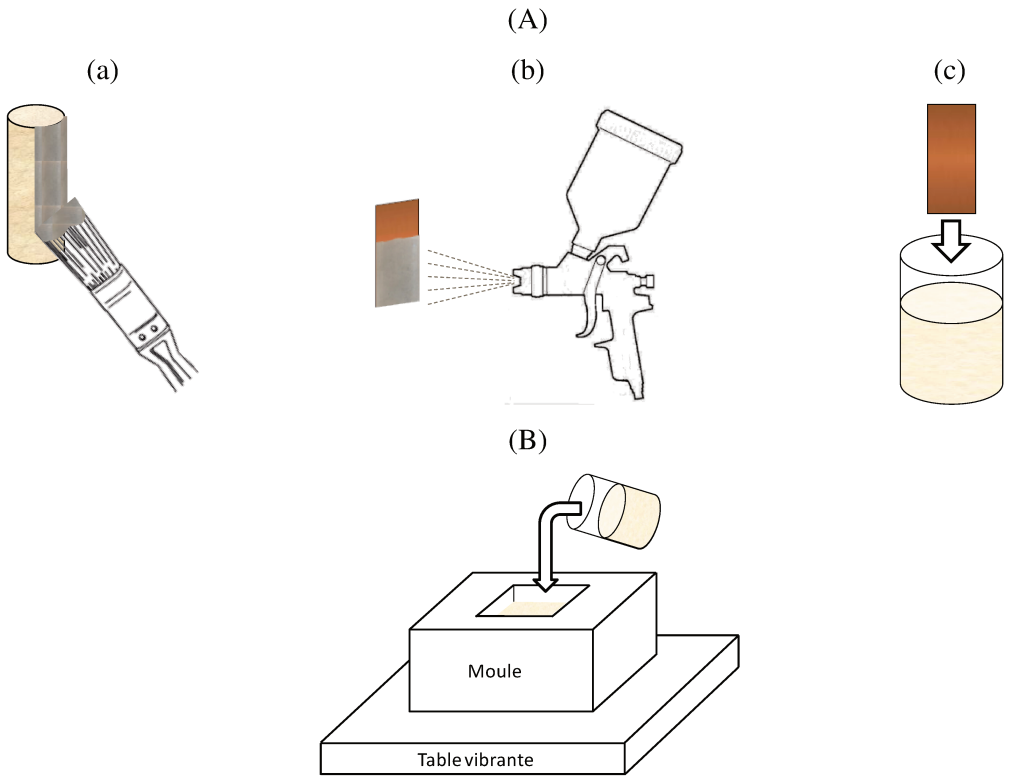

Figure 4 : (A) méthodes de dépôt de liants géopolymères sur des blocs de sable aggloméré ou des métaux et **(B)** coulage de liants géopolymères dans un moule.

Une **deuxième méthode** de mise en forme correspond **au coulage** du mélange réactif dans un moule **(Figure 4B).** Le coulage du mélange a été effectué avec un angle de 30° sur une table vibrante afin d'ôter les bulles d'air. Des pièces de différentes formes ont été réalisées (plaque ou corps de fusible). Dans le cas des plaques, les échantillons ont été démoulés après 24 heures de séchage. Les échantillons ont ensuite été conservés dans des sachets plastiques.

Dans le cas des corps de fusible, les échantillons ont été partiellement démoulés après 4 à 5 heures de séchage en fonction de la composition. Les échantillons ont ensuite été placés dans une enceinte hermétique à température ambiante et 85 % d'humidité pendant 12 heures. Puis, les pièces ont été démoulées et placées dans des sachets plastiques.

IV. NOMENCLATURES

Plusieurs nomenclatures ont été utilisées pour désigner les différents échantillons tels que les solutions de silicate (**Annexe II-2-A**), les blocs de sable aggloméré (**Annexe II-2-B**), les liants géopolymères (**Annexe II-2-C**), les blocs de sable enrobés (**Annexe II-2-D**) ainsi que les échantillons enrobés (**Annexe II-2-E**).

Les nomenclatures générales des différents types d'échantillons sont répertoriées dans le **Tableau 3**.

Tableau 3 : *nomenclatures utilisées pour les différents types d'échantillons.*

Echantillonnage	Nomenclature
Solutions	${}^{dl}_{a}M^{b}_{M^{c}\text{-}dMo}$
Blocs de sable aggloméré	$(Eau + {}^{dl}_{a}M^{b})\text{-}({}^{e}S_{x}{}^{f})^{T}_{g}$
Liants géopolymères	$({}_{a}M^{b}_{dMo}\text{-}{}^{h}My_{ij})^{T\text{-}t}$
Dépôts de liant sur des blocs de sable	$({}^{dl}_{a}M^{b}\text{-}S_{x})^{t}\text{-}NaK\text{-}({}_{a}M^{b}_{M^{c}}\text{-}{}^{h}My)^{k\text{-}t}$
Dépôt de liant sur des métaux	$P_{S}\text{-}({}_{a}M^{b}_{M^{c}}\text{-}{}^{h}My)^{k\text{-}t}$

Les différents paramètres sont :

- « **dl** » le taux de dilution de la solution (dl = 30, 50 ou 70 %),
- « **a** » la méthode de préparation de la solution (a = C (commerciale) ou L (laboratoire)),
- « **M** » le cation alcalin de la solution (M = Na, K ou Li),
- « **b** » le rapport Si/M initial (b allant de 0,2 à 1,7),
- « **c** » le rapport Si/M final (c allant de 0,35 à 1,0),
- « **dMo** » la quantité de molybdate d'ammonium ajoutée (d = 0,40, 0,80 ou 1,57 %),
- « **Eau** » lorsque de l'eau a été ajoutée avant l'imprégnation avec la solution,
- « **e** » la méthode d'imprégnation (e = goutte à goutte (G), mélange (mel) ou capillarité (cap)),
- « $\mathbf{S_x}$ » le type de sable ($S_x = S_2$, S_4, S_8 ou S_9),
- « **f** » le type de filtre utilisé (f = N (filtre en nylon) ou T_v (tissu de verre)),
- « **T** » la température (blocs de sable : T = 70, 110 ou 150 °C ; liants : T = 800, 1000 ou 1400 °C),
- « **g** » le mode de séchage (g = Conv (conventionnel) ou MO (micro-ondes)),
- « **h** » la quantité de métakaolin ajoutée (h variant de 0,5 à 20 g),
- « **My** » le type de métakaolin (My = M1, M2, MT ou M5),

- « **ij** » la quantité et le type d'ajout (i = 1, 5, 10, 40 ou 55 % ; j = S (sable), V (fibres de verre) ou Zr (sable de zircon),
- « **t** » le temps (liants : t = 1, 4 ou 24 h ; blocs de sable: t = 0, 1, 3 ou 7 j ; dépôts : t = 1 ou 24 h),
- « **NaK** » lorsqu'une couche de transition a été réalisée à l'aide de la solution $_{C}KNa^{1,6}$,
- « **k** » l'épaisseur de liant (z = 1c (une couche) ou 2c (deux couches)),
- « **P** » la plaque métallique utilisée (P = Cu, CuNi et CuSn),
- « **s** » est ajouté lorsque la plaque métallique a été sablée.

V. TECHNIQUES DE CARACTERISATION

1. Caractérisations structurales et microstructurales

a. Spectroscopie infrarouge à transformée de Fourier (IRTF)

La spectroscopie infrarouge permet de caractériser le matériau (à l'état liquide ou solide) à partir de son interaction avec le rayonnement infrarouge. Lorsqu'un échantillon est irradié, les liaisons chimiques qui sont excitées à leur énergie de vibration propre absorbent sélectivement le signal. Ainsi, le spectre obtenu permet d'identifier les différents groupements moléculaires présents dans l'échantillon. Les solutions de silicate ainsi que les matériaux géopolymères sont composés d'un cation alcalin (noté M), de silicium et d'aluminium. La présence de ces trois éléments va induire un grand nombre de liaisons possibles (Si-O-Si, Si-O-Al, Si-O, Si-O-M, O-Si-O) possédant chacune différents modes vibrationnels.

Les mesures par spectroscopie infrarouge ont été réalisées sur un appareil ThermoFisher Scientific Nicolet 380 en mode ATR (Attenuated Total Reflectance). La poudre, la solution ou le mélange à étudier sont simplement déposés sur le diamant de l'appareil avant les acquisitions. Les acquisitions sont réalisées entre 500 et 4000 cm^{-1}, le nombre de scans est de 64 et la résolution de 4 cm^{-1}. Les données sont ensuite traitées grâce au logiciel OMNIC (Nicolet instrument). Le dioxyde de carbone de l'air produisant des perturbations du signal entre 2400 et 2280 cm^{-1}, une ligne droite est substituée à cette portion du spectre afin d'éliminer ce bruit de fond. Une correction automatique de la ligne de base et une normalisation des spectres sont également effectuées afin de permettre la comparaison des différents résultats.

Les solutions ont été étudiées par des mesures ponctuelles en déposant quelques gouttes de solution sur le diamant (**Figure 5a**). Des analyses au cours de la formation d'un liant ont été réalisées en déposant quelques gouttes de milieu réactif sur le diamant. Les acquisitions se

font alors toutes les 10 minutes pendant 13 heures. L'évolution des liaisons au sein du matériau est ainsi décrite par la superposition des 72 spectres obtenus (**Figure 5b**). Suite au traitement des spectres, il est possible de tracer l'évolution de la position de la bande Si-O-M (M = Si ou Al), traduisant la substitution des liaisons Si-O-Si par les liaisons Si-O-Al. La pente de la courbe durant les premières minutes de réaction permet d'évaluer la cinétique de substitution.

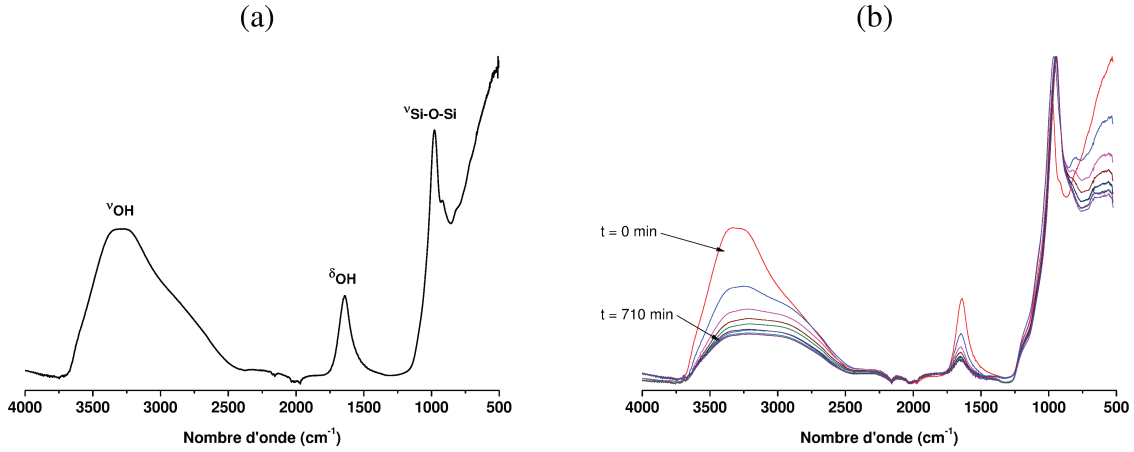

Figure 5 : (a) spectre IRTF de la solution ${}_{L}K^{0,7}$ et **(b)** suivi *de la formation de l'échantillon* ${}_{L}K^{0,7}$-${}^{12}M1$.

b. Spectroscopie Raman

La spectroscopie Raman permet de caractériser le matériau (liquide ou solide) à partir de son interaction avec une source excitatrice monochromatique de type laser. L'appareil utilisé est un spectromètre Raman Horiba-Jobin-Yvon T64000. L'excitation est réalisée à une longueur d'onde de 514 nm. Pour les échantillons solides, un réseau triple 1800 ainsi qu'un objectif 50 LWD (Long Work Distance) sont utilisés. Les acquisitions sont effectuées entre 100 et 1200 cm^{-1} avec un temps d'acquisition de 60 s sur chaque domaine spectral et une puissance de 300 mW (30 mW sur l'échantillon). Les échantillons ont été broyés préalablement à l'analyse.

Pour les solutions de silicate, un réseau triple 1800 avec un montage spécifique pour les liquides sont utilisés. Les acquisitions sont effectuées entre 300 et 1400 cm^{-1}. Le temps d'acquisition est de 60 accumulations de 15 s sur chaque domaine spectral et la puissance de sortie du laser est de 300 mW (30 mW sur l'échantillon).

Les spectres obtenus pour les solutions ont été traités puis décomposés à l'aide du logiciel Wire (Renishaw) (**Figure 6**). Le protocole utilisé pour le traitement et la décomposition des spectres Raman est présenté en **Annexe II-3**. Le **Tableau 4** présente les positions et les attributions des différentes contributions.

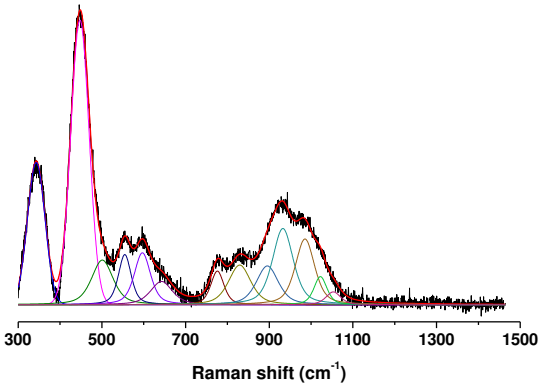

Figure 6 : exemple de décomposition de spectre Raman obtenue pour la solution $_{L}Na^{0,5}$.

Tableau 4 : position des différentes contributions détectées sur les solutions de silicate par spectroscopie Raman.

Contribution	Shift Raman (cm^{-1})	Références
ν_s (Si-O) (Q^4)	1120 – 1230	[2, 3]
ν_s (Si-O^-) (Q^3)	1000 – 1100	[4, 5]
ν_s (Si-O^-) (Q^2)	920 – 1000	[6, 7]
ν_s (Si-O^-) (Q^1)	850 – 920	[8, 9]
ν_s (Si-O^-) (Q^0)	800 – 875	[10, 11]
TO/LO (Si-O-Si)	650 – 850	[11]
ν_s (Si-O) (monomères)	639 – 649	[12]
D_2 (δ [R_3])	587 – 606	[13, 14]
ν_s (Si-O-Si) ($C_{5,6,7}$)	480 – 535	[12]
D_1 (δ [R_4])	453 – 550	[14, 15]
δ [$R_{5\ et\ plus}$]	400 – 490	[15, 16]
M--O (cation modificateur de réseau)	340 – 360	[10]

c. Résonance magnétique nucléaire (RMN)

La spectroscopie par résonance magnétique nucléaire permet de caractériser les molécules ou les espèces chimiques possédant un ou plusieurs noyaux magnétiques de spin nucléaire non nul (rapport gyromagnétique non nul). L'analyse des spectres RMN renseigne sur l'environnement électronique du noyau (sphère de coordinence). Dans le cas des différentes formulations, les environnements du silicium (^{29}Si) et de l'aluminium (^{27}Al) ont été étudiés. Leurs caractéristiques intrinsèques en solution sont regroupées dans le **Tableau 5**.

Tableau 5 : principales caractéristiques des noyaux ^{27}Al et ^{29}Si [17].

Noyau	Spin	Moment quadripolaire Q ($10^{-28}m^2$)	Abondance naturelle N (%)	Sensibilité (comparée au ^{1}H)	Rapport gyromagnétique	Fréquence de résonance (MHz) sous 9,7 T
^{27}Al	5/2	0,15	100,0	21.10^{-2}	6,976	104,26
^{29}Si	1/2	0	4,7	369.10^{-2}	-5,314	79,49

Protocole expérimental

Les solutions de silicate ont été analysées par RMN du silicium (^{29}Si). Les spectres ont été enregistrés à température ambiante sur un spectromètre Bruker AVANCE-400 avec une fréquence de résonance de 79,49 MHz. Les spectres en RMN du ^{29}Si (I = 1/2) ont été obtenus en mode statique avec une impulsion $\pi/2$ (4 µs) utilisant un filtre à 500 kHz pour améliorer le rapport signal sur bruit. Le nombre de scans collecté est de 400 et le temps entre chaque acquisition est de 10 secondes afin de minimiser les effets de saturation. Les déplacements chimiques du ^{29}Si ont été mesurés en utilisant un standard externe de tetraméthylsilane (TMS). L'erreur pour le déplacement chimique a été estimée inférieure à 0,5 ppm. L'erreur concernant la détermination des intensités relatives des différentes contributions a été évaluée inférieure à 5 %.

Afin d'être étudiés, les échantillons massifs sont broyés finement et placés dans un rotor. Les spectres RMN-MAS du ^{29}Si et ^{27}Al ont été enregistrés à température ambiante avec une sonde MAS tournant à 10 kHz. La fréquence de résonance utilisée est de 104,26 MHz pour le signal ^{27}Al et 79,49 MHz pour le signal ^{29}Si. Les spectres en RMN-MAS du ^{29}Si (I = 1/2) ont été obtenus avec une impulsion $\pi/2$ (4 µs) utilisant un filtre à 500 kHz pour améliorer le rapport signal sur bruit. Afin d'enregistrer les transitions centrales de l'aluminium (^{27}Al) (I = 5/2), une impulsion de $\pi/8$ (1,5 µs) lui a été appliquée et un filtre à 1 MHz est utilisé pour améliorer le rapport signal sur bruit.

Pour l'ensemble des échantillons, les spectres obtenus en RMN du silicium ou de l'aluminium ont été traités et décomposés à l'aide du logiciel Winfit (Bruker). Le protocole utilisé pour le traitement et la décomposition des spectres Raman est présenté en **Annexe II-4**. La **Figure 7** présente un exemple de décomposition du spectre RMN ^{29}Si de la solution $_LK^{0,7}$.

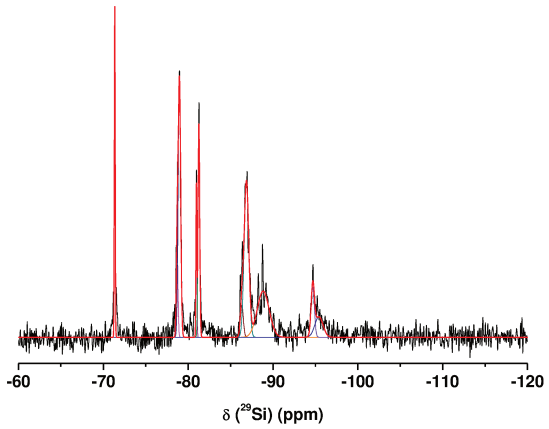

Figure 7 : décomposition du spectre RMN ^{29}Si de la solution $_{L}K^{0,7}$.

d. Microscopie électronique

Microscopie électronique à balayage (MEB)

La microscopie électronique à balayage est une technique de caractérisation de surface permettant des observations jusqu'à l'échelle de quelques nanomètres en fonction de l'appareillage. Son principe est basé sur l'interaction électron-matière. La détection des électrons secondaires et rétrodiffusés émis par l'échantillon soumis à un faisceau électronique permet de reconstituer l'image de l'objet en contraste morphologique ou chimique respectivement. Ainsi, la microstructure des matériaux consolidés et des matières premières, ou encore le comportement des renforts au sein de la matrice géopolymère ont été observés.

Les observations ont été réalisées à l'aide d'un microscope électronique à balayage Cambridge Stereoscan S260 Instruments. Les échantillons sont préalablement métallisés à l'or/palladium (Au/Pd) ou au platine (Pt) et fixés sur un porte-échantillon à l'aide de pâte ou de pastille carbone. Cette métallisation évite l'accumulation de charges à la surface de l'échantillon et diminue la profondeur de pénétration du faisceau, améliorant ainsi la qualité de l'image. Les observations morphologiques sont réalisées en électrons secondaires. Des analyses chimiques EDX (Energie Dispersive X-Ray) ont également été effectuées permettant ainsi d'identifier les différents éléments chimiques présents dans les échantillons tels que le silicium ($K\alpha$ = 1,739 eV), l'aluminium ($K\alpha$ = 1,486 eV), le potassium ($K\alpha$ = 3,312 eV) et le sodium ($K\alpha$ = 1,041 eV).

Microscopie électronique en transmission (MET)

La microscopie électronique en transmission est la seule technique susceptible de donner des informations structurales et chimiques à l'échelle nanométrique. Brièvement, les électrons produits par la source sont accélérés puis focalisés sur l'échantillon par des lentilles

condenseurs. Après l'interaction électron-matière, il apparaît à la sortie de l'échantillon un faisceau transmis et un ou plusieurs faisceaux diffractés. Il est ainsi possible de visualiser pour un même objet l'image correspondante, l'image du plan focal de la lentille objectif (diagramme de diffraction) et des analyses ponctuelles.

Les analyses ont été réalisées à l'aide d'un microscope électronique en transmission (MET) de type JEOL 2100F HR 200 kV. Cet appareil possède une imagerie conventionnelle à haute résolution (0,19 nm) et un détecteur pour la spectrométrie X (EDS). Les échantillons ont été préparés par dépôt d'une goutte sur une grille.

e. Diffraction des rayons X (DRX)

La diffraction des rayons X est une technique d'analyse structurale fondée sur l'interaction entre les rayons X et la matière, consistant à envoyer un faisceau de rayons X de longueur d'onde λ sur un échantillon solide. Lorsque cette longueur d'onde est du même ordre de grandeur que les distances inter-réticulaires (d), le faisceau est diffracté par les plans cristallins selon la loi de Bragg (**Équation 2**). Les rayons diffusés interfèrent et conduisent au phénomène de diffraction.

$$2d_{hkl}\sin\theta=\lambda \qquad \textbf{eq 2}$$

Les différents diffractogrammes ont été obtenus sur un appareil Bruker D8 équipé d'une anode en cuivre (CuKα =1,5418 Å) et d'un monochromateur arrière en graphite. Les échantillons sont préalablement broyés mécaniquement puis tamisés à 63 µm. La gamme d'analyse est comprise entre 5° et 120° (2θ). Le temps d'acquisition est de 0,5 s avec un pas de 0,014° (2θ). Les phases cristallines ont été identifiées par comparaison avec les fiches de références PDF (Power Diffraction File) du ICDD (International Center for Diffraction Data) à l'aide du logiciel EVA (Bruker-AXS). La **Figure 8** présente le diffractogramme obtenu sur le géopolymère ${}_{L}K^{0,7}\text{-}^{12}M1$ calciné à 1400 °C et fait apparaître deux phases cristallines : la leucite et la kalsilite.

Les diffractogrammes fournissent également une information sur la possible réactivité des phases au cours de la géopolymérisation de l'échantillon. En effet, un géopolymère présente une structure amorphe identifiable par la présence d'un dôme amorphe entre 20 et 35° (2θ). Seulement les impuretés qui ne participent pas (ou peu) à la formation du réseau sont encore bien cristallisées et présentent donc des pics de diffraction clairement identifiables.

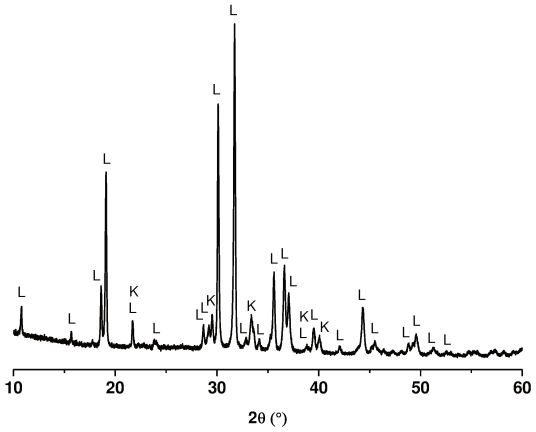

Figure 8 : diffractogramme du géopolymère ${}_{L}K^{0,7}\text{-}{}^{12}M1^{1400\text{-}4h}$ (L : leucite $KAlSi_2O_6$ (PDF : 01-085-1626), K : kalsilite $KAlSiO_4$ (PDF : 00-050-0436).

2. Caractérisations physico-chimiques

a. Mesure de la valeur de pH

Les mesures des valeurs de pH ont été réalisées à l'aide d'un appareil Schott Instrument Lab860 équipé d'une électrode pour pH basique à 25 °C.

Afin de suivre la variation de la valeur de pH au cours de la réaction de géopolymérisation, les échantillons sous forme de pastilles ont été placés dans des tubes (Ø : 35 mm et H : 70 mm) et recouverts d'eau en conservant les rapports masse de géopolymère sur masse d'eau ($m_{géopolymère}/m_{eau}$ = 0,12) pour chaque mesure. L'électrode a ensuite été placée dans le mélange et la valeur de pH a été relevée après 3 minutes.

b. Mesure d'angles de mouillage

Les angles de mouillage permettent de quantifier la qualité de mouillage. Différents phénomènes sont possibles : un mouillage total correspond à un angle de mouillage nul, un mouillage partiel correspond à l'observation d'une goutte sur la surface et un mouillage nul correspond à un angle de mouillage proche de 180° (cas spéciaux). L'appareil utilisé est un Digidrop MCAT de GBX. Il est constitué d'une caméra et d'une lampe permettant d'enregistrer le dépôt d'une goutte. Les angles de mouillage ont ensuite été mesurés à l'aide du logiciel Visiodrop de GBX (**Figure 9**).

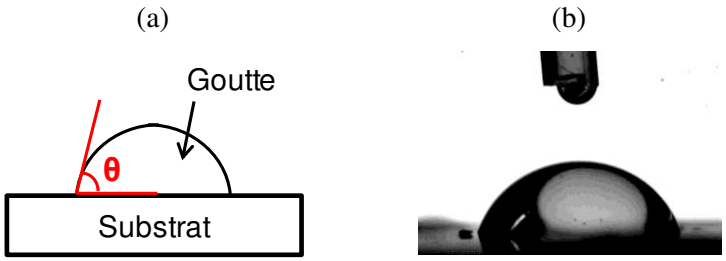

Figure 9 ***: (a) schéma de la mesure d'angle de mouillage θ et (b) exemple d'image obtenue*** **avec la solution $_{C}Na^{1,7}$ sur du cuivre nickelé.**

Des mesures d'angles de mouillage ont été effectuées avec les différentes solutions sur des substrats variés (PEHD ou métaux). Pour cela, une goutte de solution a été déposée sur le substrat et la mesure de l'angle de mouillage a été réalisée à t = 0, c'est-à-dire sur la première image où la goutte est posée sur le substrat (**Figure 9b**).

Dans le cas des mélanges réactifs, une goutte a été déposée sur différents substrats (PEHD, métaux ou blocs de sable). Pour les dépôts sur des blocs de sable aggloméré, le dépôt de la goutte a été filmé puis une photographie a été réalisée toutes les minutes pendant 3 minutes. Les valeurs d'angles de mouillage ont ensuite été relevés à t = 0, 1, 2 et 3 minutes afin d'observer l'évolution de la goutte au cours du temps.

Pour un état de mouillage partiel, le travail de cohésion du liquide (**Eq. 1**) est supérieur au travail d'adhésion du liquide sur le substrat (**Eq. 2**). Dans ce cas, le liquide formant une lentille au lieu de s'étaler montre bien que sa cohésion est supérieure à son adhésion sur le substrat [18, 19].

$$W_{cohésion} = 2\gamma_s \qquad \textbf{Eq. 1}$$

$$W_{adhésion} = \gamma_{SL} - (\gamma_{LV} + \gamma_{SV}) \qquad \textbf{Eq. 2}$$

Pour la suite de ces travaux, seul la valeur de l'angle de mouillage sera prise en compte. En effet, les liquides étudiés présenteront des compositions chimiques différentes mais des charges électrostatiques comparables.

c. Demande en eau (mouillabilité)

La demande en eau d'une poudre, exprimée en µL/g, correspond au volume d'eau qui peut être adsorbé par 1 gramme de poudre jusqu'à saturation. À cet équilibre, l'ensemble peut être représenté comme une association de particules dont les porosités intrinsèques et inter-particulaires sont comblées par le liquide. Cette grandeur dépend directement de la granulométrie, de la surface spécifique et de la morphologie des particules composant la poudre. Elle permet ainsi de caractériser la réactivité de la poudre vis-à-vis du liquide utilisé.

L'évaluation de cette demande en eau a été effectuée de la façon suivante : un gramme de poudre est pesé puis déposé sur une lame de verre. A l'aide d'une micropipette, l'eau est ajoutée à la poudre (microlitre par microlitre) jusqu'à saturation visuelle de l'ensemble granulaire.

d. Analyse chimique par fluorescence X

L'analyse par fluorescence X consiste à exciter l'échantillon afin de provoquer l'émission d'un spectre de rayons X caractéristique de sa composition. Un analyseur-détecteur de rayonnement permet d'identifier les raies composant le spectre émis et d'en déduire la composition élémentaire de l'échantillon. L'appareil utilisé est un analyseur chimique par fluorescence X XRF XMET 5500 de chez Oxford. Les échantillons sont analysés à l'état brut ou sous forme de poudre pastillée.

e. Analyse thermique différentielle et thermogravimétrique (ATD-ATG)

Ce type d'analyse permet de déterminer l'évolution thermique d'un échantillon en fonction du temps ou de la température. L'analyse thermique différentielle (ATD), couplée à l'analyse thermogravimétrique (ATG), met en évidence les changements d'états physico-chimiques des composés soumis à des variations de température. Ces changements d'états se traduisent par des phénomènes exothermiques ou endothermiques. L'analyse thermique différentielle mesure la différence de température entre l'échantillon et un creuset vide servant de référence. Il est ainsi possible de suivre les transformations qui ont lieu aux différentes températures au sein de l'échantillon. L'analyse thermogravimétrique permet quant à elle de suivre l'évolution de la masse de l'échantillon lors d'un cycle thermique, révélant la perte d'eau ou d'espèces gazeuses. Elle permet de déterminer la nature de certains pics et la contribution de ces derniers.

Protocole expérimental

Les analyses ont été réalisées avec un appareil SDT Q600 TA Instruments, dans des creusets en platine sous un flux d'air de 100 cm^3/min. Les données sont ensuite traitées grâce au logiciel TA Universal Analysis.

Le comportement thermique des liants géopolymères consolidés est analysé sur des matériaux préalablement broyés. Le cycle thermique utilisé est une rampe de 10 °C/min jusqu'à une température comprise entre 800 et 1400 °C. Les courbes ATD-ATG (**Figure 10a**)

obtenues permettent de déterminer le pourcentage d'eau contenu au sein du matériau consolidé.

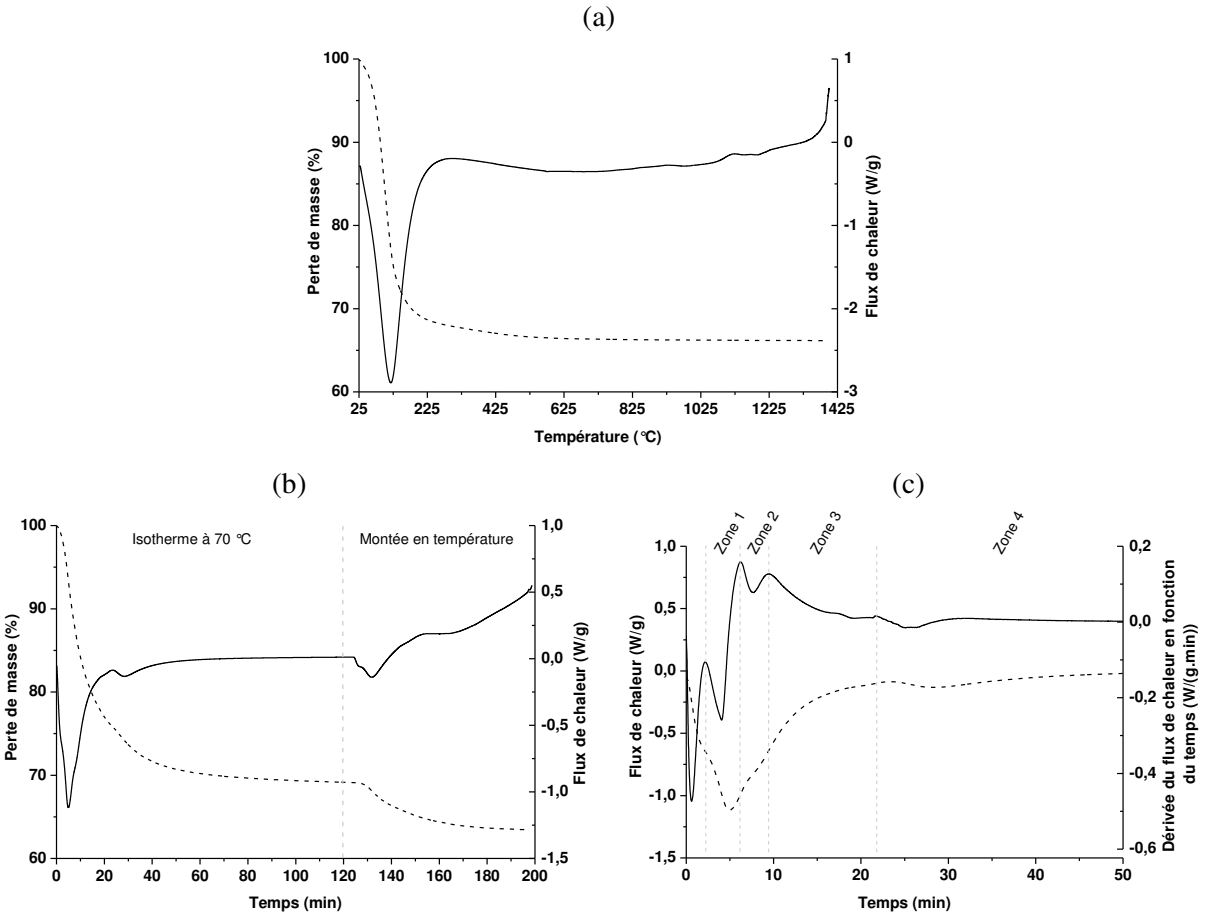

Figure 10 : (a) courbes ATD-ATG obtenues sur le géopolymère ${}_{L}K^{0,7}\text{-}{}^{12}M1$ sous forme de poudre, **(b)** courbes ATD-ATG dans le cas du géopolymère ${}_{L}K^{0,7}\text{-}{}^{12}M1$ consolidé à 70 °C et **(c)** définition des différentes zones lors de la formation du géopolymère ${}_{L}K^{0,7}\text{-}{}^{12}M1$.

Afin d'étudier la formation des liants ainsi que leur comportement en température après consolidation, les analyses ont été réalisées selon le cycle suivant : un palier à 70 °C durant deux heures suivi d'une montée à 800 °C à une vitesse de 10 °C/min. À l'aide de la dérivée première du flux de chaleur en fonction du temps, il est possible de définir plusieurs phénomènes endothermiques intervenant lors de la formation du matériau (**Figure 10b, c**).

f. Analyse dilatométrique

L'analyse dilatométrique est une technique de caractérisation qui permet d'étudier les variations dimensionnelles d'un échantillon dans une direction donnée en fonction de la température (**Annexe II-5**). Les mesures dilatométriques ont été effectuées sous air, à l'aide d'un dilatomètre vertical à contact (TMA Setsys Evolution Setaram), sur des échantillons

massifs à géométrie cylindrique (H = 7 mm, Φ = 0,7 mm). Deux cales en platine ont été placées à chaque extrémité des échantillons pour éviter les phénomènes de diffusion à haute température entre l'échantillon et les cales en alumine. Un essai de calibration à vide (sans échantillon) a été réalisé et enregistré. L'enregistrement à vide est ensuite soustrait à celui effectué avec l'échantillon afin d'éliminer la contribution liée à l'appareillage. Le cycle thermique utilisé se compose d'une montée en température de 25 °C à 1400 °C et d'une descente de 1400 °C à 25 °C à une vitesse de 5 °C/min.

3. Essais mécaniques (compression)

Les essais de compression réalisés imposent la rupture de l'échantillon par un chargement dans une seule direction. Il permet de déterminer dans la direction de sollicitation, le module d'élasticité E et la contrainte maximale σ_{max} à la rupture nommée parfois résistance mécanique.

Les différents échantillons sont placés dans des pots cylindriques (Φ = 15 mm et H = 49 mm pour les liants géopolymères et Φ = 15 mm et H = 49 mm ou Φ = 9 mm et H = 25 mm pour les blocs de sable aggloméré). Les cylindres obtenus servent d'éprouvettes pour les essais de compression et sont démoulés juste avant l'essai. Ils sont rectifiés à l'aide d'une meule diamantée afin d'obtenir un élancement (hauteur/diamètre) au minimum égal à 2 [20] et des faces parfaitement parallèles et planes. Après rectification, l'éprouvette est centrée sur la presse d'essai. Pour pallier aux défauts de planéité des plateaux de la presse, du papier multi-plis est appliqué entre l'éprouvette et les deux plateaux. La répétition des essais permet de vérifier la répétabilité des résultats et d'éliminer les valeurs aberrantes liées à la présence de défauts au sein des éprouvettes.

Pour chaque composition de géopolymères, cinq éprouvettes sont démoulées, rectifiées et testées après 7 jours. Pour les blocs de sable, cinq échantillons ont été testés après leur séchage. Les tests de compression sont réalisés à l'aide d'un appareil LLOYD EZ20 Instrument (AMETEK, UK) équipé d'une cellule de charge de 20 kN. Les éprouvettes sont soumises à une charge croissante jusqu'à la rupture à la vitesse de 0,1 mm.min^{-1}. La **Figure 11** présente les profils de contrainte, en fonction de la déformation, obtenus lors des essais sur les échantillons ${}_{L}K^{0,7}\text{-}{}^{12}M2$ et ${}_{L}Na^{1,0}\text{-}{}^{12}M1$ âgés de 7 jours et $({}^{50}{}_{C1}Na^{1,7}\text{-}{}^{cap}S_4)^{150}{}_{conv}$. À partir de ces données, il est possible de calculer une valeur moyenne de contrainte avec une erreur de plus ou moins 4 MPa.

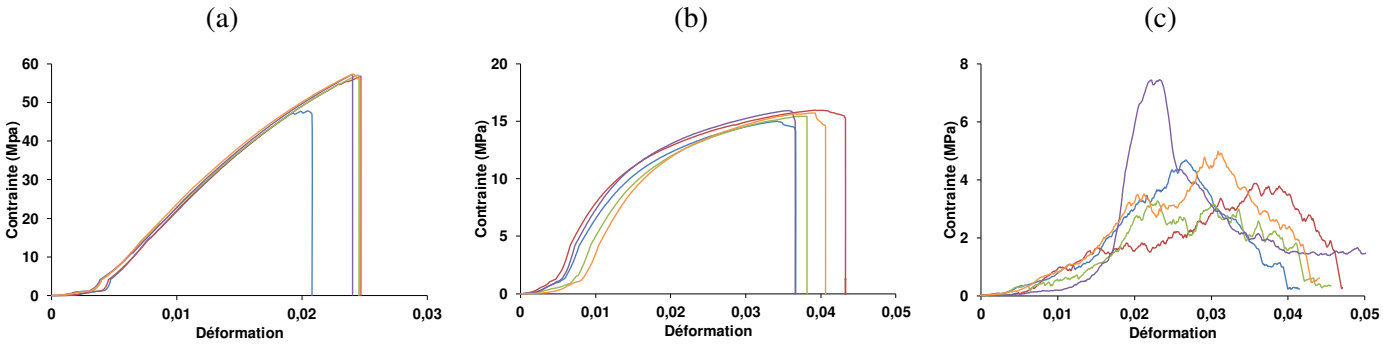

Figure 11 : courbe de contrainte à la rupture en fonction de la déformation pour une série de géopolymères **(a, b)** ${}_{L}K^{0,7}\text{-}{}^{12}M2$ - ${}_{L}Na^{1,0}\text{-}{}^{12}M1$ et **(c)** une série de blocs de sable aggloméré $({}^{50}{}_{C1}Na^{1,7}\text{-}{}^{capillarité}S_4)^{150}{}_{Conv}$.

VI. BIBLIOGRAPHIE

[1] E. Rouèche. Influence des paramètres de vibrations sur la rhéologie d'un milieu granulaire : Application au remplissage des fusibles. Thèse de doctorat, Ecole Nationale Supérieure des Mines de Saint-Etienne, 2005.

[2] J. Tan, S. Zhao, W. Wang, G. Davies, X. Mo. The effect of cooling rate on the structure of sodium silicate glass. Materials Science and Engineering B, 2004, vol. 106, p. 295-299.

[3] W.J. Malfait, V.P. Zakaznova-Herzog, W.E. Walter. Quantitative Raman spectroscopy: high temperature speciation of potassium silicate melts. Journal of Non-Crystalline Solids, 2007, vol. 353, p. 4029-4042.

[4] B.O. Mysen, G.D. Cody. Solution mechanisms of H_2O in depolymerized peralkaline melts. Geochimica et Cosmochimica Acta, 2005, vol. 69, p. 5557-5566

[5] J.D. Hunt, A. Kavner, E.A. Schauble, D. Snyder, C.E. Manning. Polymerization of aqueous silica in H_2O-K_2O solutions at 25-200 °C and 1 bar to 20 kbar. Chemical Geology, 2011, vol. 283, p. 161-170.

[6] E.V. Belova, Y.A. Kolyagin, I.A. Uspenskaya. Structure and glass transition temperature of sodium silicate glasses doped with iron. Journal of Non-Crystalline Solids, 2015, vol. 423-424, p. 50-57.

[7] A.J.G. Ellison, P.C. Hess. Raman study of potassium silicate glasses containing Rb^{+}, Sr^{2+}, Y^{3+}, and Zr^{4+}: Implications for cation solution mechanisms in multicomponent silicate liquids. Geochimica et Cosmochimica Acta, 1994, vol. 58, p. 1877-1887.

[8] W.J. Malfait, V.P. Zakaznova-Herzog, W.E. Halter. Quantitative Raman spectroscopy: speciation of Na-silicate glasses and melts. American Mineralogist, 2008, vol. 93, p. 1505-1518.

[9] B.O. Mysen, L.W. Finger, D. Virgo, F.A. Seifert. Curve-fitting of Raman spectra of silicate glasses. American Mineralogist, 1982, vol. 67, p. 686-695.

[10] B. Hehlen, D.R. Neuville. Raman response of network modifier cations in alumino-silicate glasses. Journal of Physical Chemistry B, 2015, vol. 119, p. 4093-4098.

[11] M. Chligui. Etude des propriétés optiques et mécaniques des verres binaires silicatés d'alcalins lourds. Thèse de doctorat, Université d'Orléans, 2010.

[12] A. Depla, E.Verheyen, A. Veyfeyken, M. Van Houteghem, K. Houthoofd, V. Van Speybroeck, M. Waroquier, C.E.A. Kirschhock, J.A. Martens. UV-Raman and ^{29}Si NMR spectroscopy investigation of the nature of silicate oligomers formed by acid catalyzed hydrolysis and polycondensation of tetramethylorthosilicate. Journal of Physical Chemistry C, 2011, vol. 115, p. 11077-11088.

[13] C. Le Losq, D.R. Neuville. Effect of the Na/K mixing on the structure and the rheology of tectosilicate silica-rich melts. Chemical Geology, 2013, vol. 346, p. 57-71.

[14] N. Zotov, I. Ebbsjö, D. Timpel, H. Keppler. Calculation of Raman spectra and vibrational properties of silicate glasses: comparison between $Na_2Si_4O_4$ and SiO_2 glasses. Physical Review B, 1999, vol. 60(9), p. 6383-6397.

[15] A.E. Geissberger, F.L. Galeener. Raman studies of vitreous SiO_2 versus fictive temperature. Physical Review B, 1983, vol. 28(6), p. 3266-3271.

[16] H. Aguiar, J. Serra, P. González, B. León. Structural study of sol-gel silicate glasses by IR and Raman spectroscopies. Journal of Non-Crystalline Solids, 2009, vol. 355, p. 475-480.

[17] R.K. Harris, B.E. Mann. Introduction in NMR and the periodic table. Editions Academic Press of London, New York, San Francisco, 1978.

[18] E. Bertrand. Transitions de mouillage des alcanes sur l'eau : rôle des interactionsentre interfaces. Thèse de doctorat, Université Pierre et Marie Curie, 2000.

[19] C. Goalard. Etude physico-chimique du procédé de dispersion des poudres libres et agglomérées en milieu liquide. Thèse de doctorat, Institut National Polytechnique de Toulouse, 2005.

[20] ASTM D1633 – 00. Standard Test Methods for Compressive Strength of Molded Soil Cement Cylinders. 2007.

CHAPITRE III

Synthèse des résultats expérimentaux issus des différentes publications

I. INTRODUCTION

Ce chapitre est consacré à la caractérisation des solutions de silicate et à l'étude des interactions entre une solution et du sable pour l'obtention d'un bloc de sable aggloméré. Ensuite, des essais de faisabilité pour la réalisation d'un fusible en une seule étape seront effectués. Finalement, une étude concernant la tenue en température des liants et les interactions entre un liant et des métaux sera réalisée en vue d'une rupture technologique pour la fabrication d'un busbar.

II. INTERACTIONS ENTRE LE SABLE ET LA SOLUTION

1. Les solutions de silicate

Afin de comprendre la réactivité des différentes solutions, diverses analyses ont été réalisées sur des solutions de nature différente.

a. Etudes spectroscopiques : IRTF, Raman et RMN ^{29}Si

Les divers spectres (IRTF, Raman et RMN) des solutions $_{C1}K^{1,7}$, $_{C}K^{0,7}$ et $_{L}K^{0,7}$ sont présentés sur la **Figure 1** (**Livre – Chapitre 1**).

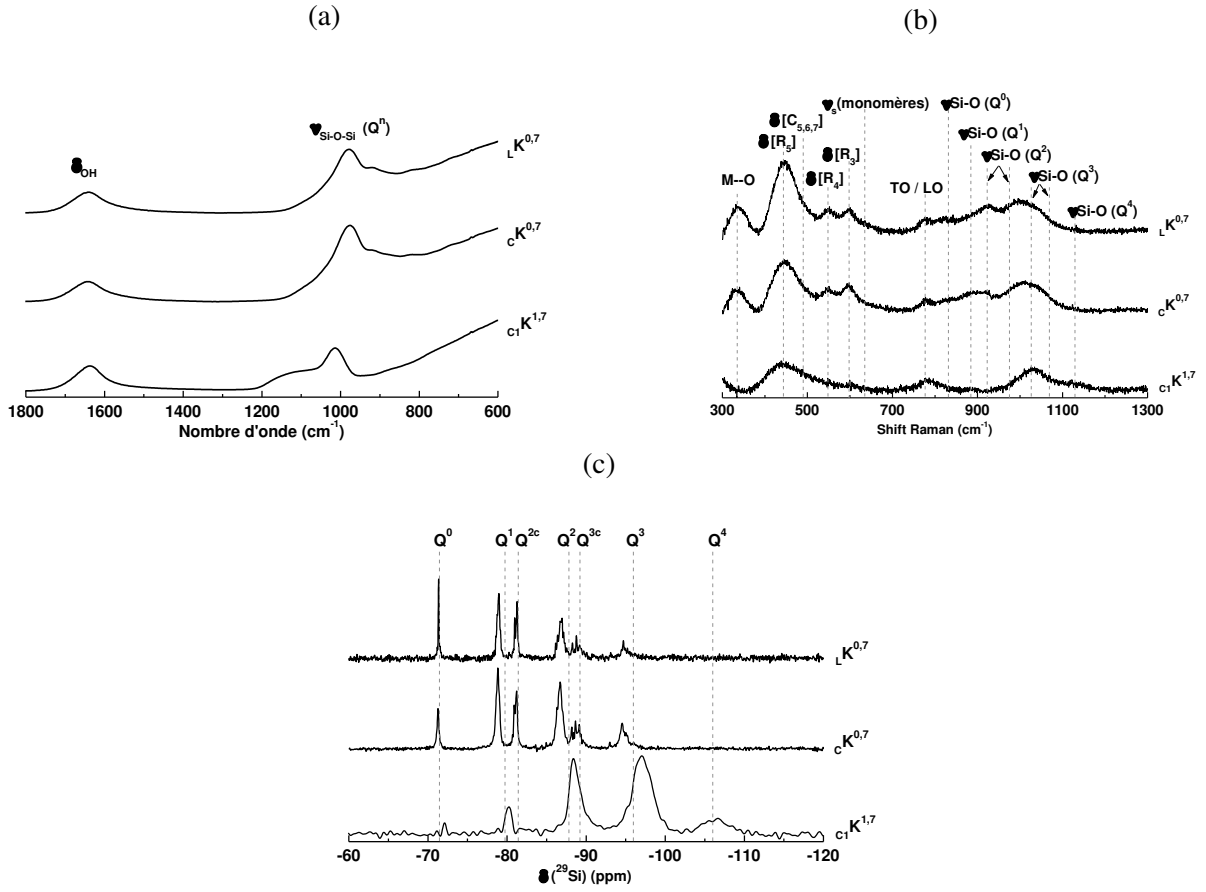

Figure 1 : spectres **(a)** IRTF, **(b)** Raman et **(c)** RMN ^{29}Si des solutions $_{C1}K^{1,7}$, $_{C}K^{0,7}$ et $_{L}K^{0,7}$.

Quelle que soit la solution considérée, les spectres IRTF présentent des contributions situées vers 1640 cm^{-1} ainsi qu'une large bande vers 1000 cm^{-1} attribuées respectivement à la déformation des molécules d'eau (δ_{OH}) et à l'élongation des liaisons Si-O-Si ($\nu_{Si\text{-}O\text{-}Si}$) des espèces silicatées Q^n [1, 2] (**Figure 1a**). Les contributions des espèces SiO_2O^{2-} (Q^2) et $SiO_{3/2}O^-$ (Q^3) respectivement à 1014 et 1100 cm^{-1} (épaulement) sont majoritaires pour une valeur de rapport Si/K = 1,7. A l'inverse, pour un rapport Si/K = 0,7, les contributions majoritaires sont celles attribuées respectivement aux espèces $SiO_{1/2}O^{3-}$ (Q^1) et $Si(O^-)_4$ (Q^0) à 980 et 920 cm^{-1} En accord avec les travaux de Gharzouni et al. [3], ces évolutions caractérisent le phénomène de dépolymérisation des solutions pour des rapports Si/M faibles. La faible différence d'intensité observée pour les solutions ${}_CK^{0,7}$ et ${}_LK^{0,7}$ pourrait être expliquée par des méthodes de préparation différentes (commerciale et laboratoire).

Les spectres Raman présentent les différentes contributions attribuées aux chaînes, aux anneaux et aux espèces Q^n (cf. **Chapitre II**) (**Figure 1b**). Pour la solution ${}_CK^{1,7}$, les contributions majoritaires sont attribuées aux espèces Q^4, Q^3 et aux anneaux de grande taille ($R_{5\text{ et plus}}$). Comme attendu, pour un rapport Si/M de 0,7 (${}_CK^{0,7}$ et ${}_LK^{0,7}$), les bandes associées aux espèces Q^0, Q^1 et Q^2, aux anneaux R_3 et R_4 et à la vibration M--O sont prédominantes au détriment des contributions liées aux espèces polymérisées ($C_{5,6,7}$, TO/LO et Q^3). Ces données révèlent que le phénomène de dépolymérisation est associé à la formation d'anneaux de petite taille (3 et 4 tétraèdres). Les quantifications de ces contributions seront exploitées par la suite.

De même, les spectres RMN présentent les contributions des différentes espèces Q^n (**Figure 1c**). La solution ${}_CK^{1,7}$ est caractérisée par de larges bandes dues aux espèces Q^2, Q^3 et Q^4 respectivement situées vers -88, -97 et -106 ppm. A l'inverse pour les solutions ${}_CK^{0,7}$ et ${}_LK^{0,7}$, les espèces prédominantes sont les entités Q^0, Q^1 et Q^2 respectivement observées à -71, -79, et -87 ppm et l'apparition d'espèces cycliques Q^{2c} et Q^{3c} est notée. L'information complémentaire est la présence des espèces cycliques.

Afin de déterminer l'influence du rapport molaire Si/M et du taux de dilution, la position du pic Si-O-Si (950 – 1020 cm^{-1}), déterminée par spectroscopie IRTF, a été tracée en fonction de la concentration en silicium pour les différentes solutions (**Figure 2**) (**ACL 4**). Quel que soit le cation considéré, pour un rapport Si/M donné, il est noté une variation linéaire de la valeur de la position en fonction de la concentration en silicium. La valeur absolue des pentes des droites varie entre 3 et 6,8 pour des rapports molaires respectivement égaux à 1,7 et 0,35 et les pentes les plus élevées sont obtenues pour des rapports Si/M faibles. Ces variations traduisent que :

- Pour une concentration en silicium donnée, l'augmentation du nombre d'onde associé au rapport Si/M est liée à la présence d'espèces plus polymérisées au sein de la solution [4, 5].
- Pour un rapport Si/M donné, la nature du cation alcalin entraîne une modification du nombre d'onde indiquant la présence d'espèces plus ou moins polymérisées.
- Plus la concentration est faible (augmentation du taux de dilution), plus le phénomène de polymérisation est exacerbé [6].

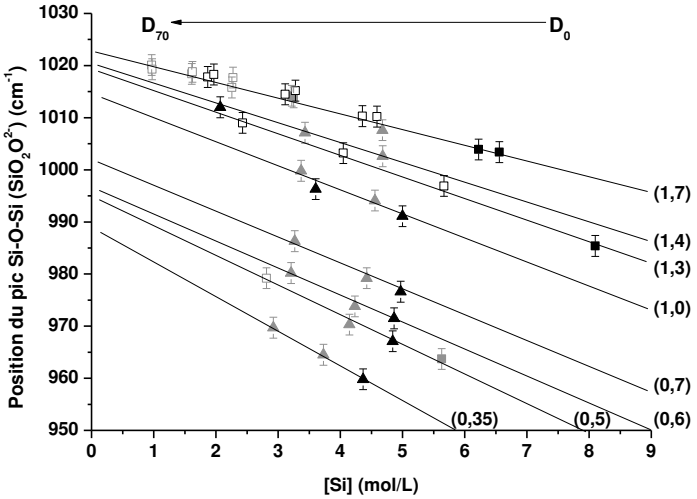

Figure 2 : position du pic Si-O-Si (Q^2) en fonction de la concentration en silicium pour les solutions (■) $_{C}K^{b}$, (□) $^{dl}{}_{C}K^{b}$, (▲) $_{L}K^{b}$, (■) $_{C}Na^{b}$, (□) $^{dl}{}_{C}Na^{b}$ et (▲) $_{L}Na^{b}$ (nombre entre parenthèses (Si/M)).

Afin de mettre en évidence l'état de polymérisation des différentes solutions, le nombre d'atomes d'oxygène non-pontant par tétraèdre (NBO) a été calculé. La **Figure 3** présente la variation du pourcentage d'espèces Q^0 et du NBO, obtenus par RMN ^{29}Si, en fonction du rapport Si/M. Il est noté une diminution du NBO associé au nombre d'entités Q^0 pour une valeur de Si/M comprise entre 1 et 1,7 en accord avec une polymérisation progressive des espèces. Pour une valeur Si/M < 1, les espèces étant plus dépolymérisées, il y a une croissance accrue des espèces Q^0. Concernant la valeur du NBO, le comportement est différent puisque un maximum est atteint pour une valeur de Si/M compris entre 0,5 et 0,8. Ce maximum traduit la présence de nombreuses espèces de nature très différentes caractéristiques de la réactivité des solutions. De plus, ce comportement peut être généralisé quels que soient le cation alcalin et le mode de préparation de la solution.

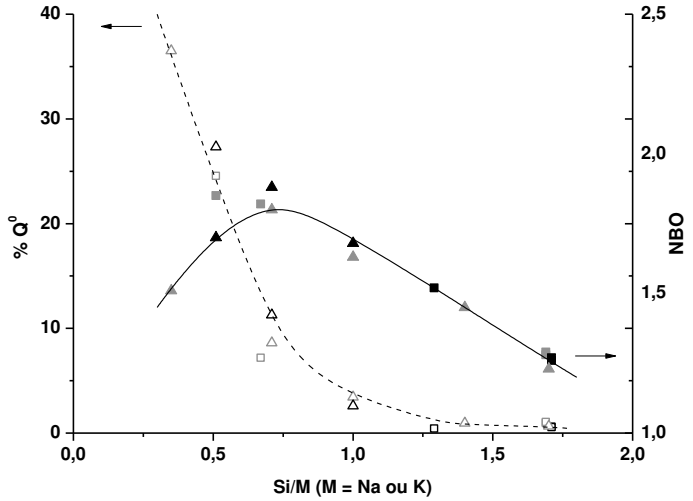

Figure 3 : variation (—) du NBO $(3Q^1+2Q^2+Q^3)/100)$ et (---) *du pourcentage d'espèces* Q^0 en fonction du rapport molaire Si/M pour les différentes solutions de silicate ((■) $_{C}K^{b}$, (▲) $_{L}K^{b}$, (■) $_{C}Na^{b}$ et (▲) $_{L}Na^{b}$ et (□) $_{C}K^{b}$, (△) $_{L}K^{b}$, (□) $_{C}Na^{b}$ et (△) $_{L}Na^{b}$).

b. Effet des différents paramètres

Afin de déterminer l'influence du cation et de la teneur en eau, les valeurs des angles de mouillage corrigées par le rapport Si/M et du NBO ont été tracées en fonction de la concentration en cation alcalin corrigée par la distance M-O [7] pour les solutions $_{C}KNa^{1,6}$, $_{C}K^{1,7}{}_{K}{}^{0,6}$, $_{C}K^{1,7}{}_{Na}{}^{0,6}$, $_{C}K^{0,7}{}_{K}{}^{0,5}$, $_{C}K^{0,7}{}_{Na}{}^{0,5}$, $_{C}Na^{1,7}{}_{Na}{}^{0,7}$ et $_{C}Na^{1,7}{}_{K}{}^{0,7}$ (**Figure 4**). La correction de l'angle de mouillage par le rapport Si/M permet de tenir compte de l'état initial de la solution.

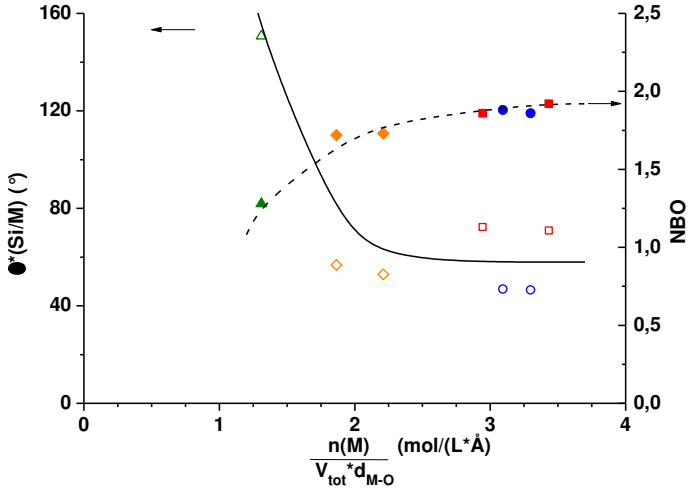

Figure 4 : variation (—) *de l'angle de mouillage corrigé par le rapport Si/M et du* (---) NBO en fonction de la concentration en cation alcalin pour les solutions (△, ▲) $_{C}KNa^{1,6}$, (◇, ◆) $_{C}K^{1,7}{}_{M}{}^{0,6}$, (○, ●) $_{C}K^{0,7}{}_{M}{}^{0,5}$ et (□, ■) $_{C}Na^{1,7}{}_{M}{}^{0,7}$.

L'augmentation de la concentration en cation alcalin entraîne une diminution de la valeur de l'angle de mouillage ainsi qu'une augmentation du NBO. L'augmentation du NBO est associée à un phénomène de dépolymérisation des espèces silicatées et donc à une augmentation de la réactivité des solutions en accord avec les résultats précédents (**Figure 3**). De plus, la diminution de la valeur de l'angle de mouillage est liée à un phénomène de dépolymérisation puisque les solutions de concentration élevée en cation alcalin contiennent des espèces dépolymérisées. Ces espèces fortement chargées sont en perpétuel mouvement et les interactions électrostatiques induisent des répulsions conduisant à un angle de mouillage faible. En présence d'espèces polymérisées, les répulsions diminuent et l'angle de mouillage est donc plus élevé. Ainsi, la valeur de l'angle de mouillage pourrait permettre de déterminer la réactivité des solutions de silicate.

Afin de déterminer l'influence du procédé de fabrication, les contributions Raman (ramenées à une mole de silicium) des chaînes ($C_{5,6,7}$), des anneaux ($R_{3,4,5\ et\ plus}$) et des espèces Q^n (n = 0 - 2) ont été tracées en fonction de la concentration en cation corrigée par la distance M-O [7] pour les solutions commerciales et laboratoire (**Figure 5A, B**) (**Annexe II-3**) (**ACL5**). Les entités Q^3 et Q^4 n'ont pas été considérées du fait de leur degré de polymérisation élevé. Quel que soit le procédé de fabrication, les mêmes tendances sont observées.

- L'augmentation de la quantité de cations alcalins entraîne une décroissance des anneaux et une variation inversement proportionnelle des chaînes et des espèces Q^n, traduisant une rupture des chaînes au profit des entités de plus petite taille (Q^0, Q^1 et Q^2).
- Le mode de préparation induit des variations au niveau des anneaux en relation avec la quantité de cation alcalin puisque une forte décroissance est notée pour les solutions laboratoire ($_LK^b$ et $_LNa^b$) par rapport aux solutions commerciales $_CK^b$ et $_CNa^b$. Ce paramètre entraîne également un déplacement de la zone d'inversion entre les entités Q^n et les chaînes.
- Le taux d'anneaux formés est dépendant de la concentration en alcalin.

Toutes ces variations peuvent être expliquées par la vitesse de diffusion des cations [8]. En effet, le potassium possède une vitesse de diffusion élevée et entraîne une formation plus rapide des anneaux impliquant la rupture des chaînes au profit d'espèces Q^n plus dépolymérisées. Les mêmes phénomènes se produisent pour le cation sodium mais pour des taux plus élevés de façon à atteindre un régime diffusionnel identique.

D'autre part, les résultats semblent indiquer que les solutions commerciales et laboratoire présenteront une réactivité importante pour des quantités de cations alcalins supérieures à 2 mol/(L*Å). En effet, c'est à partir de cette valeur que les espèces Q^n, les chaînes et les anneaux semblent stables. Cependant, pour des concentrations plus élevées ([M] > 4 mol/(L*Å)), les solutions sont très dépolymérisées et d'autres phénomènes comme une viscosité élevée pourraient induire une baisse de la réactivité [9].

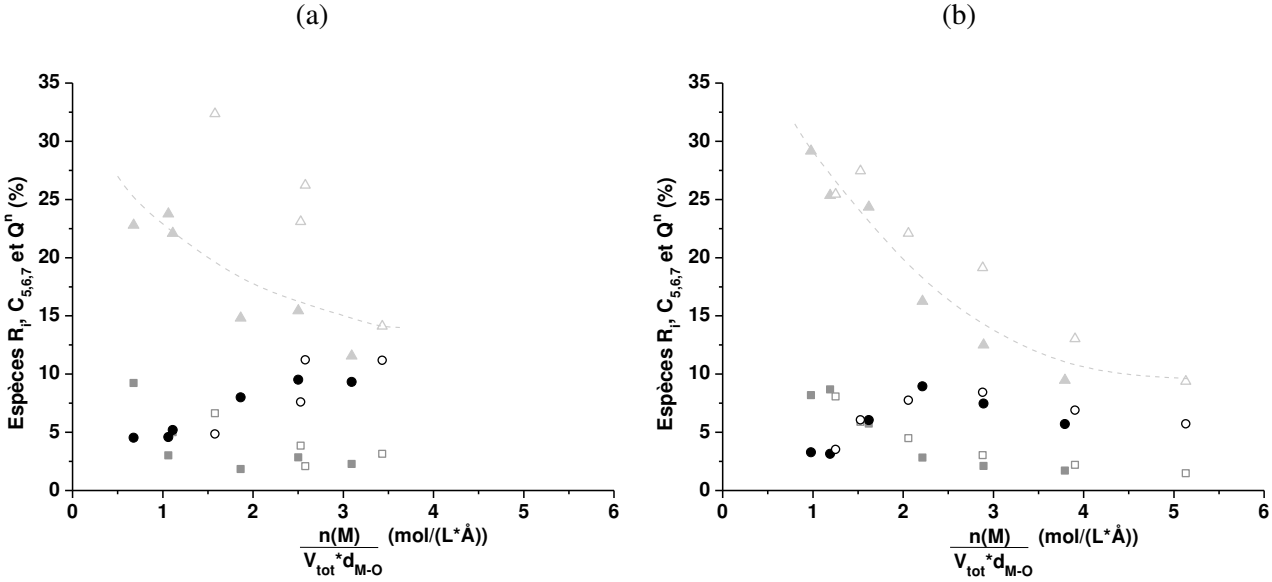

Figure 5 : variation de la contribution (■) des chaînes ($C_{5,6,7}$), (▲) des anneaux R_i et (●) des espèces Q^n (n = 0 - 2) en fonction de la concentration en cation alcalin pour les solutions **(a)** commerciales ${}_CM^x{}_{M^y}$ et **(b)** laboratoire ${}_LM^x{}_{M^y}$ avec M = (■, ▲, ●) K et (□, △, ○) Na.

c. Bilan

Afin de déterminer le degré de polymérisation et la réactivité des solutions, la **Figure 6** présente les variations des différentes espèces Q^n (n = 0, 1 et 4 ; spectroscopies RMN et Raman) en fonction du rapport Si/M et du pourcentage massique d'eau déduit. Les pourcentages plus faibles observés dans le cas de la spectroscopie Raman s'expliquent par la normalisation des différentes contributions par rapport à l'aire totale du spectre (cf. **Chapitre II**).

Les données obtenues par spectroscopies RMN du ^{29}Si et Raman présentent des tendances similaires pour les différentes espèces Q^n. La diminution du rapport Si/M et du taux d'eau entraîne une augmentation des espèces dépolymérisées (Q^0 et Q^1) au détriment des entités polymérisées Q^4 traduisant la dépolymérisation des espèces silicatées.

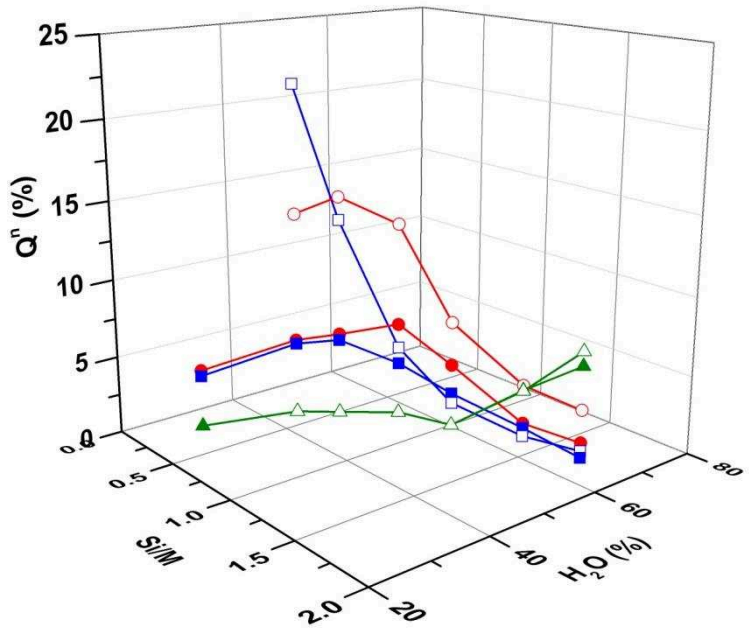

Figure 6 : variation des différentes espèces Q^n obtenues par spectroscopies (■, ●, ▲) Raman et (□, ○, △) RMN ^{29}Si avec (■, □) Q^0, (●, ○) Q^1 et (▲, △) Q^4.

Par conséquent, toutes ces données spectroscopiques permettent d'établir des abaques concernant le degré de polymérisation de n'importe quelle solution de silicate alcalin.

2. Agglomération du sable par une solution de silicate

Les solutions de silicate ont ensuite été mélangées à du sable afin d'obtenir des blocs de sable aggloméré. Afin de comprendre les interactions entre les solutions de silicate et le sable, différentes analyses ont été réalisées sur les matériaux consolidés dépendant du taux de dilution, de la nature du cation alcalin, du sable, de la méthode d'imprégnation et du séchage. Les données sur ces matériaux sont présentées en **Annexe III-1** et **Annexe III-2** puisque l'objectif de cette partie est de présenter les principaux résultats.

a. Mode de préparation

Différentes méthodes d'imprégnation (mélange, capillarité ou goutte à goutte) ont été utilisées pour la préparation des échantillons (cf. **Chapitre II**). La solution à base de phénolphtaléine a été utilisée afin de quantifier la répartition du silicate alcalin au sein du matériau consolidé, testé également par des essais de compression (**Figure 7**).

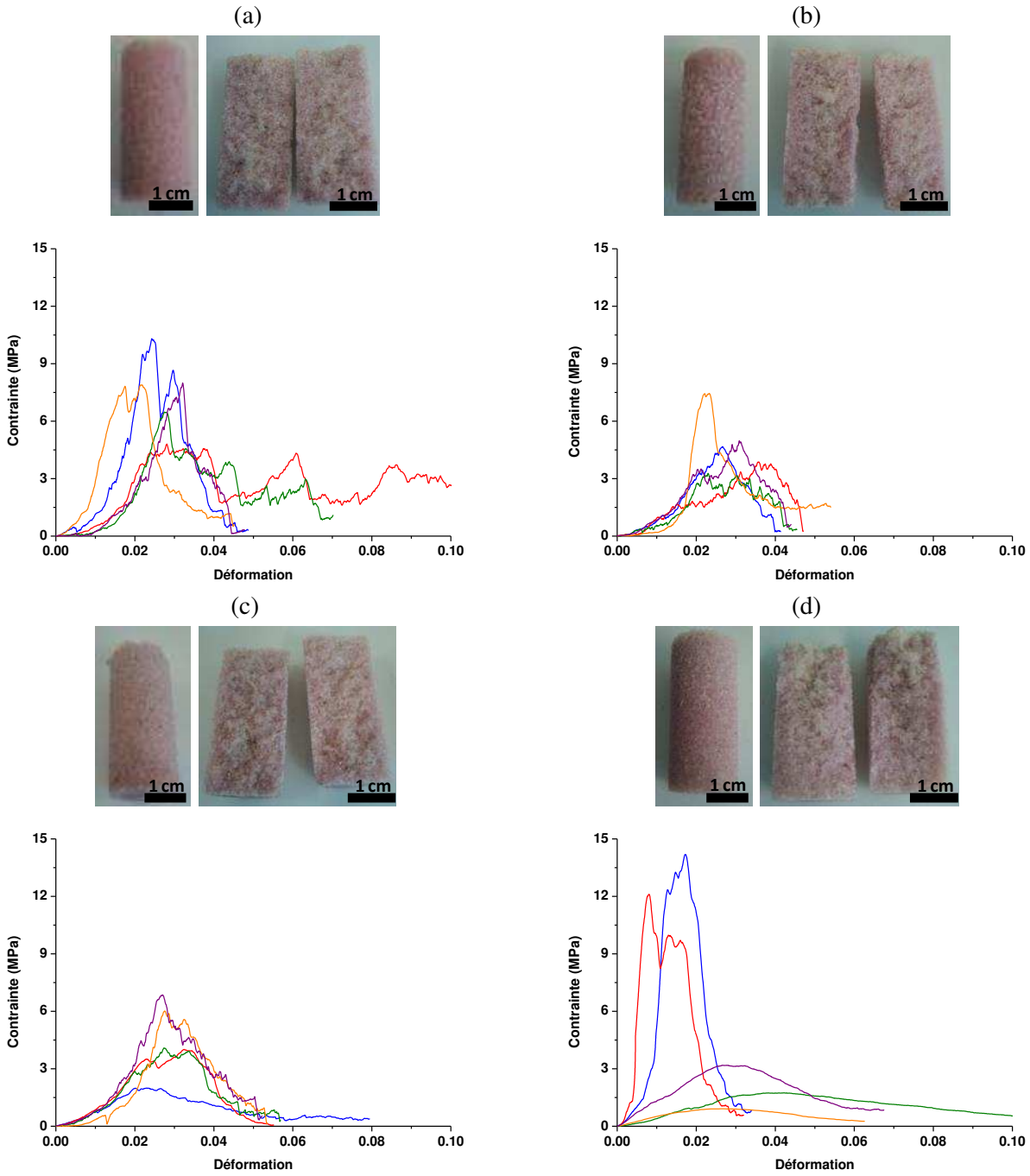

Figure 7 : photographies et courbes de compression des échantillons **(a)** $(^{50}_{C1}Na^{1,7})$-$(^{mel}S_4)^{150}_{conv}$, **(b)** $(^{50}_{C1}Na^{1,7})$-$(^{cap}S_4)^{150}_{conv}$, **(c)** $(^{50}_{C1}Na^{1,7})$-$(^{G}S_4)^{150}_{conv}$ et **(d)** (Eau + $_{C1}Na^{1,7}$)-$(^{G}S_4)^{150}_{conv.}$ ((—) a, (—) b, (—) c, (—) d, et (—) e).

Les différences de répartition du silicate observées pour les différentes méthodes d'imprégnation reflètent deux types d'imprégnation, (i) l'une quasi homogène ($(^{50}_{C1}Na^{1,7})$-$(^{mel.}S_4)^{150}_{conv}$) et (ii) l'autre où le cœur de l'échantillon ($(^{50}_{C1}Na^{1,7})$-$(^{cap.}S_4)^{150}_{conv}$ et $(^{50}_{C1}Na^{1,7})$-$(^{G}S_4)^{150}_{conv}$) ou la partie inférieure du bloc de sable est colorée ((Eau + $_{C1}Na^{1,7}$)-$(^{G}S_4)^{150}_{conv}$).

Les valeurs de contrainte à la rupture peu dispersées des échantillons $(^{50}_{C1}Na^{1,7})$-$(^{mel}S_4)^{150}_{conv}$ sont en relation avec une mouillabilité quasi homogène du sable. En effet, dans

ce cas, la solution de silicate et le sable ont été mélangés préalablement au remplissage des moules. Cette technique permet ainsi d'obtenir une imprégnation quasi homogène en favorisant la pénétration du silicate au sein de l'empilement granulaire.

Les essais $(^{50}{}_{C1}Na^{1,7})$-$(^{cap.}S_4)^{150}{}_{conv}$ et $(^{50}{}_{C1}Na^{1,7})$-$(^{G}S_4)^{150}{}_{conv}$ présentent des valeurs de contrainte à la rupture similaires et légèrement plus faibles que les échantillons précédents ($(^{50}{}_{C1}Na^{1,7})$-$(^{mel.}S_4)^{150}{}_{conv}$). Ces valeurs sont certainement dues à une imprégnation insuffisante du bloc de sable. En effet, les essais de coloration ont mis en évidence une absence de coloration au sein du bloc de sable pouvant être due à une faible imprégnation de cette zone.

Les échantillons (Eau + $_{C1}Na^{1,7}$)-$(^{G}S_4)^{150}{}_{conv}$ présentent des valeurs de contrainte très hétérogènes. Ce phénomène peut être expliqué par des chemins de diffusion différents dus à des interactions différentes avec l'eau introduite au préalable. En effet, des mesures d'angles de mouillage de l'eau et de la solution $_{C1}Na^{1,7}$ sur du sable tassé par pluviation ont démontré que l'eau est absorbée dès qu'elle entre en contact avec la surface tandis que la solution forme une goutte à la surface du sable (**Annexe III-1-A**). De plus, des travaux au laboratoire ont démontré que du sable mouillé est difficilement imprégnable par un liant (**Annexe III-1-B**). L'eau préalablement introduite semble donc diminuer la capillarité entraînant une diffusion du silicate plus difficile au sein de l'empilement granulaire.

Toutes ces différentes méthodes d'imprégnation soulignent la difficulté d'obtenir des blocs de sable aggloméré homogènes.

b. Séchage

Des essais de séchage ont été réalisés afin de déterminer l'influence de plusieurs paramètres sur la microstructure des blocs de sable aggloméré et les échantillons obtenus ont été observés au microscope électronique à balayage (**Figure 8**). Les différents paramètres étudiés sont le taux de dilution et le cation de la solution, le type de sable ainsi que le type et la température de séchage (**Livre – Chapitre 1**).

Ces paramètres permettent d'obtenir des microstructures variées. L'augmentation du taux de dilution entraîne une augmentation de la quantité de silicate à la surface des grains de sable (**Figure 8A**). Cependant, l'échantillon $(^{70}{}_{C1}Na^{1,7})$-$(^{G}S_8)^{150}{}_{MO}$ présente une meilleure répartition du silicate et un phénomène de cristallisation est noté entre les grains de sable. Ce phénomène pourrait être dû à la formation d'espèces polymérisées, favorisées par la dilution de la solution, permettant ainsi une meilleure élimination de l'eau lors du séchage et favorisant l'apparition de phénomène de cristallisation [10]. Ainsi, le taux de dilution a une influence sur la microstructure des blocs de sable aggloméré.

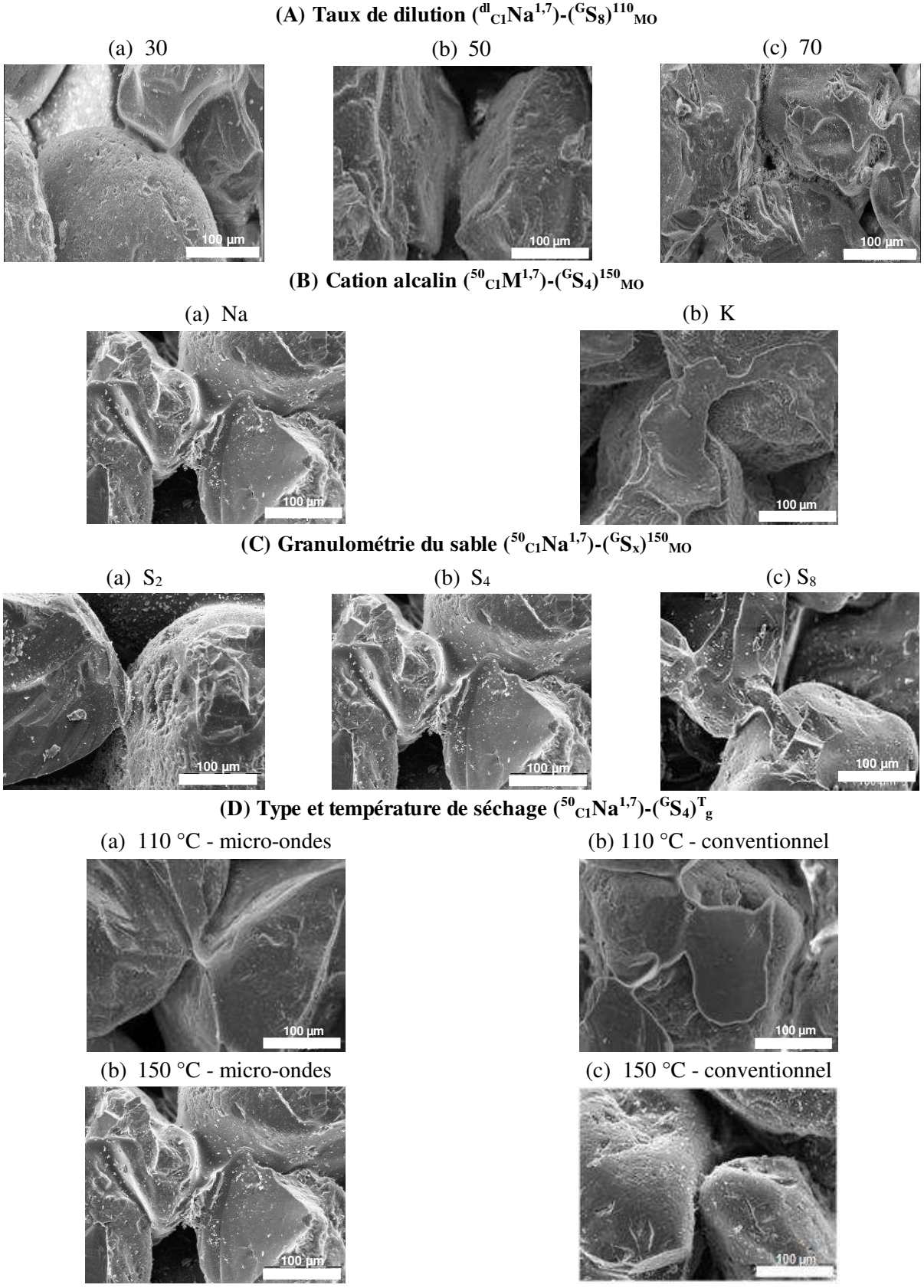

Figure 8 : images MEB des blocs de sable aggloméré pour différents **(A)** taux de dilution (dl), **(B)** cations alcalins (M), **(C)** granulométries de sable (S_x) et **(D)** types et températures de séchage (T et g).

Le cation alcalin ne semble pas avoir d'effet sur la répartition du silicate (**Figure 8B**). Cependant, les deux solutions présentent des aspects différents à la surface des grains de sable. Ainsi, le cation potassium entraîne un phénomène de démixtion qui n'apparaît pas en présence de sodium. Ces observations sont en accord avec les diagrammes de phase SiO_2-K_2O et SiO_2-Na_2O [11]. En effet, dans le cas du cation potassium, le point eutectique étant à une température plus faible que pour le sodium pourrait favoriser ainsi un phénomène de démixtion à plus basse température.

Quel que soit le type de sable, les morphologies des échantillons sont comparables (**Figure 8C**). En effet, les grains de sable semblent être enrobés par la solution de silicate quelle que soit la granulométrie du sable. Ainsi, le type de sable n'a pas d'influence notable sur la microstructure des échantillons.

Le type et la température de séchage conduisent à des répartitions différentes de la solution de silicate (**Figure 8D**) entraînant des microstructures différentes. En effet, le séchage par micro-ondes semble favoriser l'enrobage des grains de sable, tandis que l'utilisation du séchage conventionnel entraîne la présence du liant seulement au niveau des ponts entre les grains. Ce phénomène pourrait être expliqué par le fait que le séchage par convection permet l'évaporation d'une quantité plus importante d'eau que le séchage par micro-ondes [12]. Ces différences sont dues à des interactions différentes pour les deux séchages. En effet, lors du séchage par micro-ondes, les interactions dipolaires vont favoriser l'élimination de l'eau sans détériorer le silicate. Dans ce cas, le silicate enrobe les grains de sable. En revanche, dans le cas d'un séchage conventionnel, l'eau est éliminée et un phénomène de dissolution / reprécipitation apparaît entraînant ainsi la formation de ponts entre les grains.

De plus, l'élévation de la température de 110 à 150 °C permet de diminuer la quantité de silicate à la surface des grains. Ce phénomène pourrait être expliqué par des teneurs en eau différentes en fonction de la température de séchage. En effet, le séchage à 150 °C permet d'éliminer une plus grande quantité d'eau qu'à 110 °C [12, 13]. Ainsi, les échantillons séchés à 110 °C contiennent une plus grande quantité d'eau et le silicate semble donc être en plus grande quantité à la surface des grains de sable. Ainsi, le type et la température de séchage ont une influence sur la répartition du silicate au sein des blocs de sable.

Les effets des différents paramètres ont également été étudiés par des essais de compression. La valeur de la contrainte à la rupture a été tracée en fonction de la masse volumique des échantillons pour les deux types de séchage (**Figure 9**). Les résultats obtenus pour les autres paramètres sont présentés en **Annexe III-2**.

Les deux types de séchage permettent d'obtenir des valeurs de contrainte à la rupture proches. Cependant, le séchage convectif semble favoriser l'obtention de valeurs légèrement plus élevées. De récentes études par Granat et al. ont démontré que le séchage micro-ondes de blocs de sable à 700 W pendant 240 secondes permet d'obtenir des propriétés mécaniques similaires, voire légèrement supérieures, au séchage conventionnel [14]. Les différences observées pour les échantillons $(^{30}_{C1}K^{1,7})$-$(^{G}S_8)^{150}_{MO}$ séchés à 150 W pendant 45 minutes, par rapport aux études de Granat et al., pourraient être dues à la puissance de micro-ondes différente [15]. La nature du séchage induit des différences au niveau de la résistance mécanique qui peut être contrôlée par la température de séchage et la puissance associée.

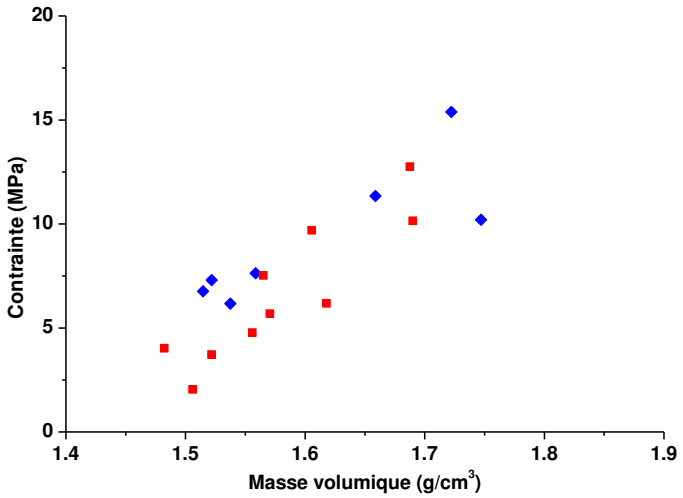

Figure 9 : valeurs de contrainte à la rupture en fonction de la masse volumique pour les échantillons $(^{30}_{C1}K^{1,7})$-$(^{G}S_8)^{150}_{g}$ avec g = (◆) convectif et (■) micro-ondes

Afin de mieux appréhender les différentes interactions, des essais d'agglomération d'un sable de zircon ont été réalisés avec la solution $^{50}_{C1}Na^{1,7}$. Les blocs de sable imprégnés ont été séchés à 110 et 150 °C par séchage conventionnel et analysés au microscope électronique à balayage (**Figure 10**). Les deux échantillons présentent des microstructures différentes. L'échantillon $(^{50}_{C1}Na^{1,7})$-$(^{G}Zr)^{110}_{conv}$ ne présente pas de phénomène de dissolution / reprécipitation (**Figure 10a**) suggérant des répulsions entre le sable de zircon et les entités silicatées. La présence de l'élément zirconium entraîne des répulsions de par sa valeur de PEI (point isoélectrique) de 4,7 [16] vis-à-vis des espèces réactives par comparaison avec une surface de silice de PEI de 2 [17]. Ceci induit un problème d'adhérence du silicate sur le sable de zircon. En revanche, à 150 °C, il est noté un phénomène de démixtion dû à l'agitation thermique. En effet, les phénomènes précédents sont atténués puisqu'une partie d'eau va s'évaporer (**Figure 10b**). Les espèces silicatées vont toujours interagir avec les surfaces

siliceuses et l'excès de silicate alcalin n'ayant pas réagi va cristalliser. Ceci conduit à un matériau homogène pour le sable siliceux alors que, pour le sable de zircon, il y a des hétérogénéités. Ceci démontre que la nature du sable contrôle en partie l'agglomération en présence d'espèces siliceuses.

Figure 10 : images MEB des blocs de sable de zircon ($^{50}_{C1}Na^{1,7}$)-(^{G}Zr)$^{T}_{conv}$ avec T = **(a)** 110 et **(b)** 150 °C.

Les différentes analyses réalisées sur les blocs de sable aggloméré ont démontré que les paramètres importants pour l'agglomération du sable sont le type et la température de séchage induisant un enrobage des grains ou un phénomène de dissolution / reprécipitation. La **Figure 11** présente une cartographie des microstructures obtenues en fonction de la température et du type de séchage utilisé pour la préparation des blocs de sable aggloméré.

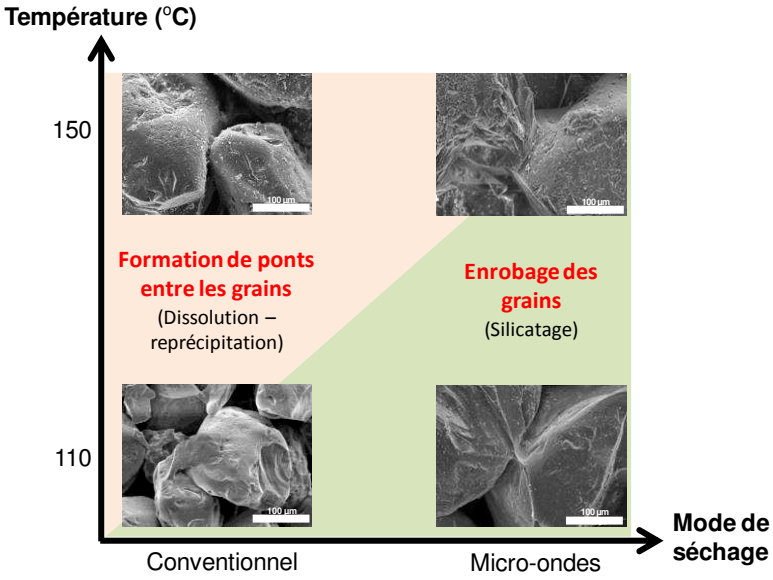

Figure 11 : *résumé de l'influence de la température et du mode de séchage sur la* microstructure des blocs de sable aggloméré.

Un enrobage des grains de sable est noté pour de faibles températures ainsi qu'avec un séchage par micro-ondes. En revanche, l'augmentation de la température et l'utilisation d'un séchage conventionnel favorisent l'apparition de phénomènes de dissolution / reprécipitation

et la formation de ponts entre les grains de sable. Ainsi, il semble préférable de sécher les blocs de sable imprégnés à 150 °C par un séchage conventionnel afin de former des ponts entre les grains de sable.

***Les différentes méthodes d'imprégnation soulignent la difficulté d'obtenir une répartition homogène de la solution au sein de l'empilement granulaire. Un séchage* conventionnel à 150 °C apparaît *être une alternative afin d'obtenir une microstructure et* des propriétés mécaniques satisfaisantes.**

III. LE FUSIBLE EN UNE SEULE ÉTAPE : ESSAIS DE FAISABILITÉ

A. REMPLACEMENT DE LA PIÈCE CÉRAMIQUE

Afin de remplacer le corps en céramique par un liant géopolymère, deux pistes d'investigation ont été envisagées. La première consiste à enrober un bloc de sable à l'aide d'un liant géopolymère et la seconde à réaliser une pièce par coulage pour ensuite l'ensabler. L'objectif de cette partie est donc d'étudier les différentes interfaces entre le liant de type géopolymère et le bloc de sable, ainsi que la réalisation d'un bloc de sable enrobé à partir d'une pièce géopolymère.

1. Agglomération du sable par un liant géopolymère

a. Enrobage du sable

Afin de réaliser un fusible en une seule étape, des essais d'enrobage ont été réalisés sur des blocs de sable aggloméré. L'influence de la composition du liant et des paramètres qui influent sur l'épaisseur déposée, i.e. le temps de séchage et le nombre de couches, a été étudiée.

Effet de la composition

Afin d'identifier les interactions entre un liant géopolymère et un bloc de sable, il a été procédé à l'évaluation de l'interface par la détermination des angles de mouillage de façon comparative. Pour cela, des compositions connues du laboratoire ont été sélectionnées (**ACL2**, **ACL3** et **ACLN3**). Les blocs de sable utilisés sont réalisés à partir de la solution $^{50}{}_{C1}Na^{1,7}$ et du sable S_9 afin de diminuer l'erreur due à la rugosité et à la présence de porosité en surface [18, 19].

La **Figure 12** présente l'évolution de la valeur d'angle de mouillage en fonction du temps pour différentes compositions. Les principales différences sont liées à la composition. La

formulation $(_{C1}K^{1,7}{}_{K^{0,7}}\text{-}^{12}M1)^{25}$ présente une faible valeur initiale d'angle de mouillage qui diminue au cours du temps. En effet, la valeur initiale de l'angle est de 85,0°, puis elle diminue jusqu'à 60,2° et reste stable pour des temps supérieurs à 1 minute. Cette variation de l'angle pourrait être expliquée par la pénétration du liant au sein du bloc de sable par le liant. En effet, la faible viscosité de cette formulation, due à la faible réactivité du métakaolin, favorise la migration vers le sable [20]. En présence de la même solution, un métakaolin plus réactif [20] entraîne une importante augmentation de la valeur de l'angle, respectivement de 85,0° à 124,7° et 113,1° pour les liants $(_{C1}K^{1,7}{}_{K^{0,7}}\text{-}^{12}M1)^{25}$, $(_{C1}K^{1,7}{}_{K^{0,7}}\text{-}^{12}MT)^{25}$ et $(_{C1}K^{1,7}{}_{K^{0,7}}\text{-}^{12}M2)^{25}$, et évoluant peu au cours du temps. La valeur plus élevée de l'angle peut être expliquée par la réactivité plus importante des métakaolins M2 et MT favorisant les réactions de polycondensation, et entraînant donc des interactions électrostatiques plus fortes dues à la consolidation plus rapide du liant [20, 21]. L'utilisation d'un métakaolin plus réactif induit également une augmentation de la viscosité limitant la pénétration du liant au sein du bloc de sable, et permettant d'expliquer la faible variation de la valeur de l'angle de mouillage au cours du temps [20].

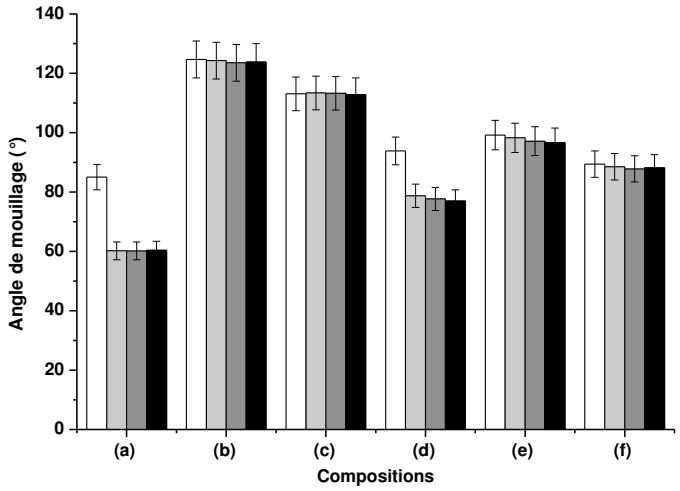

Figure 12 : *valeur de l'angle de mouillage sur du sable aggloméré* $(^{50}{}_{C1}Na^{1,7})\text{-}(^{mel}S_9)^{70}{}_{conv}$ pour les formulations **(a)** $(_{C1}K^{1,7}{}_{K^{0,7}}\text{-}^{12}M1)^{25}$, **(b)** $(_{C1}K^{1,7}{}_{K^{0,7}}\text{-}^{12}MT)^{25}$, **(c)** $(_{C1}K^{1,7}{}_{K^{0,7}}\text{-}^{12}M2)^{25}$, **(d)** $(_{C1}Na^{1,7}{}_{Na^{0,7}}\text{-}^{12}M1)^{25}$, **(e)** $(_{C1}Na^{1,7}{}_{Na^{0,7}}\text{-}^{12}MT)^{25}$ et **(f)** $(_{C1}Na^{1,7}{}_{Na^{0,7}}\text{-}^{12}M2)^{25}$ à t = (□) 0, (▒) 1, (▒) 2 et (■) 3 minutes.

La modification du cation alcalin entraîne une augmentation de la valeur de l'angle de mouillage (respectivement de 85,0° à 93,9° pour $(_{C1}K^{1,7}{}_{K^{0,7}}\text{-}^{12}M1)^{25}$ et $(_{C1}Na^{1,7}{}_{Na^{0,7}}\text{-}^{12}M1)^{25}$). Cependant, un comportement similaire à celui du liant $(_{C1}K^{1,7}{}_{K^{0,7}}\text{-}^{12}M1)^{25}$ est noté au cours du temps. L'augmentation de l'angle de mouillage peut être expliqué par un état de

dépolymérisation plus important pour la solution $_{C1}Na^{1,7}{}_{Na}{}^{0,7}$, par rapport à la solution $_{C1}K^{1,7}{}_{K}{}^{0,6}$, induisant de fortes interactions entre les espèces. La faible variation de l'angle au cours du temps peut, à nouveau, être expliquée par une faible viscosité du liant limitant l'imprégnation du sable aggloméré. Dans le cas d'un métakaolin réactif, la valeur de l'angle de mouillage varie peu (de 93,9° à 99,2° et 89,4° pour $(_{C1}Na^{1,7}{}_{Na}{}^{0,7}\text{-}{}^{12}M1)^{25}$, $(_{C1}Na^{1,7}{}_{Na}{}^{0,7}\text{-}{}^{12}MT)^{25}$ et $(_{C1}Na^{1,7}{}_{Na}{}^{0,7}\text{-}{}^{12}M2)^{25}$) et n'évolue pas au cours du temps. Cette faible variation est à corréler à l'ajout d'eau lors de la phase de préparation pour les mesures. En effet, les mélanges présentaient des viscosités très élevées et il était difficile d'obtenir une goutte pour la mesure de l'angle. L'ajout d'eau entraîne une légère polymérisation de la solution et diminue par conséquent les interactions entre les espèces, induisant ainsi une diminution de la valeur de l'angle de mouillage.

La mesure de l'angle de mouillage permet d'évaluer la réactivité du liant.

Compte tenu de ces données, des essais d'adhésion ont ensuite été réalisés avec les différentes compositions. Pour cela, deux couches de liant, espacées de 60 min de séchage, (cf. **Chapitre II**) ont été déposées sur des blocs de sable ; excepté pour la formulation $_{C1}K^{1,7}{}_{K}{}^{0,5}\ \text{-}{}^{20}M1^{25}$ très visqueuse et difficilement applicable. La **Figure 13** présente les photographies des échantillons obtenus à différents temps ainsi que le taux de fissures en fonction du temps pour les différentes formulations. D'importantes différences sont notables en fonction de la formulation du liant. En effet, seulement la composition $(_{C1}K^{1,7}{}_{K}{}^{0,6}\text{-}{}^{12}M1)^{25}$ n'entraîne pas de fissuration du dépôt, alors que, pour les liants $(_{C1}K^{1,7}{}_{K}{}^{0,6}\text{-}{}^{12}MT)^{25}$, $(_{C1}K^{1,7}{}_{K}{}^{0,6}\ \text{-}{}^{12}M1\text{-}{}^{12}MT)^{25}$ et $(_{C1}K^{1,7}{}_{K}{}^{0,5}\ \text{-}{}^{20}M1)^{25}$, l'apparition de fissures est visible dès le premier jour de séchage.

Le changement de la source aluminosilicate M1 ($(_{C1}K^{1,7}{}_{K}{}^{0,5}\ \text{-}{}^{12}M1)^{25}$) par MT ($(_{C1}K^{1,7}{}_{K}{}^{0,6}\text{-}{}^{12}MT)^{25}$) entraîne une couche de liant plus épaisse qui va induire des fissures. La réalisation de deux couches de compositions différentes ($(_{C1}K^{1,7}{}_{K}{}^{0,6}\ \text{-}{}^{12}M1\text{-}{}^{12}MT)^{25}$) entraîne également l'apparition de fissures sur la couche supérieure. Ces différences de comportements sont en accord avec les variations des angles de mouillage et sont dues aux réactivités différentes des métakaolins [20]. En effet, l'utilisation du métakaolin M1 induit une diffusion vers le sable favorisant l'ancrage, alors que le métakaolin MT, très réactif, limite la diffusion du liant fragilisant ainsi le dépôt avec l'apparition de fissures. Un taux de charge de métakaolin M1 ($(_{C1}K^{1,7}{}_{K0,5}\ \text{-}{}^{20}M1)^{25}$) entraîne également un dépôt d'épaisseur plus importante mais fissurant.

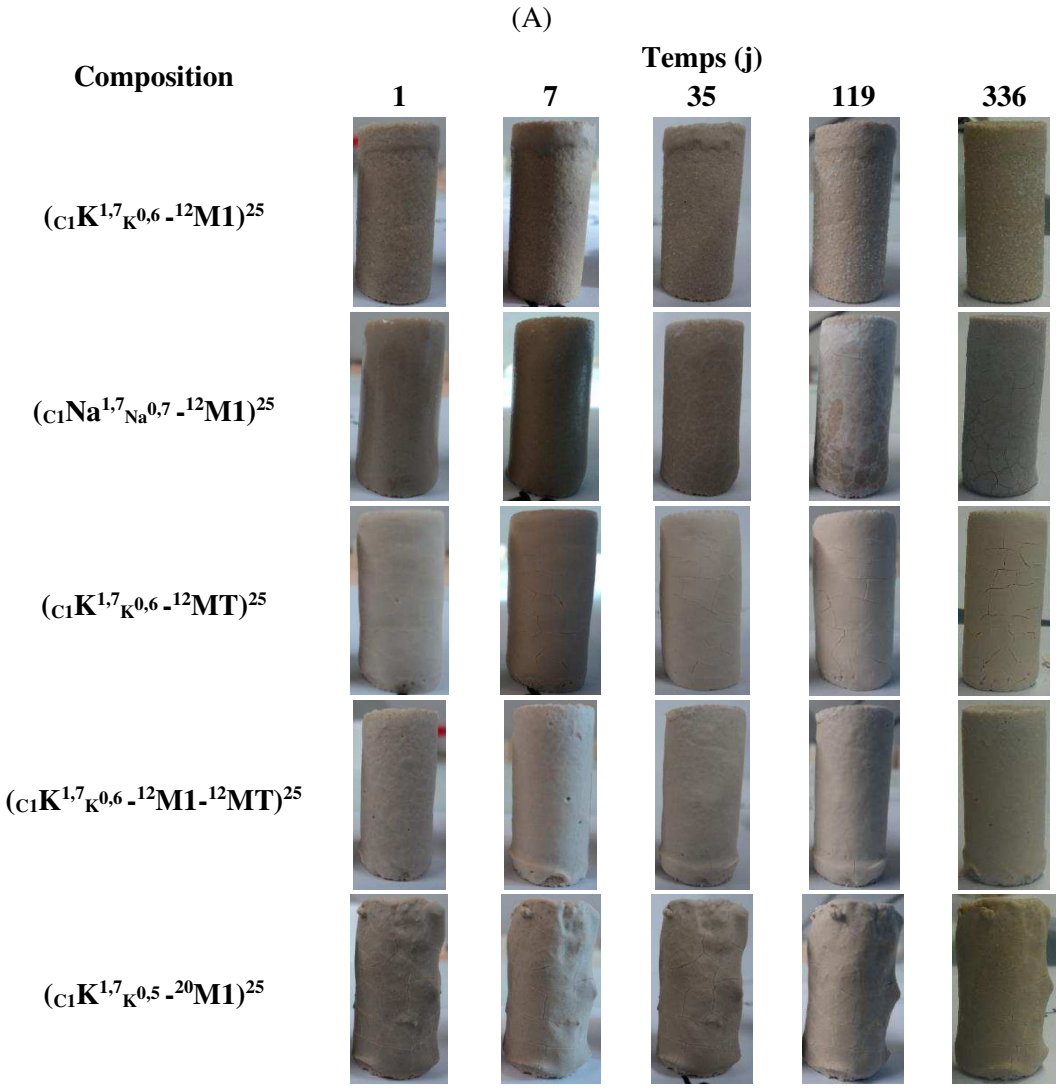

Figure 13 : (A) *photographies des essais d'adhésion (Ø =* 15 mm) et **(B)** taux de fissuration au cours du temps (▬) $(C_1K^{1,7}{}_{K}{}^{0,6}\text{-}{}^{12}M1)^{25}$, (▬) $(C_1K^{1,7}{}_{K}{}^{0,6}\text{-}{}^{12}MT)^{25}$, (▬) $(C_1K^{1,7}{}_{K}{}^{0,6}\text{-}{}^{12}M1\text{-}{}^{12}MT)^{25}$ et (▬) $(C_1K^{1,7}{}_{K}{}^{0,5}\text{-}{}^{20}M1)^{25}$ et (▬) $(C_1Na^{1,7}{}_{Na}{}^{0,7}\text{-}{}^{12}M1)^{25}$.

Une viscosité plus élevée limite la diffusion du liant au sein du bloc de sable en accord avec les données des angles de mouillage. De plus, la nature du cation alcalin et donc la concentration (respectivement 5,5 et 8,7 mol/L pour $_{C1}K^{1,7}{}_{K}{}^{0,6}$ et $_{C1}Na^{1,7}{}_{Na}{}^{0,7}$) induit une variation de l'épaisseur du dépôt. Le dépôt est plus conséquent pour la formulation à base de sodium $_{C1}Na^{1,7}{}_{Na}{}^{0,7}$-$^{12}M1^{25}$ que pour celle à base $_{C1}K^{1,7}{}_{K}{}^{0,5}$ -$^{20}M1^{25}$ de potassium. Ce phénomène est à corréler à la quantité d'eau plus importante pour la solution $_{C1}K^{1,7}{}_{K}{}^{0,6}$ [22].

Il est possible de contrôler l'apparition de fissures **en modifiant la source aluminosilicate et le cation alcalin.**

Influence du temps de séchage et du nombre de couches

L'influence de l'épaisseur du liant, contrôlée par le temps de séchage et le nombre de couches déposées, a ensuite été étudiée. La **Figure 14** présente l'influence de l'épaisseur du liant pour les différents échantillons obtenus à différents temps (**ACL7**).

Les quatre formulations présentent des comportements différents en accord avec les résultats précédents. En effet, le mélange $(_{C1}K^{1,7}{}_{K}{}^{0,6}$-$^{12}M1)^{25}$ ne présente pas de fissures quels que soient l'épaisseur et le temps de séchage du liant alors que des fissures sont observées pour l'échantillon $(^{50}{}_{C1}Na^{1,7}$-$S_4)^0$-$(_{C1}K^{1,7}{}_{K}{}^{0,6}$ -$^{12}MT)$ dès 24h de séchage. Ce phénomène est accentué par un temps de séchage plus long avant le dépôt de la deuxième couche (24h). L'apparition de fissures peut être reliée à la réactivité du métakaolin. Le métakaolin MT très réactif, conduisant à un liant de faible porosité finale, ne permet pas l'ancrage d'une seconde couche [23]. Ceci a pour conséquence d'entraîner l'accentuation des fissures pour un dépôt après 24 heures de séchage. Les interactions entre les deux couches de ce liant semblent être légèrement plus favorables pour un dépôt après 1 heure de séchage, i.e. lorsque le dépôt n'est pas totalement consolidé. L'ajout d'une seconde couche de composition différente $((_{C1}K^{1,7}{}_{K}{}^{0,6}$-$^{12}M1$-$^{12}MT)^{25})$ entraîne l'apparition d'une légère fissuration dès 24 heures de séchage. Le dépôt de deux couches de formulations différentes semble légèrement améliorer le comportement de la composition à base de métakaolin MT. En effet, la composition à base de métakaolin M1, très poreuse, facilite l'ancrage de la composition $(_{C1}K^{1,7}{}_{K}{}^{0,6}$-$^{12}MT)^{25}$ [23].

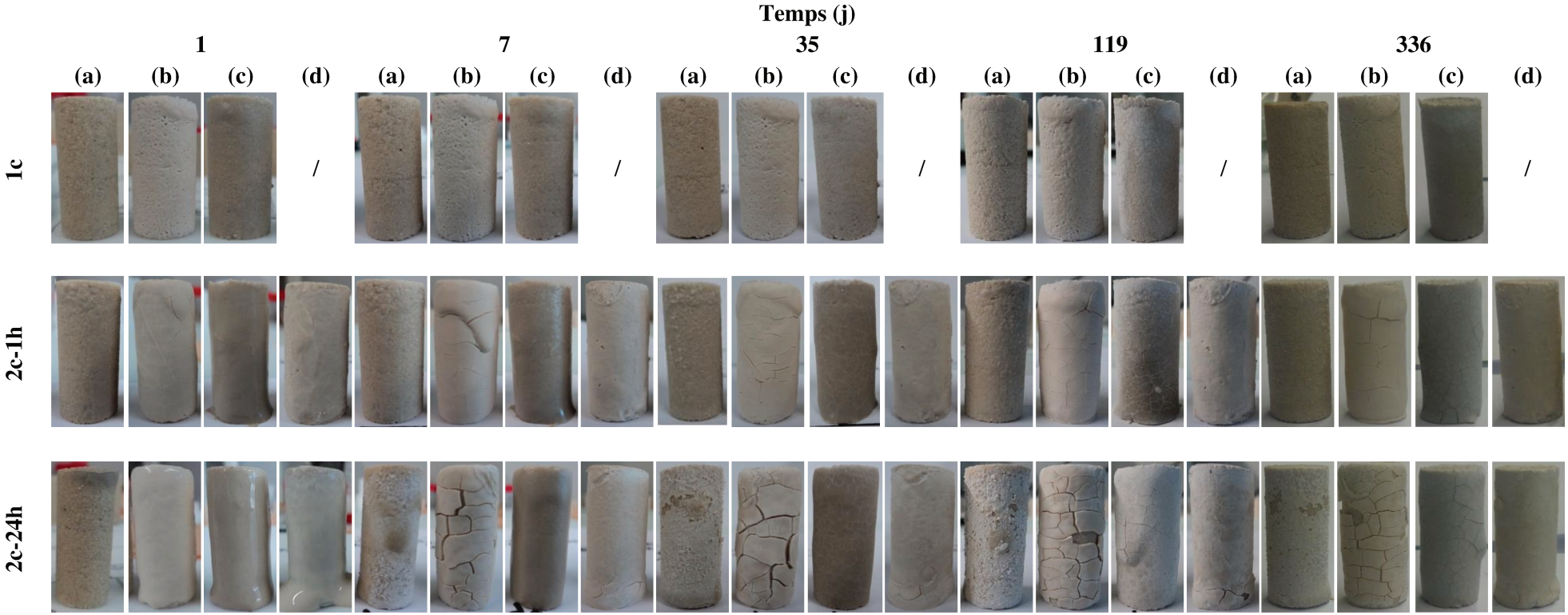

Figure 14 : photographies des dépôts en fonction du temps de séchage entre les couches (2c-1h et 2c-24h) de liants pour les formulations **(a)** $(_{C1}K^{1,7}{}_{K^{0,6}}\text{-}{}^{12}M1)^{25}$, **(b)** $(_{C1}K^{1,7}{}_{K^{0,6}}\text{-}{}^{12}MT)^{25}$, **(c)** $(_{C1}Na^{1,7}{}_{Na^{0,7}}\text{-}{}^{12}M1)^{25}$ et **(d)** $(_{C1}K^{1,7}{}_{K^{0,6}}\text{-}{}^{12}M1\text{-}{}^{12}MT)^{25}$ (Ø = 15 mm).

La modification du cation alcalin de la solution en présence du métakaolin M1 ($(_{C1}Na^{1,7}{}_{Na}0,7\text{-}{}^{12}M1)^{25}$) induit la formation de fissures après 35 jours de séchage pour les échantillons comportant deux couches. Ceci est aussi à corréler soit à une porosité moindre, soit à la présence de carbonates de surface inhibant l'ancrage de la seconde couche et entraînant la formation de fissures.

L'apparition d'efflorescences a également été notée pour les échantillons $(^{50}{}_{C1}Na^{1,7}\text{-}S_4)^0\text{-}(_{C1}K^{1,7}{}_{K}0,6\text{-}{}^{12}M1)^{2c\text{-}1h}$, $(^{50}{}_{C1}Na^{1,7}\text{-}S_4)^0\text{-}(_{C1}K^{1,7}{}_{K}0,6\text{-}{}^{12}M1)^{2c\text{-}24h}$, $(^{50}{}_{C1}Na^{1,7}\text{-}S_4)^0\text{-}(_{C1}Na^{1,7}{}_{Na}0,7\text{-}{}^{12}M1)^{2c\text{-}1h}$, $(^{50}{}_{C1}Na^{1,7}\text{-}S_4)^0\text{-}(_{C1}Na^{1,7}{}_{Na}0,7\text{-}{}^{12}M1)^{2c\text{-}24h}$ s'accentuant avec l'augmentation du temps entre les deux couches. Ces efflorescences sont dues à la formation de carbonates et peuvent être expliquées par la présence de cations alcalins en excès pouvant réagir avec le CO_2 [24].

Les dépôts présentant la meilleure tenue au cours du temps sont réalisés avec la composition $(_{C1}K^{1,7}{}_{K}0,6\text{-}{}^{12}M1)^{25}$ dont l'épaisseur et le temps de séchage sont contrôlables.

Caractérisation de l'interface

L'interface entre le bloc de sable aggloméré et le liant géopolymère a ensuite été observée au microscope électronique à balayage pour la composition $(_{C1}K^{1,7}{}_{K}0,6\text{-}{}^{12}MT)$ (**Figure 15**).

Le liant semble imprégner le bloc de sable selon une épaisseur d'environ 500 µm (**Figure 15a**). Ceci est dû à la porosité du bloc de sable et à la faible viscosité du mélange. De plus, ceci permet une meilleure isolation du bloc de sable en colmatant les couches externes du bloc de sable. La microstructure observée à l'interface entre le liant et le grain de sable est similaire à celle d'un géopolymère [25] (**Figure 15b**). En effet, le liant géopolymère n'est pas en interaction avec le grain de sable, dû à sa nature faiblement réactive de par la couche de silicate alcalin issue des conditions de séchage (cf. **Chapitre II**). La forte concentration des éléments Al et K (**Figure 15c**), observée à l'intérieur du bloc de sable, correspond à la formulation du liant géopolymère confirmant l'imprégnation du sable par le liant.

Afin de compléter ces résultats, des mesures d'angles de mouillage de différentes compositions sur des blocs de sable aggloméré pourraient être réalisées. Des observations au microscope électronique à balayage sur d'autres dépôts pourraient également être effectuées.

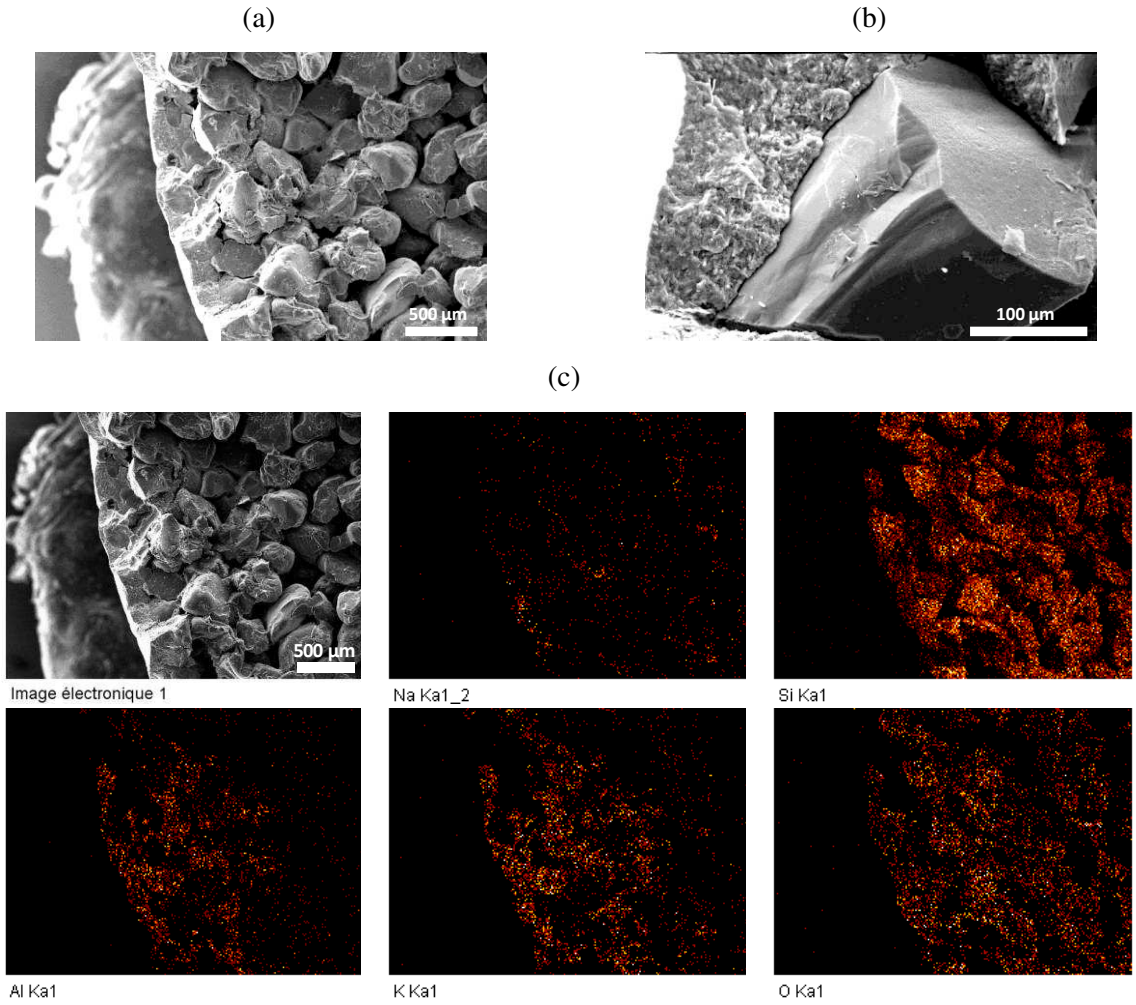

Figure 15 : images MEB **(a)** *d'un bloc de sable enrobé de liant géopolym*ère ($_{C1}K^{1,7}{}_{K^{0,6}}$ - ^{12}MT), **(b)** *zoom sur l'interface et* **(c)** cartographie X des éléments Na (K_α = 1,041 eV), Si (K_α = 1,739 eV), Al (K_α = 1,486 eV), K (K_α = 3,312 eV) et O (K_α = 0,525 eV).

La diffusion du liant géopolymère au sein du bloc de sable aggloméré permet de *favoriser la tenue du dépôt. Cependant, il faudrait déterminer l'impact de l'ajout d'une* faible quantité de métakaolin afin de réaliser une couche progressive.

b. Détermination des interactions avant la formation de géopolymères

Dans le but d'identifier les interactions entre une formulation aluminosilicate alcalin et le bloc de sable aggloméré, différents mélanges contenant des teneurs variables en métakaolin ont été étudiés par spectroscopie IRTF (**ACL 7**). La **Figure 16** présente la variation de la valeur de shift corrigée par le taux d'eau (shift/H_2O) en fonction de la concentration en aluminium corrigée par le pourcentage d'amorphe. Cette correction a été appliquée du fait de la mise en solution très rapide des atomes d'aluminium responsables, par conséquent, de la formation des réseaux.

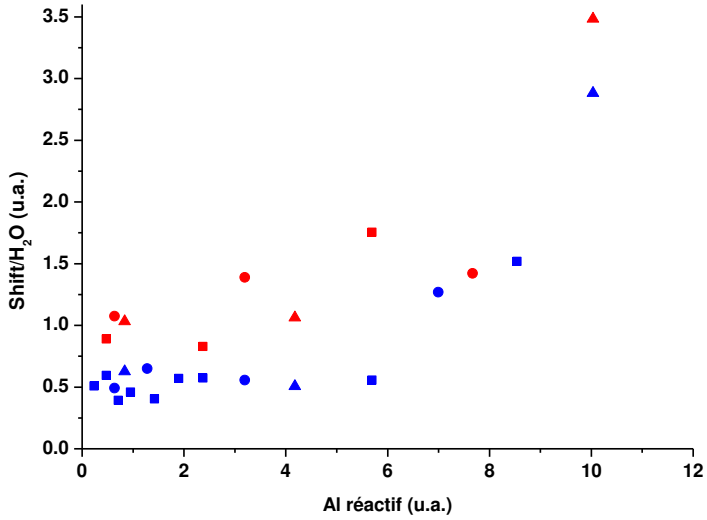

Figure 16 : *valeur de shift (spectroscopie IRTF) corrigé par le taux d'eau en fonction de la concentration en aluminium corrigée par le taux d'amorphe (DRX métakaolin) pour les* mélanges (■) $({}_{L}M^{0,7}\text{-}{}^{h}M1)^{25}$, (●) $({}_{L}M^{0,7}\text{-}{}^{h}M2)^{25}$, (▲) $({}_{L}M^{0,7}\text{-}{}^{h}MT)^{25}$ avec M = (▬) K et (▬) Na et h variant de 0,5 à 18 g.

Quel que soit le mélange réactionnel, les valeurs du rapport shift/H_2O sont constantes jusqu'à une valeur seuil d'aluminium réactif de 5 u.a., puis il est observé une augmentation significative pour les solutions ${}_{L}K^{0,7}$ et ${}_{L}Na^{0,7}$, respectivement de 0,5 à 2,8 et de 1,0 à 3,5 u.a. Cependant, les mélanges à base de sodium présentent des valeurs de rapport shift/H_2O légèrement plus élevées que ceux à base de potassium (respectivement 0,5 et 1,0 pour les solutions ${}_{L}K^{0,7}$ et ${}_{L}Na^{0,7}$), dues à la réactivité plus importante de la solution ${}_{L}Na^{0,7}$ [23]. Dans ce cas, la valeur de pH des mélanges $({}_{L}Na^{0,7}\text{-}{}^{1}My)^{25}$ est plus faible, de l'ordre de 13,6, signifiant que certaines réactions de polycondensation ont eu lieu, résultant en une valeur de shift élevée. Pour des quantités d'aluminium réactif inférieures à 5 u.s, les valeurs de shift/H_2O faibles sont dues à des quantités d'eau au sein du mélange réactionnel élevées (entre 40 à 55 % pour des quantités variant de 0,2 à 4,2 u.a.). Dans ce domaine de quantité d'aluminium réactif, la solution est très diluée, les espèces se comportent comme dans un état dilué conduisant à la formation de différentes espèces [26]. En revanche, pour des quantités supérieures à 5 u.a., l'enrichissement en atomes d'aluminium favorise la formation d'un réseau plus ordonné [27]. Il a donc été mis en évidence pour la formation des géopolymères à la fois, (i) l'existence d'une valeur d'aluminium réactif limite (5 mol/L) et (ii) une valeur du rapport shift/H_2O = 1,4.

La concentration en espèces étant un paramètre déterminant, il a été procédé à l'évaluation du volume réactif par le calcul de la différence entre le volume d'eau de la solution et le volume d'eau nécessaire pour mouiller la quantité de métakaolin ajoutée. Cette donnée sera notée ΔV. Afin de corroborer ce résultat au domaine d'existence des géopolymères mis en évidence par Gharzouni et al. [23], cette variable a été reportée en fonction des rapports molaires Si/Al et M/Al (M = Na, K) du mélange total (**Figure 17**). Les valeurs positives sont caractéristiques d'une quantité d'eau en excès pour mouiller le métakaolin alors que celles négatives soulignent un déficit en eau. Les mêmes variations sont notables pour les rapports molaires sélectionnés, à savoir un régime dynamique pour des valeurs positives et un régime invariant pour des valeurs de ΔV négatives.

L'évolution observée pour des valeurs de rapports molaires ($3 < Si/Al < 15$ et $2 < M/Al < 20$) est caractéristique d'un mélange dilué en présence d'une faible quantité de métakaolin. Le volume de liquide introduit est toujours excédentaire, les atomes d'aluminium et les atomes de silicium libérés vont interagir avec les espèces siliceuses de la solution en formant des espèces très riches en atomes de silicium, dues à la faible variation de la bande des Q^2. Ces espèces pourraient être amenées à précipiter, ce qui est vérifié par la formation d'un précipité.

Pour des rapports Si/Al = 2 et M/Al = 1,2, la valeur nulle de ΔV est relative à un état d'équilibre physicochimique, où les réactions de polycondensation vont prendre le relais et conduire à un réseau polymérique. De plus, cette valeur correspond à la limite de la zone d'existence des géopolymères.

Pour des valeurs de ΔV négatives, le volume de solution force la dissolution du métakaolin et favorise l'enrichissement du milieu réactionnel par les colloïdes aluminosilicates. Ceci induit une saturation du milieu favorisant ainsi les réactions de polycondensation et de géopolymérisation [23].

Dans ce domaine de concentration, la nature du cation alcalin n'est pas prépondérante. La faible différence entre le cation sodium et le cation potassium est à corréler à la viscosité du milieu qui régit le déplacement des espèces. En effet, les caractéristiques de la solution sodique de viscosité élevée, où le cation sodium diffuse moins vite, sont équivalentes à celle de la solution potassique, où le cation va diffuser plus vite.

Par conséquent, cette donnée ΔV facilement calculable peut être utilisée pour valider la faisabilité d'un liant géopolymère associée aux concentrations et de rapports molaires Si/Al et M/Al.

(a)

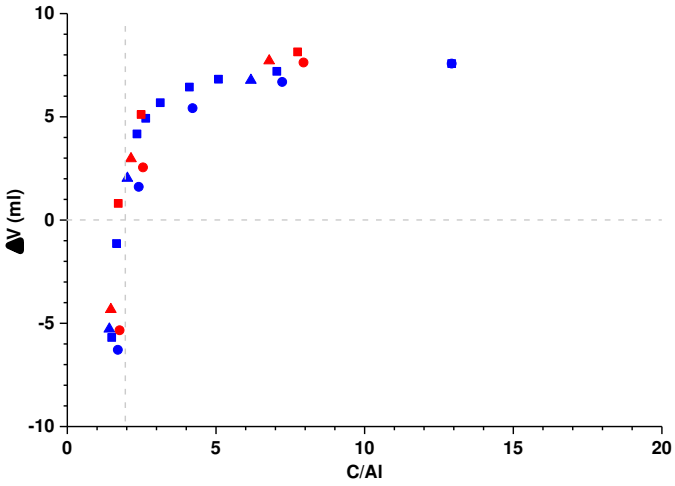

(b)

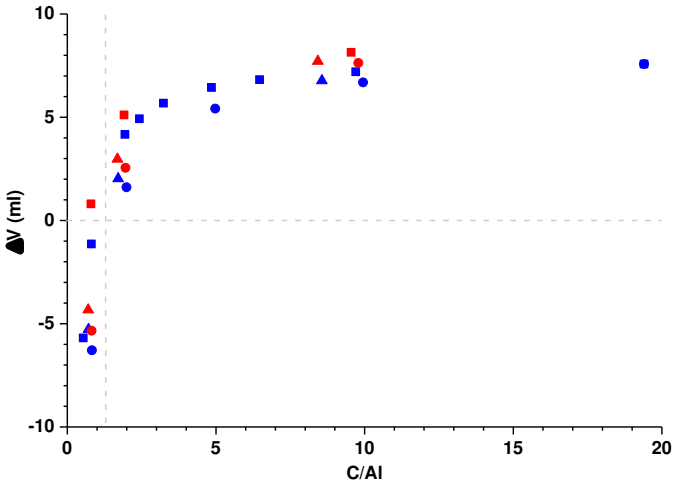

Figure 17 : *valeur de ΔV en fonction du rapport molaire C/Al avec* **(a)** C = Si et **(b)** C = K ou Na pour les mélanges (■) $(_{L}M^{0,7}\text{-}^{h}M1)^{25}$, (●) $(_{L}M^{0,7}\text{-}^{h}M2)^{25}$, (▲) $(_{L}M^{0,7}\text{-}^{h}MT)^{25}$ avec M = (▬) K et (▬) Na et h variant de 0,5 à 18 g.

2. Mise en forme d'une pièce

Afin de remplacer les corps de fusible actuels, des essais de mise en forme à température ambiante ont été réalisés à l'aide de plusieurs formulations.

a. Coulage de pièces en géopolymère

Neuf compositions ont été retenues et coulées sous forme de tubes, de plaques et de corps de fusible (**Tableau 1**). Les formulations utilisées (**Annexe III-3**) diffèrent de par la solution alcaline (mode de préparation, cation et rapport molaire Si/M différents), le métakaolin

(réactivité et pureté différentes) et le type de renfort (fibres de verre, sablon ou sable de zircon).

Tableau 1 : mise en forme par coulage des différentes compositions.

Composition	Tube (Ø = 15 mm)	Plaque (Lxlxh = 80x80x5 mm)	Corps de fusible (Lxlxh = 50x50x40 mm)
$_{C1}K^{1,7}{}_{K}{}^{0,6}\text{-}{}^{12}MT$		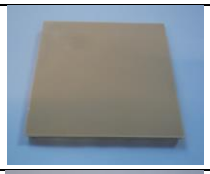	
$_{L}K^{0,7}\text{-}{}^{4}M1^{8}MT_{10s\text{-}10f}$		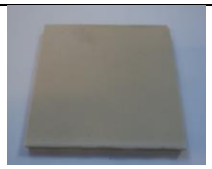	
$_{C1}Na^{1,7}{}_{Na}{}^{0,7}\text{-}{}^{6}M1^{6}M2_{40s\text{-}10f}$		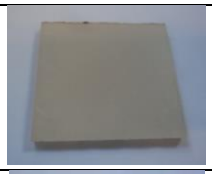	
$_{C1}K^{1,7}{}_{K}{}^{0,6}\text{-}{}^{6}M1^{6}M2_{40s\text{-}10f}$		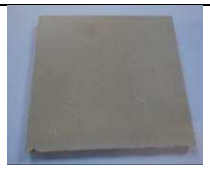	
$_{L}Na^{0,7}\text{-}{}^{8}M1^{4}M2_{40s\text{-}1f}$		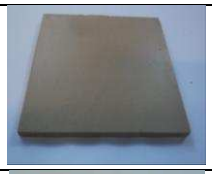	
$_{C1}Na^{1,7}{}_{Na}{}^{0,7}\text{-}{}^{16}M5_{40s}$			
$_{C1}Na^{1,7}{}_{Na}{}^{0,7}\text{-}{}^{16}M5_{40Zr}$		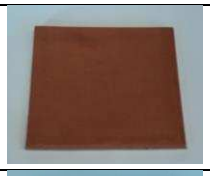	
$_{C1}K^{1,7}{}_{K}{}^{0,6}\text{-}{}^{16}M5_{40s}$		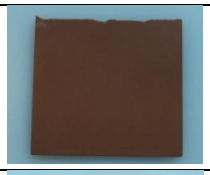	
$_{C1}K^{1,7}{}_{K}{}^{0,6}\text{-}{}^{22}M5_{55s}$		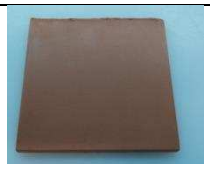	

Les différentes compositions permettent d'obtenir des pièces de forme différente sans défauts. Cependant, des modes opératoires distincts sont nécessaires pour obtenir ces différentes pièces.

En effet, pour les formes pleines (plaque et tube), le liant peut consolider au sein du moule avant le démoulage. Ces pièces ont donc été démoulées 24 heures après le coulage excepté pour les compositions $_{C1}K^{1,7}{}_{K}{}^{0,6}\text{-}{}^{16}M5_{40s}$ et $_{C1}K^{1,7}{}_{K}{}^{0,6}\text{-}{}^{22}M5_{55s}$ qui ont été démoulées après 6 heures. En effet, au-delà de ce temps de séchage, l'apparition de fissures a été notée. En revanche, pour les pièces creuses, la partie centrale du moule doit être ôtée avant que le matériau ne soit totalement consolidé, dû à l'existence d'un retrait au cours des réactions de géopolymérisation, afin d'éviter les fissurations. Le temps nécessaire pour l'enlèvement de la partie centrale du moule diffère en fonction de la composition, dû aux temps de consolidation différents. Les pièces, toujours contenues dans la partie supérieure du moule, ont ensuite été conservées dans une atmosphère à 85 % d'humidité puis elles ont été totalement démoulées 24 heures après le coulage.

Les résultats mettent en évidence que, quelle que soit la composition, la mise en forme et l'obtention de formes complexes à l'aide de liants géopolymères sont possibles. De plus, quel que soit le type de renfort, l'ajout au sein du mélange réactif n'inhibe pas la mise en forme de ces matériaux ($_{C1}Na^{1,7}{}_{Na}{}^{0,7}\text{-}{}^{16}M5_{40s}$, $_{C1}Na^{1,7}{}_{Na}{}^{0,7}\text{-}{}^{16}M5_{40Zr}$, $_{C1}K^{1,7}{}_{K}{}^{0,6}\text{-}{}^{16}M5_{40s}$ et $_{C1}K^{1,7}{}_{K}{}^{0,6}\text{-}{}^{22}M5_{55s}$). De même, la mise en forme des matériaux n'est pas affectée par le mélange de deux métakaolins de réactivité différente ($_{L}K^{0,7}\text{-}{}^{4}M1^{8}MT_{10s\text{-}10f}$, $_{C1}Na^{1,7}{}_{Na}{}^{0,7}\text{-}{}^{6}M1^{6}M2_{40s\text{-}10f}$, $_{C1}K^{1,7}{}_{K}{}^{0,6}\text{-}{}^{6}M1^{6}M2_{40s\text{-}10f}$ et $_{L}Na^{0,7}\text{-}{}^{8}M1^{4}M2_{40s\text{-}1f}$).

La mise en forme des liants géopolymères, réalisable par coulage, nécessite la connaissance du retrait au cours de la prise.

Afin de déterminer le retrait à température ambiante des liants, des mesures dilatométriques ont été effectuées entre 24 et 48 heures après la préparation du mélange pour les différentes formulations. Les échantillons ont été traités suivant un cycle de 24 heures à température ambiante suivi d'une montée en température jusqu'à 700 °C puis d'une descente jusqu'à 25 °C à 10 °C/min. Les résultats obtenus lors du traitement thermique seront présentés ultérieurement. Les courbes dilatométriques de trois compositions représentatives de l'ensemble des mélanges étudiés sont reportées sur la **Figure 18**.

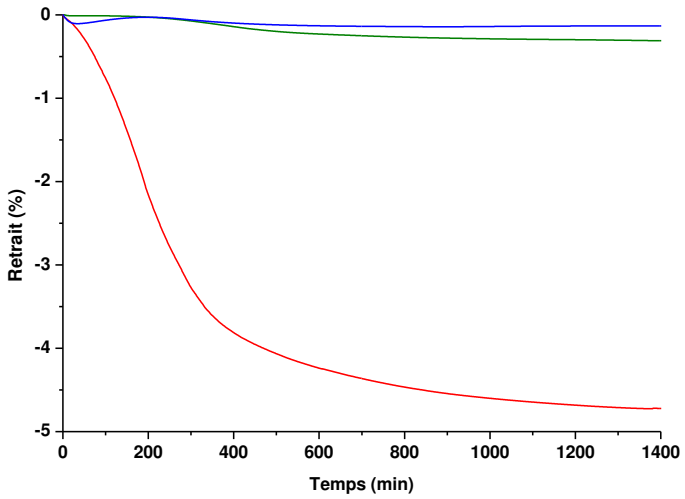

Figure 18 : courbes dilatométriques entre 24 et 48 heures à température ambiante pour les échantillons (—) $_{L}Na^{0,7}$-$^{8}M1^{4}M2_{40s\text{-}1f}$, (—) $_{C1}Na^{1,7}{}_{Na}{}^{0,7}$-$^{16}M5_{40Zr}$, (—) $_{C1}K^{1,7}{}_{K}{}^{0,6}$-$^{22}M5_{55s}$.

Différents comportements entraînant des valeurs de retrait différentes sont observables. L'échantillon $_{C1}Na^{1,7}{}_{Na}{}^{0,7}$-$^{16}M5_{40Zr}$ présente la valeur de retrait la plus élevée (-4,73 %) alors qu'un retrait de -0,31 % est observé pour la formulation $_{L}Na^{0,7}$-$^{8}M1^{4}M2_{40s\text{-}1f}$. Enfin, pour l'échantillon $_{C1}K^{1,7}{}_{K}{}^{0,6}$-$^{22}M5_{55s}$, un léger retrait est observé entre 0 et 50 minutes, puis une légère expansion jusqu'à t = 200 minutes suivie d'un faible retrait, le retrait final étant de -0,13 %. La valeur de retrait diminue lorsque la quantité de cation alcalin diminue respectivement de -4,73, -0,31 et -0,13 % pour des concentrations de 22,6, 19,4 et 10,3 mol/L relatives aux compositions $_{C1}Na^{1,7}{}_{Na}{}^{0,7}$-$^{16}M5_{40Zr}$, $_{L}Na^{0,7}$-$^{8}M1^{4}M2_{40s\text{-}1f}$ et $_{C1}K^{1,7}{}_{K}{}^{0,6}$-$^{22}M5_{55s}$. Ceci souligne l'importance de la teneur en alcalin nécessaire pour compenser la charge négative du réseau aluminosilicate en relation donc avec la valeur du retrait total.

De plus, comme précédemment démontré, cette charge positive dépend de la nature des espèces de la solution de silicate. Afin de mieux comprendre, les quantités d'anneaux R_3 et R_4 (déduites de la spectroscopie Raman) au sein de la solution alcaline sont respectivement de 7,06 / 5,85, 8,24 / 9,74 et 3,81 / 3,66 pour les solutions $_{C1}K^{1,7}{}_{K}{}^{0,6}$, $_{L}Na^{0,7}$ et $_{C1}Na^{1,7}{}_{Na}{}^{0,7}$. Lorsque la solution initiale contient des quantités égales d'espèces R_3 et R_4, le mélange ($_{C1}Na^{1,7}{}_{Na}{}^{0,7}$) présente un retrait important entre 24 et 48 heures. En revanche, lorsqu'il y a compétition entre les entités R_3 et R_4 (i.e. $R_3 < R_4$ ou $R_3 > R_4$), la valeur de retrait à température ambiante est inférieure à 2 %. D'autre part, la quantité d'anneaux R_4 supérieure à la quantité d'espèces R_3 est à corréler à l'expansion du mélange $_{C1}K^{1,7}{}_{K}{}^{0,6}$-$^{22}M5_{55s}$ entre 100 et 300 minutes et à une valeur de rapport molaire Si/M > 2 (**Annexe III-4**).

L'existence de ce phénomène d'expansion peut être due à la formation d'une phase métastable qui évolue par la suite. Pour rappel, au sein du diagramme binaire K_2O-SiO_2, les mélanges de rapport molaire Si/M supérieur à 2 sont situés dans la zone comprise entre les phases $K_2Si_4O_9$ et SiO_2 [28]. Ainsi, au sein du mélange réactionnel, la présence de germes de composition $K_2Si_4O_9$ semblerait être à l'origine de ce phénomène. Ceci ne serait pas observable pour les compositions à base de sodium puisque de telles phases n'existent pas. A nouveau, ces mélanges de faible rapport molaire Si/Al vont nécessiter une compensation de charge plus faible par les cations potassium. Le mélange réactionnel est donc plus dilué favorisant la formation de phase métastable par de premières réactions de polycondensation.

Le contrôle du retrait à température ambiante est dépendant du rapport Si/Al et de la compensation de charge par le cation alcalin.

b. Réalisation d'un fusible

Afin de déterminer la faisabilité de fusibles à partir d'un corps en liant géopolymère, un ensablage par un mélange de sable S_4 et de solution $^{50}{}_{C1}Na^{1,7}$ suivi d'un séchage à 70 °C (24 h) ont été réalisés. Les photographies (**Figure 19**) montrent que, quelle que soit la formulation, il est possible d'ensabler des corps de fusible en géopolymère afin de remplacer les corps de fusible en céramique. De plus, le bloc de sable aggloméré semble adhérer au corps de fusible en géopolymère.

(a) (b)

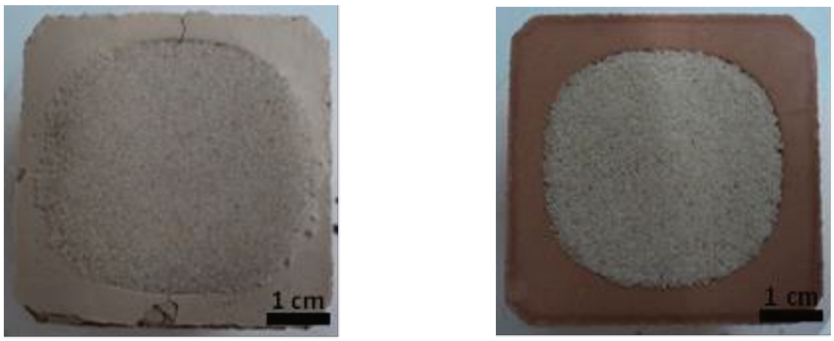

Figure 19 : photographies des corps de fusible ensablés réalisés avec les liants géopolymères **(a)** $_{C1}Na^{1,7}{}_{Na}{}^{0,7}$-$^{6}M1^{6}M2_{40s\text{-}10f}$ et **(b)** $_{C1}K^{1,7}{}_{K}{}^{0,6}$-$^{22}M5_{55s}$.

L'interface entre le corps de fusible $_{C1}Na^{1,7}{}_{Na}{}^{0,7}$-$^{6}M1^{6}M2_{40s\text{-}10f}$ et le sable aggloméré a été observée au microscope électronique à balayage (**Figure 20**). Une nette démarcation est notée à l'interface entre le liant et le bloc de sable aggloméré. Le sable aggloméré est constitué de grains de sable enrobés de silicate en accord avec les observations précédentes. Le liant fissuré apparaît en faible interaction avec le bloc de sable aggloméré où la formation de ponts

entre les grains de sable et l'enveloppe géopolymère est observée. La présence de pont entre les grains dû au nappage par le silicate est caractéristique du séchage à basse température (70 °C).

Des essais supplémentaires d'ensablage des corps de fusible en géopolymère permettraient d'optimiser les interactions entre le corps de fusible et le bloc de sable aggloméré.

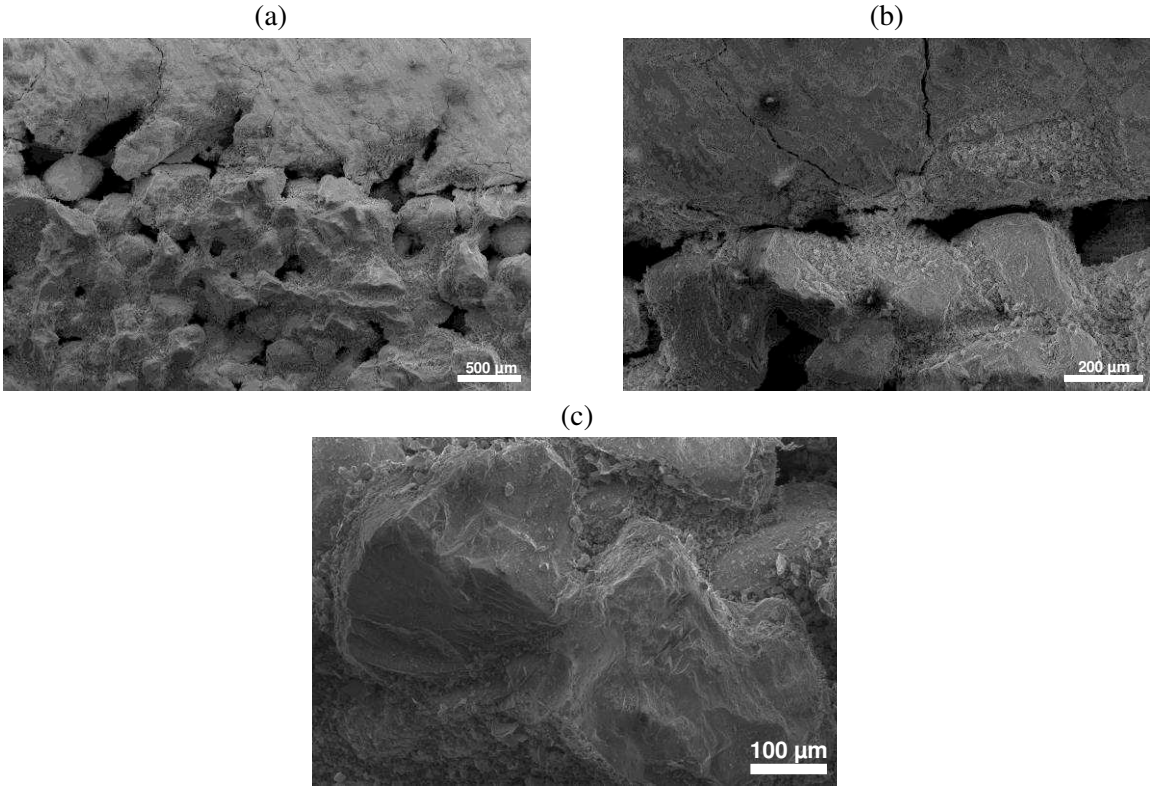

Figure 20 : images MEB **(a)** *d'un corps de fusible en géopolymère ensablé*, **(b)** zoom à *l'interface entre le bloc de sable aggloméré et le liant géopolymère* et **(c)** zoom sur un pont entre deux grains de sable.

Ainsi, les différents résultats ont mis en évidence la possibilité de créer une couche progressive entre un bloc de sable *aggloméré et un liant géopolymère ou d'ensabler un* corps de fusible en géopolymère obtenu par coulage.

B. TENUE EN TEMPÉRATURE DES PIÈCES CÉRAMIQUES

Le corps du fusible devant résister à des températures supérieures à 150 °C en conditions d'usage, les futures céramiques développées doivent donc tenir dans ces conditions [29]. Afin de pouvoir remplacer les enveloppes céramiques actuelles par des géopolymères, il est donc nécessaire de déterminer le comportement en température de ces liants aluminosilicates [30, 31]. Pour répondre à ce critère deux voies ont été explorées à savoir la modification de la

solution alcaline et la formulation avec différents renforts. Les nomenclatures utilisées sont répertoriées dans le **Chapitre II**.

1. Modification de la solution alcaline

Différents ajouts de molybdate d'ammonium, capable de complexer des espèces siliceuses et alumineuses [32, 33], ont été effectués (**ACL1**, **ACL6**, **ACLN1** et **ACLN2**).

Dans un premier temps, les mélanges réactionnels ont été suivis par analyse spectroscopique IRTF et par analyse thermique (**ACL6**). Les valeurs des pentes et des déplacements (**Figure 21**), déduits des suivis IRTF des différents liants ($(_LK^{0,7}{}_{xMo}\text{-}{}^{12}M1)^{25}$ et $(_LK^{0,7}{}_{xMo}\text{-}{}^{12}M2)^{25}$), sont situées respectivement dans la zone où plusieurs réseaux coexistent ou dans la zone des géopolymères selon les travaux précédents [34]. Les échantillons $(_LK^{0,7}{}_{xMo}\text{-}{}^{12}M1)^{25}$ sont localisés dans la zone de coexistence de différents réseaux. Cependant, l'ajout de molybdène dans les liants $(_LK^{0,7}{}_{1,57Mo}\text{-}{}^{12}M1)^{25}$ entraîne une diminution de la valeur du déplacement et de la pente traduisant une meilleure réorganisation des espèces, permettant ainsi de favoriser la dissolution de la source aluminosilicate. Par conséquent, la présence d'anions molybdiques de par leur répartition électrostatique va induire des modifications des espèces siliceuses favorisant ainsi la formation d'un réseau géopolymère. Pour les formulations à base de métakaolin M2, il y a peu de modifications.

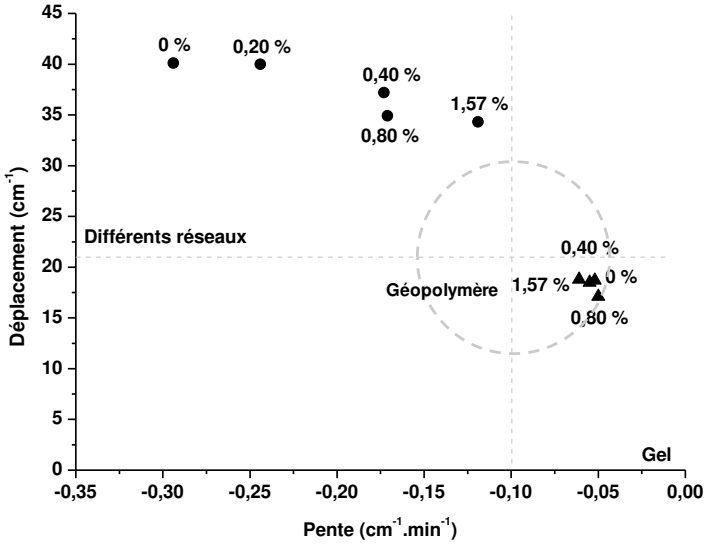

Figure 21 : variation du déplacement total en fonction de la valeur de la pente déterminés par spectroscopie IRTF pour les échantillons (●) $(_LK^{0,7}{}_{xMo}\text{-}{}^{12}M1)^{25}$ *et (▲)* $(_LK^{0,7}{}_{xMo}\text{-}{}^{12}M2)^{25}$.

Des analyses thermiques permettent de suivre les différentes étapes de formation des géopolymères [35,36]. Quatre zones ont ainsi pu être identifiées à partir des thermogrammes (cf. **Chapitre II**) en accord avec des travaux précédents. La zone I est attribuée à la réorganisation des différentes espèces (i.e. aux équilibres de spéciation), la zone II correspond à la dissolution du métakaolin, la zone III est associée à la formation des oligomères et la zone IV est due aux réactions de polycondensation (**Figure 22**). La quantité d'eau consommée, caractérisant l'énergie associée, lors de la première zone est similaire pour tous les mélanges (≈ 28 %). Concernant la zone II, l'énergie associée à la dissolution du métakaolin est la plus importante pour le mélange $({}_{L}K^{0,7}\text{-}{}^{12}M2)^{70}$ en accord avec sa réactivité puisqu'il y a libération rapide des espèces aluminosilicates [20]. L'ajout de molybdène $(({}_{L}K^{0,7}{}_{1,57Mo}\text{-}{}^{12}M2)^{70})$ entraînant une légère diminution de l'énergie suggère une réaction cinétiquement favorable. En présence du mélange $({}_{L}K^{0,7}\text{-}{}^{12}M1)^{70}$, le métakaolin M1 moins réactif est dépendant de la solution alcaline et l'énergie associée est moindre du fait d'une réaction plus difficile [20]. L'échantillon $({}_{L}K^{0,7}{}_{1,57Mo}\text{-}{}^{12}M1)^{70}$ d'énergie légèrement plus élevée souligne à nouveau que la modification de la solution alcaline entraîne une meilleure dissolution du métakaolin. Par ailleurs, lorsque la dissolution du métakaolin est favorisée, l'énergie de formation des oligomères (zone III) sera plus faible. Ceci est notable pour le mélange $({}_{L}K^{0,7}\text{-}{}^{12}M2)^{70}$. [20, 21]. La faible différence observée entre $({}_{L}K^{0,7}\text{-}{}^{12}M2)^{70}$ et $({}_{L}K^{0,7}{}_{1,57Mo}\text{-}{}^{12}M2)^{70}$ peut être attribuée au désordre des entités siliceuses demandant plus d'énergie. Des phénomènes similaires sont notables pour les compositions $({}_{L}K^{0,7}\text{-}{}^{12}M1)^{70}$ et $({}_{L}K^{0,7}{}_{1,57Mo}\text{-}{}^{12}M1)^{70}$ puisque les énergies associées sont toujours plus élevées. Finalement, pour la zone IV, l'énergie nécessaire aux réactions de polycondensation est minimale lorsque la formation des oligomères est facilitée. En présence de molybdate, il y a de nouveau une petite augmentation lorsque la formation des oligomères demande plus d'énergie. Les mêmes conclusions sont notables pour le métakaolin M1.

Les différents résultats ont mis en évidence l'existence de réactions de polycondensation différentes en fonction de la quantité de molybdène ajoutée et du type de métakaolin, pouvant entraîner la formation de réseaux différents au sein du matériau consolidé.

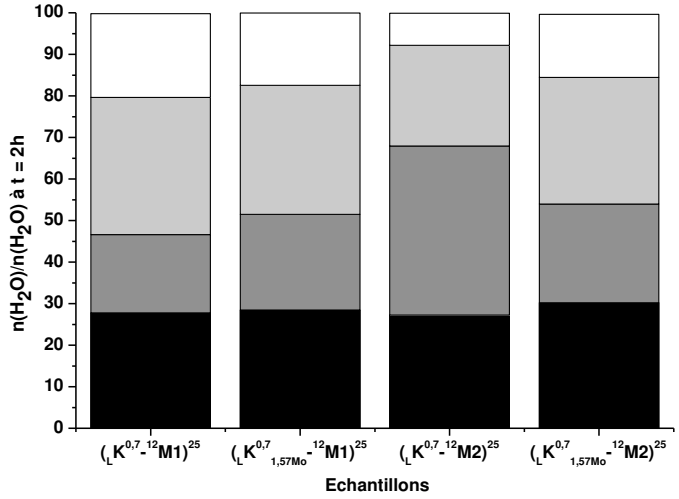

Figure 22: *nombres de moles d'eau consommées lors de la formation des échantillons* ($_LK^{0,7}$-$^{12}M1)^{70}$, ($_LK^{0,7}{}_{1,57Mo}$-$^{12}M1)^{70}$, ($_LK^{0,7}$-$^{12}M2)^{70}$ et ($_LK^{0,7}{}_{1,57Mo}$-$^{12}M2)^{70}$. La consolidation a été *réalisée à 70 °C pendant 2 heures. (*■ réorganisation des espèces (zone I), ■ dissolution du métakaolin (zone II), ■ formation des oligomères (zone III)*,* □ *polycondensation* (zone IV)).

Afin de valider le traitement en température, des analyses dilatométriques ont été réalisées sur les échantillons contenant différentes quantités de molybdate d'ammonium (cf. **Chapitre II**) (**ACL1**). La **Figure 23** présente la variation de la valeur de $\Delta L_{ech}/\Delta L_{ref}$ (où ΔL représente le retrait et ref, la référence, est l'échantillon sans ajout de molybdène) en fonction de la quantité de molybdène ajoutée au mélange.

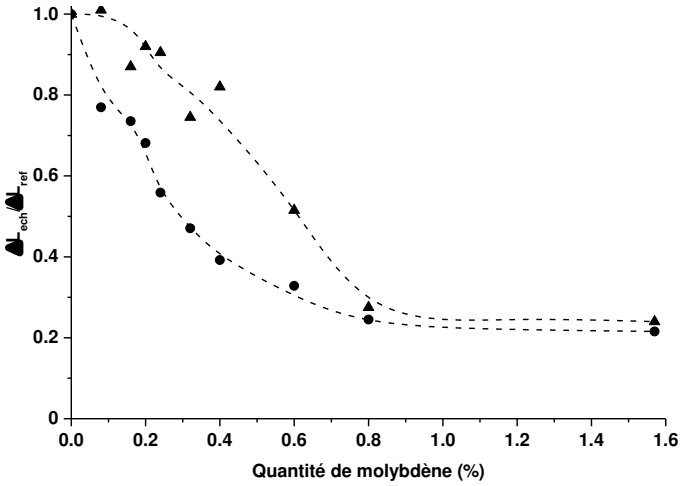

Figure 23 : *$\Delta L_{ech}/\Delta L_{ref}$ en fonction de la quantité de molybdène pour les échantillons (●)* ($_LK^{0,7}{}_{xMo}$-$^{12}M1)^{1400}$ *et (▲)* ($_LK^{0,7}{}_{xMo}$-$^{12}M2)^{1400}$ ((---) courbes de tendance).

Deux types de comportements sont observés en relation avec le métakaolin et l'ajout de molybdate. Pour une teneur en molybdène inférieure à 0,24 %, la valeur de retrait diminue

rapidement pour les mélanges $({}_{L}K^{0,7}{}_{xMo}\text{-}{}^{12}M1)^{1400}$ alors que la diminution est plus faible pour les compositions $({}_{L}K^{0,7}{}_{xMo}\text{-}{}^{12}M2)^{1400}$. Entre 0,24 et 0,80 % de teneur en molybdène, les mélanges $({}_{L}K^{0,7}{}_{xMo}\text{-}{}^{12}M1)^{1400}$ et $({}_{L}K^{0,7}{}_{xMo}\text{-}{}^{12}M2)^{1400}$ présentent des comportements similaires avec une décroissance quasi linéaire pouvant être attribuée à des mécanismes similaires. Ensuite, pour un ajout supérieur à 0,80 %, les deux géopolymères présentent les mêmes valeurs de retrait. Ces comportements peuvent être expliqués par deux paramètres, i.e. la solution alcaline ou la réactivité du métakaolin, pouvant induire deux comportements différents. Compte tenu des résultats précédents, pour l'échantillon $({}_{L}K^{0,7}\text{-}{}^{12}M1)^{25}$, les espèces siliceuses ou alumineuses sont libérées progressivement et de façon aléatoire entraînant l'apparition d'une compétition entre les deux réseaux désordonnés (réseaux riche en silicium et riche en aluminium). Les analyses Raman des différentes solutions ont révélé que l'ajout de faibles teneurs de molybdène (< 0,40 %) entraîne à la fois un phénomène de polycondensation des espèces et un phénomène de dépolymérisation, dû à la formation d'espèces oxo-molybdiques (**ACL 6**). Pour des teneurs de molybdène plus élevées, un phénomène de dépolymérisation associé à la formation d'anneaux et l'existence d'interactions entre les anneaux et les espèces molybdiques ont été identifiées telles que les entités MoO_4^{2-} [37]. Pour de faibles ajouts de molybdène, la solution est peu réactive et la réactivité du métakaolin va donc prédominer. Ce phénomène induit l'existence de comportements différents en fonction de la réactivité du métakaolin. En effet, le métakaolin M1, favorisant la formation de différents réseaux, entraîne des valeurs de retrait plus élevées dues à la présence de réseaux riches en silicium. En revanche, le métakaolin M2, favorisant la formation d'un réseau géopolymère riche en aluminium, présente des valeurs de retrait plus faibles. Ceci est en relation avec la présence de flux visqueux silicatés différents [38]. L'augmentation de la quantité de molybdène améliorant la réactivité de la solution, les réactions de polycondensation sont contrôlées par la solution et la réactivité du métakaolin va être inhibée. Ceci a pour conséquence la formation d'un seul réseau proche d'un réseau géopolymère pour les deux métakaolins. Ce phénomène permet donc d'expliquer les comportements similaires observés pour les deux métakaolins pour des teneurs de molybdène supérieures à 0,80 %.

***Il est donc possible d'avoir un matériau stable en température en fonctionnalisant une* solution alcaline peu réactive avec différents métakaolins.**

2. Modification de la composition : ajout de renforts

Afin d'améliorer les propriétés des liants au cours des traitements thermiques, l'influence de l'ajout de renforts a été étudiée.

Les compositions (cf. **Chapitre III – III.A.2**) ont été étudiées en température. Les photographies des échantillons relatives aux compositions utilisées pour la mise en forme, avant et après traitement thermique à 800 °C, sont reportées dans le **Tableau 2**. Trois comportements sont notables. Les échantillons à base de sodium présentent (i) soit une fissuration à la surface et un changement de couleur ($_{C1}Na^{1,7}{}_{Na}{}^{0,7}$-$^{16}M5_{40Zr}$), (ii) soit un début de fusion ($_{C1}Na^{1,7}{}_{Na}{}^{0,7}$-$^{16}M5_{40Zr}$). A l'inverse, l'échantillon $_{C1}K^{1,7}{}_{K}{}^{0,6}$-$^{22}M5_{55s}$ ne présente pas de modification avec seulement un changement de couleur. Les changements de couleur sont dus à la présence des oxydes de fer contenus dans le sablon ou le métakaolin.

Tableau 2 : photographies des échantillons avant et après traitement thermique à 800 °C (Ø = 35 mm).

	$_{L}Na^{0,7}$-$^{8}M1^{4}M2_{40s-1f}$	$_{C1}Na^{1,7}{}_{Na}{}^{0,7}$-$^{16}M5_{40Zr}$	$_{C1}K^{1,7}{}_{K}{}^{0,6}$-$^{22}M5_{55s}$
Avant traitement thermique			
Après traitement thermique			

Afin de comprendre les différents comportements, des analyses dilatométriques ont été réalisées jusqu'à 700 °C sur les différentes compositions (**Figure 24**). Trois types de retraits sont notés en fonction de la composition en accord avec les observations précédentes. A savoir un premier retrait qui est observé entre 100 et 200 °C et, au-delà de cette température, un phénomène spécifique pour chaque formulation.

Le retrait entre 100 et 200 °C est dû à l'évaporation de l'eau contenue au sein du matériau et sa valeur dépend de la composition (respectivement 1, 4 et 1 % pour les mélanges $_{C1}K^{1,7}{}_{K}{}^{0,6}$-$^{22}M5_{55s}$, $_{L}Na^{0,7}$-$^{8}M1^{4}M2_{40s-1f}$ et $_{C1}Na^{1,7}{}_{Na}{}^{0,7}$-$^{16}M5_{40Zr}$) [39, 40]. Ces valeurs de retrait sont en accord avec les pertes d'eau déterminées par ATD (respectivement égales à 21,6, 28,0 et

22,5 % pour les compositions $_{C1}K^{1,7}{}_{K}{}^{0,6}$-$^{22}M5_{55s}$, $_{L}Na^{0,7}$-$^{8}M1^{4}M2_{40s-1f}$ et $_{C1}Na^{1,7}{}_{Na}{}^{0,7}$-$^{16}M5_{40Zr}$). Ensuite, pour les compositions $_{C1}K^{1,7}{}_{K}{}^{0,6}$-$^{22}M5_{55s}$ et $_{L}Na^{0,7}$-$^{8}M1^{4}M2_{40s-1f}$, une légère diminution de la valeur de retrait est observée entre 200 et 500 °C due à des réorganisations structurales au sein du matériau [39]. Concernant la composition $_{C1}Na^{1,7}{}_{Na}{}^{0,7}$-$^{16}M5_{40Zr}$, l'expansion de l'ordre de 5,5 % observée dans le domaine de température (250 - 400 °C) est caractéristique de la formation de phases entre les différentes espèces en présence.

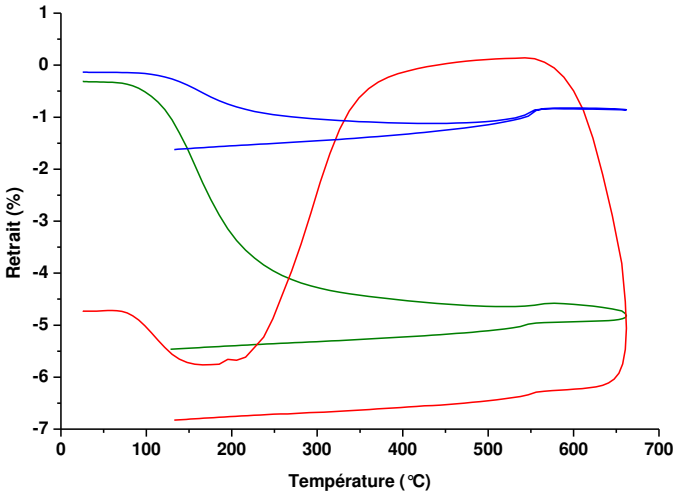

Figure 24 : *courbes dilatométriques jusqu'à 700 °C pour les échantillons (—)* $_{L}Na^{0,7}$-$^{8}M1^{4}M2_{40s-1f}$, (—) $_{C1}Na^{1,7}{}_{Na}{}^{0,7}$-$^{16}M5_{40Zr}$, (—) $_{C1}K^{1,7}{}_{K}{}^{0,6}$-$^{22}M5_{55s}$

En effet, il pourrait se former une phase à base de silicium responsable de cette expansion comme mentionné par Konon et al. [41]. La diminution importante de la valeur du retrait (≈ 6 %) traduit l'apparition d'un flux visqueux au sein du matériau. De plus, quelle que soit la formulation, la transformation de phase du quartz est observée vers 550 °C et peut être expliquée par la présence du sablon siliceux au sein du mélange [42].

La valeur du retrait total diffère en fonction de la composition, respectivement de -1,5, -5,5 et -7,0 % pour les liants $_{C1}K^{1,7}{}_{K}{}^{0,6}$-$^{22}M5_{55s}$, $_{L}Na^{0,7}$-$^{8}M1^{4}M2_{40s-1f}$ et $_{C1}Na^{1,7}{}_{Na}{}^{0,7}$-$^{16}M5_{40Zr}$, et peut être corrélée à la valeur du rapport molaire Si/(Al+M). En effet, pour un rapport Si/(Al+M) inférieur à 1, les compositions présentent une valeur de retrait élevée à haute température alors que si le rapport est supérieur à 1, une faible valeur de retrait est notable.

Par conséquent, la fissuration de la composition $_{L}Na^{0,7}$-$^{8}M1^{4}M2_{40s-1f}$ pourrait être expliquée par l'évaporation de l'eau entraînant un retrait élevé lors du traitement thermique. Dans le cas du liant $_{C1}Na^{1,7}{}_{Na}{}^{0,7}$-$^{16}M5_{40Zr}$, le début de fusion observé est dû à une quantité importante de cation alcalin au sein du mélange, ainsi qu'à la présence d'impuretés au sein du métakaolin

entraînant l'apparition d'un flux visqueux vers 600 °C. Finalement, la tenue en température de l'échantillon $_{C1}K^{1,7}{}_{K^{0,6}}{}^{-22}M5_{55s}$ pourrait être due à une teneur élevée en silicium et en aluminium.

Il est reporté sur la **Figure 25** le comportement en température en fonction des nombres de moles en aluminium, silicium et cation alcalin pour les différentes compositions étudiées. Trois zones, associées à des comportements différents, ont pu être isolées en fonction des différentes concentrations. Pour des pourcentages molaires Al > 0,50, Si < 0,50 et M < 0,75, l'apparition de fissures est observée à la surface des échantillons. Les échantillons fondent lors d'un traitement thermique pour des teneurs respectives en Al < 0,25, Si < 0,75 et M > 0,75. Enfin, dans la dernière zone (Al < 0,50, Si > 0,75 et M < 0,25 mol), les échantillons présentent une tenue en température correcte. Il a donc été possible de déterminer une cartographie de la tenue en température des liants géopolymères en fonction des nombres de moles en aluminium, silicium et cation alcalin.

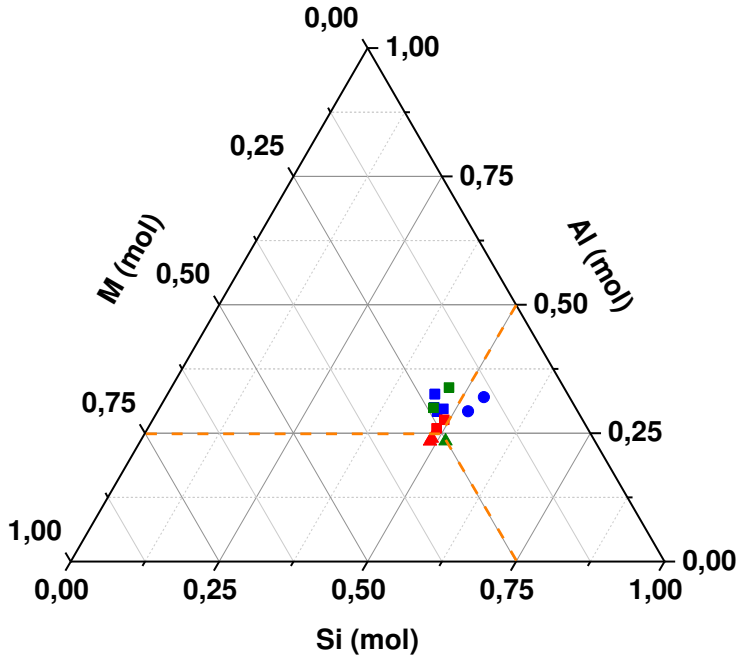

Figure 25 : tenue en température en fonction des nombres de moles en aluminium, silicium et cation alcalin (—) sodium, (—) potassium et (—) mixte pour les échantillons présentant (■) une fissuration, (▲) un début de fusion et (●) une tenue en température correcte.

Le domaine de tenue en température des pièces mises en forme en liant géopolymère est fonction de la formulation et du rapport Si/(Al+M) > 1.

IV. AVANCÉE TECHNOLOGIQUE

Dans le cas d'une rupture technologique telle que la réalisation d'un busbar (cf. **Chapitre I**), cette partie est consacrée à l'étude de l'interface entre différents supports métalliques et différentes formulations de liant.

1. Essais préliminaires

Afin de pouvoir déposer le liant sur les métaux, des essais préliminaires de projection à l'aide d'un pistolet ont été réalisés avec deux compositions présentant de faibles viscosités (cf. **Chapitre II**). L'aspect des dépôts des différentes formulations (**Figure 26**) est fonction de la nature des supports métalliques.

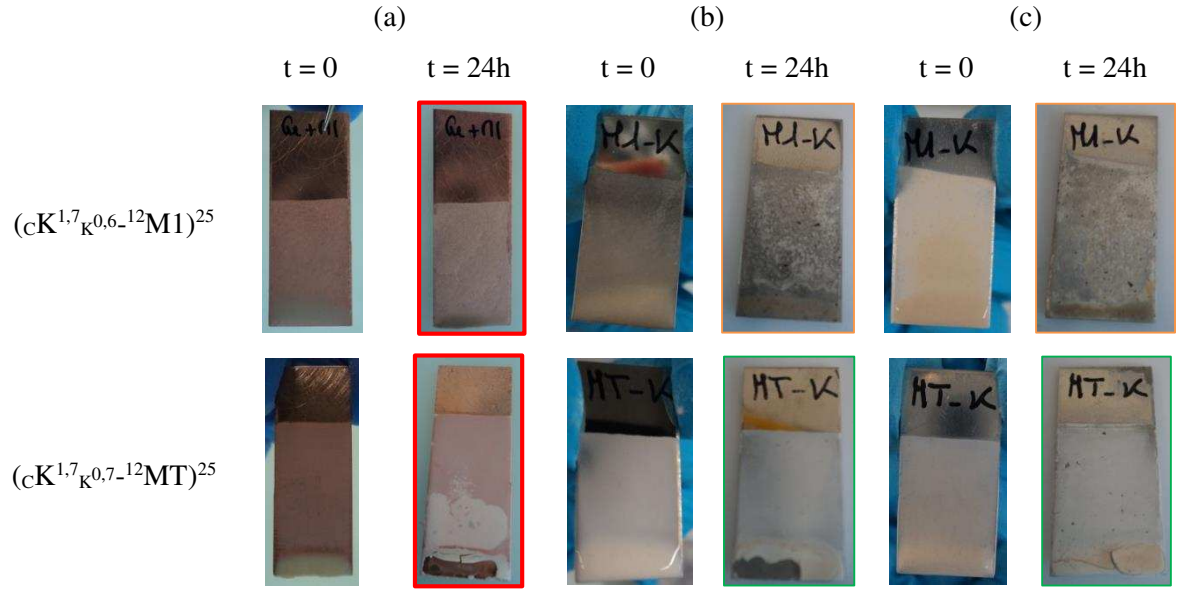

Figure 26 : *photographies des essais d'adhésion des différentes formulations de liant* géopolymère sur une plaque de cuivre **(a)** pur, **(b)** nickelé et **(c)** étamé.

Dans le cas du cuivre (**Figure 26a**), quelle que soit la composition du liant, le dépôt se décolle après 24 heures de séchage pour les échantillons Cu-($_{C1}K^{1,7}{}_{K}{}^{0,6}\text{-}{}^{12}M1$) et Cu-($_{C1}K^{1,7}{}_{K}{}^{0,7}\text{-}{}^{12}MT$). Le cuivre métallique en présence d'une solution basique entraîne l'oxydation du cuivre et / ou la formation d'hydroxyde de cuivre (CuO) / $Cu(OH)_4^{2-}$ ne favorisant pas l'adhésion [43]. La limite de la formation de cette phase étant pour une valeur de pH de l'ordre de 12,5, il sera donc difficile de déterminer l'espèce responsable. Quoiqu'il advienne, le dépôt de liant géopolymère ne pourra pas adhérer au support.

L'ajout de nickel au cuivre modifie la réactivité et donc l'aspect des dépôts. En effet, l'échantillon CuNi-($_{C1}K^{1,7}{}_{K}{}^{0,6}\text{-}{}^{12}M1$) présente un dépôt hétérogène (**Figure 26b**). Le

changement de métakaolin de réactivité supérieure ($_{C1}K^{1,7}{}_{K}{}^{0,7}$-^{12}MT) permet l'obtention d'un dépôt sans fissures et homogène. Ce phénomène est à corréler aux valeurs de pH des liants. En effet, une étude a démontré que la valeur de pH du mélange $_{C1}K^{1,7}{}_{K}{}^{0,6}$-^{12}M1 varie de 12,8 à 11,5 alors que pour la composition $_{C1}K^{1,7}{}_{K}{}^{0,6}$-^{12}MT, la valeur de pH évolue de 12,2 à 11,0 [21]. Ainsi, la composition $_{C1}K^{1,7}{}_{K}{}^{0,6}$-^{12}M1, de pH = 12,8, entraîne la formation d'espèces $HNiO_2^-$ [44]. Cette dernière espèce s'insérant dans le mélange perturbe les réactions de polycondensation, responsable de l'hétérogénéité du dépôt. A l'inverse, le mélange $_{C1}K^{1,7}{}_{K}{}^{0,7}$-^{12}MT de valeur de pH (12,2) favorise la formation de $Ni(OH)_2$ passivant le métal et facilitant ainsi l'ancrage du liant.

Le même comportement est observé sur la plaque de cuivre étamé (**Figure 26c**). Dans ce cas, des espèces SnO_3^{2-} sont formées au contact du liant $_{C1}K^{1,7}{}_{K}{}^{0,6}$-^{12}M1 induisant la formation d'un dépôt hétérogène. Au contraire, le liant $_{C1}K^{1,7}{}_{K}{}^{0,7}$-^{12}MT entraîne la formation d'espèces $Sn(OH)_2$ favorisant la formation d'un dépôt homogène.

Les meilleurs résultats semblent être obtenus avec les plaques de cuivre étamé et de cuivre nickelé ainsi qu'avec le liant $_{C1}K^{1,7}{}_{K}{}^{0,7}$-^{12}MT.

Le contrôle de l'adhésion entre le métal et le liant a été réalisé par des observations au microscope électronique à balayage (**Figure 27**). L'échantillon Cu-($_{C1}K^{1,7}{}_{K}{}^{0,6}$-^{12}MT) n'a pas pu être observé car le dépôt était totalement décollé de la plaque métallique. Quel que soit le support métallique, il est toujours noté un interstice entre le support et la couche de liant soulignant l'absence de réaction chimique. Plus précisément, l'échantillon Cu-($_{C1}K^{1,7}{}_{K}{}^{0,6}$-^{12}M1) présentant une fissure et le décollement qui en découle devra être corrélé à la tension interfaciale. Comme précédemment, la formation d'espèces $HNiO_2^-$ et SnO_3^{2-} à l'interface entre le liant et le métal, respectivement nickelé et étamé, favorise un dépôt plus hétérogène de faible fissuration. De même, les échantillons CuNi-($_{C1}K^{1,7}{}_{K}{}^{0,7}$-^{12}MT) et CuSn-($_{C1}K^{1,7}{}_{K}{}^{0,7}$-^{12}MT) présentant de meilleures adhésions sont à corréler à la formation d'une phase $Ni(OH)_2$ ou $Sn(OH)_2$ à l'interface entre les deux matériaux favorisant ainsi l'ancrage du dépôt.

***Les différences d'adhésion entre le liant géo*polymère et le métal sont essentiellement maîtrisables par la formulation.**

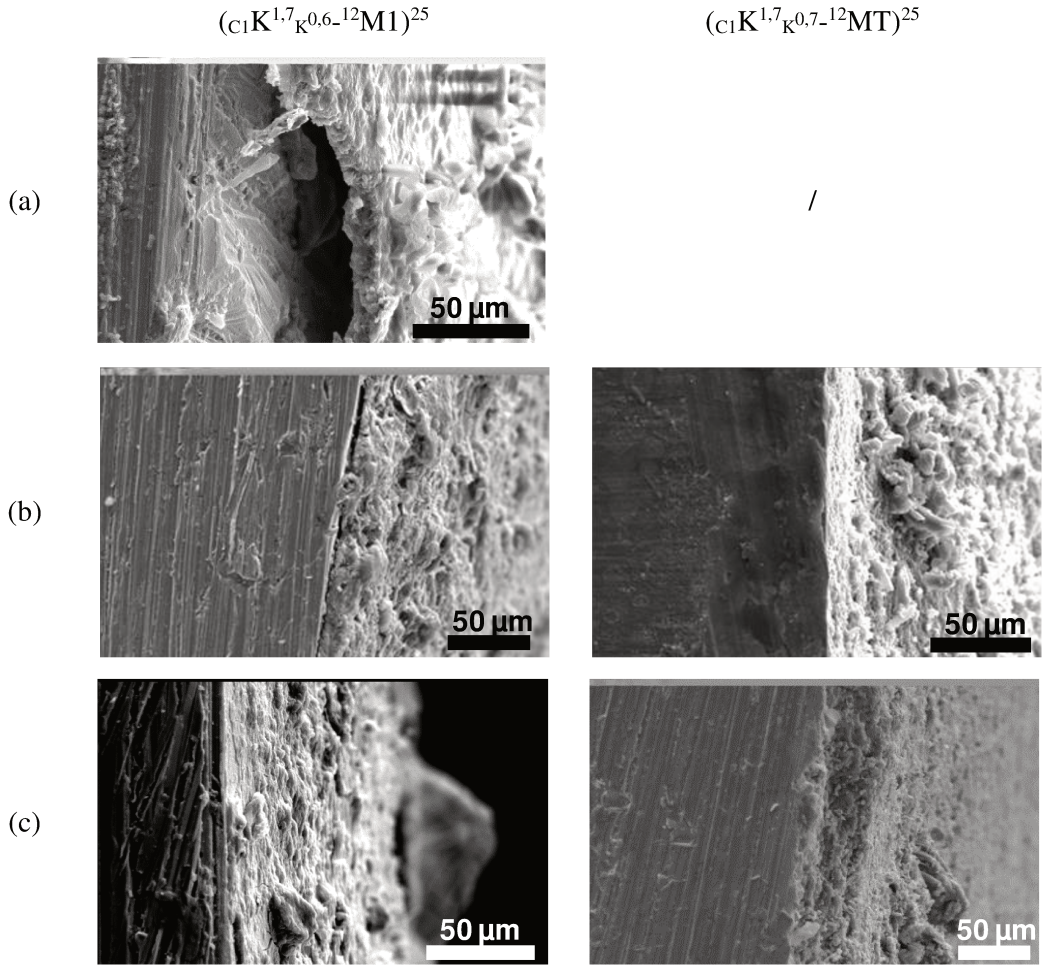

Figure 27 : images MEB des dépôts de $(_{C1}K^{1,7}{}_{K}{}^{0,6}\text{-}{}^{12}M1)^{25}$ et $(_{C1}K^{1,7}{}_{K}{}^{0,7}\text{-}{}^{12}MT)^{25}$sur les plaques de cuivre **(a)** pur, **(b)** nickelé et **(c)** étamé.

2. Contrôle de l'interface

Afin d'évaluer les interactions entre les liants et les différents supports métalliques, il a été étudié le comportement des différents liants en fonction des trois grandes familles des matériaux : à savoir polymère (polyéthylène), céramique (plaque de verre) et métallique (plaque de cuivre). Il a été également étudié deux supports métalliques étamé et nickelé (**ACL7**).

La **Figure 28** regroupe les valeurs des angles de mouillage, pour les deux familles de liants retenues, en fonction des trois supports. Pour rappel, plus la valeur de l'angle est élevée, plus les interactions au sein du liant sont fortes. De plus, celles-ci sont dépendantes du type de métakaolin et du cation alcalin.

Les valeurs d'angle de mouillage sont toujours plus élevées, quel que soit le support, pour les compositions à base de sodium induisant plus de réactivité (cf. **Chapitre III - III.A.1**). Dans le cas de la plaque de verre usuelle (**Figure 28a**), les différences observées sont propres à la

nature du cation alcalin. En effet, les valeurs d'angle de mouillage des compositions $(_{L}K^{0,7}\text{-}^{12}M1)^{25}$ et $(_{L}Na^{0,7}\text{-}^{12}M1)^{25}$ sont respectivement égales à 25,5 et 43,2°. En présence du cation K^+, le phénomène observé peut être assimilé aux échanges chimiques utilisés lors de la trempe chimique des verres [45]. Il existe un échange du cation Na^+ en surface vers le liant et inversement, transfert du cation K^+ vers la surface du verre, ceci ayant pour effet de diminuer la valeur de l'angle de mouillage.

Les autres différences sont dues aux métakaolins. En effet, les mélanges $(_{L}K^{0,7}\text{-}^{12}M1)^{25}$, $(_{L}K^{0,7}\text{-}^{6}M1^{6}MT)^{25}$ et $(_{L}K^{0,7}\text{-}^{12}MT)^{25}$ ont respectivement des valeurs d'angle de mouillage de 25,5°, 33,4° et 52,6°. Plus particulièrement, la valeur de l'angle plus élevée pour la formulation $(_{L}K^{0,7}\text{-}^{12}MT)^{25}$ s'explique par un début de géopolymérisation au sein du liant. La valeur de pH plus élevée de l'échantillon $(_{L}K^{0,7}\text{-}^{12}M1)^{25}$ (12,8), par comparaison à l'échantillon $(_{L}K^{0,7}\text{-}^{12}MT)^{25}$ (12,2), favorise l'échange des cations Na-K en surface, induisant une diminution de l'angle. La combinaison des deux métakaolins induit une plus faible valeur de pH toujours caractéristique du degré d'avancement des réactions de géopolymérisation. L'angle de mouillage obtenu est donc compris entre les valeurs obtenues pour les mélanges $(_{L}K^{0,7}\text{-}^{12}M1)^{25}$ et $(_{L}K^{0,7}\text{-}^{12}MT)^{25}$. Pour les échantillons à base de sodium, les valeurs de pH plus faibles (respectivement 11,8, 11,5 et 11,8 pour les compositions $(_{L}Na^{0,7}\text{-}^{12}M1)^{25}$, $(_{L}Na^{0,7}\text{-}^{6}M1^{6}MT)^{25}$ et $(_{L}Na^{0,7}\text{-}^{12}MT)^{25}$) sont dues à une réactivité plus importante entraînant une augmentation de la valeur de l'angle de mouillage.

En présence du polyéthylène (**Figure 28b**), seul l'effet du cation est observé alors que l'effet du métakaolin est inhibé par la surface hydrophobe du polyéthylène. En effet, la valeur de l'angle est similaire quelle que soit la composition (environ 99° et 118° pour les compositions $(_{L}K^{0,7}\text{-}^{12}My)^{25}$ et $(_{L}Na^{0,7}\text{-}^{12}My)^{25}$).

En présence du cuivre (**Figure 28c**), l'effet du cation sodium est à nouveau notable (respectivement 49,0° et 77,7°) pour les compositions $(_{L}K^{0,7}\text{-}^{12}M1)^{25}$ et $(_{L}Na^{0,7}\text{-}^{12}M1)^{25}$. De la même façon, les valeurs d'angle vont être caractéristiques des échanges d'espèces entre le cuivre et le liant (cf. **Chapitre III – IV.1**). La principale différence est notable pour les compositions $(_{L}K^{0,7}\text{-}^{6}M1^{6}MT)^{25}$ (respectivement 49,0°, 49,1° et 98,9° pour les mélanges $(_{L}K^{0,7}\text{-}^{12}M1)^{25}$, $(_{L}K^{0,7}\text{-}^{12}MT)^{25}$ et $(_{L}K^{0,7}\text{-}^{6}M1^{6}MT)^{25}$). En effet, pour ces mélanges, il existe la formation de $Cu(OH)_4^{2-}$, ou de CuO en compétition avec le degré d'avancement des réactions de géopolymérisation. Pour les liants $(_{L}K^{0,7}\text{-}^{12}M1)^{25}$ ou $(_{L}K^{0,7}\text{-}^{12}MT)^{25}$, ce sont essentiellement les phénomènes d'altération du support qui interviennent, alors qu'en présence des métakaolins M1 et MT, c'est la réaction de géopolymérisation qui gouverne, imposant une valeur élevée de l'angle.

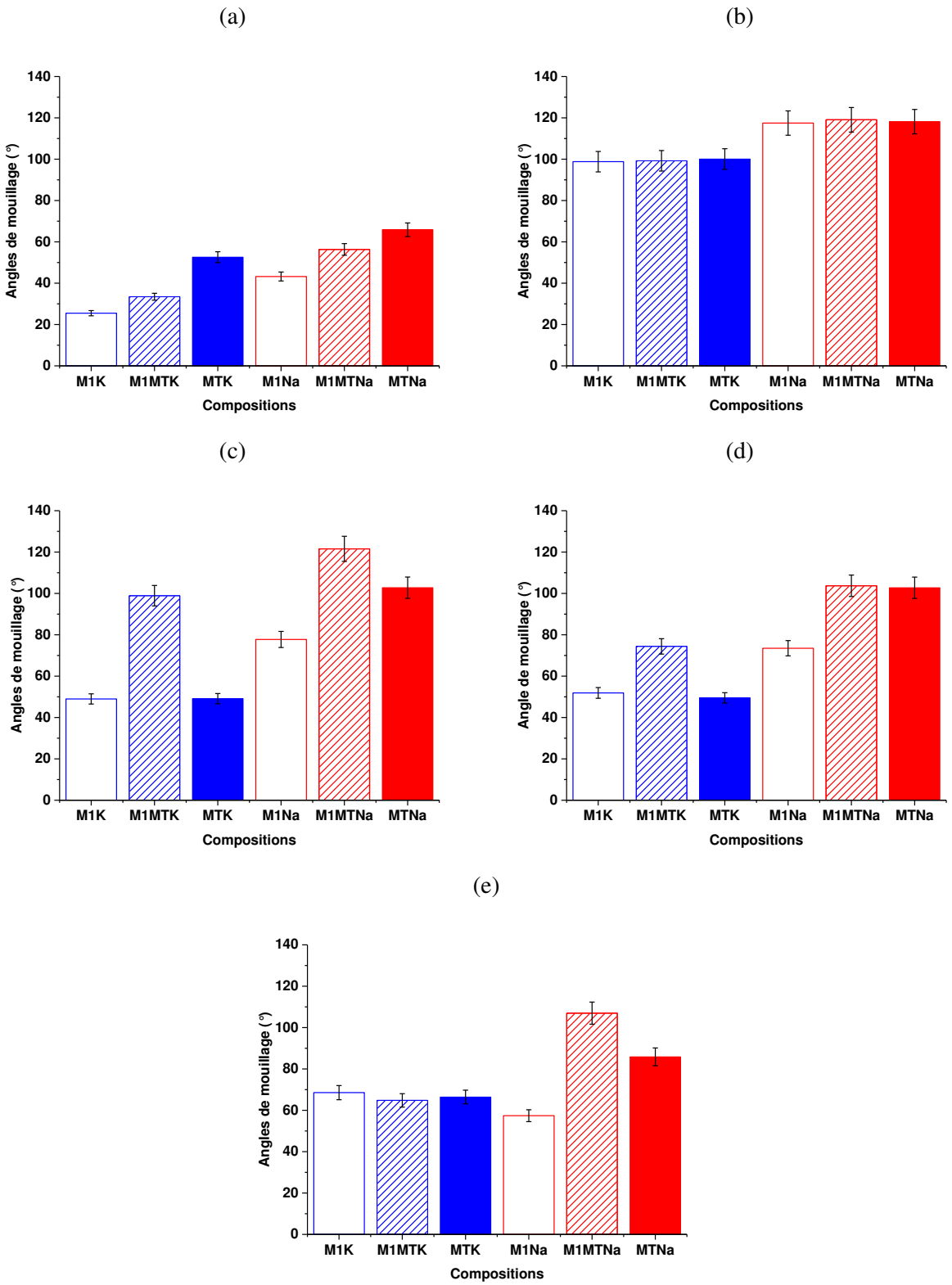

Figure 28 : *variation de la valeur de l'angle de mouillage sur* **(a)** du verre, **(b)** du polyéthylène, **(c)** du cuivre, **(d)** du cuivre étamé et **(e)** du cuivre nickelé pour les compositions (□) $({}_{L}K^{0,7}\text{-}{}^{12}M1)^{25}$, (▨) $({}_{L}K^{0,7}\text{-}{}^{6}M1{}^{6}MT)^{25}$, (■) $({}_{L}K^{0,7}\text{-}{}^{12}MT)^{25}$, (□) $({}_{L}Na^{0,7}\text{-}{}^{12}M1)^{25}$, (▨) $({}_{L}Na^{0,7}\text{-}{}^{6}M1{}^{6}MT)^{25}$ et (■) $({}_{L}K^{0,7}\text{-}{}^{12}MT)^{25}$.

En présence du cation sodium, les mêmes phénomènes sont observés. Néanmoins, la différence observée pour ($_{L}Na^{0,7}$-$^{6}M1^{6}MT$)^{25} est due au caractère cinétique plus élevé de la réaction de géopolymérisation (cf. **Annexe III-5-A**).

Le dernier point à aborder concerne la modification de la surface métallique. Des essais d'angles de mouillage ont donc été réalisés sur des plaques de cuivre étamé et de cuivre nickelé. L'effet du cation alcalin est notable quel que soit le support métallique. En présence de cuivre étamé (**Figure 28d**), le comportement des différents liants est similaire à celui observé sur le cuivre. En effet, il est observé une valeur d'angle plus élevée pour les compositions contenant un mélange de métakaolins M1 et MT (respectivement 51,9°, 49,5° et 74,4° pour les compositions ($_{L}K^{0,7}$-$^{12}M1$)^{25}, ($_{L}K^{0,7}$-^{12}MT)^{25} et ($_{L}K^{0,7}$-$^{6}M1^{6}MT$)^{25}). Comme pour le cuivre, les valeurs plus élevées indiquent que la réaction de géopolymérisation contrôle la valeur de l'angle.

Dans le cas du cuivre nickelé (**Figure 28e**), le métakaolin ne semble pas avoir d'influence sur la valeur de l'angle en présence d'une solution à base de potassium (respectivement 68,5°, 64,8° et 66,4° pour les formulations ($_{L}K^{0,7}$-$^{12}M1$)^{25}, ($_{L}K^{0,7}$-$^{6}M1^{6}MT$)^{25} et ($_{L}K^{0,7}$-^{12}MT)^{25}). Les différences observées pourraient être dues aux zones d'existence des différentes espèces au sein des diagrammes de Pourbaix. En revanche, en présence de sodium, la valeur de l'angle de mouillage semble dépendre de la réactivité du métakaolin. A nouveau, le mélange ($_{L}Na^{0,7}$-$^{6}M1^{6}MT$)^{25} présente la valeur d'angle la plus élevée (respectivement 57,4°, 107,0° et 85,9° pour les compositions ($_{L}Na^{0,7}$-$^{12}M1$)^{25}, ($_{L}Na^{0,7}$-$^{6}M1^{6}MT$)^{25} et ($_{L}Na^{0,7}$-^{12}MT)^{25}). L'adhésion du liant sur la surface est conditionnée par la valeur de pH du liant et les zones d'existence des différentes espèces réactives métalliques, qui conditionnent également la valeur finale de l'angle de mouillage.

Ainsi, les différentes interactions sont contrôlables à la fois par le cation alcalin et le métakaolin qui jouent un rôle sur la réaction de géopolymérisation, mais aussi par la valeur de pH qui a une influence sur la libération des espèces par le support.

Les plaques de cuivre étamé étant les plaques les plus souvent utilisées pour les applications électriques [29], les essais d'enrobage seront réalisés sur celles-ci. De plus, les compositions retenues pour la suite de l'étude sont les formulations ($_{L}K^{0,7}$-$^{6}M1^{6}MT$)^{25} et ($_{L}Na^{0,7}$-$^{6}M1^{6}MT$)^{25} compte tenu de la valeur de l'angle de mouillage la plus élevée. Les éprouvettes constituées de la plaque de cuivre étamé enrobée à l'aide des liants (($_{L}K^{0,7}$-$^{6}M1^{6}MT$)^{25} et ($_{L}Na^{0,7}$-$^{6}M1^{6}MT$)^{25}) sont stockées pendant 7 jours selon trois conditions, à

savoir en moule ouvert, en moule fermé et à une humidité de 85 %. La **Figure 29** présente les photographies des différents échantillons enrobés de liants géopolymères. Les échantillons présentent des aspects différents en fonction des conditions de stockage.

Quel que soit le cation alcalin, le séchage en moule ouvert entraîne une fissuration importante de l'échantillon au niveau des bords de la plaque métallique et le liant n'adhère pas au métal. Ceci pourrait être dû aux tensions interfaciales très fortes existant à la surface de l'échantillon, causées par la présence de la plaque et de l'humidité relative ambiante, induisant donc des contraintes [46]. En effet, la pression capillaire de la partie supérieure de l'échantillon est en traction pour évacuer l'eau porale sachant que la force exercée par l'humidité relative ambiante est plus élevée.

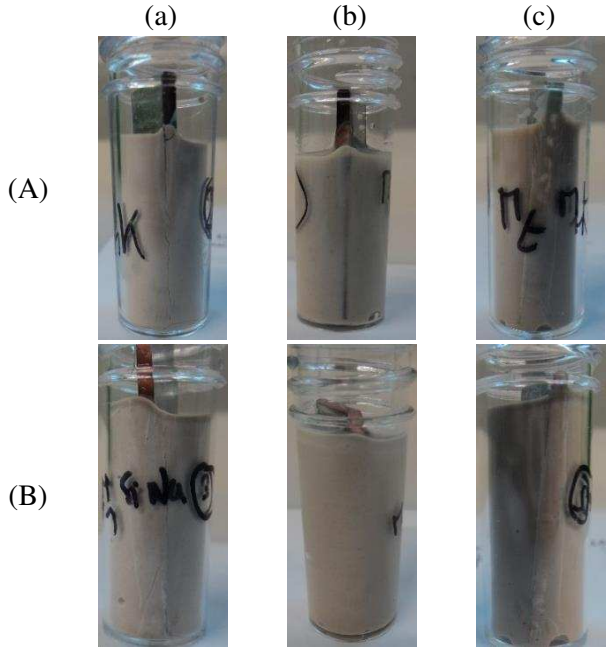

Figure 29 : photographies des plaques de cuivre étamé enrobées *d'un liant géopolym*ère **(A)** $({}_{L}K^{0,7}\text{-}{}^{6}M1^{6}MT)^{25}$ et **(B)** $({}_{L}K^{0,7}\text{-}{}^{6}M1^{6}MT)^{25}$ conservées pendant 7 jours **(a)** en moule ouvert, **(b)** en moule fermé et **(c)** *à 85 % d'humidité (Ø = 15 mm).*

Dans le cas du séchage en moule fermé, aucune fissure n'est visible indiquant une adhésion correcte du liant sur la plaque métallique en accord avec un séchage plus homogène du matériau. En effet, la fermeture du moule permet de contrôler les échanges hydriques à la surface, les pressions de vapeur saturante s'équilibrent limitant ainsi l'évaporation de l'eau du matériau [46].

Finalement, l'apparition de fissures seulement d'un côté de la plaque métallique pour les échantillons conservés à 85 % d'humidité révèle que l'adhésion entre le liant et le métal n'est peut-être pas totale. Dans ce cas, les échanges de pression de vapeur saturante favorisent le séchage de façon homogène [46].

L'apparition de fissures a également été notée lorsque l'épaisseur de liant recouvrant le métal est faible, et ce pour les atmosphères humides et le moule ouvert. Ce phénomène pourrait être dû à l'existence de contraintes à l'interface entre le métal et le liant, et à la résistance moins élevée d'une faible épaisseur de liant dans cette zone. Un gradient de contraintes assez prononcé et réparti sur une faible épaisseur favorise le décollement. Dans le cas des échantillons séchés en moule fermé, l'absence de fissures pourrait être expliquée par une épaisseur et donc une résistance plus importante du liant, étayant à nouveau l'importance des équilibres de pression de vapeur saturante.

***Le séchage en atmosphère contrôlée permet d'obtenir une adhésion entre le liant et le* support métallique adéquate.**

Les découpes des échantillons ont été analysées au microscope optique (avec un objectif x20) et par profilométrie (**Annexe III-5-B**). Il n'a pas été possible d'analyser par microscopie électronique à balayage les échantillons compte tenu de la difficulté d'obtenir un vide suffisant. Des différences d'adhésion sont observées en fonction de la composition du liant et de l'atmosphère de stockage (**Figure 30**). Quelle que soit la formulation, une faible adhésion est notée entre le liant géopolymère et la surface métallique lorsque les échantillons sont conservés en moule ouvert (**Figure 30 Aa, Ba**) comme évoqué précédemment. L'adhésion semble être favorisée par un stockage en moule fermé, bien que quelques zones de fractures soient notables à l'interface (**Figure 30 Ab, Bb**). Celles-ci pourraient être dues à un arrachement du liant lors de la découpe du composite. Finalement, de légères différences d'adhésion sont observées pour les matériaux conservés à 85 % d'humidité (**Figure 30 Ac, Bc**) avec toujours l'apparition de défauts d'adhésion pour le liant $({}_{L}K^{0,7}\text{-}{}^{6}M1^{6}MT)^{25}$, attribuables à la préparation de l'échantillon lors de la découpe. Le liant $({}_{L}Na^{0,7}\text{-}{}^{6}M1^{6}MT)^{25}$ semble adhérer à la plaque métallique sans défauts à l'interface. Ces données ont été corroborées par profilométrie (**Annexe III-5-B**).

***Il est donc possible de favoriser l'adhésion d'un liant à base sodium et de deux* métakaolins sur une plaque étamé en atmosphère humide.**

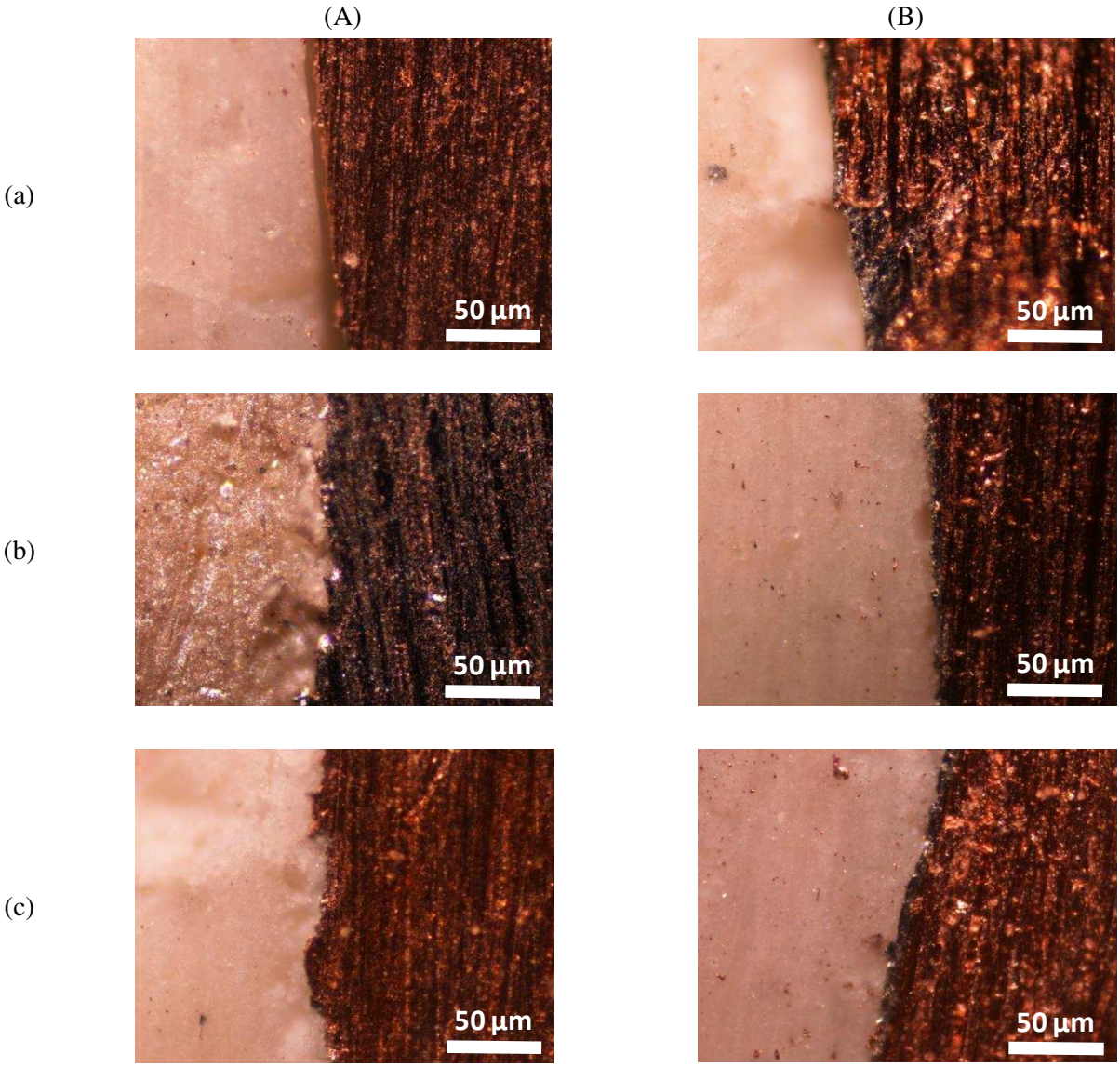

Figure 30 : *observation au microscope optique de l'interface entre un support en cuivre et un* liant géopolymère **(A)** $(_{L}K^{0,7}\text{-}^{6}M1^{6}MT)^{25}$ et **(B)** $(_{L}Na^{0,7}\text{-}^{6}M1^{6}MT)^{25}$ conservés pendant 7 jours **(a)** en moule ouvert, **(b)** en moule fermé et **(c)** *à 85 % d'humidité.*

3. Réalisation du busbar

Afin de réaliser un busbar à l'aide d'un liant géopolymère, la composition retenue est la formulation $(_{L}Na^{0,7}\text{-}^{6}M1^{6}MT)^{25}$. La pièce obtenue par coulage a été partiellement démoulée après 48 heures et maintenue à 30 °C et 85 %HR pendant 72h avant le démoulage total.

La photographie de la pièce obtenue est présentée sur la **Figure 31**. Les résultats montrent qu'il est possible de réaliser un busbar enrobé de liant géopolymère. Une étude approfondie des interactions entre les métaux et les liants géopolymères devrait permettre d'optimiser les paramètres d'obtention de la pièce et, plus particulièrement, le temps nécessaire au démoulage.

(a) (b)

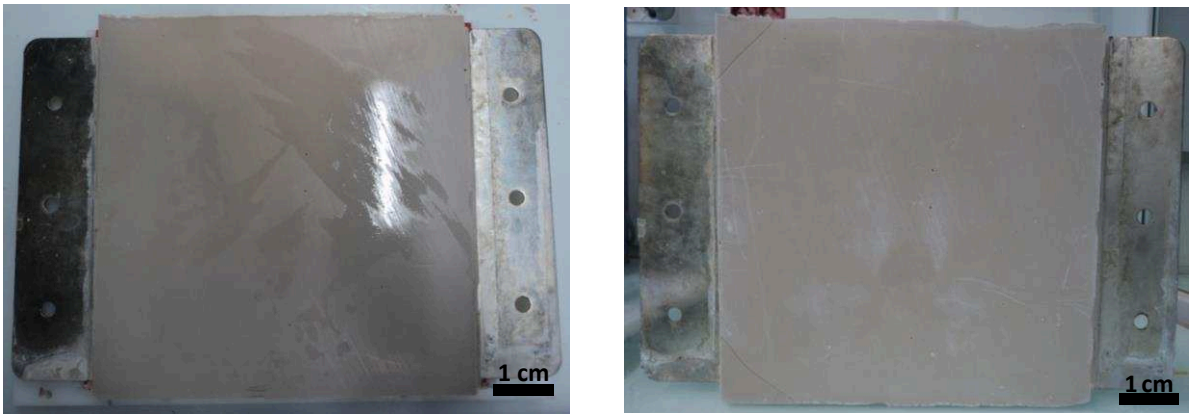

Figure 31 : photographies du busbar obtenu par coulage de la formulation ($_{L}Na^{0,7}$-$^{6}M1^{6}MT$)^{25} et conservation en atmosphère humide à t = **(a)** 2 jours et **(b)** 1 semaine après coulage.

V. CONCLUSION

Cette étude a été réalisée depuis la caractérisation des matières premières jusqu'à l'obtention du produit fini en contrôlant les différentes étapes de la fabrication.

La caractérisation des solutions de silicate par différentes méthodes spectroscopiques a permis d'identifier les espèces réactives et notamment la réalisation d'une cartographie en fonction du taux d'eau et du cation alcalin. L'agglomération du sable est maîtrisée par la dilution de la solution de silicate et l'utilisation d'un séchage conventionnel à 150 °C.

La réalisation d'une couche de transition peut être réalisée par des liants géopolymères à partir des critères suivants, à savoir une solution de silicate de rapport Si/M compris entre 0,5 et 0,8 et un métakaolin permettant d'obtenir des rapports molaires Si/Al < 2 et M/Al < 1,2.

L'enrobage d'un bloc de sable aggloméré ou d'un métal par un liant géopolymère peut être maîtrisé en modifiant la formulation du liant et plus particulièrement le cation alcalin ou le métakaolin.

Finalement, il a été démontré que l'obtention de composants électriques avec des liants géopolymères est possible.

VI. BIBLIOGRAPHIE

[1] M.T. Tognonvi, J. Soro, S. Rossignol. Physical-chemistry of silica/alkaline silicate interactions during consolidation. Part 1: Effect of cation size. Journal of Non-Crystalline Solids, 2012, vol. 358, p. 81-87.

[2] M. Muroya. Correlation between the formation of silica skeleton and Fourier transform reflection infrared absorption spectroscopy spectra. Colloids and Surfaces A, 1999, vol. 157, p. 147-155.
[3] A. Gharzouni, E. Joussein, B. Samet, S. Baklouti, S. Pronier, I. Sobrados, J. Sanz, S. Rossignol. The effect of an activation solution with siliceous species on the chemical reactivity and mechanical properties of geopolymers. Journal of Sol-Gel Science and Technology, 2014, vol. 73, p. 250-259.
[4] I.L.Svensson, S. Sjöberg, L.-O. Öhman. Polysilicate equilibria in concentrated sodium silicate solutions. Journal of the Chemical Society, Faraday Transactions, 1986, vol. 82, p. 3635-3646.
[5] J.L. Bass, G.L. Turner, M.D. Morris. Vibrational and ^{29}Si NMR spectroscopies of soluble silicate oligomers. Macromolecular Symposia, 1999, vol. 140, p. 263-270.
[6] J. Nordström, E. Nilsson, P. Jarvol, M. Nayeri, A. Palmqvist, J. Bergenholtz, A. Matic. Concentration- and pH-dependence of highly alkaline sodium silicate solutions. Journal of Colloid and Interface Science, 2011, vol. 356, p. 37-45.
[7] J. Mähler, I. Persson. A study of the hydration of the alkali metal ions in aqueous solutions. Inorganic Chemistry, 2012, vol. 51, p. 425-438.
[8] T. Melkior, S. Yahiaoui, D. Thoby, S. Motellier, V. Barthès. Diffusion coefficients of alkaline cations in Bure mudrock. Physics and Chemistry of the Earth, 2007, vol. 32, p. 453-462.
[9] X. Yang, W. Zhu, Q. Yang. The viscosity properties of sodium silicate solutions. Journal of Solution Chemistry, 2008, vol. 37, p. 73-83.
[10] R.K. Iler. The chemistry of silica. John Wiley and Sons, New York, 1979.
[11] M.D. Allendorf, K.E. Spear. Thermodynamic analysis of silica refractory corrosion in glass-melting furnaces. Journal of the Electrochemical Society, 2001, vol. 148 (2), p. B59-B67.
[12] Y.A. Owusu. Application of thermal energy in curing sodium silicate bonded sand. Proceedings of Condensed Papers - 16th Southeastern Seminar on Thermal Sciences, 1982, p. 1071-1084.
[13] L.T. Zhuravlev. The surface chemistry of amorphous silica. Zhuravlev model. Colloids and Surfaces A, 2000, vol. 173, p. 1-38.
[14] K. Granat, D. Nowak, M. Pigiel, M. Stachowicz, R. Wikiera. Microwaves energy in curing process of water glass molding sands. Archives of Foundry Engineering, 2007, vol. 7 (1), p. 183-188.
[15] M. Stachowicz, K. Granat, D. Nowak. Dielectric hardening method of sandmixes containing hydrated sodium silicate. Metalurgija, 2013, vol. 52 (2), p. 169-172.
[16] M. Bjelopavlic, J. Ralston, G. Reynolds. Adsorption of monoalkyl phosphates at the zircon-aqueous solution interface. Journal of Colloid and Interface Science, 1998, vol. 208, p. 183-190.
[17] M. Kosmulski. Positive electrokinetic charge of silica in the presence of chlorides. Journal of Colloid and Interface Science, 1998, vol. 208, p. 543-545.

[18] O. Dezellus. Contribution à l'étude des mécanismes de mouillage réactif. Institut National Polytechnique de Grenoble, Grenoble, 2005.
[19] A. Alghunaim, S. Kirdponpattara, B.Z. Newby. Techniques for determining contact angle and wettability of powders. Powder Technology, 2016, vol. 287, p. 201-215.
[20] A. Autef, E. Joussein, A. Poulesquen, G. Gasgnier, S. Pronier, I. Sobrados, J. Sanz, S. Rossignol. Influence of metakaolin purities on potassium geopolymer formulation: the existence of several networks. Journal of Colloid and Interface Science, 2013, vol. 408, p. 43-53.
[21] A. Gharzouni, E. Joussein, B. Samet, S. Baklouti, S. Rossignol. Effect of the reactivity of alkaline solution and metakaolin on geopolymer formation. Journal of Non-Crystalline Solids, vol. 410, p. 127-134.
[22] J. Temuujin, W. Rickard, M. Lee, A. van Riessen. Preparation and thermal properties of fire resistant metakaolin-based geopolymer-type coatings. Journal of Non-Crystalline Solids, 2011, vol. 357, p. 1399-1404.
[23] A. Gharzouni, I. Sobrados, E. Joussein, S. Baklouti, S. Rossignol. Predictive tools to control the structure and the properties of metakaolin based geopolymer materials. Colloids and Surfaces A, submitted.
[24] X.X. Gao, A. Autef, E. Prud'homme, P. Michaud, E. Joussein, S. Rossignol. Synthesis of consolidated materials from alkaline solutions and metakaolin: existence of domains in the Al-Si-K/O ternary diagram. Journal of Sol-Gel Science Technology, 2013, vol. 65, p. 220-229.
[25] E. Prud'Homme. Rôles du cation alcalin et des renforts minéraux et végétaux sur les mécanismes de formation de géopolymères poreux ou denses. Thèse d'Université, Université de Limoges, 2011.
[26] M. Henry, J.-P. Jolivet, J. Livage. Aqueous chemistry of metal cations: hydrolysis, condensation and complexation. Structure and Bonding, 1990, p. 1-64.
[27] J.T.G. Overbeek. Recent developments in the understanding of colloid stability. Journal of Colloid and Interface Science, 1977, vol. 58, p. 408-422.
[28] M.D. Allendorf, K.E. Spearb. Thermodynamic analysis of silica refractory corrosion in glass-melting furnaces. Journal of the Electrochemical Society, 2001, vol. 148, p. 59-67.
[29] J.-L. Gelet. Informations pour présenter le fusible et le busbar. Document interne MERSEN, 2016.
[30] P. Duxson, G.C. Lukey, J.S.J. van Deventer. Thermal evolution of metakaolin geopolymers: Part 1 – Physical evolution. Journal of Non-Crystalline solids, 2006, vol. 352, p. 5541-5555.
[31] P. He, D. Jia, M. Wang, Y. Zhou. Thermal evolution and crystallization kinetics of potassium-based geopolymer. Ceramics International, 2011, vol. 37, p. 59-63.
[32] D.P. Debecker, M. Stoyanova, U. Rodemerck, E.M. Gaigneaux. Preparation of MoO3/SiO2-Al2O3 metathesis catalysts via wet impregnation with different Mo precursors. Journal of Molecular Catalysis A: Chemical, 2011, vol. 340, p. 65-76.

[33] P. Sarrazin, B. Mouchel, S. Kasztelan. ^{95}Mo NMR study of the interaction of heptamolybdate solutions with alumina and silica. Journal of Physical Chemistry, 1989, vol. 93, p. 904-908.
[34] F. Gouny, F. Fouchal, P. Maillard, S. Rossignol. Study of the effect of siliceous species in the formation of a geopolymer binder: Understanding the reaction mechanisms among the binder, wood, and earth brick. Industrial and Engineering Chemistry Research, 2014, vol. 53 (9), p. 3559-3569.
[35] A. Autef, E. Joussein, G. Gasgnier, S. Rossignol. Role of the silica source on the geopolymerization rate. Journal of Non-Crystalline Solids, 2012, vol. 358, p. 2886-2893.
[36] A. Autef, E. Joussein, G. Gasgnier, S. Rossignol. Role of the silica source on the geopolymerization rate: A thermal analysis study. Journal of Non-Crystalline Solids, 2013, vol. 366, p. 13-21.
[37] J. Jiang, I. May, M.J. Sarsfield, M. Ogden, D.O. Fox, C.J. Jones, P. Mayhew. A spectroscopic study of the dissolution of cesium phosphomolybdate and zirconium molybdate by ammonium carbamate. Journal of Solution Chemistry, 2005, vol. 34, p. 443-468.
[38] N. Essaidi, B. Samet, S. Baklouti, S. Rossignol. Effect of calcination temperature of tunisian clays on the properties of geopolymers. Ceramics – Silikáty, 2013, vol. 57 (3), p. 251-257.
[39] J.L. Provis, R.M. Harrex, S.A. Bernal, P. Duxson, J.S.J. van Deventer. Dilatometry of geopolymers as a means of selecting desirable fly ash sources. Journal of Non-Crystalline Solids, 2012, vol. 358, p. 1930-1937.
[40] P. Duxson, G.C. Lukey, J.S.J. van Deventer. Physical evolution of Na-geopolymer derived from metakaolin up to 1000 °C. Journal of Materials Science, 2007, vol. 42 (9), p. 3044-3054.
[41] M.Y. Konon, S.V. Stolyar, L.F. Dikaya, I.G. Polyakova, I.A. Drozdova, T.V. Antropova. Physicochemical properties of glasses of the Na_2O-B_2O_3-SiO_2-Fe_2O_3 system in the $8Na_2O/70SiO_2$ section. Glass Physics and Chemistry, 2015, vol. 41 (1), p. 116-121.
[42] L. Zuda, R. Černý. Measurement of linear thermal expansion coefficient of alkali-activated aluminosilicate composites up to 1000 °C. Cement and Concrete Composites, 2009, vol. 31, p. 263-267.
[43] Y. Zeng, K. Bai, H. Jin. Thermodynamic study on the corrosion mechanism of copper wire bonding. Microelectronics Reliability, 2013, vol. 53, p. 985-1001.
[44] M. Pourbaix. Atlas d'équilibres électrochimiques à 25 °C. Gauthier-Villars, Paris, 1963.
[45] R. Gy. Ion exchange for glass strengthening. Materials Science and Engineering B, 2008, vol. 149, p. 159-165.
[46] R.W. Ford. Drying. Institute of Ceramics, textbook series, MacLaren and Sons, Londres, Angleterre, 1964.

CHAPITRE IV

Publications

Publication 1 (ACL 1)

L. Vidal, E. Joussein, M. Colas, J. Absi, S. Rossignol

"Effect of the addition of ammonium molydabte on metakaolin-based geopolymer formation: Shrinkage and crystallization"

Powder Technology, 2015, vol. 275, p. 211-219.

Powder Technology 275 (2015) 211–219

Contents lists available at ScienceDirect

Powder Technology

journal homepage: www.elsevier.com/locate/powtec

Effect of the addition of ammonium molybdate on metakaolin-based geopolymer formation: Shrinkage and crystallization

L. Vidal [a,b], E. Joussein [c], M. Colas [a], J. Absi [b], S. Rossignol [a,*]

[a] Science des Procédés Céramiques et de Traitements de Surface (SPCTS), Ecole Nationale Supérieure de Céramique Industrielle, 12 rue Atlantis, 87068 Limoges Cedex, France
[b] Groupe d'Etude des Matériaux Hétérogènes (GEMH), Ecole Nationale Supérieure de Céramique Industrielle, 12 rue Atlantis, 87068 Limoges Cedex, France
[c] Université de Limoges, GRESE EA 4330, 123 avenue Albert Thomas, 87060 Limoges, France

ARTICLE INFO

Article history:
Received 28 November 2014
Received in revised form 10 January 2015
Accepted 7 February 2015
Available online 14 February 2015

Keywords:
Metakaolin reactivity
Ammonium molybdate
Silicate species
Shrinkage
Raman spectroscopy

ABSTRACT

This paper focuses on the influence of the addition of ammonium molybdate to geopolymer mixtures to better understand the formation of geopolymer structural networks and the effect of Mo-based additive on the thermal behavior of material. Several geopolymers were synthesized between two metakaolins and various amounts of ammonium molybdate. The microstructure of samples was determined by SEM, the structural evolution (depending on the amount of molybdenum added) was investigated using Raman spectroscopy and XRD analyses, and the temperature behaviors of materials by DTA–TGA and dilatometric analyses. The results showed that (i) both metakaolins react differently in the presence of ammonium molybdate, (ii) molybdenum induces decrease of shrinkage value at high temperatures, and (iii) the crystallization seems to be favored with ammonium molybdate. This work shows that ammonium molybdate controls polycondensation reactions highlighting the modifier or former role played by the molybdenum atoms depending on the amount of ammonium molybdate added.

1. Introduction

Geopolymers are aluminosilicate materials synthesized at ambient temperature or slightly higher temperature by the alkaline activation of aluminosilicate sources. These materials were previously discussed in the 1960s by Glukhovsky [1]. Due to the high interest of geopolymer materials in industry, a large number of studies were conducted, and it was found that the main role of the aluminosilicate source was as the alumina source for Al–Si polycondensation, and the alkaline solution acted as an activating agent [2,3]. The aluminosilicate sources could be derived from natural clay minerals, calcined clays or industrial by-products [4]. Even if metakaolins are the major aluminosilicate source used around the world due to their high reactivities, it is also possible to work with other Al-rich sources, such as montmorilllonite, illite or non-dehydroxylated kaolin [5]. But it was shown that the geopolymerization is much less complete with unreactive non-dehydroxylated kaolinite or 2:1 clay minerals [6,7]. Previous studies on aluminosilicate sources showed the influence of the reactivity and purity of different metakaolins on the formation of various networks in the strengthened materials [8,9]. Thermal treatments were performed on various potassium-based geopolymers to identify these different networks, and the analyses highlighted the crystallization of compounds identified as leucite ($KAlSi_2O_6$) and kalsilite ($KAlSiO_4$) for all of the samples [10]. The various metakaolins used will lead to differences between the strengthened materials. Indeed, the authors demonstrated that a more reactive metakaolin will form a single geopolymer network due to the very fast dissolution of the metakaolin. A less pure and reactive metakaolin leads to two "geopolymer" networks: a Si-rich network and an Al-rich network with a partial dissolution of the metakaolin.

Concerning the alkaline solution, there are various parameters that could influence the polycondensation reactions such as the alkali cation, the water content, the Si/M ratio (where M = Na or K) or the siliceous species present in the solution. Indeed, Steins et al. [11] studied the influence of three cations (sodium, potassium and cesium) as alkali activators. They demonstrated that the dissolution of the metakaolin is more rapid with a small cation. They demonstrated that the alkali hydration sphere could play a role in the local organization and consolidation of the geopolymer. Moreover, other authors showed the influence of the silicate solution used [12,13]. Indeed, they studied two different potassium silicate solutions; the first one was prepared by adding KOH pellets to a commercial potassium silicate solution, and the second one was obtained by the dissolution of silica in a solution containing water and KOH pellets. The authors demonstrated that the second solution contained more Q^0 species than the first one. Because Q^0 species are more reactive than other Q^n species, this solution has a higher reactivity. So, these solutions will lead to different polycondensation reactions. According to this, the quality of the alkaline solution and therefore its reactivity are in accordance with the purity and the reactivity of the metakaolin (see before) because the various networks formed in these

* Corresponding author. Tel.: +33 5 87 50 25 64.
E-mail address: sylvie.rossignol@unilim.fr (S. Rossignol).

http://dx.doi.org/10.1016/j.powtec.2015.02.012
0032-5910/

materials are essentially based on silicate compounds. So, the control of the siliceous species in the reaction mixture could influence the formation of a specific network.

Some studies highlighted that the formation of silicomolybdic entities was possible thanks to the reaction between siliceous species and ammonium molybdate ($(NH_4)_2Mo_2O_7$) [14]. The formation of α and β silicomolybdic acid ($H_4SiMo_{12}O_{40}$) was demonstrated by Truesdale and Smith [15]. These entities could be used for the determination of the silica thanks to a colorimetric method [16]. Indeed, in water, the reaction between silica and molybdate will form yellow or blue silicomolydic acid. The intensity of the color, measured by spectrophotometric analysis, allows the determination of the concentration of silicomolybdic entities in the material. Other authors determined the size of colloidal silica in alkali–silicate solutions depending on the pKa of $H_3SiO_4^-$ by a reaction with molybdic acid [17]. Some studies showed the stability of different molybdic species as a function of the pH value. Thus, Jiang et al. [18] determined that in the presence of phosphorus or zirconium, MoO_4^{2-} entities exist for pH values between 6 and 10.5 while $Mo_7O_{24}^{6-}$ species exist between pH values of 6 and 7.5. Others authors [19] showed the presence of $Ag_2Mo_2O_7$ for a pH value near 5 and the existence of Ag_2MoO_4 for pH values between 6.5 and 12. It was highlighted that alumina could react with molybdic species to change the isoelectric point whereas silica reacts with molybdic compounds to form various species. The interaction of the Oxo molybdenum species with alumina is irreversible, whereas with silica the species remain labile [20]. In some recent studies, the molybdate method and spectroscopic measurements were used to follow the various interactions between an alkaline solution and aluminosilicates [21]. They showed that the formation of different structural units depends on the reaction time. The same methods were also used to determine the structure of the geopolymer formed [22]. Studies on various types of silicate glass showed that crystallization in these materials is favored by these molybdic compounds [23]. In silicate glass, the molybdenum atoms are in a four-fold environment ($[MoO_4]^{2-}$). These tetrahedrons cannot bridge with silicon polyhedrons [24]. Thus, the molybdenum atoms are located in zones rich in alkali or alkaline earth metals. Therefore, the silica network is impoverished in alkaline cations and contains fewer non-bridging oxygen atoms. When potassium atoms are present in the system, the crystallization of potassium bimolybdate ($K_2Mo_2O_7$) and potassium molybdate (K_2MoO_4) occur at 460 °C and 925 °C, respectively, during thermal treatments [25,26].

The molybdate compounds could be used to modify siliceous species from the alkaline solution. Because geopolymers are alkaline activated materials based on silica species, the aim of this study is to control these siliceous species in the potassium silicate solution by adding ammonium molybdate. Finally, the role of molybdic species on the formation of different structural networks in geopolymer materials was determined. To do this, various geopolymer samples synthesized from two different metakaolin sources were realized with Mo-addition and were studied by spectroscopic, microscopic and dilatometric analyses.

2. Material and methods

2.1. Raw materials and sample preparation

Samples were synthesized using an alkaline silicate solution (Si/K = 0.7) and two metakaolins (denoted Mk1 and Mk2) from the supplier Imerys (Table 1) [27]. The alkaline silicate solution was obtained by the dissolution of KOH pellets (85.2% purity) and amorphous silica (99.9% purity) in osmotically purified water at room temperature as described in a previous work [28]. Syntheses were performed by mixing the alkaline silicate solution and metakaolins. Then, the samples were placed in a closed mold at room temperature (25 °C). The geopolymer characteristics are presented in Table 1. Other samples were realized with the addition of anhydrous ammonium molybdate (99.9% purity) to the alkaline solution before the addition of the metakaolins. The amounts added were between 0.08 and 1.57% molar of molybdenum.

Table 1
Chemical characteristics of raw materials and geopolymers.

	Raw materials		Geopolymers		
	Chemical composition (weight %)		Si/Al	Al/K	% H_2O
	SiO_2	Al_2O_3			
M1	55.0	40. 0	1.80	1.12	32.8
M2	55.0	39.0	1.84	1.09	32.8

Some of these samples were heated at 1400 °C using a 5 °C/min ramp after consolidation. The nomenclature used for the various samples is reported in Table 2.

2.2. Sample characterization

Raman spectroscopy was performed on powder samples using a T64000 Horiba–Jobin–Yvon spectrophotometer with 514 nm laser excitation operating at a power of 30 mW at the sample. Scattered light was collected in the backscattering mode using a long working distance objective (×50) with a triple diffraction grating (1800 lines/mm). The spectral range was 100 to 1200 cm^{-1}, and the acquisition time was 60 s.

X-ray patterns were collected from powder samples after they were crushed to 63 μm in size and were obtained from 5 to 80° (2θ) using a Brücker D8 apparatus equipped with a graphite-backed monochromator. The device was equipped with a cobalt anode (λ = 1.79026 Å). The XRD patterns were obtained using a dwell time of 0.5 s and a step size of 0.01° (2θ). The crystalline phases were identified by comparing the patterns with powder diffraction file (PDF) standards from the International Center for Diffraction Data (ICDD).

The morphologies of the final products were determined using a Cambridge Stereoscan S260 scanning electron microscope (SEM). The samples were broken and carbon coated.

Differential thermal analysis (DTA) and thermogravimetric analysis (TGA) were performed on an SDT Q600 apparatus from TA Instruments in a flowing dry air atmosphere (100 mL/min) in platinum crucibles. The signals were measured using Pt/Pt-10% Rh thermocouples. Milligram aliquots of the samples were placed in platinum crucibles, and the analyses were performed from 30 to 1400 °C at 20 °C/min for the consolidated geopolymer samples obtained at room temperature. All of the samples were crushed prior to analysis.

Dilatometric measures were made under air, by means of a contact vertical dilatometer (TMA Setsys Evolution Setaram), on bulk samples with a cylindrical geometry (H = 7 mm; Ø = 6.5 mm). Two platinum holders were placed at the surface end contacts of the samples to avoid high-temperature diffusion between the samples and the alumina holders. A calibration cycle (without the sample) was performed and registered. The calibration data were then subtracted from the data collected for each sample to eliminate the contribution of the device. The thermal cycle used consisted of heating from 30 to 1400 °C and cooling from 1400 to 30 °C, both at a rate of 5 °C/min. Then, the $\Delta L_{sample}/\Delta L_{reference}$, where the reference is the sample without the addition of ammonium molybdate, was calculated for every composition. For example, for the $^{25}M2_{1.57}$ geopolymer, the total shrinkage is equal to 4.8%. The shrinkage of the reference ($^{25}M2$) is 20%. So, the $\Delta L_{sample}/\Delta L_{reference}$ value is equal to 0.24.

Table 2
Nomenclature of samples.

Molar % of Mo	Mk1		Mk2	
	25 °C	1400 °C	25 °C	1400 °C
0	$^{25}M1$	$^{1400}M1$	$^{25}M2$	$^{1400}M2$
0.40	$^{25}M1_{0.40}$	$^{1400}M1_{0.40}$	$^{25}M2_{0.40}$	$^{1400}M2_{0.40}$
1.57	$^{25}M1_{1.57}$	$^{1400}M1_{1.57}$	$^{25}M2_{1.57}$	$^{1400}M2_{1.57}$

3. Results and discussion

3.1. Impact of the addition of a fixed percentage of ammonium molybdate on geopolymer formulation

To study the influence of ammonium molybdate on consolidated materials, thermal analyses and scanning electron microscopy observations were performed on the two extreme compositions (with or without molybdenum (1.57%)).

Fig. 1 presents the DTA and TGA curves of the four samples. All of the samples exhibit the same phenomena. First, an endothermic peak is observed between 30 and 200 °C and then, exothermic peaks, which are centered on different temperatures, are noted at high temperatures (above 800 °C). The endothermic peak is associated with an important weight loss (between 25 and 35%) and can be explained by the loss of the water in the porous network as demonstrated in geopolymer compounds [29]. For the ^{25}M1 and ^{25}M2 samples (Fig. 1a, c), the weight losses are equal to 34 and 36% respectively. The incorporation of ammonium molybdate in the ^{25}M1 geopolymer (Fig. 1b) does not have a significant effect on the quantity of water contained in the sample, which is equal to 35%. In the case of the $^{25}M2_{1.57}$ sample (Fig. 1d), the weight loss is near 28%. So, this sample seems to contain less water than without the ammonium molybdate. This phenomenon could be due to some different polycondensation reactions. Indeed, the two metakaolins have different reactivities according to Autef et al. [8]. Moreover, in the case of samples containing ammonium molybdate, the small amount of molybdenum can modify the alkaline solution. Consequently, these two phenomena have an impact on the geopolymerization mechanisms (unpublished work). Then, exothermic peaks are noted for the four samples between 900 and 1400 °C. For sample ^{25}M1 (Fig. 1a), the two peaks located at 1120 and 1170 °C can be attributed to various structural rearrangements, which lead to the formation of two phases: the leucite and the kalsilite [8,10]. The presence of these phases was also determined by XRD analysis (Fig. 3b). The ^{25}M2 geopolymer (Fig. 1c) also presents two exothermic peaks, but they are centered on different temperatures. The first one is located at approximately 980 °C and may be due to spinel-phase formation [30,31]. The second is located at 1230 °C and may be related to the crystallization of leucite ($KAlSi_2O_6$) as shown by Autef et al. [8]. The incorporation of ammonium molybdate into the ^{25}M1 geopolymer (Fig. 1b) seems to modify the exothermic peaks located at 1000 and 1140 °C. The first peak at 1000 °C could be explained by the formation of a spinel-phase or by the crystallization of another compound because the composition must be identical. The second peak at 1140 °C is the same as the one for the ^{25}M1 geopolymer. In the case of the $^{25}M2_{1.57}$ geopolymer, the presence of only one peak at 1015 °C is noted (Fig. 1d). This peak could correspond to the peak observed at 980 °C for sample ^{25}M2, indicating that crystallization occurs at a higher temperature. So, the addition of ammonium molybdate seems to delay the crystallization phenomena in this geopolymer.

These results indicate that the addition of ammonium molybdate has an influence on the crystallization of phases at high temperatures and on the amount of water contained in the porous network. So, the addition of this compound may have an effect on the structural data of the geopolymers.

As a way to determine the impact of the addition of ammonium molybdate on the structures of the samples, SEM investigations were performed (Fig. 2). The ^{25}M1 and ^{25}M2 materials show typical geopolymer morphologies [32] (Fig. 2a, e). Some minor differences can be observed between these two samples and can be linked to the reactivities of the two metakaolins leading to distinct networks [8]. The addition of ammonium molybdate into the ^{25}M1 geopolymer (Fig. 2c) implies changes in the properties of the microstructure, such as a more pronounced texture as can be observed in the presence of various

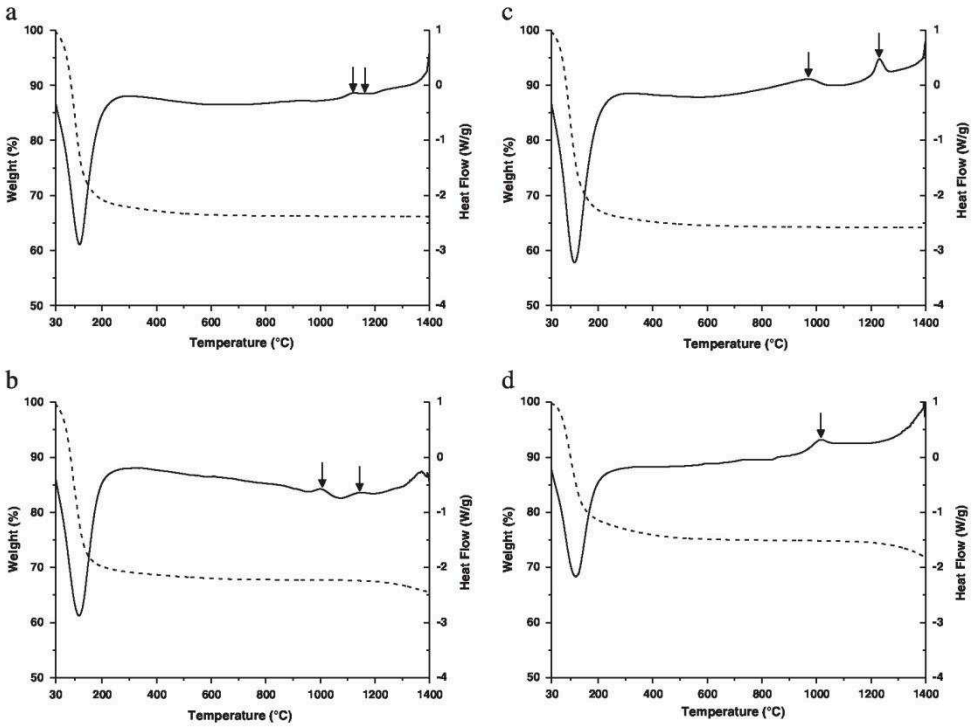

Fig. 1. (- - -) Weight loss and (–) heat flow curves versus time for (a) ^{25}M1, (b) $^{25}M1_{1.57}$, (c) ^{25}M2 and (d) $^{25}M2_{1.57}$ samples.

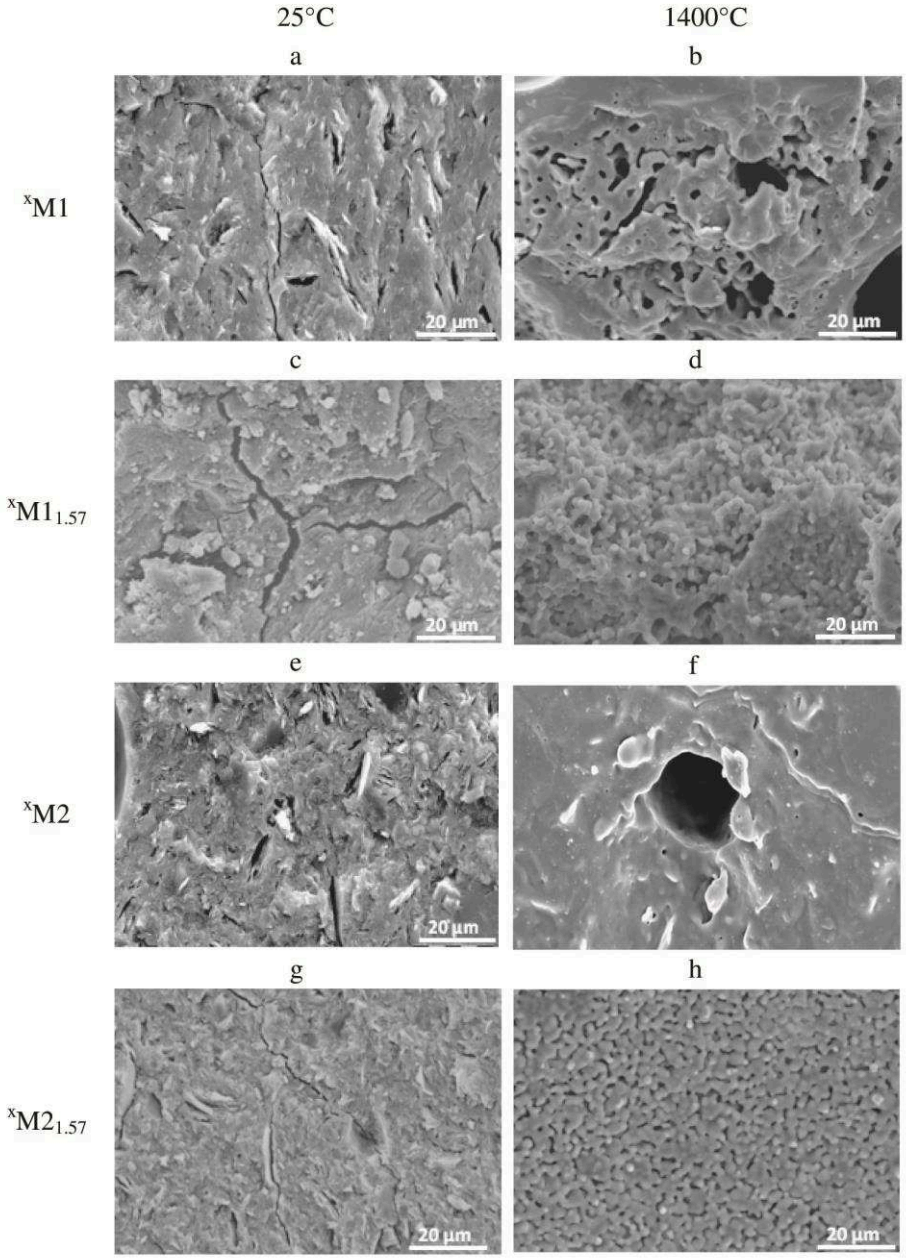

Fig. 2. SEM images (a) ^{25}M1, (b) ^{1400}M1, (c) ^{25}M1$_{1.57}$, (d) ^{1400}M1$_{1.57}$, (e) ^{25}M2, (f) ^{1400}M2, (g) ^{25}M2$_{1.57}$, and (h) ^{1400}M2$_{1.57}$ samples.

alkaline solutions [33]. This feature is related to the alkaline solution specificity, implying that different polycondensation reactions are occurring. The same phenomenon could be observed for the SEM image of the ^{25}M2$_{1.57}$ sample (Fig. 2g). Moreover, some cracks could be observed for the ^{25}M1$_{1.57}$ sample (Fig. 2c) due to the fact that the observation was done on the broken zone. In the case of the ^{1400}M1 and ^{1400}M2 samples (Fig. 2b, f), different microstructures are observed. The ^{1400}M1 sample exhibits a vitreous aspect associated with the presence of some crystallization features whereas the ^{1400}M2 sample displays a homogeneous vitreous feature [34,35]. The observations for the ^{1400}M1 sample could be explained by the presence of two interconnected networks. The homogenous structure of the ^{1400}M2 geopolymer could be due to the existence of a single geopolymer network in this sample [8]. Then, for the ^{1400}M1$_{1.57}$ and ^{1400}M2$_{1.57}$ samples (Fig. 2d, h), the vitreous phase seems to disappear, and the presence of small crystallites is noted. Nevertheless, the ^{1400}M2$_{1.57}$ geopolymer displays an almost perfect distribution, which could be linked to the only exothermic peak observed by DTA analysis, as opposed to ^{1400}M1$_{1.57}$, which exhibits a heterogeneous distribution, where several exothermic peaks are detected.

These observations reveal that in the presence of ammonium molybdate, the texture is more compact (a little deeper) for unheated samples. During heat treatment, the crystallization is enhanced in the presence of this ammonium molybdate, which acts as a catalyst of crystallization.

All of these observations focus on the effects of various amounts of molybdenum between 0 and 1.57% because it is not possible to obtain a consolidated geopolymer when the amount of Mo is superior to 1.57%. The difficulty of obtaining consolidated materials with Mo additions superior to 1.57% could be due to the fact that this compound influences the geopolymerization reactions. This phenomenon could be explained by the fact that molybdic species may either react with SiO_4 tetrahedrons as it is the case for determining silica in silicates [15–17] or be counterbalanced by potassium ions like in silicate glasses [23,24].

3.2. Effect of a variable percentage of ammonium molybdate on the geopolymer crystallized phases

X-ray diffraction was performed on samples containing various amounts of molybdenum (Fig. 3), namely ^{25}M1 (Fig. 3a), ^{1400}M1 (Fig. 3b), ^{25}M2 (Fig. 3c) and ^{1400}M2 (Fig. 3d) containing various amounts of this compound (0, 0.40 and 1.57%).

As expected, the XRD patterns of the ^{25}M1 and ^{25}M2 samples are quite similar and characteristic of geopolymer materials with an amorphous dome centered near 33° (2θ) (CoKα). As expected, some crystallized phases are present and attributed to impurities in the metakaolins such as quartz, anatase and muscovite. The addition of ammonium molybdate does not seem to have an effect on the XRD pattern obtained. Indeed, the $^{25}M1_{0.40}$, $^{25}M1_{1.57}$, $^{25}M2_{0.40}$ and $^{25}M2_{1.57}$ patterns are similar to those obtained for the ^{25}M1 and ^{25}M2 samples. This result is most likely due to that (i) the impact of ammonium molybdenum is essentially on amorphous phases, and this impact is difficult to show by XRD, and (ii) the amount of ammonium molybdenum added into the mixture (up to 1.2 wt.%) is very small, which does not allow modifications to be seen on the XRD. After thermal treatment, both the ^{1400}M1 and ^{1400}M2 samples display similar XRD patterns with the presence of crystallized phases such as leucite ($KAlSi_2O_6$) and kalsilite ($KAlSiO_4$). Whatever the metakaolin raw material used, with the incorporation of 0.40% molybdenum ($^{1400}M1_{0.40}$ and $^{1400}M2_{0.40}$), the leucite phase is still present. However, there is a decrease of the kalsilite phase, and the appearance of a potassium bimolybdate phase ($K_2Mo_2O_7$) is observed. The kalsilite phase disappears moving from the addition of 0.40 to 1.57% molybdenum for both the $^{1400}M1_{1.57}$ and $^{1400}M2_{1.57}$ samples. Moreover, the potassium bimolybdate phase is always observed with the presence of an alumina phase which may be Mo-doped. Consequently, as was previously observed, the ammonium molybdate plays a role on the structure and the formation of the various networks in materials at low temperatures. This phenomenon is also found during heat treatment, inhibiting the formation of the kalsilite phase in favor of potassium bimolybdate and Mo-doped alumina. This could be explained by the complexation of the potassium with the molybdenum atoms to form the potassium bimolybdate phase. The remaining aluminum atoms react to create an Al-rich phase doped with molybdenum atoms. So, the ^{25}M1 and ^{25}M2 samples display an amorphous dome characteristic of geopolymer materials with some crystallized phases due to impurities in the metakaolins. After thermal treatment, the XRD patterns are similar for both samples without the addition of Mo; crystallized phases identified as leucite and kalsilite are present. With the addition of ammonium molybdate, a potassium bimolybdate phase is also observed. For the addition of 1.57% of molybdenum, the kalsilite phase totally disappears whereas in the presence of potassium bimolybdate, Mo-doped alumina and leucite are observed.

The presence and evolution of the phases in the geopolymers are confirmed by Raman spectroscopy (Fig. 4) on these different samples. Raman frequencies of some molybdic compounds are given in Table 3 [36–39]. In fact, for the ^{25}M1 and ^{25}M2 samples (Fig. 4a, c), the Raman spectra are similar, and they present contributions at 150 (E_g), 200 (E_g), 392 (B_{1g}), 510 (A_{1g}) and 634 cm^{-1} (E_g) [40,41]. In order to better see the weak bands, the contribution located at 150 cm^{-1}, which is very strong, is not presented in Fig. 4a and c. All of these bands are attributed to anatase, which comes from the metakaolin and was unaltered either by the calcination or by the alkaline attack [8]. This compound was also observed by the XRD analyses (Fig. 3) in all of the samples. After the addition of 0.40% molybdenum, in the $^{25}M1_{0.40}$ and $^{25}M2_{0.40}$ materials, only the contribution of anatase is observed. The same bands are observed for the $^{25}M1_{1.57}$ and $^{25}M2_{1.57}$ geopolymers, but there are also other contributions due to Mo–O bonds that are detected at 315 and 884 cm^{-1}. These bands are attributed to the δ(Mo–O) and the ν_s(Mo–O), respectively, for the MoO_4^{2-} anion (Table 3). This phenomenon seems to indicate that, in an alkaline medium, the $Mo_2O_7^{2-}$ anions are not stable and will form MoO_4^{2-} entities as reported by Jiang et al. [18]. Indeed, the authors have shown that in an alkaline medium (pH > 9), only MoO_4^{2-} ions are detected. After thermal treatment, new bands appear at 150, 379, 495 and 529 cm^{-1} in all of the samples, and an enlargement at approximately 1000 cm^{-1} is also observed. The contribution at 379 cm^{-1} could be attributed to kalsilite, and the others are associated with δ (T–O–T), where T = Si or Al, for the leucite [42]. The large band at approximately 1000 cm^{-1} can be attributed to disordered phases such as an aluminous network associated with some leucite weak modes [42–44]. In the case of the ^{1400}M2 sample, bands assigned to leucite and kalsilite are also observed. However, the contribution at approximately 1000 cm^{-1} is smaller for this material than for ^{1400}M1. This result can also be explained by the presence of disordered phases, most likely due to the different reactivities of the two metakaolin precursors used. For the $^{1400}M1_{0.40}$ sample, the contributions due to the presence of leucite and kalsilite are found. Moreover, the large bands between 600 and 1200 cm^{-1} are still observed. The same observations are observed for the $^{1400}M2_{0.40}$ geopolymer. Finally, for the addition of ammonium molybdate up to 1.57%, the kalsilite contribution at 379 cm^{-1} disappears, and the bands attributed to leucite are still present for $^{1400}M1_{1.57}$ material, as shown by the XRD analyses. Moreover, the band at approximately 1000 cm^{-1} is smaller for this sample. This phenomenon confirms the previous results (see above) about the presence of less disordered phases. The same observations regarding the kalsilite and leucite phases were made for the $^{1400}M2_{1.57}$ geopolymer. To conclude, the analyses on unheated samples showed the presence of MoO_4^{2-} species with the addition of 1.57% molybdenum, which can be explained by the fact that $Mo_2O_7^{2-}$ entities are not stable in alkaline medium. After thermal treatments, all of the samples present contributions of leucite. The presence of kalsilite is detected in the samples without ammonium molybdate. However, the contribution of kalsilite disappears when 1.57% ammonium molybdate is added. According to some studies [45,46], the molybdenum atoms could play the role of either network modifiers or network formers in various types of silicate glass. In effect, these authors have demonstrated that in phosphate glass at low concentrations the molybdenum oxide plays the role of a network modifier, and at high concentrations, it acts as a network former. Indeed, it has been shown that in these types of glass molybdenum atoms will preferentially bridge with oxygen atoms to form units such as MoO_6. It was also demonstrated that molybdenum oxide has an effect on the nucleation kinetics in glass. Therefore, it is clear that the molybdenum atoms may have an impact on crystallization during thermal treatment inducing drastic modifications in the geopolymer mixtures.

3.3. Mechanisms versus the reactivities of the metakaolins

Dilatometric analyses were performed on the samples containing various amounts of ammonium molybdate. Fig. 5 presents the dilatometric curves obtained for the samples of various compositions with both metakaolins Mk1 (Fig. 5a) and Mk2 (Fig. 5b) containing 0 to 1.57% of molybdenum.

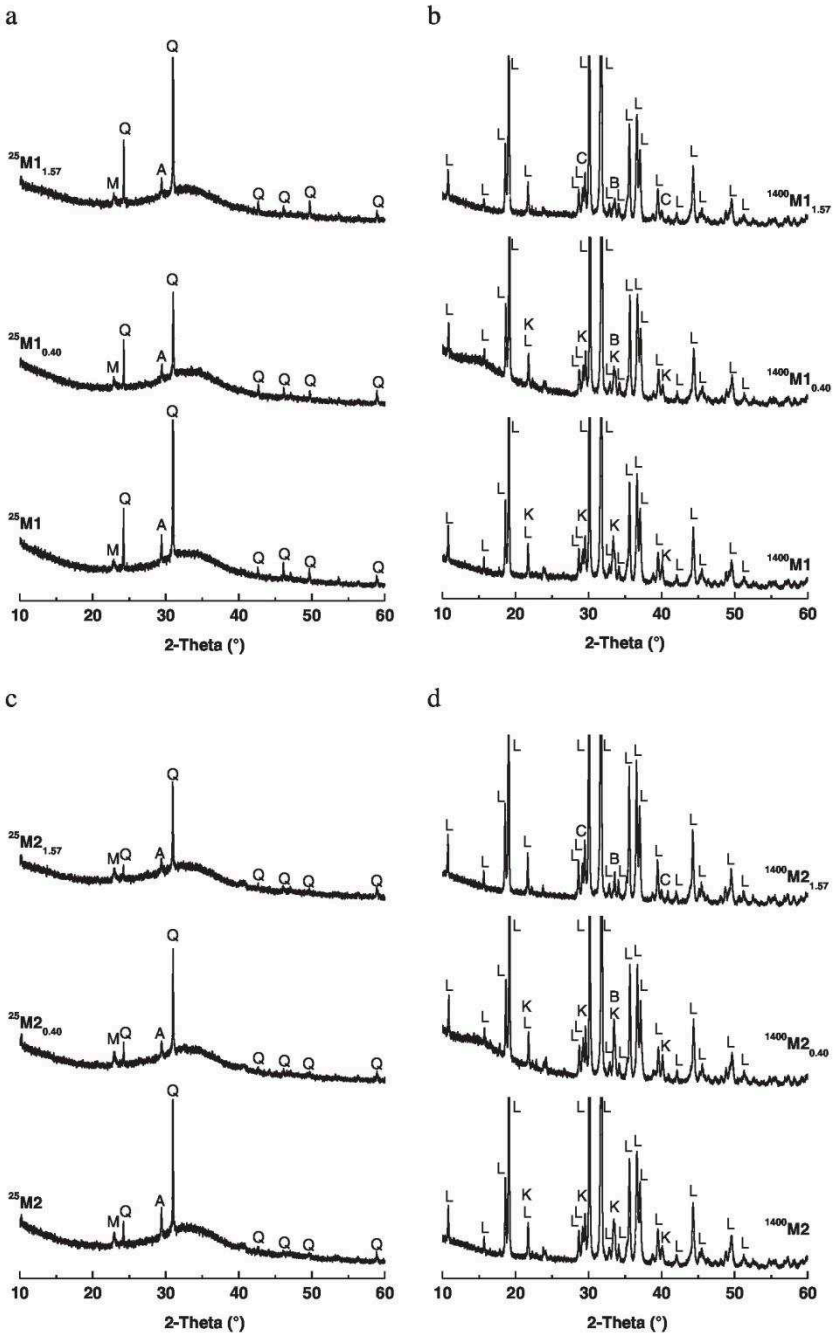

Fig. 3. XRD patterns of (a) ^{25}M1, (b) ^{1400}M1, (c) ^{25}M2 and (d) ^{1400}M2 geopolymers with various amounts of ammonium molybdate. (A: anatase (PDF: 00-021-1272), Q: quartz (PDF: 04-012-0490, M: muscovite (PDF: 04-015-4251), L: leucite (PDF: 01-085-1626), K: kalsilite (PDF: 00-050-0436), B: potassium bimolybdate (PDF: 00-036-0347), C: corundum (PDF: 00-010-0173).

The dilatometric curve obtained for the ^{25}M1 sample displays a total shrinkage near 20%, and two phenomena are observed. The first one between 30 and 200 °C, linked to an approximately 5% dimensional variation [29,47], could be associated with the loss of the water in the porous network [10,29,47] as was demonstrated by the DTA and TGA analyses. Then, a second dimensional variation near 15% appears between 900 and 1000 °C and could be attributed to a viscous sintering [10]. This phenomenon is characteristic of the two contributions corresponding to the two networks identified by Autef et al. [8]. The first has been attributed to a relatively amorphous network in which the potassium and aluminum atoms lead to the formation of non-bridging oxygen atoms whereas in the second network, aluminum atoms could

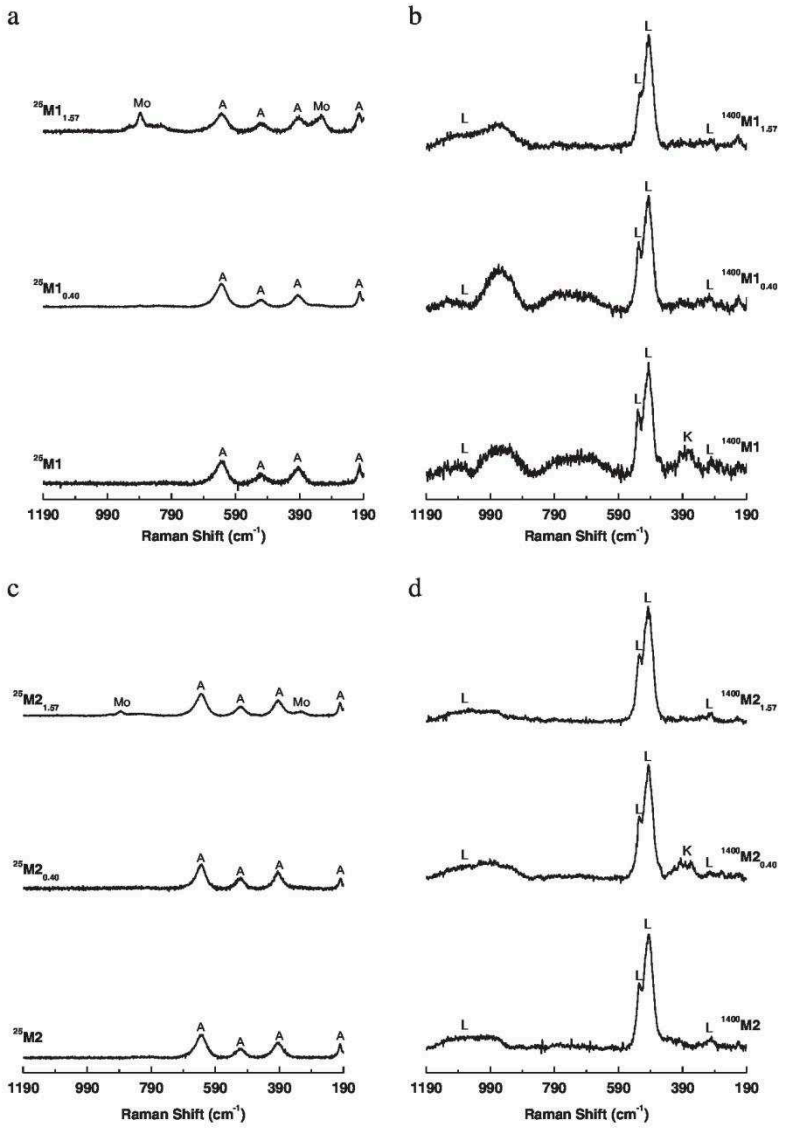

Fig. 4. Raman spectra of (a) ^{25}M1, (b) ^{1400}M1, (c) ^{25}M2 and (d) ^{1400}M2 geopolymers with various amounts of ammonium molybdate (A: anatase, Mo: MoO_4^{2-}, L: leucite and K: kalsilite).

play the role of network formers, and therefore, only the potassium atoms are responsible for the presence of non-bridging atoms. For the ^{25}M2 geopolymer, the same behavior is observed with two stages in the dimensional variation, the first between 30 and 200 °C and the second between 900 and 1150 °C. However, this sample differs from the ^{25}M1 sample because in the second phenomenon three contributions appear. The first one at 950 °C could be explained by the occurrence of a viscous flow from the geopolymer network according to the TEM observations [8]. Then, the second one near 1000 °C could be associated with a delay due to the appearance of siliceous species from the transformation of some residual aluminosilicate, which increases the viscous flow. Finally, the third contribution at 1100 °C could be explained as another delay due to the presence of quartz in the material enriching the viscous flow [48]. So, this sample also displays a total shrinkage equal to 20%. In conclusion, these two samples display the same shrinkage values, but they have different behaviors during thermal treatment in agreement with their exothermic peaks detected by thermal analyses.

Then, the effects of molybdenum additions of 0.40% on the dimensional variations of these two compositions were studied. The dilatometric curve of the $^{25}M1_{0.40}$ sample (Fig. 5a) shows that the first 5% shrinkage is present. The second contribution at 950 °C is also visible, but the shrinkage value associated with this contribution is less important (near 5% compared to 15% for the ^{25}M1). In this case, the total shrinkage of only 10% implies that the incorporation of ammonium molybdate seems to decrease the shrinkage. Regarding the $^{25}M2_{0.40}$ sample, there are also two stages in the dimensional variation. The first one occurs between 30 and 200 °C and is equal to 5%. The second one occurs at 990 °C (11%). The three contributions observed for the ^{25}M2 sample are no longer measurable, and only one phenomenon occurs at the higher temperature. This phenomenon is associated with an

Table 3
Raman frequencies of molybdic compounds.

Compounds	Raman frequencies (cm^{-1})				
	MoO_4^{2-}	$Mo_2O_7^{2-}$	$Mo_7O_{24}^{6-}$	$(NH_4)_6Mo_7O_{24}\cdot 4H_2O$	$[MoO_2Cl_3(H_2O)]^-$
Reference	[31]	[31]	[32]	[33]	[34]
ν_s (Mo–O)	888	929 [O] 908 [T]	959 [O]	934 905 890 881 859 838	946
ν_{as} (Mo–O)	852	873 [O] 860 [T]	911	–	896
δ (Mo–O)	317	–	360 [O]	–	–
ν and δ (Mo–O–Mo)	–	–	225	–	253
ν_{as} (Mo–OH_2)	–	–	–	–	391

11% shrinkage value, and the total dimensional variation of this sample is equal to 16%. So, the effect of 0.40% molybdenum is more significant for the samples prepared with the Mk1 metakaolin. Whatever the metakaolin used, Mk1 or Mk2, the 5% shrinkage between 30 and 200 °C is also observed when the amount of molybdenum is increased up to 1.57%. Moreover, the contribution at high temperature disappears and the total shrinkage is near 5% for the $^{25}M1_{1.57}$ and $^{25}M2_{1.57}$ geopolymers. So, it seems that, whatever the metakaolin used, a limited value of ammonium molybdate must be used to observe behavior differences between samples using the different metakaolins. Above this limit, both geopolymers seem to have the same behavior.

The results evidenced that the incorporation of ammonium molybdate in geopolymer reactive mixture caused changes on the morphology, on the structure and on the thermal behavior of the strengthened materials.

Further investigations were made to determine how the geopolymers containing various amounts of ammonium molybdate react during heat treatments. Fig. 6 presents the variation of the $\Delta L_{sample}/\Delta L_{reference}$ values (where ΔL represents the shrinkage and the reference is the sample without any Mo addition) as a function of the amount of molybdenum added to the mixture. Two different behaviors are observed for both metakaolins. Indeed, for an amount of molybdenum inferior to 0.24%, the shrinkage value will decrease rapidly for the Mk1 metakaolin whereas the diminution is less pronounced for the Mk2 metakaolin. Between 0.24 and 0.80% molybdenum, both geopolymers display almost the same behavior with a quasi linear decrease, which could be attributed to the same mechanism. Then, for an addition above 0.80%, both geopolymers display the same shrinkage value. These two different behaviors must be explained by two parameters, such as the alkaline solution or the metakaolin reactivity, and two different phenomena may occur depending on these parameters. First, if it is the solution that controls the polycondensation reactions, the decrease in the shrinkage value would be similar for both materials, but the results do not seem to confirm this hypothesis. The second factor is in relation to the ability of each metakaolin to release aluminosilicate species in the presence of the alkaline solution. Indeed, the Mk2 compound will have the aptitude to rapidly release aluminosilicate species whereas the release is more progressive for the Mk1 metakaolin [49]. The addition of ammonium molybdate into the solution leads to the formation of MoO_4^{2-} species. These entities will locally disrupt the siliceous species, which could react with the potassium or aluminum species modifying the silicate species, as has already been shown in the laboratory (unpublished work). In the case of the $^{25}M1$ sample, siliceous or aluminous species will be randomly released, and a competition between the two networks (Si-rich and Al-rich networks) occurs. For small amounts of ammonium molybdate, a network where the potassium and aluminum atoms are modifiers will be favored. Then, when the amounts of ammonium molybdate increase in the mixture, the aluminum and molybdenum atoms play the role of network formers as can be observed in various types of glass [45,46]. In the case of the $^{25}M2$ geopolymer, the Mk2 metakaolin releases siliceous and aluminous species very rapidly. The dilatometric curves show that for additions above 0.24%, the dimensional variations at high temperature occur at higher temperatures than for additions below 0.24%. This phenomenon could be explained by the formation of a former-rich network, which shifts the contribution to higher temperature (950 to 1015 °C; Fig. 5). Indeed, as it was previously mentioned, the molybdenum atoms will bridge with oxygen atoms and act as network co-formers. So, a network where the aluminum and molybdenum atoms play the role of network formers predominates. Thus, in this case it also seems possible that the network could be enriched in network formers such as the molybdenum and aluminum atoms.

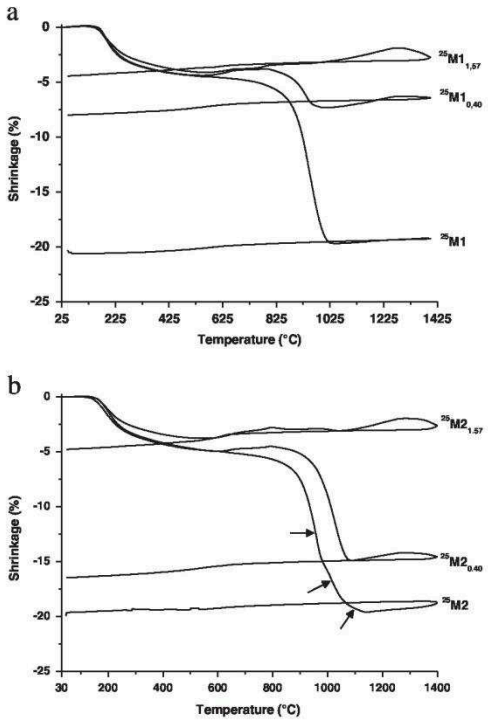

Fig. 5. Dilatometric curves of (a) M1 and (b) M2 geopolymers with various amounts of ammonium molybdate.

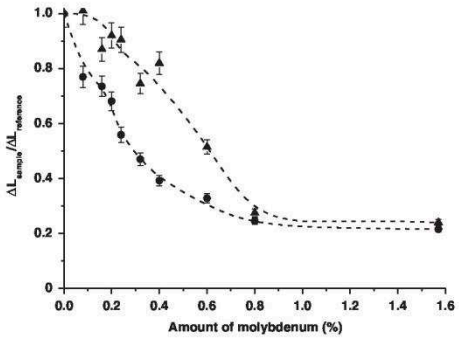

Fig. 6. $\Delta L_{sample}/\Delta L_{reference}$ versus the amount of ammonium molybdate for (●) M1 and (▲) M2 (trendline).

So, the addition of ammonium molybdate into the geopolymer mixture seems to be able to control the formation of the networks in the strengthened materials, and depending on the amount of this compound added, different networks can be observed. According to this, the molybdenum atoms play the role of modifiers when small amounts of ammonium molybdate are added and the role of formers when greater amounts are added.

4. Conclusion

The effects of the addition of various amounts of ammonium molybdate into geopolymer mixtures have been studied for compositions made with two various metakaolins. The experiments have shown that molybdenum can be added up to 1.57% whatever the metakaolin used. Above this amount, it is difficult to obtain a consolidated material.

The results demonstrated that the addition of ammonium molybdate into geopolymer mixtures induces decreases in the shrinkage values and increase the temperature of crystallization. The addition of this compound into the solution implies the presence of MoO_4^{2-} entities, which will disrupt siliceous species inducing a modification of the reactivity of the alkaline solution. For small amounts of molybdenum (<0.24%), the aluminosilicate source controls the polycondensation reactions whereas this is the alkaline solution for higher amounts of ammonium molybdate. Consequently, for small amounts of molybdenum, the molybdenum atoms may play the role of network modifiers whereas above 0.24%, the molybdenum atoms are network formers.

Finally, the addition of ammonium molybdate allows control of the formation of specific networks, then the geopolymerization one and could also improve the thermal behavior of the geopolymers.

References

[1] V.D. Glukhovsky, Soil silicates, their properties, Technology and Manufacturing and Fields of Application, PhD Thesis, Civil Engineering Institute, Kiev, Ukraine, 1965.
[2] J.L. Provis, J.S.J. van Deventer, Geopolymers, Structure, Processing and Industrial Applications2009.
[3] H. Xu, Geopolymerisation of Aluminosilicate Minerals, PhD Thesis, Department of Chemical Engineering, University of Melbourne, Australia, 2001.
[4] J. Davidovits, Geopolymer: Chemistry and Applications, 2nd ed. Institut Géopolymère, St-Quentin, 2008.
[5] E. Prud'homme, P. Michaud, E. Joussein, C. Peyratout, A. Smith, S. Rossignol, In situ inorganic foams prepared from various clays at low temperature, Appl. Clay Sci. 51 (2011) 15–22.
[6] K.J.D. MacKenzie, D.R.M. Brew, R.A. Fletcher, R. Vagana, Formation of aluminosilicate geopolymers from 1:1 layer-lattice minerals pre-treated by various methods: a comparative study, J. Mater. Sci. 42 (2007) 4667–4674.
[7] K.J.D. MacKenzie, S. Komphanchai, R. Vagana, Formation of inorganic polymers (geopolymers) from 2:1 layer lattice aluminosilicates, J. Eur. Ceram. Soc. 28 (2008) 177–181.
[8] A. Autef, E. Joussein, A. Poulesquen, G. Gasgnier, S. Pronier, I. Sobrados, J. Sanz, S. Rossignol, Influence of metakaolin purities on potassium geopolymer formulation: the existence of several networks, J. Colloid Interface Sci. 408 (2013) 43–53.
[9] E. Prud'homme, P. Michaud, E. Joussein, A. Smith, C. Peyratout, I. Sobrados, J. Sanz, S. Rossignol, Geomaterial foams: role assignment of raw materials in the network formation, J. Sol–Gel Sci. Technol. 61 (2012) 436–448.
[10] P. He, D. Jia, M. Wang, Y. Zhou, Thermal evolution and crystallization kinetics of potassium-based geopolymer, Ceram. Int. 37 (2011) 59–63.
[11] P. Steins, A. Poulesquen, O. Diat, F. Frizon, Structural evolution during geopolymerization from an early age to consolidated material, Langmuir 28 (2012) 8502–8510.
[12] X.X. Gao, A. Autef, E. Prud'homme, P. Michaud, E. Joussein, S. Rossignol, Synthesis of consolidated materials from alkaline solutions and metakaolin: existence of domains in the Al–Si–K/O ternary diagram, J. Sol–Gel Sci. Technol. 65 (2013) 220–229.
[13] E. Prud'homme, A. Autef, N. Essaidi, P. Michaud, B. Samet, E. Joussein, S. Rossignol, Defining existence domains in geopolymers through their physicochemical properties, Appl. Clay Sci. 73 (2013) 26–34.
[14] F. Parmentier, Sur les silicomolybdates, Ann. Sci. Ec. Norm. Super. 2e série (11) (1882) 187–218.
[15] V.W. Truesdale, C.J. Smith, The formation of molybdosilicic acids from mixed solutions of molybdate and silicate, Analyst 100 (1975) 203–212.
[16] L.H. Andersson, Studies in the determination of silica, Acta Chem. Scand. 12 (1958) 495–502.
[17] J.-E.A. Otterstedt, M. Ghuzel, J.P. Sterte, Colloidal components in solutions of alkali silicates, J. Colloid Interface Sci. 115 (1987) 95–103.
[18] J. Jiang, I. May, M.J. Sarsfield, M. Ogden, D.O. Fox, C.J. Jones, P. Mayhew, A spectroscopic study of the dissolution of cesium phosphomolybdate and zirconium molybdate by ammonium carbamate, J. Solut. Chem. 34 (2005) 443–468.
[19] E.K. Fodjo, D.-W. Li, N.P. Marius, T. Albert, Y.-T. Long, Low temperature synthesis and SERS application of silver molybdenum oxides, J. Mater. Chem. 1 (2013) 2558–2566.
[20] P. Sarrazin, B. Mouchel, S. Kasztelan, 95Mo NMR study of the interaction of heptamolybdate solutions with alumina and silica, J. Phys. Chem. 93 (1989) 904–908.
[21] C.H. Rüscher, E. Mielcarek, Weakening of alkali-activated metakaolin during aging investigated by the molybdate method and infrared absorption spectroscopy, J. Am. Ceram. Soc. 93 (2010) 2585–2590.
[22] W. Lutz, A. Ritzmann, Detection of geopolymer structure by spectroscopic and molybdate measurements, Z. Anorg. Allg. Chem. 639 (2013) 1776–1781.
[23] C. Cousi, F. Bart, J. Phalippou, Phase separation and crystallization induced by adding molybdenum and phosphorus to a soda–lime–silica glass, Glass Technol. 45 (2004) 65–67.
[24] M. Le Grand, Les platinoïdes et le molybdène dans des verres d'intérêt nucléaires: étude structurale, PhD Thesis, University of Paris 7, France, 1999.
[25] G.-Q. Zhang, J. Guo, L. He, D. Zhou, H. Wang, J. Koruza, M. Kosec, Preparation and microwave dielectric properties of ultra-low temperature sintering ceramics in K_2O–MoO_3 binary system, J. Am. Ceram. Soc. 97 (2014) 241–245.
[26] Z.A. Kochkarov, R.A. Zhizhuev, Interactions of salts in ionic melts of the ternary reciprocal systems Na, K/BO_2, MoO_4 and Na, K/BO_2, WO_4, Russ. J. Inorg. Chem. 59 (2014) 387–393.
[27] A. Autef, Formulation géopolymère: influence des rapports molaires Si/K et Si/Al sur les réactions de polycondensation au sein de gels aluminosilicatés, PhD thesis, University of Limoges, 2013.
[28] A. Autef, E. Joussein, G. Gasgnier, S. Rossignol, Role of the silica source on the geopolymerization rate, J. Non-Cryst. Solids 358 (2012) 2886–2893.
[29] P. Duxson, G.C. Lukey, J.S.J. van Deventer, Thermal evolution of metakaolin geopolymers: part 1 — physical evolution, J. Non-Cryst. Solids 352 (2006) 5541–5555.
[30] T.M.B. Campos, L.S. Cividanes, D.D. Brunelli, K.K. Sakane, G.P. Thim, Effect of ethylene glycol on the mullite crystallization, J. Eur. Ceram. Soc. 32 (2012) 835–842.
[31] T. Iwahiro, Y. Nakamura, R. Komatsu, K. Ikeda, Crystallization behavior and characteristics of mullites formed from alumina–silica gels prepared by the geopolymer technique in acidic conditions, J. Eur. Ceram. Soc. 21 (2001) 2515–2519.
[32] E. Prud'homme, P. Michaud, E. Joussein, C. Peyratout, A. Smith, S. Arri-Clacens, J.-M. Clacens, S. Rossignol, Silica fume as porogent agent in geo-materials at low temperature, J. Eur. Ceram. Soc. 30 (2010) 1641–1648.
[33] E. Prud'homme, P. Michaud, E. Joussein, J.-M. Clacens, S. Rossignol, Role of alkaline cations and water content on geomaterial foams: monitoring during formation, J. Non-Cryst. Solids 357 (2011) 1270–1278.
[34] J.L. Bell, P.E. Driemeyer, W.M. Kriven, Formation of ceramics from metakaolin-based geopolymers. Part II: K-based geopolymer, J. Am. Ceram. Soc. 92 (2009) 607–615.
[35] S.A. Bernal, E.D. Rodríguez, R.M. de Gutiérrez, M. Gordillo, J.L. Provis, Mechanical and thermal characterization of geopolymers based on silicate-activated metakaolin/slag blends, J. Mater. Sci. 46 (2011) 5477–5486.
[36] A. Erdőhelyi, K. Fodor, F. Solymosi, Partial oxidation of methane on supported potassium molybdate, J. Catal. 166 (1997) 244–253.
[37] S.L. González-Cortés, S. Rugmini, T. Xiao, M.L.H. Green, S.M. Rodulfo-Baechler, F.E. Imbert, Deep hydrotreating of different feedstocks over a highly active Al_2O_3-supported NiMoW sulfide catalyst, Appl. Catal. A Gen. 475 (2014) 270–281.
[38] R. Murugan, H. Chang, Thermo-Raman investigations on thermal decomposition of $(NH_4)_6Mo_7O_{24}\cdot 4H_2O$, J. Chem. Soc. Dalton Trans. (2001) 3125–3132.
[39] M.J. Taylor, C.E.F. Rickard, L.A. Kloo, Vibrational and crystallographic studies of dioxohalogenomolybdenum(VI) complexes with crown ethers, J. Chem. Soc. Dalton Trans. (1998) 3195–3198.
[40] M.J. Šćepanović, M. Grujić-Brojčin, Z.D. Dohčević-Mitrović, Characterization of anatase TiO_2 nanopowder by variable-temperature raman spectroscopy, Sci. Sinter. 41 (2009) 67–73.
[41] L. Ćurković, D. Ljubas, S. Šegota, I. Bačić, Photocatalytic degradation of Lissamine Green B by using nanostructured sol–gel TiO_2 films, J. Alloys Compd. 604 (2014) 309–316.
[42] D.A. McKeown, A.C. Buechele, C. Viragh, Ian L. Pegg, Raman and X-ray absorption spectroscopic studies of hydrothermally altered alkali–borosilicate nuclear waste glass, J. Nucl. Mater. 399 (2010) 13–25.
[43] H.D. Ruan, R.L. Frost, J.T. Kloprogge, Comparison of Raman spectra in characterizing gibbsite, bayerite, diaspore and boehmite, J. Raman Spectrosc. 32 (2001) 745–750.
[44] R.L. Frost, J.T. Kloprogge, S.C. Russell, J.L. Szetu, Vibrational spectroscopy and dehydroxylation of aluminum (oxo)hydroxides: gibbsite, Appl. Spectrosc. 53 (1999) 423–434.
[45] I. Penkov, I. Gutzow, Nucleation kinetics in glass–ceramic enamel, J. Mater. Sci. 19 (1984) 233–244.
[46] D. Toloman, R. Ciceo-Lucacel, D.A. Magdas, A. Regos, A.R. Biris, C. Leostean, I. Ardelean, The modifier/former role of MoO_3 in some calcium–phosphate glasses, J. Alloys Compd. 556 (2013) 67–70.
[47] P. Duxson, G.C. Lukey, J.S.J. van Deventer, Physical evolution of Na-geopolymer derived from metakaolin up to 1000 °C, J. Mater. Sci. 42 (2007) 3044–3054.
[48] N. Essaidi, B. Samet, S. Baklouti, S. Rossignol, Effect of calcination temperature of Tunisian clays on the properties of geopolymers, Ceram. -Silik. 57 (2013) 251–257.
[49] A. Autef, E. Joussein, G. Gasnier, S. Pronier, I. Sobrados, J. Sanz, S. Rossignol, Role of metakaolin dehydroxylation in geopolymer synthesis, Powder Technol. 250 (2013) 33–39.

Publication 2 (ACL 2)

N. Essaidi, A. Gharzouni, L. Vidal, F. Gouny, E. Joussein, S. Rossignol

"Recycling of aluminosilicate waste: impact onto geopolymer formation"

The European Physical Journal: Special Topics, 2015, vol. 224, p. 1707-1713.

Eur. Phys. J. Special Topics **224**, 1707–1713 (2015)

DOI: 10.1140/epjst/10.1140/epjst/e2015-02492-9

THE EUROPEAN PHYSICAL JOURNAL SPECIAL TOPICS

Regular Article

Recycling of aluminosilicate waste: impact onto geopolymer formation

N. Essaidi[1], A. Gharzouni[1], L. Vidal[1,2], F. Gouny[1], E. Joussein[3], and S. Rossignol[1]

[1] Science des Procédés Céramiques et de Traitements de Surface (SPCTS) UMR 7315 CNRS, Ecole Nationale Supérieure de Céramique Industrielle, 12 rue Atlantis, 87068 Limoges Cedex, France.
[2] Groupe d'Etude des Matériaux Hétérogènes (GEMH), Ecole Nationale Supérieure de Céramique Industrielle, 12 rue Atlantis, 87068 Limoges Cedex, France
[3] Université de Limoges, GRESE EA 4330, 123 avenue Albert Thomas, 87060 Limoges, France.

Received 28 November 2014 / Received in final form 21 May 2015
Published online XX July 2015

Abstract. Geopolymers are innovative ecomaterials resulting from the activation of an aluminosilicate source by an alkaline solution. Their properties depend on the used raw materials. This paper focuses on the possibility to obtain geopolymer materials with aluminosilicate laboratory waste. The effect of these additions on the geopolymer properties was studied by FTIR spectroscopy and mechanical test. It was evidenced a slowdown of the polycondensation reaction as well as the compressive strength due to the addition of laboratory waste which decrease the Si/K ratio of mixture.

1 Introduction

Geopolymer materials have a lot of attention [1] as suitable binder because they are environmentally friendly and require less energy during their manufacturing process. These ecomaterials can be synthesized by the alkaline activation of aluminosilicates obtained from calcined clays, natural minerals and industrial wastes at room temperature. The properties of geopolymers are affected by two important factors which are the alkaline solution and the aluminosilicate source [2,3]. Autef et al. [2,4] highlighted that the purity and the reactivity of the metakaolin can lead to the formation of one or several networks which influence the working performances of the final material. Generally, for metakaolin-based geopolymers, the compressive strengths and Young's moduli ranged from 20 to 80 MPa and 2.5 to 5.5 GPa respectively [5]. In the case of fly ash based geopolymer, the compressive strength is about 61 MPa and the Young's modulus is 2.9 GPa [6].

Recently, economical and environmental demands encourage waste recycling in order to reduce the consumption of natural resources. Taking this into account, some studies focused on recycled aggregates incorporation in the geopolymer materials [7–9]. Indeed, Sata et al. [7] compared materials obtained with natural and recycled

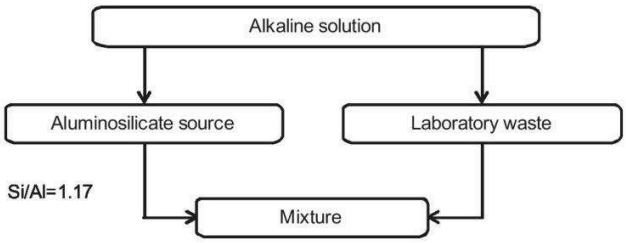

Fig. 1. Synthesis protocol of geopolymer samples.

coarse aggregates. They proved that recycled aggregates could be reused to make pervious geopolymer concretes. However, a loss in compressive strength was observed.

In this context, the aim of the current study is to investigate the influence of laboratory waste addition on geopolymer formation in order to minimize the cost and to focus on the life cycle of material. For this, different amounts of laboratory waste were added to geopolymer reactive mixture. The synthesized materials were characterized by FTIR spectroscopy and compression tests.

2 Experimental part

2.1 Raw materials and sample preparation

The experimental protocol of geopolymer synthesis is described in Fig. 1 [10]. The alkaline solution was obtained by dissolving potassium hydroxide pellets (VWR, 85.2% pure) in a commercial potassium silicate solution in order to maintain the $Si/K_{solution}$ molar ratio to 0.58. Then, laboratory aluminosilicate waste ($Si/Al = 1.66$), previously crushed and sieved through 80 μm, and metakaolin were added. The mass proportion of SiO_2, Al_2O_3 and K_2O in the waste is respectively 53, 28 and 19%. The waste proportion ranged from 10 to 30% of total mass. The reactive mixtures were placed in open polystyrene molds at room temperature. Samples are denoted as G^x, where x refers to the percentage of laboratory waste added. For example, G^{20} corresponds to a geopolymer with 20% of waste.

2.2 Technical characterization

Fourier-transform infrared (FTIR) spectroscopy in ATR mode was used to investigate the structural evolution of the geopolymer mixtures. The FTIR spectra were obtained using a ThermoFisher Scientific Nicolet 380 infrared spectrometer. The IR spectra were gathered over a range of 400 to 4000 cm^{-1} with a resolution of 4 cm^{-1}. The atmospheric CO_2 contribution was removed with a straight line between 2400 and 2280 cm^{-1}. To monitor the geopolymer formation, a software was used to acquire a spectrum (64 scans) every 10 minutes for 250 minutes. For comparison, the spectra were baseline-corrected and normalized [10].

X-ray patterns were collected from raw materials after they were crushed to 80 μm in size and were obtained from 5 to 70° (2θ) using a Brücker-AXS D5005 apparatus ($\lambda = 1.54056$ Å) equipped with a graphite-backed monochromator. The XRD patterns were obtained using a dwell time of 2 s and a step size of 0.04°(2θ). The crystalline phases were identified by comparing the patterns with powder diffraction file (PDF) standards from the International Center for Diffraction Data (ICDD).

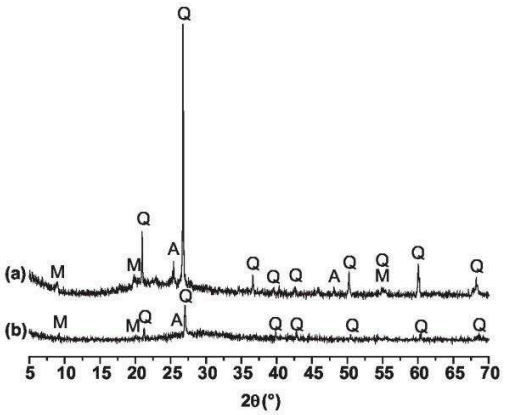

Fig. 2. X-rays patterns of (a) metakaolin and (b) laboratory waste (A: Anatase (PDF: 00-021-1272), M: Muscovite (PDF: 00-046-0741), and Q: Quartz (PDF: 00-046-1045)).

The compressive strengths were tested using a LLOYD EZ20 universal testing machine with a crosshead speed of 0.1 mm/min. The compressive tests were made on five samples for every composition. The samples were cylindrical in shape with a diameter (Φ) of 15 mm and a height (h) of approximately 30 mm, and were aged for 7 days in an open mold at room temperature. The compressive strength values represent the average of the obtained values and were expressed in MPa.

3 Results and Discussion

3.1 Feasibility of consolidated material

The raw materials were previously characterized by XRD analysis. The results are given in the Fig. 2. Briefly, the metakaolin pattern clearly evidence the presence of amorphous phases (dome at $2\theta = 22°$). All the main peaks are relative to presence of impurities such as quartz, anatase and micas. The waste laboratory displays also an amorphous component which is shifted to higher angle (dome at $2\theta = 30°$) traducing a more disturbed network [11]. This fact is in accordance with the BET values (17 and 50 m^2/g for the metakaolin and the laboratory waste respectively). All these data reveals the different reactivity of the materials.

A preliminary feasibility study of consolidated materials with different amounts of laboratory waste was carried out. The initial composition G^0 was based on the Prud'homme et al. studies [12]. Then, the laboratory waste was progressively added to the mixture up to 30%. The obtained materials were consolidated, homogeneous and show a geopolymer feature (Fig. 3a). The different compositions are reported in Si-Al-K ternary diagram (Fig. 3b). Previous studies [13] have evidenced the existence of various domains which are (A) geopolymer, (B) hardening material, (C) sedimented material and (D) gel. Whatever the amount of laboratory waste added, the studied compositions are still located in the geopolymer domain. To understand the effect of aluminosilicate laboratory waste addition on geopolymer formation, FTIR spectroscopy and mechanical test were performed.

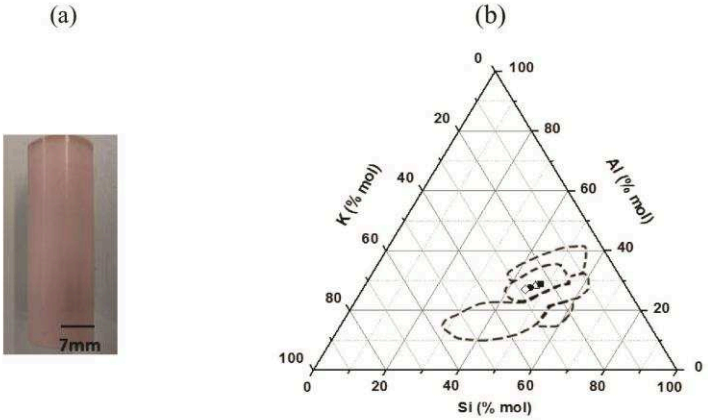

Fig. 3. (a) Photo of G^{20} geopolymer (Ø = 14 mm) and (b) position of the different G^x compositions with x = (■) 0, (Δ) 10, (•) 20 and (◇) 30% of laboratory waste. The various domains correspond to (A) geopolymer, (B) hardening material, (C) sedimented material and (D) gel.

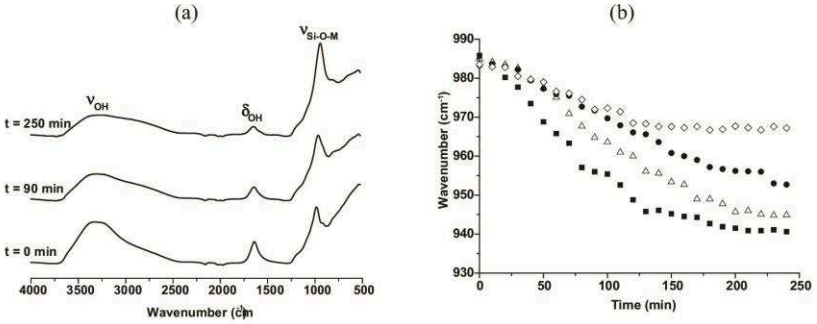

Fig. 4. (a) In situ FTIR spectra obtained at t = 0, 90 and 250 min and (b) Q^2 position versus time for the G^x samples with x = (■) 0, (Δ) 10, (•) 20 and (◇) 30% of laboratory waste added.

3.2 Effect of laboratory waste addition on the polycondensation rate

The various compositions were followed by FTIR spectroscopy. Examples of the obtained spectra for G^0 composition are shown in Fig. 4a. For the spectra at t = 0 min, the bands at 3200 and 1640 cm^{-1} were attributed to ν_{OH} and δ_{OH} respectively. The bands assigned to Si-O-M bonds (M = Si, Al, K) were located in the 1100-950 cm^{-1} range [12]. Over the time, the decrease of OH bands and the shift of Si-O-M band indicate the dissolution of metakaolin by the basic environment [14] and the occurrence of polycondensation reaction leading to the formation of specific networks [12,15,16].

The displacement of the Si-O-M band versus time was plotted in Fig. 4b for all samples. The slope at the beginning of the curve gives information about the kinetic of the reaction [12]. The displacement and the slope values relative to G^0 composition were approximately 45 cm^{-1} and -0.31 cm^{-1}/min. The addition of waste involves a

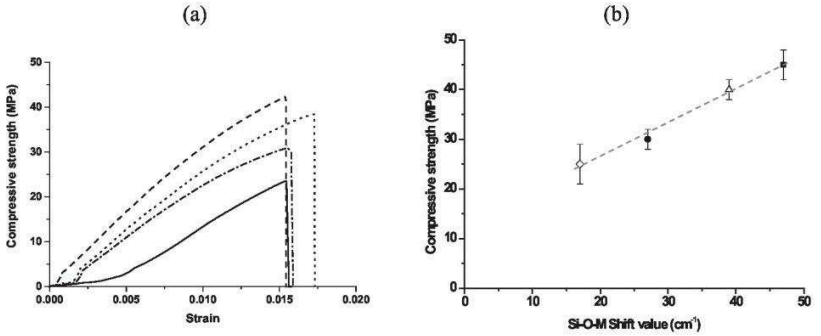

Fig. 5. (a) Variation of compressive strength versus strain for G^x reactive mixture with x = (- - -) 0, (• • •) 10, (-•-) 20 and (—) 30% of laboratory waste added and (b) evolution of the shift value as a function of the compressive strength for (■) G^0, (Δ) G^{10}, (•) G^{20} and (◇) G^{30}.

decrease of the shift from 39 to 17 cm^{-1} and the slope from −0.26 to −0.12 cm^{-1}/min for G^{10} and G^{30} respectively. The variation of the shift value indicates the presence of various geopolymer networks [4]. Indeed, the low reactivity of laboratory waste may lead to a geopolymer network associated with unreacted waste coated by the alkaline solution. The presence of non-reactive species provided by the aluminosilicate laboratory waste will disrupt the exchange between reactive aluminous and siliceous species. This phenomenon is exacerbated by the increase of waste in the reactive mixture. Moreover, the waste addition affects the kinetic of the reaction. In fact the decrease of the slope value evidences the slowdown of the polycondensation reaction due to the presence of inactive species provided from the laboratory wastes which disturb the reaction. To sum up, these data show the effect of waste addition on the geopolymerization reaction rate and suggest different mechanical properties.

3.3 Effect of laboratory waste addition on the mechanical properties and correlation with polycondensation rate

The influence of laboratory waste on the mechanical properties was evaluated by compression test. The variation of the compressive strength values as a function of strain is presented in Fig. 5a. Regardless of the sample, the obtained curves presented a linear variation characteristic of elastic regime followed by a slight plastic deformation and a brittle failure. The waste addition implied a lower stiffness suggesting a decrease of the Young's modulus [17]. To verify this hypothesis, the Young's modulus of each sample was calculated from the linear stress / strain response [6,18]. The mechanical strengths and Young's moduli decreased from 45 to 25 MPa and from 2.9 to 2.3 ± 0.2 GPa respectively. The standard deviation for the compressive strength is approximately 2 MPa. These values are in agreement with literature [19]. Previous studies about the incorporation of sand in geopolymers show the same evolution [20]. The authors explained this phenomenon by the fact that the sand is not dissolved and does not participate to the reaction. Consequently, in the case of waste addition, the loss of strength can be due to the non or poor reactivity of the waste compared to metakaolin in an alkaline environment. To confirm this hypothesis and exacerbate the reactivity of the aluminosilicate laboratory wastes, a composition based on only

laboratory waste was prepared. This composition did not lead to consolidate materials which corroborate the low reactivity of the waste.

In order to better understand these phenomena, a correlation between the FTIR and mechanical results was established. The evolution of the compressive strength versus the shift is presented in Fig. 5b. The compressive strength values seem to vary linearly with the shift values and decrease as the amount of laboratory waste increases. This may be due to the decrease of the $Si/K_{composition}$ molar ratio in the alkaline solution taking into account the amount of potassium released from the waste (0.58, 0.53, 0.48 and 0.44 for G^0, G^{10}, G^{20} and G^{30} respectively). It seems that an excess of potassium (lower Si/K ratio) can inhibit the polymerization of the species in the solution and consequently limit the formation of a geopolymer network leading to lower shift values and compressive strengths [21]. Indeed, Autef et al. [2] have demonstrated that the decrease of the Si/K molar ratio from 0.8 to 0.35 induces the decrease of the mechanical properties from 45 MPa to 5 MPa. In these conditions, an excess of the alkali prevents the polymerization of species in solution which affects the reactivity of the mixture and alters the structure, then the mechanical properties of formed materials. These results are in accordance with FTIR analysis.

4 Conclusion

This study evidenced the possibility of re-using aluminosilicate laboratory waste to synthesize consolidated materials. It was shown that the laboratory waste addition influences the polycondensation rate as well as the mechanical strength, still acceptable to consolidated materials. The low reactivity of these incorporated materials disturbs the geopolymerization reactions and lead to the formation of different networks. These networks induce the presence of some weaknesses into the final material due to a lower Si/K ratio in the mixture. However, this hypothesis needs to be confirmed by microstructural characterization in further work.

The authors thank the Limousin council and the FEDER for financing this study.

References

1. J.S.J. Van Deventer, J.L. Provis, P. Duxson, Miner. Eng **29**, 89 (2012)
2. A. Autef, PhD thesis, University of Limoges (2013)
3. A. Gharzouni, E. Joussein, S. Baklouti, S. Pronier, I. Sobrados, J. Sanz, S. Rossignol, J. Sol-Gel Sci. Technol. Article in press (2014)
4. E. Prud'homme, P. Michaud, E. Joussein, A. Smith, C. Peyratout, I. Sobrados, J. Sanz, S. Rossignol, J. Sol-Gel Sci. Technol **61**, 436 (2012)
5. P. Duxson, J.L. Provis, G.C. Lukey, S.W. Mallicoat, W.M. Kriven, J.S.J. Van Deventer, Colloids Surf. A **269**, 47 (2005)
6. E. Ul Haq, S. Kunjalukkal Padmanabhan, A. Licciulli, Ceram. Int. **40**, 2965 (2014)
7. V. Sata, A. Wonsga, P. Chindaprasirt, Constr. Build. Mater. **42**, 33 (2013)
8. X.S. Shi, F.G. Collins, X.L. Zhao, Q.Y. Wang, J. Hazard. Mater. **237-238**, 20 (2012)
9. A.R.M. Ridzuan, M.M. Al Bakri Abdullah, M.F. Arshad, M.F. Mohd Tahir, A.A. Khairulniza, Mater. Sci. Forum **803**, 194 (2014)
10. E. Prud'homme, P. Michaud, E. Joussein, J.M. Clacens, S. Rossignol, J. Non-Cryst. Solids **357**, 1270 (2011)
11. E. Prud'homme, P. Michaud, E. Joussein, J-M. Clacens, S. Arii-Clacens, I. Sobrados, C. Peyratout, A. Smith, J. Sanz, S. Rossignol, J. Non-Cryst. Solids **357**, 3637 (2011)
12. E. Prud'homme, PhD thesis, University of Limoges, (2011)

13. X.X. Gao, A. Autef, E. Prud'homme, P. Michaud, E. Joussein, S. Rossignol, J. Sol-Gel Sci. Technol. **65**, 220 (2013)
14. W.K.W. Lee, J.S.J. Van Deventer, Langmuir **19**, 8726 (2003)
15. C.A. Ress, J.L. Provis, G.C. Luckey, J.S.J. Van Deventer, Langmuir **23**, 8170 (2007)
16. C.A. Ress, J.L. Provis, G.C. Luckey, J.S.J. Van Deventer, Langmuir **23**, 9076 (2007)
17. J. He, J. Zhang, Y. Yu, G. Zhang, Constr. Build. Mater. **30**, 80 (2012)
18. M. Zhang, H. Guo, T. El-Korchi, G. Zhang, M. Tao, Constr. Build. Mater. **47**, 1468 (2013)
19. P. Duxson, J.L. Provis, G.C. Lukey, S.W. Mallicoat, W.M. Kriven, J.S.J. Van Deventer, Colloids Surf. A **269**, 47 (2005)
20. A. Autef, E. Joussein, G. Gasgnier, S. Rossignol, J. Non-Cryst. Solids **358**, 2886 (2012)
21. A. Autef, E. Joussein, G. Gasgnier, S. Rossignol, Ceram. Eng. Sci. Proc. **34**, 3 (2014)

Publication 3 (ACL 3)

A. Gharzouni, L. Vidal, N. Essaidi, E. Joussein, S. Rossignol

"Recycling of geopolymer waste: Influence on geopolymer formation and mechanical properties"

Materials and Design, 2016, vol. 94, p. 221-229.

Materials and Design 94 (2016) 221–229

Contents lists available at ScienceDirect

Materials and Design

journal homepage: www.elsevier.com/locate/matdes

Recycling of geopolymer waste: Influence on geopolymer formation and mechanical properties

A. Gharzouni [a], L. Vidal [a], N. Essaidi [a], E. Joussein [b], S. Rossignol [a,*]

[a] Univ Limoges, CNRS, ENSCI, SPCTS, UMR7315, F-87000 Limoges, France
[b] Univ Limoges, GRESE, EA 4330, F-87000 Limoges, France

ARTICLE INFO

Article history:
Received 18 November 2015
Received in revised form 8 January 2016
Accepted 9 January 2016
Available online 12 January 2016

Keywords:
Recycling
Geopolymer waste
Alkaline solution
Metakaolin
Mechanical properties
Reactivity

ABSTRACT

Geopolymers are new binders resulting from the activation of an aluminosilicate source by an alkaline solution. These binders are economically and environmentally profitable since they have the advantage of reusing recycled waste and industrial by-products as aluminosilicate sources. In this context, this paper focuses on the geopolymer wastes incorporation in different formulations and their effect on geopolymer formation and the properties of the final materials. For this purpose, the geopolymer wastes were at first characterized. Three compositions differing in the used alkaline solution and the amount of metakaolin added were investigated. A feasibility study allowed retaining 20% as the waste percentage added or substituted to the metakaolin to still obtain geopolymer materials. Moreover, it was shown that the incorporation of the geopolymer waste may disturb the polycondensation rate which was proven to strongly depend on the solid to liquid ratio and the Si/K ratio of the alkaline solution. Finally, relationships were demonstrated between the compressive strengths and the chemical compositions of the different samples. The low reactivity of geopolymer waste can be compensated with the use of highly reactive alkaline solution or the increase of the amount of metakaolin in the mixture.

1. Introduction

In recent years, the growth of waste production associated with the awareness of the environmental problems and the need of sustainable development make waste management a priority [1]. Recycling has drawn great interest as a way to solve waste problems, reduce environmental pollutions and preserve natural resources. For example, the glasses are reused in glass or enamel compositions as cullet and allow lowering the energy and the raw material consumption [2]. Others examples are concretes or ceramics which are crushed and used as aggregates in new concretes [3,4]. In this context, geopolymer materials are a new class of binders having the advantage of using industrial byproducts and recycled waste. These binders are generated from the activation of an aluminosilicate source with an alkaline solution [5,6]. Their formation implies the dissolution of aluminosilicate species in an alkaline environment to form an amorphous three-dimensional geopolymer network by polycondensation reaction. Based on such a unique structure, geopolymers may exhibit good mechanical, chemical and thermal properties making them a promising alternative for a variety of applications [7]. Diverse industrial by-products were proven to be suitable for producing geopolymer materials such as fly ash [8,9], furnace slag [9,10,11], red mud [12], mine waste mud [13], waste concrete [14] and construction and demolition waste [15]. He et al., [12] established a comparative study between two types of geopolymers based on metakaolin and a mixture of red mud and fly ash. The lower strength obtained for a mixture of red mud and fly ash sample were attributed to the reactivity of the raw materials. The final materials were composed of a geopolymer binder and unreacted phases present as inactive fillers. This fact was also evidenced by Komnitsas et al. [15], in the case of construction and demolition waste-based geopolymers. Indeed, they observed a heterogeneous matrix containing grains of various sizes and attributed this to the partial reaction of the initial concrete. Similarly, Gao et al. [16], demonstrated that the compressive strength firstly increased up to 20% of fly ash content and then decreased as the fly ash content increased into metakaolin-slag blends.

Nazari and Sanjayan [17] proved the possibility of producing geopolymers using aluminum and cast iron slags. They highlight that the silica to alumina ratio is the most important parameter governing the mechanical properties. Onutai et al. [18] evidenced that 40 wt.% of Al waste content in geopolymer mixture lead to a dense structure and therefore optimal compressive strength. Moreover, investigation study about the influence of different types of aggregates, such as lime stone, schist and granite, on the properties of geopolymeric mine waste mud binder was undertaken. It was demonstrated that the aggregate dimensions affect the tensile strength. Ferone et al. [19] have shown the suitability of calcined clay sediments for geopolymer synthesis and evidenced the role of heat treatment temperature on the reactivity. In addition to that, the immobilization of heavy metals in municipal solid waste incineration fly ash based geopolymer was evidenced [20]. The mechanical properties

* Corresponding author.
E-mail address: sylvie.rossignol@unilim.fr (S. Rossignol).

http://dx.doi.org/10.1016/j.matdes.2016.01.043
0264-1275/

and microstructure of the resulting materials were directly linked to the alkaline solution dosage and the Si/Al molar ratio. According to these studies, there are different remaining problems to consider. Indeed, the authors evidenced that the use of wastes implies a decrease of the compressive strength, a contamination coming from the wastes and the low reactivity of these materials. In order to improve the results, it seems to be necessary to determine the optimum amount of wastes for the addition or the substitution of raw materials.

So far, as extensive research on geopolymer has been conducted, the generation of geopolymer waste increases. In this context, an innovative use of geopolymer waste is their incorporation in different geopolymer formulations which is in accordance with the "cradle to cradle" concept. Moreover, reusing these geopolymers allow reducing the amount of raw materials used. Recycling of waste and their use as aluminosilicate sources seems to be profitable since it economical and environmental benefits, leading to greener manufacturing and global sustainable development. Recent investigations using recycling aggregates produced in laboratory point out to the fact that the use of fine recycled aggregates must not exceed 30%, otherwise the performance could be at risk [14]. Current recycled aggregates have particles of impurities such as soil, plastics, wastepaper wood, metals and organic matter. Organic matter leads to lower mechanical performance and lower concrete durability. Moreover, Park and Noguchi [21] studied concrete containing metal impurities and it was found that aluminum caused performance degradation.

The present work aims to evaluate the suitability of using crushed geopolymer in addition or substitution of metakaolin to produce geopolymers materials. For this, the used raw materials were characterized. Then, the feasibility of consolidated materials was evaluated. Several samples were prepared by varying the proportion of geopolymer waste. The structural evolution of the reactive mixtures was monitored by FTIR spectroscopy. Finally, the consolidated materials were characterized by compression tests.

2. Experimental part

2.1. Raw materials and sample preparation

The consolidated materials were prepared by mixing the metakaolin (MK) and the geopolymer, crushed and sieved at 80 μm, in an alkaline solution (AS) as described in Fig. 1 [22,23]. The reactive mixtures were placed in open polystyrene molds at room temperature for 7 days. Three formulations, differenced by the amount of metakaolin and the starting silicate solution were studied. The two silicate solutions, denoted as S1 and S3, differ in terms of the Si/K molar ratio (1.7 for S1and 0.7 for S3) and the water contents (79% for S1 and 59% for S3) [24,25].

For each composition, the effect of the substitution of an amount of metakaolin (MK) by crushed geopolymer (CG) or the addition of this compound was investigated. So, three sets are synthesized. Samples were synthesized either by adding the crushed geopolymer to metakaolin or substituting an amount of metakaolin by crushed geopolymer. Samples are denoted as $^{x,Si}G^{y}$ or $^{x,Si}G^{Sy}$ where x refers to the quantity of metakaolin, Si is the type of the used silicate solution, y the percentage of crushed geopolymer added to the mixture and ^{Sy} the percentage of crushed geopolymer which substitutes an amount of metakaolin mass. For example $^{12,S1}G^{S20}$ refers to the geopolymer obtained from the substitution of 20% of 12 g of metakaolin by crushed geopolymer using S1 as a silicate solution. The nomenclature and the composition of the samples analyzed are presented in the Table 1.

2.2. Technical characterization

The chemical composition of the precursors was determined using X-ray fluorescence (XRF). This technique allows the quantification of the atomic elements.

The particle size distributions of the raw materials were measured using a laser particle size analyzer (Mastersizer 2000). The mixture contained 1 g of aluminosilicate precursor in 20 ml of water, mixed by ultrasound to eliminate any aggregation. The measured particle sizes are in the range 0.05–880 μm. Additionally, the concentration of the solution should not be too large (obscuration < 35%).

Powder BET surface areas were determined by N_2 adsorption at −195.85 °C using a Micrometrics Tristar II 3020 volumetric adsorption/desorption apparatus. Prior to the measurement, the samples were degassed at 200 °C under vacuum for 4 h.

Bulk density was measured by pycnometer method. Numerically, it represents the mass per unit volume of matter. The SI unit of density is kg/m^3.

The wettability (water demand) of a powder is the volume of water that can be absorbed by 1 g of powder until saturation. This quantity depends directly on the particle size, the specific surface and the morphology of powder. One gram of powder is weighted and then deposited on a glass slide. Using a micropipette, the water is added to the powder (microlite by microlite) until visual saturation of the granular.

The pH values were measured using a Schott Instrument Lab860 pH-meter at 25 °C during the first 400 min of the geopolymer formation. A 2.4 g sample was immersed in 30 mL of osmosed water, which provided a solid to liquid ratio of 0.08 [26].

The mineral phases were identified by powder X-ray diffraction (XRD) with a BRUKERAXS D8 Advance powder diffractometer using CuKα radiation (λKα = 0.154186 nm). The analytical range used was between 5° and 70° with a step size of 0.04° and an acquisition time of 2 s. JCPDS (Joint Committee Powder Diffraction Standard) files were used for phase identification.

Fourier-transform infrared (FTIR) spectroscopy in ATR mode was used to investigate the structural evolution of the geopolymer mixtures. The FTIR spectra were obtained using a ThermoFisher Scientific Nicolet

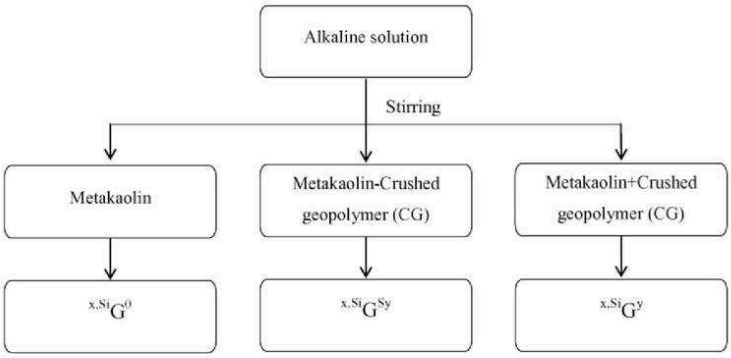

Fig. 1. Synthesis protocol of the various consolidated samples.

Table 1
Nomenclature and compositions of the different studied mixtures.

Set	Nomenclature	Mass of metakaolin (g)	Solution type	% geopolymer waste	Si/Al	Si/K
1	$^{12,S1}G^0$			0	1.66	2.09
	$^{12,S1}G^{20}$	12	S1	20		
	$^{12,S1}G^{S20}$			20	1.76	1.80
2	$^{12,S3}G^0$			0	1.72	1.67
	$^{12,S3}G^{20}$	12	S3	20		
	$^{12,S3}G^{S20}$			20	1.84	1.45
3	$^{20,S1}G^0$			0	1.41	3.09
	$^{20,S1}G^{20}$	20	S1	20		
	$^{20,S1}G^{S20}$			20	1.45	2.63

380 infrared spectrometer. The IR spectra were gathered over a range of 400 to 4000 cm^{-1} with a resolution of 4 cm^{-1}. The atmospheric CO_2 contribution was removed with a straight line between 2400 and 2280 cm^{-1}. To monitor the geopolymer formation, a software was used to acquire a spectrum (64 scans) every 10 min for 13 h. For comparison, the spectra were baseline-corrected and normalized.

The compressive strengths were tested using a LLOYD EZ20 universal testing machine with a crosshead speed of 0.1 mm/min. The compressive tests were made on five samples for every composition. The compressive strength values represent the average of the five obtained values and were expressed in MPa. The samples were cylindrical in shape with a diameter (Φ) of 15 mm and a height (h) of approximately 30 mm, and they were aged for 7 days in an open mold at room temperature.

3. Results

3.1. Raw materials characterization

The properties of the geopolymers are strongly influenced by the raw materials used for their synthesis. In this study, the raw materials used in the preparation of the samples, such as the metakaolin (MK) and various crushed geopolymers (CG), are characterized using several methods.

The Si/K and Si/Al molar ratios and physical data of the precursors, such as the specific surface, the D_{50} (particle size) and the wettability values are reported in Table 2. The Si/Al ratio is deduced from their chemical composition. It is about 1.17 for MK whereas for the $^{12,S1}CG^0$, $^{12,S3}CG^0$ and $^{20,S1}CG^0$ crushed geopolymers, these ratios are 1.66, 1.72 and 1.41 respectively. These higher values for CG compared to MK are due to the additional silicon provided by the silicate solution. In the case of $^{20,S1}CG^0$, the lower value can be explained by the higher amount of metakaolin. The Si/K ratio is about 2.09, 1.67 and 3.09 for $^{12,S1}CG^0$, $^{12,S3}CG^0$ and $^{20,S1}CG^0$ respectively. These differences are related to the Si/K molar ratio of the alkaline solution (0.58, 0.51 and 0.47 for $^{12,S1}CG^0$, $^{12,S3}CG^0$ and $^{20,S1}CG^0$ respectively), to the different silicate solutions used (S1 or S3) and to the various metakaolin contents (12 or 20 g).

The d_{50} values of $^{12,S1}CG^0$, $^{12,S3}CG^0$ and $^{20,S1}CG^0$ are 5.9, 3.6 and 3.6 μm respectively while MK has a slightly greater D_{50} of approximately 10 μm. According to the BET measurements, the $^{12,S1}CG^0$ exhibits the highest specific surface area (125 m^2/g) followed by $^{12,S3}CG^0$ and $^{20,S1}CG^0$ which have similar specific surface areas (≈53 m^2/g). MK has the lowest specific surface area (17 m^2/g). The wettability values are 611, 523, 744 and 758 μl/g for $^{12,S1}CG^0$, $^{12,S3}CG^0$, $^{20,S1}CG^0$ and MK respectively. The bulk densities of these precursors are 2.24, 2.15, 2.35 and 2.63 g/cm^3 for $^{12,S1}CG^0$, $^{12,S3}CG^0$, $^{20,S1}CG^0$ and MK respectively. These values are almost similar. The crushed geopolymers $^{12,S1}CG^0$, $^{12,S3}CG^0$ and $^{20,S1}CG^0$ indicate a pH value of about 11 which is the common pH value of geopolymer materials in compliance with the work of Aly et al. [27]. The metakaolin has a pH value of 7 [28]. The measured pH value denotes the presence of alkaline species in solution released from geopolymers. The physicochemical characterizations have shown similar results for the three CG samples. The main differences are due to the different chemical composition of the starting geopolymer materials. This may also be indicative of various amorphous phase contents in the three samples.

To validate this hypothesis, XRD analyses were performed. The resulting XRD patterns (Fig. 2) display a broad peak characteristic of an amorphous material and peaks relative to crystalline phases such as quartz, muscovite and anatase. These phases present in the crushed geopolymer are explained by the fact that there were not altered as in metakaolin. The shift of the amorphous dome position between MK ($2\theta \approx 23°$) and the crushed geopolymer ($2\theta \approx 30°$) indicates the dissolution of SiO_4 and AlO_4 tetrahedra in alkaline solution [29]. Furthermore, the amorphous dome is more pronounced for $^{12,S1}CG^0$ evidencing higher amorphization in comparison with the other precursors. This phenomenon explained the higher BET value obtained for this sample.

All these distinct data suggest that the various precursors (metakaolin and crushed geopolymers) might have different reactivities in the alkaline solution and therefore on the feasibility of consolidated materials based on these precursors.

3.2. Feasibility of consolidated materials

In order to evaluate the feasibility of consolidated materials using crushed geopolymer, several formulations were synthesized. Three compositions denoted as $^{12,S1}G^0$, $^{12,S3}G^0$ and $^{20,S1}G^0$ were considered as reference materials. They differ in terms of the amount of metakaolin (12 g of metakaolin for $^{12,S1}G^0$ and $^{12,S1}G^0$, $^{12,S3}G^0$ vs 20 g for $^{20,S1}G^0$) and the type of the solution as detailed in Table 1.

Then, for each composition, a set of samples was synthesized either by addition or substitution of crushed geopolymer up to 100% of metakaolin's mass. Based on their visual aspects and consolidated states, the domains of feasibility of consolidated materials as well as geopolymers were defined in function of the amount of crushed geopolymer in the mixture and the Si/K molar ratio of the activating solution in Fig. 3(A).

For the first set ($^{12,S1}G^y$), the Si/K molar ratio of the alkaline solution is about 0.58. The consolidated materials were obtained until 90% of crushed geopolymer substituting the metakaolin. Above this value, sedimented materials showing different layers were obtained. Indeed, the crushed geopolymer remains in the bottom layer and the excess of solution is in the upper layer. This fact suggests differences in reactivity between the metakaolin and the crushed geopolymer in an alkaline media. On the other hand, when crushed geopolymer is added to the mixture, consolidated materials were obtained up to 50% of crushed geopolymer. Above this percentage, there is an excess of aluminosilicate

Table 2
Physical and chemical properties of the raw materials.

Raw materials	Molar ratios		D_{10} (μm)	D_{50} (μm)	D_{90} (μm)	BET value (m^2/g)	pH value	Wettability w (μl/g)	Bulk density (g/cm^3)
	Si/Al	Si/K							
MK	1.17	–		10.0		17	7.92	758	2.63
$^{12,S1}G^0$	1.66	2.09	2.0	5.9	15.1	125	10.67	611	2.24
$^{12,S3}G^0$	1.72	1.67	1.3	3.6	9.3	54	10.61	523	2.15
$^{20,S1}G^0$	1.41	3.09	1.3	3.6	9.6	51	10.83	744	2.35

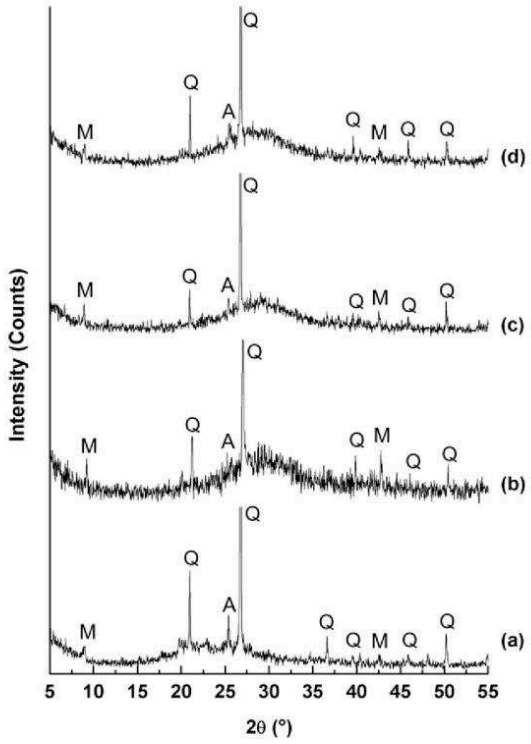

Fig. 2. XRD patterns of raw materials (a) MK, (b) $^{12,S1}G^0$, (c) $^{12,S3}G^0$, and (d) $^{20,S1}G^0$. Q: quartz, M: muscovite, and A: anatase.

source. The amount of species coming out from the solution is not enough to wet and completely alter the aluminosilicate source to initiate a polycondensation reaction. The materials exhibiting geopolymer features, homogenous and brilliant aspect were only obtained up to 50% of crushed geopolymer substituting the metakaolin or added to the mixture. For the second set ($^{12,S3}G^y$), with a Si/K molar ratio of 0.51, 50% of crushed geopolymer for both substitution and addition permit to obtain consolidated materials. The percentage of substitution is lower than the first set ($^{12,S1}G^y$) regarding the lower water content in S3 starting solution. Taking this fact into account, above 50% of crushed geopolymer, there is not enough silicate to dissolve the entire aluminosilicate source. In fact, the water content in silicate solutions is known to play a crucial role during and after synthesis since it affects the viscosity and the workability during mixing as well as the structure and the properties of the materials [30]. Indeed, the increase of the water content in the solution leads to the polymerization of the silicate species which will have an influence on the polycondensation reactions. The geopolymer zone extends only to 40% and 25% of crushed geopolymer for substitution and addition respectively. For the last set ($^{20,S1}G^y$), with a Si/K molar ratio of 0.47, consolidated materials are feasible up to 50% of substitution of metakaolin by crushed geopolymer and only up to 20% of addition. The percentage of addition is lower than the two others sets because the reference composition ($^{20,S1}G^0$) was already charged in metakaolin compared to $^{12,S1}G^0$ and $^{12,S3}G^0$ samples.

Furthermore, it is noticed that the feasibility of consolidated and geopolymer materials increases as the Si/K molar ratio of the alkaline solution increases. In fact, it was demonstrated that the Si/K molar ratio controls the nature and the amount of siliceous species present in the solution. The increase of this ratio from 0.35 to 0.60 leads to the formation of oligomers to the detriment of monomers and the increase of the non-bridging oxygen atom (NBO). According to Autef et al. [31],

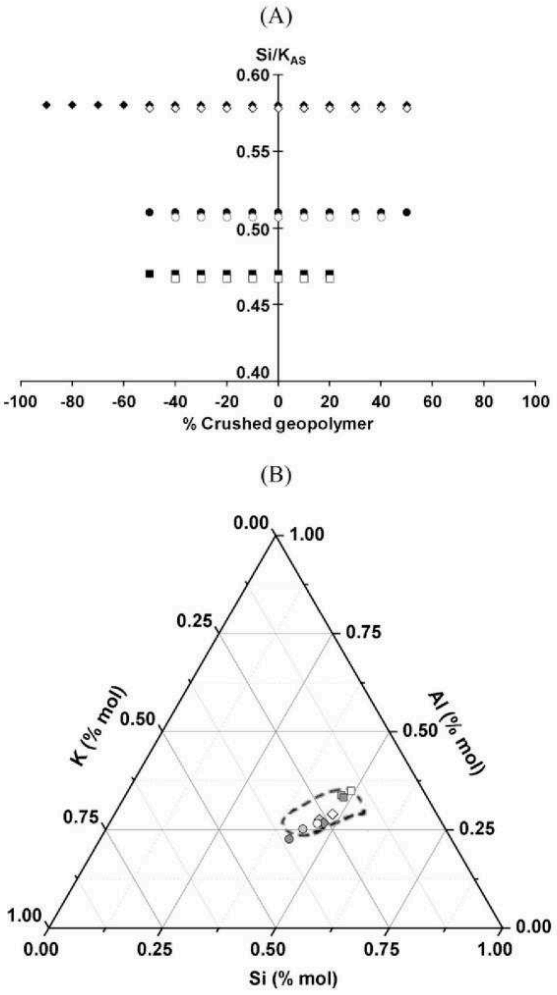

Fig. 3. (A) Feasibility domains for (♦) $^{12,S1}G^y$, (●) $^{12,S3}G^y$ and (■) $^{20,S1}G^y$ and geopolymer domains for (◊) $^{12,S1}G^y$, (○) $^{12,S3}G^y$ and (□) $^{20,S1}G^y$ and (B) position of the different compositions (◊) $^{12,S1}G^0$, (♦) $^{12,S1}G^{20}$, (♦) $^{12,S1}G^{S20}$, (○) $^{12,S3}G^0$, (●) $^{12,S3}G^{20}$, (●) $^{12,S3}G^{S20}$, (□) $^{20,S1}G^0$, (■) $^{20,S1}G^{20}$, (■) $^{20,S1}G^{S20}$ on the Si—Al—K/O ternary.

an increase of the Si/K ratio from 0.35 to 0.60 favors the formation of the geopolymer phase. This fact was explained by a decrease of the connectivity of the silicate anions and, consequently, inhibits the network polymerization due to the very high alkalinity of the solution. In the following sections, to exacerbate the effect of addition and substitution of crushed geopolymer on the polycondensation rate and the working properties of the final materials, only the compositions ($^{12,S1}G^0$, $^{12,S1}G^{20}$ and $^{12,S1}G^{S20}$), ($^{12,S3}G^0$, $^{12,S3}G^{20}$ and $^{12,S3}G^{S20}$) and ($^{20,S1}G^0$, $^{20,S1}G^{20}$ and $^{12,S1}G^{S20}$) were chosen for characterization.

To validate the previously discussed data, the chosen samples were reported in Al–Si–K–O ternary diagram as presented in Fig. 3(B). According to previous work [32], it was evidenced the existence of various domains depending on the Si/Al and Si/K molar ratios which are (A) geopolymer, (B) hardening material, (C) sedimented material and (D) gel. It was confirmed that all samples, for both addition and substitution of 20% of crushed geopolymer, were located in the geopolymer zone.

In order to investigate the effect of aluminosilicate waste on geopolymer formation, FTIR spectroscopy and mechanical tests were performed.

3.3. Characterization of selected compositions

3.3.1. Effect of the crushed geopolymer on the polycondensation rate

The formation of the geopolymer was the result of a geopolymerization reaction involving the restructuration of material which could be followed by FTIR spectroscopy. Example of the spectra obtained at different time for $^{12,S1}G^0$ sample are shown in Fig. 4(A). All the spectra exhibit the contributions at 3200 and 1640 cm^{-1} attributed to the ν_{OH} and δ_{OH} respectively. A broad band is also observed in the 1100–950 cm^{-1} range and is assigned to the Si—O—M (M = Si, Al) bond. Over time, the intensity of the ν_{OH} and δ_{OH} bands gradually decreases whereas the Si—O—M contribution shifts towards lower wavenumber. This variation reveals a polycondensation reaction and is characteristic of the formation of a specific network [33,34]. The evolution of Si—O—M band position versus time is plotted in Fig. 4(B). A displacement of this band to lower wavenumber is noticed. Indeed, the Si—O—M peak position shifts from 969 cm^{-1} to 940 cm^{-1} during 250 min. This is in agreement with the literature data [29] and it evidences the dissolution of the metakaolin species by the basic environment. Furthermore, the shift value denotes the replacement of Si—O—Si by Si—O—Al bonds during the geopolymerization and the calculated slope value at the beginning of the curve gives information about the kinetic of the reaction.

In order to understand the effect of the presence of crushed geopolymer in the mixture, the displacement of the Si—O—M band versus time for all samples was plotted in Fig. 5. All the samples show a shift of Si—O—M band to lower wavenumber. The initial peak positions are similar for the $^{12,S1}G^y$ and $^{20,S1}G^y$ samples (986 and 980 cm^{-1} respectively) whereas it is lower for $^{12,S3}G^y$ mixtures (969 cm^{-1}). This difference is explained by the different initial alkaline solutions. Indeed, the similar initial peak position for $^{12,S1}G^y$ and $^{20,S1}G^y$ geopolymers are due to the use of S1 solution contrary to $^{12,S3}G^y$ sample. These two solutions have different silicate species as shown by Gharzouni et al. [24,25]. Then, for $^{12,S1}G^y$ mixtures (Fig. 5(A)), the addition of CG implies a diminution of the shift value (from 47 to 27 cm^{-1} for $^{12,S1}G^0$ and $^{12,S1}G^{20}$ samples respectively) slowing down the polycondensation reactions. This fact may reveal a low or non-reactivity of the CG. Indeed, according to previous work [15], the presence of low or non-reactive species provided by the waste disrupts the exchanges between reactive aluminous and siliceous

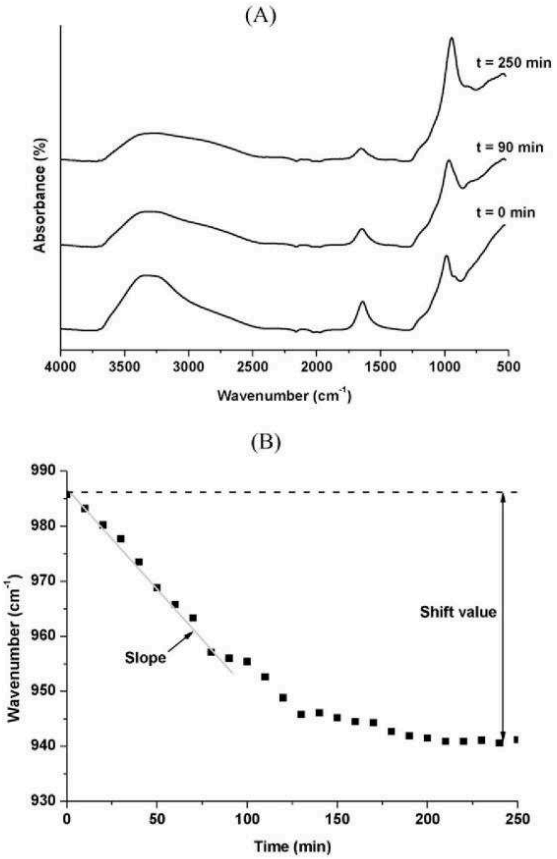

Fig. 4. In situ FTIR spectra obtained at t = 0, t = 90 and t = 250 min for the (A) $^{12,S1}G^0$ and (B) Q^2 position shift and slope from IR spectra versus time for the $^{12,S1}G^0$ sample.

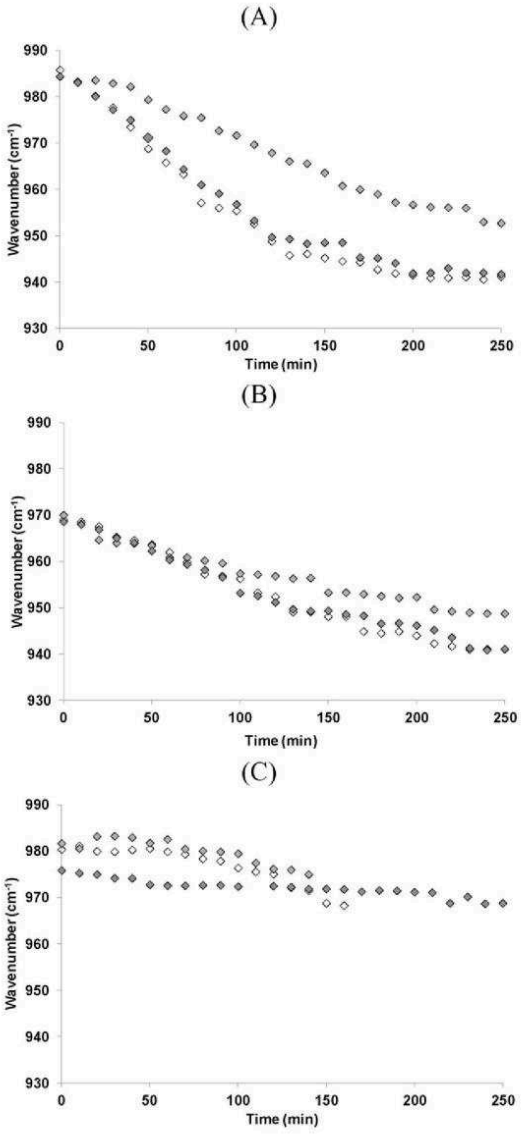

Fig. 5. Evolution of the shift of Q^2 position from FTIR spectra versus time for (A) $^{12,S1}G^X$, (B) $^{12,S3}G^X$ and (C) $^{20,S1}G^{SX}$ reactive mixtures with x = (◇) 0, (◈) 20 and (◆) S20% of crushed geopolymer.

species leading to a slowdown of the reactions. In the case of $^{12,S3}G^{y}$ samples (Fig. 5(B)), the addition of CG has no effect on the shift values (28 and 29 cm^{-1} for $^{12,S3}G^{0}$ and $^{12,S3}G^{20}$ mixtures respectively). The unchanged values observed are due to the fact that the alkaline solution governs the reactions. In fact, Gharzouni et al. [25] demonstrated that, when S3 is used, close shift values were observed for four metakaolins differing in terms of reactivity. Consequently, S3 solution governs the reactivity of the mixtures regardless the metakaolin properties. The addition of crushed geopolymers in the $^{20,S1}G^{y}$ mixtures (Fig. 5(C)) lead to weak variations of the shift values (21 and 13 cm^{-1} for $^{20,S1}G^{0}$ and $^{20,S1}G^{20}$ geopolymers respectively). In this case, the slight decrease of the shift values evidences that the effect of the presence of CG is associated to the influence of the high amount of metakaolin in these compositions. Some authors [26,35] showed that a high amount of metakaolin leads to a lack of reactive silicate species to completely react with the MK. A geopolymerization reaction took place but the attack of the MK being incomplete, the final material may exhibit a geopolymer network with unreacted MK particles. This is the phenomenon observed for the $^{20,S1}G^{0}$ sample. When CG is added, the reactions are also incomplete and the final material may contain unreacted CG and MK particles in a geopolymeric matrix.

Contrary to the addition, the substitution of an amount of metakaolin by crushed geopolymer does not have a significant effect on the various samples. For the $^{12,S1}G^{S20}$ sample, the unchanged shift values (44 cm^{-1} instead of 47 cm^{-1} for $^{12,S1}G^{0}$ mixture) may be explained by the low or non-reactivity of the waste. Indeed, the CG has a limited effect on the polycondensation degree of the network according to Gao et al. [16]. The authors showed that the substitution of a small amount of slag by fly ash leads to unchanged infrared band position and attributed this to the small influence of fly ash inclusions on the networks. Then, for the $^{12,S3}G^{y}$ set, the unchanged shift values (28 and 35 cm^{-1} for $^{12,S3}G^{0}$ and $^{12,S3}G^{S20}$ samples) may be due to the fact that the alkaline solution governs the geopolymerization reactions as it was observed for the addition. For the $^{20,S1}G^{y}$ samples, the shift values are also unchanged (21 and 16 cm^{-1} for $^{20,S1}G^{0}$ and $^{20,S1}G^{S20}$ samples) and this phenomenon could be explained by the low or non-reactivity of the waste as well as the small amount of CG substituting the metakaolin as previously seen. All these data evidenced a more pronounced effect of the geopolymer waste on the $^{12,S1}G^{y}$ mixtures. For the other two compositions, the limited effect of the waste is attributable at the use of a highly reactive solution or the higher amount of metakaolin.

The evolution of the shift versus the slope values calculated for all the samples is presented in Fig. 6. Different zones were determined depending on the shift and slope values [36]. For a slope and a shift higher than -0.10 cm^{-1}/min and 22 cm^{-1} respectively, there is the coexistence of several networks. The existence of a gel was determined for a shift and a slope lower than 22 cm^{-1} and -0.10 cm^{-1}/min respectively. Then, the junction of these two zones seems to be characteristic of geopolymer materials. According to the shift and slope values, different types of networks were identified for the studied samples [37]. All the samples from the $^{12,S1}G^{y}$ set are located in the zone were several networks coexists whereas the mixtures from the $^{12,S3}G^{y}$ and $^{20,S1}G^{y}$ sets are placed in the geopolymer domain. These results are in accordance with the previously discussed results and with the works of Gharzouni et al. [25]. However, for the first set ($^{12,S1}G^{y}$), the $^{12,S1}G^{0}$ sample is far from the geopolymer zone and the $^{12,S1}G^{20}$ mixture is closer to the geopolymer domain (decrease of the shift and slope values). The addition of CG seems to modify the behavior of the mixture and to lead to the presence of several networks different from those in the $^{12,S1}G^{0}$ sample. This fact may be explained by the low or non-reactivity of the waste which disrupts and slows down the exchanges between the reactive species during the geopolymerization process [22]. For the second and third set ($^{12,S3}G^{y}$ and $^{20,S1}G^{y}$), the $^{12,S3}G^{0}$, $^{12,S3}G^{20}$, $^{20,S1}G^{20}$ and $^{20,S1}G^{0}$ samples are located in the geopolymer zone. As it was seen previously, the waste addition does not seem to have a significant effect on the behavior of these materials. For the $^{12,S3}G^{y}$ set, this phenomenon is

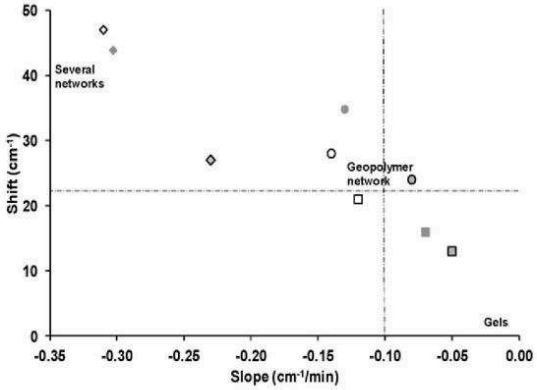

Fig. 6. Evolution of the shift versus the slope for different compositions (◇) $^{12,S1}G^{0}$, (◈) $^{12,S1}G^{20}$, (◆) $^{12,S1}G^{S20}$, (○) $^{12,S3}G^{0}$, (●) $^{12,S3}G^{20}$, (◉) $^{12,S3}G^{S20}$, (□) $^{20,S1}G^{0}$, (■) $^{20,S1}G^{20}$ and (▣) $^{20,S1}G^{S20}$ samples.

explained by the reactions governed by the alkaline solution. For the $^{20,S1}G^{y}$ set, the behavior is due to the high amount of MK in the reactive mixture. In fact, Liew et al. [35] showed that for a high quantity of metakaolin, the polycondensation reactions are incomplete. According to this, for the $^{20,S1}G^{20}$ sample, the effect of the CG may be associated to the influence of the amount of MK. Whatever the considered set, the substitution of an amount of MK by CG has no significant effect on the behavior of the different mixtures. Indeed, the $^{12,S1}G^{S20}$, $^{12,S3}G^{S20}$ and $^{20,S1}G^{S20}$ samples are located close to the reference samples ($^{12,S1}G^{0}$, $^{12,S3}G^{0}$ and $^{20,S1}G^{0}$ respectively). According to Gao et al. [16], the behavior of the three samples with substitution may be explained by the small amount of MK substituted by the waste which has a weak influence on the reactions.

So, the effect of the crushed geopolymer on the polycondensation rate can be counterbalanced by the use of a reactive alkaline solution or by the increase of the amount of metakaolin in the mixture. These differences in reactivity suggest the existence of variations on the mechanical properties of these compositions.

3.3.2. Effect of on geopolymer waste the mechanical properties

The influence of crushed geopolymer on the mechanical properties was evaluated by compressive test. The variation of compressive strength values as a function of strain for the three sets is illustrated in Fig. 7(A). Regardless of the sample, the obtained curves exhibited a linear variation characteristic of elastic regime followed by a slight plastic deformation and a brittle failure. The compressive strength value of samples, considered as reference, increased from 45, 68 to 76 MPa ± 0.2 for $^{12,S1}G^{0}$, $^{12,S3}G^{0}$ and $^{20,S1}G^{0}$ respectively. It is noticed, firstly, that the increase of the metakaolin amount from $^{12,S1}G^{0}$ to $^{20,S1}G^{0}$ seems to improve the mechanical properties. Then, the $^{20,S1}G^{0}$ display the highest compressive strength because it contains a high amount of metakaolin [38].

In the case of the addition 20% of crushed geopolymer and compared to reference samples, for the first set ($^{12,S1}G^{20}$), the compressive strength value decreases to 30 MPa ± 0.2. However, the mechanical properties of the second set ($^{20,S3}G^{20}$) are quite identical while 20% is added (about 70 MPa ± 0.2). The $^{20,S1}G^{20}$ has a compressive strength of 65 MPa ± 0.2 which is lower than $^{20,S1}G^{0}$. Consequently, it seems that the addition of crushed geopolymer decreases the compressive strength value especially for the first and third set. The loss of strength can be due to the non- or poor reactivity of the geopolymer crushed compared to metakaolin in an alkaline environment. This behavior is in agreement with the literature [12,39] since the aluminosilicate source based on metakaolin and crushed geopolymer as filler has been modified. The close values of mechanical properties for the second set ($^{12,S3}G^{20}$), can

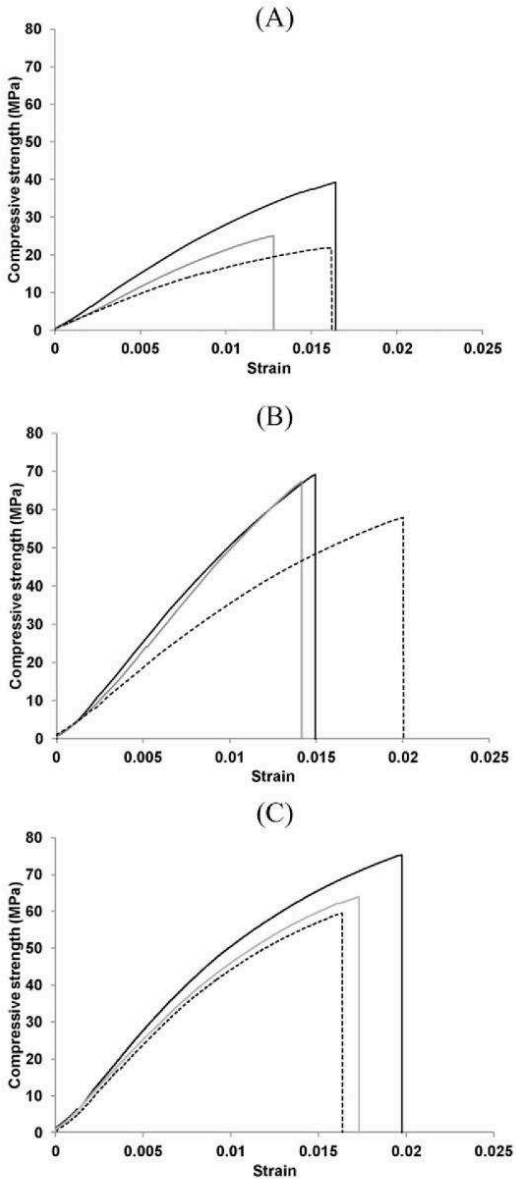

Fig. 7. Variation of compressive strength as a function of strain for (A) $^{12,S1}G^{x}$, (B) $^{12,S3}G^{Sx}$ and (C) $^{20,S1}G^{x}$ reactive mixtures with x = (—) 0, (---) 20, and (–) S20 of crushed geopolymer added.

be related to the use of highly reactive alkaline solution (S3) which govern the working properties as it was proved by Gharzouni et al. [25].

In the case of metakaolin substitution by crushed geopolymer, the compressive strength values decrease to (25, 60 to 62 MPa ± 0.2) for $^{12,S1}G^{S20}$, $^{12,S3}G^{S20}$ and $^{20,S1}G^{S20}$ respectively revealing that the mechanical properties decreased also with the substitution of metakaolin by crushed geopolymer. For the ($^{20,S1}G^{20}$ and $^{20,S1}G^{S20}$) compositions, the similar values are in relation with the crushed geopolymer source of aluminosilicate in presence of alkaline solution. Indeed, the $^{20,S1}G^{20}$ behaves as a geopolymer containing reinforcements in which the reactivity metakaolin is slowed in the presence of the alkaline solution, while for the $^{20,S1}G^{S20}$ sample, although metakaolin rate is lower, the alkaline solution allows dissolution which also leads to further enhanced geopolymer.

From these data, both the addition and the substitution of metakaolin by the crushed geopolymer diminish the compressive strength of the obtained materials.

4. Discussion

In order to understand the effect of crushed geopolymer incorporation in the different compositions on the polycondensation rate, the shift values were plotted versus the solid to liquid ratio (S/L) of each mixture normalized by the S/L of $^{12,S1}G^{0}$ sample (exhibiting the lowest S/L ratio) in Fig. 8(A). Typically, the shift values decreased with increasing the solid to liquid ratio (S/L). This ratio increased from 0.97 for $^{12,S1}G^{0}$ to 1.28 for $^{12,S3}G^{0}$ due to the lower water content in S3 solution and to 2.11 in the case of $^{20,S1}G^{0}$ higher amount of metakaolin in the case of $^{20,S1}G^{0}$. Whatever the composition, the substitution of metakaolin by crushed geopolymer maintains the same S/L ratio which explains the close obtained shift values (47 and 44 cm^{-1} for $^{12,S1}G^{0}$ and $^{12,S1}G^{S20}$ having a S/L ratio of about 0.97). However, the addition of crushed geopolymer increases the amount of aluminosilicate source and therefore increases the S/L ratio which corresponds to lower shift values compared to the reference compositions (27 cm^{-1} for $^{12,S1}G^{20}$ having a S/L ratio of 1.47). High shift values corresponding to low S/L suggest the existence of higher number of bonds between dissolved species and impurities of metakaolin engendering the formation of several networks as has been previously demonstrated by Autef et al. [37]. In fact, the high amount of activating liquid increases the mobility of species and, hence, facilitates the interaction between them. Liew et al. [35] have shown that low S/L

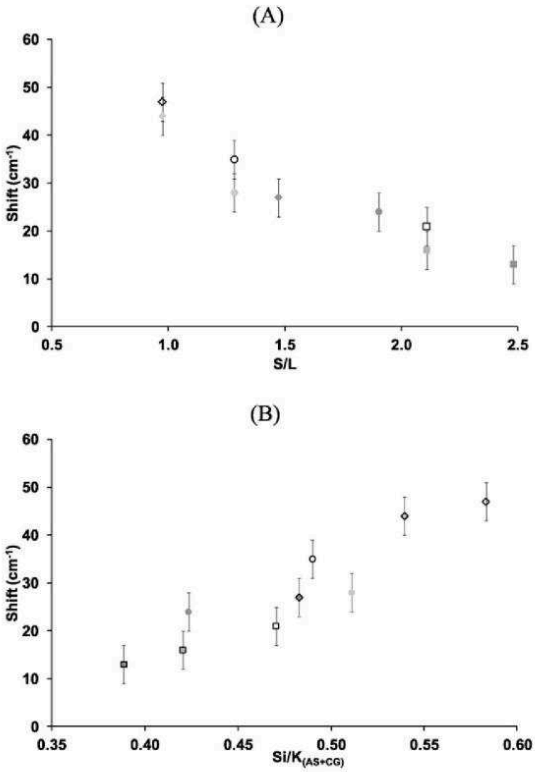

Fig. 8. Evolution of the shift values versus (A) the solid to liquid ratio (S/L) and (B) the Si/K molar ratio of the alkaline solution for (◇) $^{12,S1}G^{0}$, (◆) $^{12,S1}G^{20}$, (◆) $^{12,S1}G^{S20}$, (○) $^{12,S3}G^{0}$, (●) $^{12,S3}G^{20}$, (●) $^{12,S3}G^{S20}$, (□) $^{20,S1}G^{0}$, (■) $^{20,S1}G^{20}$ and (■) $^{20,S1}G^{S20}$ samples.

ratio favors the dissolution rate. However, it prevents the polycondensation rate because the diffusion of dissolved species is difficult. On the other hand, the relatively lower shift values corresponding to high S/L ratios indicate that the increase of the amount of solid in the mixture reduce the mobility of species at the interface charged region [40] leading to the formation of a unique network. Consequently, in addition to controlling the workability of the mixture, the S/L ratio is a crucial parameter which governs the type of formed networks in the resulting materials. To thoroughly understand this evolution, the shift values were plotted as function of the Si/K molar ratio of the activating solution in Fig. 8(B). The shift value decreases as the Si/K molar ratio decreases. The substitution of metakaolin by CG and in a greater extent the CG addition decreases the Si/K molar ratio of the activating solution due to the additional amount of potassium species released from crushed geopolymer causing therefore the decrease of the shift values. This fact can be explained by different extent of depolymerization of alkaline solution after the CG incorporation. In fact, the decrease of the Si/K ratio increases the depolymerization of the solution by increasing the number of non-bridging oxygen and the amount of low order siliceous species (Q^0 and Q^1) known to be more reactive than the other species [41]. Less depolymerized solution (high Si/K) induces the combination of Si—O—M (M = Si, Al or K) from dissolved species and from the impurities of metakaolin leading to high shift values and formation of different networks as discussed previously. In contrast, the decrease of the Si/K ratio increases the depolymerization of the solution by increasing the number of non-bridging oxygen and the amount of low order siliceous species (Q^0 and Q^1) known to be more reactive than the other species. The quickly released siliceous species reach speciation equilibrium and then react with the aluminous species because of their high reactivity inducing low shift values and formation of a geopolymer network. However, it should be mentioned that a very high alkalinity can act negatively on the polymerization due to lower connectivity between silicate anions.

To correlate the mechanical properties with the chemical compositions of the different samples, the specific compressive strength values were plotted versus the $(nSi/nK)_{AS}/(nSi/nAl)_{CG\ +\ MK}$ molar ratio in Fig. 9. Whatever the composition, the specific compressive strength values decreases with the decrease of $(nSi/nK)_{AS}/(nSi/nAl)_{CG\ +\ MK}$ molar ratio as a result of the CG incorporation by addition or by substitution. Using S1 alkaline solution, a linear relationship is observed between $^{12,S1}G^y$ and $^{20,S1}G^y$ series of samples evidencing the decrease of the compressive strength values with the decrease of aluminum availability. This finding is in accordance with the literature [30,42]. In fact, a strong correlation between the chemical composition and the mechanical properties was demonstrated. With a low Si/Al ratio, the geopolymer exhibits a weak porous structure. However, the increase of the Si/Al ratio leads to an homogenous microstructure and hence an increase in strength. For $^{12,S3}G^y$ samples, S3 alkaline solution seems to govern the compressive strengths. This fact can be explained by the differences in the distribution of silicon atoms and potassium availability between the two solutions inducing different reactivities [43]. Reactive released siliceous species from S3 solution [25] react quickly with the aluminous species leading to the formation of a perfect geopolymer network which enhance the mechanical properties of the strengthened materials.

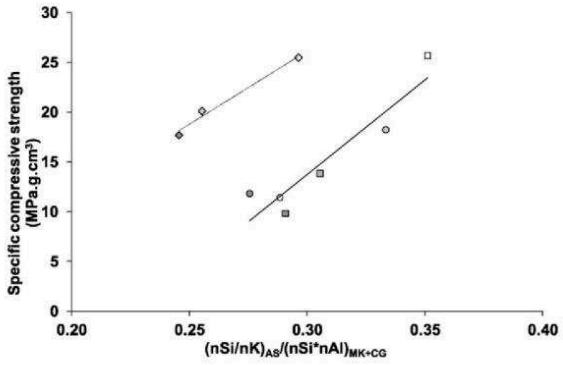

Fig. 9. Evolution of the specific compressive strength values versus the chemical composition ($(nSi/nK)_{AS}/(nSi/nAl)_{(CG\ +\ MK)}$ for (◇) $^{12,S1}G^0$, (◆) $^{12,S1}G^{20}$, (◆) $^{12,S1}G^{S20}$, (○) $^{12,S3}G^0$, (●) $^{12,S3}G^{20}$, (●) $^{12,S3}G^{S20}$, (□) $^{20,S1}G^0$, (■) $^{20,S1}G^{20}$ and (■) $^{20,S1}G^{S20}$ samples.

5. Conclusion

This study evidenced the possibility of recycling geopolymer wastes to synthesize new geopolymer materials. Three compositions differing in the used alkaline solution and the amount of metakaolin were investigated. The geopolymer wastes characterization has evidenced different physico-chemical properties suggesting different reactivities in contact with an alkaline solution. A feasibility study allowed determining the waste amount which could be added or substituted to the metakaolin to obtain geopolymer materials. 20% of geopolymer waste was the retained percentage of both addition and substitution. Furthermore, it was shown that the incorporation of the geopolymer waste may hinder the polycondensation rate and decreases the mechanical strengths of the final materials due to its low or non-reactivity. Indeed, correlations were established on one hand, between the polycondensation rate and solid to liquid ratio ($1.41 \le S/L \le 1.72$) and Si/K molar of the alkaline solution and on the other hand, between the compressive strengths and the chemical compositions of the different samples. Nevertheless, the effect of geopolymer waste incorporation can be counterbalanced with the use of a highly reactive alkaline solution or the increase of the amount of metakaolin in the mixture.

References

[1] L.A. Guerrero, G. Mass, W. Hogland, Solid waste management challenges for cities in developing countries, Waste Manag. 33 (2013) 220–232.
[2] M. Ruth, P. Dell'Anno, An industrial ecology of the US glass industry, Res. Policy 23 (3) (1997) 109–124.
[3] M. Gomes, J. De Brito, Structural concrete with incorporation of coarse recycles concrete and ceramic aggregates: durability performance, Mater. Struct. 42 (5) (2009) 663–675.
[4] A. Gonzalez-Corominas, M. Etxeberria, Properties of high performance concrete made with recycled fine ceramic and coarse mixed aggregates, Constr. Build. Mater. 68 (2014) 618–626.
[5] P. Duxson, A. Fernández-Jiménez, J.L. Provis, G.C. Lukey, A. Palomo, J.S.J. van Deventer, Geopolymer technology: the current state of the art, J. Mater. Sci. 42 (2007) 2917–2933.
[6] J. Davidovits, Geopolymer: Chemistry and Applications, second ed. Institut Géopolymère, St-Quentin, 2008.
[7] C.A. Rees, J.L. Provis, G.C. Lukey, J.S.J. van Deventer, The mechanism of geopolymer gel formation investigated through seeded nucleation, Colloids Surf. A 318 (2008) 97–105.
[8] W.D.A. Rickard, R. Williams, J. Temuujin, A.v. Riessen, Assessing the suitability of the three Australian fly ashes as an aluminosilicate source for geopolymers in high temperature applications, Mater. Sci. Eng. A 528 (2011) 3390–3397.
[9] F. Messina, C. Ferone, F. Colangelo, R. Cioffi, Low temperature alkaline activation of weathered fly ash: influence of mineral admixtures on early age performance, Constr. Build. Mater. 86 (2015) 169–177.
[10] I. Ismail, S.A. Bernal, J.L. Provis, R. San Nicolas, S. Hamdan, J.S.J. van Deventer, Modification of phase evolution in alkali-activated blast furnace slag by the incorporation of fly ash, Cem. Concr. Compos. 45 (2014) 125–135.
[11] H. Xu, W. Gong, L. Syltebo, K. Izzo, W. Lutze, I.L. Pegg, Effect of blast furnace slag grades on fly ash based geopolymer waste forms, Fuel 133 (2014) 332–340.
[12] J. He, J. Zhang, Y. Yu, G. Zhang, The strength and microstructure of two geopolymers derived from metakaolin and red mud-fly ash admixture: a comparative study, Constr. Build. Mater. 30 (2012) 80–91.
[13] F. Pacheco-Torgal, J. Castro-Gomes, S. Jalali, Investigations about the effect of aggregates on strength and microstructure of geopolymeric mine waste mud binders, Cem. Concr. Res. 37 (6) (2007) 933–941 (Cem. Concr. Res. 37(6) (2007) 933-941).
[14] L. Evangelista, J. de Brito, Mechanical behaviour of concrete made with fine recycled concrete aggregates, Cem. Concr. Compos. 29 (5) (2007) 397–401.
[15] K. Komnitsas, D. Zaharaki, A. Vlachou, G. Bartzas, M. Galetakis, Effect of synthesis parameters on the quality of construction and demolition wastes (CDW) geopolymers, Adv. Powder Technol. 26 (2) (2015) 368–376.
[16] X. Gao, Q.L. Yu, H.J.H. Brouwers, Reaction kinetics, gel character and strength of ambient temperature cured alkali activated slag–fly ash blends, Constr. Build. Mater. 80 (2015) 105–115.

[17] A. Nazari, J.G. Sanjayan, Synthesis of geopolymer from industrial wastes, J. Clean. Prod. 99 (2015) 297–304.
[18] S. Onutai, S. Jiemsirilers, P. Thavorniti, T. Kobayashi, Aluminium hydroxide waste based geopolymer composed of fly ash for sustainable cement materials, Constr. Build. Mater. 101 (2015) 298–308.
[19] C. Ferone, B. Liguori, I. Capasso, F. Colangelo, R. Cioffi, E. Cappelletto, R. DiMaggio, Thermally treated clay sediments as geopolymer source material, Appl. Clay Sci. 107 (2015) 195–204.
[20] L. Zheng, W. Wang, Y. Shi, The effects of alkaline dosage and Si/Al ratio on the immobilization of heavy metals in municipal solid waste incineration fly ash-based geopolymer, Chemosphere 79 (6) (2010) 665–671.
[21] W. Park, T. Noguchi, Influence of metal impurity on recycled aggregate concrete and inspection method for aluminum impurity, Constr. Build. Mater. 40 (2013) 1174–1183.
[22] N. Essaidi, A. Gharzouni, L. Vidal, F. Gouny, E. Joussein, S. Rossignol, Recycling of aluminosilicate waste: impact onto geopolymer formation, Eur. Phys. J. 224 (2015) 1707–1713.
[23] N. Essaidi, L. Vidal, F. Gouny, E. Joussein, S. Rossignol, Recycled geopolymer on new formulations, Ceram. Eng. Sci. Proc. 36 (8) (2015) 49–60.
[24] A. Gharzouni, E. Joussein, B. Samet, S. Baklouti, S. Pronier, I. Sobrados, J. Sanz, S. Rossignol, The effect of an activation solution with siliceous species on the chemical reactivity and mechanical properties of geopolymers, J. Sol-Gel Sci. Technol. 73 (2015) 250–259.
[25] A. Gharzouni, E. Joussein, B. Samet, S. Baklouti, S. Rossignol, Effect of the reactivity of alkaline solution and metakaolin on geopolymer formation, J. Non-Cryst. Solids 410 (2015) 127–134.
[26] E. Prud'homme, P. Michaud, A. Smith, C. Peyratout, I. Sobrados, J. Sanz, S. Rossignol, Geomaterial foams: role assignment of raw materials in the network formation, J. Sol-Gel Sci. Technol. 61 (2) (2012) 436–448.
[27] Z. Aly, E.R. Vance, D.S. Perera, J.V. Hanna, C.S. Griffith, J. Davis, D. Durce, Aqueous leachability of metakaolin-based geopolymers with molar ratios of Si/Al = 1.5–4, J. Nucl. Mater. 378 (2) (2008) 172–179.
[28] E. Moulin, P. Blanc, D. Sorentino, Influence of key cement chemical parameters on the properties of metakaolin blended, Cem. Concr. Compos. 23 (2001) 463–469.
[29] E. Prud'homme, P. Michaud, E. Joussein, J.M. Clacens, S. Rossignol, Role of alkaline cations and water content on geomaterial foams: monitoring during formation, J. Non-Cryst. Solids 357 (2011) 1270–1278.
[30] M. Lizcano, A. Gonzalez, S. Basu, K. Lozano, M. Radovic, Effects of water content and chemical composition on structural properties of alkaline activated metakaolin-based geopolymers, J. Am. Ceram. Soc. 95 (7) (2012) 2169–2177.
[31] A. Autef, E. Joussein, G. Gasgnier, S. Rossignol, Effect of alkaline solutions Si/K ratio on mechanical properties of geomaterial components, Ceram. Eng. Sci. Proc. 35 (8) (2014) 29–38.
[32] X.X. Gao, A. Autef, E. Prud'homme, P. Michaud, E. Joussein, S. Rossignol, Synthesis of consolidated materials from alkaline solutions and metakaolin: existence of domains in the Al–Si–K/O ternary diagram, J. Sol-Gel Sci. Technol. 65 (2) (2013) 220–229.
[33] C.A. Rees, J.L. Provis, G.C. Lukey, J.S.J.v. Deventer, Attenuated total reflectance Fourier transform infrared analysis of fly ash geopolymer gel aging, Langmuir 23 (15) (2007) 8170–8179.
[34] C.A. Rees, J.L. Provis, G.C. Lukey, J.S.J.v. Deventer, In situ ATR-FTIR study of the early stages of fly ash geopolymer gel formation, Langmuir 23 (17) (2007) 9076–9082.
[35] Y.M. Liew, H. Kamarudin, A.M. Mustafa Al Bakri, M. Bnhussain, M. Luqman, I. Khairul Nizar, C.M. Ruzaidi, C.Y. Heah, Optimization of solids-to-liquid and alkali activator ratios of calcined kaolin geopolymeric powder, Constr. Build. Mater. 37 (2012) 440–451.
[36] F. Gouny, F. Fouchal, P. Maillard, S. Rossignol, Study of the effect of siliceous species in the formation of a geopolymer binder: understanding the reaction mechanisms among the binder, wood, and earth brick, Ind. Eng. Chem. Res. 53 (9) (2014) 3559–3569.
[37] A. Autef, E. Joussein, A. Poulesquen, G. Gasgnier, S. Pronier, I. Sobrados, J. Sanz, S. Rossignol, Influence of metakaolin purities on potassium geopolymer formulation: the existence of several networks, J. Colloid Interface Sci. 408 (2013) 43–53.
[38] P. Duxson, J.L. Provis, G.C. Lukey, S.W. Mallicoat, W.M. Kriven, J.S.J. Van Deventer, Understanding the relationship between geopolymer composition, microstructure and mechanical properties, Colloids Surf. A 269 (1–3) (2005) 47–58.
[39] X.S. Shi, F.G. Collins, X.L. Zhao, Q.Y. Wang, Mechanical properties and microstructure analysis of fly ash geopolymeric recycled concrete, J. Hazard. Mater. 237-238 (2012) 20–29.
[40] F.K. Crundwell, The mechanism of dissolution of the feldspars: part I. Dissolution at conditions far from equilibrium, Hydrometallurgy 151 (2015) 151–162.
[41] F. Liebau, Structural Chemistry of Silicates, first ed. Springer-Verlag, Berlin, Germany, 1985.
[42] J.S.J. Van Deventer, J.L. Provis, P. Duxson, Technical and commercial progress in the adoption of geopolymer cement, Miner. Eng. 29 (2012) 89–104.
[43] A.S. Brykov, V.V. Danilov, E.Y. Aleshunina, State of silicon in silicate and silica-containing solutions and their binding properties, Russ. J. Appl. Chem. 81 (10) (2008) 1717–1721.

Publication 4 (ACL 4)

L. Vidal, E. Joussein, M. Colas, J. Cornette, J. Sanz, I. Sobrados, J.-L. Gelet, J. Absi, S. Rossignol

"Controlling the reactivity of silicate solution: A FTIR, Raman and NMR study"

Colloids and Surfaces A: Physicochemical and Engineering Aspects, 2016, vol. 503, p. 101-109.

Colloids and Surfaces A: Physicochem. Eng. Aspects 503 (2016) 101–109

Contents lists available at ScienceDirect

Colloids and Surfaces A: Physicochemical and Engineering Aspects

journal homepage: www.elsevier.com/locate/colsurfa

Controlling the reactivity of silicate solutions: A FTIR, Raman and NMR study

L. Vidal[a], E. Joussein[b], M. Colas[a], J. Cornette[a], J. Sanz[c], I. Sobrados[c], J-L. Gelet[d], J. Absi[a], S. Rossignol[a,*]

[a] Science des Procédés Céramiques et de Traitements de Surface (SPCTS), Ecole Nationale Supérieure de Céramique Industrielle, Université de Limoges, 12 rue Atlantis, 87068 Limoges Cedex, France
[b] Université de Limoges, GRESE EA 4330, 123 avenue Albert Thomas, 87060 Limoges, France
[c] Instituto de Ciencia de Materiales de Madrid, Consejo Superior de Investigaciones Científicas (CSIC), C/Sor Juana Inés de la Cruz, 3, 28049 Madrid, Spain
[d] MERSEN, 15 Rue Jacques Vaucanson, 69720 St Bonnet de Mure Cedex, France

HIGHLIGHTS

- The number of non-bridging oxygen atoms (NBOs) is directly linked to the Si/M molar ratio.
- The higher reactivity, i.e. the higher number of non-bridging oxygen, is obtained for $0.5 < Si/M < 1$.
- Raman spectroscopy provides additional information to FTIR and NMR data.

GRAPHICAL ABSTRACT

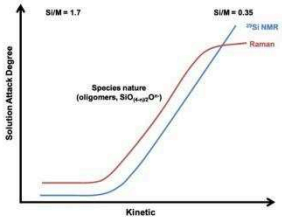

ARTICLE INFO

Article history:
Received 28 January 2016
Received in revised form 15 April 2016
Accepted 11 May 2016
Available online 12 May 2016

Keywords:
Silicate solutions
Reactivity
Raman spectroscopy
Potassium
Sodium
NMR

ABSTRACT

Alkaline silicate solutions are of great interest for several industrial applications. Previous studies demonstrated the influence of different parameters such as the Si/M (Na, K) molar ratio, the dilution level, the cation size and the manufacturing process on the silicate species. The aim of this study was to complete the data from previous works. This study focuses on the effects of these various parameters on the polymerization and the reactivity of silicate solutions. To evaluate the effects, several solutions obtained from various processes with different cations and Si/M ratios were studied. All the solutions were characterized using spectroscopic investigations (FTIR, Raman and NMR). FTIR spectroscopy was used to define the polymerization state of the various solutions. The experiments revealed that increases in the Si/M molar ratio, the dilution level and the cation size lead to the polymerization of the species. However, the effect of the cation is less pronounced. Moreover, Raman spectroscopy revealed an increase in oligomers for Si/M molar ratios less than 1. It was also shown that the manufacturing process causes a slight variation in the amount of the different silicate species responsible of the reactivity of the solution. Knowledge of these key parameters is important for different applications, including geopolymer fabrication. Moreover, it was shown a correlation between the results obtained by NMR and Raman spectroscopy.

1. Introduction

Alkaline silicate solutions, also called water glass, are of great interest for several industrial applications (e.g., sealants, deflocculants or binders [1,2]. More recently, one of the main applications

* Corresponding author.
E-mail address: sylvie.rossignol@unilim.fr (S. Rossignol).

http://dx.doi.org/10.1016/j.colsurfa.2016.05.039
0927-7757/

is related to the use of geopolymer materials [3–5] as alkaline reactants. Alkaline silicate solutions play an efficient role in the various reaction since the amount of each species (i.e., the monomers or oligomers) will lead to different behaviors. Studies indicate that the reactions between oligomers and reactive aluminous species are more favorable than with the monomers [6,7]. The various solutions are aqueous solutions containing silicate dioxide (SiO_2) and alkali oxide (such as Li_2O, Na_2O, K_2O) and are commonly prepared by dissolution of an alkali-silicate glass in water or by using steam or pressure [2]. Alkali-silicate glasses are prepared through a reaction between silica and sodium carbonate or sodium sulfate [8]. This process is typically used for the industrial manufacture of alkaline silicate solutions. Another method to prepare these solutions is to dissolve silica fume in an alkaline solution [5,9]. Authors [14,10,11] have demonstrated that for the same Si/M ratio, a commercial potassium silicate solution with KOH pellets and a lab-prepared potassium silicate solution present the same silicate species. This fact was also evidenced by Svensson et al. [16], who studied various solutions prepared using four different methods. Brykov et al. [12] reported the weak influence of the preparation method on the silicon atom connectivity for similar Si/M molar ratios and silica concentrations.

Different types of analyses can be used to determine the presence of the various silicate species in the solutions. Fourier transform infrared (FTIR) spectroscopy was used in various studies to determine the species present in the silicate solutions by following the broad peak attributed to the asymmetric stretching of the Si-O-Si bond [13,14]. The position of the Si-O-Si peak depends on the Si/M molar ratio of the silicate solutions. However, FTIR spectroscopy is not a quantitative analysis. ^{29}Si NMR has been widely used to characterize the alkaline silicate solutions [2,6,15,16]. This approach distinguishes and quantifies the different Q^n species. The Q^n notation for silicate species was introduced by Engelhardt et al. [17]. In this notation, Q refers to the silicon atom, and n = 0–4 refers to the bridging oxygen atoms. Moreover, the number of non-bridging oxygens can be calculated due to the quantification of the different silicate species. Raman spectroscopy has been used in several studies on silicate glasses [18–20] and on silicate solutions [21–23] to investigate the effects of different parameters such as the contributions of monomers and oligomers [23,24]. Another point is the possibility to obtains additional information about the entities such as the vibrations of 3-, 4- or 5-membered rings [20,24,25]. Malfait et al. [26] evidenced the variation of Q^n species depending on the amount of M_2O (M = Na or K) by Raman spectroscopy. Indeed, the authors observed a decrease of Q^4 and Q^3 species and an increase of Q^2 and Q^1 species when the Na_2O or the K_2O content increases in glasses. Hunt et al. [23] also highlighted the effect of the total silica concentration and the K_2O/SiO_2 ratio on the polymerization of silica. Finally, Hehlen et al. [27] identified a vibrational mode related to cations at modifier's place in glasses. This vibration was attributed to $—O^-Na^+$ or $—O^-Ca^{2+}O^-$ motions in sodo-silicate or lime-silicate glasses and increases as the amount of cation increases. Moreover, Le Losq et al. [20] demonstrated a variation in the Raman spectra depending on the amount of sodium or potassium. Indeed, they observed that the intensity of the peak located at 450 cm^{-1}, attributed to the vibration of the Si—O—Si bonds in five- six- or higher-membered rings, decreases when the potassium is replaced by the sodium cation. This phenomenon might be explained by the M–O distance (where M is the alkali cation). In fact, Mähler and Persson [28] showed that the distance K–O (2.81 Å) is larger than Na–O (2.43 Å).

Previous studies have shown that the presence of various silicate species in silicate solutions depends on several parameters, such as the Si/M (or SiO_2/M_2O) molar ratio, the dilution level and the alkaline cation [3,5]. The Si/M molar ratio controls the silicate species in the silicate solutions [16,12,29] such that an increase in this ratio leads to the polymerization of the silicate solution. Several authors have demonstrated that for a high Si/M molar ratio (>1), the principal species in the solutions are the Q^2 and Q^3 units; however, the Q^4 species are also observed. According to Couty and Fernandez [29], when the Si/M ratio decreases, the Q^4 entities lead to the formation of Q^3 species associated with linear chains (i.e., $Q^1 + Q^2$). For a Si/M molar ratio less than 1, the Q^0 and Q^1 species are formed to the detriment of the Q^3 and Q^2 entities [14,30]. However, this phenomenon is associated with the appearance of Q^2 and Q^3 cyclic species (Q^{2c} and Q^{3c}) [31,32]. Another parameter influencing the silicate species is the dilution level [30,33] inducing a slight polymerization of the silicate anions to higher polymeric species or colloids [2,34].

To control the reactivity of such solutions, i.e. its capacity to react with other species such as aluminosilicate species to create Si-O-Al colloidal species, few authors highlighted the effect of a very low Si/M molar ratio (<0.5) on alkaline silicate solutions, particularly on those containing potassium [12]. In addition, only a few works studied the alkaline silicate solutions with Raman spectroscopy [21,23], and none of these investigated the influence of the alkali cation on the oligomers and monomers. The effect of the dilution level has been observed by FTIR spectroscopy in only a few studies [33], and no works have been performed on the dilution level of alkaline silicate solutions with a Si/M molar ratio less than 1. Moreover, none of these authors determined correlations between the three FTIR, Raman and NMR spectroscopies. Consequently, the aim of this study was to correlate the effects of various parameters (Si/M ratio, dilution level, alkali cation) on the silicate species nature responsible of the reactivity of the solution. For this purpose, various sodium and potassium silicate solutions were used with different Si/M molar ratios and were then characterized by FTIR, ^{29}Si NMR and Raman spectroscopies.

2. Materials and methods

2.1. Raw materials and sample preparation

Various sodium and potassium alkaline silicate solutions were studied and are referenced in Table 1. The main parameters studied are the cation, Si/M molar ratio with M = K or Na (from 0.35 to 1.7), the dilution level and the manufacturing process. Moreover, the effect of dilution was obtained by diluting the silicate solution through the addition of 30–70% water. To study the manufacturing process, commercial and lab-prepared solutions were used. The commercial solutions were supplied by Woellner[1] and Mersen.[2] The lab-prepared solutions were obtained by the dissolution of KOH or NaOH pellets (85.2% and 99% purity, respectively) and amorphous silica (99.9% purity) in osmotically purified water at room temperature, as described in a previous work [4]. The nomenclature used (Table 1) is $^{x}SiM_{y(-dlz)}$, where x is the Si/M molar ratio (from 0.35 to 1.7), M is the cation (Na or K), y is the manufacturing process (C = commercial, L = lab-prepared and dl = dilution) and z is the dilution level (z = 30, 50 or 70). C1 and C2 correspond to two different commercial silicate solutions.

2.2. Sample characterization

FTIR spectroscopy in ATR (attenuated total reflectance) mode was used to characterize the solutions. FTIR spectra were obtained using a ThermoFisher Scientific Nicolet 380 infrared spectrometer. The IR spectra were collected over a wavenumber range of 500–4000 cm^{-1} with a resolution of 4 cm^{-1}. The atmospheric CO_2

[1] Wöllner GmbH, Wöllnerstraße 26, D-67065 Ludwigshafen, Germany.
[2] Mersen, 15 Rue Jacques Vaucanson, 69720 St Bonnet de Mure Cedex, France.

Table 1
Nomenclature of the various studied solutions (C = commercial, L = laboratory, dl = dilution), water content and FTIR slope.

Cation	Si/M	% water	pH value	Nomenclature	Slope (FTIR) (L/cm mol)
Na	0.35	49.6		$^{0.35}SiNa_L$	6.8
	0.5	55.3	14.0	$^{0.5}SiNa_L$	5.3
	0.6	57.5		$^{0.6}SiNa_L$	5.0
	0.7	59.6		$^{0.7}SiNa_L$	4.9
	1.0	63.0	13.0	$^{1.0}SiNa_L$	4.7
	1.3	55.5	12.0	$^{1.3}SiNa_C$	4.1
		65.2	11.8	$^{1.3}SiNa_{C\text{-}dl30}$	
		73.1	11.7	$^{1.3}SiNa_{C\text{-}dl50}$	
		82.4	11.6	$^{1.3}SiNa_{C\text{-}dl70}$	
	1.4	66.0	12.0	$^{1.4}SiNa_L$	3.7
		83.7	12.0	$^{1.4}SiNa_{L\text{-}dl}$	
	1.7	62.7	11.4	$^{1.7}SiNa_{C1}$	3.0
		71.6	11.3	$^{1.7}SiNa_{C1\text{-}dl30}$	
		78.4	11.3	$^{1.7}SiNa_{C1\text{-}dl50}$	
		86.2	11.2	$^{1.7}SiNa_{C1\text{-}dl70}$	
		64.2	11.3	$^{1.7}SiNa_{C2}$	
		72.8	11.3	$^{1.7}SiNa_{C2\text{-}dl30}$	
		79.4	11.2	$^{1.7}SiNa_{C2\text{-}dl50}$	
		86.8	11.1	$^{1.7}SiNa_{C2\text{-}dl70}$	
	0.35	41.0		$^{0.35}SiK_L$	6.8
		59.6		$^{0.35}SiK_{L\text{-}dl}$	
	0.5	47.7	14.0	$^{0.5}SiK_L$	5.7
		48.0		$^{0.5}SiK_C$	
		67.6		$^{0.5}SiK_{C\text{-}dl50}$	
K	0.6	50.4		$^{0.6}SiK_L$	5.0
		73.3		$^{.6}SiK_{L\text{-}dl}$	
	0.7	53.0		$^{0.7}SiK_L$	4.9
		77.2		$^{0.7}SiK_{L\text{-}dl}$	
		59.4		$^{0.7}SiK_C$	
	1.0	57.8	13.8	$^{1.0}SiK_L$	4.7
		84.1	13.6	$^{1.0}SiK_{L\text{-}dl}$	
	1.4	61.7	12.2	$^{1.4}SiK_L$	3.7
		89.7	12.2	$^{1.4}SiK_{L\text{-}dl}$	
		63.6	12.0	$^{1.7}SiK_L$	
	1.7	76.0	11.4	$^{1.7}SiK_{C1}$	3.0
		82.4	11.3	$^{1.7}SiK_{C1\text{-}dl30}$	
		87.0	11.3	$^{1.7}SiK_{C1\text{-}dl50}$	
		91.9	11.2	$^{1.7}SiK_{C1\text{-}dl70}$	
		76.0	11.5	$^{1.7}SiK_{C2}$	
		82.4	11.4	$^{1.7}SiK_{C2\text{-}dl30}$	
		87.0	11.3	$^{1.7}SiK_{C2\text{-}dl50}$	
		91.9	11.2	$^{1.7}SiK_{C2\text{-}dl70}$	

contribution was removed using a straight line between 2400 and 2280 cm^{-1}. To allow comparisons of the spectra, they were corrected using a baseline and were normalized.

NMR experiments were performed on silicate solutions at room temperature on a Bruker AVANCE-400 spectrometer operating at 79.49 MHz (^{29}Si signal). The ^{29}Si (I = 1/2) NMR spectra were acquired after a $\pi/2$-pulse irradiation (4 μs), and a 500 kHz filter was used to improve the signal/noise ratio. The number of scans collected was 400, and the time between acquisitions was set at 10 s to minimize saturation effects. The ^{29}Si chemical shifts were measured using external standard of tetramethylsilane (TMS). The error in chemical shift values was estimated to be lower than 0.5 ppm. Errors in determination of relative band intensities were estimated as lower than 5%. The quantitative analysis of NMR spectra was carried out with the Winfit software package (Bruker). This program allows the position, line width, and intensity of components to be determined.

Raman spectroscopy was performed on solutions using a T64000 Horiba-Jobin-Yvon spectrophotometer with 514 nm laser excitation operating at a power of 30 mW. Scattered light was collected in the backscattering mode using a long working distance objective (×50) with a triple diffraction grating (1800 lines/mm). The spectral range was 300–1400 cm^{-1}, and the exposure time of the solutions was 60 accumulations of 15 s each. The acquired spectra were corrected by subtracting the baseline, which was modeled by a 5° polynomial curve. Then, the spectra were decomposed using Wire software.

3. Results

3.1. Silicate solution characterization from FTIR spectroscopy

The FTIR spectra obtained for some of the sodium silicate solutions are shown in Fig. 1. The effects of the Si/Na molar ratio (1.7 and 0.5) and the dilution level are clearly observed (Fig. 1.A). The various contributions observed on the different spectra are shown in Table 2 [13,21,22,35]. All the samples exhibit a contribution near 1640 cm^{-1} and a broad band near 1000 cm^{-1} due to the bending of water molecules (δOH) and the asymmetric stretching of Si-O-Si bonds (ν_{as}Si-O-Si), respectively [13,35]. The $^{1.7}SiNa_{C1}$ solution shows a peak at 1003 cm^{-1} with a shoulder at 1100 cm^{-1}, which is characteristic of the SiO_2O^{2-} and $SiO_{3/2}O^-$ units, respectively [13,14]. For the $^{0.5}SiNa_L$ solution, there are two contributions located at 967 and 914 cm^{-1}, which are assigned to the stretching of Si-O-Si bonds for $SiO_{1/2}O^{3-}$ and $Si(O^-)_4$ respectively. The Si-O-Si band displacement to a lower wavenumber and the appearance of the $Si(O^-)_4$ band are due to a depolymerization phenomenon. Lucas et al. [36] demonstrated that an increase in the pH value (i.e., a decrease of the Si/M ratio) favors depolymerization by breaking the Si—O—Si bonds to create Si—O^- groups. Thus, for a low Si/Na ratio,

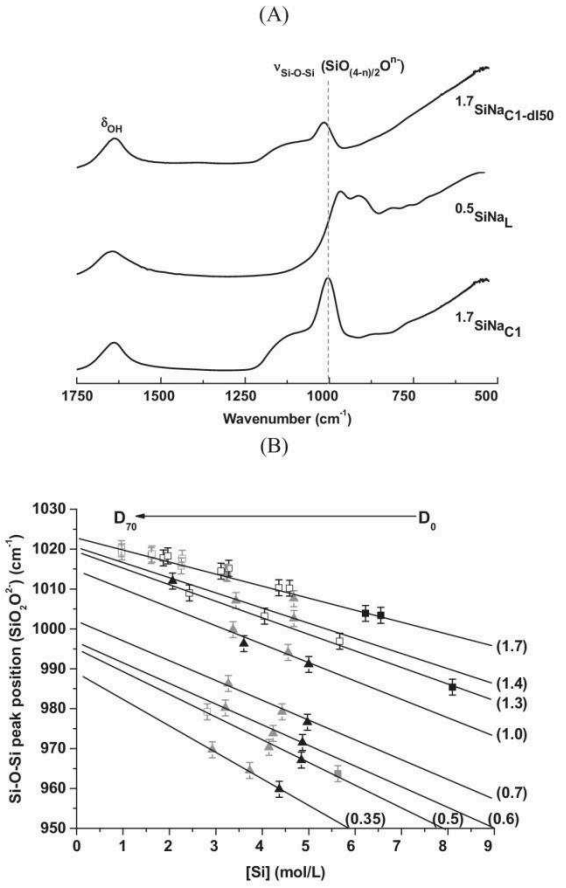

Fig. 1. (A) FTIR spectra of sodium silicate solutions with different Si/Na molar ratios and dilutions and (B) variation of the Si-O-Si peak position as a function of the Si concentration for (■) $^{x}SiNa_{C}$, (□) $^{x}SiNa_{C\text{-}dlz}$, (▲) $^{x}SiNa_{L}$, (■) $^{x}SiK_{C}$, (□) $^{x}SiK_{C\text{-}dlz}$ and (▲) $^{x}SiK_{L}$ solutions (numbers in brakets (Si/M)).

the solution is depolymerized and contains a majority of $Si(O^-)_4$ and $SiO_{1/2}O^{3-}$ species [14]. However, for a high Si/Na ratio, the solution is more polymerized, and the majority of the species are SiO_2O^{2-} and $SiO_{3/2}O^-$.

The $^{1.7}SiNa_{dl50}$ solution presents the same contributions as $^{1.7}SiNa_{C1}$ (1015 cm^{-1} for SiO_2O^{2-} and 1100 cm^{-1} for $SiO_{3/2}O^-$ entities), but the intensity is less substantial. The displacement of the Si—O—Si peak to a higher wavenumber could be explained by a slight polymerization of the silicate solution [13]. Thus, the increase in the dilution level implies a polymerization phenomenon. Therefore, for a higher Si/M molar ratio or dilution level, the silicate solutions contain more polymerized species.

To further investigate the influences of the Si/M molar ratio and the dilution level, the variation of the Si-O-Si peak position as a function of the silicon concentration is plotted in Fig. 1B for the different solutions. For each considered cation, the Si—O—Si peak position decreases for a lower Si/M molar ratio. Moreover, for a given Si/M ratio, the increase of the silicon concentration leads to a shift of the Si—O—Si peak to lower wavenumber. All these variations are in agreement with a depolymerisation phenomenon.

For a similar Si/M molar ratio of 1.7, the Si concentration (mol/L) vs. Si-O-Si (SiO_2O^{2-}) peak positions (cm^{-1}) are [6.5–1003], [4.7–1008] and [3.2–1014] for $^{1.7}SiNa_{C1}$, $^{1.7}SiK_{L}$ and $^{1.7}SiK_{C}$, respectively. For $^{1.7}SiK_{C}$ the position of the Si-O-Si band at a slightly higher wavenumber is linked to the presence of more polymerized species in this solution [14].

Table 2
Vibrational frequencies of silicate species (IR = FTIR spectroscopy, R = Raman spectroscopy).

Contribution	Position (cm^{-1})		References
δOH	1640 (IR)		[36]
ν_sSi-O-Si (Q^4)	1120–1230 (R)	1154 (IR)	[8,13]
ν_sSi-O-Si (Q^3)	1000–1100 (R)	1099 (IR)	[8,18]
ν_sSi-O-Si (Q^2)	920–1000 (R)	1011–1014 (IR)	[8,40]
νSi-O^-(M^+)	885–928 (IR)		[8]
ν_sSi-O-Si (Q^1)	850–920 (R)		[41,45]
ν_sSi-O^- (Q^0)	800–875 (R)		[42,44]
ν_s(Na)O-Si-O(Na)	830 (IR)		[16,17]
ν_sSi-O-Si	820 (IR)		[36]
TO/LO (Si-O-Si)	650–850 (R)		[42]
ν_s (Si-O) (monomers)	639–649 (R)		[41]
D_2 (δ[T_3])	587–606 (R)		[15,43]
ν_s (Si-O-Si) ($C_{5,6,7}$)	515–535 (R)		[41]
D_1 (δ[T_4])	453–550 (R)		[20,43]
δ[$T_{5and more}$]	400–490 (R)		[19,20]
M-O (–M^+ O^-–)(network modifiers)	340–360 (R)		[44]

Similarly, for a Si concentration of approximately 5 mol/L, the $^{0.5}SiNa_{L}$, $^{0.6}SiNa_{L}$, $^{0.7}SiNa_{L}$, $^{1.4}SiK_{L}$ and $^{1.7}SiK_{L}$ solutions exhibit a Si—O—Si band at 967, 972, 977, 1003 and 1008 cm^{-1}, respectively. Thus, for a constant Si concentration, an increase in the wavenumber is observed when the Si/M ratio increases. Bass et al. [37] showed that at a constant silica concentration, the Si—O—Si peak shifted to a lower frequency as the silica/alkali ratio decreased. This result was attributed to the condensation of monomers to more complex anions when the silica/alkali ratio increased. Other authors also observed that the increase in the Si/M ratio implied the presence of more polymerized species in the solutions [16,24]. Thus, for the same concentration and for each considered cation, a higher Si/M ratio indicates a more polymerized solution. The slope values are an indicator of the reactivity kinetic of the solutions; the higher the slope is, the more reactive is the solution.

Moreover, the decrease in the Si concentration is directly linked to the increase in the dilution level for the solutions, leading to a shift of the Si—O—Si peak to the higher wavenumbers [38], as evidenced for the Si/M molar ratio of 1.3 ([8 mol/L – 985 cm^{-1}], with values of [5.7 mol/L – 997 cm^{-1}], [4 mol/L – 1003 cm^{-1}] and [2.4 mol/L – 1009 cm^{-1}] for $^{1.3}SiNa_{C}$, $^{1.3}SiNa_{dl30}$, $^{1.3}SiNa_{dl50}$ and $^{1.3}SiNa_{dl70}$, respectively). This phenomenon is observed regardless of the Si/M molar ratio or the cation used (K or Na). This increase in the wavenumber reveals that the more diluted the solution is, the more the polymerization phenomenon will be exacerbated.

To qualify the various Si/M ratios, the slope values have been calculated by linear regression (Table 1).

Thus, increases in the Si/M molar ratio and the dilution level appear to lead to the polymerization of the solution. The use of the potassium cation implies the presence of slightly more polymerized species. Thus, the polymerization state of the silicate solutions depending on the various parameters (cation size, Si/M molar ratio and dilution level) is known. However, the FTIR investigations do not allow for the quantification of the different silicate species.

3.2. *Quantification of silicate species from ^{29}Si NMR*

To obtain information about the amounts of the various silicate species for the different solutions and Si/M molar ratios, ^{29}Si NMR analyses were performed and are reported in Fig. 2. For each of the considered solutions, the spectra presents the contributions of the different Q^0, Q^1, Q^2, Q^3 and Q^4 species near −72, −80, −88, −97, and −106 ppm, respectively [3,38]. Fig. 2.A presents the obtained

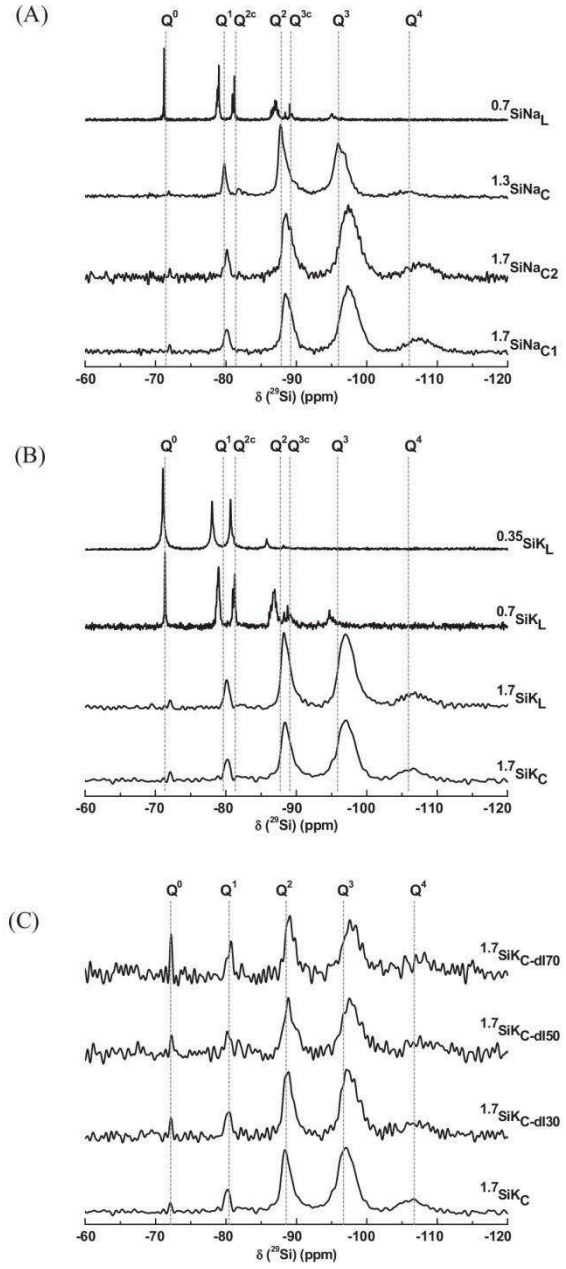

Fig. 2. ^{29}Si NMR spectra of (A) $^{x}SiNa_{y}$ (x = 0.7, 1.3 and 1.7 and y = L and C) solutions, (B) $^{x}SiNa_{y}$ (x = 0.35, 0.7, 1.4 and 1.7 and y = L and C) solutions, and (C) $^{1.7}SiK_{C(-dlz)}$ (z = 30, 50 and 70) solutions.

spectra for some of the sodium silicate solutions with various Si/Na molar ratios. The $^{1.7}SiNa_{C1}$ solution exhibits the Q^0, Q^1, Q^2, Q^3 and Q^4 species. When the Si/Na ratio decreases from 1.7 to 0.7, a shift in the contributions to a higher chemical displacement is observed, and the Q^{2c} and Q^{3c} species appear to the detriment of the Q^4 species. For Si/Na greater than 1, the presence of Q^2, Q^3 and Q^4 species indicates that the solutions are polymerized. For Si/Na less than 1, the majority of the species are Q^0 and Q^1 entities, indicating that the solutions are depolymerized [16].

The chemical shift (δ) and the percentage area (%A) of the different contributions obtained by deconvolution of each solution spectra are presented in Table 3. With the increase in the Si/Na molar ratio, the amount of depolymerized species decreases from approximately 10–0.5% (Q^0) and from 30 and 5.5% (Q^1) for Si/Na between 0.35 and 1.7, respectively. However, there is an increase in the more polymerized species Q^2, Q^3 and Q^4 when the Si/Na increases from 0.35 to 1.7 (Table 3). Moreover, the decrease in the Si/Na molar ratio implies an increase in the cyclic silicate species. For Si/Na equal to 1.7, there are no cyclic species, whereas for a Si/Na of 0.35, the Q^{2c} and Q^{3c} entities are present (27 and 3.5%, respectively). Therefore, the decrease in the Si/Na ratio implies the depolymerization of the silicate species in the solution. This phenomenon is linked to the formation of cyclic species. All these observations are in accordance with the works of Jansson et al. [39].

Moreover, the contribution attributed to the Q^3 species is located at −97.5 and −96.3 ppm for $^{1.7}SiNa_{C1}$ and $^{1.3}SiNa_{C}$, respectively, whereas in the literature data, it is located at −97 ppm [2,38]. This slight shift corresponds to the variation of the protonation degree of silicon atoms [3,16]. The protonation degree corresponds to the number of hydrogen atoms linked to the silicon atoms and it depends on the pH value. This displacement is also observed for the other Q^n species, and it increases when the Si/Na molar ratio decreases (Q^3 species located at −95.1 ppm for $^{0.7}SiNa_{L}$ instead of −97 ppm in the literature data). This phenomenon is explained by a variation of the oligomer protonation, depending on the Si/Na molar ratio. As this ratio decreases (Si/Na from 1 to 0.35) the more alkaline the solution becomes and the more deprotonated are the oligomers. Therefore, the silicon atoms appear more deprotonated in the spectra [3,5]. Furthermore, the $^{1.7}SiNa_{C1}$ and $^{1.7}SiNa_{C2}$ solutions exhibit similar spectra with slight intensity variations [12]. These slight variations could be due to the distinct manufacturing processes of the two suppliers.

The same observations are revealed in the potassium silicate solutions spectra (Fig. 2B) as well as for the two commercial solutions ($^{1.7}SiK_{C}$ and $^{1.7}SiK_{L}$). For the same Si/K molar ratio (1.7), the potassium and sodium silicate solutions display similar spectra, which is in accordance with the works of Bourlon [3]. Thus, the Si/M molar ratio of the solution has an important influence on the silicate species, whereas the effect of the cation is less pronounced. The effect of the Si/M molar ratio on the Q^0/Q^1 and Q^2/Q^1 ratios is discussed later.

The dilution effect, for example, for $^{1.7}SiK_{C}$ solutions, shows the contributions previously observed for the Na solution (Fig. 2C). The Q^3 species contribution is centered at −97 and −97.9 ppm for the $^{1.7}SiK_{C}$ and $^{1.7}SiK_{dl70}$ solutions, respectively. This is also characteristic of a variation of the protonation of silicon atoms [3,15]. Thus, for $^{1.7}SiK_{C1}$ the obtained percentages are 6.7, 29.0, 51.2 and 12.1 for Q^1, Q^2, Q^3 and Q^4 species respectively whereas for $^{1.7}SiK_{C1\text{-}dl70}$, the percentages are 7.2, 23.0, 49.4 and 18.1 for Q^1, Q^2, Q^3 and Q^4 species respectively. So, an increase in the Q^4 species and a decrease in the Q^2 species are observed. These variations can be explained by a slight polymerization of the solution when the solutions are diluted. Yang et al. [40] have also observed a variation in the particle size with dilution of the solutions. Thus, the dilution level has an effect on the silicate species.

Therefore, these experiments provide information about the influence of the Si/M molar ratio on the silicate species present in the alkaline silicate solution, and an important change of these entities is observed for a Si/M of approximately 1. The existence of monomers or oligomers was revealed; however, the type of cyclic entities was not distinguished. The presence of these species in the solution allows the determination of the degree of reactivity of the

Table 3
Deconvolutions of ^{29}Si NMR spectra of silicate solutions.

		Silicate species						
		% Area			(δ (ppm))			
		Q^0	Q^1	Q^{2c}	Q^2	Q^{3c}	Q^3	Q^4
Solutions	$^{1.7}$**SiNa**$_{C1}$	0.6	6.1	/	29.0	/	50.5	13.8
		(−72.0)	(−80.1)		(−88.8)		(−97.6)	(−107.6)
	$^{1.7}$**SiNa**$_{C2}$	0.6	5.3	/	29.4	/	51.5	13.2
		(−72.0)	(−80.1)		(−88.9)		(−97.6)	(−107.6)
	$^{1.7}$**SiK**$_L$	0.7	5.7	/	27.8	/	50.7	15.1
		(−72.1)	(−80.1)		(−88.6)		(−97.2)	(−106.9)
	$^{1.7}$**SiK**$_C$	1.0	6.7	/	29.0	/	51.2	12.1
		(−72.1)	(−80.2)		(−88.6)		(−97.1)	(−106.4)
	$^{1.7}$**SiK**$_{dl30}$	1.0	5.6	/	27.5	/	51.1	14.8
		(−72.2)	(−80.3)		(−88.9)		(−97.7)	(−107.2)
	$^{1.7}$**SiK**$_{dl50}$	2.2	5.3	/	25.9	/	49.0	17.6
		(−72.3)	(−80.3)		(−89.0)		(−97.8)	(−107.8)
	$^{1.7}$**SiK**$_{dl70}$	2.3	7.2	/	23.0	/	49.4	18.1
		(−72.2)	(−80.5)		(−89.1)		(−97.9)	(−108.0)
	$^{1.3}$**SiNa**$_C$	0.4	7.6	2.9	38.8	/	46.6	4.0
		(−71.9)	(−79.8)	(−81.9)	(−88.2)		(−96.3)	(−105.5)
	$^{0.7}$**SiNa**$_L$	11.3	29.0	18.8	22.1	11.1	7.7	/
		(−71.2)	(−78.9)	(−81.1)	(−87.0)	(−89.0)	(−95.2)	
	$^{0.7}$**SiK**$_L$	8.6	24.1	24.7	15.4	10.2	17.0	/
		(−71.4)	(−78.9)	(−81.2)	(−86.8)	(−88.9)	(−95.0)	
	$^{0.35}$**SiK**$_L$	36.5	27.3	26.8	6.1	3.3	/	/
		(−71.0)	(−78.0)	(−80.7)	(−85.9)	(−88.4)		

solution that means the species which would react with another cation.

3.3. Evaluation of the reactivity of silicate solution by Raman spectroscopy

To determine the presence of monomers and oligomers in the different silicate solutions depending on the Si/M ratio and the cation, Raman spectroscopy was performed, and the results are reported in Fig. 3. Moreover, the various contributions observed in the different spectra are presented in Table 2 [23,24,41].

For Si/Na greater than 1, the $^{1.7}SiNa_{C1}$ and $^{1.4}SiNa_L$ spectra (Fig. 3A) show the contributions due to the stretching of Q^2 ($Si(OH)_2O_2^{2-}$), Q^3 ($Si_2O(OH)_5O^-$, $Si_3O_3(OH)_4O_2^{2-}$) and Q^4 species [23,26,42]. The TO/LO modes are noted at 787 cm^{-1} [43]. The bands located near 600, 490 and 450 cm^{-1} are assigned to the ring breathing mode of the 3, 4 and 5 or more-membered ring (denoted as $\delta[T_3]$, $\delta[T_4]$ and $\delta[T_5]$) [20,24,44]. Weak contribution attributed to the M—O bonds is located near 325 cm^{-1} [27]. The presence of the Q^3 and Q^4 contributions reveals the fact that the solutions are polymerized, which is in accordance with the previous results obtained by FTIR and ^{29}Si NMR analyses. For the $^{1.4}SiNa_L$ solution, the disappearance of the Q^4 species contribution highlights a polymerization state less significant than for the $^{1.7}SiNa_{C1}$ solution. Indeed, this solution contains a higher amount of alkali cation which implies the disappearance of the Q^4 species to the profit of lower polymerized species.

For a Si/Na lower than 1 ($^{0.7}SiNa_L$ and $^{0.35}SiNa_L$), it appears that the bands of M—O bonds and $\delta[T_5]$ are more intense. An increase in the TO/LO modes and Q^2 species contributions and a decrease in the Q^3 species bands are also observed. The increase of the $\delta[T_{3and4}]$ (3- and 4-membered rings) bands and the stretching of oligomer contributions is noted [23,24]. The appearance of Q^1 and Q^0 species is also observed at 825 and 880 cm^{-1} respectively [43,45]. These data reveal the depolymerized state of the solutions. In the case of $^{0.35}SiNa_L$, the contributions attributed to the Q^2 species, the oligomers and the $[T_3]$ or $[T_4]$ rings appear to be more intense, in contrast to the band assigned to the Q^3 species, which appears to decrease. For this solution, the results reveal a substantial depolymerization of the solution and confirm the previous observations. As expected, the potassium-based silicate solutions present similar trends (Fig. 3.B) such as the decrease of the Q^4 and Q^3 species and the increase of Q^2 and Q^1 species or the increase of the M—O band when the Si/M molar ratio decreases

The Raman spectra of the various silicate solutions have been decomposed. The Fig. 4A. presents an example of decomposition obtained for the $^{0.7}SiK_L$ solution. All samples have been decomposed with the same contributions but with various amounts. This study focuses on the M—O bond because the alkali cation M^+ will break the Si—O—Si bonds inducing a depolymerization phenomenon. The position of the M—O band was plotted as a function of the Si/M molar ratio for the various solutions (Fig. 4B). The position of the M—O contribution increases when the Si/M molar ratio decreases. Indeed, this band is located at 325 cm^{-1} for $^{1.7}SiNa_{C1}$ solution whereas it is observed at 350 cm^{-1} for $^{0.35}SiNa_L$ solution. This phenomenon is also noted for the K-based solutions (310 and 345 cm^{-1} for $^{1.7}SiK_{C1}$ and $^{0.35}SiK_L$ respectively). The increase of the peak position of the M—O band may be linked to the presence of more covalent bonds when the solution is depolymerized. This behavior might be due to the fact that, for Si/M molar ratio above 1, the polysilicate species are predominant leading to a structure similar to silica. Conversely, for Si/M molar ratio below 1, the predominant species are rings and dimers. The presence of these species is relevant with a low polymerization degree due to isolated silicate species counterbalanced by the alkali cations M^+ [16].

Thus, the Raman spectroscopy provides information that is complementary to the previous results and reveals the presence of M–O bonds associated with the oligomers for Si/M ratios less than 1, i.e., for highly depolymerized solutions. The presence of the oligomers may be an important factor concerning the reactivity of the silicate solutions (Fig. 5).

4. The range of silicate solution reactivity

To better quantify the effects of the Si/M molar ratio and the cation size on the solution reactivity, the $Si(O^-)_4/SiO_{1/2}O^{3-}$ (corresponding to Q^0/Q^1) and the $SiO_2O^{2-}/SiO_{1/2}O^{3-}$ (corresponding to Q^2/Q^1) contributions area ratios obtained from ^{29}Si NMR deconvolution (see Table 3) were plotted in Fig. 4A For each cation (Na or K) and for each manufacturing process, an increase in the Si/M molar

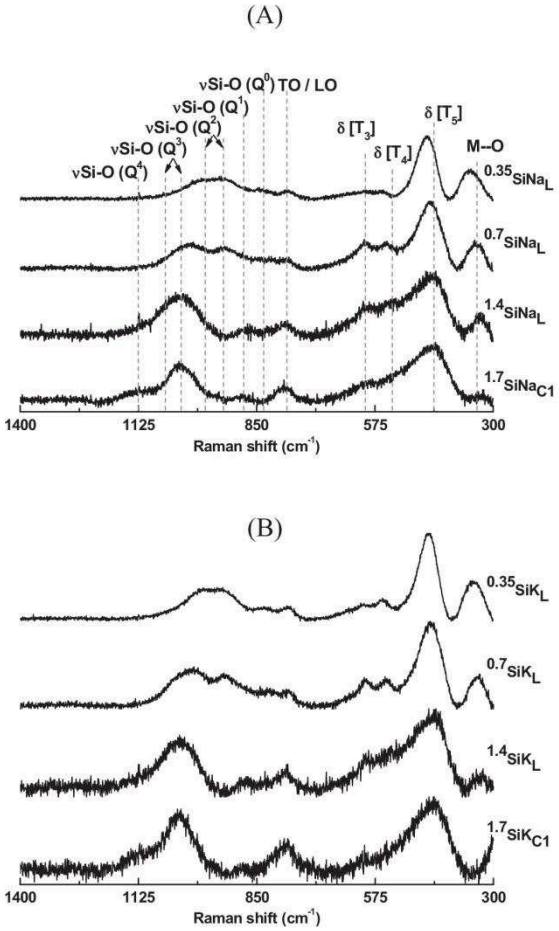

Fig. 3. Raman spectra of (A) $^{x}SiNa_{y}$ solutions and (B) $^{x}SiK_{y}$ solutions (x = 0.35, 0.7, 1.4 and 1.7 and y = L and C).

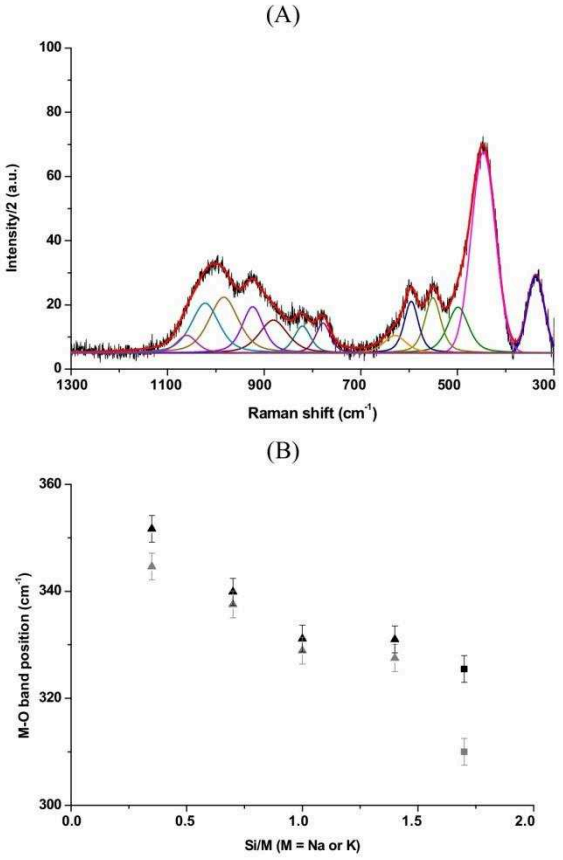

Fig. 4. (A) Decomposition of Raman spectra of $^{0.7}SiK_{L}$ solution and (B) variation of the M—O band position versus the Si/M molar ratio for (■) $^{x}SiNa_{C}$, (▲) $^{x}SiNa_{L}$, (■) $^{x}SiK_{C}$ and (▲) $^{x}SiK_{L}$ solutions.

ratio leads to a decrease in the Q^0/Q^1 ratio and an increase in the Q^2/Q^1 ratio. The Q^0/Q^1 and Q^2/Q^1 ratios vary from 1.3 to 0.2 and 1.2–5, respectively, for a Si/M molar ratio from 0.35 to 1.7. These variations indicate that the Q^2 will be dissociated into less polymerized species (Q^0 and Q^1 entities) because the Si/M ratio decreases. Moreover, it appears that the Q^2 species disappear faster compared with the formation of the Q^0 species. This phenomenon reveals the depolymerization mechanisms (the dissociation of two Q^n units and the formation of one Q^{n-1} and Q^{n+1} entities, as was previously observed in alkali silicate glasses [46]. The decrease in the Si/M ratio implies an increase in M^+ cations ($M^+ = Na^+$ or K^+) for a given silicon concentration, and these cations will break the Si-O-Si bonds, creating Si—O— bonds. This observation is in accordance with the decrease in the polymerization degree of the solutions when the Si/M ratio decreases from 1.7 to 0.35 [3,16].

To highlight the different polymerization states of the various silicate solutions, the number of NBOs (non-bridging oxygen atoms) per tetrahedron was calculated using the percentage of the Q^n species previously determined ($NBO = (3 \times Q^1 + 2*Q^2 + Q^3)/100$) [47]. The variation in the number of NBO and the percentage of the Q^0 species were plotted as a function of the Si/M molar ratio in Fig. 4B. NBO appears to be at its maximum for 0.5 < Si/M ratio < 1. For 1 < Si/M < 1.7, the increase of the NBO is characteristic of the depolymerization observed by ^{29}Si NMR (Fig. 2.A, B). This phenomenon indicates the transformation of the Q^4 species into Q^3, Q^2 and Q^1 species [12,29]. Moreover, the Q^0 percentage slightly varies for Si/M molar ratios between 1.7 and 1. This is correlated to an increase in the pH value when the Si/M molar ratio decreases (Table 1). Nordström et al. [38] showed a slight polymerization of the solutions (ie. an increase of Q^4 and Q^3 species and a decrease in Q^0 and Q^1 species) with the decrease of the pH values. For a value of 0.5 < Si/M < 1, the silicate solutions are already depolymerized, and the presence of the Q^0 species is effective in these solutions. Thus, there is nearly no depolymerization of the silicate species in the solution, and few variations of the NBO are noted. For a Si/M < 0.5, the solutions are depolymerized and contain a large amount of Q^0 entities. A fast variation of the Q^0 percentage (Si/M = 1.7, Q^0 = 1%; Si/M = 0.35, Q^0 = 36.5%) and a decrease in the NBO are observed. Then, for Si/M molar ratio below 1, the solutions present a pH value equal to 14. This fact tends to reveal the presence of a limiting value for 0.5 < Si/M ratio < 1. In this range, the silicate solutions may be more reactive. For Si/M < 0.5 or 1 < Si/M < 1.7, the reactivity of the silicate solution decreases. Moreover, the non-bridging oxygen atoms become more reactive for a Si/M molar ratio equal to 1. Thus, the sodium or potassium cation may break the Si—O—Si bonds, inducing the depolymerization of the solution. For a 0.5 < Si/M molar ratio < 1,

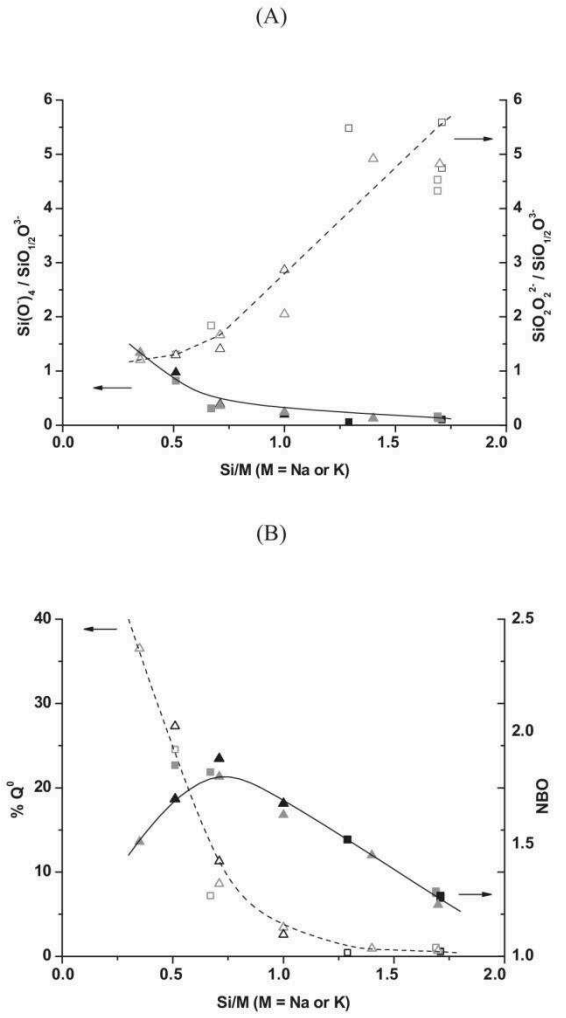

Fig. 5. Variation of the (A) (—) the $Si(O^-)_4/SiO_{1/2}O^{3-}$ (corresponding to Q^0/Q^1) and (--) the $SiO_2O^{2-}/SiO_{1/2}O^{3-}$ (corresponding to Q^2/Q^1) contributions area ratios and (B) (—) NBO (NBO = $(3Q^1 + 2Q^2 + Q^3)/100$ = and (-) Q^0 percentage versus the Si/M ratio for the various silicate solutions ((■) $SiNa_C$, (▲) $SiNa_L$, (■) SiK_C and (▲) SiK_L and (□) $SiNa_C$, (△) $SiNa_L$, (□) SiK_C and (△) SiK_L).

the solution contains more than one alkali cation for one silicon atom. Thus, the silicate species in the solution are already depolymerized, and the decrease of the Si/M ratio leads to a slight variation of the polymerization degree of the solution [3,12]. When the Si/M ratio is greater than 1, there is less than one alkali cation for each silicon atom. The silicate solution contains more polymerized species, and the increase of the Si/M ratio implies a slight polymerization of the solution [3,12]. According to these observations, it appears that 0.5 < Si/M molar ratio < 1 is the limiting range for the depolymerization. Regardless of the cation and the manufacturing process considered, the same tendencies are observed for the variation of the NBO and the Q^0 species.

Then, it was shown that the various spectroscopic analyses (FTIR, ^{29}Si NMR and Raman) allowed obtaining similar results concerning the polymerization degree of the different studied silicate solution. Now, it could be interesting to determine if Raman spectroscopy might substitute ^{29}Si NMR to identify the polymerization state of the solution and thus, their reactivity or attack degree. To achieve this, the M—O contribution area (Raman spectroscopy) was plotted as a function of the $Q^0 + Q^1$ species amount (^{29}Si NMR) (Fig. 6) and the variation is linear whatever the solution. The M–O contribution area and the $Q^0 + Q^1$ species vary from 1.5 to 15% and from 6 to 76% for a Si/M (M = Na or K) ratio between 1.7 and 0.35 respectively. The existence of this behavior between these two parameters suggests that Raman spectroscopy and ^{29}Si NMR give similar data about the polymerization degree of the various solutions. This evidences that it is possible, thanks to Raman spectroscopy, to determine the reactivity of a solution as ^{29}Si NMR spectroscopy.

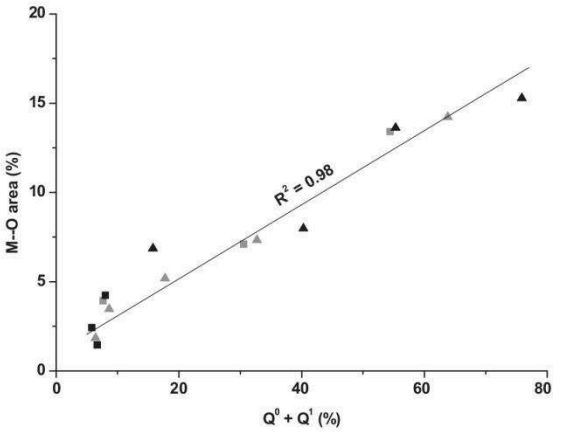

Fig. 6. Variation of the M—O contribution area (Raman) versus the $Q^0 + Q^1$ species amount (NMR) for the different silicate solutions ((■) $SiNa_C$, (▲) $SiNa_L$, (■) SiK_C and (▲) SiK_L).

Finally, it is possible to use Raman spectroscopy to substitute ^{29}Si NMR in order to predict polymerization state and thus, the reactivity of the silicate solution for any potential use.

5. Conclusion

In this work, several sodium and potassium silicate solutions with 0.35 < Si/M < 1.7 were studied by FTIR, Raman and ^{29}Si NMR spectroscopies. Only a few authors have studied highly alkaline solutions (Si/M < 0.5). NMR data revealed the increase of Q^0 and Q^1 species as the Si/M molar ratio decreased (Si/M < 1) and the high depolymerization state of the silicate entities for Si/M < 0.5. In addition, few works have studied the alkaline silicate solutions by Raman spectroscopy. This method revealed the presence of M—O bonds and oligomers for Si/M molar ratios less than 1. The effect of the dilution level was observed for solutions with values of 0.5 < Si/M < 1.7. In the literature, this effect was observed only for Si/M > 1. A linear correlation between the Si concentration and the Si—O—Si peak position obtained by FTIR was evidenced for the various Si/M ratios.

The results demonstrate that the number of non-bridging oxygens (NBOs) presents a maximum value for a Si/M molar ratio between 0.5 and 1. Above this value, the solutions mostly contain polymerized species (Q^2, Q^3 and Q^4). Below this value, the solutions are depolymerized, and the major species are the Q^0 and Q^1 species. Finally, the highly depolymerized solutions present a high amount of monomers and are highly reactive. This investigation revealed that the different studied parameters influence the reactivity of the alkaline silicate solutions. The most reactive solutions

are obtained with a Si/M molar ratio of 0.5–1. This complete work is quite important for understanding the key parameters involving in the geopolymer materials. This study also highlighted that Raman spectroscopy and ^{29}Si NMR give similar results for the determination of the reactivity of alkaline silicate solution.

Acknowledgments

The authors gratefully acknowledge the FEDER agency, the Limousin regional council and the FUI program for their financial support.

References

[1] A.C.J.H. Johnson, P. Greenwood, M. Hagström, Z. Abbas, S. Wall, Aggregation of nanosized colloidal silica in the presence of various alkali cations investigated by the electrospray technique, Langmuir 24 (2008) 12798–12806.
[2] M.T. Tognonvi, D. Massiot, A. Lecomte, S. Rossignol, J.-P. Bonnet, Identification of solvated species present in concentrated and dilute sodium silicate solutions by combined ^{29}Si NMR and SAXS studies, J. Colloid Interface Sci. 352 (2010) 309–315.
[3] Bourlon A., Physico-chimie et rhéologie des géopolymères frais pour la cimentation des puits pétroliers. Ph.D. Thesis, University of Pierre et Marie Curie (2011).
[4] A. Autef, E. Joussein, G. Gasgnier, S. Rossignol, Role of the silica source on the geopolymerization rate, J. Non-Cryst. Solids 358 (2012) 2886–2893.
[5] Steins P., Influence des paramètres de formulation sur la texturation et la structuration des géopolymères. Ph.D. Thesis, University of Limoges (2014).
[6] H. Xu, J.S.J. Van Deventer, The geopolymerization of alumino-silicate minerals, Int. J. Miner. Process. 59 (2000) 247–266.
[7] L. Weng, K. Sagoe-Crentsil, Dissolution processes, hydrolysis and condensation reactions during geopolymer synthesis: part I. –Low Si/Al ratio systems, J. Mater. Sci. 42 (2007) 2997–3006.
[8] R.K. Iler, The Chemistry of Silica: Solubility, Polymerization, Colloid and Surface Properties, and Biochemistry, Wiley-Interscience, New York, 1979, pp. 63.
[9] R.K. Harris, C.T.G. Knight, Silicon-29 nuclear magnetic resonance studies of aqueous silicate solutions Part 5. First-order patterns in potassium silicate solutions enriched with silicon-29, J. Chem. Soc. Faraday Trans. 2 79 (1983) 1525–1538.
[10] Autef A. Formulation géopolymère: influence des rapports molaires Si/K et Si/Al sur les réactions de polycondensation au sein des gels aluminosilicatés. Ph.D. Thesis, University of Limoges (2013).
[11] E. Prud'homme, A. Autef, N. Essaidi, P. Michaud, B. Samet, E. Joussein, S. Rossignol, Defining existence domains in geopolymers through their physicochemical properties, Appl. Clay Sci. 73 (2013) 26–34.
[12] A.S. Brykov, V.V. Danilov, E.Y. Aleshunina, State of silicon in silicate and silica-containing solutions and their binding properties, Russ. J. Appl. Chem. 81 (2008) 1717–1721.
[13] M.T. Tognonvi, J. Soro, S. Rossignol, Physical-chemistry of silica/alkaline silicate interactions during consolidation: part 1: Effect of cation size, J. Non-Cryst. Solids. 358 (2012) 81–87.
[14] A. Gharzouni, E. Joussein, B. Samet, S. Baklouti, S. Pronier, I. Sobrados, J. Sanz, S. Rossignol, The effect of an activation solution with siliceous species on the chemical reactivity and mechanical properties of geopolymers, J. Sol-Gel Sci. Technol. 73 (2014) 250–259.
[15] R.K. Harris, C.T.G. Knight, Silicon-29 nuclear magnetic resonance studies of aqueous silicate solutions Part 6. Second order patterns in potassium silicate solutions enriched with silicon-29, J. Chem. Soc. Faraday Trans. 2. 79 (1983) 1539–1561.
[16] I.L. Svensson, S. Sjöberg, L.-O. Öhman, Polysilicate equilibria in concentrated sodium silicate solutions, J. Chem. Soc. Faraday Trans. 82 (1986) 3635–3646.
[17] G. Engelhardt, D. Zeigan, H. Jancke, D. Hoebbel, Z. Weiker, High resolution ^{29}Si NMR of silicates and zeolites, Z. Anorg. Allg. Chem. 418 (1975) 17–28.
[18] J. Tan, S. Zhao, W. Wang, G. Davies, X. Mo, The effect of cooling rate on the structure of sodium silicate glass, Mater. Sci. Eng. B 106 (2004) 295–299.
[19] B.O. Mysen, G.D. Cody, Solution mechanisms of H_2O in depolymerized peralkaline melts, Geochim. Cosmochim. Ac. 69 (2005) 5557–5566.
[20] C. Le Losq, D.R. Neuville, Effect of the Na/K mixing on the structure and the rheology of tectosilicate silica-rich melts, Chem. Geol. 346 (2013) 57–71.
[21] I. Halasz, M. Agarwal, R. Li, N. Miller, Vibrational spectra of aqueous Na_2SiO_3 solutions, Catal. Lett. 117 (2007) 34–42.
[22] I. Halazs, M. Agarwal, R. Li, N. Miller, What can vibrational spectroscopy tell about the structure of dissolved sodium silicate, Microporous Mesoporous Mat. 135 (2010) 74–81.
[23] J.D. Hunt, A. Kavner, E.A. Schauble, D. Snyder, C.E. Manning, Polymerization of aqueous silica in H2O-K2O solutions at 25–200 °C and 1 bar to 20 kbar, Chem. Geol. 283 (2011) 161–170.
[24] H. Aguiar, J. Serra, P. González, B. León, Structural study of sol-gel silicate glasses by IR and Raman spectroscopies, J. Non-Cryst. Solids 355 (2009) 475–480.
[25] A.E. Geissberger, F.L. Galeener, Raman studies of vitreous SiO_2 versus fictive temperature, Phys. Rev. B. 28 (6) (1983) 3266–3271.
[26] W.J. Malfait, V.P. Zakaznova-Herzog, W.E. Halter, Quantitative Raman spectroscopy: speciation of Na-silicate glasses and melts, Am. Mineral. 93 (2008) 1505–1518.
[27] B. Hehlen, D.R. Neuville, Raman response of network modifier cations in alumino-silicate glasses, J. Phys. Chem. B 119 (2015) 4093–4098.
[28] J. Mähler, I. Persson, A study of the hydration of the alkali metal ions in aqueous solutions, Inorg. Chem. 51 (2012) 425–438.
[29] R. Couty, L. Fernandez, Etude du passage de l'état colloïdal à l'état ionique de solutions de silicates sodiques par spectroscopie RMN ^{29}Si et infrarouge, J. Chim. Phys. Phys. –Chim. Biol. 95 (1998) 384–387.
[30] J.L. Bass, G.L. Turner, Anion distributions in sodium silicate solutions Characterization by ^{29}Si NMR and infrared spectroscopies, and vapor phase osmometry, J. Phys. Chem. B 101 (1997) 10638–10644.
[31] C.F. Weber, R.D. Hunt, Modeling alkaline silicate solutions at 25 °C, Ind. Eng. Chem. Res. 42 (2003) 6970–6976.
[32] J.L. Provis, P. Duxson, G.C. Lukey, F. Separovic, W.M. Kriven, J.S.J. van Deventer, Modeling speciation in Highly concentrated alkaline silicate solutions, Ind. Eng. Chem. Res. 44 (2005) 8899–8908.
[33] D. Böschel, M. Janich, H. Roggendorf, Size distribution of colloidal silica in sodium silicate solutions investigated by dynamic light scattering and viscosity measurements, J. Colloid Interface Sci. 267 (2003) 360–368.
[34] M.A. McGarry, J.F. Hazel, Electron microscopy of labile alkali silicate solutions, J. Colloid Sci. 20 (1965) 72–80.
[35] M. Muroya, Correlation between the formation of silica skeleton and Fourier transform reflection infrared absorption spectroscopy spectra, Colloid Surf. A 157 (1999) 147–155.
[36] S. Lucas, M.T. Tognonvi, J.-L. Gelet, J. Soro, S. Rossignol, Interactions between silica sand and sodium silicate solution during consolidation process, J. Non-Cryst. Solids. 357 (2011) 1310–1318.
[37] J.L. Bass, G.L. Turner, M.D. Morris, Vibrational and ^{29}Si NMR spectroscopies of soluble silicate oligomers, Macromol. Symp. 140 (1999) 263–270.
[38] J. Nordström, E. Nilsson, P. Jarvol, M. Nayeri, A. Palmqvist, J. Bergenholtz, A. Matic, Concentration- and pH-dependence of highly alkaline sodium silicate solutions, J. Colloid Interface Sci. 356 (2011) 37–45.
[39] H. Jansson, D. Bernin, K. Ramser, Silicate species of water glass and insights for alkali-activated green cement, AIP Adv. 5 (2015) 067167.
[40] X. Yang, W. Zhu, Q. Yang, The viscosity properties of sodium silicate solutions, J. Solution Chem. 37 (2008) 73–83.
[41] A. Depla, E. Verheyen, A. Veyfeyken, M. Van Houteghem, K. Houthoofd, V. Van Speybroeck, M. Waroquier, C.E.A. Kirschhock, J.A. Martens, UV-Raman and ^{29}Si NMR spectroscopy investigation of the nature of silicate oligomers formed by acid catalyzed hydrolysis and polycondensation of tetramethylorthosilicate, J. Phys. Chem. C 115 (2011) 11077–11088.
[42] E.V. Belova, Y.A. Kolyagin, I.A. Uspenskaya, Structure and glass transition temperature of sodium silicate glasses doped with iron, J. Non-Cryst. Solids 423–424 (2015) 50–57.
[43] Chligui M., Etude des propriétés optiques et mécaniques des verres binaires silicatés d'alcalins lourds. Ph.D. Thesis. University of Orléans (2010).
[44] N. Zotov, I. Ebbsjö, D. Timpel, H. Keppler, Calculation of Raman spectra and vibrational properties of silicate glasses: comparison between $Na_2Si_4O_4$ and SiO_2 glasses, Phys. Rev. B 60 (9) (1999) 6383–6397.
[45] B.O. Mysen, L.W. Finger, D. Virgo, F.A. Seifert, Curve-fitting of Raman spectra of silicate glasses, Am. Mineral. 67 (1982) 686–695.
[46] J. Macháček, O. Gedeon, Q-species in alkali-disilicate glasses, Ceram. Silik. 47 (2003) 45–49.
[47] W.J. Malfait, W.E. Halter, Y. Morizet, B.H. Meier, R. Verel, Structural control on bulk melt properties: single and double quantum ^{29}Si NMR spectroscopy on alkali-silicate glasses, Geochim. Cosmochim. Ac. 71 (2007) 6002–6018.

Publication 5 (ACL 5)

L. Vidal, E. Joussein, M. Colas, J. Cornette, J. Absi, S. Rossignol

"Identification of chains and rings in alkaline silicate solutions by Raman spectroscopy: Effect of alkali cation"

Spectrochimica Acta Part A: Molecular and Biomolecular Spectroscopy, submitted.

IDENTIFICATION OF CHAINS AND RINGS IN ALKALINE SILICATE SOLUTIONS BY RAMAN SPECTROSCOPY: EFFECT OF ALKALI CATION

L.Vidal[1], E. Joussein[2], M. Colas[3], J. Cornette[3], J.Absi[3], S. Rossignol[1]

[1] SPCTS, ENSCI, 12 rue Atlantis, 87068 Limoges Cedex, France.
[2] Université de Limoges, GRESE EA 4330, 123 avenue Albert Thomas, 87060 Limoges, France.

[3] Université de Limoges, SPCTS, 12 rue Atlantis, 87068 Limoges Cedex, France.

■ corresponding author: sylvie.rossignol@unilim.fr, tel.: 33 5 87 50 25 64

Abstract:
Alkaline silicate solutions are used for different industrial applications. Structural studies of these solutions performed by FTIR and NMR spectroscopies have shown the presence of cyclic species. However, variations in ring and chain size as a function of the content of alkali cations and water cannot be determined with these techniques. The objective of this study was thus to use Raman spectroscopy to obtain additive information with regard to these species and to the reactivity of the silicate solutions. For this, several solutions were prepared according to different preparation methods (commercial or laboratory) with different cations and Si/M ratios (M = Na and/or K). The structural results obtained by Raman spectroscopy showed the effect of the Si/M ratio on the different species and in particular the formation of rings at the expense of chains. The preparation method also influenced the variation of the rings with 3 and 4 tetrahedra. It has thus been demonstrated that the cation had a stronger effect on the variations of these rings for commercially available solutions compared to their laboratory-made counterparts. Moreover, in the case of mixed solutions (M = Na + K), the alkali cation also influenced the formation of this type of rings. Finally, this study has demonstrated that Raman spectroscopy is a crucial technique for understanding the structure of silicate solutions and their reactivity.

Keywords

Silicate solution	Alkaline nature	Ring
Raman spectroscopy	Reactivity	Water

1. Introduction

Alkaline silicate solutions (also called water glass) are part of the silicate family. These solutions can be used in many industrial applications including binders, gel formers, coatings, deflocculants or corrosion inhibitors [1,2]. For the last few decades, they have also been used as binders for the agglomeration of sand in the electrical industry [3,4] and as reagents for the production of geopolymers [5]. The solutions used for these two applications do not have the same characteristics with regard to the water content and the Si/M molar ratio (M = Na or K). Thus, for the agglomeration of sand, the solutions are used as they are while in the case of geopolymers, the Si/M ratio of commercially available solutions is reduced with alkali hydroxides. The various applications for which these solutions are employed will depend on their reactivity based on the cation M and the water content.

To understand the above-mentioned parameters, several authors have conducted structural studies with FTIR and ^{29}Si NMR. The various siliceous species are identified as Q^n according

to the nomenclature by Engelhardt et al [6]; where Q represents the silicon atom with n bridging oxygen atoms. It has been shown that high Si/M ratios and water contents contribute to the formation of Q^2 and Q^3 species [4,7]. Their presence could indicate the existence of simple and branched chains. The formation of cyclic Q^{2c} and Q^{3c} species has also been demonstrated by NMR [7,8]. Such species may perhaps reveal the formation of rings. These solutions thus appear to be composed of chains and rings. To supplement these data, 2D NMR analyses have been performed on solutions with Si/M ratios ranging from 1.7 to 0.5 [2,9]. Tognonvi et al. [2] have thus demonstrated that the Q^n species are preferably connected to Q^n or Q^{n+1} entities. Cho et al. [9] also revealed that is was possible to use 2D NMR to identify, in the intervals between -88 and -91 ppm and -96 and -98 ppm, new and small oligomer structures undetected by 1D NMR in a sodium silicate solution with a Si/M ratio close to 0.6. The presence of these entities indicated the existence of stereoisomers in silicate solutions with different chemical properties.

However, this technique is difficult to implement, which is not the case for Raman spectroscopy which could be a fast complementary technique. Indeed, studies on glass have shown that this method made it possible to obtain information on the size of the rings (at low frequency) and on the Q^n species (at high frequency) [10,11]. Since the technique requires long acquisition times in order for useful contributions to be obtained, it has not been widely developed when it comes to characterizing silicate solutions [12,13]. Contributions attributed to ring breathing mode as well as the vibration of the monomers and oligomers and their variations as a function of the Si/M ratio have been observed [12,13]. Indeed, an increase in the quantity of alkali cations was found to lead to an increase in 3-memberred rings and monomers, associated with a reduction in 4-membered rings and oligomers [12,14]. Trcera [15] noted a shift to higher wavenumbers of the band attributed to the rings with 5 tetrahedra or more when the amount of alkali ions increased. This shift has been linked to a reduction of the Si-O-Si angles and thus to a decrease in the size of the rings in accordance with the work by Galeener [11]. Furthermore, a study has shown that increasing the water content in sodium-silicate glass leads to the disappearance of the 3-membered rings [16]. Depolymerization phenomena have also been noted thanks to the variations in the Q^n silicate species. Indeed, increasing the quantity of alkali cations led to reduced Q^4 species in favor of Q^3 species [10,13]. For higher amounts of alkali cations, the formation of Q^2 entities at the expense of Q^3 species was observed, indicating a phenomenon of depolymerization.

Few authors have compared data obtained by Raman spectroscopy and 2D NMR [17]. However, Le Losq [17] used Raman spectroscopy and 2D NMR to demonstrate that the proportion of Si-O-Si bonds in sodium glass is greater than in potassium glass. This is due to a less orderly distribution of silicon and aluminum atoms in potassium glass; a phenomenon that can be explained by the greater size of the potassium cation. Indeed, the sites available in the silicate network are small while potassium has a large radius. Thus, the introduction of potassium within the network results in the distortion of the latter. Variations of the different Q^n species cannot be correlated to the reactivity of the silicate solutions [8,13]. Indeed, a study performed in the laboratory showed a maximal reactivity for Si/M ratios between 0.5 and 1.0 [13]. However, the presence of only cyclic species was noted for this range of Si/M ratios [8,13]. Raman spectroscopy could thus be used to determine the reactivity (or attack capability) of the solutions. These solutions must thus be analyzed using a technique that can identify and determine the size of the rings that they comprise.

Structural analyses by FTIR and NMR spectroscopies have shown that the degree of polymerization depends on the Q^n species, rings and chains present in the solutions. These species in turn depend on the preparation method, the alkali cation, the Si/M ratio and the water content, and will therefore affect the degree of polymerization of the solutions [18,19]. The method used to prepare the solution has an effect on the silicate species. Several authors

[20,21,22] have demonstrated that, for the same Si/M ratio, a commercial silicate solution in which KOH pellets were dissolved and a laboratory solution have the same silicate species in different amounts. Moreover, diluting a solution causes slight polymerization of the silicate anions. Indeed, Lucas et al. [3] have shown that dilution promotes the polycondensation of the silicate species. Thus, the preparation method results in the presence of Q^n species in different amounts and a higher water content promotes the polymerization of the solution.
The alkali cation also has a slight influence on the silicate species. Increasing the size of the cation promotes the formation of silicate species that are slightly more polymerized as well as Q^{2c} and Q^{3c} species [18,23]. This phenomenon is due to the fact that the hydration shell radius decreases as the cation size increases. Mähler and Persson [24] estimated the radius of the Na^+ and K^+ cations and showed that the Na-O distance was slightly smaller than the K-O distance. According to Melkior et al. [25], the potassium cation has a faster diffusion rate than its sodium counterpart due to the Stokes radius of the cation.
For high Si/M ratios, the solutions contain predominantly Q^2 and Q^3 species associated with Q^4 entities in small quantities [19,26]. A decrease of the Si/M ratio leads to the formation of Q^0 and Q^1 species associated with the appearance of cyclic Q^{2c} and Q^{3c} species for Si/M ratios smaller than 1 [27,28], thus promoting depolymerization. Consequently, several parameters can be used to control the rate of polymerization and therefore the reactivity of the silicate solutions.

Studies using FTIR spectroscopy [29,30] and NMR ^{29}Si [29,31] on silicate glass have therefore assessed the changes in Q^n species as a function of the alkali content [14] as well as the presence of monomers and oligomers [32]. Therefore, it seemed appropriate to carry out Raman analysis of the silicate solutions in order to identify the presence of chains and rings to determine the reactivity of the solutions. Various parameters were studied, such as the preparation mode (commercial or laboratory), the alkali cation (K, Na and NaK mixture) and the Si/M ratio (from 0.2 to 1.7). These parameters were systematically compared as a function of the different contributions determined from the spectra.

2. Materials and methods

2.1 Raw materials and sample preparation

Various potassium, sodium or mixed (K and Na) silicate solutions were used for this study and are presented in Table 1. The parameters studied were the alkali cation (K and/or Na), the Si/M molar ratio with M = K and/or Na (from 0.2 to 1.7) and the manufacturing process. In order to study the influence of this process, commercially available and lab-prepared solutions were used. The commercial silicate solutions were supplied by the companies Woellner[1] and MERSEN[2]. The lab-prepared solutions were obtained by the dissolution of KOH or NaOH pellets (85.2% and 97% purity, respectively) and amorphous silica (99.9% purity) in osmotically purified water at room temperature, as described elsewhere [5]. To compare the various solutions, MOH pellets (M = K or Na) were dissolved in the commercially available or laboratory-made solutions. The nomenclature used for these different solutions is listed in Table 1 and can be seen in Fig. 1.

[1] Woellner GmbH, Wöllnerstraße 26, D-67065 Ludwigshafen, Germany.
[2] MERSEN, 15 Rue Jacques Vaucanson, 69720 St Bonnet de Mure Cedex, France.

Table 1: Characteristics and nomenclature of the studied K-based solutions (C = commercial, L = laboratory). The characteristics for the other solutions are reported in the supplementary file.

Cation	Manufacturing method	Si/M	Nomenclature	Symbols
K	Laboratory	1.7	$_{L}K^{1.7}$	◇
	Commercial	1.7	$_{C}K^{1.7}$	□
		1.5	$_{C}K^{1.5}$	
	Laboratory	1.4	$_{L}K^{1.4}$	◇
		1.0	$_{L}K^{1.0}$	
	Commercial		$_{C}K^{1.7}{}_{K}{}^{1.0}$	×
	Laboratory	0.7	$_{L}K^{0.7}$	◇
	Commercial		$_{C}K^{0.7}$	□
		0.6	$_{C}K^{1.7}{}_{K}{}^{0.6}$	×
		0.5	$_{C}K^{1.5}{}_{K}{}^{0.5}$	
			$_{C}K^{0.7}{}_{K}{}^{0.5}$	
			$_{C}K^{0.5}$	□
	Laboratory		$_{L}K^{0.5}$	◇
		0.35	$_{L}K^{0.35}$	
		0.2	$_{L}K^{0.2}$	

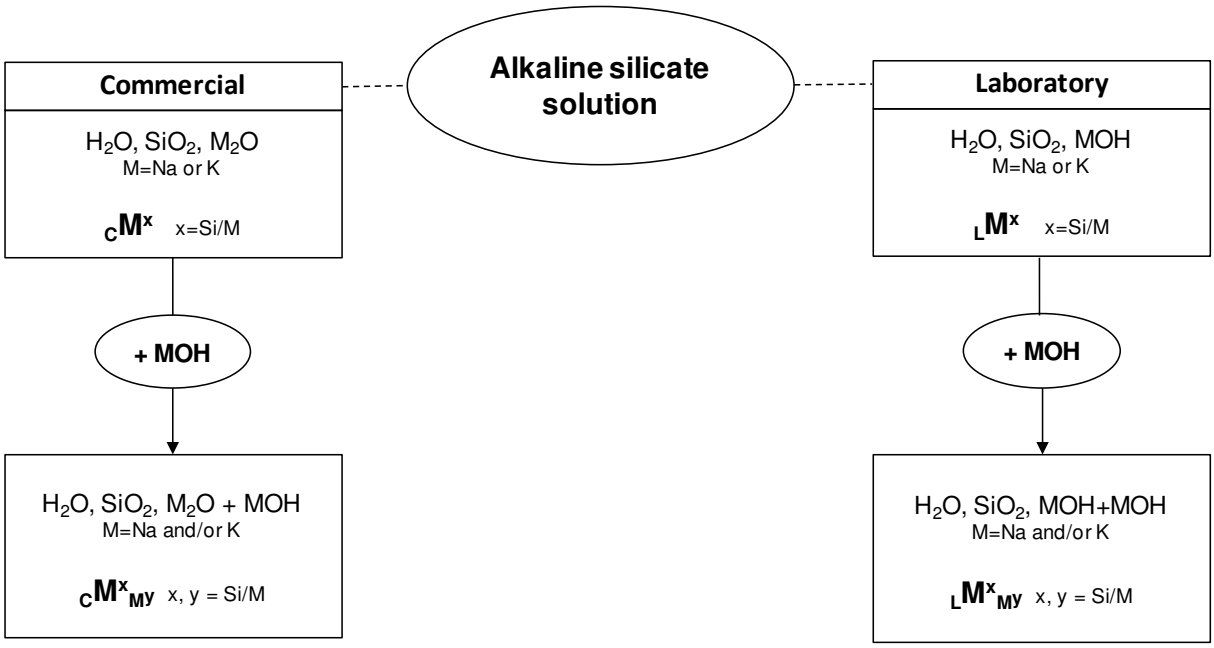

Fig. 1. Schema presenting the various alkaline silicate solutions studied and their nomenclatures.

For the commercially available solutions, the nomenclature was ${}_{C}M^{x}$ where M denoted the alkali cation (Na and/or K), x was the Si/M molar ratio (from 0.2 to 1.7) and C stood for commercial. For example, a commercially available potassium-based silicate solution with a Si/M ratio equal to 1.7 was named ${}_{C}K^{1.7}$. Concerning the lab-prepared solutions, the nomenclature used was ${}_{L}M^{x}$ where M denoted the alkali cation (Na or K), x was the Si/M ratio (from 0.2 to 1.7) and L stood for laboratory. For example, a lab-prepared sodium-based silicate solution with a Si/M ratio equal to 0.5 was called ${}_{L}Na^{0.5}$. Finally, the mixed solutions were given the designation ${}_{y}M^{x}{}_{Mz}$ where M denoted the alkali cation (M = K and/or Na), x was the initial Si/M molar ratio (from 0.7 to 1.7), y described the manufacturing process (y = C for commercial or L for laboratory) and z corresponded to the final Si/M molar ratio (from 0.2 to 1.0). For example, a lab-prepared sodium-based silicate solution, with an initial Si/M molar ratio of 1.7, in which KOH pellets were added to obtain a final Si/M molar ratio equal to 0.5 was named ${}_{L}Na^{1.7}{}_{K0.5}$. A commercial potassium-based silicate solution, with an initial Si/M molar ratio of 0.7, in which NaOH pellets were added to obtain a final Si/M molar ratio equal to 0.5 was called ${}_{C}K^{0.7}{}_{Na0.5}$.

2.2 Sample characterization

Raman spectroscopy was performed on the solutions using a T64000 Horiba-Jobin-Yvon spectrophotometer with a 514-nm laser excitation operating at a power of 30 mW at the sample. Scattered light was collected in backscattering mode using a specific assembly for liquid samples with a triple diffraction grating (1800 lines/mm). The spectral range was 300 to 1300 cm^{-1}, and 60 scans of 15 s each were carried out for the acquisition. The subtracted baseline was modeled by a five-degree polynomial curve. Then, Raman spectra were decomposed using the Wire 4.0 software from Renishaw. The contributions were modeled by a pseudo-Voigt function. In order to compare the different solutions, the areas obtained for all the contributions were normalized by the total area of the spectrum. This way, the areas could be determined as percentages. The various contributions observed by Raman spectroscopy are listed in Table 2, and Raman spectra obtained for ${}_{L}K^{0.7}$ and ${}_{L}Na^{0.7}$ solutions are presented in Fig. 2. It can be seen that the used method for collecting Raman data made it possible to distinguish the various contributions. Moreover, the Raman spectrum of the amorphous silica used to prepare the laboratory solutions is presented in Fig. 2.

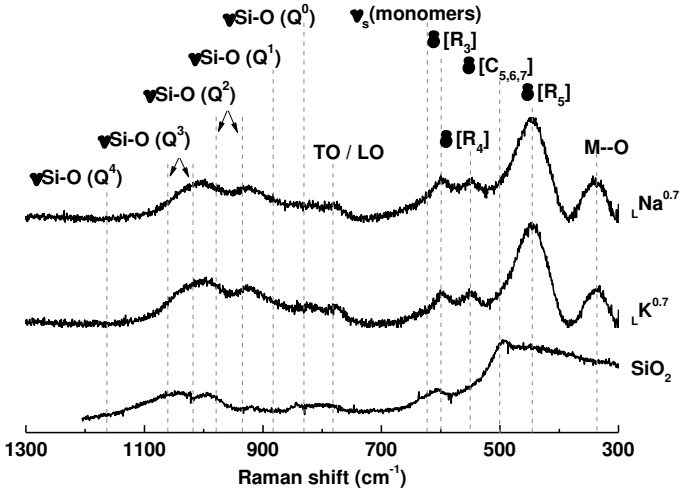

Fig. 2. Raman spectra of the amorphous silica and the solutions ${}_{L}K^{0.7}$ and ${}_{L}Na^{0.7}$.

Table 2: Vibrational frequencies of silicate species for Raman spectroscopy.

Contribution	Raman shift (cm^{-1})	References
ν_s (Si-O) (Q^4)	1120 – 1230	[30,33]
ν_s (Si-O^-) (Q^3)	1000 – 1100	[16,30]
ν_s (Si-O^-) (Q^2)	920 – 1000	[14,16]
ν_s (Si-O^-) (Q^1)	850 – 920	[35,39]
ν_s (Si-O^-) (Q^0)	800 – 875	[34,35]
TO/LO (Si-O-Si)	650 – 850	[35]
ν_s (Si-O) (monomers)	639 – 649	[36]
D_2 (δ [R_3])	587 – 606	[14,32]
ν_s (Si-O-Si) ($C_{5,6,7}$)	515 – 535	[36]
D_1 (δ [R_4])	453 – 550	[10,32]
δ [$R_{5\ or\ more}$]	400 – 490	[10,34]
M--O (network modifiers)	340 – 360	[34]

3. Results and discussions

3.1 Decomposition of the various Raman spectra

In order to determine each contribution, such as monomers and rings, from the various silicate solutions, the Raman spectra had been decomposed taking into account the literature data of the frequencies (Table 2) and the previous paper by Vidal et al. [13] regarding silicate solutions.

3.1.1. Si/M (M=K, Na) molar ratios for the laboratory solution

The objective was to determine the effect of the Si/M molar ratio and the alkali cation on the polymerization of the silicate species present in the solutions. In order to do so, spectra of six laboratory-made Na- and K-silicate solutions with varying Si/M ratios ($_LK^{1.7}$, $_LK^{1.0}$, $_LK^{0.5}$, $_LNa^{1.7}$, $_LNa^{1.0}$ and $_LNa^{0.5}$, see nomenclature Table 1) were studied and are shown in Fig. 3.

Regardless of the cation (Na or K) for a Si/M ratio = 1.7 ($_LK^{1.7}$ and $_LNa^{1.7}$), the decomposed Raman spectra showed the same contributions with variable intensities: the contributions due to the stretching of Q^1 ($SiO_{1/2}O_3^{3-}$), Q^2 ($SiO_2O_2^{2-}$), Q^3 ($Si_2O_{3/2}O^-$) and Q^4 (SiO_4) species can be evidenced near 875, 1000, 1060 and 1120 cm^{-1} respectively [12,14,33]. Weak contributions attributed to the bending of M--O bonds and to the TO/LO vibration modes were observed at 320 and 785 cm^{-1}, respectively [34,35]. Finally, all the contributions in the low-frequency range (300-800 cm^{-1}) were effective. For example, the bands observed near 440, 550, 600, 500 and 645 cm^{-1} were attributed, respectively, to the ring breathing mode of the ring with 5 or more tetrahedra (denoted $\delta[R_{5\ or\ more}]$), to $\delta[R_3]$ (3-membered rings), to $\delta[R_4]$ (4-membered rings), to the stretching of ν_S(Si-O-Si) of the chains ($C_{5,6,7}$) and to monomer contributions (ν_S(Si-O)) [10,31,36]. The curve-fitting results of the Raman spectra are reported in Table 3 and show that the cation effect was relatively limited when the Si/M ratio was high. However, the presence of Q^3 and Q^4 contributions were proof that the solution was polymerized which is consistent with previous results by Vidal et al. [13].

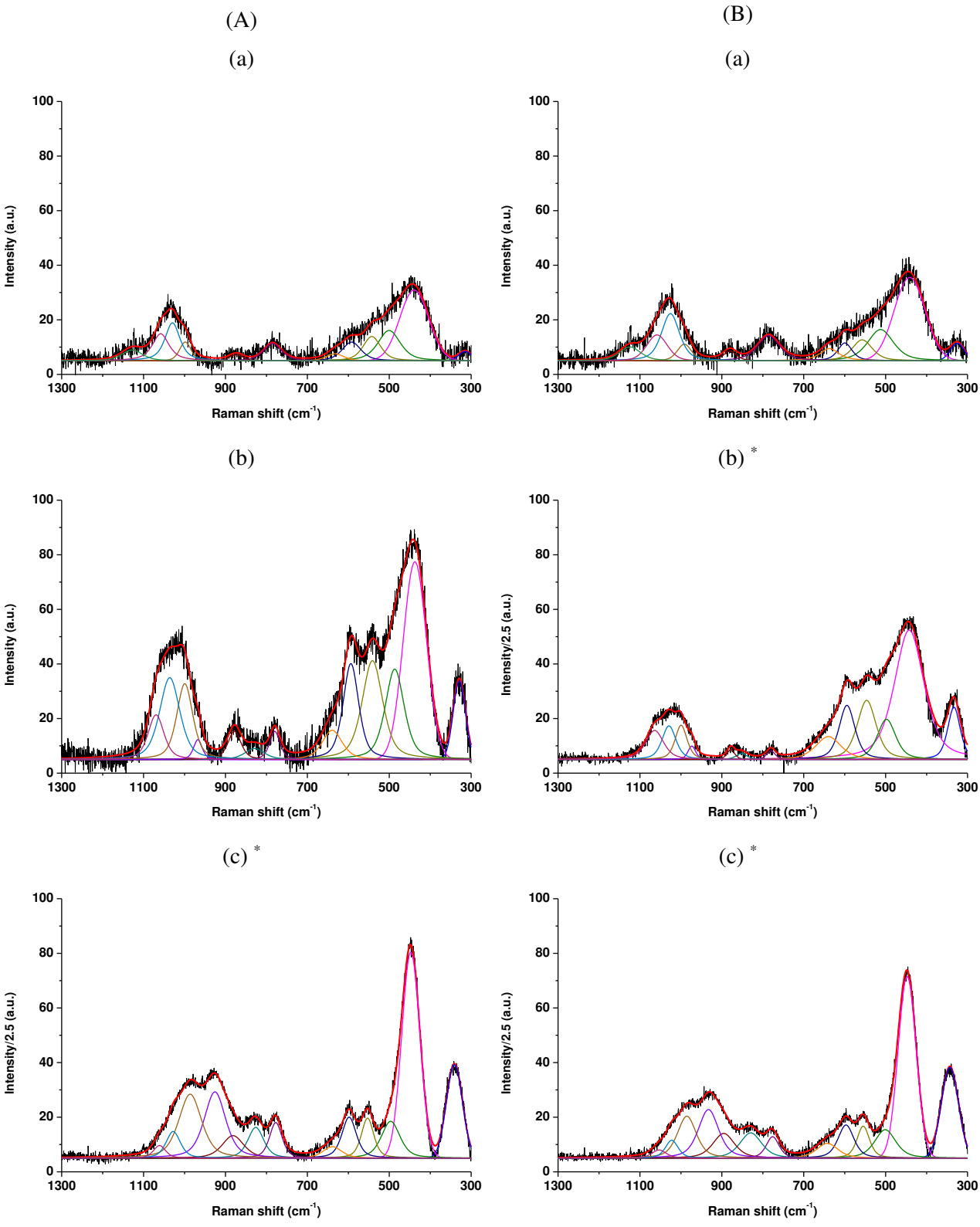

Fig. 3. Curve-fitting of Raman spectra for (A) (a) $_{L}K^{1.7}$, (b) $_{L}K^{1.0}$, (c) $_{L}K^{0.5*}$ solutions and (B) (a) $_{L}Na^{1.7}$, (b) $_{L}Na^{1.0*}$ and (c) $_{L}Na^{0.5\,*}$ solutions based on potassium and sodium respectively (* Intensity divided by 2.5).

Table 3: Curve-fitting results of Raman spectra of the various silicate solutions (a) in the low frequency range (300 – 800 cm^{-1}) and (b) in the high frequency range (800 – 1200 cm^{-1}) (- : No contribution).

(a)

		Raman contributions						
		Area (%) (Position (cm^{-1}) (± 2.5 cm^{-1}))						
		M--O	**δ [$R_{5\ or\ more}$]**	**ν_s (Si-O-Si) ($C_{5, 6, 7}$)**	**D_1 (δ [R_4])**	**D_2 (δ [R_3])**	**ν_s (Si-O) (monomers)**	**TO/LO (Si-O-Si)**
Solution	$_LK^{1.7}$	1.9 (315)	31.1 (439)	12.9 (500)	8.2 (542)	7.0 (592)	2.8 (629)	6.1 (785)
	$_LNa^{1.7}$	3.1 (326)	30.1 (440)	11.4 (504)	7.5 (550)	5.9 (600)	3.2 (644)	8.7 (786)
	$_CNa^{1.35}$	4.2 (329)	25.3 (445)	3.7 (498)	9.5 (539)	11.7 (595)	2.9 (655)	1.8 (782)
	$_LNa^{1.35}$	5.0 (331)	25.8 (440)	10.0 (496)	11.0 (540)	10.4 (595)	3.8 (645)	3.7 (784)
	$_LK^{1.0}$	5.2 (329)	24.9 (437)	11.5 (487)	13.7 (541)	10.1 (594)	3.9 (639)	2.0 (779)
	$_LNa^{1.0}$	6.9 (333)	40.3 (442)	7.8 (498)	11.8 (546)	9.0 (594)	6.1 (640)	0.8 (780)
	$_CK^{0.7}$	7.1 (335)	24.0 (445)	7.0 (499)	6.5 (549)	8.4 (596)	3.2 (640)	2.6 (779)
	$_LK^{0.7}$	7.4 (338)	27.7 (446)	6.8 (499)	6.4 (551)	5.2 (595)	2.8 (629)	3.1 (778)
	$_LK^{0.5}$	10.9 (341)	27.1 (447)	6.2 (497)	4.5 (553)	5.4 (598)	2.0 (639)	4.1 (777)
	$_LNa^{0.5}$	13.6 (343)	28.5 (447)	6.5 (501)	4.4 (555)	5.7 (597)	3.5 (642)	3.0 (776)
	$_LK^{1.7}{}_{Na}{}^{0.5}$	12.0 (342)	28.0 (446)	7.3 (492)	6.2 (552)	5.9 (600)	1.9 (643)	2.8 (777)
	$_LNa^{1.7}{}_K{}^{0.5}$	10.8 (341)	27.5 (446)	7.6 (491)	7.2 (555)	2.8 (598)	3.6 (628)	2.8 (777)
	$_LK^{0.7}{}_{Na}{}^{0.5}$	12.2 (339)	25.0 (446)	6.3 (490)	4.9 (553)	2.6 (597)	4.3 (624)	4.2 (778)
	$_LNa^{0.7}{}_K{}^{0.5}$	12.3 (343)	28.5 (447)	6.1 (495)	6.5 (554)	4.8 (599)	3.2 (640)	3.0 (777)

(b)

		Raman contributions						
		Area (%) (Position (cm^{-1}) (± 2.5 cm^{-1}))						
		ν_s (Si-O^-) (Q^0)	ν_s (Si-O^-) (Q^1)	ν_s (Si-O^-) (Q^{2c})	ν_s (Si-O^-) (Q^2)	ν_s (Si-O^-) (Q^{3c})	ν_s (Si-O^-) (Q^3)	ν_s (Si-O) (Q^4)
Solution	${}_LK^{1.7}$	-	1.4 (874)	-	3.9 (999)	13.3 (1033)	6.3 (1062)	5.2 (1122)
	${}_LNa^{1.7}$	-	1.9 (880)	-	3.8 (993)	12.8 (1026)	6.8 (1057)	4.7 (1123)
	${}_CNa^{1.35}$	2.6 (859)	5.6 (892)	-	11.7 (987)	13.5 (1027)	5.2 (1065)	2.3 (1123)
	${}_LNa^{1.35}$	0.9 (825)	1.6 (872)	-	7.9 (1001)	13.5 (1040)	3.2 (1073)	3.1 (1119)
	${}_LK^{1.0}$	1.5 (829)	2.5 (878)	1.1 (967)	8.1 (999)	11.0 (1036)	4.7 (1070)	-
	${}_LNa^{1.0}$	0.7 (852)	0.8 (878)	1.1 (973)	4.3 (999)	5.0 (1029)	5.6 (1064)	-
	${}_CK^{0.7}$	3.4 (824)	7.0 (878)	6.2 (917)	13.3 (993)	9.0 (1034)	2.5 (1063)	-
	${}_LK^{0.7}$	3.2 (821)	6.7 (881)	6.7 (924)	11.7 (984)	9.8 (1022)	2.5 (1060)	-
	${}_LK^{0.5}$	4.4 (826)	4.4 (882)	12.9 (926)	13.3 (986)	3.5 (1028)	1.4 (1061)	-
	${}_LNa^{0.5}$	6.0 (829)	5.8 (896)	10.7 (933)	8.6 (985)	2.5 (1022)	1.3 (1053)	-
	${}_LK^{1.7}{}_{Na}{}^{0.5}$	5.3 (824)	5.2 (891)	9.8 (928)	10.2 (985)	3.0 (1018)	2.3 (1046)	-
	${}_LNa^{1.7}{}_K{}^{0.5}$	5.8 (825)	4.9 (892)	11.3 (931)	10.8 (990)	3.6 (1022)	1.4 (1066)	-
	${}_LK^{0.7}{}_{Na}{}^{0.5}$	4.9 (827)	5.8 (888)	12.6 (930)	12.4 (991)	3.4 (1028)	1.5 (1065)	-
	${}_LNa^{0.7}{}_K{}^{0.5}$	5.2 (825)	4.0 (886)	11.2 (927)	10.9 (986)	2.9 (1025)	1.3 (1061)	-

For the solutions with a Si/M ratio equal to 1 (${}_LK^{1.0}$ and ${}_LNa^{1.0}$), changes were clearly effective. Indeed, all the contributions seemed to be more intense than for the ${}_LK^{1.7}$ and ${}_LNa^{1.7}$. However, this phenomenon was less pronounced with the curve-fitting results due to the fact that these data were normalized. Moreover, the Q^4 band disappeared whereas a Q^0 band near 830 cm^{-1} was observed. The disappearance of the contribution from the Q^4 species highlights a less significant polymerization state compared to the ${}_LK^{1.7}$ and ${}_LNa^{1.7}$ solutions. Equivalent contributions were observed in the low-frequency range (see Table 3 and previous results). Globally, the curve fitting gives evidence of an increase in the area of the $\delta[R_{3,4}]$ and M--O with the decrease of the Si/M ratio for both cations. The contributions attributed to the Q^2 and Q^3 species appeared to be more intense for low Si/M ratios. However, it seemed that these latter species were more pronounced in the case of the K-based silicate solution compared to its Na-based counterpart (Table 3 and Fig. 3). Moreover, an increased content of alkali cation

led to a decrease of the TO/LO and $C_{5,6,7}$ contributions, thus indicating that these solutions were less polymerized.

The decrease of the Si/M molar ratio to 0.5 ($_LK^{0.5}$ and $_LNa^{0.5}$) led to an increase of the Q^0, Q^1 and Q^2 bands to the detriment of the Q^3 contribution. Moreover, in the low-frequency range, the contributions attributed to $\delta[R_{3,4}]$ decreased. The relative intensity of the $\delta[R_{5 \text{ and more}}]$ and M--O contributions were exacerbated in the case of the solution with a Si/M ratio = 0.5 which suggests that the M--O bonds may be associated with the oligomers for low Si/M ratios, i.e., for very depolymerized solutions. This fact reveals that the solutions were highly depolymerized. Moreover, the contributions attributed to Q^0 and Q^1 silicate species were slightly more pronounced for $_LNa^{0.5}$ than for $_LK^{0.5}$. This fact highlights that sodium silicate solutions may be slightly more depolymerized than their potassium silicate counterparts.

The increased amount of oligomer species with the decrease of the Si/M ratio may be an important factor concerning the attack capacity of the silicate solutions.

3.1.2. Influence of the preparation method: commercial versus laboratory

In order to understand the effect of the preparation method, i.e., commercially available vs. laboratory-made solutions, Raman spectra of Na and K-based silicate solutions were decomposed. The spectra of $_CK^{0.7}$, $_LK^{0.7}$, $_CNa^{1.35}$ and $_LNa^{1.35}$ are shown in Fig. 4. Previously, the decision was made to present spectra of the K-based solution with a low Si/M ratio (equal to 0.7) since this solution is more depolymerized than its Na-based counterpart (Si/M ratio = 1.35). However, it was assumed that the spectra were representative of all tested silicate solutions and that they give a global vision of the impact of the preparation method as a function of the alkali cation and Si/M ratio. The $_CK^{0.7}$ and $_LK^{0.7}$ spectra present the same contributions but their intensity seems to be more significant for the $_LK^{0.7}$ solution (for this solution, the intensity of the spectrum was divided by 2.5 in the figure) (Fig. 4 Aa and Bb respectively) due to the slight difference in water content. Indeed, the $n(Si)/n(H_2O)$ molar ratio was 0.09 and 0.10 for the $_CK^{0.7}$ and $_LK^{0.7}$ solutions, respectively. Thus, the $_LK^{0.7}$ solution contained less water, implying slightly more intense contributions. Moreover, it seemed that the contributions of the $\delta[R_3]$ and Q^2 species in the commercial solution were slightly more intense than in the laboratory-made one. In addition, the M--O and $\delta[R_{5 \text{ and more}}]$ contributions appeared to be slightly more pronounced for the $_LK^{0.7}$ solution.

In the case of the Na-based silicate solution ($_CNa^{1.35}$ and $_LNa^{1.35}$; Si/M ratio = 1.35), the spectra (Fig. 4 Ac and Bd) were different in comparison with its potassium-based counterpart. Indeed, the contributions of the Q^0, Q^1 and Q^2 species were more intense for the commercially available solution as opposed to the laboratory-made one whereas the opposite was true for the contributions attributed to the stretching ν_S(Si-O-Si) $C_{5,6,7}$. These results were evidence of differences between each preparation method even if these differences were much more limited in the case of the K-based silicate solution as opposed to the Na one. In fine, the preparation method plays an important role in terms of reactive species evidenced in the solution. This last point is important and also indicates that the commercial Na-based and K-based silicate solutions are not obtained by the same preparation method.

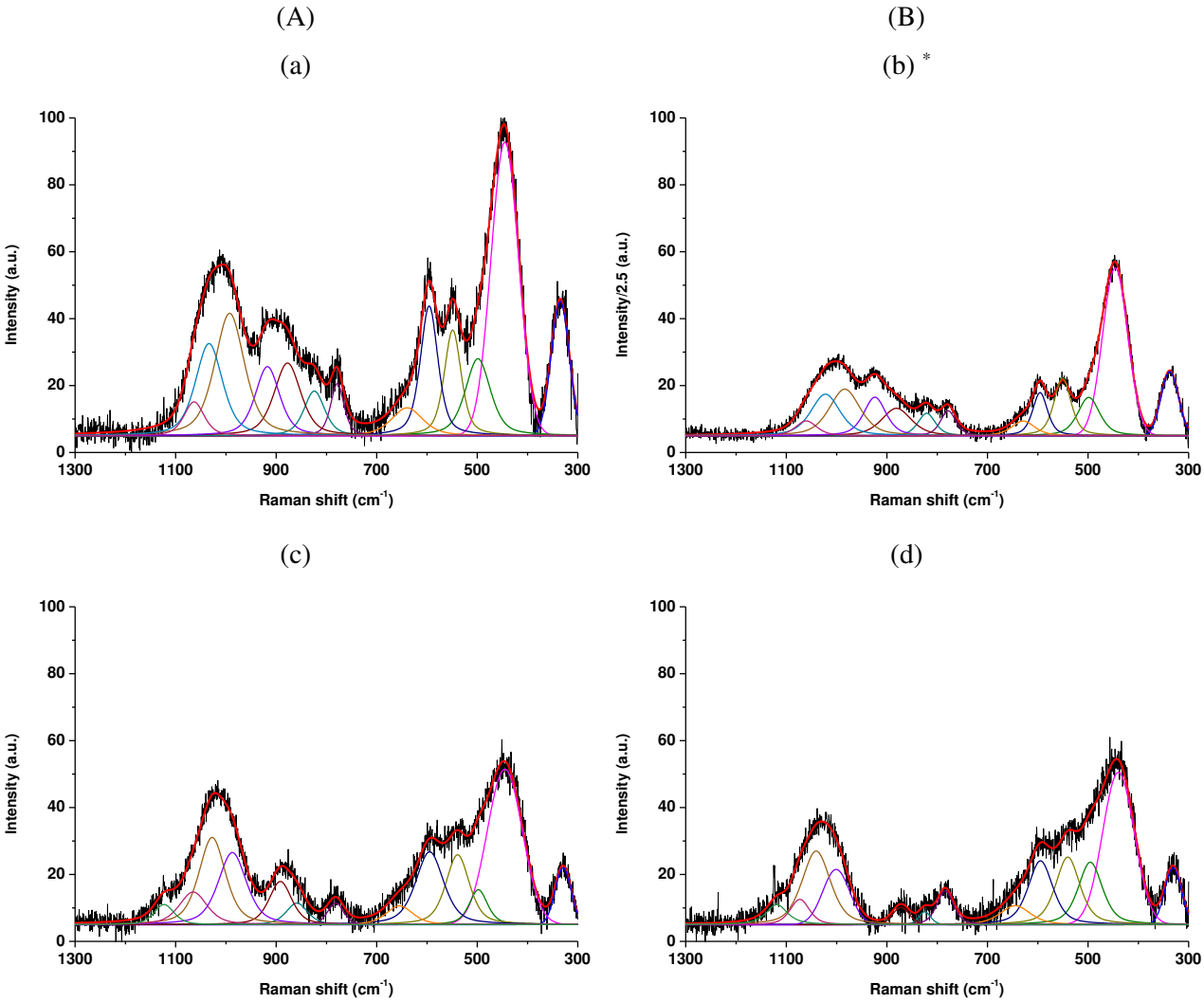

Fig. 4. Curve-fitting of Raman spectra for the (A) commercial and (B) laboratory solutions ((a) $_{C}K^{0.7}$, (b) $_{L}K^{0.7*}$, (c) $_{C}Na^{1.35}$ and (d) $_{L}Na^{1.35}$ (* Intensity divided by 2.5)).

3.1.3. Mixed solution (NaK) with similar Si/M ratio: cation effect

Fig. 5 displays the Raman spectra of the mixed cation solutions $_{L}K^{1.7}{}_{Na0.5}$, $_{L}K^{0.7}{}_{Na0.5}$, $_{L}Na^{1.7}{}_{K0.5}$ and $_{L}Na^{0.7}{}_{K0.5}$ (laboratory-based) for a single Si/M ratio = 0.5. All the spectra resemble the one obtained for a solution with a Si/M molar ratio equal to 0.5. Even though the same contributions were observed, their relative intensity varied slightly. Fig. 5a and 5b present the Raman spectra for the K-based silicate solution with the addition of NaOH ($_{L}K^{1.7}{}_{Na0.5}$ and $_{L}K^{0.7}{}_{Na0.5}$) and Fig. 5c and 5d show the SiNa-based solutions where KOH was added in order to obtain a NaK solution ($_{L}Na^{1.7}{}_{K0.5}$ and $_{L}Na^{0.7}{}_{K0.5}$).

It seems that the addition of Na to a K-based solution with an initial Si/M molar ratio equal to 1.7 ($_{L}K^{1.7}{}_{Na0.5}$) gave rise to slightly more intense M--O and $\delta[R_{3,4}]$ contributions in addition to a less significant monomer contribution as opposed to the more depolymerized solution $_{L}K^{0.7}{}_{Na0.5}$. These observations were less noticeable in the case of the $_{L}Na^{1.7}{}_{K0.5}$ and $_{L}Na^{0.7}{}_{K0.5}$ solutions. Moreover, the Q^1 contribution appeared to be slightly more intense for $_{L}K^{0.7}{}_{Na0.5}$ than for $_{L}Na^{0.7}{}_{K0.5}$. Thus, it seemed that, for a similar Si/M molar ratio, the K-based solutions with addition of NaOH were somewhat more depolymerized than their Na-based counterparts with KOH addition.

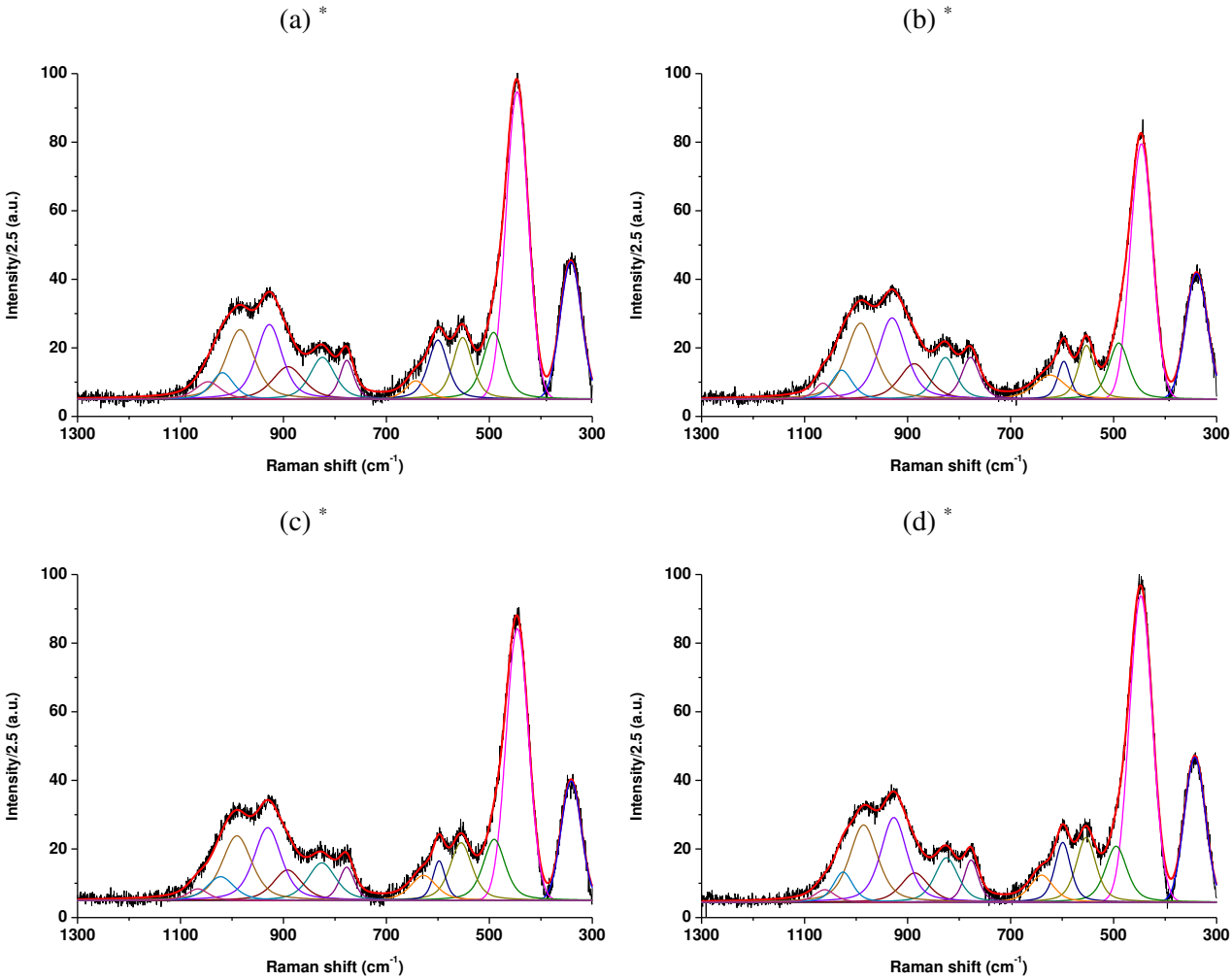

Fig. 5. Curve-fitting of Raman spectra for the mixed cation solutions (a) ${}_{L}K^{1.7}{}_{Na}{}^{0.5*}$, (b) ${}_{L}K^{0.7}{}_{Na}{}^{0.5*}$, (c) ${}_{L}Na^{1.7}{}_{K}{}^{0.5*}$ and (d) ${}_{L}Na^{0.7}{}_{K}{}^{0.5*}$ (* Intensity divided by 2.5).

For better interpretations, the $\delta[C_{5,6,7}]$ and $\delta[R_3 + R_4]$ intensities corrected by the higher intensity were plotted as a function of the cation mole number corrected by the cation radius relative to the volume of the solution $((n(M)/r(M))/V_{tot})$ for various solutions (Fig. 6). Regardless of the solution and the alkali cation, the intensity of the contribution attributed to $C_{5,6,7}$ decreased. However, the sum of the R_3 and R_4 intensities increased and then decreased with increasing cation concentration. Indeed, the $\delta[C_{5,6,7}]$ intensity band decreased from 0.6 to 0.25 (Fig. 6a) for a cationic concentration reaching 4 mol/(L*Å). When the concentration was above 4 mol/(L*Å), the $\delta[C_{5,6,7}]$ intensity seemed to be relatively stable.

In the case of the evolution of the intensity of the $\delta[R_3 + R_4]$ band, the opposite phenomenon was observed (Fig. 6b): the intensity of the $\delta[R_3 + R_4]$ band increased up to 0.6 (1 to 4 mol/(L*Å) cationic concentration range), then decreased for the highest cationic concentration. These variations indicate an influence of the alkali cation. Moreover, the presence of the sodium cation in the solutions appeared to give rise to the formation of rings (R_3 and R_4) for alkali cation concentrations that were higher than for the potassium cation.

This phenomenon could be related to the size of the cation. Indeed, the radius of the sodium ion was smaller than that of potassium [24], and for an increasing alkali cation concentration, potassium would then cause the rupture of rings at lower concentrations than for sodium. Another explanation for this phenomenon could be linked to the diffusion of species. Indeed,

Melkior et al. [25] have shown that the potassium diffusion rate is greater than that of sodium. This difference in diffusion rate could therefore explain the breaking of rings for lower concentrations in the case of potassium. Thus, the cation contained in the solution appeared to have an influence on the degree of polymerization of silicate species and therefore on the solution.

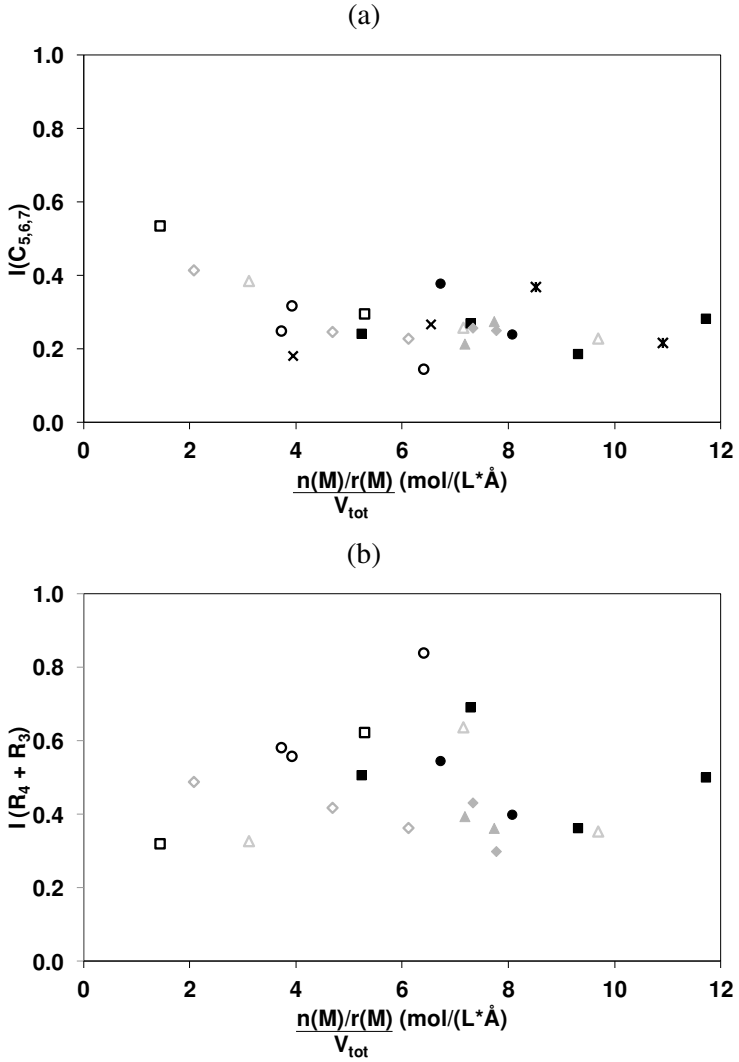

Fig. 6. Variation of the (a) $C_{5,6,7}$ and (b) R_3+R_4 contribution intensities corrected by the higher contribution intensity versus the cation concentration corrected by the cation radius [18] for (□) ${}_C K^x$, (○) ${}_C Na^x$, (◇) ${}_L K^x$, (△) ${}_L Na^x$, (×) ${}_C K^x{}_{K^y}$, (✱) ${}_C Na^x{}_{Na^y}$, (■) ${}_C K^x{}_{Na^y}$, (●) ${}_C Na^x{}_{K^y}$, (◆) ${}_L K^x{}_{Na^y}$ and (▲) ${}_L Na^x{}_{K^y}$ solutions (Table 1).

The decomposition of the spectra has made it possible to detect contributions that have yet to be identified, such as the contribution attributed to M--O bonds. Since the key parameter of the solutions is the alkali cation, Fig. 7 shows the percentage of the M--O contribution, determined by decomposition, as a function of the alkali cation concentration corrected by the distance M-O. Regardless of the cation and the solution in question, there was an increase in the M--O contribution when the content of alkali cation increased; however, the variation was not linear over the considered concentration range. It increased linearly for a concentration ranging from 0.5 to about 4 mol/(L*Å), then leveled off for higher concentrations. Indeed, for the solutions ${}_C K^x$ and for a concentration of approximately 0.7 mol/(L*Å) (${}_C K^{1.7}$), the M--O contribution was about 4% whereas for a concentration close to 4 mol/(L*Å) (${}_C K^{0.5}$), the

contribution increased to 13.5%. This phenomenon was also observed for $_LNa^x$ solutions where the M--O contribution varied from 2% to 13.5% at concentrations ranging from 1 to 4 mol/(L*Å). Subsequently, this contribution remained constant at about 15.5% for concentrations greater than 4.5 mol/(L*Å). The existence of a plateau can be correlated with a state of complete dissociation of the siliceous species [19]. Indeed, when the M--O content was stable, the silicate species were completely dissociated. This complete dissociation was due to pH values of 14 or higher and Si/M ratios below 0.5. Indeed, for Si/M ratios below 0.5, highly depolymerized species (Q^0) predominated. Svensson et al. [21] have demonstrated that for low SiO_2/M_2O ratios, the predominate silicate species were Q^0 entities. Other authors have also observed these changes [19,26]. The change in the M--O contribution seemed to depend on the water content and the content of alkali cation. This suggests that the reactivity of silicate species and thus silicate solutions can be controlled by knowledge of the alkali cation, the preparation method and the water content of these solutions. A curve chart of the reactivity of the silicate species in relation to these parameters has thus been obtained.

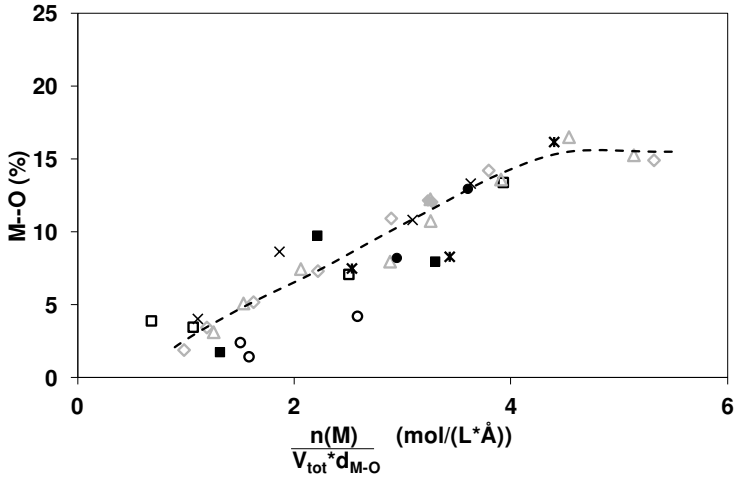

Fig. 7. M--O contribution area versus the alkali concentration corrected by the M-O distance ($n(M)/(V_{tot}*d_{M-O})$) for (□) $_CK^x$, (○) $_CNa^x$, (◇) $_LK^x$, (△) $_LNa^x$, (✕) $_CK^x{}_{K^y}$, (✳) $_CNa^x{}_{Na^y}$, (■) $_CK^x{}_{Na^y}$, (●) $_CNa^x{}_{K^y}$, (◆) $_LK^x{}_{Na^y}$ and (▲) $_LNa^x{}_{K^y}$ solutions (Table 1).

3.2 Global behavior and tendencies obtained from all solutions by Raman spectroscopy

The decomposition of different solutions as well as bibliographic data has helped identify the various contributions observed by Raman spectroscopy. Some contributions were also detected by ^{29}Si NMR, including the bands attributed to Q^n species [21,37]. It was deemed beneficial to compare the results obtained by Raman spectroscopy with literature data when it comes to variations of different Q^n species as a function of the amount of introduced alkali cation. Given the previous results, this part focuses on the contribution of all identified species. All contributions are expressed as a function of the alkali cation concentration corrected by the M-O distance proposed in the work of Mähler and Persson [24].

The contributions observed at high frequencies (800 - 1300 cm^{-1}) were attributed to the vibration of Si-O bonds in the Q^n species. Fig. 8 shows the variation of these different species as a function of the alkali concentration corrected by the M-O distance. Upon introduction of the M cation and regardless of the cation and solution in question, the polymerized species (Q^3 and Q^4) disappeared in favor of more depolymerized species (Q^2). When the cation concentration became larger, the amount of depolymerized species (Q^0 and Q^1) increased at the expense of more polymerized ones (Q^3).

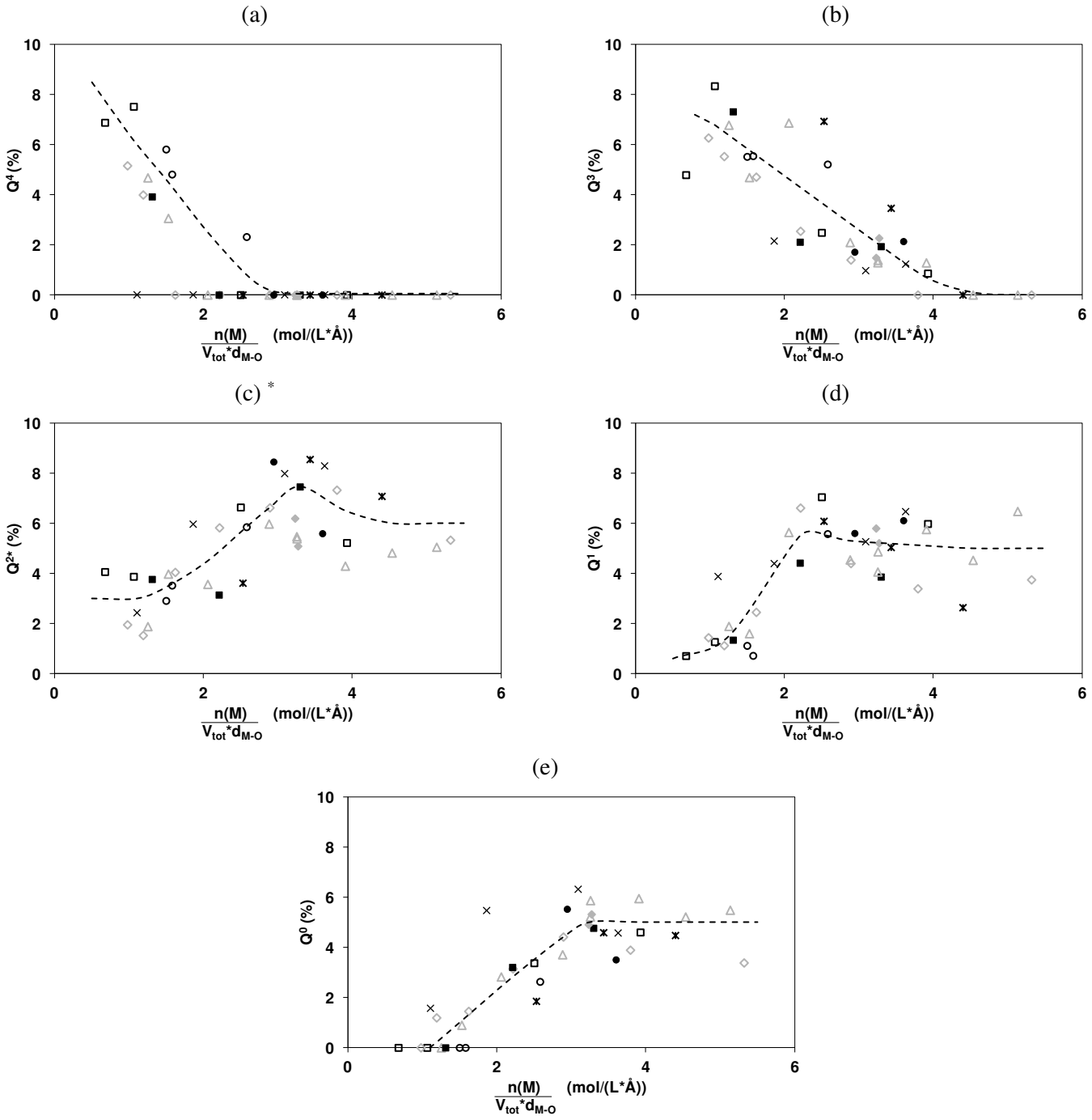

Fig. 8. Variation of the area of (a) Q^4, (b) Q^3, (c) Q^{2*}, (d) Q^1 and (e) Q^0 silicate species as a function of the alkali concentration corrected by the M-O distance ($n(M)/(V_{tot}*d_{M-O})$) for (□) ${}_{C}K^{x}$, (○) ${}_{C}Na^{x}$, (◇) ${}_{L}K^{x}$, (△) ${}_{L}Na^{x}$, (×) ${}_{C}K^{x}{}_{K}{}^{y}$, (∗) ${}_{C}Na^{x}{}_{Na}{}^{y}$, (■) ${}_{C}K^{x}{}_{Na}{}^{y}$, (●) ${}_{C}Na^{x}{}_{K}{}^{y}$, (◆) ${}_{L}K^{x}{}_{Na}{}^{y}$ and (▲) ${}_{L}Na^{x}{}_{K}{}^{y}$ solutions (Table 1) (*Area divided by 2).

The amount of Q^4 species (Fig. 8a) decreased when the alkali cation concentration increased and the species disappeared for concentrations higher than 3 mol/(L*Å). A difference was noted between commercial solutions (${}_{C}M^{x}$) and laboratory counterparts (${}_{L}M^{x}$) for Q^4 species. This is consistent with the decomposition results presented earlier (Fig. 4 and Table 3). Indeed, for the same cation concentration, the solutions prepared in the laboratory did not contain any Q^4 species while these entities were present in the commercial solutions. For example, at a concentration of 2.5 mol/(L*Å), the commercially available solution contained

2% Q^4 species while its laboratory counterpart did not contain any. This difference may be due to the various preparation methods of the solutions. Indeed, the commercial solutions were prepared by dissolving glass containing a large amount of polymerized units while the laboratory solutions were prepared by dissolving amorphous silica containing a smaller amount of polymerized species [38]. As a matter of fact, the Raman spectrum of the amorphous silica used for the preparation of the laboratory solutions highlights a small amount of Q^4 species together with a lower polymerization rate for these solutions (Fig. 2).
The same trend was observed for Q^3 species (Fig. 8b). In fact, the amount of these species decreased with an increasing cation concentration and they disappeared completely above 4.5 mol/(L*Å). More particularly, the point at 0.7 mol/(L*Å) corresponding to the ${}_CK^{1,7}$ solution had a smaller amount of Q^3 species (of the order of 5%) than the ${}_CK^{1,5}$ solution at 1 mol/(L*Å) (approximately 8.5%). This can be explained by the formation of Q^3 species at the expense of Q^4 species for low cation concentrations, and when the amount of alkali cations increases, the Q^3 and Q^4 species also disappear in favor of more depolymerized species [19,26]. This phenomenon is consistent with the depolymerization of the solution and has also been observed in the case of silicate glass [29,39]. However, in the case of glass, the disappearance of Q^3 and Q^4 species in favor of more depolymerized species (Q^2) occurred for slightly higher contents of alkali cation (Si/M ranging from 1.5 to 0.75) [14,39].

The variation of Q^2 species (Fig. 8c) was consistent with the variations of the preceding species. Indeed, when the amount of Q^3 and Q^4 species decreased, the Q^2 species increased to a concentration of about 3.5 mol/(L*Å) after which a slight decrease to a limit value (about 6%) was observed. The commercial and laboratory solutions no longer showed such differences with regard to the variation of these species. In addition, the amount of Q^2 species reached a maximum value before the disappearance of the Q^3 entities. This suggests the presence of branched chains in the solutions. Indeed, these species reveal the presence of siliceous polymerized entities. Moreover, since the Q^2 species had only two Si-O-Si bonds, their presence indicates the existence of chains in these solutions.

The same phenomenon was observed for Q^1 species (Fig. 8d). In fact, the contribution attributed to these species increased when the amount of alkali cations increased to 2.5 mol/(L*Å). Beyond this value, the Q^1 species appeared to decrease slightly and reach a limit value of 5%.

Finally, the variation of Q^0 species (Fig. 8e) was similar to that of the Q^1 entities. Indeed, the amount of Q^0 species increased when the quantity of alkali cations increased respectively to 3 mol/(L*Å). Above this concentration, the amount of these species appeared to become stabilized. For low alkali cation concentrations, the commercial solutions did not contain any Q^0 species. This phenomenon can be explained by the high initial polymerization rate. Thus, the major differences between the commercial and laboratory solutions can be identified from changes in Q^0 and Q^4 species.

All these observations were consistent with a depolymerization phenomenon. Indeed, for concentrations below 3.5 mol/(L*Å), the Q^3 and Q^4 species disappeared while the amount of Q^2, Q^1 and Q^0 species increased. Then, as the concentration increased, the amount of Q^2 species decreased in favor of Q^0 and Q^1 species. These changes were consistent with the observations made by ^{29}Si NMR of alkaline silicate solutions. Indeed, Svensson et al. [21] performed NMR analysis on various silicate solutions and demonstrated that for high SiO_2/Na_2O ratios (i.e., for low alkali cation concentrations), Q^4 were the predominate species. When the SiO_2/Na_2O ratio decreased slightly, the Q^4 species declined and the Q^3 species became predominate. For low SiO_2/Na_2O ratios, the Q^0, Q^1 and Q^2 species increased to the detriment of more polymerized species (Q^3 et Q^4). The same trends have also been reported

by Provis et al. [19]. On the other hand, the Raman analysis of silicate glass has also helped to highlight similar patterns for Q^n silicate species as a function of the alkaline level [14,39].

Formation of rings and silicate chains

The variations in Q^2 and Q^3 entities have aroused scientific curiosity. These variations may indicate the presence of previously unobserved phenomena and in particular the creation and disappearance of chains and rings. The above-mentioned results suggest that NMR and Raman spectroscopy (800 - 1300 cm^{-1}) produce similar outcomes regarding variations of silicate species as a function of the amount of alkali cations. However, additional information on the variations in the silicate chains and rings could be obtained by Raman spectroscopy (300 – 800 cm^{-1}).

Fig. 9 shows the variation of species linked to silicon tetrahedra (TO/LO, $R_{5\text{ or more}}$, R_4, R_3 and $C_{5,6,7}$) as a function of the cation concentration corrected by the M-O distance. Contributions attributed to TO/LO mode and $C_{5,6,7}$ decreased when the content of alkali cation increased whereas the band attributed to R_5 remained constant. Meanwhile, the contributions associated with R_3 and R_4 demonstrated an increase and then a decrease when the alkali cation concentration increased.

The contribution attributed to the decrease in TO/LO mode as the alkali cation concentration increased (Fig. 9Aa) was comparable with that of the Q^4 silicate species (Fig. 8a). This development is consistent with the literature [34]. The band attributed to the chains ($C_{5,6,7}$) also decreased as the cation concentration increased and then became stabilized (Fig. 9Ab). The stable contribution corresponded to the fact that large rings (i.e., rings with 5 or more tetrahedra) were present in substantial amounts in the solutions (Fig. 9Ba) [17,39]. This band is made up of contributions attributed to rings with 5 or more tetrahedra. The stability of this contribution could thus be explained by a different composition and a reorganization of the rings in these solutions. Thus, for high Si/M ratios, very large rings would be present and a decrease in the Si/M ratio would result in the formation of smaller rings such as R_5.

Fig. 9Bb shows the evolution of the position of the band attributed to rings with 5 tetrahedra or more as a function of the Si/M molar ratio of the solution. A shift of the contribution toward lower wavenumbers occurred as the Si/M ratio increased, regardless of the solution under consideration. Indeed, for solutions with a Si/M ratio of 0.5, the band was around 355 cm^{-1} while it was located at about 320 cm^{-1} for a Si/M ratio of 1.7. This phenomenon has also been observed in silicate glass [39]. Trcera [15] noticed a shift of the bands attributed to the rings and linked this to a decrease in the value of the Si-O-Si angles. However, Galeener [11] showed that the values of the Si-O-Si angles were related to the ring size. Thus, Trcera [15] put forward the theory that the shift of the bands attributed to the rings may be due to the reduction in the size of the latter. Thus, in the case of silicate solutions, the shift of the band associated with $R_{5\text{ or more}}$ was consistent with the reorganization of rings corresponding to a reduction of their size. Large rings were broken and smaller rings were formed.

The R_4 and R_3 species (Fig. 9Bc,d) had the same variations, namely an increase up to a concentration of between 1.5 and 2 mol/(L*Å) followed by a decrease. However, the maximum was reached at different concentrations (1.5 and 2 mol/(L*Å) for the R_4 and R_3 contributions, respectively). The R_4 rings decreased at slightly lower concentrations than their R_3 counterparts (1.5 and 2 mol/(L*Å) for respectively the R_4 and R_3 rings). Indeed, these rings would be transformed faster than the rings of smaller size because of steric hindrance.

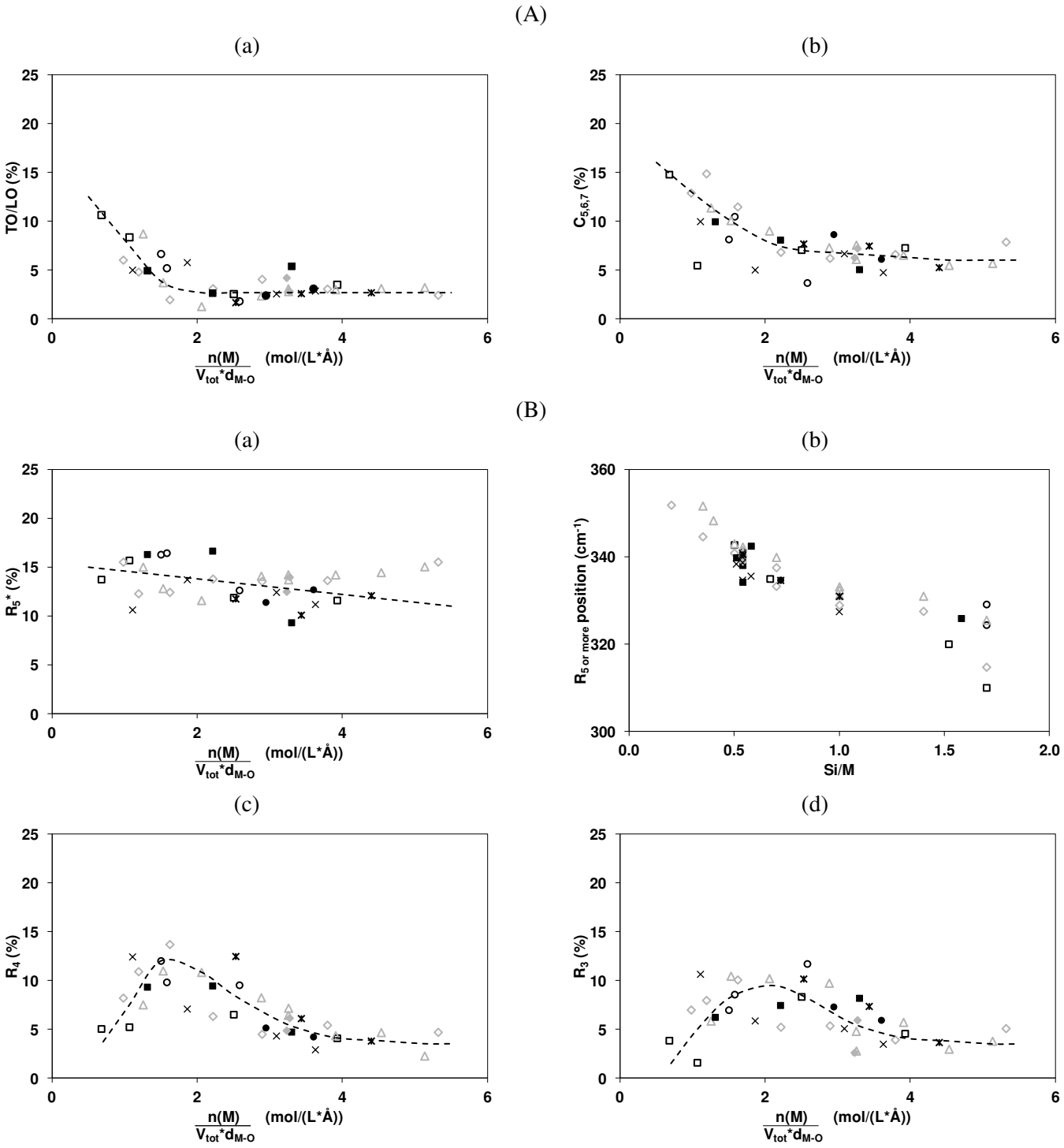

Fig. 9. Variation of (A) the area of the contributions due to (a) TO/LO and (b) $C_{5,6,7}$ and (B) (a) the $R_{5\ or\ more}$ contribution area, (b) the $R_{5\ or\ more}$ contribution position, the contribution areas of (c) the R_4 and (d) the R_3 as a function of the alkali concentration corrected by the M-O distance ($n(M)/(V_{tot}*d_{M-O})$) for (□) ${}_{C}K^{x}$, (○) ${}_{C}Na^{x}$, (◇) ${}_{L}K^{x}$, (△) ${}_{L}Na^{x}$, (×) ${}_{C}K^{x}{}_{K}{}^{y}$, (∗) ${}_{C}Na^{x}{}_{Na}{}^{y}$, (■) ${}_{C}K^{x}{}_{Na}{}^{y}$, (●) ${}_{C}Na^{x}{}_{K}{}^{y}$, (◆) ${}_{L}K^{x}{}_{Na}{}^{y}$ and (▲) ${}_{L}Na^{x}{}_{K}{}^{y}$ (Table 1).

The small amount of rings at low concentrations could be due to the large amount of water in these solutions. Indeed, Zotov and Keppler [16] have shown that increasing the amount of water in sodium-silicate glass results in the disappearance of the bands attributed to the R_3 rings. This could explain the low amount of rings observed for very low alkali cation

concentrations (about 1 mol/(L*Å)). The observed increase in R_3 and R_4 can be correlated to the decrease in chains and was thus due to the closing of chains as soon as the alkali cation was added. Indeed, when the alkali cation concentration increased, the stresses exerted by the cations became more significant and promoted a folding of the chains onto themselves. This consequently led to ring formation. These phenomena can be explained by the equilibrium of the dissociation of siliceous species [19,27]. In fact, the solutions with high Si/M ratios contained a majority of Q^3 species which is consistent with previous findings and the literature [26,27]. Their presence might be explained by the fact that the solutions contained branched chains based on Q^3. Therefore, when the alkali cation concentration increased, the stresses exerted by the cations on the chains caused them to close thus leading to the formation of rings.

Given these different variations and large concentration ranges, the reactivity of the solutions can be demonstrated by the variation of the rings and chains at a fixed concentration of silicon atoms. The contributions of the chains ($C_{5,6,7}$), rings (R_3+R_4+R_5) and Q^n species (Q^0+Q^1+Q^2) for one silicon atom were plotted against the cation concentration corrected by the M-O distance for the commercial and laboratory solutions (Fig. 10). The Q^3 and Q^4 species have not been considered in this section because of their polymerization state.
In this case, regardless of the alkali cation concentration, the same trends were found. Indeed, a significant decrease in rings was observed when the cation concentration increased. In addition, the amounts of chains and Q^n species evolved in an inversely proportional manner. When the chains decreased, an increase in Q^n species was observed. This phenomenon suggests that the chains broke to form smaller entities (Q^0, Q^1 and Q^2). For the laboratory-made solutions at a concentration of 1 mol/(L*Å), the amount of chains was 8% and the amount of Q^n species was 3%. When the concentration reached 1.5 mol/(L*Å), the percentage of $C_{5,6,7}$ and Q^n was around 5.5 %. Increasing the concentration to 3 mol/(L*Å) gave rise to quantities of chains and Q^n species of 8% and 2%, respectively. This phenomenon was also observed with the commercially available solutions, and these developments were consistent with dissociation.

With regard to the variation of the rings, it became more pronounced depending on the preparation method and the alkali cation. Indeed, for the laboratory-made solutions, there was a significant decrease of 30% to 10% respectively for concentrations of 1 and 5.2 mol/(L*Å). In addition, sodium- and potassium-based solutions exhibited similar trends. However, in the case of the commercially available solutions, significant differences were observed for ${}_C K^x$ and ${}_C Na^x$. The number of rings went from 24% to 12% and from 32% to 14% respectively when the concentration increased from 0.8 to 3.1 and from 1.5 to 3.4 mol/(L*Å) for the ${}_C K^x$ and ${}_C Na^x$ solutions. The variation in the rings was, as before, certainly due to the dissociated siliceous species. The rings broke when the amount of alkali cations increased.

Regardless of the preparation method, the same quantity of rings was obtained at lower concentrations for the potassium-based solutions compared to those based on sodium. However, this phenomenon was more pronounced in the case of the commercially available solutions. Thus, in commercial solutions, in order to obtain 23% of chains, concentrations of 1.0 and 2.5 mol/(L*Å) were required for respectively the ${}_C K^x$ and ${}_C Na^x$ solutions. The fact that the same number of rings was obtained at a lower concentration for potassium as opposed to sodium may be due to the size of the cation [24] as well as the diffusion rate [25]. Thus, potassium would give rise to a faster formation of rings by forcing chains to close at lower concentrations due to its rapid diffusion. Then, the K^+ cation, which has a greater radius than its sodium counterpart, would lead to the destruction of the rings in favor of more depolymerized Q^n species. In the case of sodium, the same phenomena would occur at higher concentrations due to the slower diffusion of the cation and its smaller radius. Thus, the

diffusion speed and the size of the alkali cation appear to have an influence on the depolymerization phenomena of the solutions.

In addition, the results suggest that commercially available and laboratory-made silicate solutions present differences in reactivity for concentrations between 2 and 4 mol/(L*Å). These differences were not observed by ^{29}Si NMR. Therefore, these results show that Raman spectroscopy makes it possible to understand the depolymerization phenomena involved with different cations and for different solutions when this is not possible by NMR.

(A)

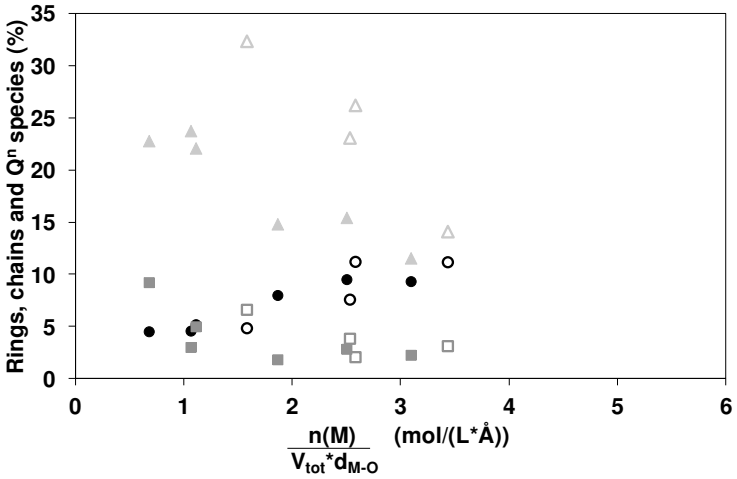

(B)

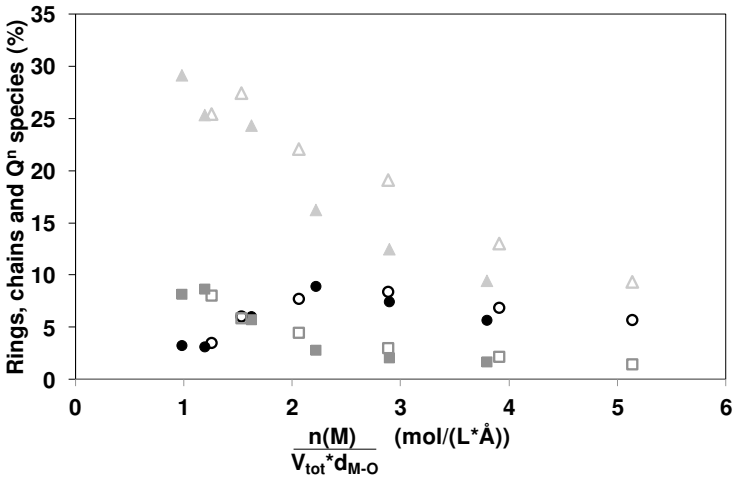

Fig. 10. Variation of the amount of (■) chains ($C_{5,6,7}$), (▲) rings (R_3 + R_4 + R_5) and (●) Q^n species (Q^0 + Q^1 + Q^2) versus the alkali concentration corrected by the M-O distance ($n(M)/(V_{tot}*d_{M-O})$) for (A) commercial $SiM^x_{C\text{-}M}{}^y$ and (B) laboratory $SiM^x_{L\text{-}M}{}^y$ solutions with M = (■, ▲, ●) K and (□, △, ○) Na.

4. Conclusion

Various commercially available and laboratory-made alkaline silicate solutions based on potassium, sodium or a mixture of the two were studied by Raman spectroscopy. The results show that:

1) Increasing the cation concentration to 5.5 mol/(L*Å), i.e., decreasing the Si/M ratio from 1.7 to 0.2 resulted in the depolymerization of the solution. Meanwhile, the contribution of R_3 and R_4 rings went through a maximum for cation concentrations of 2 and 1.5 mol/(L*Å), respectively.

2) The preparation method (commercial or laboratory) affected the silicate species and especially the R_3 and R_4 rings that were preferentially dependent on the alkali cation for the commercially available solutions. Their reactivity can be identified from the variations in the rings as well as in the Q^0 and Q^4 species.

3) The nature of the alkali cation had an effect on the formation of the rings, particularly for potassium.

This study also showed that Raman spectroscopy can be used to obtain additive information, especially with regard to changes in chains ($C_{5,6,7}$), silicate-containing rings (R_3, R_4 and R_5), and the TO/LO mode. These data rendered it possible to determine the depolymerization phenomena involved, which is not the case for NMR spectroscopy.

Thus, Raman spectroscopy is a promising tool for determining the reactivity of silicate solutions, which greatly contributes to the use of such solutions in numerous applications.

Acknowledgments

The authors gratefully acknowledge the FEDER agency, the Limousin regional council, the DIRECCTE agency and the FUI program for their financial support.

References

[1] A.C.J.H. Johnson, P. Greenwood, M. Hagström, Z. Abbas, S. Wall, Aggregation of nanosized colloidal silica in the presence of various alkali cations investigated by the electrospray technique, Langmuir 24 (2008) 12798-12806.
[2] M.T. Tognonvi, D. Massiot, A. Lecomte, S. Rossignol, J.-P. Bonnet, Identification of solvated species present in concentrated and dilute sodium silicate solutions by combined ^{29}Si NMR and SAXS studies, J. Colloid Interface Sci. 352 (2010) 309-315.
[3] S. Lucas, M.T. Tognonvi, J.-L. Gelet, J. Soro, S. Rossignol, Interactions between silica sand and sodium silicate solution during consolidation process, J. Non-Cryst. Solids 357 (2011) 1310-1318.
[4] M.T. Tognonvi, J. Soro, S. Rossignol, Physical-chemistry of silica/alkaline silicate interactions during consolidation. Part 1: Effect of cation size, J. Non-Cryst. Solids 358 (2012) 81-87.
[5] A. Autef, E. Joussein, G. Gasgnier, S. Rossignol, Role of the silica source on the geopolymerization rate, J. Non-Cryst. Solids. 358 (2012) 2886-2893.
[6] G. Engelhardt, D. Zeigan, H. Jancke, D. Hoebbel, Z. Weiker, High resolution ^{29}Si NMR of silicates and zeolites, Z. Anorg. Allg. Chem. 418 (1975) 17-28.
[7] J.L. Bass, G.L. Turner, Anion distributions in sodium silicate solutions. Characterization by ^{29}Si NMR and infrared spectroscopies, and vapor phase osmometry, J. Phys. Chem. B. 101 (1997) 10638-10644.
[8] A. Bourlon, Physico-chimie et rhéologie des géopolymères frais pour la cimentation des puits pétroliers, Ph.D. Thesis, University of Pierre et Marie Curie, 2011.
[9] H. Cho, A.R. Felmy, R. Craciun, J.P. Keenum, N. Shah, D.A. Dixon, Solution state structure determination of silicate oligomers by ^{29}Si NMR spectroscopy and molecular modeling, J. Am. Chem. Soc. 128 (2006) 2324-2335.
[10] C. Le Losq, D.R. Neuville, Effect of the Na/K mixing on the structure and the rheology of tectosilicate silica-rich melts, Chem. Geol. 346 (2013) 57-71.
[11] F.L. Galeener, Planar rings in vitreous silica, J. Non-Cryst. Solids. 49 (1982) 53-62.

[12] J.D. Hunt, A. Kavner, E.A. Schauble, D. Snyder, C.E. Manning, Polymerization of aqueous silica in H2O-K2O solutions at 25-200 °C and 1 bar to 20 kbar, Chem. Geol. 283 (2011) 161-170.
[13] L. Vidal, E. Joussein, M. Colas, J. Cornette, J. Sanz, I. Sobrados, J.-L. Gelet, J. Absi, S. Rossignol, Controlling the reactivity of silicate solutions: a FTIR, Raman and NMR study, Colloid Surf. A 503 (2016) 101-109.
[14] W.J. Malfait, V.P. Zakaznova-Herzog, W.E. Halter, Quantitative Raman spectroscopy: high-temperature speciation of potassium silicate melts, J. Non-Cryst. Solids 353 (2007) 4029-4042.
[15] N. Trcera, Etude de la structure des verres magnésio-silicatés : approche expérimentale et modélisation, Ph.D. Thesis, University of Paris-Est, 2010.
[16] N. Zotov, H. Keppler, The influence of water on the structure of hydrous sodium tetrasilicate glasses, Am. Mineral. 83 (1998) 823-834.
[17] C. Le Losq, Rôle des éléments alcalins et de l'eau sur les propriétés et la structure des aluminosilicates fondus et vitreux : implications volcanologiques, Ph.D. Thesis, University Paris-Diderot, 2012.
[18] P. Steins, Influence des paramètres de formulation sur la texturation et la structuration des géopolymères, Ph.D. Thesis, University of Limoges, 2014.
[19] J.L. Provis, P. Duxson, G.C. Lukey, F. Separovic, W.M. Kriven, J.S.J. van Deventer, Modeling speciation in Highly concentrated alkaline silicate solutions, Ind. Eng. Chem. Res. 44 (2005) 8899-8908.
[20] A. Gharzouni, E. Joussein, B. Samet, S. Baklouti, S. Pronier, I. Sobrados, J. Sanz, S. Rossignol, The effect of an activation solution with siliceous species on the chemical reactivity and mechanical properties of geopolymers, J. Sol-Gel Sci. Technol. 73 (2014) 250-259.
[21] I.L. Svensson, S. Sjöberg, L.-O. Öhman, Polysilicate equilibria in concentrated sodium silicate solutions, J. Chem. Soc., Faraday Trans. 1 82 (1986) 3635-3646.
[22] E. Prud'homme, A. Autef, N. Essaidi, P. Michaud, B. Samet, E. Joussein, S. Rossignol, Defining existence domains in geopolymers through their physicochemical properties, Appl. Clay Sci. 73 (2013) 26-34.
[23] N.H. Ray, R.J. Plaisted, The constitution of aqueous silicate solutions. J. Chem. Soc. Dalton Trans, (1983) 475-481.
[24] J. Mähler, I. Persson, A study of the hydration of the alkali metal ions in aqueous solutions, Inorg. Chem. 51 (2012) 425-438.
[25] T. Melkior, S. Yahiaoui, D. Thoby, S. Motellier, V. Barthès, Diffusion coefficients of alkaline cations in Bure mudrock, Phys. Chem. Earth. 32 (2007) 453-462.
[26] C.F. Weber, R.D. Hunt, Modeling alkaline silicate solutions at 25 °C, Ind. Eng. Chem. Res. 42 (2003) 6970-6976.
[27] A.S. Brykov, V.V. Danilov, E.Y. Aleshunina, State of silicon in silicate and silica-containing solutions and their binding properties, Russ. J. Appl. Chem. 81 (2008) 1717-1721.
[28] G.D. Cody, B.O. Mysen, S.K. Lee, Structure vs. composition: a solid-state ^{1}H and ^{29}Si NMR study of quenched glasses along the Na_2O-SiO_2-H_2O join, Geochim. Cosmochim. Ac. 69 (9) (2005) 2373-2384.
[29] W.J. Malfait, W.E. Halter, Y. Morizet, B.H. Meier, R. Verel, Structural control on bulk melt properties: single and double quantum ^{29}Si NMR spectroscopy on alkali-silicate glasses, Geochim. Cosmochim. Ac. 71 (2007) 6002-6018.
[30] B.O. Mysen, G.D. Cody, Solution mechanisms of H_2O in depolymerized peralkaline melts, Geochim. Cosmochim. Ac. 69 (2005) 5557-5566.

[31] N. Zotov, I. Ebbsjö, D. Timpel, H. Keppler, Calculation of Raman spectra and vibrational properties of silicate glasses: comparison between $Na_2Si_4O_4$ and SiO_2 glasses, Phys. Rev. B 60 (9) (1990) 6383-6397.
[32] H. Aguiar, J. Serra, P. González, B. León, Structural study of sol-gel silicate glasses by IR and Raman spectroscopies, J. Non-Cryst. Solids. 355 (2009) 475-480.
[33] E.V. Belova, Y.A. Kolyagin, I.A. Uspenskaya, Structure and glass transition temperature of sodium silicate glasses doped with iron, J. Non-Cryst. Solids 423-424 (2015) 50-57.
[34] B. Hehlen, D.R. Neuville, Raman response of network modifier cations in alumino-silicate glasses, J. Phys. Chem. B 119 (2015) 4093-4098.
[35] M. Chligui, Etude des propriétés optiques et mécaniques des verres binaires silicatés d'alcalins lourds, Ph.D. Thesis. University of Orléans.
[36] A. Depla, E. Verheyen, A. Veyfeyken, M. Van Houteghem, K. Houthoofd, V. Van Speybroeck, M. Waroquier, C.E.A. Kirschhock, J.A. Martens, UV-Raman and 29Si NMR spectroscopy investigation of the nature of silicate oligomers formed by acid catalyzed hydrolysis and polycondensation of tetramethylorthosilicate, J. Phys. Chem. C 115 (2011) 11077-11088.
[37] R.K. Harris, E.K.F. Bahlmann, Quantitative Silicon-29 NMR investigations of highly concentrated high-ratio sodium silicate solutions, Magn. Res. Chem. 31 (1993) 743-747.
[38] J.L. Koenig, P.T.K. Shih, Raman and infrared spectroscopic studies of the reactions of silica and glass surfaces, Mat. Sci. Eng. 20 (1975) 127-135.
[39] W.J. Malfait, V.P. Zakaznova-Herzog, W.E. Halter, Quantitative Raman spectroscopy: speciation of Na-silicate glasses and melts, Am. Miner. 93 (2008) 1505-1518.

Publication 6 (ACL 6)

L. Vidal, E. Joussein, I. Sobrados, J. Absi, S. Rossignol

"How to counteract the low reactivity of an alkaline solution"

Journal of Non-Crystalline Solids, 2016, vol. 452, p. 220-230.

Journal of Non-Crystalline Solids 452 (2016) 220–230

Contents lists available at ScienceDirect

Journal of Non-Crystalline Solids

journal homepage: www.elsevier.com/locate/jnoncrysol

How to counteract the low reactivity of an alkaline solution

L. Vidal [a], E. Joussein [b], I. Sobrados [d], J. Absi [c], S. Rossignol [a,*]

[a] SPCTS, ENSCI, 12 rue Atlantis, 87068 Limoges Cedex, France
[b] Université de Limoges, GRESE EA 4330, 123 Avenue Albert Thomas, 87060 Limoges, France
[c] Université de Limoges, SPCTS, 12 rue Atlantis, 87068 Limoges Cedex, France
[d] Instituto de Ciencia de Materiales de Madrid, Consejo Superior de Investigaciones Científicas (CSIC), C/Sor Juana Inés de la Cruz, 3, 28049 Madrid, Spain

ARTICLE INFO

Article history:
Received 13 July 2016
Received in revised form 29 August 2016
Accepted 31 August 2016
Available online xxxx

Keywords:
Geopolymer
Ammonium molybdate
Silicate species
Metakaolin reactivity
Raman spectroscopy

ABSTRACT

This study is focused on understanding the role of molybdic species during polycondensation reactions. For this purpose, several geopolymers were synthesized using two metakaolins of different reactivities and various amounts of ammonium molybdate (0.40, 0.80 and 1.57% molar molybdenum). The reactions involved were investigated by FTIR, Raman, DTA and MAS-NMR. The results showed that the addition of Mo induces the modification of (i) the silica species negative charge balance and (ii) their nature and size, and favors perturbations toward the polycondensation reactions, which differ in terms of metakaolin reactivity. The addition of Mo species to the silicate solution counterbalances the metakaolin reactivity (the presence of an Al-rich or Si-rich network). This highlights the modification and formation roles played by molybdenum atoms, depending on the amount of ammonium molybdate added.

1. Introduction

Geopolymer materials are prepared at room temperature by alkaline activation of aluminosilicate sources [1]. These materials have many applications due to their temperature resistance [2] and their mechanical characteristics. To increase their mechanical strength, reinforcements may be added to the matrix [3]. For example, concrete reinforced with glass fibers exhibits higher fire strength than conventional concrete. Masi et al. [4] showed that the addition of basalt fibers to a geopolymer matrix improves the temperature resistance of these materials. Likewise, it is possible to add refractory compounds to promote thermal resistance [5]. Another possibility is based on the addition of compounds, including boron or phosphorus, to the formulation of various types of materials. For example, Xia et al. [6] showed that the addition of boron to lithium aluminosilicate reinforced with carbon fibers improves the temperature stability of this material, resulting in zero thermal expansion. The addition of these additives requires perfect control of the interactions between the binder and reinforcement [7] and leads to local changes in the composition. Therefore, it is ideal to introduce compounds whose influence is known in advance.

In the case of geopolymer binders, the final structure of the material depends on the nature of the oligomers formed during polycondensation reactions. The formation of these oligomers is influenced by the sources of the raw materials. Many studies have shown that the properties of raw materials, i.e., the alkaline solution and metakaolin, influence the structure of the final materials. Autef et al. [8] demonstrated that in the consolidated materials, the metakaolin reactivity influences the kinetics of reactions and the formation of networks. Regarding the silicate solution, Singh et al. [9] studied the influence of the alkaline solution on the reactions and demonstrated the appearance of different phenomena depending on the alkaline solution. It was also noted that the nature and the concentration of the alkaline cation influences the polycondensation reactions and therefore the properties of the consolidated materials [10,11].

Oligomer formation and polycondensation reactions, which are the origin of geopolymer binder formation, can be evaluated by various characterization techniques, including NMR and FTIR spectroscopies and thermal analysis. Polycondensation reactions followed by FTIR spectroscopy are related to the evolution of the Si-O-M peak, which indicates the replacement of Si—O—Si by Si—O—Al bonds [12]. Autef et al. [13] followed the formation of geopolymers maintained at 70 °C for 2 h by thermal analysis. The various stages of the formation of these materials, such as the reorganization of the species, metakaolin dissolution, oligomer formation and polycondensation reactions made it possible to identify the formation energies. An ^{1}H NMR study also revealed the existence of four stages in the geopolymerization reactions [14]. ^{27}Al NMR analysis was used to study the formation of these materials, particularly the changing amounts of Al (IV), Al (V) and Al (VI) during polycondensation reactions [9]. Another study by X-ray scattering at small angles showed that the alkaline cation influences the reaction rate and the arrangement of oligomers [15].

Previous work on geopolymer binders made from different metakaolins [16], conducted in our laboratory, highlighted the monitoring of the final shrinkage vs temperature in the presence of ammonium molybdate. The molybdenum cation in basic medium can react with

* Corresponding author.
E-mail address: sylvie.rossignol@unilim.fr (S. Rossignol).

http://dx.doi.org/10.1016/j.jnoncrysol.2016.08.045
0022-3093/

silica, alumina or potassium to form various complexes. Debecker et al. [17] demonstrated the formation of $Al(OH)_6Mo_6O_{18}^{3-}$ entities when a solution of ammonium heptamolybdate is added to an aluminosilicate compound. Other authors have shown the formation of K_2MoO_4 or $K_2Mo_2O_7$ species [18,19] when interactions between molybdic and potassium species occur. However, molybdenum only reacts with silica in an acid medium to form Keggin ions with the formula $SiMo_{12}O_{40}^{4-}$ [20]. Sarrazin et al. [20] showed that only MoO_4^{2-} entities exist in basic media, and this fact was confirmed by Jiang et al. [21]. This information provides insight into the phenomena occurring during the formation of polycondensation reactions that are responsible for improving the thermal resistance of samples.

The objective of this work is to investigate the impact of the molybdenum cation on the final structure of the binders. For this purpose, reactive mixtures prepared from two metakaolins presenting different reactivity and different amounts of molybdate were analyzed to determine the influence of this compound on polycondensation reactions in different solutions. Finally, the correlation between the characteristics of the raw materials and the final geopolymer structure will also be presented.

2. Experimental section

2.1. Sample preparation

Samples were synthesized using an alkaline silicate solution (Si/K = 0.7) and two metakaolins (denoted M1 and M2) from the supplier Imerys, AGS Clerac, France (Table 1). The alkaline silicate solution was obtained by dissolving KOH pellets (85.2% purity) and amorphous silica (99.9% purity) in osmotically purified water at room temperature, as described in previous works [22]. Two types of alkaline silicate solution were studied: pure potassium silicate solution and solutions with various amounts of anhydrous ammonium molybdate $(NH_4)_2Mo_2O_7$ (99.9% purity). The amounts added were 0.40, 0.80 and 1.57% molar molybdenum. The pH value of these various solutions was 14.

Syntheses were performed by mixing the alkaline silicate solution and metakaolins. Then, the samples were placed in a closed mold at room temperature (25 °C) [13].

Table 2 presents the nomenclature of the various solutions and geopolymers studied. The nomenclature used for the silicate solutions is ${}_LK^{0.7}{}_x$, where L represents a lab-prepared solution, 0.7 is the Si/K molar ratio and x is the amount of molybdenum added. For example, ${}_LK^{0.7}{}_{0.40}$ corresponds to an alkaline silicate solution with 0.40% molybdenum. For the geopolymers, the nomenclature used is ${}^TMy_x$, where x is the amount of molybdenum added, My is the metakaolin used and T is the temperature. For example, a geopolymer made with M1 metakaolin with 0.80% molybdenum prepared at ambient temperature is denoted ${}^{25}M1_{0.80}$.

2.2. Characterization

Fourier-transform infrared (FTIR) spectroscopy in ATR mode was used to monitor the geopolymerization. FTIR spectra were obtained using a ThermoFisher Scientific Nicolet 380 infrared spectrometer. The IR spectra were collected over a wavenumber range of 400 to 4000 cm^{-1} with a resolution of 4 cm^{-1}. To follow the evolution of the bonds over time, software was used to acquire a spectrum every 10 min for 8 h. The atmospheric CO_2 contribution was removed by a straight line between 2400 and 2280 cm^{-1}. To allow comparison of the spectra, they were corrected using a baseline and were normalized.

Table 1
Chemical characteristics of raw materials and geopolymers.

	Metakaolin		Geopolymer mixture		
	Chemical composition (weight %)		Si/Al	K/Al	Water (weight %)
	SiO_2	Al_2O_3			
M1	55.0	40. 0	1.80	0.89	32.8
M2	55.0	39.0	1.84	0.92	32.8

Table 2
Nomenclature of samples.

Mo amount (mol %)	Solution	M1	M2
0	${}_LSiK^{0.7}$	${}^TM1_0$	${}^TM2_0$
0.40	${}_LSiK^{0.7}{}_{0.40}$	${}^TM1_{0.40}$	${}^TM2_{0.40}$
0.80	${}_LSiK^{0.7}{}_{0.80}$	${}^TM1_{0.80}$	${}^TM2_{0.80}$
1.57	${}_LSiK^{0.7}{}_{1.57}$	${}^TM1_{1.57}$	${}^TM2_{1.57}$

Raman spectroscopy was performed on the solutions using a T64000 Horiba-Jobin-Yvon spectrophotometer with 514 nm laser excitation operating at a power of 30 mW at the sample. Scattered light was collected in backscattering mode using a specific assembly for liquid samples with a triple diffraction grating (1800 lines/mm). The spectral range was 250 to 1300 cm^{-1}, and 60 scans of 15 s each were performed for the acquisition. The subtracted baseline was modeled by a five-degree polynomial curve. The contributions in the range 700–1300 cm^{-1}, attributed to silicate species, were difficult to decompose due to the molybdenum contributions, which are very intense. Thus, the Raman spectra were decomposed in the range 250–700 cm^{-1} using Wire 4.0 software from Renishaw [23] (Fig. 1). The contributions were modeled by a pseudo-Voigt function. To compare the different solutions, the intensity of each contribution was normalized by the intensity of the contribution located at 446 cm^{-1} (attributed to $R_{5\ or\ more}$, i.e., rings with 5 or more tetrahedra). The same observations were made on solutions prepared a few minutes or 24 h before being analyzed. The various contributions observed by Raman spectroscopy are listed in Table 3 [24,25,26].

NMR experiments were performed on silicate solutions and crushed geopolymer samples at room temperature on a Bruker AVANCE-400 spectrometer operating at 79.49 and 104.26 MHz (^{29}Si and ^{27}Al signals, respectively). For the solutions, the ^{29}Si (I = 1/2) NMR spectra were acquired after a π/2-pulse irradiation (4 μs), and a 500 kHz filter was used to improve the signal/noise ratio. The number of scans collected was 400, and the time between acquisitions was 10 s to minimize saturation effects. The ^{29}Si chemical shifts were measured using an external standard of tetramethylsilane (TMS). The error in the chemical shift values was estimated to be <0.5 ppm. Errors in the determination of the relative band intensities were estimated as lower than 5%. For the geopolymer sample ^{27}Al (I = 5/2) MAS-NMR signals, spectra were

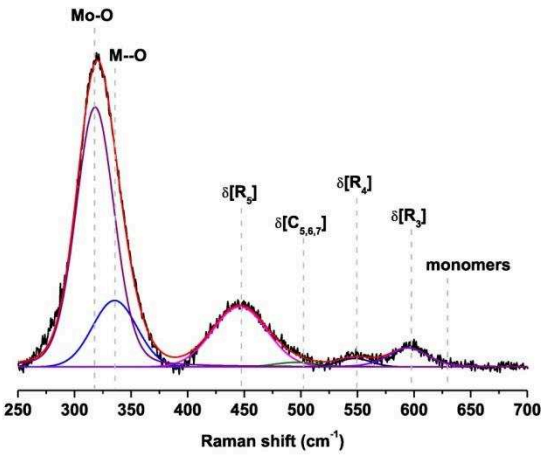

Fig. 1. Example of decomposition of Raman spectra obtained for ${}_LK^{0.7}{}_{0.40}$.

Table 3
Vibrational frequencies of various species for Raman spectroscopy.

Species	Contribution	Raman shift (cm^{-1})	References
Silicate	ν_s (Si-O) (Q^4)	1120–1230	[32,33]
	ν_s (Si-O^-) (Q^3)	1000–1100	[32,33]
	ν_s (Si-O^-) (Q^2)	920–1000	[32]
	ν_s (Si-O^-) (Q^1)	850–920	[25]
	ν_s (Si-O^-) (Q^0)	800–875	[24,25]
	TO/LO (Si-O-Si)	650–850	[25]
	ν_s (Si-O) (monomers)	639–649	[31]
	D_2 (δ [R_3])	587–606	[25,33]
	ν_s (Si-O-Si) ($C_{5,6,7}$)	515–535	[31]
	D_1 (δ [R_4])	453–550	[24,25]
	δ [$R_{5\ or\ more}$]	400–490	[24,25]
Alkali cation	M-O (network modifiers)	340–360	[24]
Molybdate	ν_s (Mo-O) (MoO_4^{2-})	888–892	[34,36]
	($Mo_2O_7^{2-}$)	929 [O]	[36]
	($Mo_7O_{24}^{6-}$)	908 [T]	
		959 [O]	[26]
	ν_{as} (Mo-O) (MoO_4^{2-})	837–852	[34,36]
	($Mo_2O_7^{2-}$)	873 [O]	[36]
	($Mo_7O_{24}^{6-}$)	860 [T]	
		911	[26]
	δ (Mo-O) (MoO_4^{2-})	317	[36]
	($Mo_7O_{24}^{6-}$)	360 [O]	[26]

recorded after π/8 pulse irradiation (1.5 μs) using a 1 MHz filter to improve the signal/noise ratio. In the MAS experiments, powder samples were spun at 10 kHz. The number of scans was 50 for aluminum. The ^{29}Si (I = 1/2) MAS-NMR spectra were recorded after π/2-pulse irradiation (4 μs) using a 500 kHz filter to improve the signal/noise ratio. In each case, 400 scans were collected. The time between acquisitions was set to 10 s to minimize the saturation effects. Quantitative analysis of the NMR spectra was carried out with the Winfit software package (Bruker). This program allows the position, line width, and intensity of components to be determined.

The pH measurements were made using a Schott Instrument Lab860 at room temperature. To follow the variation of the pH during geopolymerization, a small amount of the reactive mixture was placed in a mold, water was added and the electrode was placed in the mixture. The geopolymer/water mass ratio was 0.12. The pH value was recorded after 3 min.

Wetting angles were measured with a Digidrop MCAT from GBX composed of a camera and a lamp to record the deposition of a drop. A solution drop was deposited on an HDPE substrate, and the wetting angle was estimated at t = 0, i.e., on the first image where the drop is deposited on the substrate, using Visiodrop software from GBX. The solutions were prepared 24 h before analysis. Wetting angle measurements were performed 5 times with an estimated error of 4%.

Differential thermal analysis (DTA) and thermogravimetric analysis (TGA) were performed on an SDT Q600 apparatus from TA Instruments in a flowing dry air atmosphere (100 mL/min) in platinum crucibles. The signals were measured using Pt/Pt-10% Rh thermocouples. Milligram aliquots of the samples were placed in platinum crucibles. The reactive mixtures were heated to 70 °C, maintained at this temperature for 120 min and then heated to 800 °C at a rate of 10 °C/min.

3. Results

3.1. Effect of molybdate on geopolymerization

The influence of molybdic species on geopolymerization mechanisms was evaluated by (i) infrared spectroscopy, (ii) changes in pH values and (iii) thermal analysis.

The infrared spectra of the $^{25}M1_x$ and $^{25}M2_x$ binder formulations, with x varying from 0 to 1.57%, were similar to those obtained in previous studies [8]. Consequently, only the displacement of the Si-O-M peak position (M = Si or Al) was plotted as a function of time for the different compositions (Fig. 2A). Regardless of the mixture, more or less pronounced displacement of the Si-O-M peak is observed in relation to the polycondensation reactions [27].

A slight increase of the initial peak wavenumber is noted when the amount of added ammonium molybdate increases from 981 to 987 cm^{-1} for mixtures $^{25}My_0$ and $^{25}My_{1.57,}$ respectively. Although this variation remains within the measurement error bars, the molybdenum addition modifies the wavenumber and therefore the interactions in the chemical bonds. The initial Si-O-M peak position is linked to the siliceous species and the number of non-bridging oxygen atoms (NBO) [28]. The addition of molybdenum therefore induces a change in the distribution of the negative charges of siliceous species. The total displacement values are also influenced by the addition of molybdate to the $^{25}M1_x$ binders (Fig. 2Aa) and change from 40 to 34 cm^{-1}, respectively, for the $^{25}M1_0$ and $^{25}M1_{1.57}$ samples. In contrast, in the presence of $^{25}M2_x$ binders (Fig. 2Ab), there are minimal changes. This highlights the importance of the alkaline solution, which is distinguished only in the case of the low-reactive metakaolin M1 [8,28], whereas for M2, highly reactive metakaolin, the effect of the solution is almost negligible.

The slopes and displacement values (Fig. 2B) deduced from the monitoring of binders $^{25}M1_x$ and $^{25}M2_x$ are located in the region where several networks coexist or in the geopolymer area according to previous works [29]. The $^{25}M1_x$ samples are located in the zone where several networks coexist. However, the addition of molybdenum to the $^{25}M1_0$ and $^{25}M1_{1.57}$ binders decreases the displacement and the slope values from 40 cm^{-1} and −0.29 $cm^{-1}.min^{-1}$ to 34 cm^{-1} and −0.12 $cm^{-1}.min^{-1}$, respectively. This reflects the impact of the modified alkaline solution, which induces better reorganization of the species, promoting the dissolution of the aluminosilicate source. Therefore, the presence of molybdic anions, due to their charge, changes the siliceous species, thereby promoting the formation of a geopolymer network.

For the $^{25}M1_x$ and $^{25}M2_x$ (x = 0, 0.40 and 1.57) binders, the variation in the pH value and its evolution (Fig. 3) determines the unreacted species. A faster or slower decrease of the pH indicates composition-dependent reactivity. The $^{25}M1_0$ sample has an initial pH value greater than that of geopolymer $^{25}M2_0$ (13 and 12.5, respectively) due to the different reactivity of the metakaolin. M2 metakaolin, which is more reactive than M1 and promotes polycondensation reactions, leads to the presence of few basic species, explaining the fast decrease of the pH value. In the presence of metakaolin M1, the reactions are slower. The addition of ammonium molybdate to the mixtures $^{25}M1_{0.40}$ and $^{25}M1_{1.57}$ decreases the initial pH value and favors geopolymerization reactions. However, the difference in the observed time needed for the decrease, induced by the addition of molybdenum, suggests the formation of species with different size/charge and blocks the diffusion of other species. The change in the reactions due to increased molybdate content suggests that these species react with other alkaline cations or entities produced by the dissolution of metakaolin. Keggin ions and compounds based on potassium or aluminum can be formed [17,18,19]. In the presence of M2 metakaolin, polycondensation reactions are slightly affected because the variations are similar. A small change in pH from 11.8 to 10.7 is noted for the $^{25}M2_{1.57}$, binder which also indicates a change in the steric hindrance of silicate species.

These data indicate that the molybdate addition disturbs siliceous or alkaline species and modifies the polycondensation reactions from a thermodynamic point of view in the presence of a very reactive metakaolin, whereas in the presence of a less-reactive metakaolin, there is just a kinetic order change.

The formation steps of different binders were followed by thermal analysis as a function of time at 70 °C (Fig. 4). This temperature was selected for technical reasons [13]. The room temperature experiment lasted 72 h, whereas at 70 °C, the experiment lasted only 4 h. Previous studies validated this temperature difference [30]. Given the experimental conditions, the curves show two different areas, A and B, which characterize the steps of binder forming and behavior during

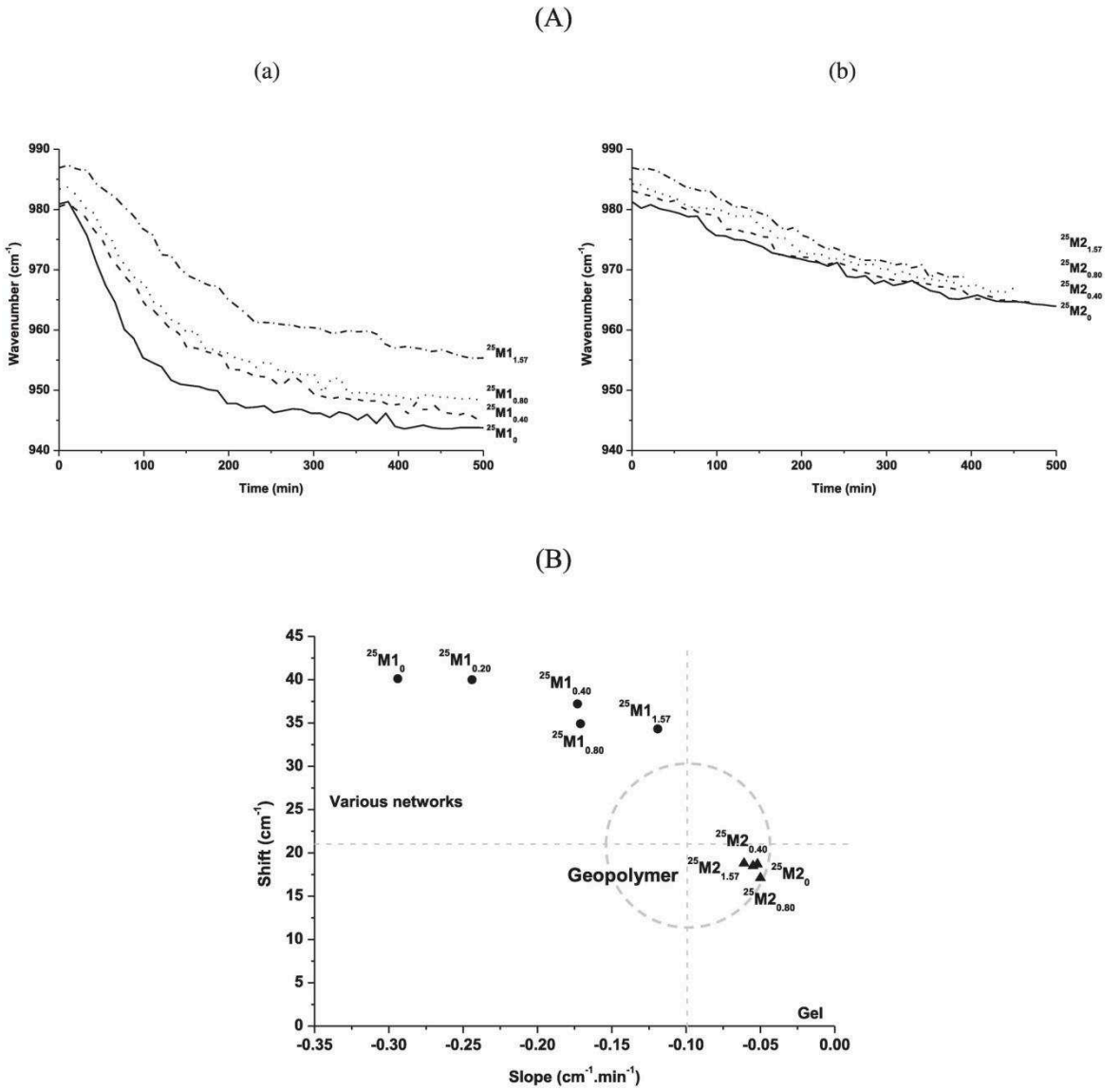

Fig. 2. (A) Shift values of Q^2 position from FTIR spectra versus the time at room temperature for (a) $^{25}M1_x$ and (b) $^{25}M2_x$ geopolymers with x = (—) 0, (–) 0.40, (····) 0.80 and (---) 1.57 and (B) variation of shift value in function of the slope for (●) $^{25}M1_x$ and (▲) $^{25}M2_x$ (± 4 cm^{-1}).

heat treatment, respectively, revealing the water content of the material [30]. The $^{70}M1_0$ and $^{70}M2_0$ compositions show similar weight losses of approximately 5.7%, and the molybdate addition induces a slight decrease to 4.90% for the $^{70}My_0$ and $^{70}My_{1.57}$ samples. The heat flow curves and their time derivative for the $^{70}M2_0$ mixture show four areas defined by the inflection points [30] (Fig. 5a). Zone I is attributed to the reorganization of the different species (i.e., speciation equilibrium), zone II corresponds to the dissolution of metakaolin, zone III is associated with oligomer formation and zone IV is due to polycondensation reactions. The number of moles of water used during the various stages of formation was calculated and normalized to the total water loss from area A (Fig. 5b). For the first area, the consumed water amount, characterizing the associated energy, is similar for all mixtures (≈28%). For zone II, the energy associated with the dissolution of metakaolin is the most important for the $^{70}M2_0$ mixture, according to its reactivity, because there is rapid release of aluminosilicate species. The addition of molybdenum ($^{70}M2_{1.57}$) causes a slight decrease in energy, which can be explained by a previously mentioned kinetic effect. In the presence of $^{70}M1_0$, the M1 metakaolin, which is less reactive, is dependent on the alkaline solution, and the associated energy is reduced due to the more difficult reaction [8]. The $^{70}M1_{1.57}$ sample has slightly higher energy, suggesting that the modification of the alkaline solution leads to better metakaolin dissolution. In this case, the different entities containing molybdenum attract siliceous and aluminous species, favoring metakaolin dissolution. Metakaolin dissolution impacts oligomer formation (zone III); therefore, the $^{70}M2_0$ mixture has the lowest energy [8,28]. The small difference in presence of molybdenum can be attributed to the siliceous entity disorder requiring more energy. Similar

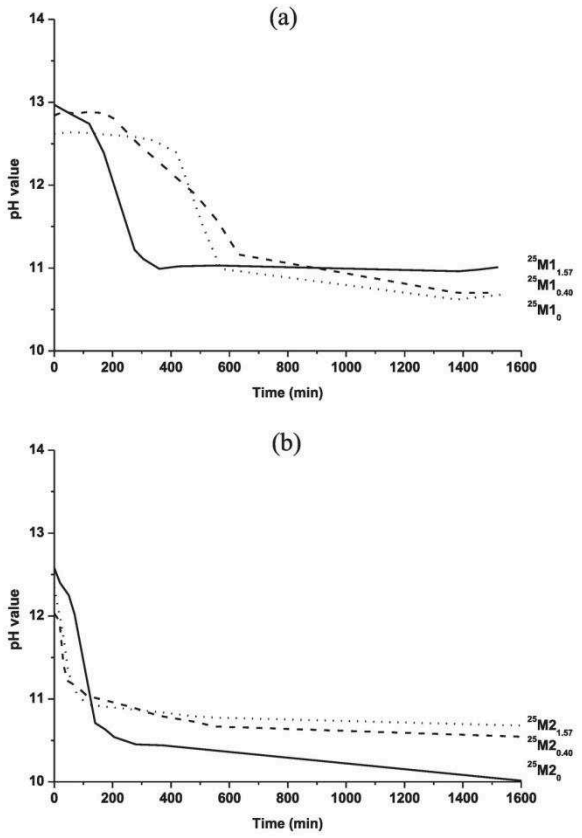

Fig. 3. Variation of the pH value as a function of time for (a) $^{25}M1_x$ and (b) $^{25}M2_x$ samples with x = (—) 0, (–) 0.40 and (····) 1.57 (pH error ± 0.1).

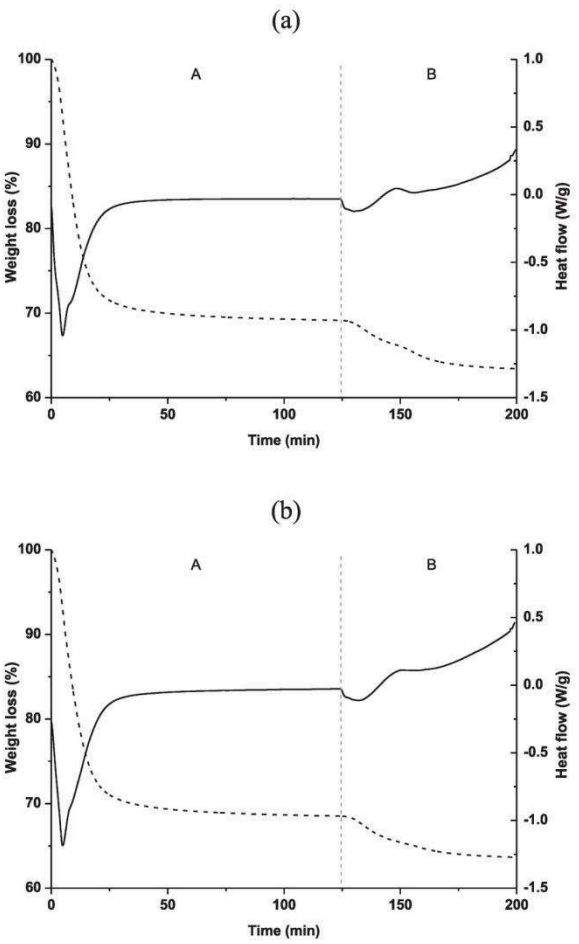

Fig. 4. (–) Weight loss and (—) heat flow versus time for the (a) $^{70}M2_0$ and (b) $^{70}M2_{1.57}$ mixtures.

phenomena are notable for $^{70}M1_0$ and $^{70}M1_{1.57}$ because the associated energies are higher. Finally, for zone IV, the energy required for polycondensation reactions is minimal when the formation of oligomers is facilitated. In the presence of molybdate, there is a small increase when the oligomer formation requires more energy. The same conclusions apply to M1 metakaolin.

Therefore, it has been shown that silicate solutions have different polymerization states depending on the molybdate content. Furthermore, the addition of molybdate delays polycondensation reactions for highly reactive metakaolin, and for low-reactive metakaolin, there are thermodynamic changes.

3.2. Effect of molybdate addition on alkaline silicate solution reactivity

To identify the species responsible for the observed differences, this section is devoted to the identification of species in solution by spectroscopic studies [22,23]. The $_LK^{0.7}{}_x$ (x varying from 0 to 1.57%) were characterized by Raman spectroscopy and ^{29}Si NMR (Figs. 6 and 7).

The Raman spectra of the various solutions (Fig. 6a) present the contributions assigned to the various silicate species reported in Table 3 [31,32,33]. Those containing molybdenum have bands located at 317, 838 and 896 cm^{-1}, whose intensity increases with the molybdenum content, that are, respectively, due to the δ(Mo-O), ν_{as}(Mo-O) and ν_s(Mo-O) vibrations of the MoO_4^{2-} entities [34,35,36] (Fig. 6). The presence of MoO_4^{2-} entities indicates that $Mo_2O_7^{2-}$ species are not stable in basic medium and are transformed in accordance with the works of Jiang et al. [21], who showed that in alkaline media, only the MoO_4^{2-} species exist (Eq. 1).

$$Mo_2O_7{}^{2-} + 2OH^- = 2MoO_4{}^{2-} + H_2O \quad (1)$$

The Raman spectra were then decomposed in the 300–700 cm^{-1} range due to the high intensity of the Mo-O contributions located at 838 and 896 cm^{-1}, leading to a pronounced decrease in the silicate species contributions. Fig. 6b shows the variations of the Mo-O/$R_{5\ and\ more}$ and $C_{5,6,7}/R_{5\ and\ more}$ intensity ratios and the R_3/R_4 contribution intensity ratio as a function of the added molybdenum amount. These contributions were chosen because they are characteristic of the species responsible for the reactivity. The linear increase of the Mo-O/$R_{5\ and\ more}$ ratio is due to the increase in the molybdenum concentration. The $C_{5,6,7}/R_{5\ and\ more}$ and R_3/R_4 values have inverse trends. When the chain contribution ($C_{5,6,7}/R_{5\ and\ more}$) decreases, an increase in the R_3/R_4 ratio is noted. However, the opposite occurs for the $_LK^{0.7}{}_{0.40Mo}$ composition. The decrease in chain contributions ($C_{5,6,7}/R_5$) favors ring formation (R_3/R_4), which reflects a reorganization of siliceous species. The increase of the R_3/R_4 ratio, reflecting a decrease of 4-membered rings (R_4) in favor of smaller rings (R_3), emphasizes the formation of small entities [23]. This phenomenon can be explained by the presence of a small amount of water released by the formation of MoO_4^{2-} species (Eq. 1). The

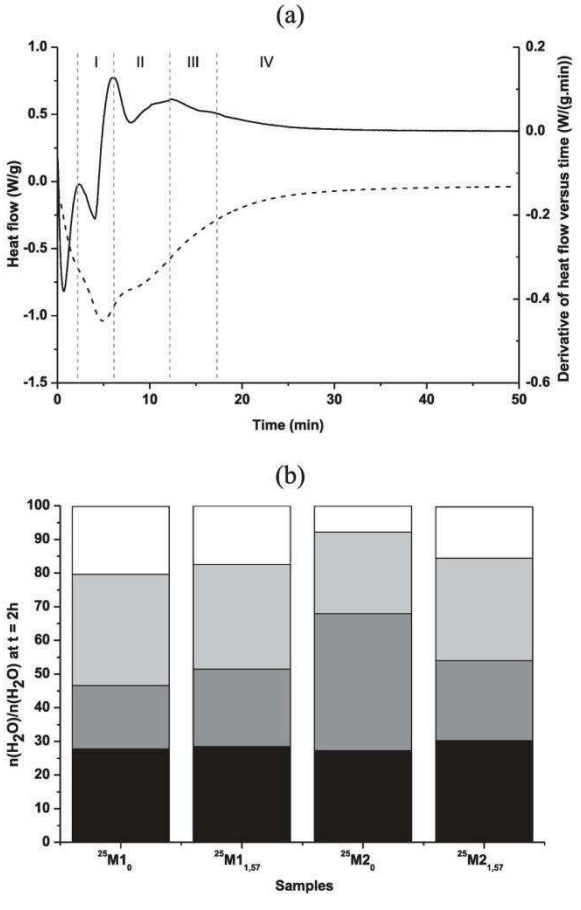

Fig. 5. (a) (—) Heat flow and (—) derivative of heat flow versus time for $^{70}M2_0$ geopolymer and (b) number of moles of water consumed for each samples (±2%). (■ reorganization of species, ■ dissolution of metakaolin, ■ formation of oligomers, □ polycondensation).

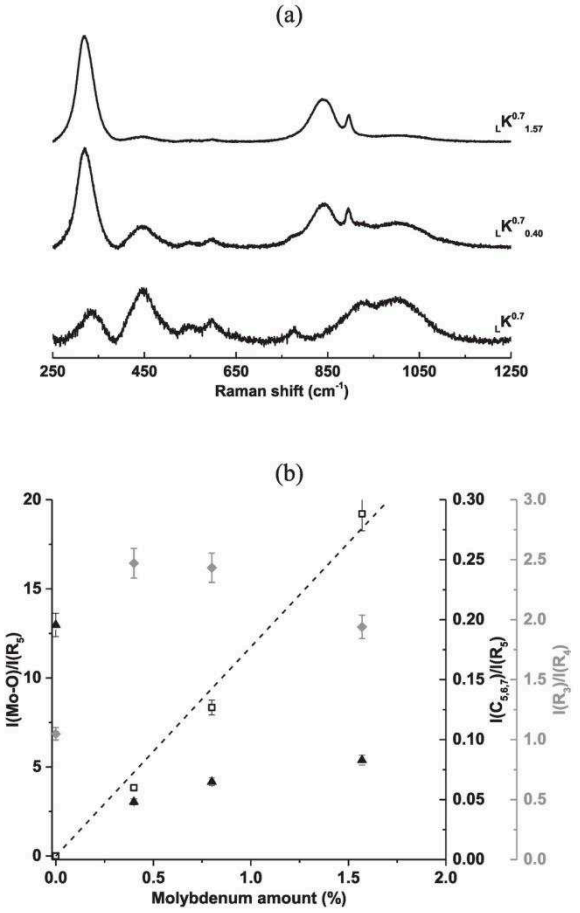

Fig. 6. (a) Raman spectra of SiK solution with various amounts of ammonium molybdate ($_LK^{0.7}$, $_LK^{0.7}_{0.40}$, $_LK^{0.7}_{1.57}$). (b) (-□-) I(Mo-O)/I(T_5), (▲) I($C_{5,6,7}$)/I(T_5) and (◆) I(T_3)/I(T_4) as a function of the molybdenum amount. (—) linear fit with correlation coefficient of 0.993.

addition of a small amount of $(NH_4)_2Mo_2O_7$ to the solution results in acid–base reactions, promoting the polymerization of the solution [22, 37]. However, in the presence of a larger amount, this effect is less important because compounds like K_2MoO_4 may be formed [38]. In the presence of these compounds, which consume positive charges, siliceous species polycondense as small entities to counterbalance the charge loss.

The validation of this charge loss can be calculated from the contributions of the different $C_{5,6,7}$, R_3 and R_4 species. These species are negatively charged and are compensated by alkali cations. The numbers of negative charges of the C_n chains and R_n rings are, respectively, equal to $2n + 2$ and $2n$. To perform the calculation, it was assumed that the chains and R_4 and R_3 rings were, respectively, composed of 6, 4 and 3 tetrahedra and therefore contained, respectively, 14 $(2 * 6 + 2)$, 8 $(2 * 4)$ and 6 $(2 * 3)$ negative charges. The data required for the calculation are shown in Table 4. For the $_LK^{0.7}$ solution containing 0.20 chains, 0.24 R_4 and 0.26 R_3, the number of negative charges is $14 * 0$, $20 + 8 * 0.24 + 6 * 0.26 = 6.28$. However, for the $_LK^{0.7}_{1.57}$, solution, the number of negative charges is 5.06. This hypothetical calculation demonstrates that ammonium molybdate addition to the solution reduces negative charges, indicating reorganization of the species in a cyclic structure.

The wetting angle values of $_LK^{0.7}$ and $_LK^{0.7}_{1.57}$ solutions are 98.9° and 103.1°, respectively. The slight increase in the wetting angle value is in agreement with the decrease in negative charges and will be discussed in the discussion section.

The NMR spectrum of the $_LK^{0.7}_{1.57}$ solution (Fig. 7a) is composed of various contributions attributed to Qn species [39] (Table 5). The dependence of the evolution of the Q^3/Q^2 and $(Q^1 + Q^2 + Q^{2c} + Q^{3c})/Q^3$ ratios on the amount of molybdenum is shown in Fig. 7b.

The ratio Q^3/Q^2 is characteristic of the polymerization state of silicate species, whereas $(Q^1 + Q^2 + Q^{2c} + Q^{3c})/Q^3$ can be used to estimate the amount of cyclic species able to react to construct a three-dimensional network. The $_LK^{0.7}_{0.40Mo}$ composition has a reverse effect; when the Q^3/Q^2 ratio decreases, the $(Q^1 + Q^2 + Q^{2c} + Q^{3c})/Q^3$ ratio increases, reflecting a change in the species structure.

For this composition, ring formation occurs to the detriment of chains. For higher contents, the increase of the Q^3/Q^2 ratio and the decrease of $(Q^1 + Q^2 + Q^{2c} + Q^{3c})/Q^3$ are characteristic of a rearrangement within species, as mentioned for the Raman spectroscopy results (Fig. 6b), with competition between K_2MoO_4 compounds and the water content.

The addition of molybdenum to the solution induces electrostatic interactions and solvation changes due to water formation. Siliceous

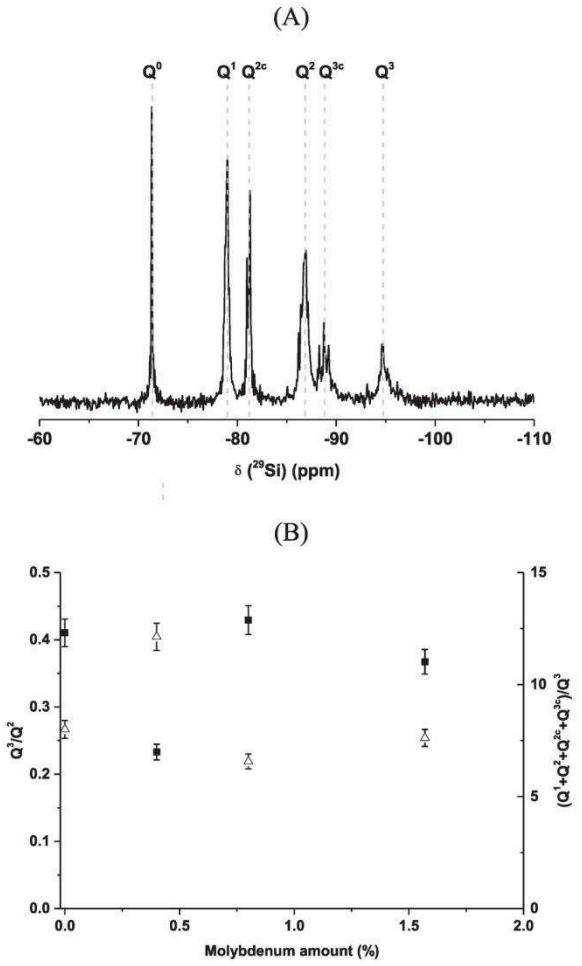

Fig. 7. (A) ^{29}Si NMR spectrum of $_{L}K^{0.7}{}_{1.57}$ and (B) (■) Q^2/Q^3 and (△) $(Q^1 + Q^2 + Q^{2c} + Q^{3c})/Q^3$ obtained from ^{29}Si NMR as a function of the amount of ammonium molybdate.

species therefore recombine and disturb the polycondensation reactions in presence of metakaolins, impacting the local network formation.

3.3. Effect of molybdate on the final material

NMR provides information about the nature of the various networks; therefore, the geopolymer structure was evaluated by ^{29}Si and ^{29}Al NMR. The untreated spectra obtained for the $^{25}M2_0$ sample are shown in Fig. 8.

The ^{27}Al NMR spectrum exhibits an intense contribution located at 55 ppm and a low-intensity contribution at 0 ppm assigned to tetrahedral aluminum (Al (IV)) and to octahedral aluminum (Al (VI)), respectively [9,40]. The high-intensity contribution due to Al (IV) agrees with the occurrence of polycondensation reactions. The aluminum V and VI from metakaolin react and are transformed into aluminum IV [9]. The presence of Al(VI) is due to non-reactive impurities from metakaolin. The widths at half maximum (FWHM) of the different samples ranged from 10.59 to 11.48, indicating the formation of more or less ordered networks depending on the metakaolin [8].

The ^{29}Si NMR spectrum has different contributions located at −106, −98, −93, −89, and −84 ppm, respectively, which are attributed to Q^4(nAl) entities with n ranging from 0 to 4 [8]. The presence of these contributions is characteristic of the formation of a geopolymer network within the material [41]. The low-intensity band at −79 ppm is associated with the existence of nesosilicates or Q^3(2Al) species within the network, as evidenced by Davidovits [42]. Previous studies identified this contribution in geopolymer binders [8].

For the four formulations, the values of the different silicate species contributions determined from the deconvolution of each spectrum are reported in Fig. 9. The observed differences reflect different connectivities depending on the aluminosilicate source and molybdate addition.

The main difference between the $^{25}M1_0$ and $^{25}M2_0$ binders is related to the two contributions (Q^4(4Al) + Q^4(3Al)). The $^{25}M1_0$ composition contains a lesser amount of these species (16.0 and 35.1%) compared to the $^{25}M2_0$ composition, which contains 20.7 and 36.2%. The $^{25}M2_0$ formulation has a geopolymer network, as evidenced by Autef et al. [8], and a slight contribution of nesosilicates or Q^3(2Al) [42]. This metakaolin reactivity allows rapid oligomers formation that polycondenses contrarily to M1 metakaolin, which reacts in a thermodynamic way. The molybdenum addition to the M1 metakaolin-based formulations ($^{25}M1_0$ and $^{25}M1_{1.57}$) decreases the nesosilicate and Q^4(3Al) species percentages from 41.7 to 34.7% and increases the silicon atom-rich species (Q^4(2Al) and Q^4(1Al)) from 37.9 to 43.6%. The reaction that occurs during molybdenum addition can be modeled by Eq. 2.

$$\text{“Nesosilicates”} + Q^4(4Al) + Q^4(3Al)Q^4(4Al) + Q^4(2Al) + Q^4(1Al) \quad (2)$$

Inversely, in the presence of M2 metakaolin ($^{25}M2_0$ and $^{25}M2_{1.57}$), the molybdenum addition increases the contributions attributed to Q^4(2Al), Q^4(1Al) and Q^4(0Al) to the detriment of Q^4(4Al) and Q^4(3Al) species. The sums of the Q^4(4Al) and Q^4(3Al) contributions and that of

Table 4
Detailed calculation of negative charges in solutions ($C_n = 2n + 2$, $R_n = 2n$) from Raman spectra decomposition (error < 1%).

Solution	Species	$\frac{I(species)}{I(R_5)}$	(−) charges per units	∑ (−) charges	∑ (−) charges in solution
$_{L}SiK^{0.7}$	Chains C_6	0.20	14	2.80	6.28
	Rings R_4	0.24	8	1.92	
	Rings R_3	0.26	6	1.56	
$_{L}SiK^{0.7}{}_{0.40}$	Chains C_6	0.05	14	0.70	3.20
	Rings R_4	0.11	8	0.88	
	Rings R_3	0.27	6	1.62	
$_{L}SiK^{0.7}{}_{0.80}$	Chains C_6	0.06	14	0.84	4.26
	Rings R_4	0.15	8	1.20	
	Rings R_3	0.37	6	2.22	
$_{L}SiK^{0.7}{}_{1.57}$	Chains C_6	0.08	14	1.12	5.06
	Rings R_4	0.20	8	1.60	
	Rings R_3	0.39	6	2.34	

Table 5
Deconvolutions of ^{29}Si NMR spectra of silicate solutions.

	Silicate species						
	% Area (δ (ppm))						
	Q^0	Q^1	Q^{2c}	Q^2	Q^{3c}	Q^3	Q^4
$_LK^{0.7}$	8.6 (−71.4)	24.1 (−78.9)	15.4 (−81.2)	24.7 (−86.8)	17.0 (−88.9)	10.2 (−94.9)	/
$_LK^{0.7}{}_{0.40}$	10.5 (−71.3)	27.2 (−78.8)	16.9 (−81.1)	29.2 (−86.7)	9.5 (−88.7)	6.8 (−94.5)	/
$_LK^{0.7}{}_{0.40}$	8.4 (−71.3)	23.9 (−78.9)	16.3 (−81.2)	27.6 (−86.8)	12.0 (−88.8)	11.8 (−94.8)	/
$_LK^{0.7}{}_{0.40}$	8.8 (−71.3)	23.6 (−78.9)	14.8 (−81.2)	28.6 (−86.8)	14.0 (−88.8)	10.2 (−94.8)	/

the Q^4(2Al), Q^4(1Al) and Q^4(0Al) bands change, respectively, from 56.9 to 44.9% and 38.5 to 51.2% for molybdenum quantities equal to 0 and 1.57%. Research on alumino-silicate compounds show that molybdenum and aluminous species can react to form $Al(OH)_6Mo_6O_{18}^{3-}$ complexes [18]. If the formation of this complex occurs in the presence of molybdenum, there are fewer aluminous species available to react and create the geopolymer network. Thus, the formation of this complex can explain why the network is richer in silicon atoms for $^{25}M2_{1.57}$. In this case, the reaction can be described by Eq. 3.

$$Q^4(4Al) + Q^4(3Al)Q^4(2Al) + Q^4(1Al) + Q^4(0Al) + 4Al(OH)_6Mo_6O_{18}{}^{3-}; 3\,K^+ \quad (3)$$

These two types of behavior are linked to the metakaolin reactivity, which in the presence of a modified alkaline solution, can form different silicon-rich or aluminum-rich networks. The spectroscopic data (Raman and NMR) showed the existence of siliceous species with smaller size or lower charge, favoring the reactivity.

The low-reactive metakaolin ($^{25}M1_0$) forms several networks. With the molybdenum addition, inducing the formation of complexes with aluminum ($Al(OH)_6Mo_6O_{18}^{3-}$) [18] and various siliceous species, the final network might be composed of a geopolymer network competing with a similar network due to the nesosilicate species, which can be grafted to aluminum-based complexes or other species. This can explain the geopolymer network enriched in aluminum atoms.

A highly reactive metakaolin in the presence of a solution modified by molybdenum promotes the formation of a network that is richer in silicon atoms.

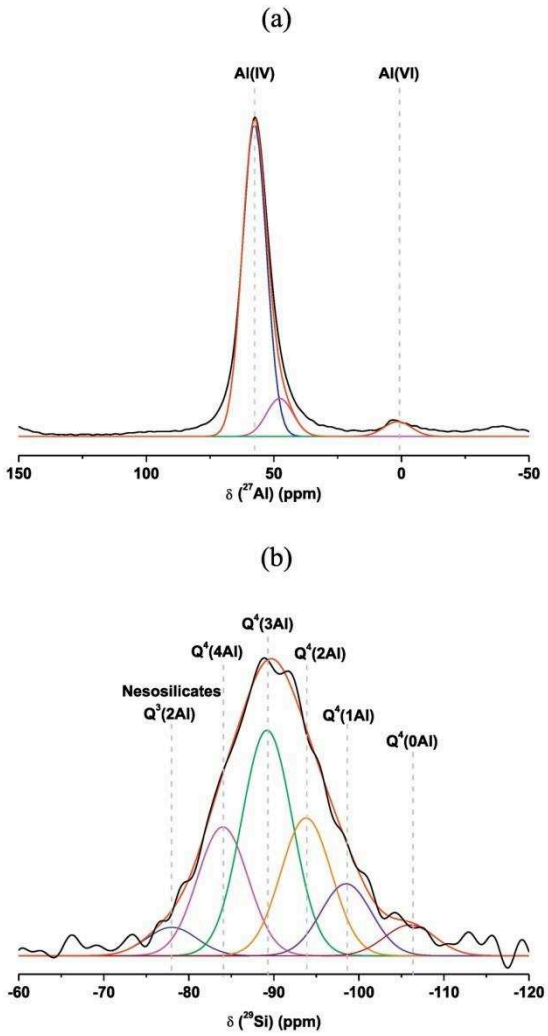

Fig. 8. (a) ^{27}Al et (b) ^{29}Si NMR spectra of the $^{25}M2_0$ geopolymers after consolidation.

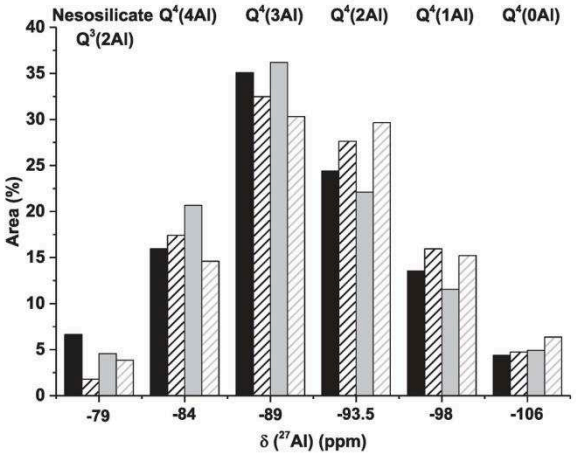

Fig. 9. Variation of the various ^{29}Si NMR contributions for (■) $^{25}M1_0$, (▨) $^{25}M1_{1.57}$, (▩) $^{25}M2_0$, (▨) $^{25}M2_{1.57}$ (error ± 1%).

The molybdenum addition in the presence of two metakaolins with different reactivity can counteract the reactivity, favoring a network rich in either aluminum or silicon atoms.

4. Discussion

The results obtained in this work indicate that the addition of molybdenum leads to differences in size and negative charges within the solution and to the formation of different networks in the final materials. It is therefore necessary to correlate the effect of raw materials to the final structure of the material.

Silicate species in the solution affect the final negative oxide network and the structure of species. NMR studies on these solutions demonstrated that the number of non-bridging oxygen atoms (NBO) is linked to the reactivity of the solution [22]. However, the calculated values vary slightly (Fig. 10) from 1.71 to 1.84. To confirm these data, they were correlated to the wetting angle values to characterize the interactions within the solution. A depolymerized solution contains many negatively charged species, causing significant repulsion and a large wetting angle [43]. However, for a polymerized solution, the interactions between species are lower due to the lower number of negative charges. The driving force of a drop is due to the competition between the interfacial and superficial energies of the mixture. As shown in Fig. 10, the wetting angle varies inversely with the NBO values. Increasing the molybdenum content induces two changes: an increase followed by a decrease in NBO, with the limit of 0.40%. The decrease in the wetting angle observed for a low molybdenum content (98.9° to 85.2° for ${}_{L}K^{0.7}$ and ${}_{L}K^{0.7}{}_{0.40}$, respectively) is characteristic of weak interactions between species and indicates a polymerization phenomenon. These observations are in agreement with the decrease in the number of negative charges in the solution (from 6.28 to 3.20 for ${}_{L}K^{0.7}$ and ${}_{L}K^{0.7}{}_{0.40}$), indicating the presence of polymerized species (Table 4). However, in the same interval, the NBO value increases slightly (from 1.80 to 1.84). This variation is in contradiction to the polymerization phenomenon highlighted previously and suggests a particular phenomenon. For molybdenum contents >0.40%, an inverse trend is observed. The wetting angle values and the number of negative charges in the solution increase (85.2° to 103.1° and 3.20 to 5.06 for ${}_{L}K^{0.7}{}_{0.40}$ and ${}_{L}K^{0.7}{}_{1.57}$ solutions, respectively). This evolution is characteristic of the presence of strong interactions within the solution, indicating a depolymerization phenomenon. In the same interval, the NBO values decrease slightly (from 1.84 to 1.71 for 0.40 and 1.57% molybdenum), indicating a polymerization phenomenon, in contrast to the previous observations.

The molybdenum addition therefore causes various phenomena. First, the NH_4^+ ions are transformed into NH_3 species, thereby releasing H_3O^+ and acidifying the medium (Eq. 4). Then, the $Mo_2O_7^{2-}$ entities, unstable in basic media, consume OH^- ions and then form MoO_4^{2-} entities and water (Eq. 1).

$$NH_4^+ + H_2O \rightarrow NH_3 + H_3O^+ \quad (4)$$

These two phenomena decreases the pH, inducing the polycondensation of the silicate species, in agreement with the variations of the negative charges and wetting angles for <0.40% molybdenum content. However, the increase in the NBO values, indicating a depolymerization phenomenon, could be explained by the formation of oxo-molybdic species that cause significant electrostatic repulsion and favor the formation of species responsible for the NBO value [44]. For higher molybdenum contents, the number of negative charges, and thus the wetting angle, increases in accordance with a depolymerization phenomenon and ring formation. The NBO value indicates that this is not a depolymerization of silicate species and that molybdenum influences the formation of K_2MoO_4 species [38]. Therefore, the changes in wetting angle and NBO values can be explained by the formation of cycles interacting with molybdic species.

These data are transposed to the geopolymer network structure. Fig. 11 shows the variation of the oligomer formation energy determined by DTA, the Si/Al ratio value [45] and the FWHM value determined by ^{29}Si and ^{27}Al NMR as a function of the different $^{25}My_x$ (x = 0 or 1.57) compositions. The same variations are observed: an increase or a decrease depending on the amount of molybdenum. For mixtures containing M1 metakaolin, the energy of oligomer formation and Si/Al ratio decrease, whereas the FWHM increases (respectively, from 33.1 to 31.1%, 1.73 to 1.68 and 9.6 to 11.5 ppm for $^{25}M1_0$ and $^{25}M1_{1.57}$ mixtures). An inverse variation is observed for mixtures containing M2 metakaolin, i.e., increases in the energy needed for oligomer formation and the Si/Al ratio, accompanied by a reduction in the FWHM value (respectively, from 24.2 to 30.5%, from 1.62 to 1.79 and from 10.6 to 9.9 ppm for $^{25}M2_0$ et $^{25}M2_{1.57}$). The increase in metakaolin reactivity is characterized by a low oligomer formation energy (33.1 to 24.2%). This reflects a decrease in the Si/Al ratio and an increase in the FWHM (from 1.73 to 1.62 and from 9.6 to 10.6 ppm for $^{25}M1_0$ and $^{25}M2_0$, respectively). As proved previously, molybdenum affects the size and charge of the species, making the solution more reactive, which causes, in the presence of low-reactive metakaolin and molybdenum, a decrease in energy linked to the formation of oligomers. The decrease in the Si/Al ratio indicates the formation of an aluminum-rich network,

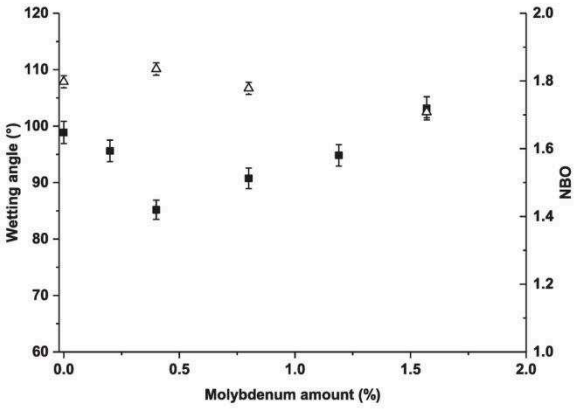

Fig. 10. Variation of (■) wetting angle on polyethylene and (△) number of non-bridging oxygen atoms (NBO) obtained from ^{29}Si NMR spectra as a function of molybdenum amount for the various ${}_{L}K^{0.7}{}_{x}$ solutions.

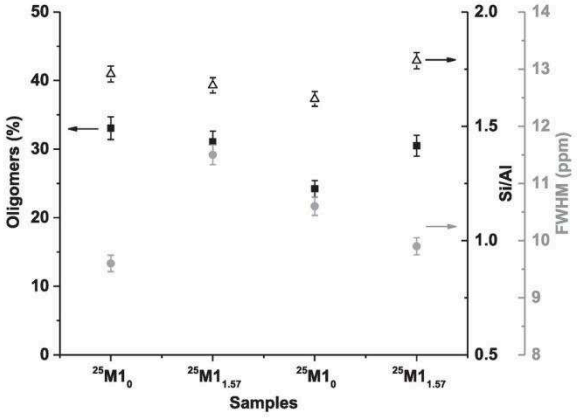

Fig. 11. Variation of (■) oligomers from DTA analysis, (●) FWHM/10 of Al(IV) contribution on ^{27}Al NMR spectra and (△) Si/Al determined from ^{29}Si NMR for the various samples.

characteristic of a network composed of a geopolymer [46]. These two phenomena suggest that the molybdenum addition favors polycondensation reactions and thus the formation of a single ordered geopolymer network. However, the FWHM increases with the formation of a more ordered network. Nevertheless, the addition of aluminum to an aluminosilicate leads to the appearance of distortions within the network and increases the FWHM [47]. In this case, the enrichment of aluminum atoms results in a higher FWHM, characteristic of the presence of distortions in the network.

Highly reactive metakaolin results in similar phenomena, in accordance with the formation of a geopolymer network that is rich in aluminum atoms [8]. The combination of a very highly reactive metakaolin and a molybdate-activated solution is detrimental to the formation of the geopolymer network, as characterized by an increase in the oligomer formation energy and a higher Si/Al ratio, in agreement with the existence of various networks. However, the decrease of the FWHM is in contradiction with this phenomenon. In this case, this variation could be explained by the presence of silicon-rich networks, which are characterized by a higher Si/Al ratio and therefore lower network distortions.

These observations suggest different behavior depending on the metakaolin reactivity. In the case of highly reactive metakaolin, dissolution is very fast, resulting in a rapid release of siliceous and aluminous species. Oligomer formation is also favored by metakaoln reactivity. Reorganizations occur between oligomers, forming a single geopolymer network that is rich in aluminum atoms. When molybdenum is added to the initial solution, the species condense and form entities with fewer negative charges, which reduces metakaolin dissolution and requires greater energy for oligomer formation. In this case, molybdenum forms large complexes and ions. These large aluminum-rich species create a more disordered network hat is depleted in aluminum atoms.

In the case of low-reactive metakaolin, the dissolution is weak due to the presence of impurities. Oligomer formation is also more difficult and requires higher energy. In this case, several disordered networks that are richer in silicon coexist. When molybdenum is added, the cyclic species formation favors the dissolution of metakaolin and the formation of oligomers. This phenomenon facilitates the formation of a three-dimensional structure that is richer in aluminum. Moreover, the fact that molybdenum traps a portion of the aluminum atoms appears to favor the formation of a single geopolymer network.

Thus, it was possible to modify a low-reactive solution by adding molybdate to counteract the metakaolin reactivity.

5. Conclusion

This study was conducted to investigate the major role of molybdic species during polycondensation reactions using two metakaolin-based geopolymers and various amounts of ammonium molybdate (0.40, 0.80 and 1.57% molar molybdenum).

The addition of molybdenum to the silicate solution (increasing the reactivity of the solution) counterbalanced the metakaolin reactivity, favoring a rich network of either aluminum or silicon. Thus, silicate solutions have different polymerization rates depending on the amount of molybdate added. The different entities containing molybdenum attract siliceous and aluminous species, favoring the dissolution of metakaolin. Finally, the addition of Mo modifies (i) the balance of negative charges in the silica species of the silicate-Mo solution and (ii) the nature and size of the species involved, which favors perturbations toward polycondensation reactions in the final material:

(i) In the case of highly reactive metakaolin, the dissolution is very fast, resulting in the rapid release of siliceous and aluminous species. When molybdenum is added to the initial solution, the species condense, reducing the dissolution rate. These large aluminum-rich species create a more disordered network and decrease the aluminum content.

(ii) In the case of low-reactive metakaolin (more classical point), oligomer formation is more difficult and requires more energy. When molybdenum is added, the formation of cyclic species favors the dissolution of metakaolin and the formation of oligomers. This phenomenon facilitates the formation of three-dimensional structure that is richer in aluminum.

Finally, it was demonstrated that it is possible to change the reactivity of the silicate solution by adding a small amount of molybdate to counteract the reactivity of metakaolin.

Acknowledgements

The authors gratefully acknowledge the FEDER Agency, the Limousin Regional Council and the FUI Program for their financial support. The authors also acknowledge M. Colas and J. Cornette for the Raman spectroscopy experiments and J. Sanz for the ^{29}Si NMR experiments.

References

[1] P. Duxson, A. Fernández-Jiménez, J.L. Provis, G.C. Lukey, A. Palomo, J.S.J. van Deventer, Geopolymer technology: the current state of the art, J. Mater. Sci. 42 (2007) 2917–2933.
[2] J.L. Provis, J.S.J. van Deventer, Geopolymers. Structure, Processing, Properties and Industrial Applications, Woodhead Publishing Limited, 2009.
[3] C. Seliin Ravikumar, T.S. Thandavamoorthy, Glass fibre concrete: investigation on strength and resistant properties, IOSR JMCE 9 (3) (2013) 21–25.
[4] G. Masi, W.D.A. Rickard, M.C. Bignozzi, A. van Riessen, The effect of organic and inorganic fibres on the mechanical and thermal properties of aluminated activated geopolymers, Composites Part B 76 (2015) 218–228.
[5] E. Kamseu, A. Rizzuti, C. Leonelli, D. Perera, Enhanced thermal stability in K_2O-metakaolin-based geopolymer concretes by Al_2O_3 and SiO_2 fillers additions, J. Mater. Sci. 45 (2010) 1715–1724.
[6] L. Xia, B. Zhong, T. Zhang, X. Hu, S. Wu, J. Yang, G. Wen, Effect of boron doping on the thermal properties of carbon fibers reinforced lithium aluminosilicate matrix composites, J. Eur. Ceram. Soc. 35 (2015) 2555–2562.
[7] S. Samal, N.P. Thanh, I. Petríková, B. Marvalová, Improved mechanical properties of various fabric-reinforced geocomposite at elevated temperature, JOM 67 (7) (2015) 1478–1485.
[8] A. Autef, E. Joussein, A. Poulesquen, G. Gasgnier, S. Pronier, I. Sobrados, J. Sanz, S. Rossignol, Influence of metakaolin purities on potassium geopolymer formulation: the existence of several networks, J. Colloid Interface Sci. 408 (2013) 43–53.
[9] P.S. Singh, M. Trigg, I. Burgar, T. Bastow, Geopolymer formation processes at room temperature studied by ^{29}Si and ^{27}Al MAS-NMR, Mater. Sci. Eng. A 396 (2005) 392–402.
[10] D. Khale, R. Chaudhary, Mechanism of geopolymerization and factors influencing its development: a review, J. Mater. Sci. 42 (2007) 729–746.
[11] P. Duxson, S.W. Mallicoat, G.C. Lukey, W.M. Kriven, J.S.J. van Deventer, The effect of alkali and Si/Al ration on the development of mechanical properties of metakaolin-based geopolymers, Colloid Surf. A 292 (2007) 8–20.
[12] C.A. Rees, J.L. Provis, G.C. Lukey, J.S.J. van Deventer, Attenuated total reflectance Fourier transform infrared analysis of fly ash geopolymer gel aging, Langmuir 23 (2007) 8170–8179.
[13] A. Autef, E. Joussein, G. Gasgnier, S. Rossignol, Role of the silica source on the geopolymerization rate: a thermal analysis study, J. Non-Cryst. Solids 366 (2013) 13–21.
[14] M. Xia, H. Shi, X. Guo, Probing the structural evolution during the geopolymerization process at an early age using proton NMR spin–lattice relaxation, Mater. Lett. 136 (2014) 222–224.
[15] P. Steins, Influence des paramètres de formulation sur la texturation et la structuration des géopolymères, Université de Limoges, Thèse de doctorat, 2014.
[16] L. Vidal, E. Joussein, M. Colas, J. Absi, S. Rossignol, Effect of addition of ammonium molybdate on metakaolin-based geopolymer formation: shrinkage and crystallization, Powder Technol. 275 (2015) 211–219.
[17] D.P. Debecker, M. Stoyanova, U. Rodemerck, E.M. Gaigneaux, Preparation of MoO_3/SiO_2-Al_2O_3 metathesis catalysts via wet impregnation with different Mo precursors, J. Mol. Catal. A Chem. 340 (2011) 65–76.
[18] N. Xu, W. Braida, C. Christodoulatos, J. Chen, A review of molybdenum adsorption in soils/bed sediments: speciation, mechanism, and model applications, Soil Sediment Contam. 22 (2013) 912–929.
[19] T. Ulrich, J. Mavrogenes, An experimental study of the solubility of molybdenum in H_2O and KCl-H_2O solutions from 500 °C to 800 °C, and 150 to 300 MPa, Geochim. Cosmochim. Acta 72 (2008) 2316–2330.
[20] P. Sarrazin, B. Mouchel, S. Kasztelan, ^{95}Mo NMR study of the interaction of heptamolybdate solutions with alumina and silica, J. Phys. Chem. 93 (1989) 904–908.
[21] J. Jiang, I. May, M.J. Sarsfield, M. Ogden, D.O. Fox, C.J. Jones, P. Mayhew, A spectroscopic study of the dissolution of cesium phosphomolybdate and zirconium molybdate by ammonium carbamate, J. Solut. Chem. 34 (2005) 443–468.

[22] L. Vidal, E. Joussein, M. Colas, J. Cornette, J. Sanz, I. Sobrados, J.-L. Gelet, J. Absi, S. Rossignol, Controlling the reactivity of silicate solutions: a FTIR, Raman and NMR study, Colloids Surf. A Physicochem. Eng. Asp. 503 (2016) 101–109.
[23] L. Vidal, E. Joussein, M. Colas, J. Cornette, J. Absi, S. Rossignol, Identification of chains and rings in alkaline silicate solutions by Raman spectroscopy: effect of alkali cation, Colloids Surf. A Physicochem. Eng. Asp. (Submitted).
[24] B. Hehlen, D.R. Neuville, Raman response of network modifier cations in alumino-silicate glasses, J. Phys. Chem. B 119 (2015) 4093–4098.
[25] M. Chligui, Etude des propriétés optiques et mécaniques des verres binaires silicatés d'alcalins lourdsPh.D. Thesis University of Orléans, 2010.
[26] R. Murugan, H. Chang, Thermo-Raman Investigations on Thermal Decomposition of $(NH_4)_6Mo_7O_{24}\cdot 4H_2O$, J. Chem. Soc, Dalton Trans, 2001 3125–3132.
[27] C.A. Rees, J.L. Provis, G.C. Lukey, J.S.J. van Deventer, In situ ATR-FTIR study of the early stages of fly ash geopolymer gel formation, Langmuir 23 (17) (2007) 9076–9082.
[28] A. Gharzouni, E. Joussein, B. Samet, S. Baklouti, S. Rossignol, Effect of the reactivity of alkaline solution and métakaolin on geopolymer formation, J. Non-Cryst. Solids 410 (2015) 127–134.
[29] F. Gouny, F. Fouchal, P. Maillard, S. Rossignol, Study of the effect of siliceous species in the formation of a geopolymer binder: understanding the reaction mechanisms among the binder, wood, and earth brick, Ind. Eng. Chem. Res. 53 (9) (2014) 3559–3569.
[30] A. Autef, E. Joussein, G. Gasgnier, S. Rossignol, Role of the silica source on the geopolymerization rate: a thermal analysis study, J. Non-Cryst. Solids 366 (2013) 13–21.
[31] A. Depla, E. Verheyen, A. Veyfeyken, M. Van Houteghem, K. Houthoofd, V. Van Speybroeck, M. Waroquier, C.E.A. Kirschhock, J.A. Martens, UV-Raman and ^{29}Si NMR spectroscopy investigation of the nature of silicate oligomers formed by acid catalyzed hydrolysis and polycondensation of tetramethylorthosilicate, J. Phys. Chem. C 115 (2011) 11077–11088.
[32] E.V. Belova, Y.A. Kolyagin, I.A. Uspenskaya, Structure and glass transition temperature of sodium silicate glasses doped with iron, J. Non-Cryst. Solids 423–424 (2015) 50–57.
[33] C. Le Losq, D.R. Neuville, Effect of the Na/K mixing on the structure and the rheology of tectosilicate silica-rich melts, Chem. Geol. 346 (2013) 57–71.
[34] A. Erdőhelyi, K. Fodor, R. Németh, A. Hancz, A. Oszkó, Partial oxidation of methane on silica-supported different alkali metal molybdates, J. Catal. 199 (2001) 328–337.
[35] T. Paul, A. Ghosh, Correlation of structure and ion conduction in $La_{2-x}Y_xMo_2O_9$ ($0 \le x \le 0.2$) oxygen ion conductors, J. Appl. Phys. 117 (2015) 235101.
[36] A. Erdőhelyi, K. Fodor, F. Solymosi, Partial oxidation of methane on supported potassium molybdate, J. Catal. 166 (1997) 244–253.
[37] E.K. Fodjo, D.W. Li, N.P. Marius, T. Albert, Y.-T. Long, Low temperature synthesis and SERS application of silver molybdenum oxides, J. Mater. Chem. A 1 (2013) 2558–2566.
[38] J. Liu, L. Yu, Z. Zhao, Y. Chen, P. Zhu, C. Wang, Y. Luo, C. Xu, A. Duan, G. Jiang, Potassium-modified molybdenum containing SBA-15 catalysts for highly efficient production of acetaldehyde and ethylene by the selective oxidation of ethane, J. Catal. 285 (2012) 134–144.
[39] I.L. Svensson, S. Sjöberg, L.-O. Öhman, Polysilicate equilibria in concentrated sodium silicate solutions, J. Chem. Soc. Faraday Trans. 1 (82) (1986) 3635–3646.
[40] A. Autef, E. Joussein, G. Gasgnier, S. Pronier, I. Sobrados, J. Sanz, S. Rossignol, Role of metakaolin dehydroxylation in geopolymer synthesis, Powder Technol. 250 (2013) 33–39.
[41] P.S. Singh, T. Bastow, M. Trigg, Structural studies of geopolymers by ^{29}Si and ^{27}Al MAS-NMR, J. Mater. Sci. 40 (2005) 3951–3961.
[42] J. Davidovits, Properties of geopolymer cements, Proceedings First International Conference on Alkaline Cements and Concretes (1994) 131–149.
[43] O. Dezellus, Contribution à l'étude des mécanismes de mouillage réactif, Thèse de doctorat, Institut National Polytechnique de Grenoble, Grenoble, 2005.
[44] D. Nikolova, R. Edreva-Kardjieva, M. Giurginca, A. Meghea, J. Vakros, G.A. Voyiatzis, C. Kordulis, The effect of potassium addition on the state of the components in the oxide precursor of the (Ni)(Mo)/γ-Al_2O_3 water-gas shift catalysts: FT-IR, diffuse reflectance and Raman spectroscopic studies, Vib. Spectrosc. 44 (2007) 343–350.
[45] J. Klinowski, C.A. Fyfe, G.C. Gobbi, High-resolution Solid-state Nuclear Magnetic Resonance studies of dealuminated zeolite Y, J. Chem. Soc. Faraday Trans. 81 (1985) 3003–3019.
[46] A. Autef, E. Joussein, G. Gasgnier, S. Rossignol, The fabrication of aluminosilicate compounds from various raw materials: a feasibility study based on chemical reactivity and mechanical properties, Mater. Sci. Eng. B, (submitted).
[47] D.M. Jenkins, B.L. Sherriff, J. Cramer, Z. Xu, Al, Si, and Mg occupancies in tetrahedrally and octahedrally coordinated sites in synthetic aluminous tremolite, Am. Mineral. 82 (1997) 280–290.

Publication 7 (ACL 7)

L. Vidal, E. Joussein, J. Absi, S. Rossignol

"Coating of unreactive and reactive surface by aluminosilicate binder"

Ceramics International, submitted.

COATING OF UNREACTIVE AND REACTIVE SURFACES BY ALUMINOSILICATE BINDER

L. Vidal[a], E. Joussein[b], J. Absi[c] and S. Rossignol[a]

[a] SPCTS, ENSCI, 12 rue Atlantis, 87068 Limoges Cedex, France.
[b] Université de Limoges, GRESE EA 4330, 123 avenue Albert Thomas, 87060 Limoges, France.
[c] Université de Limoges, SPCTS, 12 rue Atlantis, 87068 Limoges Cedex, France.

Corresponding author: sylvie.rossignol@unilim.fr, tel.: 33 5 87 50 25 64

Abstract
Currently, many applications require the assembly of different materials to improve their properties in use. This work focuses on the production of a geopolymer binder coating based on metal or agglomerated sand. For this, several compositions based on sodium or potassium and different reactivities of metakaolin and their interactions in the presence of different types of support were studied. The interactions between the binder and carrier were analysed by measurements of the wetting angles. Coating trials conducted over tin-plated copper and bonded sand highlighted the influences of the binder composition and the drying and deposition parameters. Scanning electronic and optical microscopy observations confirm the chemical adhesion between the various components. FTIR spectroscopic analyses have also identified the parameters for obtaining a geopolymer network such as the reactive aluminium concentration (5 mol / L) and the molar Si / Al and M / Al (M = K or Na) ratios (2 and 1.2, respectively). It is therefore possible, by determining the wetting angle, to control the deposition on either a metal or silica sand.

Keywords: Geopolymer; Metal; Wetting angle; Silicate solution; Aluminium content; Sand

1. Introduction

Today, many applications require understanding the interactions between different materials and the formation of composites or assemblies to optimize their working properties [1, 2, 3]. In fact, different types of interactions can occur at the interface between different materials, resulting in adhesion phenomena such as mechanical or chemical anchoring [4]. In the case of chemical anchoring, the existence of chemical reactions between the support and the binder must be determined. The mechanical anchoring corresponds to a solid surface penetrating into the surface tortuosity, leading to a consolidated layer. Studies have shown that mechanical anchoring depends on the roughness and wettability of the surface [5].

Many areas require the use of mixtures of materials such as technical ceramics or wide raw ceramics. In the field of aerospace, thermal barriers are used to protect metal from high temperatures [6]. These barriers are therefore made of a metal substrate, an undercoat layer and a ceramic deposit [7]. In the electronic domain, ceramic/metal assemblies are made for the manufacture of electronic circuit boards. Wielage et al. [8] prepared Al/Cu metal coatings on Al_2O_3 substrates by cold-gas spraying, and the analyses evidenced a good adhesion between the materials. Ceramic coatings on metal also exist and are used for biomedical applications. Huang et al. [1] studied glass-ceramic coatings on magnesium alloys for biomedical implant manufacturing and demonstrated the anticorrosion properties of these coatings. Gouny et al. [9] studied the interactions between a geopolymer foam and wood or earth brick for building materials. Mechanical tests have shown the formation of strong bonds between the binder and the wood or brick. Further analysis revealed that these interactions

were favoured by the penetration of the binder into the porosity of the mud brick or wood [10].

Geopolymer materials are environmentally friendly materials because of their low CO_2 emissions and energy consumption [11], and hence many works are interested in them and their interactions with different types of materials. Do Rego et al. [12] investigated the possibility of using a sodium-based geopolymer as an adhesive material for ceramic tiles and showed that better adhesion is obtained with these materials. Moreover, it was evidenced that higher performance is obtained when the temperature increases to 50 °C. Recently, Chandaprasirt et al. [13] used a fly ash-based geopolymer to protect cement pipes from aggressive solutions. The results revealed that the hardness of the geopolymeric covering material is reduced after being immersed in aggressive solutions for 90 days. Other authors evidenced that slag-based geopolymers can be used as protective coatings for marine concrete due to their good adhesion between the cement paste and the binder and the high anticorrosion property of these materials [14]. Irfan Khan et al. [15] applied binders based on mixtures of sodium hydroxide solution and fly ash on steel plates. The results showed that the value of the Na / Al ratio and the amount of water influenced the adhesion of the deposit on the metal substrate. Formulations with acceptable temperature stability and durability have the ratios of water / solid = 0.33 and 0.8 < Na / Al <1.2. Allison et al. [16] studied the interface between a geopolymer binder based on fly ash and steel, and the absence of an interface between the two materials was demonstrated by nanoindentation. In addition, the use of a pretreatment on the steel enamelling can promote the anchoring of the binder through a porous layer. Temuujin et al. [17] studied the use of metakaolin based-geopolymer coatings on stainless and mild steels for thermal protection. It was shown that the geopolymer chemical composition controls the adhesion of this material on the metallic substrates, and good adhesion was obtained for formulations with Si/Al = 2.5 and Na/Al = 1.

The coating of a binder on a support implies various interactions that may occur such as mechanical or chemical anchoring. The interactions between the different materials can be verified using wetting angle measurements, scanning electron microscopy observations or mechanical testing. The value of the wetting angle depends on the presence of defects on the surface of the solid, in particular the roughness of the solid and its chemical heterogeneities, and also the chemical composition of the binder [18]. Alghunaim et al. [19] showed that the surface roughness leads to different phenomena depending on the porosity. Shear or tensile tests may also be performed to determine the tensile strength in the parallel or perpendicular direction [8, 20]. Finally, the adhesion between the binder and the substrate may be characterized by scanning electron microscope observations. Gouny et al. [10] showed that the geopolymer binder penetrated within the pores of the wood support or earth brick, inducing adhesion between the materials. Ruth et al. [21] studied geopolymer coatings on plywood by SEM and observed a good adhesion between these two materials. Other authors evidenced by SEM observations that geopolymers with a Si / Al ratio = 2.5 form strong bonds with steel [17].

The aim of this work is to apply a coating on metal or agglomerated sand based on a geopolymer binder for different applications. The interactions between the binders and different substrates were evaluated by the measurement of the wetting angles. Observations by optical and scanning electron microscopy were used to study the adhesion between the binder and metal or bonded sand. Finally, the best aluminosilicate formulation binder was determined by FTIR spectroscopy.

2. Materials and methods

2.1 Sample preparation

In this work, a sodium silicate solution and a potassium silicate solution with Si/M molar ratios of 0.7 (M = K or Na) and three metakaolins (denoted M1, M2 and MT) were used. Alkaline silicate solutions were prepared by dissolving KOH (purity 85 %) or NaOH pellets (purity 97%) and amorphous silica (purity 99,9%) into osmotically purified water [22]. Reactive mixtures were prepared by adding different amounts of metakaolin (from 1 to 18 g) into the alkaline silicate solution (Table I). Then, 1 g of water was added to all the mixtures prepared with 12 g of metakaolin, except for the samples prepared with metakaolin M1 and SiK solutions.

Table I. Nomenclature and compositions of the various studied binders.

Solution	**Nomenclature**	**Solution**		**Metakaolin (g)**			**Added water (g)**
M cation		**M_2O (g)**	**SiO_2 (g)**	**M1**	**M2**	**MT**	
K	**$^{0.5}$M1K**	3.58	2.77	0.5			
	^{1}M1K			1.0			
	$^{1.5}$M1K			1.5			
	^{2}M1K			2.0			
	^{3}M1K			3.0			
	^{4}M1K			4.0			
	^{5}M1K			5.0			
	^{12}M1K			12.0			
	^{18}M1K			18.0			
K	**$^{0.5}$M2K**	3.58	2.77		0.5		
	^{1}M2K				1.0		
	^{2}M2K				2.0		
	^{5}M2K				5.0		
	^{12}M2K				12.0		1.0
K	**^{1}MTK**	3.58	2.77			1.0	
	^{5}MTK					5.0	
	^{12}MTK					12.0	1.0
K	**^{6}M1^{6}MTK**	3.58	2.77	6.0		6.0	
Na	**^{1}M1Na**	2.32	3.10	1.0			
	^{5}M1Na			5.0			
	^{12}M1Na			12.0			1.0
Na	**^{1}M2Na**	2.32	3.10		1.0		
	^{5}M2Na				5.0		
	^{12}M2Na				12.0		1.0
Na	**^{1}MTNa**	2.32	3.10			1.0	
	^{5}MTNa					5.0	
	^{12}MTNa					12.0	1.0
Na	**^{6}M1^{6}MTNa**	2.32	3.10	6.0		6.0	

The characteristics of the various substrates used in this work are reported in Table II.

Table II. Characteristics of the various substrates.

	Chemical composition (%)										Roughness
	Cu	**Ni**	**Sb**	**Sn**	**Cl**	**K**	**Si**	**S**	**Mn**	**Co**	**Ra**
Copper	98.0	-	-	-	-	-	-	-	-	-	0.200
Tin-plated copper	43.6	-	20.5	11.1	7.0	6.4	0.8	0.1	-	-	0.130
Nickel-plated copper	15.8	83.5	-	-	-	-	-	0.1	0.1	0.1	0.150
Polyethylene	-										0.130
Glass	-										0.007

The nomenclature used to identify the different mixtures is ^{x}MyM, with x the amount of added metakaolin (x = 0.5, 1, 1.5, 2, 3, 4, 5, 12 or 18 g), My the metakaolin (My = M1, M2 or MT) and M the alkaline cation (M = K or Na) (Table I).

2.2 Characterization methods

FTIR spectra were obtained using a ThermoFisher Nicolet 380 infrared spectrometer in attenuated total reflectance (ATR) mode. The IR spectra were collected over a wavenumber range of 400-4000 cm^{-1}, with 64 scans and a resolution of 4 cm^{-1}. The commercial software OMNIC was used for data acquisition and spectral analysis. The atmospheric CO_2 contribution was removed by a straight line between 2400 and 2280 cm^{-1}. To allow comparisons of the spectra, they were corrected using a baseline and normalized.

Wetting angles were measured with a Digidrop MCAT from a GBX comprising a camera and a lamp that allow the recording of drop deposition. The software Visiodrop (GBX) was used to measure the wetting angles. Measurements were performed with different reactive mixtures on different substrates (PEHD or metal). A mixture drop was deposited on the substrate, and the wetting angle was estimated at t = 0, i.e., from the first image where the drop is deposited on the substrate.

Roughness measurements were obtained using a Dektak 6M profilometer. Measurements were performed over 30 seconds on a length of 1500 µm with a resolution of 50 Å.
Interactions between the geopolymer binder and metals were observed by an optical microscope (Nikon Eclipse 50i). Various observations were obtained with a magnification of 20x.

The morphologies of the final products were determined using a Philips XL30 scanning electron microscope (SEM). The samples were broken and platinum-coated.

3. Results

3.1 Interactions between the geopolymer binders and various substrates

The interactions between the geopolymer binders and metal (copper, tinned copper and nickel-plated copper), plastic (HDPE) and inorganic (glass plate) supports were analysed by contact angle measurements. Fig. 1 shows the change in the wetting angle depending on the substrate (metal, inorganic or organic) and the binder (cation and metakaolin). The contact angles are always higher, whatever the support, for the sodium-based compositions.

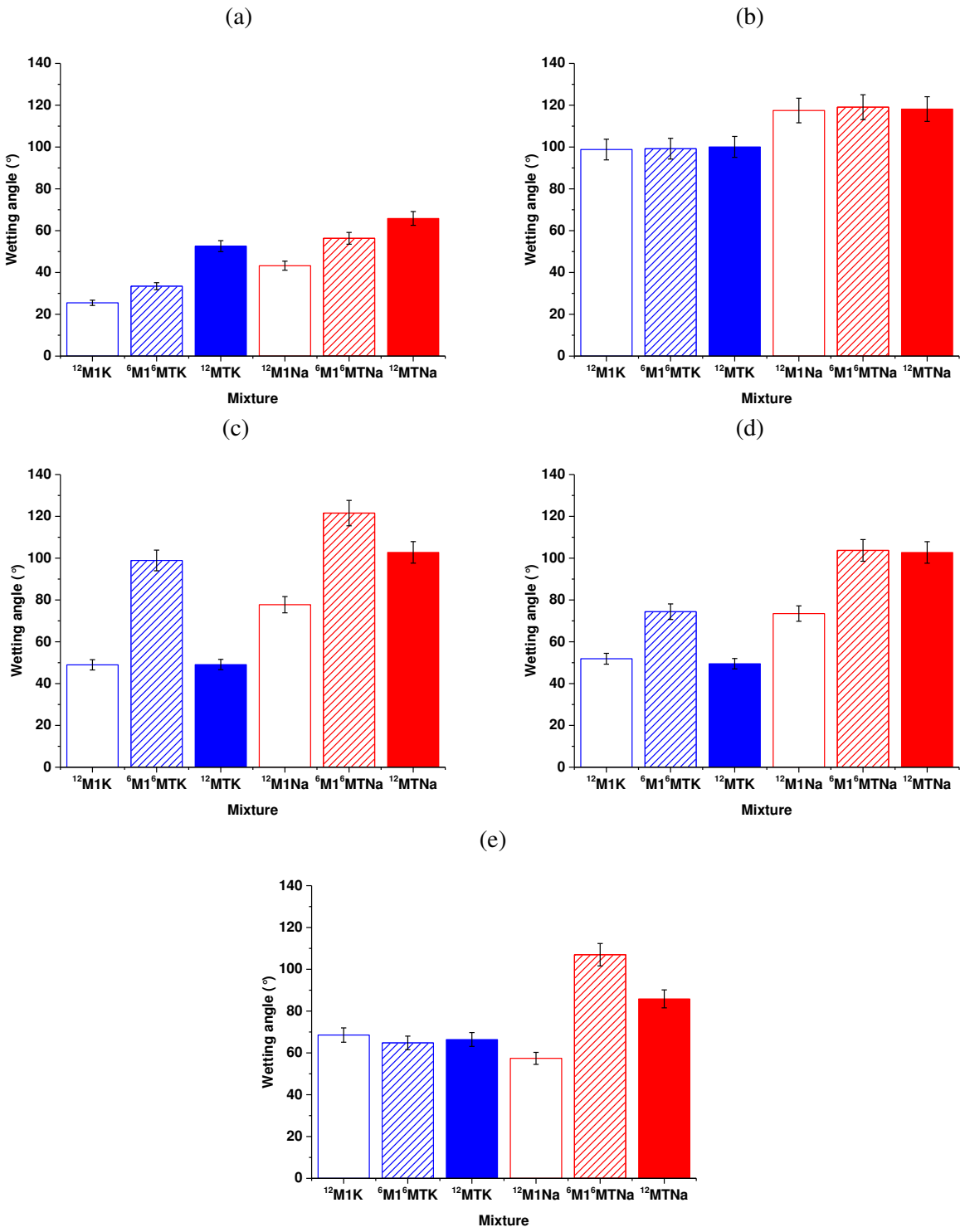

Fig. 1. Variation of the wetting angle values on (a) glass, (b) polyethylene, (c) copper, (d) tin-plated copper and (e) nickel-plated copper for the (□) ^{12}M1K, (▨) ^{6}M1^{6}MTK, (■) ^{12}MTK, (□) ^{12}M1Na, (▨) ^{6}M1^{6}MTNa and (■) ^{12}MTK formulations.

In the case of the conventional glass plate (Fig. 1a), the differences observed are specific to the nature of the alkali cation. Indeed, the wetting angles for the ^{12}M1K and ^{12}M1Na mixtures are 25.5° and 43.2°, respectively. In the presence of the K^+ cation, the observed phenomenon can be linked to chemical exchanges during the chemical cooling of the glass [23]. There is an exchange of Na^+ cations localized in the surface to the binder and vice versa, i.e., the transfer of K^+ cations to the glass surface, inducing the decrease of the value of the wetting angle.

Consequently, the ^{12}M1K, ^{6}M1^{6}MTK and ^{12}MTK mixtures have wetting angles of 25,5°, 33,4° and 52,6°, respectively. The higher value of the angle of the ^{12}MTK formulation is explained by the beginning of the geopolymerization in the binder [24]. The decrease of the wetting angle for the ^{12}M1K binder is due to the higher pH value of this sample (12.8) compared to the ^{12}MTK (12.2) binder, promoting the exchange of Na-K cations on the surface, according to a previous work [24]. The mixture of both metakaolins induces a lower pH value, characteristic of geopolymerization reactions. As expected, the obtained contact angle for this sample is between those obtained for ^{12}M1K and ^{12}MTK. For all the sodium-based samples (^{12}M1Na, ^{12}MTNa and ^{6}M1^{6}MTNa), the lower pH value (11.7) is due to a higher reactivity, enhancing the geopolymerization reaction and thus resulting in an increase in the wetting angle.

In the presence of polyethylene (Fig. 1b), only the effect of the cation is observed, while the metakaolin effect is inhibited by the hydrophobic surface of the polyethylene. Indeed, the angle value is similar regardless of the composition (approximately 99° and 118° for ^{x}MyK and ^{x}MyNa, respectively).

In the presence of copper (Fig. 1c), the effect of the sodium cation is quite notable (49.0° and 77.7° for the ^{12}M1K and ^{12}M1Na compositions, respectively). As previously evidenced, the contact angle values obtained are characteristic of species exchanges between the copper and the binder. The difference is especially notable for ^{6}M1^{6}MTK (49.0°, 49.1° and 98.9° for the ^{12}M1K, ^{12}MTK and ^{6}M1^{6}MTK mixtures, respectively). Indeed, for these mixtures, there is the formation of $Cu(OH)_4^{2-}$, or CuO, which competes with the geopolymerization reactions. For the ^{12}M1K or ^{12}MTK binders, the wetting angle can be related to an alteration phenomenon of the support, whereas in the presence of a mixture of M1 and MT metakaolins, the geopolymerization reaction governs and imposes a high value on the contact angle. In the presence of sodium cations, the same phenomena are observed. Nevertheless, the difference observed in ^{6}M1^{6}MTNa is due to the highest kinetics of the geopolymerization reaction [25].

The last point to discuss is the modification of the metal surface. Contact angles were therefore determined on tinned copper plates and nickel-plated copper, as well as the effect of the alkali metal cation. In the presence of tinned copper (Fig. 1d), the behaviour is similar to that observed on copper. Indeed, a higher angle was evidenced for compositions containing a mixture of M1 and MT metakaolins (51.9°, 49.5° and 74.4° for the ^{12}M1K, ^{12}MTK and ^{6}M1^{6}MTK mixtures, respectively). As for the copper, the higher values indicate that the geopolymerization reaction controls the contact angle. In the case of nickel-plated copper (Fig. 1e), the nature of the metakaolin does not appear to have an influence on the angle value in the presence of potassium-based solution (68.5°, 64.8° and 66.4° for the ^{12}M1K, ^{6}M1^{6}MTK and ^{12}MTK mixtures, respectively). The differences could be due to the existence of zones of different species in the Pourbaix diagrams [26, 27]. In contrast, using sodium solution, the value of the contact angle appears to depend on the metakaolin reactivity. Once again, the ^{6}M1^{6}MTNa mixture has the highest angle (57.4°, 107.0° and 85.9° for the ^{12}M1Na, ^{6}M1^{6}MTNa and ^{12}MTNa mixtures, respectively). Finally, the adhesion of the binder on the surface depends on the binder pH value and on the existence of metal reactive species zones in the range of the pH value determining the final value of the wetting angle. Indeed, the observed phenomena for sodium-based binders are explained by the largest depolymerization state of the sodium-based solutions [28]. Indeed, the presence of depolymerized species in a solution implies the existence of strong interactions between species, leading to high wetting angle values [18, 29]. A previous study showed that the number of negative charges due to the $C_{5,6,7}$, R_4 and R_3 entities can be determined by Raman spectroscopy [29]. The Raman spectra of solutions $_{L}K^{0.7}$ and $_{L}Na^{0.7}$ were decomposed in a previous work [28]. For the calculation, it was assumed that the negative charge numbers of the chains and R_4 and R_3 rings are 14, 8 and 6, respectively [29]. Table II shows the data needed for the calculation. For the $_{L}K^{0,7}$ solution,

the proportions of chains and R_4 and R_3 rings are 0.23, 0.28 and 0.26, respectively, so the number of negative charges is equal to 14 * 0.23 + 8 * 0.28 + 6 * 0.26 = 7.02. In the case of the $_LNa^{0,7}$ solution, the number of charges is 8.16. The higher value of the number of negative charges demonstrates that the $_LNa^{0,7}$ solution is more depolymerized than the $_LK^{0,7}$ solution. This leads to strong interactions between the species, inducing a higher wetting angle [29]. In this case, the increase of the wetting angle for the sodium silicate solution suggests that the silicate solution governs the interactions between the geopolymer binder and the metal support.

Table II. Detailed calculations of negative charges in solutions (C_n = 2n+2. R_n = 2n) from Raman spectra decomposition [28, 29].

Solution	Species	$\frac{I(species)}{I(R_5)}$	(-) charges per units	∑ (-) charges	∑ (-) charges in solution
$_LSiK^{0.7}$	**Chains C_6**	0.23	14	3.22	7.02
	Rings R_4	0.28	8	2.24	
	Rings R_3	0.26	6	1.56	
$_LSiNa^{0.7}$	**Chains C_6**	0.25	14	3.50	8.16
	Rings R_4	0.32	8	2.56	
	Rings R_3	0.35	6	2.10	

The samples were then observed after the consolidation of the binders (Fig. 2).

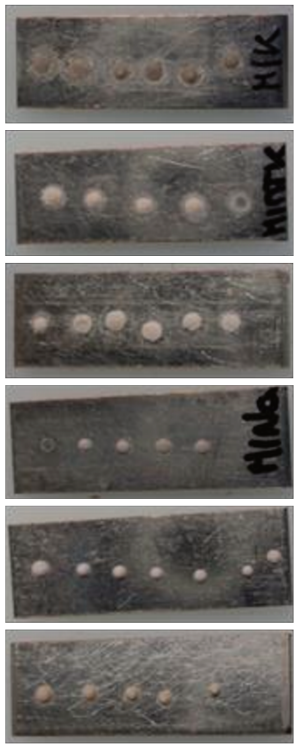

Fig. 2. Photographs of the samples after wetting angle measurements on tin-plated copper supports with the various geopolymer binder formulations.

Various behaviours are observed, depending on the formulation. In the case of ^{12}M1K, the binder drops seem to adhere to the metal surface, although a halo appears, suggesting the appearance of carbonates or the alteration of the metal surface. Indeed, the high pH value of the binder (≈12,8) promotes the formation of SnO_3^{2-} species, which can diffuse in the binder in agreement with the Pourbaix diagrams [26]. Moreover, in the case of deposits for electronic

applications, Minzari et al. [26] demonstrated during electrochemical migration tests (ECM) the formation of SnO_3^{2-} or $Sn(OH)_3^-$ species for high pH values.

The $^6M1^6MTK$ and ^{12}MTK mixtures exhibit similar behaviours, i.e., an abruption of the binder droplets and the occurrence of carbonates. The abruption of the droplets could be explained by the degradation of the metal surface due to the high pH value of the binder, leading to the formation of SnO_3^{2-} species resulting in the modification of the speciation equilibrium.

Whatever the formulation, the use of sodium cations results in a poor adhesion of the droplets of binder on the support. This phenomenon could be explained by a low contact surface, in accordance with the values of the contact angles, facilitating the pilling of the droplets.

These data will be used to evaluate the interactions between the sand assembly or metal and the geopolymer binder.

3.2 Coating

For specific applications, it is interesting to focus on the coating of geopolymer binders on tin-plated copper supports or agglomerated sand blocks. As previously discussed, the $^6M1^6MTK$ and $^6M1^6MTNa$ mixtures were selected. Samples coated by $^6M1^6MTK$ and $^6M1^6MTNa$ binders were stored for 7 days under three conditions, i.e., (i) in an open mould, (ii) in a closed mould and (ii) under 85% relative humidity. Fig. 3 shows photographs of the different samples coated with geopolymer binders.

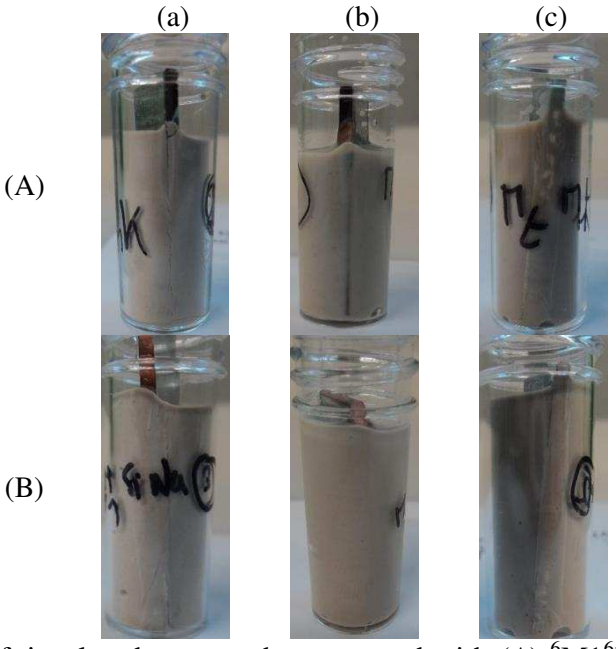

Fig. 3. Photographs of tin-plated copper sheets coated with (A) $^6M1^6MTK$ et (B) $^6M1^6MTNa$ geopolymer binders maintained for 7 days at room temperature (a) in an open mould, (b) in a closed mould and (c) under a relative humidity of 85 % (Ø = 15 mm).

The samples have different characteristics depending on the atmospheric conditions. Whatever the alkaline cation, the samples stored in an open mould exhibit significant cracking at the edges of the metal plate. In addition, the binder does not seem to adhere to the metal. This could be due to a heterogeneous drying of the consolidated material, inducing the appearance of strong stresses in the binder and consequently significant cracking [30]. There are very strong interfacial tensions at the sample surface, due to the presence of the plate as well as the atmospheric pressure that induce stresses. Indeed, the capillary pressure of the

upper part of the sample is in stress due to the pore water evaporation because the force relative to the atmospheric pressure is higher.

No cracks are evidenced on samples stored in the closed mould due to the adhesion of the binder on the metal plate, indicating a more uniform drying. Indeed, using the closed mould, the existence of a saturated atmosphere promotes water exchange at the surface and therefore minimizes the interfacial stress, limiting the evaporation of water [31]. Finally, the samples stored at 85% relative humidity exhibit cracking only on one side of the metal plate, revealing that the adhesion between the binder and the metal seems to be incomplete. In this case, the saturation vapour pressure is in perpetual equilibrium, inducing homogeneous drying [31].

The samples were then cut to investigate the interface between the metal and the binder. For practical reasons, the materials were analysed by optical microscope and by profilometry. Indeed, it was difficult to obtain sufficient vacuum to adequately observe the samples by SEM without an environmental chamber. Fig. 4 shows photographs of the different samples obtained with an optical microscope.

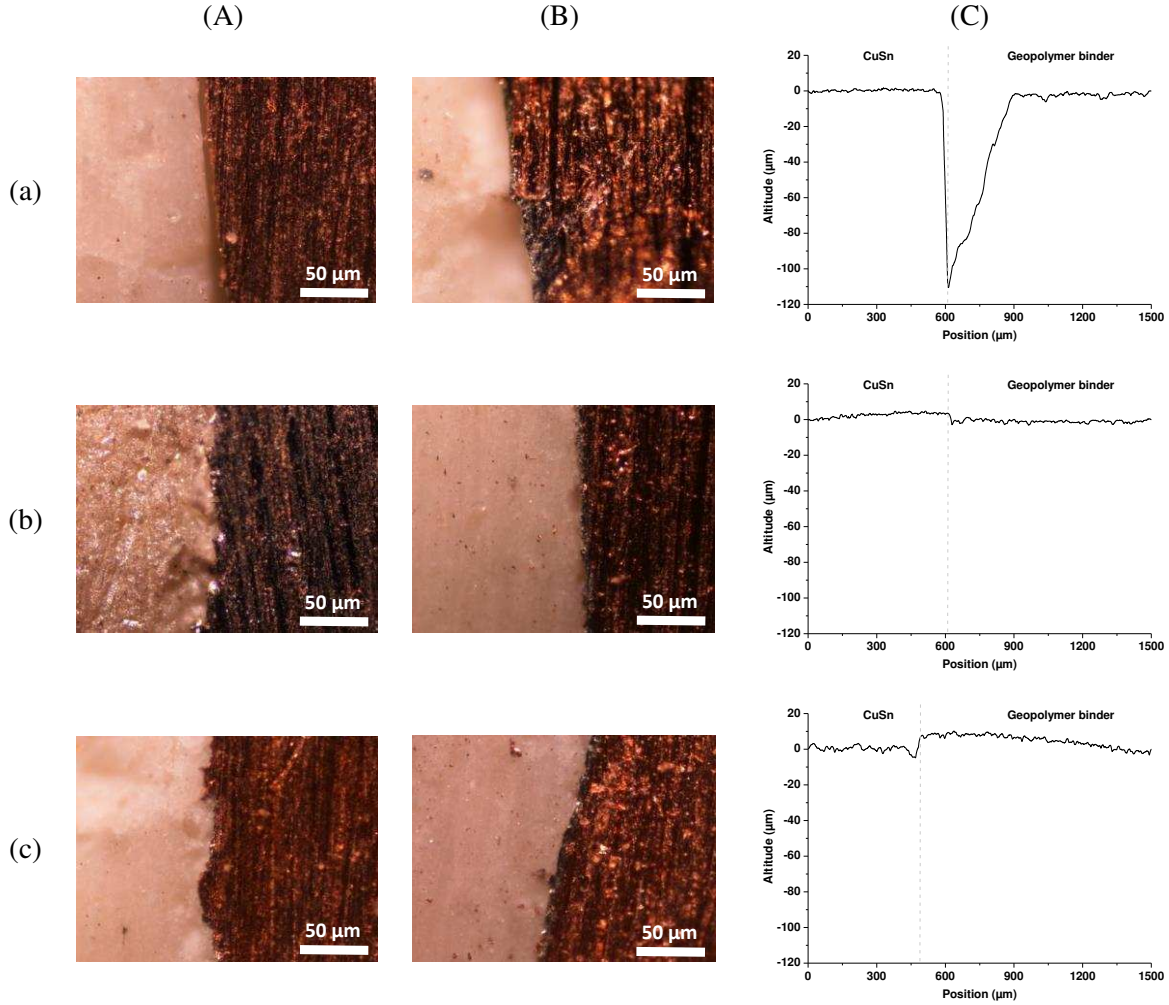

Fig. 4. Optical microscope observations at the interface between tin-plated copper and (A) ^{6}M1^{6}MTK and (B) ^{6}M1^{6}MTNa geopolymer binders and (C) profilometric curves of samples with ^{6}M1^{6}MTNa binder maintained for 7 days at room temperature (a) in an open mould, (b) in a closed mould and (c) under a relative humidity of 85% (Ø = 15 mm).

Differences in adhesion are observed depending on the binder composition and the atmosphere. Whatever the formulation, the geopolymer binder does not adhere to the metal surface when the samples are maintained in an open mould (Fig. 4 Aa and Ba). Storage in a

closed mould seems to favour adhesion. However, fracture zones are also noted at the interface (Fig. 4 Ab and Bb). The presence of such fracture zones could be due to the pilling of the binder during the sample preparation. Finally, in the case of the materials stored at an 85% relative humidity, slight adhesion differences are noted (Fig. 4 Ac and Bc). The occurrence of adhesion defects appears to be notable at the interface between the $^{6}M1^{6}MTK$ binder and the metal plate, whereas the $^{6}M1^{6}MTNa$-based binder does not have defects at the interface due to the sample preparation. Once again, these data, as well as the profilometry data, underline the importance of storage during the setting of the binder. In addition, better adhesion appears to be obtained for the sodium-based compositions.

Agglomerated sand blocks were also coated using the geopolymer binder. The samples obtained by one or two-layer deposits of the $^{6}M1^{6}MTNa$ mixture are shown in Fig. 5A.

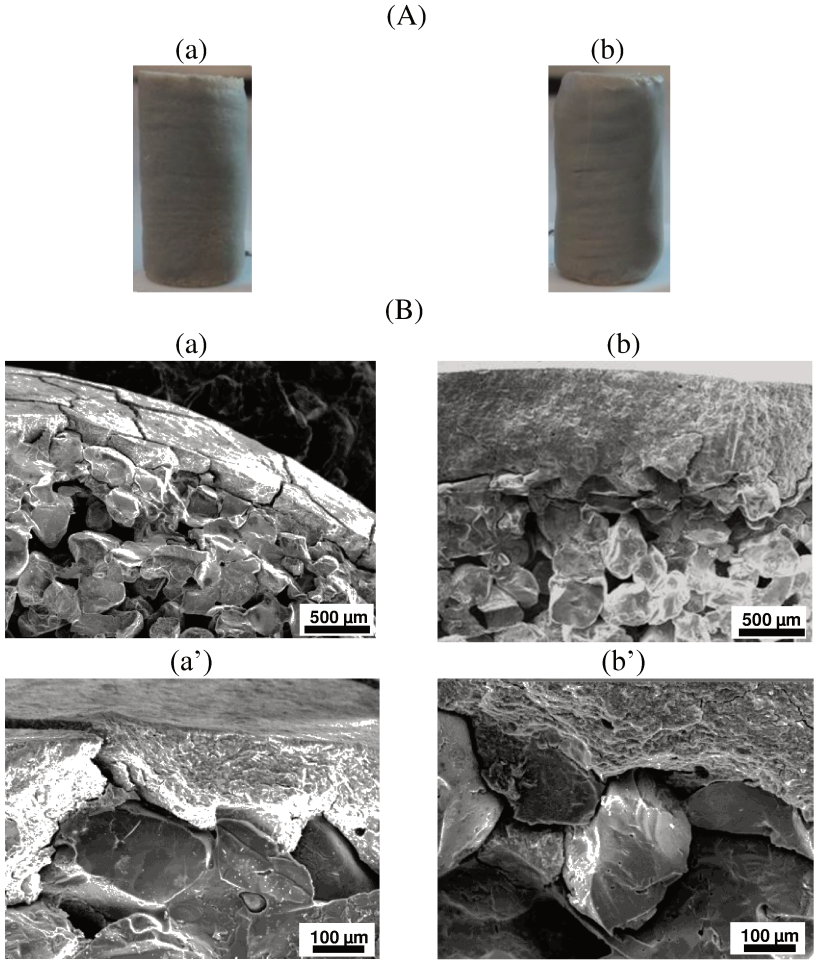

Fig. 5. (A) Photographs and (B) SEM images of an agglomerated sand block (Ø = 15 mm) *coated by (a) one layer and (b) two layers of binder and (a', b') zoom*ed in at the interface between the sand grains and the $^{6}M1^{6}MTNa$ geopolymer binder.

The binder seems to adhere to the surface of the agglomerated sand block, indicating the existence of interactions between the binder and the sand. The use of a single layer of binder seems to allow obtaining a uniform thickness of deposit. However, the deposition of two layers of binder with a 1 hour interval appears to cause small variations in the thickness and a slight cracking of the deposit. This phenomenon could be explained by the stronger interactions between the two layers of binder compared to those between the binder and the sand, inducing the cracking of the deposit [32]. During the coating, alkali cation diffusion appears between the agglomerated sand block and the binder, leading to a destabilization of

the coating and the cracking of the binder layer. Whatever the thickness of the coating, the binder seems to slightly impregnate the agglomerated sand block to a thickness of approximately 100 µm (Fig. 5Ba, b). This phenomenon can be explained by the porosity of the sand block and the viscosity of the reactive mixture. The same phenomena were observed by Gouny et al. [10] on different supports. Furthermore, no demarcation was observed between the two layers of binder, indicating a perfect adhesion between them (Fig. 5Bb). Whatever the binder thickness, the microstructure of the binder is similar to that of a geopolymer, and there are no interactions between the binder and sand grains [33] (Fig. 5Ba', b'). Consequently, the geopolymer binder is not interacting with the sand grains due to the low reactivity of the alkali silicate coating after drying [34].

Regardless of the binder formulation, it seems necessary to achieve a transition layer between the support and the binder to promote the adhesion of the deposit onto the support.

3.3 How to explain the binder-substrate adhesion?

To realize a transition layer between the substrate and the binder, various mixtures with two alkaline solutions and three metakaolins with different reactivities were studied. The interaction between the alkaline solution and metakaolin was investigated by infrared spectroscopy. The spectra at t = 0 (t_0) min and t = 720 min (t_f) are shown in Fig. 6 for several mixtures. Regardless of the formulation, all the spectra displayed two contributions at 3200 and 1640 cm^{-1}, attributed to the Si-OH and H_2O vibration bonds, respectively, [35] and a broad band located between 1100 and 950 cm^{-1} due to the Si-O-T vibration bond (T = Si or Al). For all mixtures, an intensity decrease of the 3200 and 1640 cm^{-1} bands was observed, linked to a Si-O-T shift between t = 0 and t = 720 min. For the $^{1}M1K_{t0}$ mixture, the bands at 1200, 1100, 979 and 925 cm^{-1} were attributed to the Si-O-Si vibrations of the Q^4, Q^3, Q^2 and Q^1 species, respectively [36, 37]. For the $^{1}M1K_{tf}$ formulation, the shift of the Si-O-T band at 950 cm^{-1} was assigned to the substitution of Si-O-Si bonds by Si-O-Al bonds. The appearance of the bands at 1400, 878 and 830 cm^{-1} are due to the potassium carbonate formation and the vibrations of the $Si\text{-}O^{-}M^{+}$ and Si-O-Al bonds, respectively [37, 38]. These results highlight an interaction between the metakaolin and the alkaline solution.

No major modification was observed with the increase of the metakaolin amount, as the same contributions were noted in the $^{12}M1K_{t0}$ and $^{1}M1K_{t0}$ spectra. Nonetheless, the only relative difference observed for the Q^4 species issues from the metakaolin at 1200 cm^{-1}, which is slightly more intense. At t = 720 min, only the Si-O-T shift and the increase of the Si-O-Al band, located at 941 and 830 cm^{-1}, respectively, were detected. For the $^{x}M2K$ and ^{x}MTK mixtures, the observations were similar. On the other hand, mixtures with only 1 g of metakaolin were characterized by a lower contribution due to the carbonate species, while a higher metakaolin amount in the mixture (^{12}MyK) leads to a lower shift value of the Si-O-T band. A modification of the alkaline solutions ($^{x}M1Na$, $^{x}M2Na$ and $^{x}MTNa$ mixtures) does not induce any change. With only one gram of the various metakaolins, the carbonate species appearance was not observed, and the shift of the Si-O-T band was similar for the three mixtures. The addition of 12 g of metakaolin causes a lower shift value of the Si-O-T band, regardless of the mixture, according to previous works [33].

The Si-O-T shift for the various mixtures was characteristic of the substitution of the Si-O-Si bond by a Si-O-Al bond, evidencing the dissolution of the metakaolin species by the alkaline solutions due to reactions occurring between the silicates and aluminosilicates species. With a low amount of the aluminosilicate source (1 g), few species from the metakaolin are in solution and can react with the silicate species from the alkaline solutions. In this case, the alkaline cations in excess can react with CO_2 from the air, inducing the formation of carbonate species [39]. In the case of 12 g of metakaolin, alkaline cations play a role in the reactions and are not available to form carbonate species.

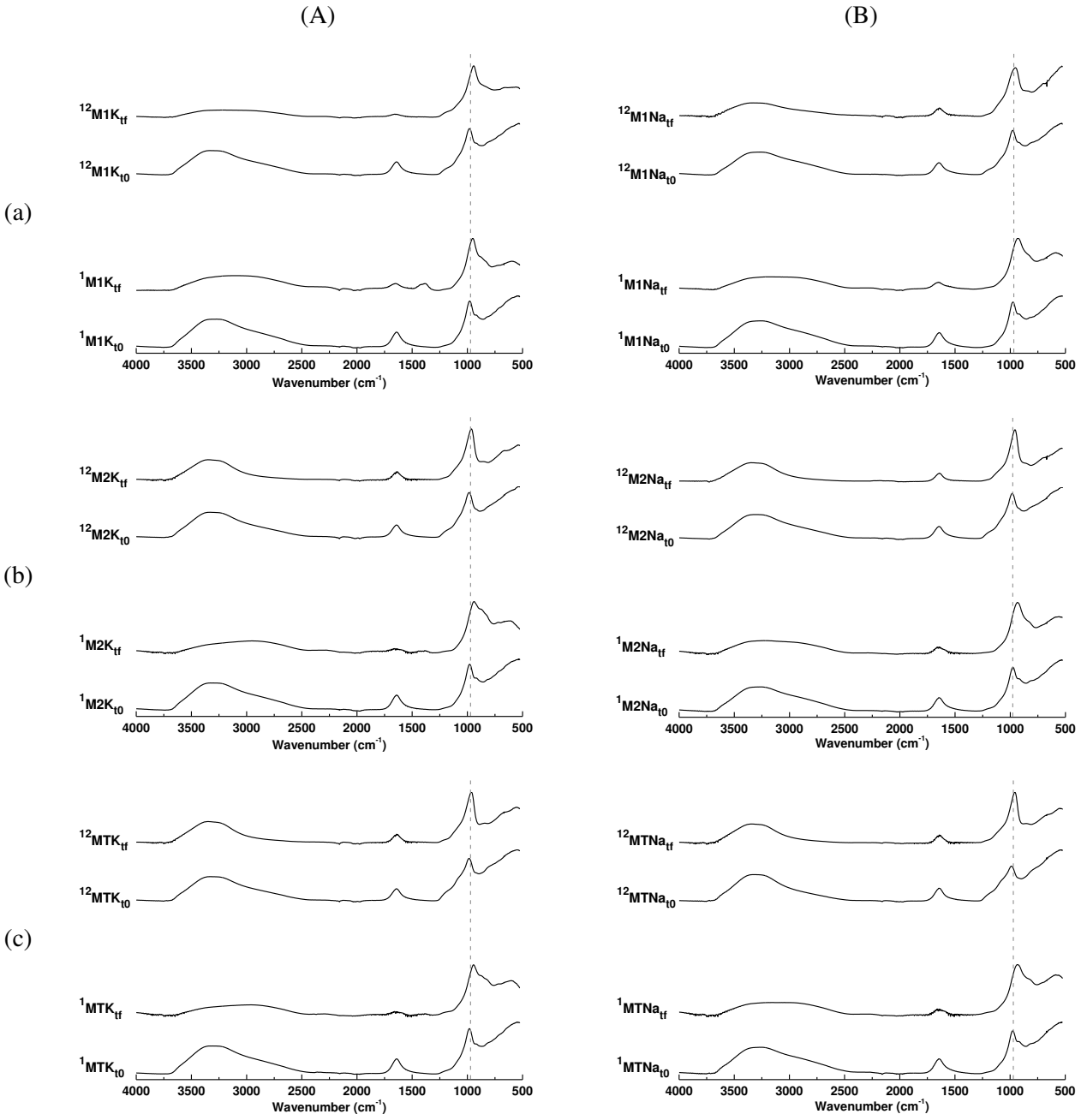

Fig. 6. FTIR spectra of (A) ^{x}MyK and (B) ^{x}MyNa compositions (x = 1 and 12 g) at t = 0 and t = 720 minutes with (a) M1, (b) M2 and (c) MT.

The shift values revised by the water content (Shift/H_2O) as a function of the reactive aluminium issuing from the metakaolin were plotted in Fig. 7. Regardless of the reactive mixture, the shift/H_2O values were constant until a threshold value of 5 a.u. Then, significant increases from 0.5 to 2.8 and from 1.0 to 3.5 a.u were observed for the $_{L}K^{0,7}$ and $_{L}Na^{0,7}$ alkaline solutions, respectively. Once again, the mixtures based on the sodium alkaline solutions show slightly higher shift/H_2O values than those based on potassium alkaline solutions (0.5 and 1.0 for the $_{L}K^{0,7}$ and $_{L}Na^{0,7}$ alkaline solutions, respectively) according to the higher reactivity of the $_{L}Na^{0,7}$ alkaline solution [28]. In this case, the pH value of the ^{1}MyNa mixture is lower, approximately 13.6, characteristic of a polycondensation reaction, thus inducing a higher shift value. For concentrations lower than 5 a.u., the shift/H_2O values are low due to the high water content in the reactive mixtures (between 40 and 55 wt% for concentrations in the range of 0.2 to 4.2 a.u., respectively). In this range of concentration, the

alkaline solution is highly diluted, so the species react as in a highly diluted medium, leading to the formation of various species [40]. However, for concentrations higher than 5 a.u., the increase in aluminium atoms leads to a more orderly network [41]. Finally, there was highlighted for the geopolymer formation (i) the existence of limiting values of reactive Al (5 a.u.) and (ii) the shift/H_2O value (1.4).

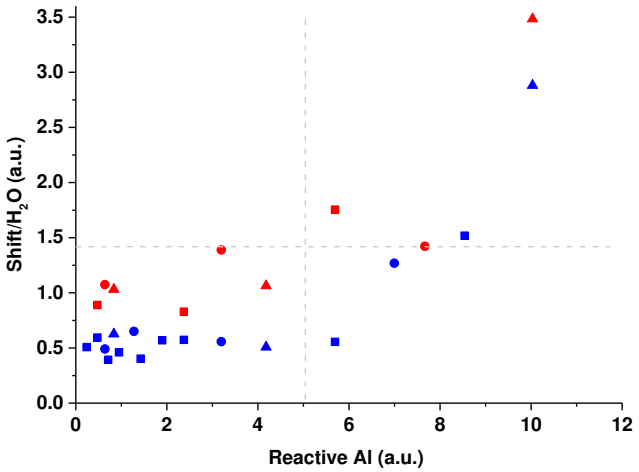

Fig. 7. Shift value corrected by the water amount obtained from FTIR spectroscopy as a function of the reactive aluminum for the (■) ^{x}M1M, (●) ^{x}M2M, (▲) ^{x}MTM mixtures, with M = (—) K and (—) Na and x varying from 0.5 to 18 g.

To demonstrate the influence of the water content in the reactive mixtures on the polycondensation reaction, the ΔV value was calculated by the difference between the water content from the solution and the water content needed to wet the added metakaolin. As an example, the volume of water necessary to wet the metakaolin depends on both the wettability of the previous solution (760, 1270 and 1190 µL/g for the M1, M2 and MT metakaolins, respectively) and the water added [42]. For the ^{1}M2K mixture, the necessary volume is 8 mL, while only 1.3 mL is sufficient to wet the metakaolin, so the ΔV value is 6.7 mL. In that case, there is an excess water content and thus a positive ΔV. Even so, for the ^{12}M2K mixture, the volume of water available is 9 mL (8 mL from the solution and 1 mL to improve the feasibility), and the water needed is 15.2 mL. The ΔV value is then – 6.2 mL, meaning that there is a lack of water in the mixture to wet the total content of metakaolin. ΔV was plotted for the various mixtures (Fig. 8) as a function of the silicon and aluminium concentrations. Whatever the alkali cation type and the metakaolin, the silicon and aluminium concentrations decrease when the ΔV value (negative or positive) increases. A threshold value in the Si and Al concentrations was determined to obtain a null ΔV (13 and 6 mol/L, respectively). The increase in the metakaolin content in the reactive mixtures leads to a diminution of the ΔV value because the water content from the alkaline solutions remains constant (8 and 9 mL for $_{L}K^{0.7}$ and $_{L}Na^{0.7}$, respectively). For high metakaolin contents in the reactive mixtures, 1 g of water was added, except for the ^{x}M1K samples. According to infrared spectroscopy, the reactive mixtures with negative ΔV values seem to lead to a geopolymer network formation, while for positive ΔV values, a formation of several networks seems to be predominant. The formation of those various networks mainly depends on the aluminium content available. For a low aluminium content, the species cannot interact and participate in the polycondensation process, as it is a dilute mixture [40]. Moreover, for an adequate aluminium content in the mixture ([Al] > 6 mol/L), the reactions lead to the geopolymer formation knowing that, for a highly concentrated system, the charges in the binder, positive or negative, will compensate [43]. However, for an even lower aluminium concentration, the formation of several networks

can be observed. Thus, there are threshold concentrations of silicon and aluminium that can allow determination of the geopolymer formation for a sample.

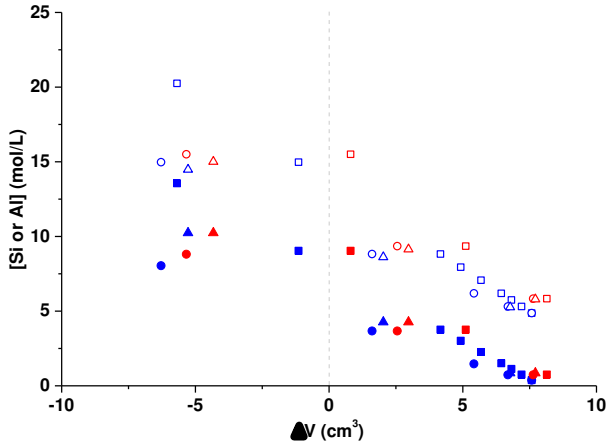

Fig. 1. Evolution of the (■) Al and (▱) Si concentrations as functions of the ΔV values (= water volume from the solution - water volume needed to wet the metakaolin) for the (■) ^{x}M1M, (●) ^{x}M2M and (▲) ^{x}MTM mixtures, with M = (▬) K and (▬) Na and x varying from 0.5 to 18 g.

To corroborate this result to the existence domains of geopolymer highlighted by Gharzouni et al. [44], the ΔV values were plotted as a function of the Si/Al and M/Al molar ratios of the total mixtures (Fig. 9). For Si/Al and M/Al molar ratios ranging from 2 to 15 and from 1.2 to 20, respectively, the ΔV value is positive and remains approximately constant. This evolution is characteristic of a dilute mixture with low metakaolin content. The volume of water introduced is always in excess, and the free silicon and aluminium atoms will interact with silicate species from the solution by forming species highly rich in silicon, due to a low variation of the Q^2 band. Those species can precipitate, which is verified by the formation of a settling phenomenon.

For Si/Al = 2 and M/Al = 1.2, the null ΔV value is relative to a physical-chemical equilibrium, where polycondensation reactions take place and will lead to a polymeric network. Plus, this value corresponds to a limit in the existence domain of geopolymers.

For negative ΔV values, the alkaline solution volume advances the metakaolin dissolution and favours the increase of aluminosilicate colloids in the reactive medium. All these facts induce a saturation of this medium, favouring the polycondensation and geopolymerization reactions [44]. In this range of concentration, the alkali cation type is not a preponderant factor. The low difference between the potassium and sodium alkali cations is to be correlated to the viscosity of this medium, which governs the species mobility. Indeed, the features of sodium alkali solutions with high viscosity, where the sodium cation diffuses less quickly, are similar to those of potassium alkali solutions, where the potassium cation diffuses more rapidly.

Thus, it was highlighted that the geopolymer binder formation can be evaluated by the ΔV value controlling the various interactions in the reactive mixture.

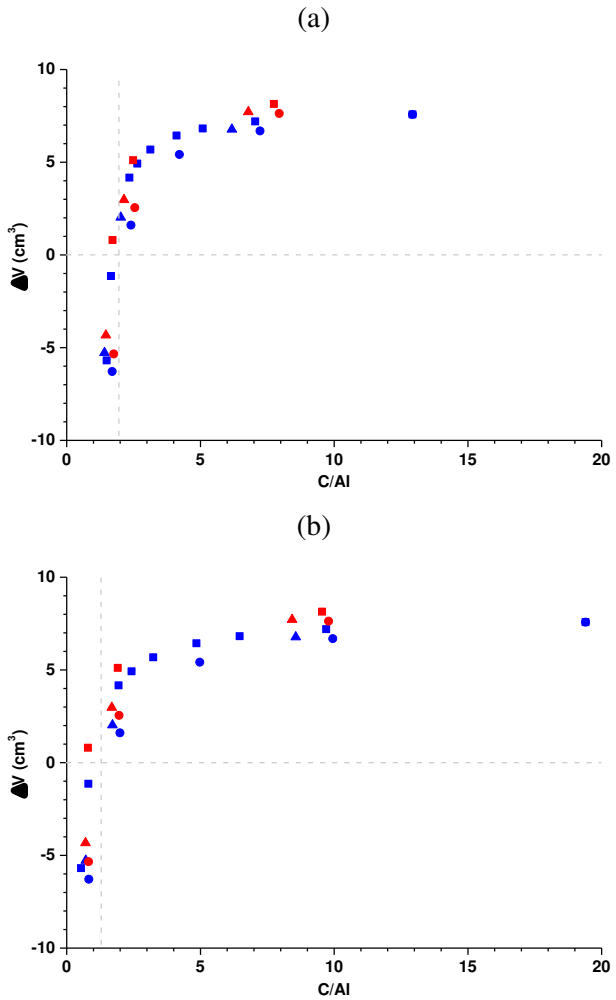

Fig. 2. Evolution of the ΔV value versus C/Al molar ratio with C = (a) Si and (b) K or Na for the (■) ^{x}M1M, (●) ^{x}M2M, (▲) ^{x}MTM formulations, with M = (—) K and (—) Na and x varying from 0.5 to 18 g.

4. Discussion

The above results have revealed various interactions between the geopolymer binders and supports. Fig. 10 shows the evolution of the wetting angle depending on the reactivity of the reactive mixture, i.e., the percentage of Al available in the mixture for the various compositions and types of support. Three behaviours can be evidenced, depending on the aluminium content and the wetting angle. These behaviours are denoted I, II, and III and correspond to (i) low interactions between the binder and the support, (ii) the creation of an interphase between the two materials and (iii) the alteration of the support, respectively. The agglomerated sand and polyethylene supports are contained in zone I due to the existence of non-reactivity or repulsion. In the case of the agglomerated sand block, the high wetting angle value is explained by the presence of alkali silicate on the surface, inducing charge repulsion [43]. Tin-plated copper supports (zone II) correspond to the adhesion between the metal and the binder by the formation of specific species such as $Sn(OH)_2$. Finally, the corrosion of the glass substrate by the binder (zone III) is characteristic of the phenomenon of chemical attack due to the alkali cation exchange [45].

For coatings on tin-plated copper, better adhesion was obtained for binders with a water/solid ratio between 0.66 and 0.74 and a Si/Al molar ratio between 1.53 and 1.58 and Na/Al = 0.75. Compared to the work of Irfan Khan et al. [15], the water-to-solid ratios of the coatings in this study are higher, the Si/Al ratio is less important and the Na/Al ratio is similar to their deposit

values. Yet, only the water/solid ratio is comparable to the study of Temuujin et al. [17], with the other ratios being inferior to their values. These differences might be partly due to the use of fly ash by Irfan Khan et al. [15] and to the silica charge by Temuujin et al. [17].

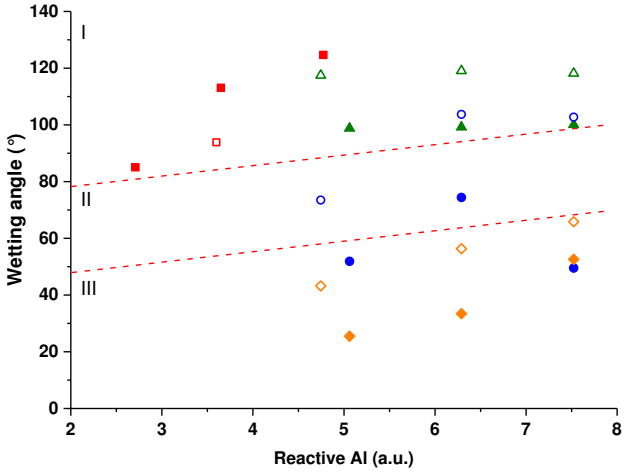

Fig. 3. Variation of the wetting angle as a function of the reactive aluminum for the various compositions with (■, ▲, ●, ◆) potassium and (□, △, ○, ◇) sodium on (■, □) agglomerated sand, (▲, △) polyethylene, (◆, ◇) tin-plated copper and (●, ○) glass.

These various interaction zones, depending on the wetting angle values, can be controlled by the amount of reactive aluminium.

5. Conclusion

Several compositions of alkali aluminosilicate binder were studied to form deposits on the metal and/ or agglomerated sand surfaces. Interactions between the different compounds evaluated by the wetting angle measurements evidenced different behaviours depending on the chemical binder composition and on the support nature. The wetting angles obtained for a composition based on sodium alkaline with two metakaolins are 43.2°, 117.5° and 77.7° for the glass, polyethylene and copper supports, respectively.

The key parameters to control the chemical interactions for producing an aluminosilicate binder deposit are for tin-plated copper plates, drying at room temperature and 85% RH, and for the agglomerated sand, blockage by two layers, which facilitates the anchoring of the geopolymer binder.

In addition, the parameters related to the formation of the geopolymer network are highlighted by the reactive [Al] > 5 mol / L and a lower volume of solution wettability. Finally, three interaction areas are evidenced depending on the value of the wetting angle and the reactive aluminium percentage in the mixture for the different carriers and binders: those with weak interactions, those with the formation of an interphase and those with the corrosion of the substrate. These interactions mean that controlling the chemical composition of the binder can produce deposits of geopolymer binders on the tin-plated copper and on bonded sand blocks.

6. Acknowledgements

The authors gratefully acknowledge the FEDER agency, the Limousin regional council and the FUI program for their financial support.

References

[1] K. Huang, S. Cai, G. Xu, X. Ye, Y. Dou, M. Ren, X. Wang, Preparation and characterization of mesoporous 45S5 bioactive glass-ceramic coatings on magnesium alloy for corrosion protection, J. Alloys Compd. 580 (2013) 290-297.
[2] Z. Zhang, X. Yao, H. Zhu, Potential application of geopolymers as protection coatings for marine concrete. I. Basic properties. Appli. Clay Sci. 49 (2010) 1-6.
[3] G. Masi, W.D.A. Rickard, M.C. Bignozzi, A. van Riessen, The effect of organic and inorganic fibres on the mechanical and thermal properties of aluminated activated geopolymers, Composites Part B 76 (2015) 218-228.
[4] J. Schultz, M. Nardin, Theories and mechanisms of adhesion, in: K.L. Mittal, A. Pizzi, Adhesion promotion techniques, Marcel Dekker, New York, 2002, pp. 1-26.
[5] J.W. McBain, D.G. Hopkins, On adhesives and adhesive action, J. Phys. Chem. 29 (2) (1925) 188-204
[6] W. Duarte, M. Vardelle, S. Rossignol, Effect of the precursor nature and preparation mode on the coarsening of La2Zr0O7 compounds, Ceram. Int. 42 (1) (2016) 1197-1209.
[7] V. Kumar, K. Balasubramanian, Progress update on failure mechanisms of advanced thermal barrier coatings: A review, Prog. Org. Coat. 90 (2016) 54-82.
[8] B. Wielage, T. Grund, C. Rupprecht, S. Kuemmel, New method for producing power electronic circuit boards by cold-gas spraying and investigation of adhesion mechanisms, Sur. Coat. Technol. 205 (2010) 1115-1118.
[9] F. Gouny, F. Fouchal, O. Pop, P. Maillard, S. Rossignol, Mechanical behavior of an assembly of wood-geopolymer-earth bricks, Constr. Build. Mater. 38 (2013) 110-118.
[10] F. Gouny, F. Fouchal, P. Maillard, S. Rossignol, A geopolymer mortar for wood and earth structures, Constr. Build. Mater. 36 (2012) 188-195.
[11] G. Habert, C. Ouellet-Plamondon, Recent update on the environmental impact of geopolymers, RILEM Technical Letters 1 (2016) 17-23.
[12] S.R. Do Rego, K.C. Gomes, A.F. Leal, N.P. Barbosa, S.M. Torres, S. De Barros, Adhesion of ceramic plates with geopolymer, Mater. Sci. Forum 643 (2010) 139-142.
[13] P. Chindaprasirt, U. Rattanasak, Improvement of durability of cement pipe with high calcium fly ash geopolymer covering, Constr. Build. Mater. 112 (2016) 956-961.
[14] Z. Zhang, X. Yao, H. Zhu, Potential application of geopolymers as protection coatings for marine concrete. I. Basic properties. Appli. Clay Sci. 49 (2010) 1-6.
[15] M. Irfan Khan, K. Azizli, S. Sufian, Z. Man. Sodium silicate-free geopolymers as coating materials: effects of Na/Al and water/solid ratios on adhesion strength, Ceram. Int. 41 (2015) 2794-2805.
[16] P.G. Allison, C.A. Weiss jr., R.D. Moser, A.J. Diaz, O.G. Rivera, S.S. Holton, Nanoindentation and SEM/EDX characterization of the geopolymer-to-steel interfacial transition zone for a reactive porcelain enamel coating, Composites Part B 78 (2015) 131-137.
[17] J. Temuujin, A. Minjigmaa, W. Rickard, M. Lee, I. Williams, A. van Riessen, Preparation of metakaolin based geopolymer coatings on metal substrates as thermal barriers, Appl. Clay Sci. 46 (2009) 265-270.
[18] O. Dezellus, Contribution à l'étude des mécanismes de mouillage réactif, Thèse de doctorat, Institut National Polytechnique de Grenoble, Grenoble, 2005.
[19] A. Alghunaim, S. Kirdponpattara, B.Z. Newby, Techniques for determining contact angle and wettability of powders, Powder Technol. 287 (2016) 201-215.
[20] R.D. Moser, P.G. Allison, B.A. Williams, C.A. Weiss Jr, A.J. Diaz, E.R. Gore, P.G. Malone, Improvement in the geopolymer-to-steel bond using a reactive vitreous enamel coating, Constr. Build. Mater. 49 (2013) 62-69.

[21] M.K. Ruth, Syamsidar, Sulfiana, H. Abdul, Subaer, Synthesis of geopolymer paste as coating material based on kaolinite and rice husk ash, Mater. Sci. Forum 841 (2016) 79-82.
[22] L. Vidal, E. Joussein, M. Colas, J. Cornette, J. Sanz, I. Sobrados, J-L. Gelet, J. Absi, S. Rossignol, Controlling the reactivity of silicate solutions: a FTIR, Raman and NMR study, Colloids Surf., A. 503 (2016) 101-109.
[23] R. Gy, Ion exchange for glass strengthening, Mater. Sci Eng. B 149 (2008) 159-165.
[24] A. Gharzouni, E. Joussein, B. Samet, S. Baklouti, S. Rossignol, Effect of the reactivity of alkaline solution and métakaolin on geopolymer formation, J. Non-Cryst. Solids 410 (2015) 127-134.
[25] A. Gharzouni, I. Sobrados, E. Joussein, S. Baklouti, S. Rossignol, Predictive tools to control the structure and the properties of metakaolin based geopolymer materials, Colloid Surf. A, submitted.
[26] D. Minzari, M.S. Jellesen, P. Møller, R. Ambat, On the electrochemical migration mechanism of tin in electronics, Corros. Sci. 53 (2011) 3366-3379.
[27] M. Pourbaix, Atlas d'équilibres électrochimiques à 25 °C, Gauthier-Villars, Paris, 1963.
[28] L. Vidal, E. Joussein, M. Colas, J. Cornette, J. Absi, S. Rossignol, Identification of chains and rings in alkaline silicate solutions by Raman spectroscopy: effect of alkali cation, Colloids Surf., A Submitted.
[29] L. Vidal, E. Joussein, I. Sobrados, J. Absi, S. Rossignol, How to counteract the low reactivity of an alkaline solution, J. Non-Cryst. Solids, Submitted.
[30] A.C. Pierre, D.R. Uhlmann, Gelation of aluminum hydroxide sols, J. Am. Ceram. Soc. 70 (1987) 28-32.
[31] R.W. Ford, Drying, Institute of Ceramics, textbook series, MacLaren and Sons, London, 1964.
[32] O. Oulanti, E. Pefferkorn, S. Champ, H. Auweter, Relaxation phenomena of polyethyleneimine molecules within saturated homogeneous and heterogeneous layers adsorbed at a silica/water interface, J. Colloid Interface Sci. 294 (2006) 87-94.
[33] E. Prud'Homme, Rôles du cation alcalin et des renforts minéraux et végétaux sur les mécanismes de formation de géopolymères poreux ou denses, Thèse d'Université, Université de Limoges, 2011.
[34] L.Vidal, A. Gharzouni, S.Rossignol, Alkaline silicate solutions: An overview of their structure, reactivity and applications, in: L. Klein, M. Aparicio, A. Jitianu, Handbook of Sol-Gel Science and Technology, submitted.
[35] I. Lancellotti, M. Catauro, C. Ponzoni, F. Bollino, C. Leonelli, Inorganic polymers from alkali activation of metakaolin: Effect of setting and curing on structure, J. Solid State Chem., 200 (2013) 341-348.
[36] L. Verdolotti, S. Iannace, M. Lavorgna, R. Lamanna, Geopolymerization reaction to consolidate incoherent pozzolanic soil, J. Mater. Sci., 43 (2008) 865-873.
[37] M.T. Tognonvi, J. Soro, S. Rossignol, Physical-chemistry of silica/alkaline silicate interactions during consolidation. Part 1: Effect of cation size, J. Non-Cryst. Solids, 358 (2012) 81-87.
[38] M. Esaifan, H. Khoury, I. Aldabsheh, H. Rahier, M. Hourani, J. Wastiels, Hydrated lime/potassium carbonate as alkaline activating mixture to produce kaolinitic clay based inorganic polymer, Appl. Clay Sci. 126 (2016) 278-286.
[39] X.X. Gao, A. Autef, E. Prud'homme, P. Michaud, E. Joussein, S. Rossignol, Synthesis of consolidated materials from alkaline solutions and metakaolin: existence of domains in the Al-Si-K/O ternary diagram, J. Sol-Gel Sci. Technol. 65 (2013) 220-229.

[40] M. Henry, J.-P. Jolivet, J. Livage, Aqueous chemistry of metal cations: hydrolysis, condensation and complexation, Struct. Bond. (1990) 1-64.
[41] J.T.G. Overbeek, Recent developments in the understanding of colloid stability, J. Colloid Interface Sci. 58 (1977) 408-422.
[42] A. Autef, Formulation géopolymère : influence des rapports molaires Si/K et Si/Al sur les réactions de polycondensation au sein de gels aluminosilicatés, PhD Thesis, University of Limoges, Limoges, France, 2013.
[43] E. Matijevic, Colloid stability and complex chemistry, J. Colloid, Interface Sci. 43 (1973) 217-245.
[44] A. Gharzouni, I. Sobrados, E. Joussein, S. Baklouti, S. Rossignol, Predictive tools to control the structure and the properties of metakaolin based geopolymer materials, Colloid Surf. A, submitted.
[45] S. Gin, P. Jollivet, M. Fournier, C. Berthon, Z. Wang, A. Mitroshkov, Z. Zhu, J.V. Ryan, The fate of silicon during glass corrosion under alkaline conditions: A mechanistic and kinetic study with the International Simple Glass, Geochim. Cosmochim. Acta 151 (2015) 68-85.

Acte de congrès 1 (ACLN 1)

L. Vidal, A. Autef, S. Selmani, E. Joussein, S. Rossignol

"Role of siliceous species in geopolymer reactant mixture: interaction with $(NH_4)_2Mo_2O_7$"

Key Engineering Materials, 2014, vol. 617, p. 46-49.

Key Engineering Materials Vol. 617 (2014) pp 46-49

doi:10.4028/www.scientific.net/KEM.617.46

Role of siliceous species in geopolymer reactant mixture: interaction with $(NH_4)_2Mo_2O_7$

Laëticia Vidal[1], Alexandre Autef[2], Samira Selmani[1], Emmanuel Joussein[3], Sylvie Rossignol[1]

[1]Groupe d'Etude des Matériaux Hétérogènes (GEMH-ENSCI) Ecole Nationale Supérieure de Céramique Industrielle, 12 Rue Atlantis, 87068 Limoges Cedex, France

[2]Imerys Ceramic Centre, 8 Rue de Soyouz, 87000 Limoges, France

[3]Université de Limoges, GRESE, EA 4330, 123 Avenue Albert Thomas, 87060 Limoges, France

sylvie.rossignol@unilim.fr

Keywords: geopolymer, aluminosilicate, infrared spectroscopy, ammonium molybdate

Abstract. Geopolymers are inorganic materials having interesting properties for many using areas. It is well known that geopolymers present various properties depending on the used aluminosilicate sources but lack of understanding are manifest. This study consists on the comprehension of the formation of different networks in geopolymers modifying the reactivity of siliceous species in the reactive mixture with ammonium molybdate. These experiments evidenced the existence of various polycondensation reactions between materials leading to the formation of different networks. Moreover the use of ammonium molybdate addition in the mixture induces a slowdown of the reaction.

Introduction

The "alkali silicates" is one of the raw materials classically used in the formulation of new materials like geopolymers. Geopolymers are amorphous three-dimensional aluminosilicate binder materials which are synthesized at ambient temperature by the alkaline activation of silica solution and aluminosilicates derived from natural minerals, calcined clay or industrial byproducts. Previous study focused on the aluminosilicate sources have shown that the presence of impurities and the reactivity of the metakaolin (aluminosilicate source) can lead to the formation of one or several networks in geopolymers materials [1]. Indeed, the different sources of metakaolins conduct to the presences of various siliceous species in the solution which react with alumina. These multiple combinations lead to the formation of different networks (then various properties of geopolymers). To understand the formation of these various networks, studies relative to the neutralization of siliceous species in solution have been done. Parmentier [2] showed that the ammonium molybdate could react with silica to create silicomolybdic compounds. More recent studies demonstrated that ammonium molybdate could also react with these species in an alkaline environment [3]. These analyses showed that ammonium molybdate could react not only with monomers and dimers, but also with larger molecules. According to this, molybdate can permit to complex siliceous species and to modify polymerization reactions. The aim of the study is to study the influence of the ammonium molybdate addition on the kinetics of the polycondensation reaction as well as on the formation of several networks.

Experimental

Sample preparation. Samples were synthesized using an alkaline silicate solution and three metakaolins (namely Mk1, Mk2 and Mk3). The alkaline silicate solution was obtained by the dissolution of KOH pellets (85.2 % purity) and amorphous silica (99.9 % purity) in water at room temperature. Syntheses were performed by mixing the alkaline silicate solution and metakaolins. The samples were named M1, M2 and M3. Other samples were realized with addition of ammonium molybdate (10 and 20% molar) to the alkaline solution before metakaolin. These samples were named M1-20, M2-10, M2-20 and M3-20.

Sample characterization. Fourier-transform infrared (FTIR) spectroscopy in ATR mode was used to monitor the geopolymerization. FTIR spectra were obtained using a ThermoFisher Scientific Nicolet 380 infrared spectrometer. The IR spectra were gathered over a wavenumber range of 400 to 4000 cm^{-1} with a resolution of 4 cm^{-1}. To follow the evolution of the involved bonds in time, a software was used to acquire a spectrum every 10 min for 13 hours. The atmospheric CO_2 contribution was removed with a straight line between 2400 and 2280 cm^{-1}. To allow comparisons of spectra, they were corrected using baseline and normalized.

Results

The influence of the addition of ammonium molybdate on the polycondensation reactions was evaluated by FTIR spectroscopy (Fig. 1). The shift of the Si-O-M band with time is characteristic of a polycondensation reaction (relative to the substitution of Si-O-Si by Si-O-Al bonds) during the geopolymer formation. According to the literature, the intensity of the Si-O-M shift for each sample is relative to different polycondensation reactions [4]. The ammonium molybdate addition in the mixture increases (up to 10 cm^{-1}) the initial displacement of the Si-O-Si peak whatever the Mk samples used. This fact evidenced a bridging between siliceous and molybdic species creating Si-O-Mo bonds [5]. The addition of ammonium molybdate slows down the shift of Si-O-M peak (M = Al or Si) and then the exchange between Al and Si. Since ammonium molybdate is added before metakaolin, the molybdate ions are complexed with Si from amorphous silica. When adding the metakaolin, the silicomolybdic complexes preferentially react with aluminum atoms leading to the presence of siliceous species in excess in the solution which come from the dissolution of the metakaolin.

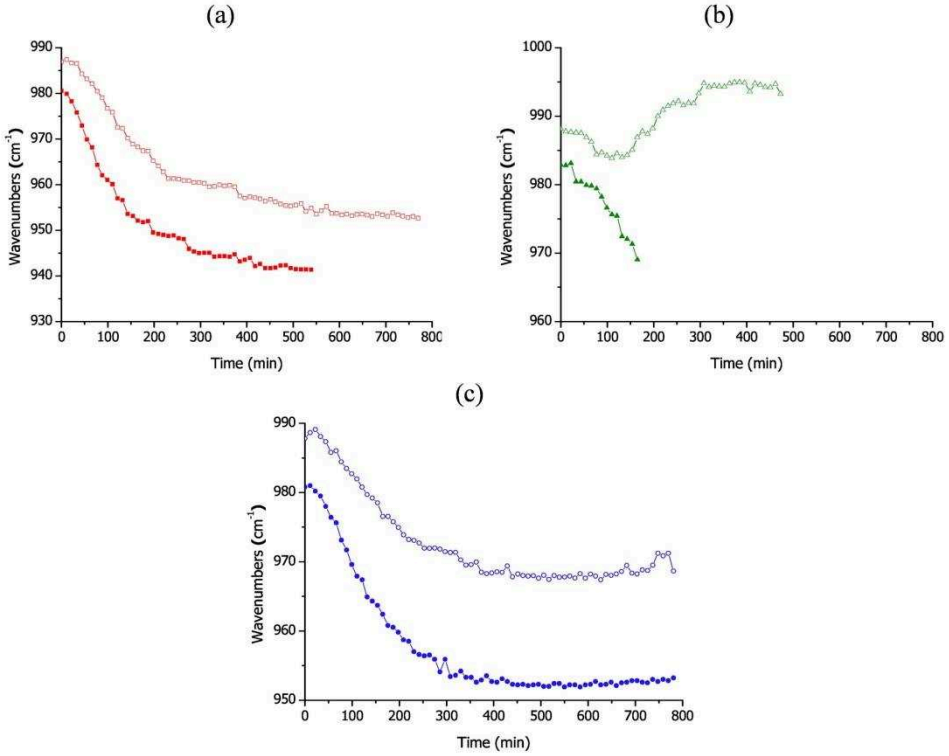

Fig. 1: Displacement of the Si-O-M (M = Al or Si) peak as a function of time for the geopolymers (a) (■) M1 and (□) M1-20, (b) (▲) M2 and (△) M2-20 and (c) (●) M3 and (○) M3-20

The shift of Si-O-M peak for the samples containing ammonium molybdate has two types of behavior: (i) a decrease of the wavenumber is observed for samples M3-20 and M1-20 compare to M3 and M1 materials, and (ii) a decrease followed by an increase for the M2-20 sample. The behavior observed for geopolymers M3-20 and M1-20 shows that addition of molybdate in the reactive mixture delays the polycondensation reactions. However, for the sample M2-20, the polycondensation reactions are very fast at the local scale, as soon as aluminous species react (decrease in the peak position). Reactions between the siliceous species are effective leading to the appearance of a siliceous compound and explaining the shift of Si-O-M peak to higher wavenumbers [1,6]. The FTIR spectroscopy highlights different polycondensation reactions for each sample. The ammonium molybdate addition leads to a modification of the reactions toward the Si-O-M bonds (M = Al or Si) creating Si-O-Mo bonds.

Discussion and conclusion

To compare the effects of ammonium molybdate on each geopolymer, the total shift of the Si-O-M (M = Al or Si) peak has been realized (Fig. 2a*)*. The total displacement is 39, 13 and 28 cm^{-1} for the geopolymers M1, M2 and M3 respectively whereas the shift is lower for the geopolymers M1-20, M2-20 and M3-20 (34, 4 and 19 cm^{-1}). The M2-10 shows a total displacement of 10 cm^{-1}.

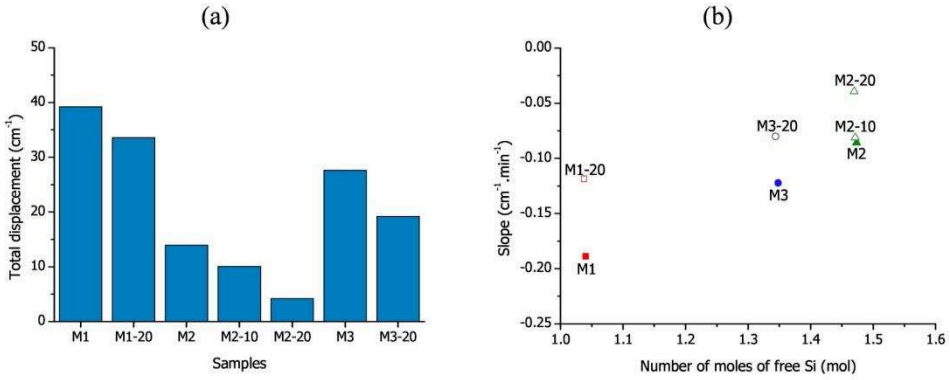

Fig. 2: (a) Total displacement and (b) evolution of the slope of the Si-O-M (M = Al or Si) peak displacement as a function of the number of silicon available in the alkaline solution for the geopolymers M1, M2 and M3 with different ammonium molybdate additions.

Whatever the sample, the addition of ammonium molybdate leads a decrease of the total displacement of the Si-O-M peak (Fig. 2a). This decrease reveals the existence of different networks [7]. The addition of 10 % of ammonium molybdate induces a quasi no effect on the reactions compare to the addition of 20 % in the reactive mixture. Therefore, a certain amount of molybdate is necessary to complex siliceous species.

The slopes values deduce from the Si-O-M peak displacement (Fig. 1) were determined. Fig. 2b shows the slopes evolution as a function of the number of moles of silicon available[1]. For each sample, the ammonium molybdate addition leads to a decrease more or less important of the slope of the Si-O-M peak displacement. However, the number of moles of available silicon in the alkaline solution slightly varies with the addition of ammonium molybdate. This is the same thing for the shift of the slope whatever the sample: -0.19 (M1) vs. -0.12 $cm^{-1}.min^{-1}$ (M1-20), -0.09 (M2) to -0.04 $cm^{-1}.min^{-1}$ M2-20 and -0.12 (M3) to -0.08 $cm^{-1}.min^{-1}$ (M3-20). As expected, the addition of 10 % of molybdate induces no effect.

[1] Number of moles of free silicon = $((n_{Si}-n_{metakaolin}-n_{Mo})*\%amorphous)/n_{Al}$

The weak variation of the number of moles of free silicon can be explained by the stoichiometry of the synthesized compounds (1 Si for 12 Mo atoms) [2]. Despite of the low influence of ammonium molybdate on the number of free silicon atoms, a strong variation of the slope is observed. In fact, a weak variation in moles number induces a strong variation on the oligomer number. It can be explained by the size of Si-Mo species creating oligomers which replace the initial $Si(OH)_4^-$ monomers. The formation of these oligomers inhibits the polycondensation reactions by an effect of oligomer polymerization [8].
These reactions are independent of the metakaolin used except in the case of the geopolymer M1 where the presence of several networks has been highlighted. These different networks imply various polycondensation mechanisms, which explains the differences observed between this sample and the other materials.

To conclude, these different observations allow to highlight the formation of oligomers from $Si(OH)_4^-$ monomers and ammonium molybdate blocking the polycondensation reactions by a polymerization effect in the alkaline solution.

References

[1] A. Autef, E. Joussein, A. Poulesquen, G. Gasgnier, S. Pronier, I. Sobrados, J. Sanz, S. Rossignol, Influence of metakaolin purities on potassium geopolymer formulation: the existence of several networks, J. of Colloïd and Interface Science, 408 (1) (2013) 43-53.

[2] F. Parmentier, Sur les silicomolybdates, Annales scientifiques de l'E.N.S., 2ème série, 11 (1882) 187-218.

[3] M. Tanakaa, K. Takahashib, Silicate species in high pH solution molybdate, whose silica concentration is determined, Analytica Chimica Acta, 429 (1) (2001) 117-123.

[4] F. Gouny, Nouveau système constructif multimatériaux bois/liant géopolymérique/brique de terre crue : formulation, caractérisation et transfert d'échelle, Thèse de doctorat, Université de Limoges, 2013.

[5] M. Chen, D.W. Goodman, Reply to comment on "The structure of monolayer SiO2 on Mo(112): A 2-D [Si-O-Si] network or isolated [SiO4] units?", Surface Science, 601 (2) (2007) 591-593.

[6] M. Tohoué Tognonvi, Physico-chimie de la gélification du silicate de sodium en milieu basique, Thèse de doctorat, Université de Limoges, 2009.

[7] E. Prud'Homme, Rôles du cation alcalin et des renforts minéraux et végétaux sur les mécanismes de formation de géopolymères poreux ou denses, Thèse de doctorat, Université de Limoges, 2011.

[8] J-E.A.Otterstedt, M. Ghuzel, J.P. Sterte, Colloidal components in solutions of alkali silicates, J. of Colloid and Interface Science, 115 (1) (1987) 95-103.

Acte de congrès 2 (ACLN 2)

L. Vidal, E. Joussein, J. Absi, S. Rossignol

"Addition of ammonium molybdate in geopolymer formulation"

Advances in Science and Technology, 2014, vol. 92, p. 8-13.

Advances in Science and Technology Vol. 92 (2014) pp 8-13
Online available since 2014/Oct/31 at www.scientific.net

doi:10.4028/www.scientific.net/AST.92.8

Addition of ammonium molybdate in geopolymer formulation

Laëticia Vidal[1,2], Emmanuel Joussein[3], Joseph Absi[2], Sylvie Rossignol[1,*]

[1] Laboratoire de Science des Procédés Céramiques et Traitements de Surface (SPCTS) UMR 7315 CNRS, Centre Européen de la Céramique, Université de Limoges, 12 Rue Atlantis, 87068 Limoges Cedex, France

[2] Groupe d'Etude des Matériaux Hétérogènes (GEMH), 12 Rue Atlantis, 87068 Limoges Cedex, France

[3]Université de Limoges, GRESE, EA 4330, 123 Avenue Albert Thomas, 87060 Limoges, France

sylvie.rossignol@unilim.fr

Keywords: geopolymer, ammonium molybdate, heat treatment

Abstract. Geopolymers are inorganic materials obtained by the alkaline activation of aluminosilicate sources. The ammonium molybdate could be used as a complexant for silica in order to complex the siliceous species in the alkaline solution. According to this, the aim of this work is to control the siliceous species and to understand the role of ammonium molybdate as a complexing agent acting on the formation of the different networks. To do this, addition of ammonium molybdate (up to 0.32% molar) in the silicate solution were realized along the formulation of geopolymer using two metakaolins. The results highlight that the addition of ammonium molybdate in geopolymer results in a decrease of the shrinkage at high temperature. Moreover, X-ray diffraction data and SEM after calcination show that geopolymers without ammonium molybdate form two phases ($KAlSi_2O_6$ and $KAlSiO_4$) while with additions of molybdate, there were only the phase $KAlSi_2O_6$ associated with Al_2O_3 doped Mo and $K_2Mo_2O_7$. Finally, SEM observations show that additions of ammonium molybdate seem to favor crystallization. The results allow to evidence the role of molybdate in the control of the polycondensation reaction in order to influence the formation of specific network

Introduction

The "alkali silicates" is one of the raw materials classically used in the formulation of new materials like geopolymers [1]. Geopolymers are amorphous three-dimensional aluminosilicate binder materials which are synthesized at ambient temperature by the alkaline activation of silica solution and aluminosilicates derived from natural minerals, calcined clay or industrial by-products [2]. The preparation of these materials depends on two parameters which are the aluminosilicate source and the alkaline solution. Previous studies [3,4] on the aluminosilicate sources (metakaolins) evidenced the influence of the purity and the reactivity of the metakaolin on the geopolymer formation which can lead to the formation of one or several networks. The existence of these different networks depends on the metakaolin used and on the silicate species available. To identify these various networks, thermal treatments were investigated and the results evidenced the formation of crystallized compounds identified as leucite ($KAlSi_2O_6$) and kalsilite ($KAlSiO_4$) [5,6]. It has been shown differences between metakaolins used (Mk1 and Mk2). Indeed, a consolidated material with a single network-type geopolymer is effective for a metakaolin Mk1 whereas there is coexistence of two systems, one rich in silicon atoms and potassium, the other rich in silicon atoms and aluminum for Mk2 metakaolin. The various networks based essentially on silicate compounds, the siliceous or silicate species must be controlled in order to influence the formation of specific network.

Some studies have shown that it was possible to obtain numerous siliceous species with ammonium molybdate ($(NH_4)_2Mo_2O_7$) to create silicomolybdic entities [7]. Victor et al. [8] has evidenced the formation of α and β molybdosilicic acid and notably their existence in acidic middle. Another study by Sarrazin et al. has investigated the interaction of heptamolydate with alumina and silica by ^{95}Mo NMR measurements [9]. It was evidenced that alumina can react with

silicomolybdic acid to change the isoelectric point while the silica react with the molybdenum compounds forming various species. The interaction of the oxomolybdenum species with alumina was irreversible whereas on silica these species remain labile. To complete these interactions, the size of some colloidal components in solutions of alkali silicates was determined [10] depending on the pKa of $H_3SiO_4^-$. The various interactions in presence of silicate middle or aluminosilicate were followed by the infrared absorption spectroscopy of molybdate method [11]. The main results indicated that different time involves formation of structural units. Moreover, these molybdate based compounds are able to favor the crystallization in silicate glasses [12]. In these compounds, the molybdenum atoms are four fold environment and the oxygen atoms cannot bridge with silicon polyhedron. Indeed, the molybdenum atoms are located in area rich on alkaline or earth alkaline. Consequently, the silica network contains less alkaline cations and more bridging oxygen atoms. Another works have mentioned the formation of $K_2Mo_2O_7$ at 460 °C during thermal treatment [13].

The ammonium molybdate could be used as a complexant for silica in order to complex the siliceous species in the alkaline solution. Consequently, the aim of the study is to control the siliceous species in the solution and to understand the role of a silicate species as a complexing agent on the formation of the different networks in temperature. This study focuses on the thermal behavior of geopolymers using two aluminosilicate species in presence of various amounts of ammonium molybdate.

Experimental

Sample preparation. Samples were synthesized using an alkaline silicate solution and two metakaolins (namely Mk1 and Mk2 already used in precedent studies) from Imerys supplier. The alkaline silicate solution was obtained by the dissolution of KOH pellets (85.2% purity) and amorphous silica (99.9% purity) in water at room temperature as described in previous work [1]. Syntheses were performed by mixing the alkaline silicate solution and metakaolins. The samples were named M1 and M2. Other samples were realized with addition of 0.02 to 0.32% molar of ammonium molybdate anhydrous (56.5% purity) to the alkaline solution before metakaolin addition. These samples were named Mx-y, where x corresponds to the metakaolin and y to the amount of ammonium molybdate. For example, a geopolymer made with the metakaolin Mk2 and 0.02% molar of ammonium molybdate is named M2-0.02.

Sample characterization.

Dilatometric measures were made under air, by means of a contact vertical dilatometer (TMA Setsys Evolution Setaram), on bulk samples with a cylindrical geometry (H = 7 mm; Ø = 6.5 mm). Two platinum holders were placed at the surface end contacts of the samples to avoid high-temperature diffusion between the sample and the alumina holders. A calibration cycle (without the sample) was performed and registered. The calibration data were then subtracted from the data collected for each sample to eliminate the contribution of the device. The thermal cycle used consisted of heating from 30 to 1400 °C and cooling from 1400 to 30 °C, each at 5 °C/min. X-ray patterns were collected from powder samples after crushing to 63 µm in size and were obtained using a Brücker D8 apparatus and a graphite-backed monochromator from 5 to 80° (2θ). The device was equipped with a cobalt anode (λ = 1.79026 Å). The XRD patterns were obtained using a dwell time of 0.5 s and a step size of 0.01° (2θ). The crystalline phases were identified by comparing the patterns with powder diffraction file (PDF) standards from the International Center for Diffraction Data (ICDD). The morphologies of final products were determined using a Cambridge Stereoscan S260 scanning electron microscope (SEM). A carbon layer was deposited on the samples prior to their analysis.

Results

To study the influence of ammonium molybdate addition in a geopolymer formulation during thermal treatment, samples containing various amounts of ammonium molybdate were characterized by dilatometric, X-Ray diffraction analysis and by scanning electron microscope observations.

Dilatometric investigations were carried out between 30 and 1400 °C on the geopolymers M1 and M2 with various amounts of ammonium molybdate (Fig. 1a, b). The geopolymer M1 displays a first dimensional variation of 5% between 30 and 200 °C also observed by thermal analysis due to water contents in the porous network [14]. Subsequently, between 300 and 800 °C, there is a low shrinkage caused by the structural reorganization due to surface hydroxyl groups. From a temperature of 940 °C, shrinkage (about 15%) due to the occurrence of a viscous flow rich in silica modified by alkali metal cations or aluminates is noted. In effect, in this composition, two network types were evidenced in which the aluminum atoms participate with the silicon as network formers (aluminum-rich) and in which the aluminum atoms play the role of compensators in a network rich in silicon. The total shrinkage of the sample is about 20%. After the temperature of 940 °C, the addition of ammonium molybdate resulted in a decreased value of the shrinkage. The dimensional variation between 30 and 200 °C is still observed. Indeed, the sample M1-0.08 has a total shrinkage of 10% while it is 4.5% for M1-geopolymer-0.32. The dilatometric curve of the sample shows the same profile M2 as M1 with a near 20% shrinkage. However, the decrease observed at 950 °C of the viscous flow is followed by two steps of viscous flow at 1000 and 1120 °C, respectively, due to impurities in the used metakaolin. The addition of ammonium molybdate induces the same behavior for the sample based on metakaolin Mk1, but the shrinkage values are different. In effect, the removal of samples M2-0.08 and M2-0.32 are respectively equal to 7.5 and 6%.

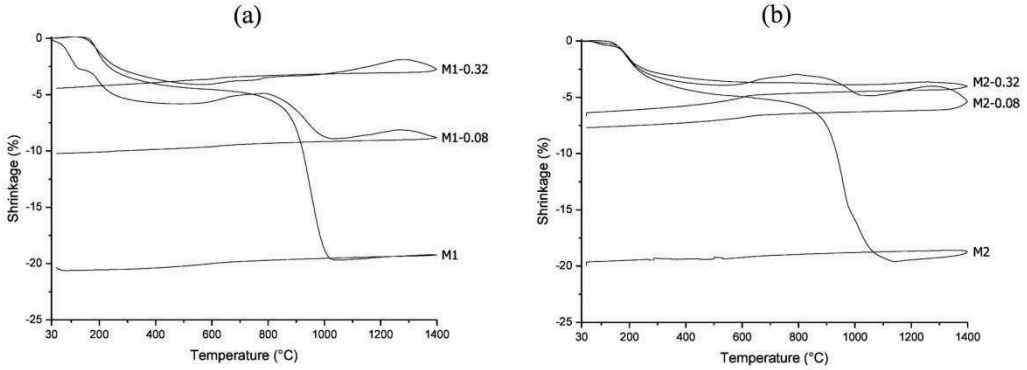

Fig. 1 : Shrinkage as a function of the temperature for (a) M1 and (b) M2 the geopolymers with various amounts of ammonium molybdate.

For sample M1, the dimensional change occurring at 940 °C could be explained by different networks rich in aluminum and silicon atoms [5] which give rise to a continuous viscous flow in accordance with the temperatures recorded by thermal analysis [5]. For the geopolymer M1-0.08, corresponding to the removal of water loss is divided into two parts which may correspond to the discharge of the water present in the pore network of the two materials. The second dimensional change, corresponding to the onset of viscous flow occurs at a temperature near 940 °C. This shrinkage less than that of M1 can also be explained by the appearance of a viscous flow. Since the shrinkage value is lower than in the M1 sample can be explain by the presence of some crystallized phases [12]. The weak variations detectable between 700 and 1250 °C can be also link to the apparition of some crystallized phases. The M1-0.32 sample shows very low variations of shrinkage from 300 °C in relation with the formation of a large amount of crystallized phases. The geopolymer M2 is characterized by the presence of three viscous flow steps at 950, 1000 and 1120 °C. The rapid decrease observed for the sample M2 is characteristic of the occurrence of a viscous

flow of the geopolymer phase. At 1000 °C, the decomposition of clay rich phases increases the amount of viscous flow delaying the apparition of temperature leading to a slowdown. At higher temperature, the same phenomenon is observed due to the fusion of part of the quartz present in the metakaolin [3]. The M2-0.08 geopolymer is characterized by a rapid decrease and a slowdown. The first corresponds to the appearance of a viscous flow within the geopolymer phase and the second corresponds to the formation of crystalline phases at higher temperatures which may be confirmed. Finally, the sample M2-0.32 has very small variations in shrinkage beyond 300 °C as the M1 compound.

The shrinkage values (Fig. 2) show that the addition of ammonium molybdate has an influence in function of the metakaolin used.

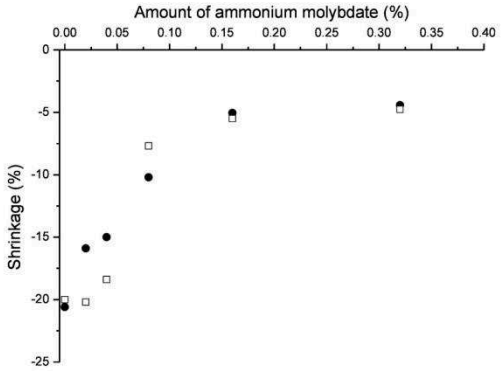

Fig. 2 : Shrinkage as a function of the amount of ammonium molybdate for the geopolymers (●) M1 and (□) M2 treated at 1400 °C.

Indeed, irrespective of the metakaolin, the same values are achieved for withdrawal rates molybdate above 0.16% while for the lower rate there are differences. Uploading molybdate in the reaction mixture M1 based on metakaolin leads to a very rapidly decreased shrinkage value whereas in the presence of metakaolin M2, the effect seems to be delayed. For the geopolymer M1, because of the availability of various aluminosilicate species within the reaction mixture, adding ammonium molybdate reacts very quickly. Indeed, there is formation of two networks, a network where the aluminum atoms are network starting and a network where the atoms of aluminum and potassium are modifiers. The formation of these two metastable networks always in challenge implies a metastable mixture in which molybdic species can react very quickly and consequently cause a decrease in the value of the shrinkage very quickly. In the case of the M2 compound, the addition of ammonium molybdate has no time to react with the siliceous or potassium species since currently there is the formation of nuclei giving rise rapidly to the geopolymer phase. In this case, the kinetics of formation of the geopolymer network, namely the formation of aluminosilicate species prevails over the possible interaction between silicomolybdic species. However, from 0.08% additions, there will be the preferential formation of silicomolybdic complex which, by steric hindrance or the formation of crystalline compounds [15,16,17] will inhibit the formation of stable geopolymer nuclei. Therefore, there will be the formation of phases that homogeneously crystallize. From a higher content (> 0.16%) of ammonium molybdate, both reaction mixtures react in the same way by the formation of different phases making the environment conducive to crystallization without the formation of viscous flow. These various interactions between species in solutions will induce different shrinkage values that are to be connected to the presence of crystalline phases. It appears that the addition of molybdate promotes the formation of crystalline phases limiting the formation of viscous flows [13].

To identify these phases, the diffractograms of each sample M1, M1-0.32, M2 and M2-0.32 were realized after calcination at 1400 °C (Fig. 3). According to XRD patterns, the geopolymers M1 and M2 present two crystalline phases, a major phase matching as leucite ($KAlSi_2O_6$) and a minor phase of kalsilite ($KAlSiO_4$). These two phases were already identified in previous work [5].

The existence of these two phases can be explained by local composition heterogeneity (variation of the Si/Al ratio) within the material obtained at room temperature. For the M1-0.32 and M2-0.32 samples, whatever the initial mixture, the XRD patterns highlight leucite phases with two others phases relative to the addition of molybdate: a small amount of potassium bimolybdate ($K_2Mo_2O_7$) and a Mo-doped corundum phases. Then these phases can be related to the presence of some Al-rich cluster before crystallization in accordance to the presence of various networks.

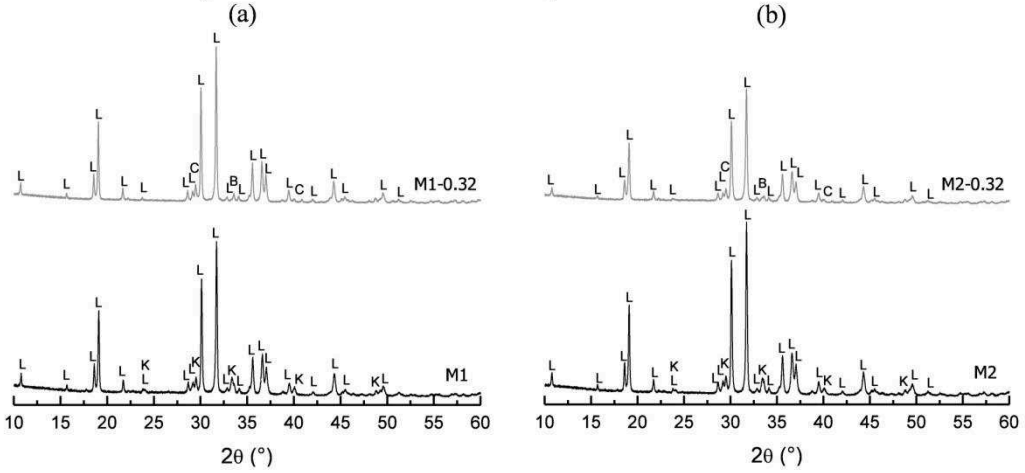

Fig. 3: X-rays patterns of calcined geopolymers (a) M1 and (b) M2, (—) without and (—) with 0.32% of ammonium molybdate. (PDF files: L: Leucite (04-013-2785), K: Kalsilite (04-015-8504), C: Corundum Mo-doped (01-075-0782), B: Potassium bimolybdate (00-036-0347)).

SEM pictures were made on samples M1, M1-0.32, M2 and M2-0.32 calcined at 1400 °C (Fig. 4). Two types of morphologies are observed. The M1 and M2 samples display geopolymer matrix containing crystallites as evidenced in previous work [3]. However, many heterogeneous crystallites are observed in M1-0.32 sample while in geopolymer M2-0.32 a homogeneous crystallization can be noted. In the case of the geopolymer M1, the sample based on two networks can lead to the formation of several phases in temperature and the addition of ammonium molybdate promotes the crystallization. The M2 based compounds containing a single geopolymeric network display a homogeneous crystallization [5].

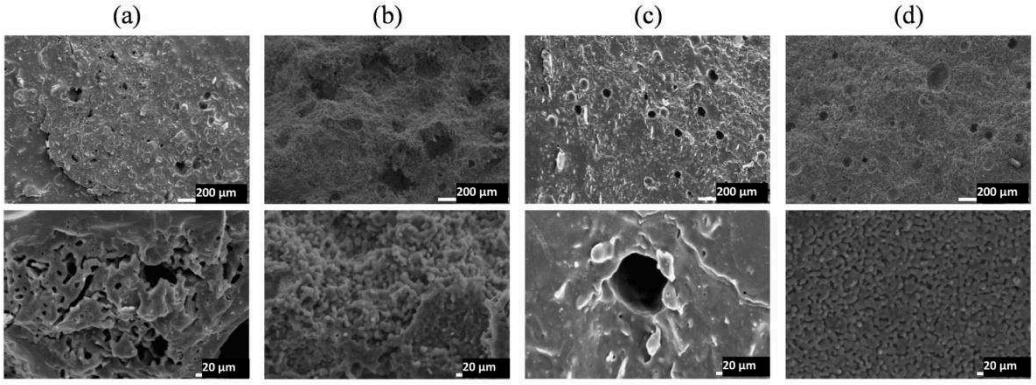

Fig. 4: SEM micrographs of geopolymers (a) M1, (b) M1-0.32, (c) M2 and (d) M2-0.32 calcined at 1400 °C.

Conclusion

This study has highlighted the role of molybdate in the geopolymer polycondensation process. The results show that the addition of ammonium molybdate in geopolymer results in a decrease of the shrinkage. It is possible to obtain at high-temperature materials with no shrinkage. Moreover, analyzes by X-ray diffraction have shown that materials containing ammonium molybdate additions lead to different compounds of those without addition. Thus, without ammonium molybdate geopolymers form two phases ($KAlSi_2O_6$ and $KAlSiO_4$) while with additions they form three compounds ($KAlSi_2O_6$, Al_2O_3 doped Mo and $K_2Mo_2O_7$). Finally, SEM observations show that additions of ammonium molybdate seem to favor crystallization.

References

[1] A. Autef, E. Joussein, G. Gasgnier, S. Rossignol, Role of the silica source on the geopolymerization rate, J. of Non-Crystalline Solids, 358 (21) (2012) 2886-2893.
[2] J. Davidovits, Geopolymer: Chemistry and Applications, second ed., Institut géopolymère, St-Quentin, 2008.
[3] A. Autef, Formulation géopolymère : influence des rapports molaires Si/K et Si/Al sur les réactions de polycondensation au sein de gels aluminosilicatés, PhD thesis, Université de Limoges, 2013.
[4] E. Prud'homme, P. Michaud, E. Joussein, A. Smith, C. Peyratout, I. Sobrados, J. Sanz, S. Rossignol, Geomaterial foams: Role assignment of raw materials in the network formation, J. of Sol-Gel Science and Technology, 61 (2) (2012) 436-448.
[5] A. Autef, E. Joussein, A. Poulesquen, G. Gasgnier, S. Pronier, I. Sobrados, J. Sanz, S. Rossignol, Influence of metakaolin purities on potassium geopolymer formulation: the existence of several networks, J. of Colloïd and Interface Science, 408 (1) (2013) 43-53.
[6] P. He, D. Jia, M. Wang, Y. Zhou, Thermal evolution and crystallization kinetics of potassium-based geopolymer, Ceramics International, 37 (1) (2011) 59.63.
[7] F. Parmentier, Sur les silicomolybdates, Annales scientifiques de l'E.N.S., 2ème série, 11 (1882) 187-218.
[8] V.W. Truesdale, C.J. Smith, The formation of molybdosilicic acids from mixed solutions of molybdate and silicate, The Analyst, 100 (1975) 203-212.
[9] P. Sarrazin, B. Mouchel, S. Kasztelan, 95Mo NMR study of the interaction of heptamolybdate solutions with alumina and silica, J. Phys. Chem, 93 (1989) 904-908.
[10] J-E.A. Otterstedt, M. Ghuzel, J.P. Sterte, Colloidal components in solutions of alkali silicates, J. of Colloid and Interface Science, 115 (1) (1987) 95-103.
[11] C.H. Rüscher, E. Mielcarek, Weakening of alkali-activated metakaolin during aging investigated by the molybdate method and infrared absorption spectroscopy, J. of the American Ceramic Society, 93 (9) (2010) 2585-2590.
[12] C. Cousi, F. Bart, J. Phalippou, Phase separation and crystallization induced by adding molybdenum and phosphorus to a soda-lime-silica glass, Glass Technology, 45 (2) (2004) 65-67.
[13] G-Q. Zhang, J. Guo, L. He, D. Zhou, H. Wang, J. Koruza, M. Kosec, Preparation and microwave dielectric properties of ultra-low temperature sintering ceramics in K_2O-MoO_3 binary system, J. of the American Ceramic Society, 97 (1) (2014) 241-245.
[14] J.L. Provis, R.M. Harrex, S.A. Bernal, P. Duxson, J.S.J. Deventer, Dilatometry of geopolymers as a means of selecting desirable fly ash sources, J. of Non-Crystalline Solids, 358 (16) (2012) 1930-1937.
[15] T. Coradin, D. Eglin, J. Livage, The silicomolybdic acid spectrophotometric method and its application to silicate/biopolymer interaction studies, Spectroscopy, 18 (4) (2004) 567-576.
[16] J. Dou, H.C. Zeng, Targeted synthesis of silicomolybdic acid (Keggin acid) inside mesoporous silica hollow spheres for Friedel-Crafts Alkylation, J. of the American Chemical Society, 134 (39) (2012) 16235-16246.
[17] L. Bi, E. Wang, R. Huang, Synthesis, properties and crystal structure of a novel organic-inorganic salt of 12-silicomolybdate, $(C_2H_5NO_2)_{3.5}H_4SiMo_{12}O_{40}\cdot 8.5H_2O$, J. of Molecular Structure, 569 (1-3) (2001) 81-88.

Acte de congrès 3 (ACLN 3)

N. Essaidi, L. Vidal, F. Gouny, E. Joussein, S. Rossignol

"Recycled geopolymer on new formulations"

Ceramic Engineering and Science Proceedings, 2016, vol. 36 (8), p. 49-60.

RECYCLED GEOPOLYMER ON NEW FORMULATIONS

N. Essaidi[1], L. Vidal[1], F.Gouny[1], E. Joussein[2] and S. Rossignol[1]

[1] Science des Procédés Céramiques et de Traitements de Surface (SPCTS) UMR 7315 CNRS, Ecole Nationale Supérieure de Céramique Industrielle, 12 rue Atlantis, 87068 Limoges Cedex, France.
[2] Université de Limoges, GRESE EA 4330, 123 avenue Albert Thomas, 87060 Limoges, France.

Abstract

Recycling is of significant importance because it counteracts the increase of waste in industrial processes and it provides other environmental advantages. Geopolymer compounds based on various precursors, such as aluminosilicate or silicate solutions, are potential candidates for study in this field. In this work, the effect of source materials on the microstructure and mechanical properties of geopolymers was studied by comparing various formulations based on the addition or substitution of metakaolin and geopolymer waste. The compressive test was conducted to assess the compounds' mechanical properties, while FTIR and scanning electron microscopy were employed to examine the geopolymerization reactions, the composition and the microstructure of the final products. The compressive test evidenced the decrease of the performance of the synthetized materials. It was observed that both the addition and the substitution decrease the reactivity and kinetics of the geopolymerization process. The difference in strength and microstructure between the synthetized compounds is attributed to the different reactivities of the source materials and the percentage of the nonreactive fillers.

Geopolymer crushed	Mechanical properties	Rate of substitution
FTIR spectroscopy	SEM	Formulation

I. Introduction

Environmental pollution and a lack of resources have been identified as global problems. Therefore, environmentally friendly products are essential and primordial. Geopolymers represent a class of synthetic silico-alumina based materials to be potentially used in several industrial areas. Many materials composed of silica and alumina can be used to synthetize geopolymers. Indeed, many investigations have used metakaolin, kaolinitic-illitique clays [1], fly ashes and blast furnace slag as raw materials [2]. Among these materials, metakaolin [3] has been used extensively because of its higher reactivity. Despite the fact that metakaolin activated by an alkaline solution [4,5] was able to promote high mechanical strength, its high price motivates the search for other ways to synthetize geopolymers. He et al [6] compared two types of geopolymers obtained from metakaolin: a non-waste material and the mixture of two types of waste (red mud and fly ash). They found that both geopolymers contain a significant amount of unreacted phases as inactive fillers. The difference in strength and microstructure of the formed geopolymers is attributed to the different reactivity of the source materials. The final products contain a gel–like geopolymer binder as the major matrix but also a small amount of unreacted source materials.

Recycled wastes used as secondary raw materials are becoming progressively more important. Using industrial by-products or wastes (fly ash [7], red mud and furnace slag) for geopolymer synthesis is another advantage of geopolymer technology because of the significantly reduced costs and the additional environmental benefits, which lead to greener manufacturing and global sustainable development. Recent investigations using recycling aggregates produced in the laboratory indicate that the use of fine recycled aggregates must

not exceed 30%, otherwise the performance of the products could be at risk [8]. Current recycled aggregates have particles of impurities, such as soil, plastics, wastepaper wood, metals and organic matter. Organic matter leads to lower mechanical performance and lower concrete durability. Park et al. [9] studied concrete containing metal impurities and found that aluminum caused performance degradation even with very low contents of less than 0.1%. Cradle to cradle is part of an environmental approach that integrates the requirements of zero pollution and 100% recycling [10]. In this context, it is interesting to reinvest a crushed geopolymer into a geopolymer formulation to test the possibility of recycling these new types of materials. To examine the possibility of reuse, the aluminosilicate must be investigated by all the analysis reported by Autef et al [11,12].

The aim of this paper is to study the effect of raw materials on the microstructure and mechanical properties of final products by comparing various formulations based on the addition or substitution of metakaolin and geopolymer waste.

II. Experimental Part

1. Raw materials and sample preparation

The consolidated materials were prepared by mixing the metakaolin (The MK is the M-1000 metakaolin supplied by AGS France, containing 55wt% of SiO_2 and 40 wt% of Al_2O_3) and the geopolymer, which was crushed and sieved at 80 µm in an alkaline solution (Si/K=0.47), as described in Figure 1. The reactive mixtures were placed in open polystyrene molds at room temperature. Samples were synthetized either by adding the geopolymer waste to metakaolin or substituting an amount of metakaolin by geopolymer waste. The synthesis of geopolymer waste was accomplish by dissolving of KOH in the SiK solution, then added MK. After stirring for 5 min at 700 rpm, a sealable polystyrene mold was used to shape the mixture, which was conserved at 25 °C during 7 days. The different ratios of the composition are Si/Al=1.41, Si/K=3.09, $Si/K_{solution}$=0.47, its value of compressive strength is 76 MPa±0.2.

The obtained materials are denoted as G^x or $G^{SX,}$ where x refers to the percentage of crushed geopolymer added and SX to the percentage of crushed geopolymer that substitutes an amount of metakaolin. For example, G^{S20} refers to the geopolymer obtained from the substitution of 20% of 12 g of metakaolin mass by geopolymer waste. Various samples were synthesized either by addition or substitution but only four compositions (G^0, G^{20}, G^{S20} and G^{S40}) are characterized. The nomenclature and the composition of the samples only studied and analyzed are presented in the Table 1.

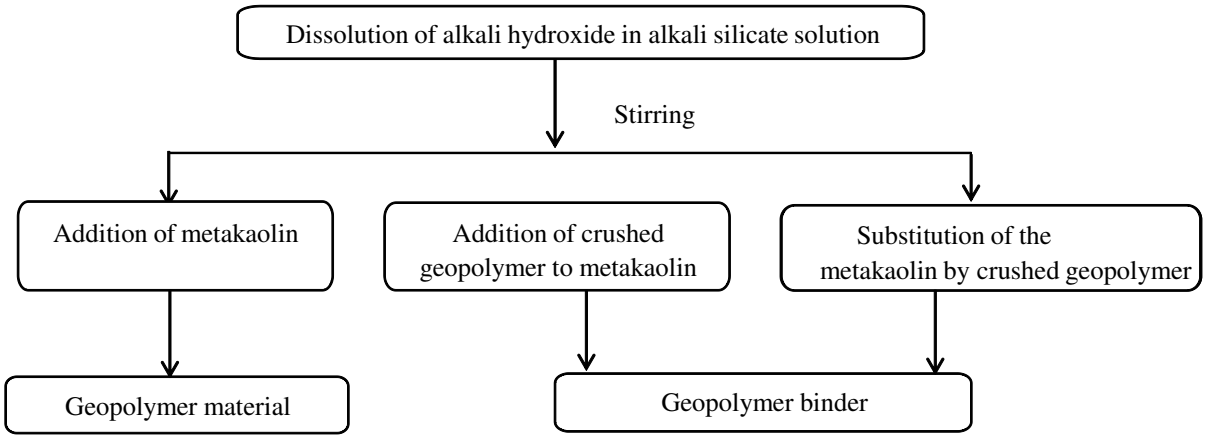

Figure 1. Synthesis protocol of geo-materials

Table 1. Nomenclature and compositions of different synthesized mixtures

Nomenclature	Metakaolin(g)	% laboratory waste	$Si/Al_{mixture}$	$Si/K_{mixture}$
G^0	20	0	1.41	3.09
G^{20}		20		
G^{S20}	16	20	1.45	2.63
G^{S40}	12	40	1.51	2.25

2. Technical characterization

Fourier-transform infrared (FTIR) spectroscopy in ATR mode was used to investigate the structural evolution of the geopolymer mixtures. The FTIR spectra were obtained using a ThermoFisher Scientific Nicolet 380 infrared spectrometer. The IR spectra were obtained over a range of 400 to 4000 cm^{-1} with a resolution of 4 cm^{-1}. The atmospheric CO_2 contribution was removed with a straight line between 2400 and 2280 cm^{-1}. To monitor the geopolymer formation, a programmed routine was used to acquire a spectrum (64 scans) every 10 minutes for 250 minutes. For comparison, the spectra were baseline-corrected and normalized [13].

Infrared spectroscopy is currently used to study the synthesis of geopolymer and their structural changes over time. Consolidation during the formation of a geopolymer is characterized by variation in the position of the Si-O-Si bond vibration band [14,15]. Geopolymerisation is characterized by a shift in the Si-O-Si vibration band to lower wavenumber, which is related to the weakening of the covalent bond due to the dissolution reaction of silicate species. This dissolution reaction promotes the formation of Q^2 units via the depolymerization of Q^4 and Q^3 units.

The compressive strengths were tested using a LLOYD EZ20 universal testing machine with a crosshead speed of 0.1 mm/min. The compressive tests were done on five samples for every composition. The samples were cylindrical in shape with a diameter (Φ) of 15 mm and a height (h) of approximately 30 mm. Additionally, the samples were aged for 7 days in an open mold at room temperature. The compressive strength values, expressed in MPa, represent the average of the five tested samples.

Dilatometric measures were made under air by means of a contact vertical dilatometer (TMA Setsys Evolution Setaram) on bulk samples with a cylindrical geometry (H = 7 mm; Ø = 6.5 mm). Two platinum holders were placed at the surface end contacts of the samples to avoid high-temperature diffusion between the samples and the alumina holders. A calibration cycle (without the sample) was performed and recorded. The calibration data were then subtracted from the data collected for each sample to eliminate artifacts from the device. The thermal cycle used consisted of heating from 30 to 1400 °C and cooling from 1400 to 30 °C, both at a rate of 5 °C/min.

III. Results and Discussion

1. Feasibility of materials

Samples were synthetized either by adding the geopolymer waste to metakaolin or substituting an amount of metakaolin by geopolymer waste. The first preliminary tests were done with the two aluminosilicate sources listed in Table 2. The main differences between the two sources reside in their natural pH and their size distribution, making the metakaolin exhibit more reactivity than the geopolymer waste. Another point of difference is the Si/Al ratio, which could modify the final composition if all the geopolymer waste is reactive in the presence of the alkaline solution.

Table 2. Chemical composition of the geopolymer waste

	Si/Al	Wettability (µl/g)	Natural pH value	Structural data	D_{50} (µm)
Geopolymer waste	1.41	744	10.83	amorphous	7
Metakaolin	1.17	758	7.93	amorphous	10

All the synthetized samples were mapped on the Al-Si-K/O ternary diagram as shown in Figure 2. In the case of the addition of geopolymer waste (G^{10}, G^{20} and G^{30}) to the mixture, the limit of the waste content is 30%. Above this limit, it is not possible to obtain a homogenous mixture without adding water. In the case of the substitution of metakaolin by geopolymer waste (G^{S10}, G^{S15}, G^{S20}, G^{S25}, G^{S30}, G^{S35}, G^{S40}, G^{S45} and G^{S50}), it is possible to substitute up to 50%. Beyond 50%, there is not enough metakaolin to ensure the consolidation of the product; the mixture stays in the liquid state and does not lead to a consolidated material. As was recently established [16], different types of materials can emerge depending on the molar composition of the reactive mixture (%Si, %Al and %K). Thus, four possible zones were identified for the obtained materials: geopolymers, gel materials, sedimented materials and hardening materials. All the samples (G^0, G^{10}, G^{20}, G^{30}, G^{S10}, G^{S15}, G^{S20}, G^{S25}, $G^{S30,}$ G^{S35}, G^{S40}, G^{S45} and G^{S50}) were expected to be located in the geopolymer zone. Indeed, the final products exhibited a consolidated and homogenous form without any shrinkage (photos of samples justified their aspects (ϕ=3 cm)).

Only four compositions (G^0, G^{20}, G^{S20} and G^{S40}) are characterized and presented in this study.

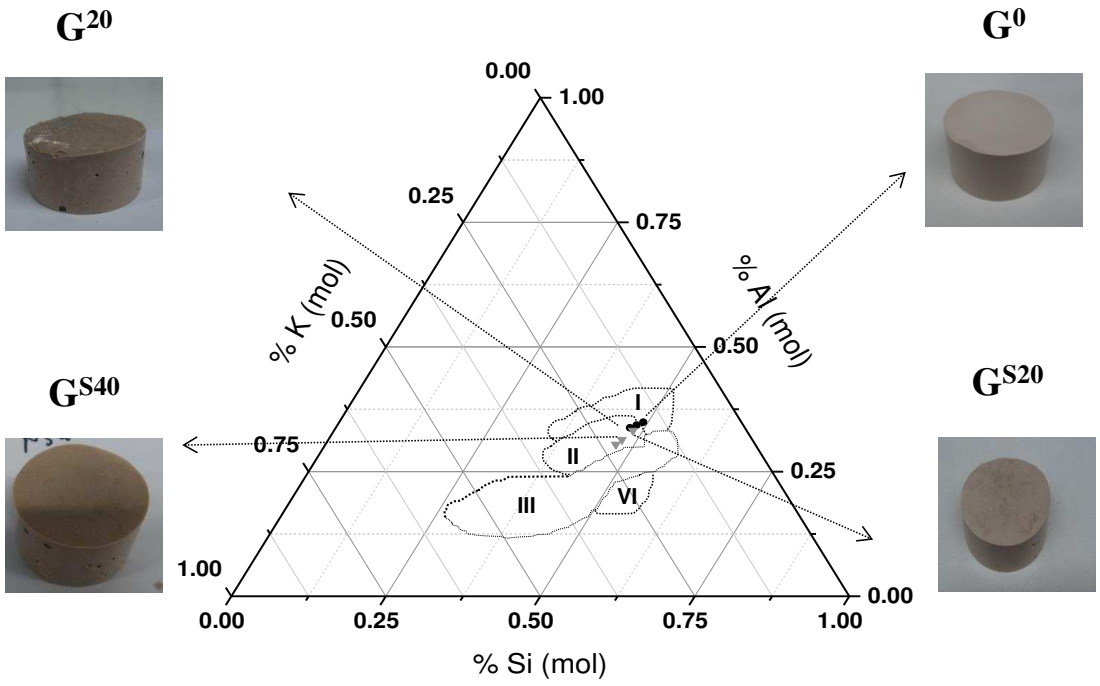

Figure 2. Position of the different compositions (■) G^X and (▼) G^{SX} on the Si-Al-K/O ternary diagram. (I) hardening material, (II) geopolymer, and (III) sedimented material and (VI) gel. Gao et al [16].

2. Following the synthesis of materials by FTIR

To understand the consolidation of materials due to the polycondensation reaction, the evolution of various mixtures were followed using FTIR in ATR mode. For different consolidation reactions, the displacement of the Si-O-M band reflects the formation of bonds characteristic of a specific type of network [17,18]. Figure 3 presents the displacement of the

Si-O-M band versus time for the synthetized compositions. The initial peak is similar for all the samples (G^0, G^{20}, G^{S20} and G^{S40}) at approximately 975 cm^{-1}.

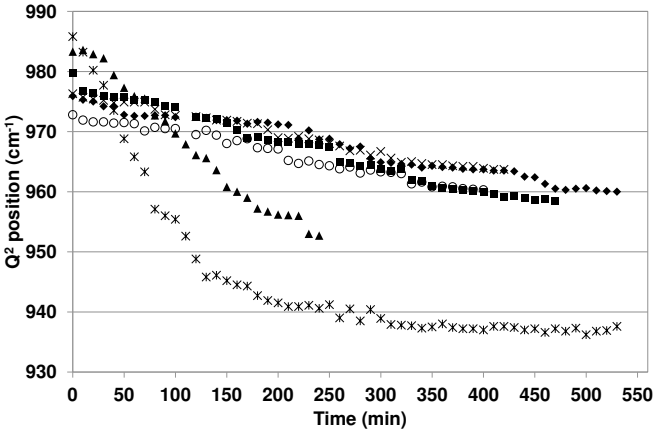

Figure 3. Q^2 position versus time for (■) G^0, (×) G^{20}, (△) G^{S20} and (○) G^{S40} as well as (∗) E^0 and (▲) E^{20}. Essaidi et al. [19]

The displacement of the reference composition G^0 is 21 cm^{-1}. For the others samples (G^{20}, G^{S20}, G^{S40}), the displacements values are 13, 16 and 12 cm^{-1}, respectively. Globally, the samples display the same behavior. The smaller displacement may be explained by either (i) the absent or weak occurrence of the polycondensation reaction or (ii) the unavailability of water in the silicate solution to wet and coat all the grains of the metakaolin, which inhibits the polycondensation reaction. However, the fact that the samples lie in the geopolymer zone means that there is a geopolymerization reaction. The data show that the slope values are -0.042, -0.032, -0.030, and -0.033 cm^{-1}/min for G^0, G^{20}, G^{S20} and G^{S40}, respectively. The waste addition could affect the kinetics of the reaction. In fact, the decrease of the slope value [7] suggests the decrease of the polycondensation reaction rate due to the disturbance caused by the presence of inactive species from the laboratory wastes. It seems that the sample G^{S40} displays another behavior in terms of reactivity, which is discussed later in the paper.

To understand this phenomenon, two samples prepared in the laboratory [18] with the same criteria were added to the study (E^0 and E^{20}). However, the amount of metakaolin introduced is lower. The relative displacements of E^0 and E^{20} were 45 and 30 cm^{-1} [18], respectively. In this case, the addition of waste involves a decrease in the shift, which underlines the low reactivity. The laboratory waste addition may lead to a geopolymer network associated with unreacted waste coated by the alkaline solution. The presence of non-reactive species provided by the aluminosilicate laboratory waste would disrupt the exchange between reactive aluminous and siliceous species.

The difference in the polycondensation reactions depends on the availability of species in the solution that will be able to interact. In the presence of a high content (G^0) of metakaolin, the silicate solution will be enriched with aluminosilicate species, which are able to participate in polycondensation reactions while the entire metakaolin has not reacted. In contrast, a low content of metakaolin will liberate those species that will interact with the alkaline solution and thus form different types of networks. The high content of metakaolin will certainly lead to differences in composition within the networks formed in the geopolymer formulation, as demonstrated by Autef et al [11]. Consequently, in the presence of a higher concentration of aluminosilicate source (G^{20}, G^{S20} and G^{S40}), the displacement does not reflect the existence of metakaolin. These data emphasize once again the role of the aluminosilicate source.

Regardless of the sample, it was observed that both the addition and the substitution decrease the reactivity and the kinetics of the geopolymerization process.

3. Evaluation of the mechanical properties and the microstructure of the obtained materials

The variation of the compressive strength values as a function of strain is presented in Figure 5. The obtained materials show a brittle failure. Sample G^0, considered the reference sample, exhibited the highest compressive strength value (76 MPa±0.2). The addition of 20% of geopolymer (G^{20}) waste decreases the compressive strength value (65 MPa±0.2). This behavior is in agreement with the literature [6, 11] because the aluminosilicate source, which is based on metakaolin and waste as filler, has been modified. For the compositions G^{S20} and G^{S40}, the compressive values are, respectively, 62 and 44 MPa±0.2, which reveal that the mechanical properties also decreased with the substitution of metakaolin by geopolymer waste. The similarity between the values of G^{20} and G^{S20} is related to the aluminosilicate source in the presence of the alkaline solution. Indeed, G^{20} behaves as a geopolymer containing reinforcements in which the reactivity of metakaolin is decreased in the presence of the alkaline solution. Meanwhile, the alkaline solution allows dissolution in G^{S20} and leads to further enhancement of the geopolymer even though the metakaolin content is lower.

It was concluded that a metakaolin based geopolymer exhibits much higher compressive strength and failure strain than a waste based geopolymer.

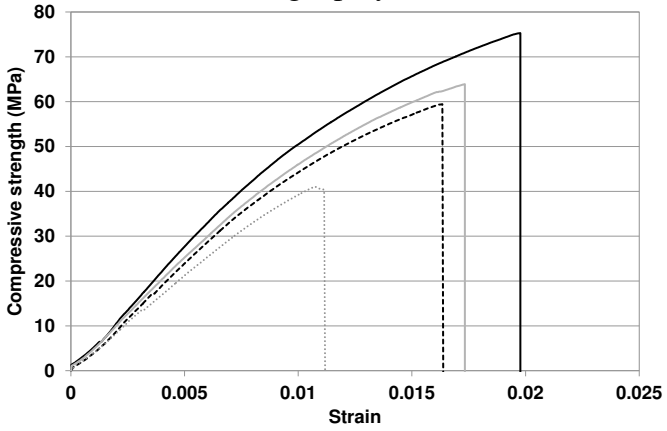

Figure 4. Variation of compressive strength versus strain for G^X reactive (–) G^0, (–) $G^{20,}$ (---) G^{S20} and (---) G^{S40} samples.

Representative Scanning Electron Microscope (SEM) images of the microstructure of different synthesized samples are shown in Figure 5. The morphological features of all these samples are characteristic of geopolymer materials [20]. However, the G^{20} and G^{S20} compositions showed the presence of a few micro-sized cracks, which can be explained by the effects of the compressive test. The G^{S40} composition has a heterogeneous microstructure, compared with the other samples, due to the high amount of waste. There is a difference between the microstructures obtained with the addition and substitution of crushed geopolymer.

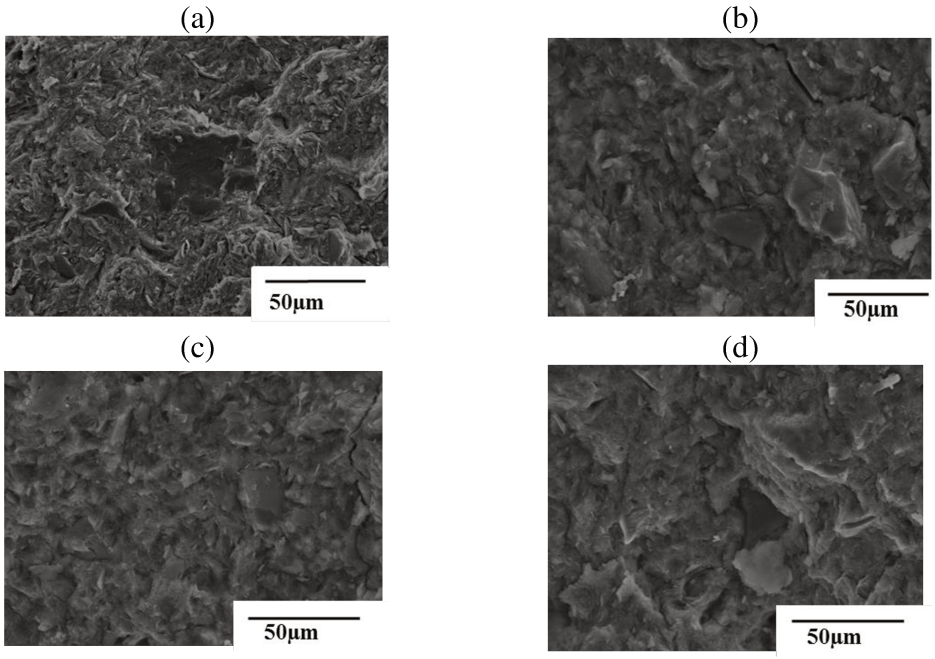

Figure 5. SEM micrographs of (a) G^0, (b) G^{20}, (c) G^{S20} and (d) G^{S40} samples.

The resulting XRD patterns (Figure 6) display a broad peak characteristic of an amorphous material and peaks relative to crystalline phases such as quartz, muscovite and anatase. The shift of the amorphous dome position ($2\theta \approx 30°$) indicates the dissolution of SiO_4 and AlO_4 tetrahedra in alkaline solution [13].

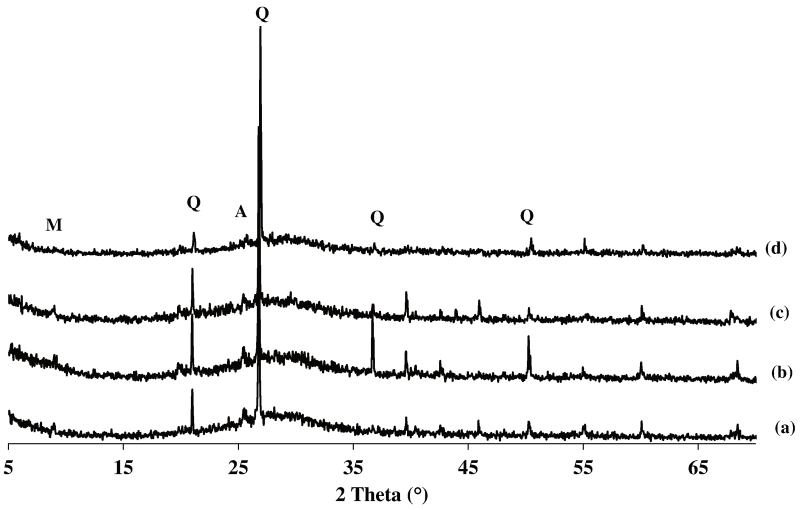

Figure 6. X-ray patterns of (a) G^0, (b) G^{20}, (c) G^{S20} and (d) G^{S40} samples (Q: quartz, A: anatase, M: muscovite)

4. Dilatometry analysis

Dilatometric investigations were carried out between 30 C and 1400 °C on the samples to highlight the local order of the structure. An example of a dilatometric curve for the composition G^0 is plotted in Figure 6 (A). The dilatometric curve obtained displays a total shrinkage of approximately 20%, and two phenomena are observed. The first one corresponds to a dimensional variation of approximately 5% between 30 and 200 °C [20], which could be associated with the loss of the water in the porous network [21]. A second dimensional variation of approximately 15% appears between 900 and 1000 °C, which could be attributed to a viscous sintering [21]. This behavior reflects the contributions corresponding to the two

networks identified by Autef et al. [22]. The first has been attributed to a relatively amorphous network in which the potassium and aluminum atoms lead to the formation of non-bridging oxygen atoms, whereas in the second network, aluminum atoms could play the role of network formers. Therefore, only the potassium atoms are responsible for the presence of non-bridging atoms. It is possible to determine the temperature of viscous flow appearance from the curves (Figure 7 (B)) of the first derivate of the linear shrinkage as a function of temperature. The peak of the G^0 sample is broad and can be attributed to the contribution of the two networks, as described previously [11]. Addition (G^{20}) and substitution (G^{S20}) lead to a decrease in the temperature of viscous flow appearance as well as in the contribution of the various networks defined previously. However, a more substantial substitution (G^{S40}) increases the temperature of viscous flow appearance.

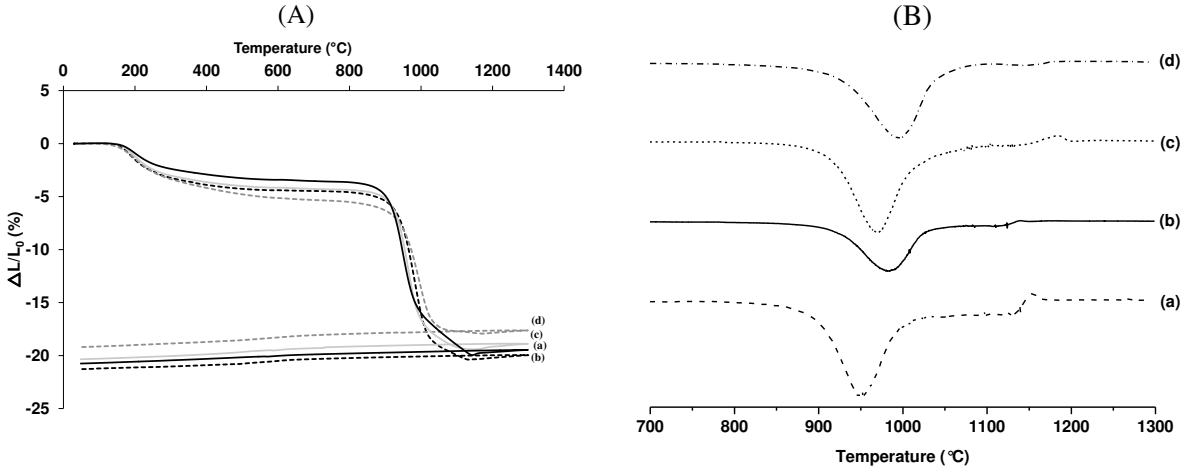

Figure 1. (A) dilatometric curves; (B) the first derivate of the linear shrinkage of (a) G^{20}, (b) G^0, (c) G^{S20} and (d) G^{S40}.

To better understand these phenomena, a correlation between the mechanical properties results and the raw materials reactivity was established. The compressive strength and the temperature deduced from dilatometric analyses, as a function of $Si_{ref}/(K_{tot}+Al_{ref})$, are presented in Figure 8. Si_{ref} and Al_{ref} represent the molarity of silicon and aluminum in metakaolin. K_{total} represents the total molarity of potassium from both the SiK alkaline solution and the geopolymer waste. The variations in compressive strength and viscous flow temperature with the ratio $Si_{ref}/ (K_{tot}+Al_{ref})$ show similar evolutions except in the case for G^{S40}. When geopolymer waste is added, it behaves as excess filler and leads to a decrease in the compressive strength value. In effect, the work of Autef et al. [22] has demonstrated that the addition cannot exceed 5% without affecting the mechanical properties. The substitution of metakaolin by geopolymer waste leads to a decrease in the compressive strength value due to a lower amount of metakaolin compared to the alkaline solution [5]. Moreover, for the G^{20} and G^{S20} samples, the temperature of viscous flow is lower than that of the reference material (G^0). This behavior emphasizes further the presence of the two sub-networks whose compositions evolve. It appears that when the degree of substitution increases, the silicon-rich network is enriched with the potassium released by the geopolymer waste, which induces the appearance of a viscous flow at a lower temperature, as in the case of glasses. Conversely, for the G^{S40} sample, a different phenomenon occurs due to the competition between the two networks previously evidenced by Autef et al [11]. The levels of the alkaline solution, being high relative to the metakaolin content, and the amount of aluminum atoms released by dissolution from metakaolin participate in the network more than potassium atoms, which has the effect of increasing the temperature of viscous flow. Moreover, a high content of

geopolymer waste also has the effect of increasing the temperature because the content of aluminum and silicon increases.

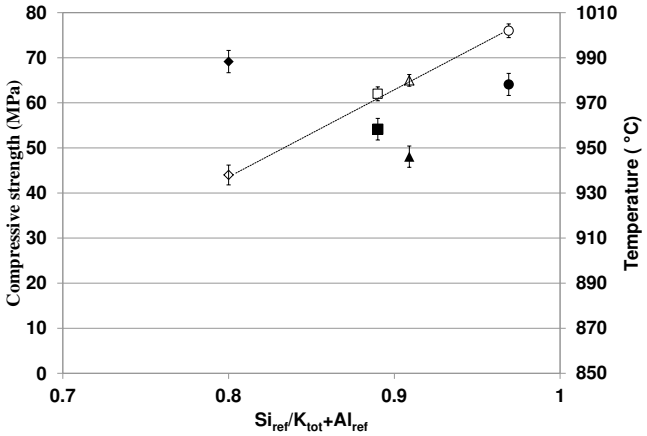

Figure 2. Evolution of Si $_{ref}$/K$_{tot}$+ Al $_{ref}$ versus the compressive strength for (○) G^0, (Δ) G^{20}, (□) G^{S20} and (◊) G^{S40} samples and (●) G^0, (▲) G^{20}, (■) G^{S20} and (♦) G^{S40} samples.

5. Conclusion

In this paper, the formulation involving the addition or substitution of crushed geopolymer with metakaolin is investigated. The results show that it is possible to synthetize geopolymer binders from recycled geopolymers within the geopolymer zone.

From FTIR analysis, it was observed that both the addition and substitution of geopolymer waste in the mixture decrease the reactivity during the geopolymerization process, emphasizing the role of the aluminosilicate source. From the results of compressive strength, both the addition and the substitution of metakaolin by the crushed geopolymer diminish the mechanical properties of the obtained materials. Nevertheless, it was demonstrated that substituting metakaolin with geopolymer waste by up to 20% or adding 20% of geopolymer waste lead to the same compound.

The relationship between the content of the source of aluminosilicate, composed of metakaolin and recycled geopolymer, and the alkaline solution is crucial to the formation of different networks within the final geopolymer.

6. References

[1] N. Essaidi, Formulation de liant aluminosilicaté de type géopolymère à base de différentes argiles Tunisiennes, PhD thesis, University of Limoges, 2013.

[2] F. Pacheco-Torgal, J.P. Castro-Gomes, S. Jalali, Alkali-activated binders: A review. Part 2. About Materials and binders manufacture, Construction and Building Materials, **22**, 1315-1322 (2008).

[3] J. Davidovits, Geopolymers – Inorganic polymeric new materials, Journal of Thermal Analysis, **37**, 1633-1656 (1991).

[4] A. Gharzouni, E. Joussein, B. Samet, S. Baklouti, S. Pronier, I. Sobrados, J. Sanz, S. Rossignol, The effect of an activation solution with siliceous species on the chemical reactivity and mechanical properties of geopolymers, Journal of Sol-Gel Science Technology, Article in press (2014).

[5] A. Gharzouni, E. Joussein, B. Samet, S. Baklouti, S. Rossignol, Effect of the reactivity of alkaline solution and metakaolin on geopolymer formation, Journal of Non-Crystalline Solids, **410**, 127-134 (2015).
[6] J. He, J. Zhang, Y. Yu, G. Zhang, The strength and microstructure of two geopolymers derived from metakaolin and red mud-fly ash admixture: a comparative study, Construction and Building Materials, **30**, 80-91 (2012).
[7] E. Prud'homme, Rôles du cation alcalin et des renforts minéraux et végétaux sur les mécanismes de formation de géopolymères poreux ou denses, PhD thesis, University of Limoges, 2011.
[8] L. Evangelista, J. de Brito, Mechanical behaviour of concrete made with fine recycled concrete aggregates, Cement and Concrete Composites, **29**, 397-401 (2007).
[9] W. Park, T. Noguchi, Influence of metal impurity on recycled aggregate concrete and inspection method for aluminum impurity, Construction and Building Materials, Article in press (2012).
[10] F. Pacheco-Torgal, Y. Ding, S. Miraldo, Z. Abdollahnejad, J. A. Labrincha, Are geopolymers more suitable than Portland cement to produce high volume recycled aggregates HPC, Construction and Building Materials, **36**, 1048-1052, 2012.
[11] A. Autef, Formulation géopolymère : influence des rapports molaires Si/K et Si/Al sur les réactions de polycondensation au sein de gels aluminosilicatés, PhD thesis, University of Limoges, 2013.
[12] A. Autef, E. Jousein, A. Poulesquen, G. Gasgnier, S. Pronier,I. Sobrados, J. Sanz, S. Rossigol, Influence of metakaolin purities on potassuim geopolymer formultaion: the existence of several networks, Journal of Colloid Interface Science, **408** (2013) 43-53.
[13] E. Prud'homme, P. Michaud, E. Joussein, J.M. Clacens, S. Rossignol, Role of alkaline cations and water content on geomaterial foams: Monitoring during formation, Journal of Non-Crystalline Solids, **357**, 1270-1278 (2011).
[14] Kouassi SS, Tohoue Tognonvi M, Soro J, Rossignol S, Consolidation mechanism of materials obtained from soduim silicate solution and silica –based aggregates. Journal of Non-Crystalline Solids, **358** (1):81-87 (2012)
[15] Tohoue Tognonvi M, Soro J, Rossignol S, Physical- chemistry of silica /alkaline silicate interactions during consolidation. Part1: Effect of cation size. Journal of of Non- Crystalline Solids **357** (15):3013-3012 (2011)
[16] X.X. Gao, A. Autef, E. Prud'homme, P. Michaud, E. Joussein, S. Rossignol, Synthesis of consolidated materials from alkaline solutions and metakaolin: Existence of domains in the Al-Si-K/O ternary diagram, Journal of Sol-Gel Science Technology, **65**, 220–229 (2013).
[17] C.A. Ress, J.L. Provis, G.C. Luckey, J.S.J. Van Deventer, Attenuated total reflectance fourier transform infrared analysis of fly ash geopolymer gel aging, Langmuir, **23**, 8170-8179 (2007).
[18] C.A. Ress, J.L. Provis, G.C. Luckey, J.S.J. Van Deventer, In situ ATR-FTIR study of the early stages of fly ash geopolymer gel formation, Langmuir, **23**, 9076-9082 (2007).
[19] Essaidi N., Gharzouni A., Vidal L., Gouny F., Joussein E., Rossignol S. Recycling of aluminosilicate waste: impact onto geopolymer formation. Eur. Phys. J., Accepted.

[20] P. Duxson, G.C. Lukey, J.S.J. Van Deventer, Thermal evolution of metakaolin geopolymers: Part 1 – Physical evolution, Journal of Non-Crystalline Solids, **352**, 5541-5555 (2006).
[21] P. He, D. Jia, M. Wang, Y. Zhou, Thermal evolution and crystallization kinetics of potassium-based geopolymer, Ceramics International, **37**, 59-63 (2011).
[22] A. Autef, E. Joussein, A. Poulesquen, G. Gasgnier, S. Pronier, I. Sobrados, J. Sanz, S. Rossignol, Influence of metakaolin purities on potassium geopolymer formulation: the existence of several networks, Journal of Colloïd and Interface Science, **408**, 43-53 (2013).

Chapitre

L. Vidal, A. Gharzouni, S. Rossignol

"Alkaline silicate solutions: An overview of their structure, reactivity, and applications"

Handbook of Sol-Gel Science and Technology, in press.

Alkaline Silicate Solutions: An Overview of their Structure, Reactivity, and Applications

L. Vidal, A. Gharzouni, and S. Rossignol

Contents

Abstract

Alkaline silicate solutions have many applications, including sand agglomeration and geopolymer production. To ensure the widespread use of these applications, it is necessary to identify the parameters controlling their reactivity and interactions with other materials, such as sand and metakaolin. It has been evidenced that the key parameters for solution reactivity are the Si/M molar ratio and the water contents. The most reactive alkaline solutions have alkali cation concentrations ranging from 4.5 to 9.5 mol/L. For the sand agglomeration application, it was shown that the used solutions are highly polymerized. In addition, the drying temperature and the method employed influence the silicate distribution in the final material. For geopolymer formation, it was evidenced that a highly reactive alkaline solution favors the formation of a geopolymer network by increasing the formation rate of $Al^{(IV)}$ up to 80 %, which improves the working properties of the final materials. Thus, knowledge of the key parameters controlling the alkaline

L. Vidal (✉) • A. Gharzouni
SPCTS, University of Limoges, Limoges, France
e-mail: laeticia.vidal@etu.unilim.fr; ameni.gharzouni@etu.unilim.fr

S. Rossignol
Ecole Nationale Superieure de Ceramique Industrielle–Limoges, Limoges, France
e-mail: sylvie.rossignol@unilim.fr

L. Klein et al. (eds.), *Handbook of Sol-Gel Science and Technology*,
DOI 10.1007/978-3-319-19454-7_88-1

silicate solution reactivity is important to determine the appropriate solution for a given application.

Introduction

Alkaline silicate solutions, also called water glass, are of great interest for several industrial applications (e.g., sealants, deflocculants, or binders) (Johnson et al. 2008; Tognonvi et al. 2010). Recently, two of the primary applications are related to their use as alkaline reactants in geopolymer materials (Bourlon 2011; Autef et al. 2012) or as a binder for sand agglomeration (Lucas et al. 2011; Tognonvi et al. 2012).

The first application concerns sand consolidation, which is primarily used in oil industries. These methods use particular alkaline silicate solutions or resins as a binder to maintain the permeability between the consolidated zones (Talaghat et al. 2009). Agglomeration of sand by sodium silicate solution is also used in fuse technology (Gurevich 1990; Vivier 2010). The purpose of the sand in an electrical fuse is to absorb the electric arc energy and disperse metal gaseous vapors when a fuse element melts during the short circuit. For high-voltage fuses, a binder is necessary to reinforce the sand cohesion within the fuse. A sodium silicate solution is commonly used to agglomerate sand because it is an economical, water-soluble, and environmentally friendly binder. Moreover, its use as a binder to consolidated sand does not generate the release of CO_2. The main parameters for silicate solutions used for agglomeration include the molar ratio of SiO_2/Na_2O, solid content, viscosity, and pH (Keeley 1983).

The second application of silicate solutions is their use as activation solutions for geopolymer materials. Geopolymers have garnered increasing interest because of their synthesis methods, high working performance (Van Jaarsveld et al. 1999), wide range of applications (Krivenko 1997), and low environmental impact (Liew et al. 2011). These binders result from the activation of an aluminosilicate source by an alkaline solution at a temperature less than 100 °C (Davidovits 2008). The mechanism consists of the dissolution of reactive aluminosilicate precursors under the effect of the alkaline solution to form oligomers ($Si[OH]_4$ and $Al[OH]^-_4$). Then, a polycondensation reaction links the oligomers, generating an amorphous three-dimensional network. Therefore, it is interesting to study the structure of an alkaline solution because it affects the working properties of the final geopolymer materials.

To ensure the widespread use of silicate applications, a deeper comprehension of the structure and the reactivity of alkaline solutions is necessary. Silicate solutions contain silicate dioxide (SiO_2) and alkali oxide (i.e., Li_2O, Na_2O, K_2O) and are commonly prepared by the dissolution of an alkali-silicate glass in water or by using steam or pressure (Tognonvi et al. 2010). Alkali-silicate glasses are prepared through a reaction between silica and sodium carbonate or sodium sulfate (Iler 1979). Another method to prepare these solutions is to dissolve silica fume in an alkaline solution (Harris and Knight 1983a; Steins 2014). Several techniques can be used to determine the various silicate species in the solutions. Fourier transform infrared

(FTIR) spectroscopy was used in various studies to determine the Q^n species in the silicate solutions by following the position of the broad peak attributed to the asymmetric stretching of the Si-O-Si bonds (Tognonvi et al. 2012). However, FTIR spectroscopy is not a quantitative analysis; thus, ^{29}Si NMR has been widely used to characterize silicate solutions (Harris and Knight 1983b; Bourlon 2011). This approach allows distinguishing and quantifying the various Q^n species. Engelhardt et al. (1975) introduced the Q^n notation for silicate species in which Q refers to the silicon atom and n (from 0 to 4) refers to the bridging-oxygen atoms. Moreover, this technique permits the detection of cyclic species and weak variations of the silicate species amounts. These solutions were also characterized using Raman spectroscopy (Halasz et al. 2007; Hunt et al. 2011). This technique revealed the contributions of monomers and oligomers in silicate solutions and glasses (Aguiar et al. 2009; Hunt et al. 2011 and allowed the identification of the vibrations of 3-, 4- or 5-membered rings (Aguiar et al. 2009; Le Losq and Neuville 2013). Thus, the Si/M molar ratio and the water content appear to be key parameters for silicate solutions. Thus, the objective of this study is to determine the main parameters controlling the reactivity of various silicate solutions and to enhance the effect of the reactivity on sand agglomeration or, in the presence of metakaolin, for geopolymerization applications.

Alkaline Solution Reactivity: Structural Investigation

To elucidate the interaction of silicate solutions with different materials (sand and clays), the structure of these solutions should be defined. Knowledge of the different entities that depend on various parameters may enable the prediction of the reactivity of these solutions. For this purpose, different spectroscopic techniques (FTIR, Raman, and ^{29}Si NMR spectroscopies) were used. FTIR spectroscopy reveals the presence of the various Q^n species in the solutions. Raman spectroscopy was used as a complementary technique. The presence of oligomers and rings was highlighted by this analysis. Finally, ^{29}Si NMR quantifies these various entities. In this study, various sodium and/or potassium alkali-silicate solutions were investigated, as referenced in Table 1. The main parameters studied are the type of cation and the Si/M molar ratio with M = K and/or Na (0.5, 1.0 and 1.7). The lab-prepared solutions were obtained by the dissolution of KOH or NaOH pellets (85.2 % and 97 % purity, respectively) and amorphous silica (99.9 % purity) in osmotically purified water at room temperature, as described in a previous study (Autef et al. 2012). The nomenclature (Table 1) is $^{x}SiM_{y}$, where x is the Si/M molar ratio, M is the alkali cation (Na or/and K), and y is the manufacturing process (C = commercially prepared and L = lab prepared).

A preliminary characterization was performed using FTIR, ^{29}Si NMR, and Raman spectroscopies to define the structure and to compare the starting silicate solutions.

FTIR spectroscopy in attenuated total reflectance (ATR) mode was performed to characterize the solutions using a Thermo Fisher Scientific Nicolet 380 infrared spectrometer. The corrected and normalized IR spectra, shown in Fig. 1a, b, were

Table 1 Nomenclature and characteristics of the various studied solutions

Cation	Si/M	Nomenclature	% water	Density
Na	1.7	$^{1.7}SiNa_C$	62.7	1.37
	1.0	$^{1.0}SiNa_L$	63.0	1.37
	0.5	$^{0.5}SiNa_L$	55.3	1.51
K	1.7	$^{1.7}SiK_C$	76.0	1.18
	1.0	$^{1.0}SiK_L$	57.8	1.36
	0.5	$^{0.5}SiK_C$	48.0	1.65
Na + K	1.7	$^{1.7}SiNaK_C$	62.0	1.38

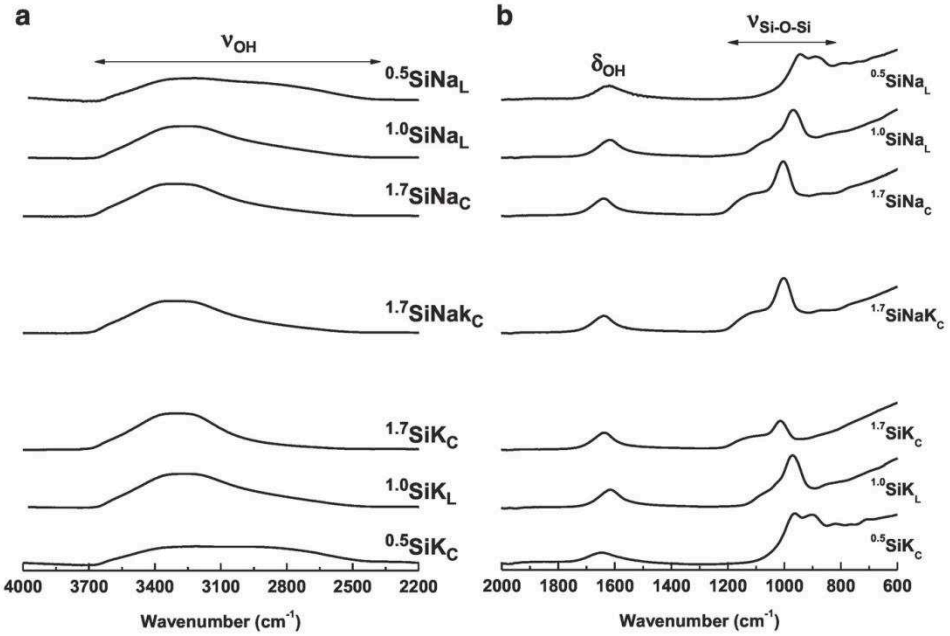

Fig. 1 FTIR spectra of sodium and/or potassium silicate solutions with different Si/M molar ratios (1.7, 1.0 and 0.35) between (**a**) 4000 and 2200 cm^{-1} and (**b**) 1800 and 600 cm^{-1}

collected over a wavenumber range of 4000–500 cm^{-1} with a resolution of 4 cm^{-1}. The various contributions observed in the different spectra are shown in Table 2 (Muroya 1999; Halasz et al. 2007, 2010; Tognonvi et al. 2012). Regardless of the solution, the bands at 3200 and 1640 cm^{-1} are attributed to the OH vibration band (ν_{OH}) and to the bending vibration of water molecules (δ_{OH}), respectively. A broad contribution near 1000 cm^{-1} due to the asymmetric stretching of Si-O-Si bonds (ν_{as}Si-O-Si) (Muroya 1999; Tognonvi et al. 2012) is observed. Moreover, $^{1.7}SiNa_C$ and $^{1.7}SiNaK_C$ exhibit similar spectra with a peak at approximately 1003 cm^{-1} and a shoulder at 1100 cm^{-1}, which are attributed to the Q^2 and Q^3 units, respectively (Tognonvi et al. 2012; Gharzouni et al. 2014). The same bands are observed in the case of $^{1.7}SiK_C$ with a slight shift of the Q^2 contribution to a higher wavenumber (1015 cm^{-1}). The $^{1.0}SiM_L$ spectra exhibit a similar trend with a decrease in the

Table 2 Vibrational frequencies of silicate species (*IR* FTIR spectroscopy, *R* Raman spectroscopy)

Contribution	Position (cm^{-1})	References
δOH	1640 (IR)	Muroya 1999
ν_sSi-O-Si (Q^4)	1120–1230 (R) 1154 (IR)	Tan et al. 2004; Tognonvi et al. 2012
ν_sSi-O-Si (Q^3)	1000–1100 (R) 1099 (IR)	Hunt et al. 2011; Tognonvi et al. 2012
ν_sSi-O-Si (Q^2)	920–1000 (R) 1011–1014 (IR)	Tognonvi et al. 2012; Belova et al. 2015
νSi-O^-(M^+)	885–928 (IR)	Tognonvi et al. 2012
ν_sSi-O-Si (Q^1)	850–920 (R)	Mysen et al. 1982; Malfait et al. 2008
ν_sSi-O^- (Q^0)	800–875 (R)	Chligui 2010; Hehlen and Neuville 2015
ν_s(Na)O-Si-O(Na)	830 (IR)	Halasz et al. 2007; 2010
ν_sSi-O-Si	820 (IR)	Muroya 1999
TO/LO (Si-O-Si)	650–850 (R)	Chligui 2010
ν_s(dimers/oligomers)	600 (R)	Hunt et al. 2011
D_2 (δ[T_3])	587–606 (R)	Zotov et al. 1999; Le Losq and Neuville 2013
D_1 (δ[T_4])	453–550 (R)	Geissberger and Galeener 1983; Zotov et al. 1999
δ[$T_{5\ and\ more}$]	400–490 (R)	Geissberger and Galeener 1983; Aguiar et al. 2009
M-O (network modifiers)	340–360 (R)	Hehlen and Neuville 2015

intensity of the Q^3 band and a slight shift of Q^2 to lower wavenumbers (991 and 994 cm^{-1} for $^{1.0}SiNa_L$ and $^{1.0}SiK_L$, respectively).

For the $^{0.5}SiNa_L$ solution, two contributions are found located near 967 and 914 cm^{-1}, which are assigned to the Si-O-Si bonds in the Q^1 and Q^0 units, respectively. The same contributions are observed in the case of $^{0.5}SiK_C$, but the Q^0 band is shifted to 902 cm^{-1}. The displacement of the Si-O-Si peak position to a lower wavenumber linked to the appearance of the Q^0 band may be explained by a depolymerization phenomenon. It was demonstrated that a decrease in the Si/M ratio (i.e., an increase in the pH value) favors depolymerization due to the breaking of the Si-O-Si bonds to create Si-O^- groups (Lucas et al. 2011). Thus, for a low Si/M ratio, the formation of lower-order siliceous species (Q^1 and Q^0) occurs to the detriment of higher-order species (Q^4, Q^3 and Q^2); the solution is depolymerized and contains a majority of Q^0 and Q^1 species (Gharzouni et al. 2014; Goudarzi 2013). However, for a high Si/M ratio, the solution is more polymerized, and the major species are the Q^2 and Q^3 entities. Moreover, regardless of the Si/M molar ratio considered, the potassium silicate solutions exhibit the Si-O-Si peak position at a higher wavenumber than the sodium silicate solutions. This phenomenon may be explained by the fact that the potassium silicate solutions are slightly more polymerized than sodium silicate solutions.

Therefore, the polymerization degree of the various silicate solutions is known, depending on the alkali cation and the Si/M molar ratio. However, the FTIR investigation does not distinguish the various silicate species.

To determine the presence of rings and oligomers in the different silicate solutions depending on the Si/M ratio and the alkali cation, Raman spectra were recorded using a T64000 Horiba-Jobin-Yvon spectrophotometer with 514 nm laser excitation operating at a power of 30 mW (Fig. 2a) (Hunt et al. 2011). The various contributions observed in the different spectra are presented in Table 2 (Aguiar et al. 2009; Hunt et al. 2011). For Si/M greater than 1 ($^{1.7}SiM_C$), (Fig. 2a) the contributions due to the stretching of the Q^2 ($Si(OH)_2O_2^{2-}$), Q^3 ($Si_2O(OH)_5O^-$, $Si_3O_3(OH)_4O_2^{2-}$), and Q^4 species are observed (Tan et al. 2004; Hunt et al. 2011). The spectra also exhibit a contribution at 787 cm^{-1}, which is attributed to the TO/LO modes. Weak contributions due to the vibrations of M-O bonds are observed near 330 cm^{-1} (Hehlen and Neuville 2015). The ring breathing modes of the 3-, 4-, 5- and more-membered rings (denoted as $\delta[T_3]$, $\delta[T_4]$, and $\delta[T_{5\ and\ more}]$) are located near 600, 490, and 450 cm^{-1}, respectively (Geissberger and Galeener 1983; Aguiar et al. 2009). The contributions of the Q^3 and Q^4 species reveal the high polymerization degree of the solutions, which is in accordance with the previous results.

For Si/M = 1 ($^{1.0}SiM_L$), an increase in the contributions of the Q^2 units, the oligomers, $\delta[T_3]$, $\delta[T_4]$, $\delta[T_{5\ and\ more}]$, and the M-O band is observed. This phenomenon is associated with the disappearance of the Q^4 species. This fact provides evidence of the depolymerization of the solutions.

For a ratio of Si/M lower than 1 ($^{0.5}SiM_y$), the bands attributed to the vibration of the M-O bonds and the $\delta[T_5]$ appear to be more intense. An increase in the Q^2 species contribution and a decrease in the TO/LO mode and Q^3 species bands are also noted. The $\delta[T_{3\ and\ 4}]$ (3- and 4-membered rings) and the stretching of oligomer contributions appear to be more intense. These data reveal that the solutions are highly depolymerized and confirm the previous observations.

Thus, Raman spectroscopy provides complementary information to the previous results. The spectra reveal the presence of the M-O bonds for Si/M ratios less than 1, i.e., for highly depolymerized solutions. The presence of the rings may be an important factor for the reactivity of the silicate solutions. Moreover, FTIR and Raman investigations provided evidence that the polymerization state of the solutions depends on the cation type and the Si/M molar ratio. However, these techniques do not quantify the different silicate species.

To obtain additional details about the molecular structure and the amounts of the various silicate species, high-resolution NMR experiments were performed at room temperature on a Bruker AVANCE-400 spectrometer operating at 79.49 MHz (^{29}Si signal). The ^{29}Si (I = 1/2) NMR spectra were recorded after a p/2 pulse irradiation (4 ls) using a 500 kHz filter to improve the signal/noise ratio. In each case, 400 scans were collected. The time between acquisitions was set to 10 s to minimize saturation effects. The ^{29}Si NMR spectra of the solutions are plotted in Fig. 2b. For all solutions, the spectra exhibit the different Q^0, Q^1, Q^2, Q^3, and Q^4 species contributions near −72, −80, −88, −97, and −106 ppm, respectively (Bourlon 2011; Nordström et al. 2011). Broad bands associated with the Q^4, Q^3, and Q^2 species

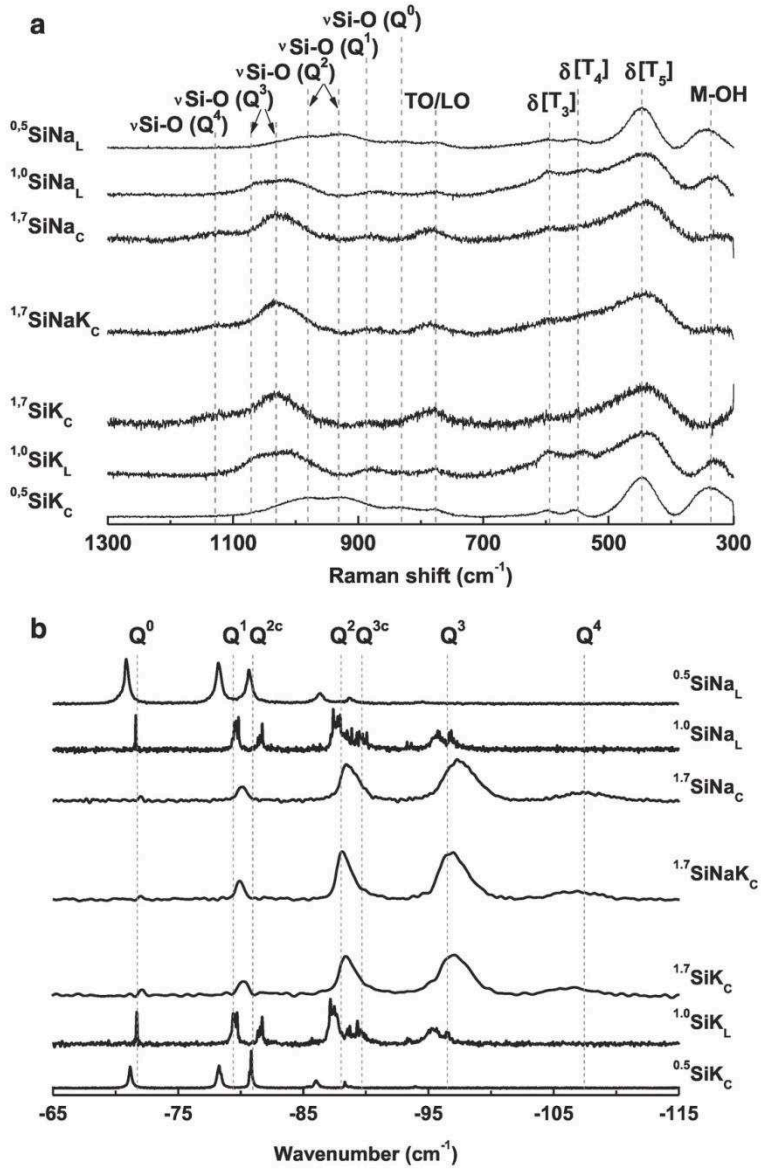

Fig. 2 (**a**) Raman spectra and (**b**) ^{29}Si NMR spectra of sodium and/or potassium silicate solutions with different Si/M (M = Na or/and K) molar ratios (1.7, 1.0, and 0.35)

are observed in the spectra of $^{1.7}SiM_C$ solutions. The broad peaks are mainly due to a continuous range in the number of bridging-oxygen atoms, with distorted sites having bonding characteristics between those of the well-defined tetrahedra in a silicate crystal (Schmidt et al. 2001). When the Si/M ratio decreases from 1.7 to 1, the contributions shift to higher chemical displacements, and Q^4 species disappear in favor of the Q^{2c} and Q^{3c} species. This fact is more pronounced in the case of

$^{0.5}SiM_C$ solutions and is characteristic of a variation in the protonation degree of the silicon atoms (Harris and Knight 1983b; Bourlon 2011). For a ratio of Si/M greater than 1, the predominance of Q^2, Q^3, and Q^4 species indicates that the solutions are polymerized. For Si/Na less than 1, the major species are Q^0 and Q^1 entities, indicating that the solutions are depolymerized (Svensson et al. 1986). The chemical shift (δ) and the percentage area (%A) of the different contributions obtained by deconvolution of each solution spectra are presented in Table 3. The decrease in the Si/M molar ratio results in the increase in the amount of depolymerized species from approximately 1 % to 25 % (Q^0) and from 6 % to 30 % (Q^1) for Si/M between 1.7 and 0.5, respectively. However, a decrease in the high-order species (more polymerized) Q^2, Q^3, and Q^4 is observed when the Si/M ratio decreases (Table 3). Moreover, the decrease in the Si/M molar ratio implies an increase in the cyclic silicate species. For Si/M equal to 1.7, no cyclic species are noted, whereas for a Si/M of 0.5, the Q^{2c} and Q^{3c} entities are observed (approximately 12 and 2 %, respectively). Thus, a decrease in the Si/M ratio leads to the depolymerization of the solutions. This fact is linked to the appearance of cyclic species. Regardless of the Si/M molar ratios, the sodium and potassium silicate solutions exhibit similar spectra. However, the contributions of the potassium silicate solutions are located at slightly higher chemical displacements than the sodium silicate solutions. This phenomenon may be explained by a variation in the protonation degree of the silicon atoms (Bourlon 2011).

Therefore, ^{29}Si MAS-NMR experiments provide information about the influence of the cation type and the Si/M molar ratio. The Si/M molar ratio is a crucial parameter that controls the amount and the nature of silicate species present in the alkaline solutions, and an important change in these entities is observed for a ratio of Si/M of approximately 1.0. Furthermore, the effect of the cation appears to be less pronounced.

Thus, the existence of monomers and/or oligomers was revealed; however, the type of cyclic entities was not distinguished. The presence of these species in the solution allows the determination of the reactivity degree of the solution.

To further investigate the influence of the Si/M molar ratio, the variation of the Si-O-Si peak position as a function of the silicon concentration is plotted in Fig. 3a for the different solutions. For each considered cation and for a given Si/M ratio, all the solutions show a linear variation with the silicon concentration. The slope values range from 3.0 to 5.7 for a Si/M molar ratio of 1.7–0.5, respectively. Furthermore, a lower Si/M ratio indicates a higher slope. For example, for a similar Si/M molar ratio of 1.7, the Si concentration (g/L) vs. Si-O-Si (Q^2) peak positions (cm^{-1}) are [175–1003] and [90–1014] for $^{1.7}SiNa_C$ and $^{1.7}SiK_C$, respectively. For $^{1.7}SiK_C$, the position of the Si-O-Si band at a slightly higher wavenumber is linked to the presence of more polymerized species in this solution (Gharzouni et al. 2014). Similarly, for an Si concentration of approximately 135 g/L, the $^{0.5}SiNa_L$, $^{1.0}SiNa_L$, and $^{1.7}SiK_L$ solutions exhibit a Si-O-Si band at 967, 991, and 1008 cm^{-1}, respectively. Thus, for a constant Si concentration, an increase in the wavenumber is observed when the Si/M ratio increases. Bass et al. (1999) showed that at a constant silica concentration, the Si-O-Si peak shifted to a lower frequency

Table 3 Deconvolutions of ^{29}SI NMR spectra of silicate solutions

		Silicate species						
		% Area (δ (ppm))						
		Q^0	Q^1	Q^{2c}	Q^2	Q^{3c}	Q^3	Q^4
Solutions	**$^{1.7}$SiNa**	0.6 (−72.0)	5.3 (−80.1)	/	29.4 (−88.9)	/	51.5 (−97.7)	13.2 (−107.6)
	$^{1.0}$SiNa	2.6 (−71.6)	13.2 (−79.6)	37.9 (−81.6)	5.9 (−87.8)	26.5 (−89.7)	13.9 (−96.2)	/
	$^{0.5}$SiNa	27.3 (−70.9)	29.7 (−78.2)	11.2 (−80.7)	26.3 (−86.3)	1.9 (−88.7)	3.6 (−94.5)	/
	SiNaK	0.7 (−72.0)	6.4 (−79.9)	/	29.2 (−88.8)	/	49.5 (−97.2)	14.3 (−106.7)
	$^{1.7}$SiK	1.0 (−72.1)	6.7 (−80.2)	/	29.0 (−88.7)	/	51.2 (−97.1)	12.1 (−106.2)
	$^{1.0}$SiK	3.4 (−71.7)	14.3 (−79.5)	31.2 (−81.6)	6.7 (−87.5)	26.7 (−89.5)	17.7 (−95.6)	/
	$^{0.5}$SiK	24.5 (−71.2)	29.9 (−78.3)	12.4 (−80.8)	26.5 (−86.0)	1.9 (−88.5)	4.8 (−94.0)	/

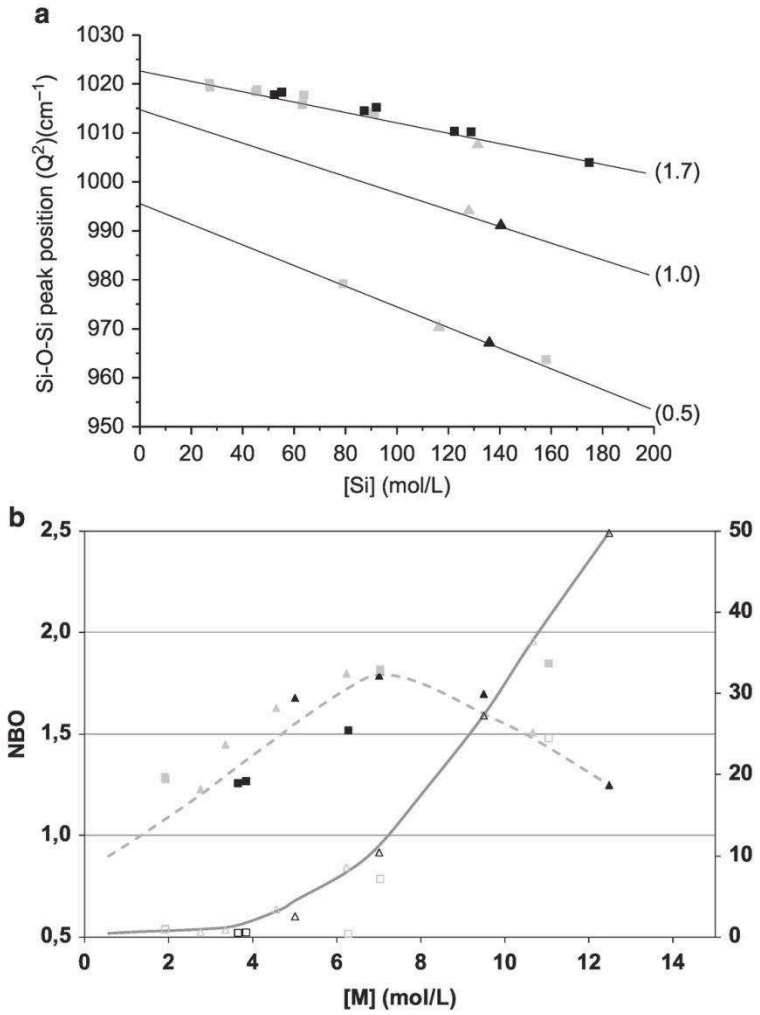

Fig. 3 Variation of the (**a**) Si-O-Si peak position as a function of the Si concentration (numbers in brackets (Si/M)) for (■) $^{x}SiNa_C$, (▲) $^{x}SiNa_L$ (◢), $^{x}SiK_C$, and (◢) $^{x}SiK_L$ solutions and (**b**) (---) NBO and (—) Q^0 percentage versus the alkali cation concentration for ((■) $SiNa_C$, (▲) $SiNa_L$ (◢), SiK_C and (▲) SiK_L and (□) $SiNa_C$, (Δ) $SiNa_L$ (▱), SiK_C, and (◿) SiK_L)

as the silica/alkali ratio decreased. This result was attributed to the condensation of monomers to more complex anions when the silica/alkali ratio increased. Other authors also observed that the increase in the Si/M ratio implied the presence of more polymerized species in the solutions (Svensson et al. 1986; Aguiar et al. 2009). Thus, for the same concentration and for each considered cation, a higher Si/M ratio indicates a more polymerized solution.

Consequently, the increase in the Si/M molar ratio leads to the polymerization of the solution. The use of the potassium cation implies the presence of slightly more polymerized species.

To highlight the effect of the different polymerization states of the various silicate solutions on the reactivity, the number of non-bridging oxygens (NBOs) per tetrahedron was calculated using the percentage of the Q^n species previously determined (Malfait et al. 2007) (Fig. 3b). The variation of the NBO appears to be at its maximum for alkali cation concentrations between 4.5 and 9.5 mol/L. For concentrations lower than 4.5 mol/L, the increase in the NBO is characteristic of the depolymerization observed by ^{29}Si NMR (Fig. 2b). This phenomenon indicates that the Q^4 species are transformed into Q^3, Q^2, and Q^1 species (Couty and Fernandez 1998; Brykov et al. 2008). Moreover, the Q^0 percentage slightly varies for concentrations below 4.5 mol/L. For a value of $4.5 < [M] < 9.5$ mol/L, the silicate solutions are already depolymerized, and the presence of the Q^0 species is effective in these solutions. Thus, there is nearly no depolymerization of the silicate species in the solution, and few variations of the NBO are noted. For an alkali cation concentration above 9.5 mol/L, the solutions are highly depolymerized and contain a large amount of Q^0 species. A rapid variation of the Q^0 percentage (Si/M = 1.7, Q^0 = 1 %; Si/M = 0.35, Q^0 = 36.5 %), and a decrease in the NBO are observed. This fact reveals the presence of a limiting value for alkali cation concentrations between 4.5 and 9.5 mol/L. In this range, the silicate solutions may be more reactive. For concentrations lower than 4.5 or higher than 9.5 mol/L, the reactivity of the silicate solutions decreases. According to these observations, it appears that regardless of the cation, $4.5 < [M] < 9.5$ mol/L is the limiting range for the depolymerization.

Once the polymerization state and the reactivity of the silicate solution is understood, it is crucial to validate the effect of the reactivity of these silicate solutions in the presence of sands or clays for new applications, such as sand agglomeration, and in the presence of metakaolin for geopolymerization. The relationship between the reactive species amount and the alkali cation concentration governs the working properties of the final material.

Applications of Alkaline Solutions

As previously mentioned, the alkaline silicate solutions have many applications, such as sand agglomeration for the fuse industry or as an activator in the presence of metakaolin for geopolymerization uses.

Sand Agglomeration

In the case of sand agglomeration, the used solutions must be diluted with various amounts of water. To better understand the effect of the dilution on the silicate species, various diluted sodium silicate solutions were studied by FTIR spectroscopy. The obtained spectra are shown in Fig. 4. All the spectra present two contributions located at 1600 and 1000 cm^{-1}, corresponding to the vibrations of the OH bonds from water and to the Si-O-Si bonds, respectively (Lucas et al. 2011). The

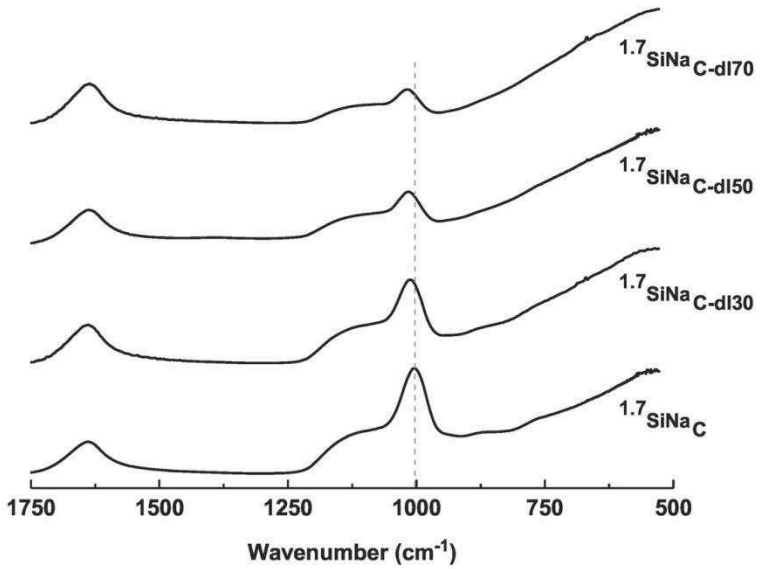

Fig. 4 FTIR spectra of sodium silicate solution with Si/M molar ratio of 1.7 and the obtained diluted solutions with various amounts of water

increase in the dilution rate leads to the displacement of the Si-O-Si peak position to higher wavenumbers. Thus, this contribution shifts from 1003 cm^{-1} for $^{1.7}SiNa_C$ to 1018 cm^{-1} for $^{1.7}SiNa_{C\text{-}dl70}$. This displacement may be explained by an increase in the Q^3 entities (1099 cm^{-1}) to the detriment of the Q^2 species (1005 cm^{-1}) (Tognonvi et al. 2012). Therefore, the dilution of a silicate solution favors the polymerization of the silicate species, regardless of the considered solution. The morphologies of agglomerated sand samples were determined using a Cambridge Stereoscan S260 scanning electron microscope (SEM). The samples were broken and platinum coated. SEM observations were performed on samples to determine the influence of various parameters on the fuse's microstructure. The different studied parameters are the dilution rate of the sodium silicate solution, the used sand, the drying mode, and the temperature.

First, the effect of the dilution rate on the morphology of the samples obtained after microwave drying at 150 °C is presented in Fig. 5A.

The amount of sodium silicate observed on the surface of the sand increased with the increase in the dilution rate. The $S_{8+}{}^{1.7}SiNa_{C\text{-}dl30}$ sample (Fig. 5A(a)) appears to present less sodium silicate on its surface than the $S_{8+}{}^{1.7}SiNa_{C\text{-}dl70}$ material (Fig. 5A (c)). However, a better distribution of the silicate is observed on the surface of the $S_{8+}{}^{1.7}SiNa_{C\text{-}dl70}$ sample. Near the grain boundaries, a precipitation phenomenon appeared to occur, leading to the formation of macroporosity. It was shown that the increase in the dilution rate of the solution favors the polymerization of the solution. Then, the macromolecule formed will facilitate the solvent release. Thus, this phenomenon enables more efficient water removal during the drying process, favoring the precipitation phenomenon (Iler 1979).

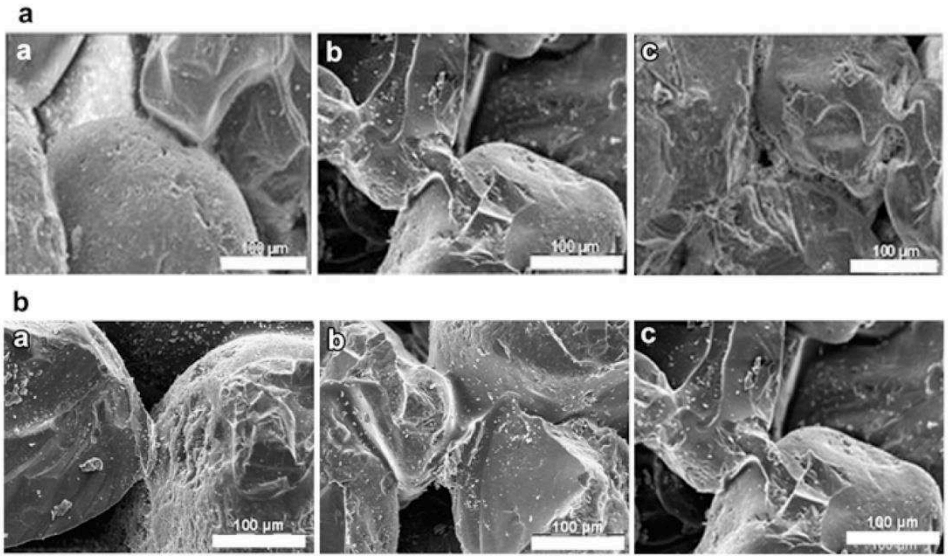

Fig. 5 SEM images of (**A**) S_8 + $^{1.7}SiNa_{C\text{-}dlz}$ with z = (**a**) 30 %, (**b**) 50 %, and (**c**) 70 % of water amount and (**B**) S_y + $^{1.7}SiNa_{C\text{-}dl50}$ with (**a**) S_2, (**b**) S_4, and (**c**) S_8 dried with microwave drying at 150 °C

Then, the effect of the sand grain size on the distribution of the silicate solution is presented in Fig. 5B. These samples were prepared with a $^{1.7}SiNa_{C\text{-}dl50}$ solution and were dried using a microwave at 150 °C.

For every sand used, the samples presented a similar silicate solution distribution. It appears that the sand grains are coated by the silicate solution regardless of the grain size (Fig. 5B (a, b, c)). Therefore, the grain size does not appear to influence the silicate distribution.

Finally, the effect of the thermal mode and the temperature used during the drying of the samples was studied. The SEM observations of the sample are presented in Fig. 6.

Different distributions of the silicate on the sand surface are observed depending on the thermal treatment used. The S_4 + $^{1.7}SiNa_{C\text{-}dl50}$ sample prepared with microwave drying at 110 °C presents an important amount of sodium silicate on the sand surface (Fig. 6a). A conventional drying at 110 °C (Fig. 6b) leads to the presence of less silicate solution on the sand grains and to the formation of grain boundaries by the silicate solution. Then, an increase of the temperature to 150 °C with microwave drying (Fig. 6c) appears to decrease the amount of silicate on the grain surface and leads to the formation of grain boundaries. Finally, conventional drying at 150 °C results in the formation of silicate grain boundaries. A comparison of these samples highlights a difference between the two drying modes. The silicate distribution is different depending on the thermal mode used. The grains appear to be coated by the solution with microwave drying, whereas conventional drying leads to the presence of this binder only at the grain boundaries. Moreover, the effect of the temperature

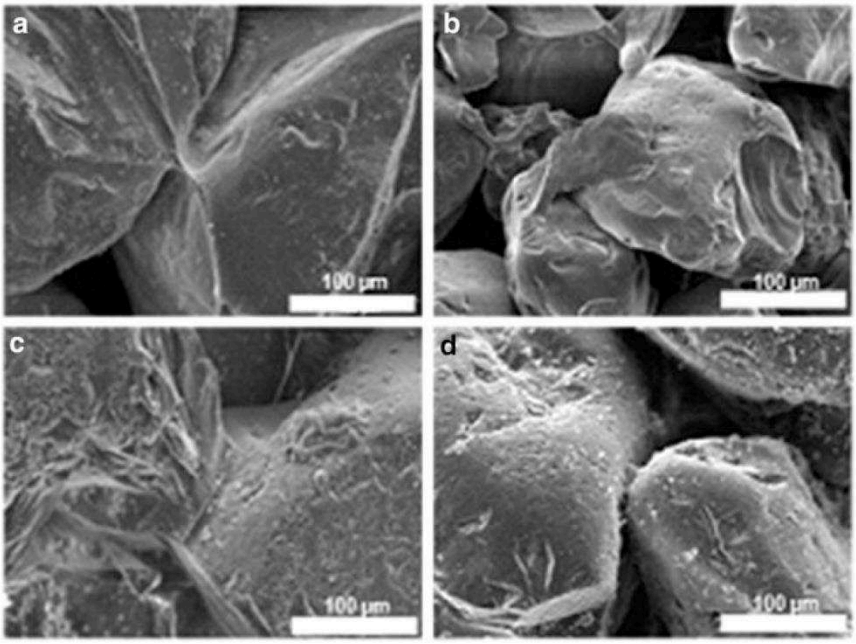

Fig. 6 SEM images of S_4 + $^{1.7}SiNa_{C\text{-}dl50}$ samples using (**a**) conventional drying at 110 °C, (**b**) microwave drying at 110 °C, (**c**) conventional drying at 150 °C, and (**d**) microwave drying at 150 °C

was revealed. Low-temperature drying leads to the presence of more silicate on the grains, whereas an increase in the temperature decreases the amount of the silicate on the sand.

Therefore, a higher temperature leads to a better distribution of the silicate, and conventional drying results in the formation of grain boundaries, whereas microwave drying leads to coating of the grains. Then, the used silicate solutions contain highly polymerized species due to the high water content.

Geopolymerization

Another innovative application of silicate solutions is their use as an activator of various aluminosilicate sources (i.e., clays, industrial waste) to produce geopolymer materials. In this section, the behavior of different silicate solutions in the presence of various metakaolins was studied. Moreover, the effect of the reactivity of the used precursors on the geopolymer formation and the final properties was increased. For this purpose, two commercial potassium silicate solutions, denoted as $^{1.7}SiK_C$ and $^{0.7}SiK_C$, with Si/K molar ratios of 1.7 and 0.7, respectively, were used. Because a comparison of solutions with different parameters is difficult, the Si/K molar ratio of the two solutions was maintained at Si/K = 0.5 by dissolving different amounts of potassium hydroxide pellets (VWR, 85.2 % pure) into the starting solutions. Then,

Table 4 Chemical and physical properties of raw metakaolins

Metakaolins	MKA	MKB	MKC
Si/Al	1.17	1.19	1.33
BET value (m^2/g)	17	22	6
Wettability (μL/g)	760	1250	670
Amorphous phase	63	87	59
Secondary minerals	Quartz, kaolinite, muscovite, and anatase		Mullite, quartz, muscovite, kaolinite and anatase

three types of metakaolins, denoted as MKA, MKB, and MKC, were used as aluminosilicate sources (Table 4).

The syntheses were performed by mixing the metakaolin and alkaline solutions until obtaining homogenous geopolymer reactive mixtures, which were placed in cylindrical closed sealable polystyrene molds at room temperature (25 °C) for 7 days. The samples were named $^{1.7}SiK_CMKA$, $^{0.7}SiK_CMKA$, $^{1.7}SiK_CMKB$, $^{0.7}SiK_CMKB$, $^{1.7}SiK_CMKC$, and $^{0.7}SiK_CMKC$.

To elucidate the primary differences between the three used metakaolins, their physical and chemical characteristics are reported in Table 4. The mineralogical compositions were also determined by X-ray diffraction. MKA and MKB showed the presence of quartz, residual kaolinite, muscovite, and anatase. For MKC, the impurity content is higher. MKC contains mullite in addition to quartz, muscovite, kaolinite, and anatase. The presence of mullite can be explained by the over-calcination of particles when passing near the flame, as in the case of the flash calcination process, as previously described by San Nicolas et al. (2013) and Cyr et al. (2014). Thus, the studied metakaolins present different mineralogical phases denoting different purity degrees. Furthermore, MKA and MKB have Si/Al molar ratios of approximately 1.17 and 1.19, respectively. However, MKC has the highest Si/Al ratios (1.44 and 1.33). This fact is in accordance with the previously discussed mineralogical data. The specific surface area (S_{BET}) is also an important parameter to study because it controls the dissolution rate of metakaolin (Weng et al. 2005). Regardless of the used metakaolin, the specific surface area values are between 6 and 22 m^2/g, which is in accordance with the literature (Konan et al. 2010; Guyot 1969). MKB exhibits the highest S_{BET} value (22 m^2/g); however, MKC has the weakest value (6 m^2/g). The differences in the specific surface area between the studied metakaolins denote the different structures of the particles. Recently, Autef (2013) demonstrated that the wettability value might be a good indicator of reactivity. Thus, it was interesting to compare the wettability values of the studied metakaolins. MKA and MKC showed low wettability values (760 and 670 μL/g, respectively), whereas MKB exhibited high wettability values (1250, 1186 and 1091 μL/g). These differences are linked to the different parent kaolin crystallinity characteristics and the various dehydroxylation processes. Finally, the amorphous phase content differs for

each metakaolin. As expected, MKB presents the highest amorphous phases content (87 %) compared to the others.

To monitor the structural evolution of the synthesized mixtures, FTIR spectroscopy in ATR mode was used. Software was used to acquire a spectrum (64 scans) every 10 min for 13 h. An example of the spectra obtained at t = 0 and t = 400 min for $^{0.7}SiK_CMKB$ sample is shown in Fig. 7a. All the spectra exhibit the contributions at 3200 and 1640 cm^{-1} attributed to ν_{OH} and δ_{OH}, respectively. A broad band is also observed in the 1100–950 cm^{-1} range and is assigned to the Si-O-M (M = Si, Al) bond. Over time, the intensity of the ν_{OH} and δ_{OH} bands gradually decreases,

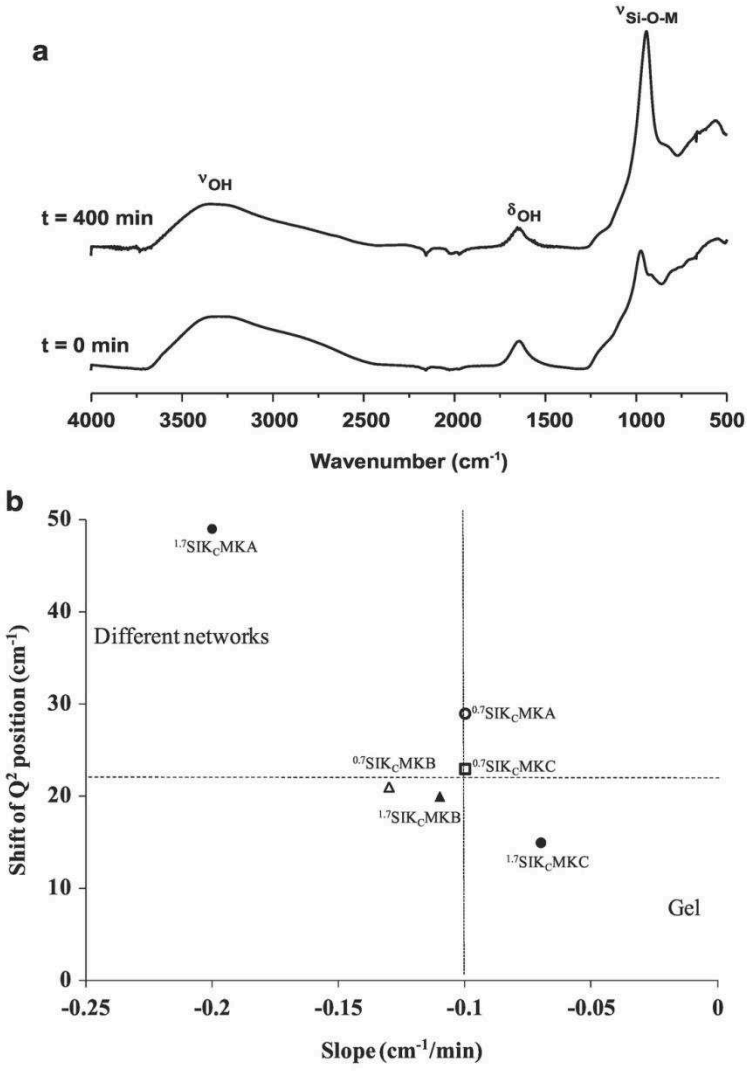

Fig. 7 (**a**) Example of in situ FTIR spectra obtained at t = 0 and t = 400 min for $^{0.7}SIK_CMKB$ sample and (**b**) Evolution of the Q^2 shift position in function of the slope value for all samples

whereas the Si-O-M contribution shifts toward lower wavenumbers. The shift value reveals a polycondensation reaction and is characteristic of the formation of a specific network (Rees et al. 2007, 2008; Duxson et al. 2007; Autef 2013). Furthermore, the slope values were calculated (the slope at the beginning of the curve of the Q^2 peak position versus time) to provide information about the kinetics of the reaction. Figure 7b shows the evolution of the Q^2 position shift versus the slope for all samples. The $^{1.7}SiK_C$MKA sample exhibits the greatest shift and slope values (49 cm^{-1} and -0.20 cm^{-1}/min, respectively). However, the use of the $^{0.7}SiK_C$ alkaline solution decreases the shift value to 29 cm^{-1} and the slope value to -0.1 cm^{-1}/min. For the MKB metakaolin, small changes are detected with the use of $^{0.7}SiK_C$, and the variation of the alkaline solution does not appear to significantly affect the reaction. In the case of MKC, the less pure metakaolin (Table 4) and weaker shift values are obtained, especially in the presence of $^{1.7}SiK_C$ (15 cm^{-1}). The use of $^{0.7}SiK_C$ increases this value to 22 cm^{-1}. The comparatively high shift and slope values observed for $^{1.7}SIK_C$MKA can be explained by a combination of Si-O-M (M = Si, Al or K) from dissolved species and the metakaolin impurities, as previously demonstrated. The weaker slope and shift values of $^{0.7}SiK_C$MKA mainly occur because of the reactivity of the $^{0.7}SiK_C$ alkaline solution. Despite the identical Si/K ratios of the two solutions (Si/K ratio = 0.5), persistent differences remain. Gharzouni et al. (2014, 2015) have demonstrated that $^{0.7}SiK_C$ contains a greater amount of Q^0 species and non-bridging oxygens than the $^{1.7}SIK_C$ solution. These differences make $^{0.7}SiK_C$ more reactive because Q^0 is the most reactive among all Q^n species, as has been previously demonstrated. Thus, highly reactive siliceous species, which are released from the $^{0.7}SiK_C$ alkaline solution, reach speciation equilibrium and react with the aluminous species (Gharzouni et al. 2014). It has been demonstrated that the monomeric silicates are exchanged much more rapidly with aluminosilicate species than with any other silicate anions (North and Swaddle and Duxson et al. 2005a). In addition, the geopolymerization reaction consequently involves the breaking of bridging-oxygen bonds with a higher number of non-bridging oxygens in the alkaline solution; hence, fewer bonds require hydrolysis before the species can be released (Rees et al. 2007, 2008). Therefore, a larger number of available reactive species are present for geopolymerization in $^{0.7}SiK_C$ because they are released more rapidly. For MKB, which is more reactive than MKA (Gharzouni et al. 2015), the effect of the alkaline solution appears negligible. The reactivity of the siliceous species released from the metakaolin controls the kinetics of the substitution of Si-O-Si by Si-O-Al bonds and the network reorganization. In fact, the more reactive metakaolin corresponds to a more favored and rapid oligomer formation. In the case of MKC, the less pure metakaolin (Table 4), the small shift value is indicative of the formation of a minor geopolymer phase blocked with impurities, such as mullite. These impurities do not participate in the polycondensation reaction and are coated by the alkaline solution (Gharzouni et al. 2016). However, the geopolymer phase is favored with the use of a highly reactive alkaline solution.

For a deeper comprehension, NMR is commonly used as an efficient and powerful technique providing structural information about silicates and aluminosilicates.

In geopolymer materials, aluminum can vary between $Al^{(IV)}$, $Al^{(V)}$ and $Al^{(VI)}$ (Rowels et al. 2007). Therefore, the change in the coordination number of aluminum can provide important information about the geopolymerization process. For fresh geopolymer reactive mixtures, ^{27}Al NMR in static mode was used. ^{27}Al is a quadrupolar nuclei (spin $I > 1/2$), which means that there is an asymmetric charge distribution in the nucleus due to the nonsymmetry of protons and neutrons. The difficulty of quadrupolar nuclei involves the quick relaxation in the liquid state and the broadening at the first and second order in the solid state (Iuga et al. 2005). The energy levels are shifted by the quadrupolar interaction, which may limit the quantitative determination of the populations (Man and Klinowski 1988). However, the quadrupolar interaction can be neglected in the liquid state, as previously reported by Favier et al. (2015). The synthesized mixtures were deposited in a zirconia rotor ($Ø = 4$ mm). The ^{27}Al ($I = 5/2$) NMR spectra were recorded after a $\pi/8$ pulse irradiation (1.5 µs) using a 1-MHz filter to improve the signal/noise ratio. In each case, 400 scans were collected. The time between acquisitions was set to 10 s to minimize the saturation effects. The six reactive mixtures were studied using ^{27}Al static NMR at different times of the formation (0, 2, 6, and 24 h, respectively). An example of the obtained spectra for the $^{1.7}SiK_CMKB$ sample is presented in Fig. 8a. The percentages of the area contributions obtained after the deconvolution of the spectra of all samples are reported in Table 5. Regardless of the sample, the spectra showed a dominant phase at 60 ppm, which is characteristic of $Al^{(IV)}$, and a minor broad peak at −10 ppm corresponding to $Al^{(VI)}$ (Fletcher et al. 2005). Moreover, it was noticed that the spectra are different from the typical ^{27}Al MAS-NMR spectra of metakaolin (Duxson et al. 2005b; Brown et al. 1985) upon immediate contact with the alkaline solution (from $t = 0$ h). The presence of $Al^{(VI)}$ denotes the possible

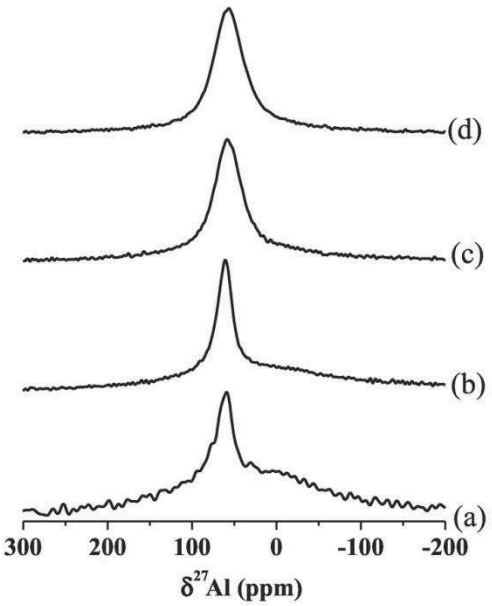

Fig. 8 Example of recorded ^{27}Al NMR spectra in static mode at (**a**) 0, (**b**) 2, (**c**) 6, and (**d**) 24 h of formation for $^{1.7}SIK_CMKB$ sample

Table 5 ^{27}AL NMR data of the various geopolymer reactive mixtures at different reaction times

Mixtures	$^{1.7}$**SiK$_C$MKA**				$^{0.7}$**SiK$_C$MKA**	
Percentage of the area curve of contribution (%)						
Time (h)	$Al^{(IV)}$		$Al^{(VI)}$	$Al^{(IV)}$		$Al^{(VI)}$
	≈70 ppm	≈60 ppm	≈ − 10 ppm	≈70 ppm	≈60 ppm	≈10 ppm
0	13.8	23.6	63.6	8.90	18.6	72.53
2	9.0	33.3	57.3	12.8	36.3	50.9
6	10.7	42.2	47.2	6.6	55.1	38.3
24	21.7	57.6	20.46	1.8	90.8	7.4
Mixtures	$^{1.7}$**SiK$_C$MKB**			$^{0.7}$**SiK$_C$MKB**		
Percentage of the area curve of contribution (%)						
Time (h)	$Al^{(IV)}$		$Al^{(VI)}$	$Al^{(IV)}$		$Al^{(VI)}$
	≈70 ppm	≈60 ppm	≈ − 10 ppm	≈70 ppm	≈60 ppm	≈10 ppm
0	8.9	9.6	81.5	8.9	41.1	50.0
2	7.4	26.7	65.9	9.8	47.6	42.6
6	10.9	60.3	28.8	6.4	76.9	16.7
24	10.5	74.8	14.7	6.4	84.7	8.9
Mixtures	$^{0.7}$**SiK$_C$MKC**			$^{0.7}$**SiK$_C$MKC**		
Percentage of the area curve of contribution (%)						
Time (h)	$Al^{(IV)}$		$Al^{(VI)}$	$Al^{(IV)}$		$Al^{(IV)}$
	≈70 ppm	≈60 ppm	≈ − 10 ppm	≈70 ppm	≈60 ppm	≈10 ppm
0	15.0	13.9	71.1	5.7	17.7	76.5
2	13.0	26.2	60.8	4.1	40.7	55.2
6	6.7	39.7	53.6	1.5	52.2	46.2
24	14.5	63.8	21.7	0.8	82.5	16.7

persistence of nondehydroxylated kaolinite and the mica phase (Autef 2013). Regardless of the mixture, when the metakaolin is mixed with the alkaline solution, an increase in the area contribution relative to $Al^{(IV)}$ causing the disappearance of $Al^{(V)}$ and a remarkable decrease in $Al^{(VI)}$ that was initially present in the metakaolin are observed. These changes reveal the rapid and strong interaction between the two precursors. As time progresses, the peak relative to $Al^{(IV)}$ broadens, denoting the formation of a geopolymer network, and the intensity of the peak relative to $Al^{(VI)}$ decreases, revealing the dissolution of metakaolin. However, $Al^{(V)}$, initially present in the metakaolin, was not observed in any spectra. The disappearance of Al $^{(V)}$ indicates that it was consumed due to its high reactivity, as has been previously demonstrated in the literature (Walther 1996).

The various behaviors of the samples detected by the FTIR and NMR experiments during the formation reveal different polycondensation rates, depending on the reactivity of the raw materials used, and suggest different mechanical properties. To elucidate this effect, the mechanical strengths were evaluated by compression tests. Then, a correlation was established between the $Al^{(IV)}$ formation rate (the difference between the amount of $Al^{(IV)}$ formed after 24 h in the geopolymer samples and the amount of $Al^{(IV)}$ initially present in the starting metakaolin) and compressive strength data, as shown in Fig. 9. Regardless of the sample, it is noted that better compressive strengths correspond to higher $Al^{(IV)}$ formation rates. Moreover, three different behaviors, depending on the reactivity of the used precursors, can be distinguished, as shown in Fig. 9. For the $^{1.7}SiK_CMKC$ sample, the $Al^{(IV)}$ formation rate did not exceed 62 %, leading to the weakest specific compressive strength value

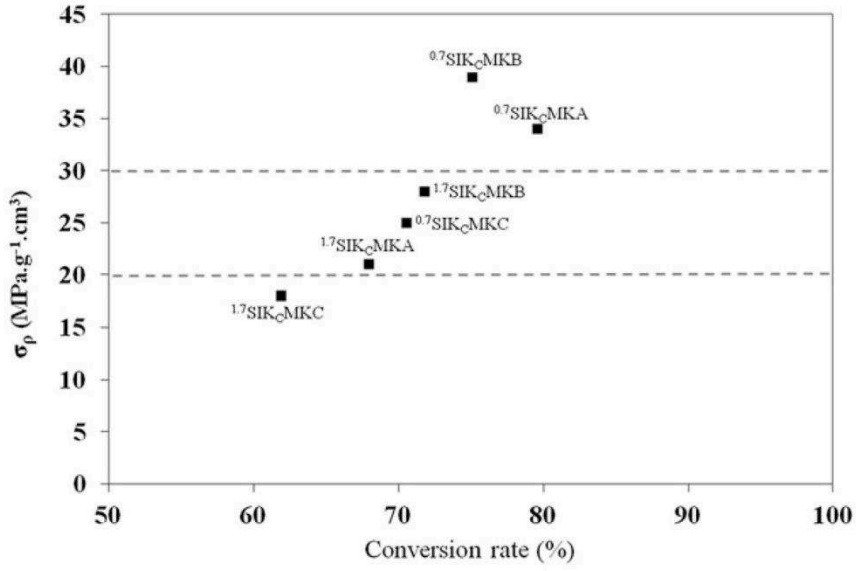

Fig. 9 The specific compressive strengths values versus the percentage of the conversion rate after 24 h $\left(\frac{Al(IV)24\ h - Al(IV)MK}{Al(IV)24\ h}\right)$ for all samples

(18 MPa.g^{-1}.cm^3). This fact can partially be explained by the low surface reactivity of metakaolin and by the low attack reactivity of the alkaline solution $^{1.7}SIK_C$ may prevent the formation of $Al^{(IV)}$ species, consequently preventing the total alteration of the metakaolin (Gharzouni et al. 2015). All of these factors inhibit the formation of a homogenous geopolymer phase, therefore decreasing the mechanical strength. The MKA and MKB metakaolins in the presence of the same solution, $^{1.7}SIK_C$, lead to a higher formation rate of $Al^{(IV)}$, which increases from 67 % to 76 % and increases the specific compressive strength values from 20 to 30 MPa.g^{-1}.cm^3. Thus, the high metakaolin reactivity favors the geopolymer phase and improves the mechanical strength. For samples using the $^{0.7}SiK_C$ solution, high formation rates (between 70 % and 80 %) were associated with high specific compressive strength values (between 36 and 41 MPa.g^{-1}.cm^3), except for the $^{0.7}SIK_CMKC$ sample (25 MPa.g^{-1}.cm^3). This is because the reactive siliceous species released from the $^{0.7}SIK_C$ solution could ensure a higher metakaolin degree of attack due, in this case, to the faster formation rate of $Al^{(IV)}$. However, the weak compressive strength observed in the case of $^{0.7}SIK_CMKC$ is due to the low reactivity of this metakaolin, in addition to the presence of mullite. Crystalline phases such as mullite are known to have higher stability in alkaline media, which may hinder the polycondensation reaction, increase the heterogeneity of the sample, and decrease the mechanical strength.

Conclusion

The various techniques used in this study allow a rapid characterization and quantification of the various species in alkaline silicate solutions. The FTIR and Raman spectroscopic data revealed the polymerization of the silicate entities when the Si/M molar ratio increases. Then, NMR analyses were used to quantify this phenomenon by determining the amount of the various silicate species. Thus, the reactivity of these solutions was found to be dependent on the Si/M ratio.

Knowledge of the reactivity of these solutions is useful for various applications, for example, the dilution of these solutions affects the silicate distribution on the sand surface. Moreover, the temperature and the drying mode influence the sample microstructure.

Alkaline solutions can be used as precursors to synthesize geopolymer materials. In this study, the behavior of three metakaolins in the presence of two potassium alkaline solutions with different reactivities was investigated using FTIR and ^{27}Al NMR during the geopolymer formation. Interactions between the silicate and aluminosilicate species were evident from an early stage of the reaction. As times progresses, the $Al^{(V)}$ and $Al^{(VI)}$ of metakaolin are converted to $Al^{(IV)}$. Different reaction rates were observed, depending on the reactivity of the used raw materials. A highly reactive alkaline solution favors the dissolution and the condensation reaction. The effect of the metakaolin reactivity is more significant when it is activated with an alkaline solution of low reactivity. Finally, a correlation was established between the amount of formed $Al^{(IV)}$ determined from ^{27}Al NMR and

the compressive strength data. The results indicate that the use of a highly reactive alkaline solution (high NBO and monomeric species content) and/or a highly reactive metakaolin (high wettability and amorphous phase) enhances the formation of the geopolymer network, which may improve the mechanical properties of the final materials. In summary, the reactivity of the alkaline solution and the metakaolin are key parameters to control the reaction rate, thereby controlling the final properties of the geopolymer materials.

References

Aguiar H, Serra J, González P, León B. Structural study of sol-gel silicate glasses by IR and Raman spectroscopies. J Non-Cryst Solids. 2009;355:475–80.

Autef A. Formulation géopolymère: influence des rapports molaires Si/K et Si/Al sur les réactions de polycondensation au sein des gels aluminosilicatés. PhD thesis. University of Limoges; 2013.

Autef A, Joussein E, Gasgnier G, Rossignol S. Role of the silica source on the geopolymerization rate. J Non-Cryst Solids. 2012;358:2886–93.

Bass JL, Turner GL, Morris MD. Vibrational and ^{29}Si NMR spectroscopies of soluble silicate oligomers. Macromol Symp. 1999;140:263–70.

Belova EV, Kolyagin YA, Uspenskaya IA. Structure and glass transition temperature of sodium silicate glasses doped with iron. J Non-Cryst Solids. 2015;423–424:50–7.

Bourlon A. Physico-chimie et rhéologie des géopolymères frais pour la cimentation des puits pétroliers. PhD thesis. University of Pierre et Marie Curie; 2011.

Brown IWM, Mackenzie KJD, Bowden ME, Meinhold RH. Outstanding problems in the kaolinite-mullite reaction sequence investigated by ^{29}Si and ^{27}Al solid-state nuclear magnetic resonance: 11, high-temperature transformations of metakaolinite. J Am Ceram Soc. 1985;68:298–301.

Brykov AS, Danilov VV, Aleshunina EY. State of silicon in silicate and silica-containing solutions and their binding properties. Russ J Appl Chem. 2008;81:1717–21.

Chligui M. Etude des propriétés optiques et mécaniques des verres binaires silicatés d'alcalins lourds. PhD thesis. University of Orléans; 2010.

Couty R, Fernandez L. Etude du passage de l'état colloïdal à l'état ionique de solutions de silicates sodiques par spectroscopie RMN ^{29}Si et infrarouge. J Chim Phys Phys Chim Biol. 1998;95:384–7.

Cyr M, Trinh M, Husson B, Casaux-Ginestet G. Effect of cement type on metakaolin efficiency. Cem Concr Res. 2014;64:63–72.

Davidovits J. Geopolymer: chemistry and applications. 2nd ed. St-Quentin: Institut Géopolymère; 2008.

Duxson P, Provis JL, Lukey GC, Mallicoat SW, Kriven WM. Understanding the relationship between geopolymer composition, microstructure and mechanical properties. Colloids Surf A. 2005a;269:47–58.

Duxson P, Lukey GC, Separovic F, van Deventer JSJ. Effect of alkali cations on aluminum incorporation in geopolymeric gels. Ind Eng Chem Res. 2005b;44:832–9.

Duxson P, Fernandez-Jimenez A, Provis JL, Lukey GC, Palomo A, Van Deventer JSJ. Geopolymer technology: the current state of the art. J Mater Sci. 2007;42:2917–33.

Engelhardt G, Zeigan D, Jancke H, Hoebbel D, Weiker Z. High resolution 29Si NMR of silicates and zeolites. Z Anorg Allg Chem. 1975;418:17–28.

Favier A, Habert G, Roussel N, De Lacaillerie JB. A multinuclear static NMR study of geopolymerisation. Cem Concr Res. 2015;75:104–9.

Fletcher RA, MacKenzie KJD, Nicholson CL, Shimada S. The composition rage of aluminosilicate geopolymers. J Eur Ceram Soc. 2005;25:1471–7.

Geissberger AE, Galeener FL. Raman studies of vitreous SiO_2 versus fictive temperature. Phys Rev B. 1983;28(6):3266–71.

Gharzouni A, Joussein E, Samet B, Baklouti S, Pronier S, Sobrados I, Sanz J, Rossignol S. The effect of an activation solution with siliceous species on the chemical reactivity and mechanical properties of geopolymers. J Sol-Gel Sci Technol. 2014;73:250–9.

Gharzouni A, Joussein E, Samet B, Baklouti S, Rossignol S. Effect of the reactivity of alkaline solution and metakaolin on geopolymer formation. J Non-Cryst Solids. 2015;410:127–34.

Gharzouni A, Joussein E, Samet B, Baklouti S, Rossignol S. Addition of low reactive clay into metakaolin-based geopolymer formulation: synthesis, existence domains and properties. Powder Technol. 2016;288:212–20.

Goudarzi N. Silicon-29 NMR spectroscopy study of the effect of tetraphenylammonium (TPA) as a template on distribution of silicate species on alkaline aqueous and alcoholic silicate solutions. Appl Magn Reson. 2013;44:469–78.

Gurevich L. Ceramic fuse wire coating. US patent 4,926,153. 1990.

Guyot J. Mesure des surfaces spécifiques des argiles par adsorption Ann. Argon. 1969;20:33–359.

Halasz I, Agarwal M, Li R, Miller N. Vibrational spectra of aqueous Na_2SiO_3 solutions. Catal Lett. 2007;117:34–42.

Halasz I, Agarwal M, Li R, Miller N. What can vibrational spectroscopy tell about the structure of dissolved sodium silicate. Microporous Mesoporous Mater. 2010;135:74–81.

Harris RK, Knight CTG. Silicon-29 nuclear magnetic resonance studies of aqueous silicate solutions. Part 5. First-order patterns in potassium silicate solutions enriched with silicon-29. J Chem Soc Faraday Trans 2. 1983a;79:1525–38.

Harris RK, Knight CTG. Silicon-29 nuclear magnetic resonance studies of aqueous silicate solutions. Part 6. Second order patterns in potassium silicate solutions enriched with silicon-29. J Chem Soc Faraday Trans 2. 1983b;79:1539–61.

Hehlen B, Neuville DR. Raman response of network modifier cations in alumino-silicate glasses. J Phys Chem B. 2015;119:4093–8.

Hunt JD, Kavner A, Schauble EA, Snyder D, Manning CE. Polymerization of aqueous silica in H_2O-K_2O solutions at 25–200 °C and 1 bar to 20 kbar. Chem Geol. 2011;283:161–70.

Iler RK. The chemistry of silica: solubility, polymerization, colloid and surface properties, and biochemistry. New York: Wiley-Interscience; 1979.

Iuga D, Morai C, Gan Z, Neuville DR, Cormier L, Massiot D. NMR heteronuclear correlation between quadrupolar nuclei in solids. J Am Chem Soc. 2005;127:11540–1.

Johnson ACJH, Greenwood P, Hagström M, Abbas Z, Wall S. Aggregation of nanosized colloidal silica in the presence of various alkali cations investigated by the electrospray technique. Langmuir. 2008;24:12798–806.

Keeley CT. Sodium silicate: the key ingredient in detergent agglomeration. J Am Oil Chem Soc. 1983;60:1370–2.

Konan KL, Soro J, Andji JYY, Oyetola S, Kra G. Etude comparative de la déshydroxylation/amorphisation dans deux kaolins de cristallinité différente. J Soc Ouest Afr Chim. 2010;30:29–39.

Krivenko P. Alkaline cements: terminology, classification, aspects of durability. In: Proceedings of the 10th International Congress on the Chemistry of Cement, Gothenburg, Sweden; 1997. 4iv046, p. 6.

Le Losq C, Neuville DR. Effect of the Na/K mixing on the structure and the rheology of tectosilicate silica-rich melts. Chem Geol. 2013;346:57–71.

Liew YM, Kamarudin H, Mustafa Al Bakri AM, Luqman M, Khairul Nizar I, Heah CY. Investigating the possibility of utilization of kaolin and the potential of metakaolin to produce green cement for construction purposes. Aust J Basic Appl Sci. 2011;5:441–9.

Lucas S, Tognonvi MT, Gelet J-L, Soro J, Rossignol S. Interactions between silica sand and sodium silicate solution during consolidation process. J Non-Cryst Solids. 2011;357:1310–8.

Malfait WJ, Halter WE, Morizet Y, Meier BH, Verel R. Structural control on bulk melt properties: single and double quantum ^{29}Si NMR spectroscopy on alkali-silicate glasses. Geochim Cosmochim Acta. 2007;71:6002–18.

Malfait WJ, Zakaznova-Herzog VP, Halter WE. Quantitative Raman spectroscopy: speciation of Na-silicate glasses and melts. Am Mineral. 2008;93:1505–18.

Man PP, Klinowski J. Quantitative determination of aluminium in zeolites by solid-state ^{27}AI N.M.R. Spectroscopy. J Chem Soc Chem Comm. 1988;19:1291–4.

Muroya M. Correlation between the formation of silica skeleton and Fourier transform reflection infrared absorption spectroscopy spectra. Colloid Surf A. 1999;157:147–55.

Mysen BO, Finger LW, Virgo D, Seifert FA. Curve-fitting of Raman spectra of silicate glasses. Am Mineral. 1982;67:686–95.

Nordström J, Nilsson E, Jarvol P, Nayeri M, Palmqvist A, Bergenholtz J, Matic A. Concentration- and pH-dependence of highly alkaline sodium silicate solutions. J Colloid Interface Sci. 2011;356:37–45.

Rees CA, Provis JL, Lukey GC, van Deventer JSJ. In situ ATR-FTIR study of the early stages of fly ash geopolymer gel formation. Langmuir. 2007;23(17):9076–82.

Rees CA, Provis JL, Lukey GC, van Deventer JSJ. The mechanism of geopolymer gel formation investigated through seeded nucleation. Colloid Surf A. 2008;318:97–105.

Rowels MR, Hanna JV, Pike KJ, Smith ME, Connor BHO. ^{29}Si, ^{27}Al, ^{1}H and ^{23}Na MAS NMR study of the bonding character in aluminosilicate inorganic polymers. Appl Magn Reson. 2007;32:663–89.

San Nicolas R, Cyr M, Escadeillas G. Characteristics and applications of flash metakaolins. Appl Clay Sci. 2013;83–84:253–62.

Schmidt BC, Riemer T, Kohn SC, Holtz F. Structural implications of water dissolution in haplogranitic glasses from NMR spectroscopy: influence of total water content and mixed alkali effect. Geochim Cosmochim Acta. 2001;65:2949–64.

Steins P. Influence des paramètres de formulation sur la texturation et la structuration des géopolymères. PhD thesis. University of Limoges; 2014.

Svensson IL, Sjöberg S, Öhman L-O. Polysilicate equilibria in concentrated sodium silicate solutions. J Chem Soc Faraday Trans. 1986;82:3635–46.

Talaghat MR, Esmaeilzadeh F, Mowla D. Sand production control by chemical consolidation. J Pet Sci Eng. 2009;67:34–40.

Tan J, Zhao S, Wang W, Davies G, Mo X. The effect of cooling rate on the structure of sodium silicate glass. Mater Sci Eng B. 2004;106:295–9.

Tognonvi MT, Massiot D, Lecomte A, Rossignol S, Bonnet J-P. Identification of solvated species present in concentrated and dilute sodium silicate solutions by combined 29Si NMR and SAXS studies. J Colloid Interface Sci. 2010;352:309–15.

Tognonvi MT, Soro J, Rossignol S. Physical-chemistry of silica/alkaline silicate interactions during consolidation. Part 1: effect of cation size. J Non-Cryst Solids. 2012;358:81–7.

Van Jaarsveld JGS, Van Deventer JSJ, Lorenzen L. The potential use of geopolymeric materials to immobilize toxic metals: part 1 theory and applications. Miner Eng. 1999;10:659–69.

Vivier G. Relations entre la microstructure des blocs agglomérés et les propriétés électriques des fusibles. PhD thesis. Institut National des Sciences Appliquées de Lyon; 2010.

Walther JV. Relation between rates of aluminosilicate mineral dissolution, pH, temperature and surface charge. Am J Sci. 1996;7:296–693.

Weng L, Sagoe-Crentsil K, Brown T, Song S. Effects of aluminates on the formation of geopolymers. Mater Sci Eng B. 2005;117:163–8.

Zotov N, Ebbsjö I, Timpel D, Keppler H. Calculation of Raman spectra and vibrational properties of silicate glasses: comparison between $Na_2Si_4O_4$ and SiO_2 glasses. Phys Rev B. 1999;60 (9):6383–97.

CONCLUSION GÉNÉRALE

Ce travail a été effectué dans le cadre du projet FE^2E dans le but de réaliser un fusible plus avantageux et plus écologique. La réponse à cette problématique nécessitait la maîtrise des différents constituants du fusible et des différentes interactions entre ces matériaux. Cette étude a donc été réalisée selon une suite d'étapes allant de la compréhension des différentes matières premières jusqu'à la réalisation d'un fusible et d'un busbar à base d'un matériau géopolymère.

Afin d'améliorer la tenue de l'agglomération du bloc de sable, il était nécessaire dans un premier temps de comprendre les solutions de silicate alcalin et notamment de déterminer les espèces réactives, puis de maîtriser les interactions entre ces espèces et le sable au cours du séchage.

L'étude des solutions, par différentes techniques spectroscopiques, a permis d'identifier les espèces réactives en fonction de différents paramètres tels que le cation alcalin, le rapport molaire Si/M et le taux d'eau. Des abaques relatifs au degré de polymérisation ont été obtenus quelle que soit la solution de silicate. A titre d'exemple, la diminution du taux d'eau et du rapport molaire Si/M entraîne une diminution du degré de polymérisation de la solution, favorisant la formation d'espèces dépolymérisées telles que les entités Q^0, Q^1 ou la formation d'espèces cycliques R_3 et R_4 et induisant par conséquent une augmentation de sa réactivité.

Afin de pallier la répartition du silicate au sein de l'empilement granulaire du sable, les essais d'imprégnation, suivis d'un séchage conventionnel ou micro-ondes à 110 et 150 °C, ont permis de révéler que seul le séchage conventionnel au-delà de 100 °C favorisait la formation de ponts entre les grains de sable. Le mélange préalable de la solution de silicate et de sable associé au séchage conventionnel à 150 °C, avec des contraintes à la rupture de l'ordre de 8 - 10 MPa, est la méthode à retenir.

La réalisation d'une pièce céramique basse température par la création d'une couche intermédiaire à base d'une source aluminosilicate ou par coulage d'un liant géopolymère a ensuite été effectuée.

Afin d'identifier les paramètres responsables de la réactivité du liant vis-à-vis du bloc de sable, les études par des mesures d'angles de mouillage ont mis en évidence une diminution de l'angle plus ou moins importante au cours du temps. Ceci souligne l'influence de la formulation du liant sur l'imprégnation du bloc de sable aggloméré par le liant géopolymère. Des essais d'enrobage ont mis en évidence que l'apparition de fissures sur les dépôts de liants géopolymères peut être contrôlée en modifiant la formulation et, plus particulièrement, le cation

alcalin et la source aluminosilicate. L'utilisation d'une solution à base de silicate de potassium et d'un métakaolin de faible réactivité s'avère pertinente pour obtenir des dépôts ne présentant pas de fissuration et de faible épaisseur. La tenue du dépôt a été expliquée par la diffusion du liant géopolymère au sein du bloc de sable aggloméré.

La mise en forme des liants géopolymères est réalisable par coulage. Cependant, cette technique nécessite la connaissance du retrait au cours de la prise. Les paramètres permettant de contrôler le retrait à température ambiante ont été identifiés. Il a ainsi été démontré que le retrait peut être contrôlé à la fois par le rapport Si/Al, et par la compensation de charge par le cation alcalin. Ceci a donc conduit à l'ensablage d'un corps de fusible en liant géopolymère.

Finalement, une rupture technologique a été envisagée via la validation de la tenue en température des nouvelles pièces en liant géopolymère et l'étude des interactions entre un liant et une surface métallique.

Les paramètres sélectionnés pour la tenue en température des liants ont été la modification de la solution alcaline par l'ajout d'un additif et la modification de la formulation.

L'obtention d'un matériau stable en température est rendue possible par la fonctionnalisation d'une solution alcaline peu réactive par l'ajout d'un additif, tel que du molybdate d'ammonium, en présence de différentes sources aluminosilicates. L'ajout de molybdène permet une diminution importante de la valeur de retrait à 1400 °C de 20 à 5 % indiquant une meilleure tenue en température de ces échantillons. De plus, des domaines de tenue en température des liants géopolymères ont été identifiés et dépendent de la formulation du liant. Il a également été démontré que des liants possédant un rapport molaire Si/(Al+M) supérieur à 1 présentent une tenue en température correcte à 800 °C.

L'adhésion d'un liant géopolymère sur du métal a ensuite été étudiée en choisissant des formulations répondant aux critères déterminés par les angles de mouillage. En effet, la nature du cation alcalin et le type de métakaolin dont dépendent les réactions de géopolymérisation, ainsi que la valeur de pH initiale du liant influençant la libération d'espèces, favorisent ou non l'adhésion. Une valeur de pH initiale élevée (cf. M1K) favorise la libération d'espèces ioniques entraînant la formation d'un dépôt hétérogène et fissuré, alors qu'un mélange de faible valeur de pH (cf. MTK) favorise la formation d'un dépôt homogène.

Des essais d'enrobage à l'aide de différentes compositions de liants géopolymères ont ensuite été réalisés sur des plaques de cuivre étamé en présence de différentes atmosphères. Le contrôle de l'eau étant un paramètre crucial, il a été démontré que le séchage en atmosphère contrôlée

(85,5 %HR et 25 °C) par rapport à un séchage en moule ouvert (65 %HR, P_{atm} et 25 °C) favorise l'adhésion entre le liant et le support métallique. Un liant géopolymère à base de sodium et d'un mélange de deux métakaolins de réactivités différentes, en atmosphère humide, doit être réalisé pour favoriser l'adhésion entre le liant et une plaque de cuivre étamé.
Finalement, compte tenu de tous ces critères, un busbar a été obtenu par coulage d'un liant géopolymère résistant jusqu'à la température de 800 °C.

Cette étude a donc démontré qu'il était possible d'envisager la réalisation d'un fusible plus écologique et plus économique par l'utilisation de liants géopolymères. La fabrication d'autres composants électriques, tels que les busbars, à base de liants géopolymères semble également envisageable. Néanmoins, afin d'améliorer les performances, il pourrait être envisagé les actions suivantes :

(i) L'obtention d'un bloc de sable aggloméré nécessitant une énergie de consolidation moindre, de propriétés mécaniques homogènes, devrait être poursuivie par le séchage micro-ondes en modifiant la puissance ainsi que par l'optimisation de la méthode d'imprégnation.

(ii) La couche de liaison pourrait être améliorée en étudiant des mélanges de viscosité différente afin d'assurer ou non une étanchéité du bloc de sable.

(iii) La fabrication d'un busbar en une étape nécessite une optimisation à la fois au niveau des interactions entre le liant et les différents métaux, mais aussi sur la façon de réaliser le bloc par coulage, par projection ou par méthode additive.

(iv) Quelle que soit la fabrication retenue, il faudrait évaluer les performances de l'assemblage en conditions d'usage.

Résumé

Cette étude s'inscrit dans le cadre du projet FE²E visant à développer un fusible plus économique et plus écologique. Ce travail a donc été réalisé selon un schéma allant de la caractérisation des matières premières à la fabrication de composants électriques à l'aide de matériaux géopolymères. La réactivité des solutions de silicate a été déterminée par spectroscopies infrarouge, Raman et résonance magnétique nucléaire. Les interactions entre les solutions et du sable ont ensuite été étudiées selon différentes méthodes d'imprégnation et différents types de séchage, afin d'optimiser les propriétés mécaniques des blocs de sable aggloméré. Le remplacement des corps de fusible par des liants géopolymères a été envisagé par la création d'un dépôt ou par coulage du liant. Ensuite, la validation des propriétés thermiques des liants et les interactions entre un liant et une surface métallique ont permis d'envisager une rupture technologique. Finalement, il a été démontré qu'il était possible d'obtenir un fusible ou un busbar à base de liants géopolymères.

Mots clés : fusible, solution de silicate, sable, géopolymère, spectroscopie Raman, traitement thermique, métal.

Abstract

This study is a part of the FE²E project and was accomplished in order to develop an economic and ecologic fuse. The methodology covers different steps going from the raw materials characterization to the manufacturing of electrical components (as fuse and busbar) with geopolymer materials. The reactive species in alkaline solutions were determined by FTIR, NMR and Raman spectroscopies. Then, the interactions between the sand and the solutions were studied using various impregnation and different curing methods in order to optimize the mechanical properties of agglomerated sand. Fuse body replacement by geopolymer binders by a coating or by casting in a mold were considered. Then, the validation of the thermal properties by thermal treatment and the interactions between a geopolymer binder and a metallic surface conduce to a technological disruptive. Finally, the possibility to obtain a geopolymer-based fuse or busbar was clearly evidenced.

Key words: fuse, silicate solution, sand, geopolymer, Raman spectroscopy, thermal treatment, metal.